State of Oregon
Oregon Department of Geology and Mineral Industries
Ian P. Madin, Interim State Geologist

SPECIAL PAPER 47

COASTAL FLOOD HAZARD STUDY, TILLAMOOK COUNTY, OREGON

by Jonathan C. Allan[1], Peter Ruggiero[2], Gabriel Garcia[2],
Fletcher E. O'Brien[3], Laura L. Stimely[1], and Jed T. Roberts[3]

2015

[1] Oregon Department of Geology and Mineral Industries, Coastal Field Office, P.O. Box 1033, Newport, OR 97365
[2] College of Earth, Ocean and Atmospheric Sciences, Oregon State University, Corvallis, OR 97331
[3] Oregon Department of Geology and Mineral Industries, 800 NE Oregon St., Ste. 965, Portland, OR 97232

DISCLAIMER

This product is for informational purposes and may not have been prepared for or be suitable for legal, engineering, or surveying purposes. Users of this information should review or consult the primary data and information sources to ascertain the usability of the information. This publication cannot substitute for site-specific investigations by qualified practitioners. Site-specific data may give results that differ from the results shown in the publication.

Cover photograph: Wave runup and overtopping during a moderate storm in Neskowin, Tillamook County. Photo taken by A. Thibault, January 9, 2008.

Oregon Department of Geology and Mineral Industries Special Paper 47
Published in conformance with ORS 516.030

For additional information:
Administrative Offices
800 NE Oregon Street #28, Suite 965
Portland, OR 97232
Telephone (971) 673-1555
Fax (971) 673-1562
http://www.oregongeology.org
http://www.oregon.gov/DOGAMI/

TABLE OF CONTENTS

LIST OF FIGURES

LIST OF TABLES

1.0 INTRODUCTION

The objective of the Tillamook County coastal flood hazard project is to develop a digital flood insurance rate map (DFIRM) and flood insurance study (FIS) report for Tillamook County, Oregon (**Figure 1-1**). A parallel effort is underway to convert the existing Tillamook County Federal Emergency Management Agency (FEMA) flood maps to a new countywide format in the North American Vertical Datum of 1988 (NAVD88); however, the scope of that project is strictly digital conversion and no new studies and/or updated floodplain boundaries are being incorporated. For this effort, the Oregon Department of Geology and Mineral Industries (DOGAMI) will be using available light detection and ranging data (lidar) to redelineate flood hazards within Tillamook County, produce revised DFIRMs and a revised FIS report, and produce other mapping products useable at the local, state, and federal level for mitigation planning, risk analysis, and disaster response.

As part of the redelineation, DOGAMI has been contracted to perform detailed coastal flood hazard studies for several stretches of beach along the Tillamook County shoreline of the Pacific Ocean. These analyses are to include assessments of the 1% annual probability, or 100-year, extreme storm wave event and the associated calculated wave setup, runup, and total water level (i.e., the wave runup superimposed on the tidal level) to help guide the determination of Special Flood Hazard Areas (SFHAs), the most significant being regions subject to high coastal flood risk (Zone VE), characterized with base flood elevations (BFEs) that are used to guide building practices. Additional modeling of the 0.2%, or 500-year, event will also be undertaken.

These detailed analyses will be limited to the following key areas (**Figure 1-1**):

- Neskowin littoral cell: extends from the north side of Cascade Head to Cape Kiwanda. This particular shore section includes the communities of Neskowin, North Neskowin, and Pacific City;
- Sand Lake littoral cell: extends from Cape Kiwanda north to Cape Lookout. This section includes the community of Tierra Del Mar;
- Netarts littoral cell: extends from Cape Lookout to Cape Meares. This sections includes Cape Lookout State Park and the communities of Happy Camp (Netarts), Oceanside, and Short Sand Beach; and
- Rockaway littoral cell: extends from the north side of Cape Meares to Neahkahnie Mountain in the north. This section includes the communities of Cape Meares, Twin Rocks, Rockaway, Nedonna Beach, Nehalem State Park, and Manzanita.

The communities noted above represent approximately 43% of the mapped Tillamook coastline; the remainder of the coast has been mapped as FEMA flood zone categories “D” (e.g., most of the spits) and “V” (e.g., Nehalem State Park). These latter areas reflect areas that were previously not mapped using detailed hydraulic analyses. As a result, this study will provide updated detailed coastal hydraulic analyses for the same communities, and will extend the detailed analyses by an additional 30% to encompass areas outside the existing areas. For the remaining 27% of the Tillamook County coast, the shoreline will be redefined as V zone (e.g., along the headlands) to better reflect the geomorphology of those areas.

The development of coastal flood maps is complicated due to its dependence on a myriad of data sources required to perform wave transformation, runup, and overtopping calculations. These challenges are further compounded by an equally wide range of potential settings in which the data and methods can be applied, which range from dune to bluff-backed beaches, sites that may be backed by coastal engineering structures such as sea walls, riprap revetments, or wooden bulkheads, to gravel and hard-rock shorelines. **Figure 1-2** broadly summarizes the steps described in the ensuing sections in order to provide a conceptual basis for the process that leads, ultimately, to the completed coastal flood hazard zones.

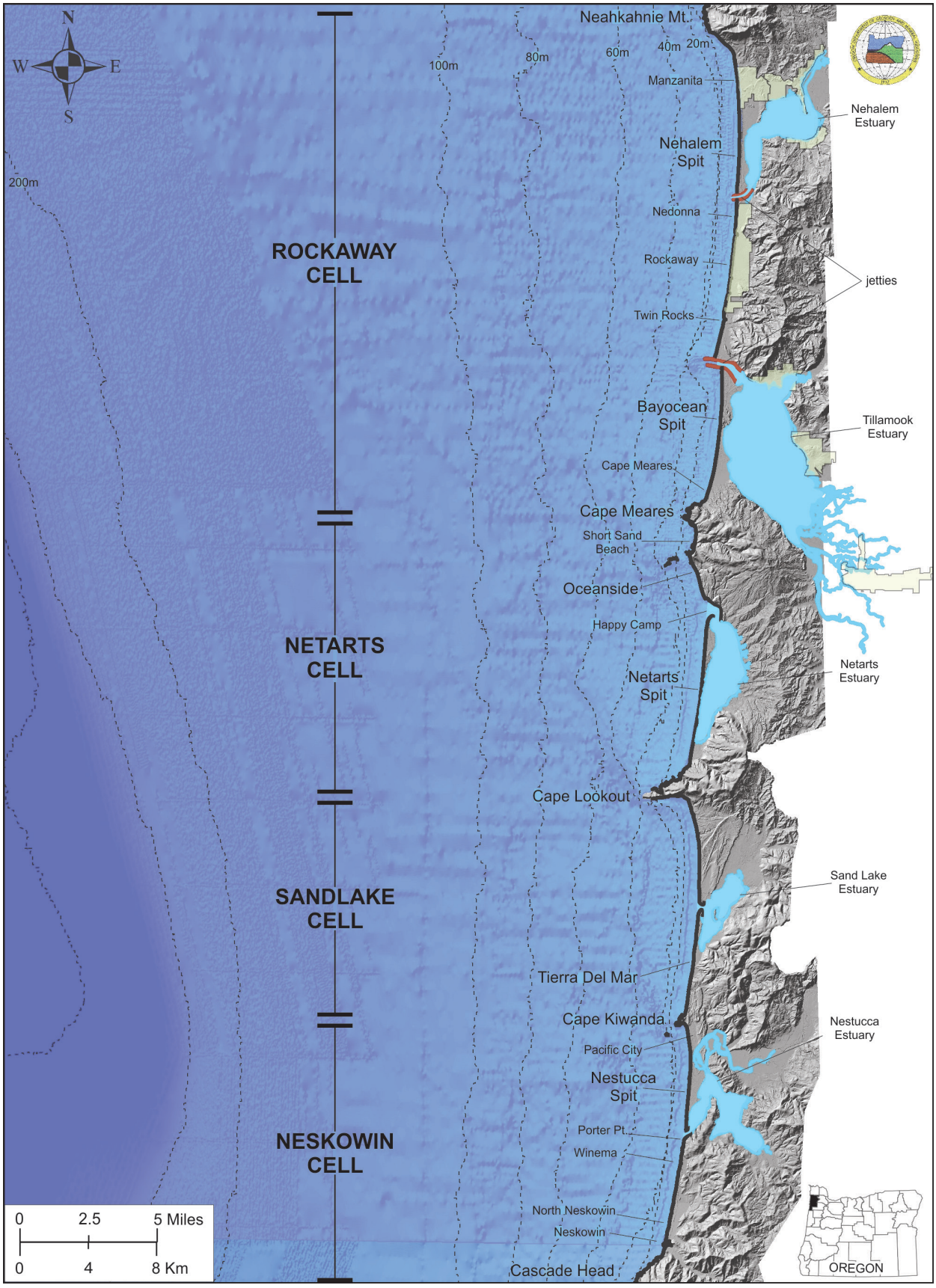

Figure 1-1. Location map of the Tillamook County, Oregon coastline.

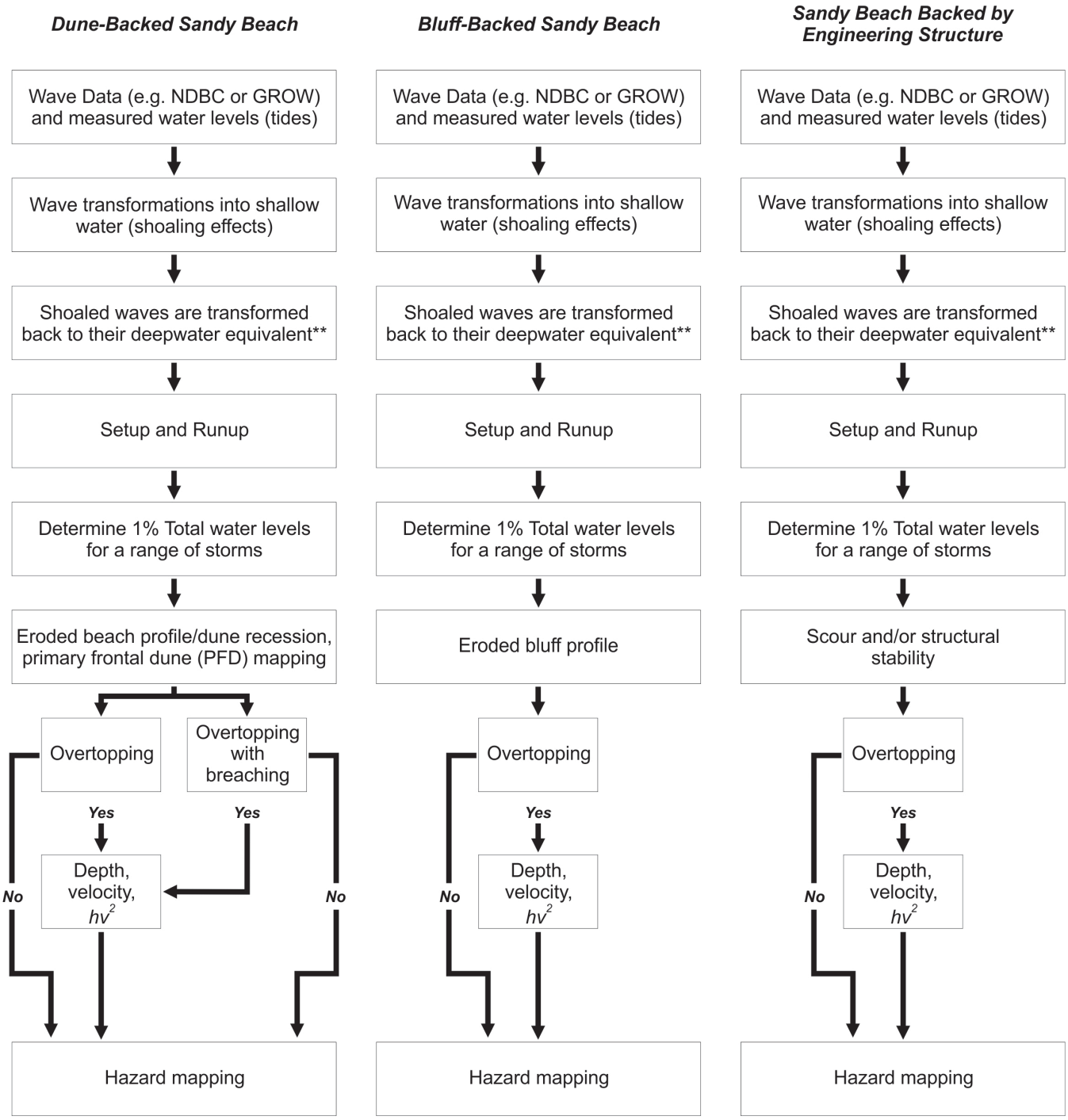

Figure 1-2. Three representative examples of the steps that may be taken to derive coastal flood hazard maps on the Pacific Northwest coast. **Note: The waves are first shoaled using numerical models in order to account for the effect of wave changes (refraction/diffraction) that take place across the shelf and in the nearshore. Because many coastal engineering equations (e.g. wave runup) require deepwater inputs, the "shoaled" waves are then converted back to their deepwater equivalence.

This report first examines the coastal geology and geomorphology of the Tillamook County shoreline, including a discussion of the erosion history of the coast. The results presented in this section will ultimately form the basis for defining the flood zones along the Tillamook coast. Section 3 presents the results of Real-Time Kinematic Differential Global Positioning Surveys (RTK-DGPS) of the detailed study sites established along the length of the Tillamook County shoreline, undertaken at the peak of the 2011-12 winter. These surveys are also compared with recent historical data derived from lidar data, which are used to help define the most eroded winter profile used in the runup calculations described in Section 6. Section 3 also documents various parameters associated with the measured beach profile data, including the beach/dune junction elevation, the beach slope and dune/bluff crest/top elevations.

Section 4 presents an examination of the tide data measured by the National Ocean Service (NOS) of the National Oceanographic Atmospheric Administration (NOAA) Garibaldi tide gauge (Tillamook Estuary) and the South Beach, Yaquina Bay tide gauges (including several other gauges), including an analysis of the 1% and 0.2% *still water levels* (SWL). Section 5 describes the steps undertaken to develop a synthesized wave climate, critical for developing the input wave statistics used in calculating the wave runup. Section 5 also examines the procedures used to refract the waves from deep water into the nearshore using the SWAN (Simulating Waves Nearshore) wave model. Analyses of the wave runup, including the calculation of the 1% and 0.2% total water levels (TWL), as well as any overtopping calculations, are presented and discussed in Section 6.

Section 7 discusses the steps used to determine the degree of erosion that might occur on the dune-backed beaches, including the approach used to define the duration-reduced erosion factor, important for further establishing the initial conditions on which the runup and overtopping calculations are ultimately performed. Similar discussions are provided describing observations of bluff erosion, characteristic of a few discrete sections of the Tillamook County shoreline. Finally, Section 8 synthesizes all of the information and describes the steps taken to draft new flood maps along the Tillamook County shoreline.

2.0 COASTAL GEOLOGY AND GEOMORPHOLOGY OF TILLAMOOK COUNTY

Tillamook County is located on the northwest Oregon coast, between latitudes 45° 45′ 49.49″ N (Cape Falcon) and 45° 3′ 54.88″ N (Cascade Head), and longitudes 124° 1′ 15.57″ W and 123° 17′ 59.88″ W. The terrain varies from low-elevation sandy beaches and dunes on the coast to elevations over 1,000 m (e.g., Rogers Peak reaches 1,130 m [3,706 ft]) farther inland. The coastal strip is approximately 104 km (65 miles) in length and varies in its geomorphology from broad, low-sloping sandy beaches backed by dunes, to beaches backed by engineered structures, cobble and boulder beaches adjacent to the headlands, and cliff shorelines. Prominent headlands formed of resistant basalt (e.g., Cascade Head, Cape Meares, Cape Lookout, and Neahkahnie Mountain) provide natural barriers to alongshore sediment transport (Komar, 1997), effectively dividing the county coastline into four littoral cells. These are:

- Neskowin littoral cell (~14.3 km), which extends from the north side of Cascade Head to Cape Kiwanda;
- Sand Lake (~13.2 km), which extends from Cape Kiwanda north to Cape Lookout;
- Netarts (~15.9 km), which extends from Cape Lookout to Cape Meares; and
- Rockaway littoral cell (~28.2 km), which extends from the north side of Cape Meares to Neahkahnie Mountain in the north.

Each of these cells is further divided into a series of subcells due to the presence of five estuaries (in order from south to north, Nestucca, Sand Lake, Netarts, Tillamook, Nehalem), two of which (Tillamook and Nehalem) are stabilized by prominent jetties (**Figure 1-1**). The county also is characterized by several major rivers (Nestucca, Nehalem, Miami, Tillamook, Trask, Kilchis, and Wilson Rivers) that terminate in the estuaries.

Due to their generally low flows and the terrain they are eroding, these rivers carry little beach sediment out to the open coast but instead deposit most of their sediment in the estuaries (Clemens and Komar, 1988; Komar and others, 2004). Hence, the beaches of Tillamook County receive very little sediment along the coast today other than from erosion of the backshore.

2.1 Local Geology

Along the Tillamook County coast the predominant geologic unit consists of latest Holocene beach sand present along the full length of the coastline (**Figure 2-1**) (Cooper, 1958). Interspersed between the sand are intrusive rocks (Tertiary age basalt), which characterize discrete areas, such as Neahkahnie Mountain at the northern end of the county coastline (**Figure 2-2**). Other volcanic rocks (Miocene age) form the prominent headlands such as at Cape Meares and Cape Lookout (Schlicker and others, 1972). These latter rocks are described as fine-grained. In all cases, rockfalls and landslides in these latter units are actively providing new material to the beaches, gravel and cobbles, albeit at relatively slow rates. These failures contribute to the formation of extensive cobble and boulder berms (**Figure 2-2**), which accumulate along their northern/southern flanks, where beaches have merged up against the headlands.

South of Cape Lookout and north of the Sand Lake estuary, much of the beach is backed by bluffs, which have an average height of 24 m (Allan and Harris, 2012) consisting of medium-grained sandstone and interbedded siltstone of the Astoria Formation (**Figure 2-3**). This particular rock formation also characterizes the geology of Cape Kiwanda, adjacent to Pacific City (**Figure 2-4**). Sandstone is also prominent along a small section of the coast adjacent to Porter Point (**Figure 1-1**), located just south of the Nestucca estuary mouth. These latter sediments are considered to be much older (Oligocene to Miocene) in age and are described as massive basaltic sandstone that is predominantly fine- to medium-grained (Schlicker and others, 1972).

Much of the beach sand present on the Oregon coast consists of grains of quartz and feldspar. The beaches also contain small amounts of heavier minerals (e.g. garnet, hypersthene, augite, and hornblende [**Figure 2-5**]), which can be traced to various sediment sources along the Pacific Northwest coast (Clemens and Komar, 1988). For example, garnet and hypersthene is derived from the Klamath Mountains located in southern Oregon and in North California. Because the headlands today extend well out in deep

water, they effectively limit sand transport around their ends under the current process regime. This suggests that these heavier minerals were probably transported northward along the coast at a time when sea level was much lower, with few barriers to interrupt their northward movement (Komar, 1997). With distance from their source, the sediments combined with other minerals derived locally from erosion processes in the coast range. As shown in **Figure 2-5**, the concentrations of garnet and hypersthene decrease to the north, while concentrations of of augite increase significantly; augite is a mineral that is prevalent in the volcanic rocks present throughout Tillamook County. At Tillamook Head, the concentration of garnet is very small, suggesting that Tillamook Head reflects its most northerly transport. North of Tillamook Head, it can be seen that concentrations of hypersthene and hornblende increase again. These latter sediments are derived from the Columbia River, which contributed to the formation of the Clatsop Plains, Long Beach Peninsula, and Grayland Plains. Thus, sediments derived from the Columbia River were transported mainly to the north, supplying the Washington coast and shelf.

With the end of the last glaciations, sea level rose rapidly and the beaches began to migrate landward. New sediments were derived from erosion of the coastal plain that makes up the continental shelf today. At around 5,000–7,000 years ago, the rate of sea level rise slowed as it approached its current level today (Komar, 1997). At this stage the prominent headlands would have begun to interrupt sediment transport. Modern barrier spits and beaches began to form within the headland bounded littoral cells that make up the present coast today.

Along the Tillamook County coast, the beaches contain abundant concentrations of augite, indicative of their having been derived locally (**Figure 2-5**). This implies that at the time, rivers and streams were carrying these sediments out to the coast where they mixed with other sediments. These concentrations likely increased during the past 150 years as human settlement accelerated leading to increased deforestation (Peterson and others, 1984; Komar and others, 2004). This correspondingly contributed to increased sediment loads in the various rivers. However, analyses of the sediment characteristics in Tillamook Bay, the largest estuary in the county, indicated that while fine sediments pass through the estuary, the bulk of the coarser sediments remain behind where they accumulate as bars and shoals in Tillamook Bay (Komar and others, 2004). Furthermore, sediments within Tillamook Bay are predominantly of a marine origin (60%), while river sediments make up 40% of the sediment in the estuary. This finding is consistent with the work of Peterson and others (1984) and Clemens and Komar (1988), who observed that because of the combination of low river discharge and high tidal regime in Oregon estuaries, the majority of the estuaries are in fact natural "sinks" for the sediment. Thus, the beaches of Oregon receive very little sediment input from rivers and streams today. Accordingly, sediment supply is essentially confined to those areas backed by coastal bluffs, particularly those areas overlain by more erosive Pleistocene marine terrace sandstones (raised ancient beach and dune sands) and more recent Holocene dune sands that drape the landscape.

Prior to the 1940s, many of the barrier spits were devoid of significant vegetation. With the introduction European beach grass (*Ammophila arenaria*) in the early 1900s and its subsequent proliferation along the Oregon coast, the grass essentially resulted in the stabilization of the dunes and barrier spits. The product today is an extensive foredune system, which consist of large "stable" dunes containing significant volumes of sand. Accompanying the stabilization of the dunes, humans have settled on them, building in the most desirable locations, typically on the most seaward foredune. As will be shown throughout this report, construction of these homes and facilities in such areas poses a significant risk as periodically storms erode into the dunes. This has resulted in many cases where the foundations of the homes are undermined, eventually requiring riprap coastal engineering structures to mitigate the erosion problem.

Figure 2-1. Looking north along Bayocean spit, the Tillamook jetties (Tillamook Bay to the right), Rockaway just north of the jetties, Nehalem Spit and Neahkahnie Mountain in the far distance (photo: E. Harris, DOGAMI, 2011).

Figure 2-2. Looking east at Neahkahnie Mountain. U.S. Highway 101 can be seen around mid photo tracking along the mountain. To the right and along the toe of the bluff is an extensive cobble/boulder berm that has formed as a result of rockfalls and landslides off the headland (photo: L. Stimely, DOGAMI, 2011).

Figure 2-3. Looking south toward Cape Kiwanda in the distance. Coastal bluffs of the Astoria Formation characterize much of the shore north of Sand Lake. Note the presence of cobbles to the left of the photo, which serve to protect the bluff toe (photo: J. Allan, DOGAMI, 2011).

Figure 2-4. Looking east across Cape Kiwanda toward the town of Pacific City. Cape Kiwanda is described as Astoria Formation sandstone. Immediately adjacent to the headland, latest Holocene dune sand have ramped up and over the headland (photo: L. Stimely, DOGAMI, 2011).

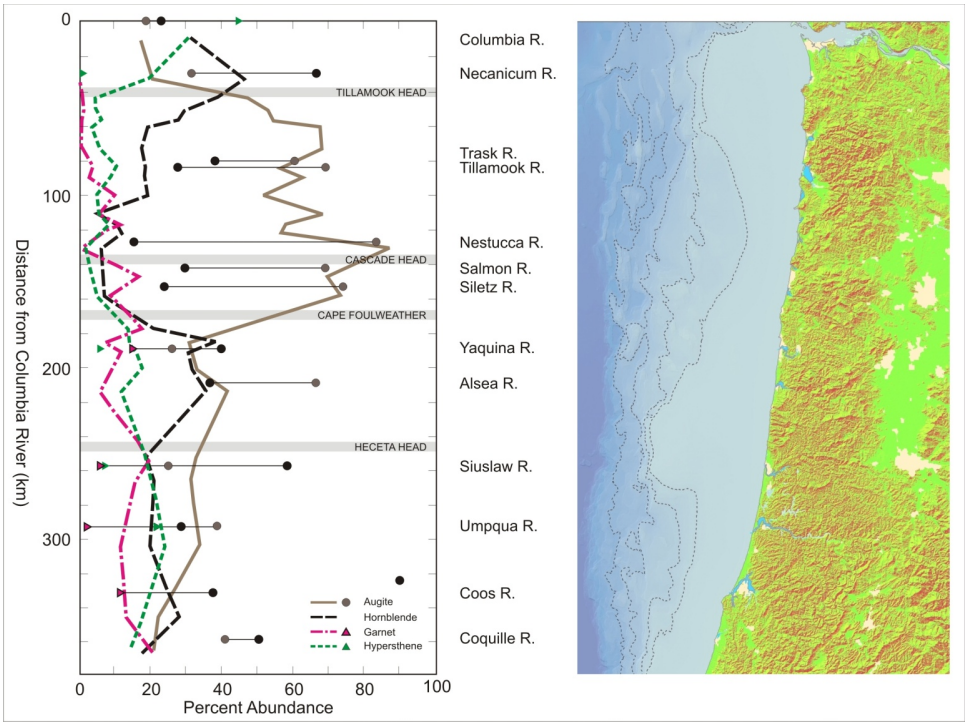

Figure 2-5. Variations in the percent abundances of various heavy minerals observed on the central to northern Oregon coast (after Clemens and Komar, 1988).

2.2 Tsunami Hazards Associated with the Cascadia Subduction Zone and from Distant Earthquake Sources

Considerable geologic data from estuaries and coastal lakes along the Cascadia subduction zone provides evidence for episodic occurrences of abrupt coastal subsidence immediately followed by significant ocean flooding associated with major tsunamis that swept across the ocean beaches and also traveled well inland through the bays and estuaries. Coastal paleoseismic records document the impacts of as many as 13 major subduction zone earthquakes and associated tsunamis over the past ~7,000 years (Witter and others, 2003; Kelsey and others, 2005; Witter and others, 2010), while recent studies of turbidite records within sediment cores collected in deep water at the heads of Cascadia submarine canyons provide evidence for at least 41 distinct tsunami events over the past ~10,000 years (Goldfinger and others, 2003; Goldfinger, 2009; Goldfinger and others, 2012). The length of time between these events varies from as short as a century to as long as 1,200 years, with the average recurrence interval for major Cascadia earthquakes (magnitude [M_W] > 9) estimated to be ~530 years (Witter and others, 2010).

The most recent Cascadia subduction zone earthquake occurred on January 26, 1700 (Satake and others, 1996; Atwater and others, 2005) and is estimated to have been a magnitude (M_W) 9 or greater based on the size of the tsunami documented along the coast of Japan. From correlations between tsunami deposits identified at multiple sites along the length of the PNW coast this event probably ruptured the full length (~1,200 km) of the subduction zone.

There is now increasing recognition that great earthquakes do not necessarily result in a complete rupture of the Cascadia subduction zone (i.e., rupture along the full 1,200 km fault zone), such that partial ruptures of the plate boundary have occurred in the paleo-records due to smaller earthquakes with magnitudes (M_W) < 9 (Witter and others, 2003; Kelsey and others, 2005). These partial segment ruptures appear to occur more frequently on the southern Oregon coast, determined from paleotsunami studies (stratigraphic coring, radiocarbon dating and marine diatom analyses) undertaken at several locations on the southern Oregon coast, including Bradley Lake located just south of Bandon, the Sixes River and the Coquille estuary. According to Kelsey and others (2005), initial estimates of the recurrence intervals of Bradley Lake tsunami incursion are typically shorter (~380–400 years) than the average recurrence intervals inferred for great earthquakes (~530 years). Furthermore, they have documented from those records that local tsunamis from Cascadia earthquakes recur in clusters (~250–400 years) followed by gaps of 700–1,300 years, with the highest tsunamis associated with earthquakes occurring at the beginning and end of a cluster.

Recent analyses of the turbidite records (Goldfinger, 2009; Goldfinger and others, 2012) suggest that of the 41 events in the geologic past:

- 20 events were probably associated with a rupture of the full Cascadia subduction zone, characterized by a magnitude (M_W) ~9 or greater earthquake;
- 2-3 events reflected a partial rupture (~75%) of the length of the subduction zone, characterized by an estimated earthquake magnitude (M_W) of ~8.5–8.8 earthquake;
- 10-11 events were associated with a partial rupture (~50%), characterized by an estimated earthquake magnitude (M_W) of ~8.3–8.5 earthquake; and
- 8 events reflected a partial rupture (~25%), with an estimated earthquake magnitude (M_W) of ~7.6–8.4.

These last 19 shorter ruptures are concentrated in the southern part of the margin and have estimated recurrence intervals of ~240–320 years. Goldfinger (2009) estimated that time-independent probabilities for segmented ruptures range from 7-9% for full margin ruptures, to ~18% in 50 years for a southern segment rupture; time dependent rupture analyses indicate that the probability increases to ~25% in 50 years for the northern zone.

Aside from local tsunamis associated with the Cascadia subduction zone, the Oregon coast is also susceptible from tsunamis generated by distant events, particularly along the coast of Japan, along the Aleutian Island chain, and from the Gulf of Alaska. The most recent distant tsunami event occurred on March

11, 2011, when a magnitude (M_W) 9.0 earthquake occurred 129 km (80 miles) offshore from the coast of Sendai, northeast Honshu, Japan (Allan and others, 2012a). This earthquake triggered a catastrophic tsunami that within minutes inundated the northeast coast of Japan, sweeping far inland; most recent reports indicate 15,854 dead and another 3,155 missing. Measurements derived from a tide gauge on the impacted shore (Ayukawa, Ishinomaki, Miyagi Prefecture) recorded a tsunami amplitude of 7.6 m, before the gauge was destroyed by the initial tsunami wave (Yamamoto, 2011), while post-tsunami surveys indicate that the tsunami water levels within the inundation zone reached as high as 19.5 m (64 ft) (Mori and others, 2011). The tsunami also propagated eastward across the Pacific Ocean, impacting coastal communities in Hawaii and along the west coast of the continental United States — Washington, Oregon, and California.

Damage in Oregon, Washington, and northern California from the tsunami was almost entirely confined to harbors, including Depoe Bay, Coos Bay, Brookings in Oregon, and in Crescent City, California, having been moderated by the arrival of the tsunami's highest waves during a relatively low tide (Allan and others, 2012a). At Crescent City, an open-coast breakwater, the to-and-fro surge of the water associated with the tsunami waves overturned and sank 15 vessels and damaged 47, while several boats were swept offshore. Flood damage also occurred during the early hours of March 12; for example, an RV park near the mouth of Elk Creek was flooded when a 1.05 m (3.4 ft) tsunami wave arrived, coinciding with high tide. The total damage to the Crescent City harbor and from the effects of the flooding has been placed at $12.5 million. At Brookings on the southern Oregon coast, 12 fishing vessels put to sea at about 6 am, prior to the arrival of the tsunami waves. However, the *Hilda*, a 220-ton fishing boat and the largest in the harbor, broke loose under the forces of the wave-induced currents, washing around the harbor and smashing into and sinking several other boats. Much of the commercial part of the harbor and about one third of the sports basin were destroyed; the total damage has been estimated at about $10 million.

Prior to the Tōhoku tsunami, the previous most significant distant tsunami occurred on March 27, 1964, when a magnitude (M_W) 9.2 earthquake occurred near Prince William Sound in Alaska. The earthquake generated a catastrophic local tsunami in Alaska, but the effects of the tsunami were also felt around the Pacific Basin. The tsunami caused significant damage to infrastructure in the coastal communities of Seaside and Cannon Beach, Oregon, and killed four people camping along Beverly Beach in Lincoln County, Oregon.

In 2009, the Oregon Department of Geology and Mineral Industries (DOGAMI) initiated a multi-year study to accelerate remapping of the Oregon coast for tsunami inundation using state of the art computer modeling and laser based terrain mapping (lidar). The outcome of this effort was the creation of new and more accurate tsunami evacuation maps for the entire length of the coast. DOGAMI, in collaboration with researchers (Zhang and Baptista) at the Oregon Health and Science University (OHSU), Oregon State University (Goldfinger) and the Geological Survey of Canada (Wang), developed a new approach to produce a suite of next-generation tsunami hazard maps for Oregon (Priest and others, 2010; Witter and others, 2010). Modeling tsunami inundation on the southern Oregon coast was initiated late in 2009 and consisted of a range of scenarios, including 15 Cascadia events and two distant earthquake source events (e.g., 1964 Prince William Sound earthquake magnitude [M_W] 9.2 earthquake [Witter, 2008]). The last of the suite of new evacuation maps (TIM series) was released in 2013; the maps are also available in an online tsunami hazard portal (http://nvs.nanoos.org/TsunamiEvac).

Associated with great Cascadia earthquakes is a near instantaneous lowering (subsidence) of the coast by ~0.4 m (1.3 ft) to as much as 3 m (9.8 ft) (Witter and others, 2003). This process equates to raising sea level by the same amount along the entire Pacific Northwest coastline. Following the earthquake, coastal erosion is expected to accelerate everywhere as the beaches and shorelines adjusted to a new equilibrium condition that, over time, would likely decrease asymptotically (Komar and others, 1991). On the southern Oregon coast, Komar and others have suggested that the extensive development of sea stacks offshore from Bandon may be evidence for that erosion response following the last major subduction zone earthquake in 1700. Over the past century, the

erosion appears to have stabilized as there is little evidence for any progressive erosion trend. This suggests that the south coast is now being uplifted (estimated to be ~0.6 to 1.1 m) due to the Cascadia subduction zone having become locked again, such that strain is now building toward the next major earthquake. With the release of that energy and land subsidence, cliff erosion along the Bandon shore (and elsewhere on the Oregon coast) would be expected to begin again.

2.3 Coastal Geomorphology

On the basis of geology and geomorphology the Tillamook County shoreline can be broadly divided into five morphological beach types. These are depicted in **Figures 2-6** to **2-10** and include:

1. ***Dune-backed beaches:*** Dune-backed beaches make up the bulk (50.9%) of the Tillamook County shoreline, much of which is associated with the barrier spits (e.g., Nestucca, Sand Lake, Netarts, Bayocean, and Nehalem Spits, **Figures 2-6** to **2-10**). The geomorphology of the beaches can be generalized as having wide, dissipative surf zones with low sloping foreshores that are backed by high dunes containing significant sand volume (**Figure 2-1**). Dune crest elevations reach their highest peak along Bayocean (39 m [128 ft]) and Netarts Spit (25 m [82 ft]) (**Figure 2-11**). However, these dunes are in part ancient parabolic dunes that are now being truncated by wave erosion. Dune crest elevations are generally lowest in the Rockaway subcell (Twin Rocks, Rockaway, and Nedonna Beach) (**Figure 1-1**). Along the length of the county, mean dune crest heights are 10.5 m (35.5 ft), with most dunes being in the range of 5 to 16 m (16 to 54 ft). The average beach slope (tan β) for dune-backed beaches is summarized in **Figure 2-12** where it is apparent that slopes vary significantly along the coast, with the lowest mean slopes occurring in the vicinity of Oceanside (mean = 0.032), and are generally steepest in the Neskowin littoral cell (mean = 0.06).
2. ***Cliffed shore:*** Cliffed shores make up the second largest (30.5%) geomorphic "type" in the county (**Figure 2-2**). Examples exist around each of the major headlands. This particular shore type generally consists of near-vertical cliffs that plunge directly into the ocean, but in some cases, the cliffs may be fronted by rock platforms and/or talus.
3. ***Bluff-backed beaches:*** Bluff-backed beaches fronted by wide, dissipative sand beaches are the third most prominent geomorphic type in Tillamook County, comprising approximately 14.3% of the shore (**Figure 2-3**). This particular geomorphic type dominates the shoreline in the vicinity of Oceanside and Short Sand Beach, south of Cape Lookout, the south end of Cape Lookout State Park, north of Cape Kiwanda and south of Tierra Del Mar, and adjacent to the mouth of Nestucca Bay. The bluffs that back the beaches vary in height from ~7 m (23 ft) to greater than 50 m (164 ft). Beach slopes (tan β) seaward of the bluffs are similar to those observed throughout Tillamook County, averaging about 0.037 ($\sigma = 0.009$). Geomorphically, these beaches may be characterized as "composite" using the terminology of Beaulieu (1973) and Jennings and Shulmeister (2002), such that the beaches consist of a wide dissipative sandy beach, backed by a steeper upper foreshore composed of gravels and cobbles. In addition, several of the bluff-backed sections are characterized by well-vegetated faces, indicating that they have not been subject to significant wave erosion processes along the toe of the bluffs for many decades.
4. ***Bluff-backed beaches fronted by gravel and sand:*** This particular geomorphic type makes up approximately 3.3% of the Tillamook County shoreline and is prevalent on the south side of Neahkahnie Mountain (north of Manzanita), immediately north of Cape Meares, Short Sand Beach (**Figure 2-13**), and immediately north of Cape Lookout. The overall morphology is essentially the same as described for bluff-backed beaches, with the only differ-

ence being the presence of a gravel berm along the toe of the bluff.

5. ***Gravel/boulder berm fronted by sand:*** In the community of Cape Meares (south end of Bayocean Spit, **Figure 2-7**), a substantial gravel/boulder beach abuts against the Cape Meares headland, where they form prominent, steep natural barriers to wave erosion (**Figure 2-14**). The berm is approximately 0.8 km (0.6 miles) long. Crest elevations of the cobble/boulder beach reach a maximum of 8.7 m (29 ft), while the mean crest elevation is 6.7 m (22 ft). The slope of the gravel berm is steep (mean = 0.187 [(σ = 0.060]), while the sand beach has a mean slope of 0.047, which is typical of much of the Tillamook County coast. Considerable flotsam exists along the crest of the berm and significant distant landward of the crest, indicating that this stretch of shore is subject to frequent wave overtopping and inundation.

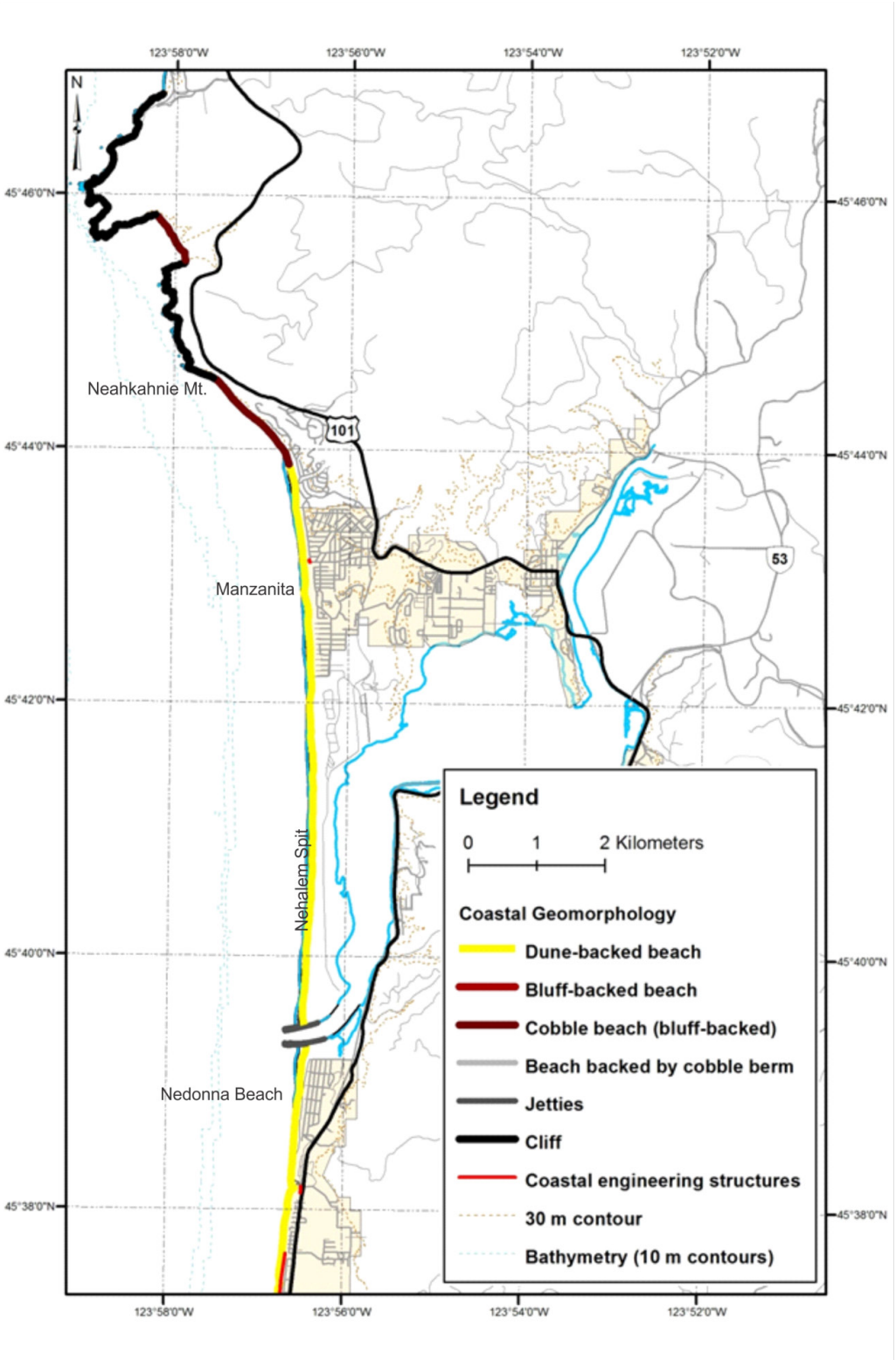

Figure 2-6. Geomorphic classification of northern Rockaway Beach/Nehalem Spit (Rockaway beach to Cape Falcon).

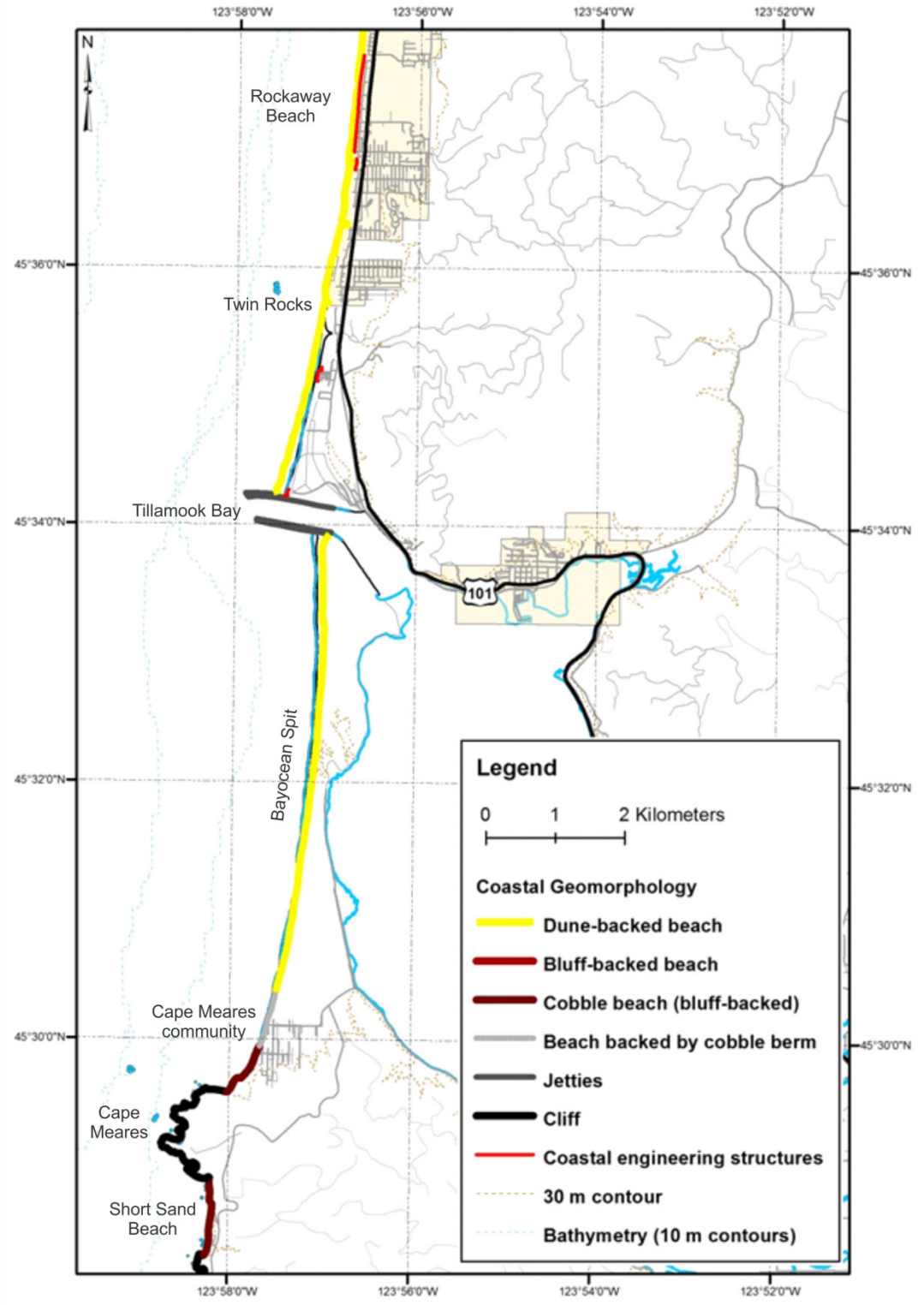

Figure 2-7. Geomorphic classification of southern Rockaway Beach/Bayocean Spit (Cape Meares to Rockaway Beach).

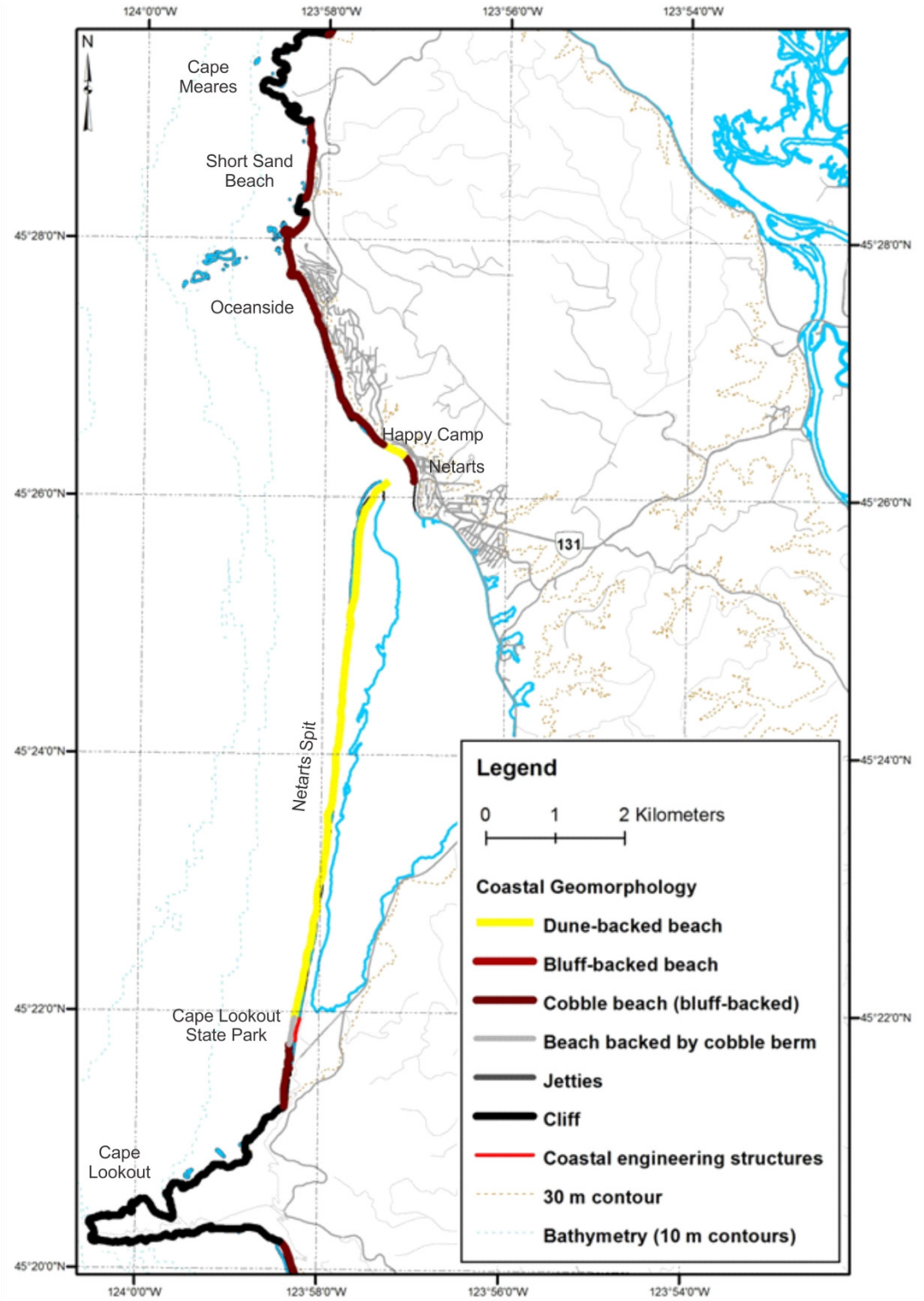

Figure 2-8. Geomorphic classification of the Netarts littoral cell (Cape Lookout to Cape Meares).

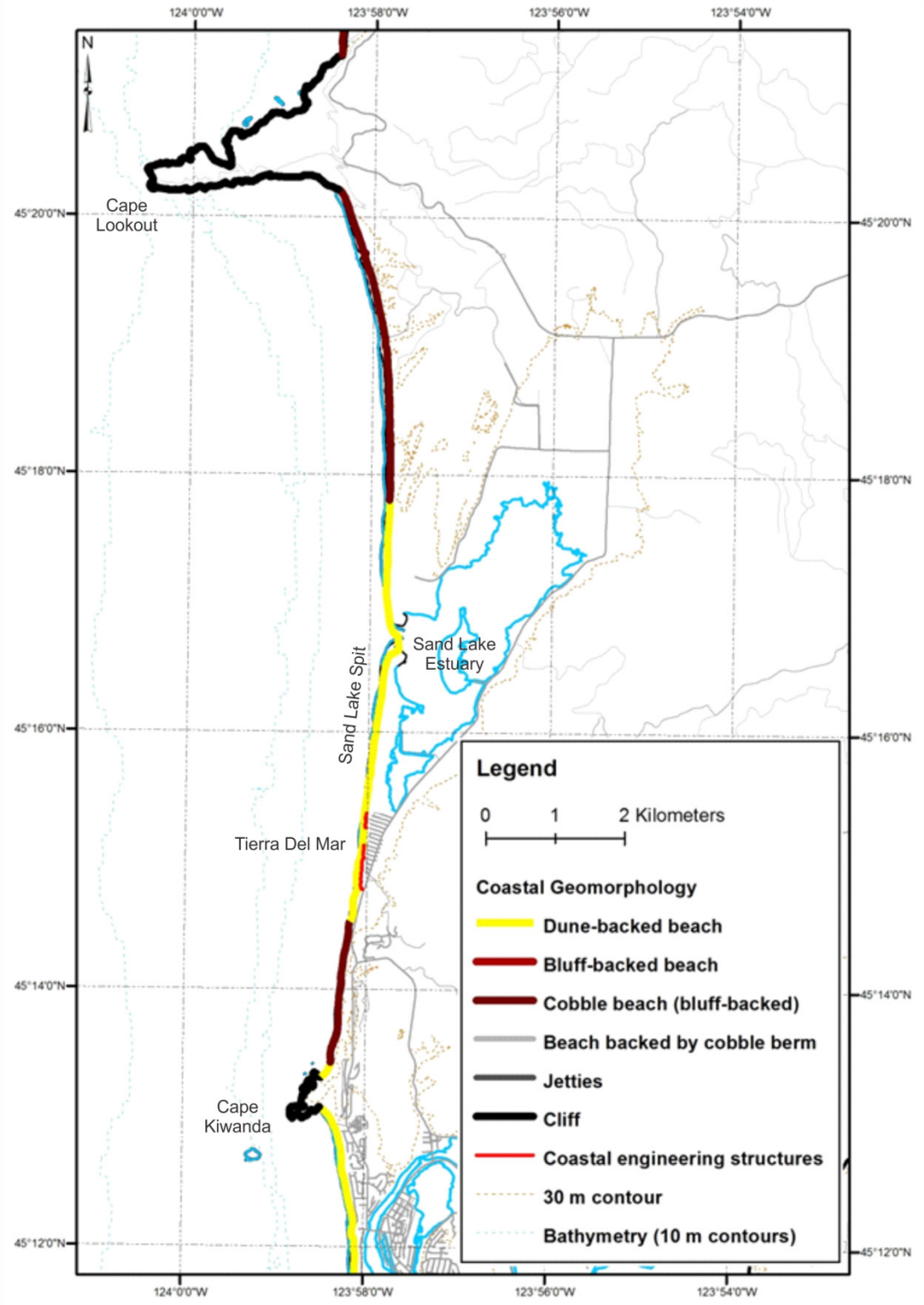

Figure 2-9. Geomorphic classification of the Sand lake littoral cell (Cape Kiwanda to Cape Lookout).

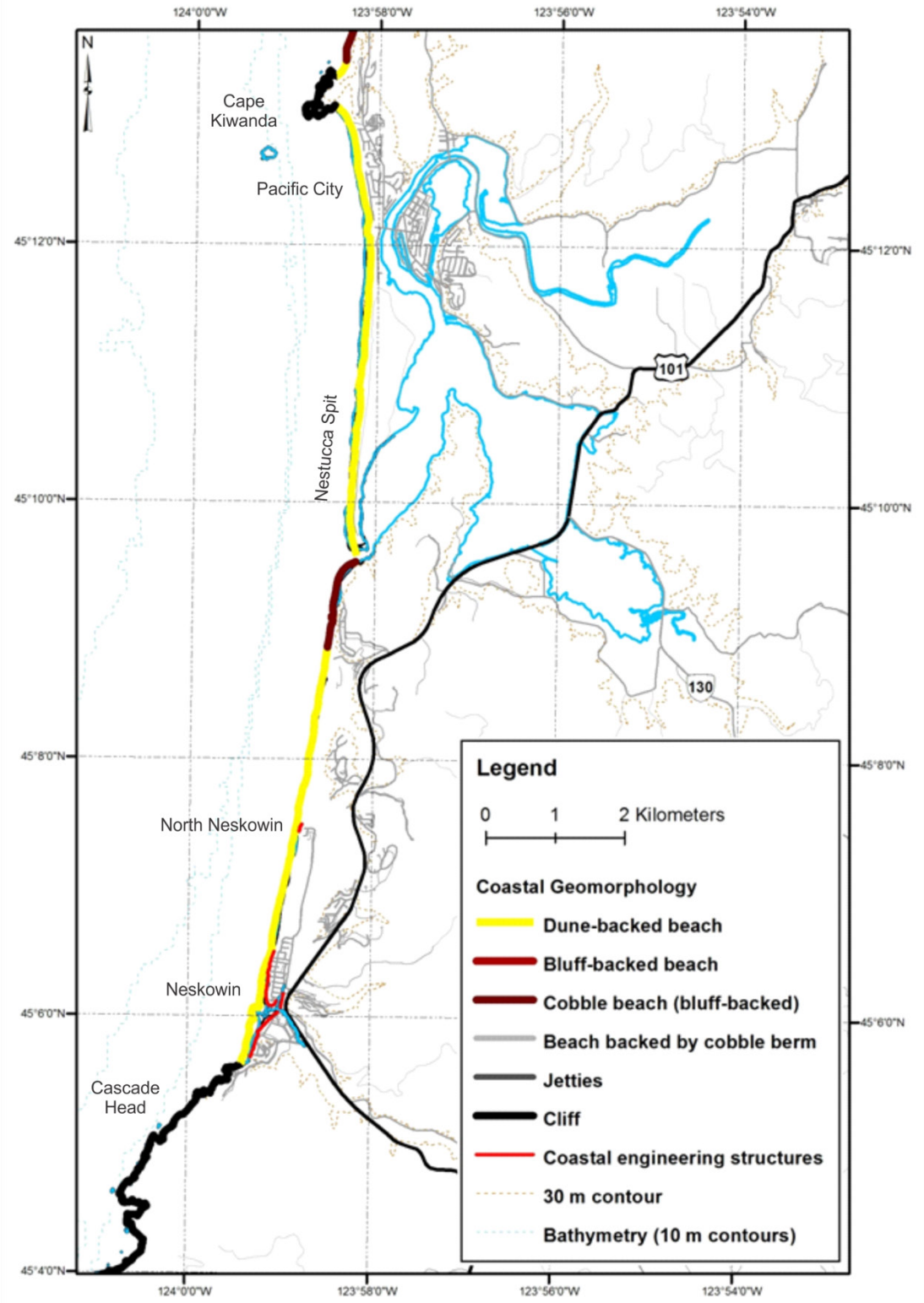

Figure 2-10. Geomorphic classification of the Neskowin littoral cell (Cascade Head to Cape Kiwanda).

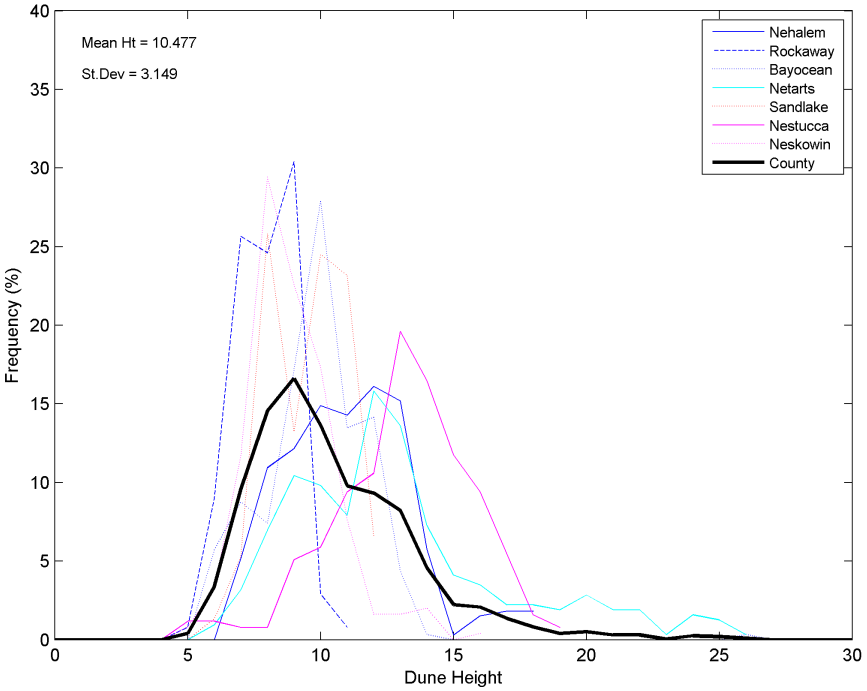

Figure 2-11. Tillamook County dune crests. Data from Allan and Harris (2012).

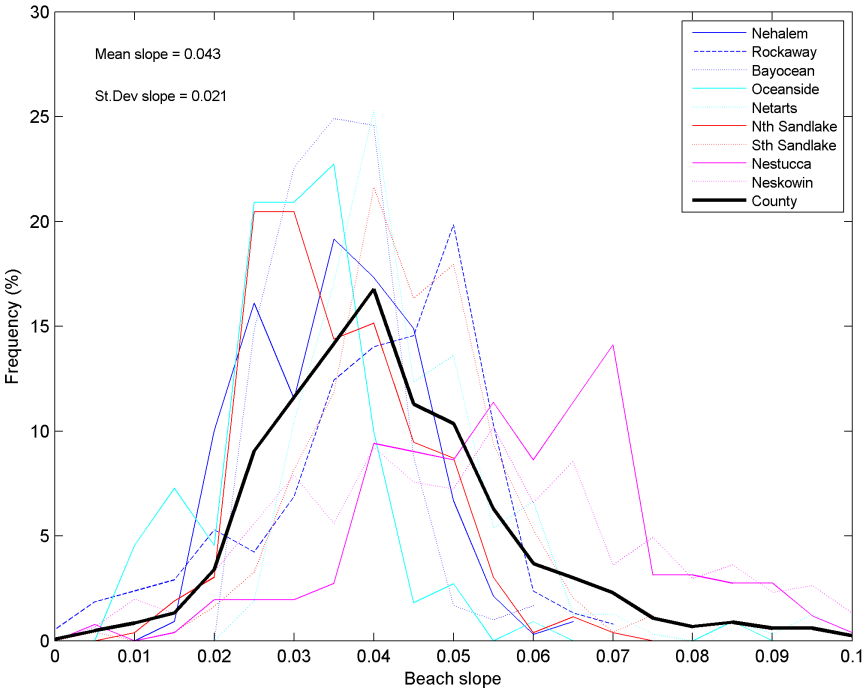

Figure 2-12. Tillamook County beach slopes. Data from Allan and Harris (2012).

Figure 2-13. An extensive gravel berm fronted by a dissipative sand beach and backed by high bluffs at Short Sand Beach, north of the community of Oceanside. Note the extensive accumulation of woody debris along the crest of the berm, which has a crest elevation that averages ~5.8 m (σ = 1.6 m) (photo: J. Allan, DOGAMI, 2003).

Figure 2-14. An extensive gravel/boulder berm that backs a dissipative sand beach in the Cape Meares community. View is looking south toward the Cape Meares headland. An exposed tree stump located in situ is exposed due to lowering of the sand beach (photo: J. Allan, DOGAMI, 2008).

2.4 Coastal Erosion and Flood History

2.4.1 Tillamook County historical shoreline positions

This section presents a qualitative discussion of large-scale morphological changes derived from analyses of historical and contemporary shorelines derived for the Tillamook County coastline. This summary stems from work undertaken by researchers at DOGAMI and OSU over the past two decades (Priest and others, 1993; Allan and Priest, 2001; Allan and others, 2003; Allan and Hart, 2007, 2008; Allan and Harris, 2012; Allan and Stimely, 2013; Ruggiero and others, 2013).

National Ocean Service (NOS) Topographic (T)-sheet shoreline positions covering the 1920s and 1950s were previously obtained from NOAA (Allan and Priest, 2001). These lines reflect the mean high water (MHW) position mapped by early NOS surveyors, on an average tide typically in mid to late summer. Additional shorelines were derived from a variety of other sources including: 1967 digital orthophotos (Ruggiero and others, 2013), 1980s era U.S. Geological Survey topographic maps, 1994 digital orthophotos, and from 1997, 1998, and 2002 lidar data (Allan and Priest, 2001). Pre-lidar historical shorelines use the high water line (HWL) as a shoreline proxy. The HWL has been used by researchers for more than 150 years because it could be visually identified in the field or from aerial photographs. In contrast, shorelines derived from lidar data are datum-based and can be extracted objectively using a tidal datum, such as MHW or mean higher high water (MHHW). Studies by Moore (2000) and Ruggiero and others (2003) note that HWL-type shoreline proxies are virtually never coincident with datum-based MHW-type shorelines. In fact they are almost universally estimated to be higher (landward) on the beach profile when compared to MHW shorelines (Ruggiero and others, 2013). According to Ruggiero and others, the average absolute horizontal offset between the HWL and MHW ranges from ~6 m (~19 ft) to as much as 50 m (164 ft), while the average is typically less than 20 m (65 ft). Offsets are typically greatest on flat, dissipative beaches where the wave runup may be large and smallest where beaches are steep (e.g., gravel beaches).

Estimates of the uncertainty of HWL shoreline measurements have been assessed in a number of studies (e.g., Moore, 2000; Ruggiero and others, 2013). These uncertainties reflect the following errors: 1) mapping methods and materials for historical shorelines (including the offset between the HWL and MHW shoreline), 2) the registration of shoreline positions relative to Cartesian coordinates, and 3) shoreline digitizing, and are summarized in **Table 2-1**.

Shorelines measured by DOGAMI staff using Real-Time Kinematic Differential Global Positioning System (RTK-DGPS) surveys of the beach are also available for the Neskowin and Rockaway littoral cells (Allan and Hart, 2007, 2008; Allan and Stimely, 2013). These latter data sets provide the most up-to-date assessments of the changes taking place along the Tillamook coastline and have been collected since 2007 in order to document the seasonal to interannual variability in shoreline positions along the county. In all cases, the GPS shorelines reflect measurements of the MHHW line located at an elevation of 2.3 m (7.5 ft). We have relied on the latter as opposed to the MHW line, because previous studies indicate that MHHW line most closely approximates the MHW line surveyed by early NOS surveyors. Errors associated with these various products are described by Moore (2000). GPS shoreline positioning errors, a function of the orientation of the GPS receiver relative to the slope of the beach, are estimated to be approximately ±0.1 to ±0.2 m (±0.3 to ±0.6 ft).

The approach adopted here is to describe the broad morphological changes identified along the

Table 2-1. Average uncertainties for Pacific Northwest shorelines (Ruggiero and others, 2013).

	NOS T-Sheets (1800s to 1950s)		DRGs (1940s to 1990s)		Aerial Photography (1960s to 1990s)		Lidar	
Total shoreline position uncertainty	18.3 m	60 ft	21.4 m	70 ft	15.1 m	50 ft	4.1 m	14 ft

coast, beginning in the south at Neskowin, and progressing northward toward Cape Falcon.

2.4.1.1 Neskowin Cell

At Neskowin, the historical shoreline positions reveal little systematic pattern, with all of the identified shorelines falling within a few hundred feet of each other (**Figure 2-15**). Many of the shorelines reveal the presence of large embayments along the coast indicative of the formation of rip currents that can result in highly localized hotspot erosion (e.g., the April 2013 shoreline in **Figure 2-15**). Along much of the southern half of the cell, the 1920s era shoreline tends to track landward of the other shorelines. This suggests that beach conditions in the 1920s reflected an eroded state following a period of large storm events. Erosion appears to have dominated much of the early existence of the Neskowin community. Probably the most significant storm on record occurred in January 1939, which affected much of the Oregon coast and caused major coastal flood hazards as well as significant erosion problems. For example, **Figure 2-16** provides an example of the damage sustained in Neskowin; one home had its foundation eroded from under it, which resulted in the house collapsing onto the beach. Within a decade, however, this process had effectively reversed itself, with much of the shore having been rebuilt as sand migrated back on to the beach. This cycle of erosion followed by accretion is typical of shoreline changes on the Oregon coast. The 1967, 1980s era, and 1994 shorelines represent the most seaward positions, implying that significant accretion had occurred adjacent to Neskowin during those years, while the early 1960s, the 1982-83 El Niño winter, and the storms of the late 1990s represent eroded states.

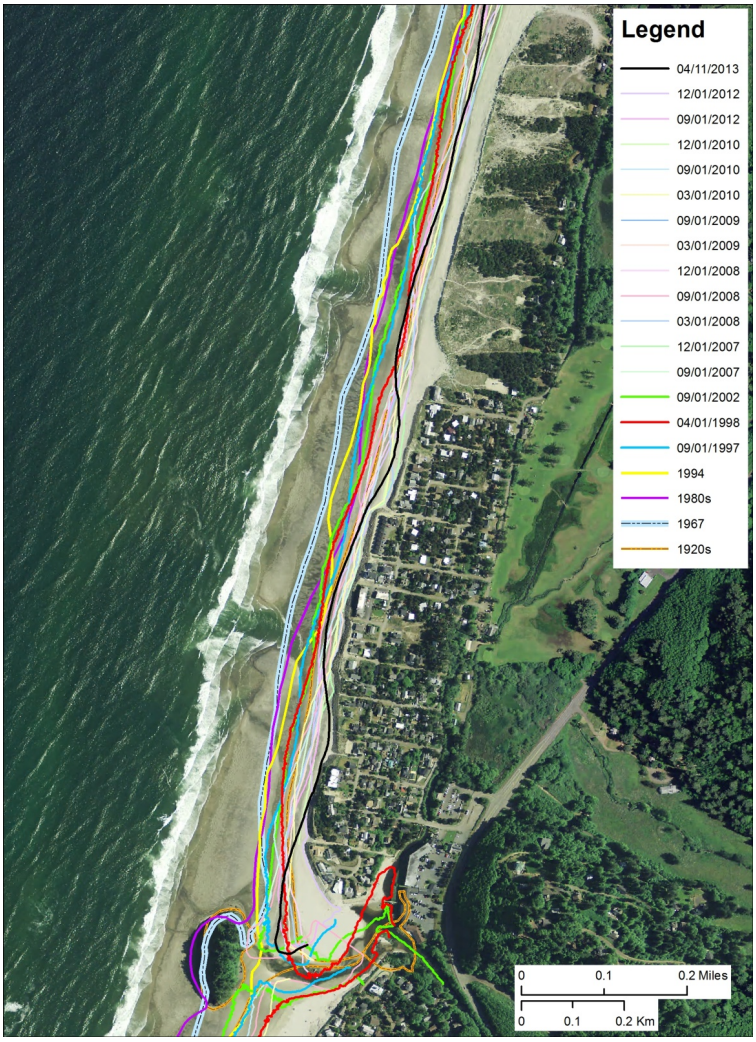

Figure 2-15. Historical and contemporary shoreline positions identified at Neskowin. Note: The 1920s (1927/28) shoreline is derived from NOS T-sheets, 1967 and 1994 are from orthorectified aerial photographs, 1980s (1985/86) is from U.S. Geological Survey topographic maps, 1997–2002 are derived from lidar, and post 2007 were measured using GPS.

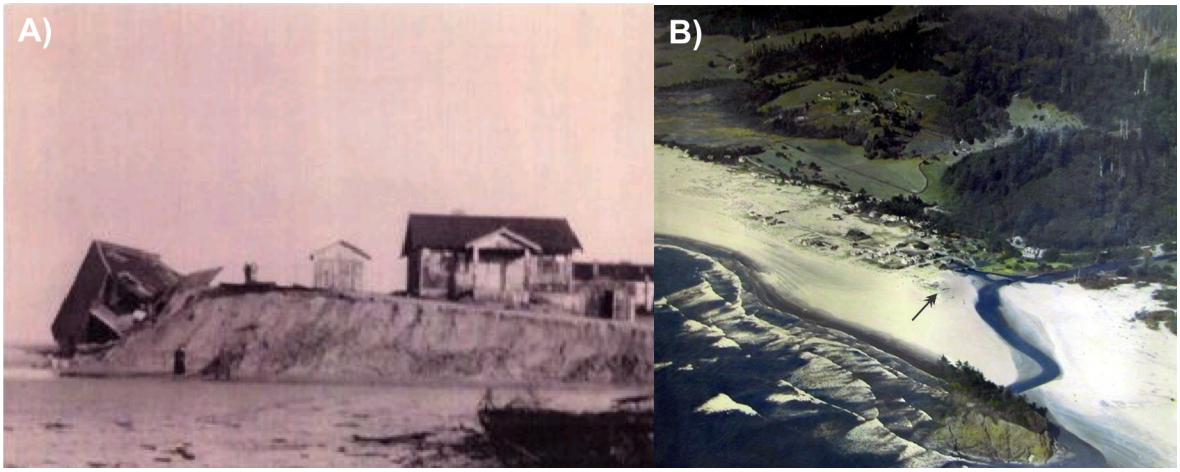

Figure 2-16. Erosion and accretion at Neskowin. A) Erosion (adjacent to the juncture between Neskowin and Hawk Creeks) following the January 1939 storm; B) Rebuilding of the sandy beach at Neskowin in 1949. Note: the arrow indicates the approximate position of the erosion shown in A). (Photos courtesy of Neskowin community archives.)

Following the major storms of the late 1990s, erosion hazards in the community of Neskowin have reached acute levels (Allan and others, 2003; Allan and Hart, 2007), with the beach and dune having eroded landward some 50 m (~150 ft) (**Figure 2-17**). Property owners responded to the hazard by installing riprap along much of the shore north of Proposal Rock. As of 2014, virtually the entire length of the community of Neskowin (including north Neskowin) is hardened with riprap. Monitoring of the beaches in Neskowin indicates that they have not fully recovered from the storms of the late 1990s (several areas have in fact continued to erode), such that the beaches today are narrower and have much less sand volume compared with the same beaches in the mid 1990s (Allan and Hart, 2008). Long-term erosion rates derived by Ruggiero and others (2013) indicate that the beaches of Neskowin have some of the highest rates of retreat in the state. Due to narrow beaches and lack of sand volume, the community of Neskowin today remains at high risk of being impacted by major winter storms and from ocean flooding.

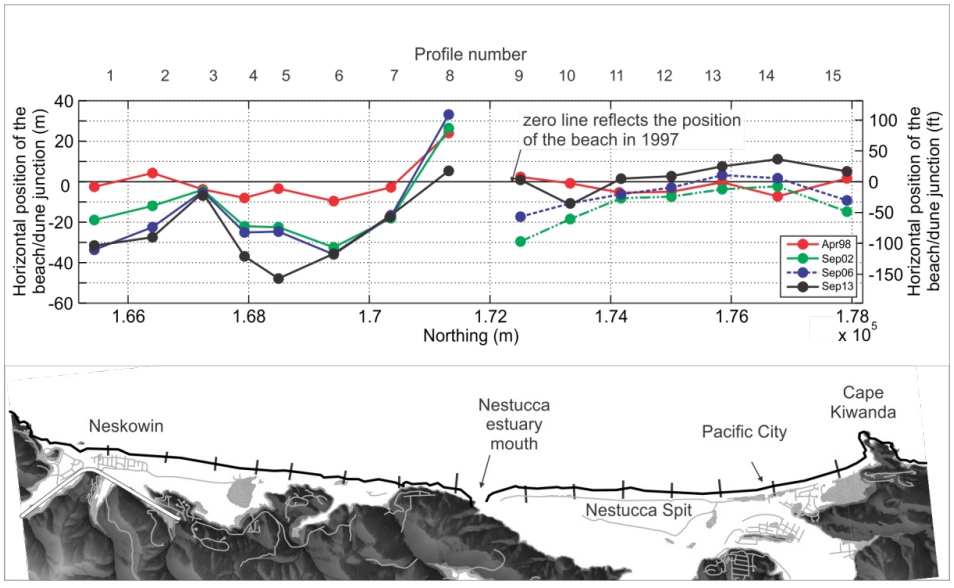

Figure 2-17. Positional changes in the beach/dune toe (elevation of 6 m) along the Neskowin cell between 1997 and 2008 derived from lidar data and RTK-DGPS measured surveys of the beach. Circles and numbers correspond to the locations of the Neskowin beach monitoring network established by DOGAMI in 2006 (after Allan and others, 2009).

Farther north along the coast, the 1994 shoreline tends to track well seaward of the other shorelines. This suggests a period of accretion and was most noticeable adjacent to Porter Point near the mouth of Nestucca Bay (**Figure 2-18** and approximate location of transect 8 in **Figure 2-17**). The pattern of accretion appears to be consistent with a general decline in wave energy and storm incidence observed during the early part of the 1990s (Allan and Komar, 2000). However, recent GPS surveys of this section of the coast by DOGAMI staff indicate a reversal from accretion back to erosion, with the shoreline now having retreated virtually back to the toe of the marine cliffs that back the beach.

Along Nestucca spit (**Figure 2-18**), the tip of the spit and the bay mouth have remained predominantly in the south, with some evidence of a northward migration in 1998. From inspection of the suite of shorelines available to us, the Nestucca spit tip has ranged over a distance of about 340 m (1,118 ft) between 1927 and 2008 and was at its most southerly position in 2008. Following the 1997-98 El Niño, the spit tip migrated northward, probably in response to a change in wave direction that is typical of El Niño events (e.g., Komar, 1986). Of interest also is the presence of a large bulge identified by the 1980s era shoreline on the eastern side of the spit (**Figure 2-18**). This feature is remnant from when the spit was breached during a major storm in February 1978 (see Figure 6.15 of Komar [1997]).

North of Nestucca spit, the 1980s era shoreline tracks landward of the other shoreline positions and extends all the way to Pacific City at the north end of the cell. This finding is likely to be a function of erosion that occurred during the 1982-83 El Niño event (P. Komar, personal communication 2001). In contrast, the 1994 and 2002 shoreline positions represent the most seaward extent of the MHWL (located some 45–76 m [150–250 ft] seaward of the 1985-1986 shoreline). This indicates that large volumes of sediment had accumulated along much of the northern half of the cell, the product of a persistent net drift of beach sediments to the north. It is highly likely that this pattern is a function of the persistent El Niño conditions that have characterized the Pacific Northwest (PNW) during the 1980s and 1990s. Similar observations of net accretion around Pacific City since about 1981 were also noted in a report by Shoreland Solutions (1998b). For example, considerable quantities of sand accumulated along much of the Pacific City shoreline, burying a large riprap revetment that was installed in 1978. Furthermore, the continued accumulation of sand at the north end of the Neskowin cell has presented major problems for homeowners since at least 1984. Of particular concern has been the inundation of homes and property by sand (Komar 1997; Shoreland Solutions, 1998b). As can be seen from **Figure 2-17**, much of the Nestucca spit has now recovered from the major storms of the late 1990s.

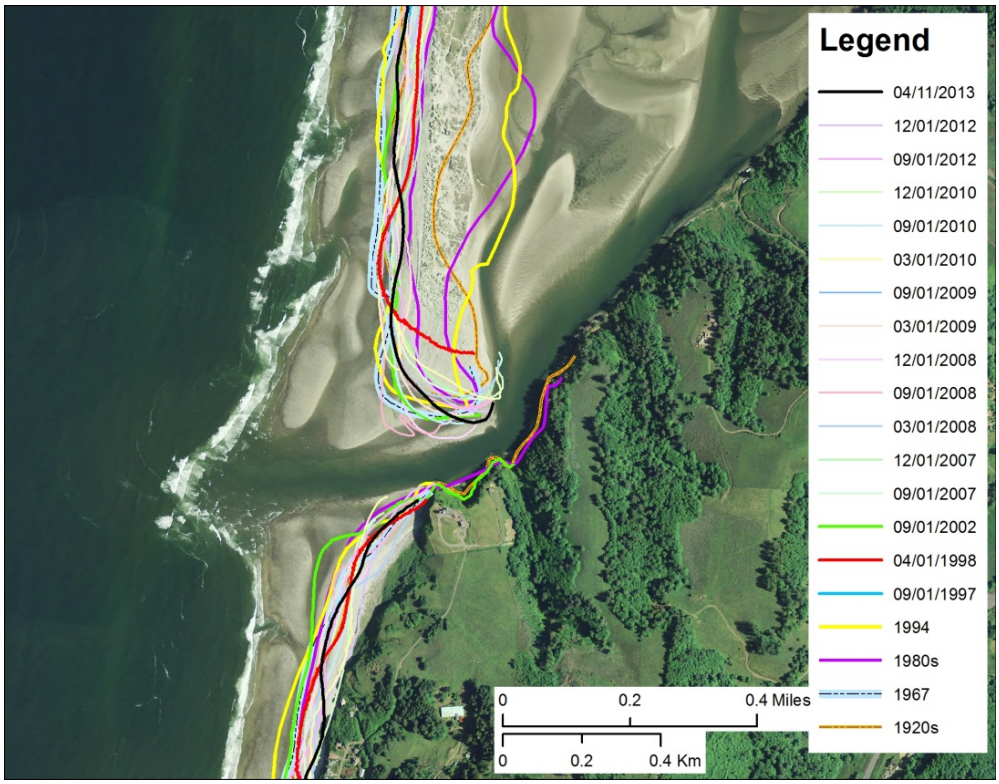

Figure 2-18. Historical and contemporary shoreline positions identified adjacent to the Nestucca Bay mouth. Note: The 1920s (1927/28) shoreline is derived from NOS T-sheets, 1967 and 1994 are from orthorectified aerial photographs, 1980s (1985/86) is from U.S. Geological Survey topographic maps, 1997–2002 are derived from lidar, and post 2007 were measured using GPS.

2.4.1.2 Sand Lake Cell

Along the Sand Lake cell, the 1920s and 1980s era shoreline positions represent the most landward extent of the MHWL (i.e., eroded state), while the 1967 and 1994 shorelines characterize the accreted state. For the most part, this pattern is broadly similar to that identified previously in the Neskowin cell. However, unlike the Neskowin cell, the 1980s era shoreline at Sand Lake indicates cell-wide coastal erosion.

Approximately 2.8 km (1.74 mi) north of Cape Kiwanda is the community of Tierra Del Mar. As with Neskowin, much of its shoreline has now been protected with coastal engineering structures (riprap). These structures appear to have been built in the early 1970s and were expanded further in 1984, probably in response to the effects of the 1982-83 El Niño. North of Tierra Del Mar, the entire spit is experiencing significant erosion. For example, analyses of lidar data from 1997 to 2009 indicate that the spit shoreline has eroded on average by 27.8 m (91 ft).

Some of the most interesting shoreline changes identified in the Sand Lake cell are found adjacent to the mouth of the estuary. As shown in **Figure 2-19**, the location of the estuary mouth has varied considerably over the past century. The 1920s era shoreline characterizes the most southerly extent of the estuary mouth (implying a period of net southerly sand transport), while the 2009 shoreline identifies its most northerly position. As a result, the estuary mouth has migrated some 0.5 km (~0.3 mi) during this period. These results clearly highlight the dynamic and unstable nature of spit ends. An examination of aerial photographs taken in 1939 (not shown) also reveals a southerly bay-mouth position, while the spit ends were much wider. These latter characteristics are broadly similar to the 1920s shoreline identified in **Figure 2-19**. In contrast, the 1980s shoreline indicates an extremely wide bay mouth (~0.5 km [~0.3 mi] wide), so that much of the inner bay was probably fully exposed to the sea. Since the 1990s the estuary mouth has migrated north up against the northern spit tip, causing the tip to be truncated, while also eroding a section of the shoreline within the estuary adjacent to Sand Lake Recreation Area park (**Figure 2-19**).

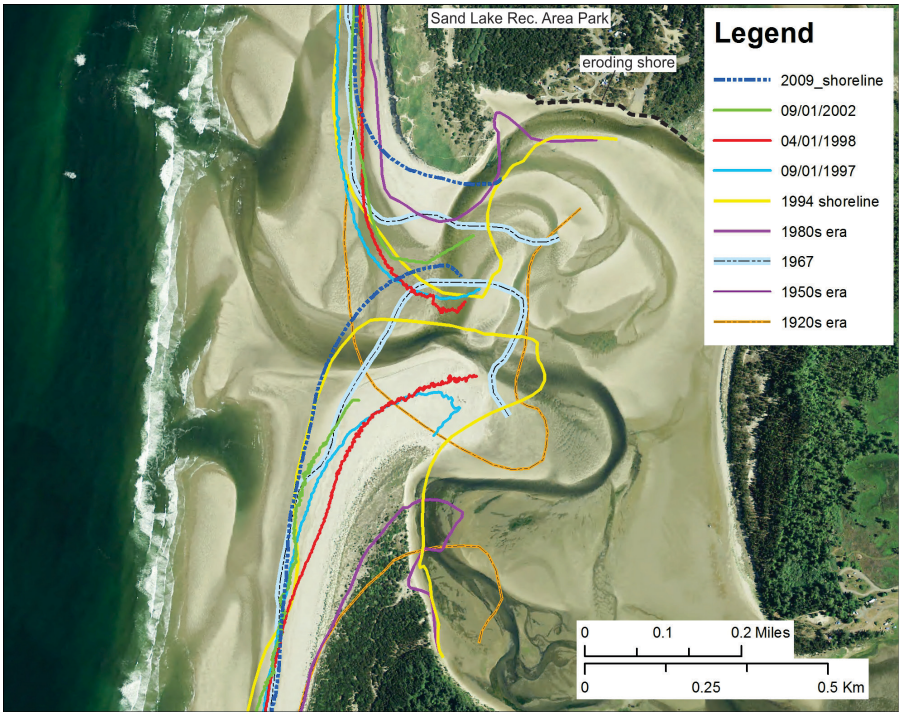

Figure 2-19. Shoreline variability adjacent to the Sand Lake estuary mouth. Note: The 1920s (1927/28) shoreline is derived from NOS T-sheets, 1967 and 1994 are from orthorectified aerial photographs, 1980s (1985/86) is from U.S. Geological Survey topographic maps, and 1997–2009 are derived from lidar.

2.4.1.3 Netarts Cell

The Netarts littoral cell is one of the smallest cells on the Oregon coast. As a result, it is particularly susceptible to variations in wave approach, particularly changes in the predominant wave direction caused by the El Niño/La Niña Southern Oscillation. The shoreline analyses presented here demonstrate a number of morphological changes that are less apparent in the other littoral cells. At Cape Lookout State Park (CLSP) located at the southern end of the cell (**Figure 2-20**), the shorelines track closely to each other. The exceptions to this are the 1994 and 2009 shorelines. The former shoreline identifies the accreted state (consistent with the other littoral cells in Tillamook County), while the 2009 shoreline reveals the most eroded state. The latter is the product of erosion along the spit that accelerated in the late 1990s, due to a series of large storms that impacted the area in the 1997-98 El Niño winter. In fact, subsequent storms over the 1998-99 La Niña winter caused even more extensive erosion of the park. In particular, a storm on March 2-3, 1999, eventually resulted in the foredune that protected the park being breached, and inundation of the campground that led to significant damage to its facilities.

According to Komar and others (1989), El Niño events have produced large spatial changes in the configuration of the Netarts cell coastline and the morphology of the beaches, especially during the 1980s and 1990s. Allan and others (2003) analyzed terrestrial lidar measured in 1997 (pre 1997-98 El Niño) and 1998 (post El Niño) in order to quantify the alongshore variance in El Niño shoreline responses (**Figure 2-21**). As can be seen in the figure, the largest extent of shoreline retreat occurred along the southern 3 km (1.86 miles) of the cell, immediately north of Cape Lookout. Erosion in that area during both the 1982-83 and 1997-98 El Niños significantly damaged Cape Lookout State Park, eroding away a high ridge of dunes that protected the park (Komar and others, 1989; Komar, 1998a). The lidar results in **Figure 2-21** also capture the northward displacement of sand during the El Niño winter. In the hotspot zone in the south, the maximum shoreline retreat reached 18 m (59 ft). Shoreline accretion otherwise prevailed along the remainder of the cell, on average 5 to 10 m (~16–33 ft), a result of sand acquired by its northward displacement from the eroded hotspot zone at the south end of the cell. There was also an occurrence of hotspot erosion along the north shore of the inlet to Netarts Bay, which threatened the loss of condominiums perched overlooking the estuary mouth on the north side of the bay (Komar, 1998a).

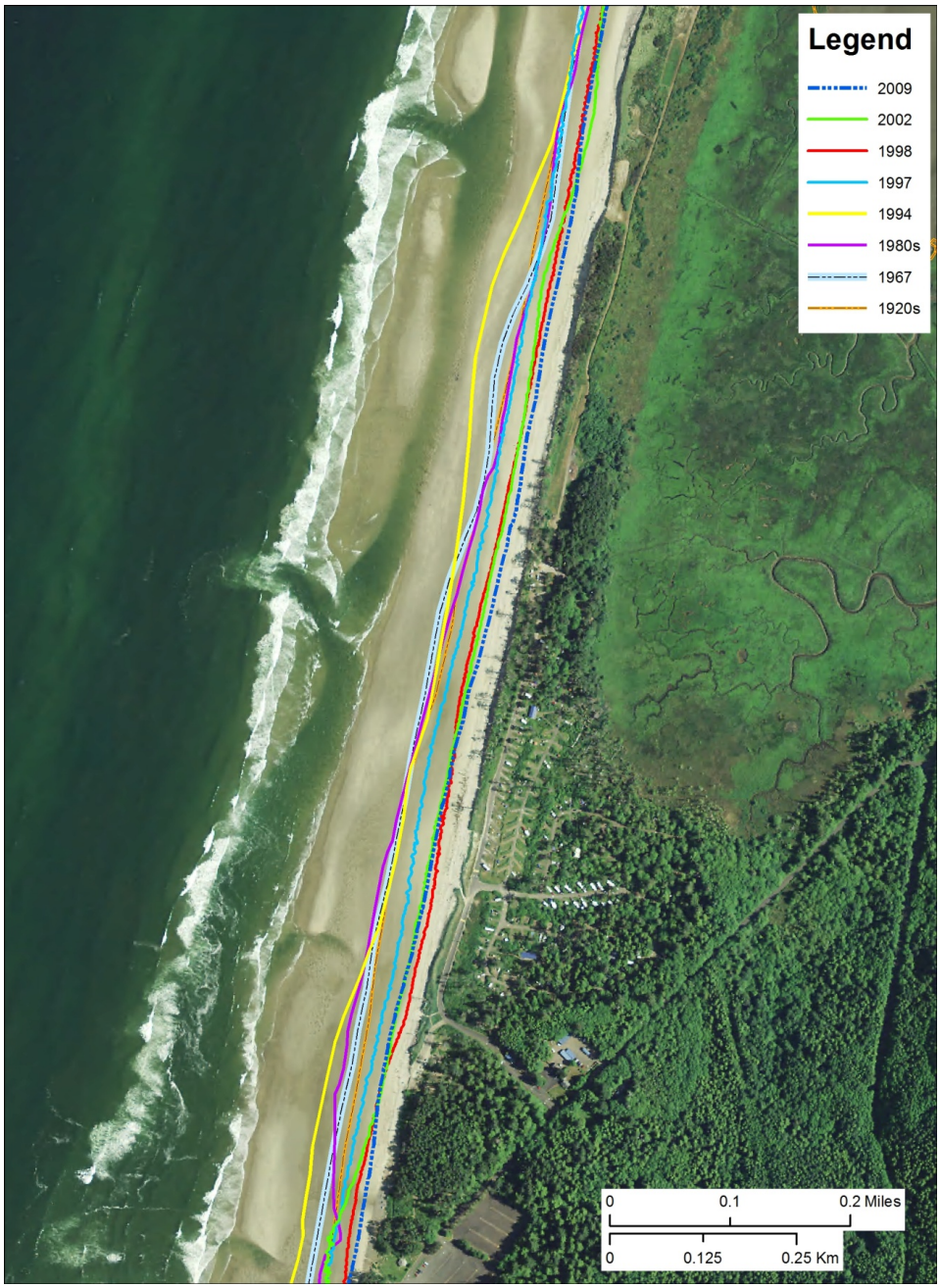

Figure 2-20. Historical and contemporary shoreline positions identified along the southern end of Netarts Spit, adjacent to Cape Lookout State Park. Note: The 1920s (1927/28) shoreline is derived from NOS T-sheets, 1967 and 1994 are from orthorectified aerial photographs, 1980s (1985/86) is from U.S. Geological Survey topographic maps, and 1997–2009 are derived from lidar.

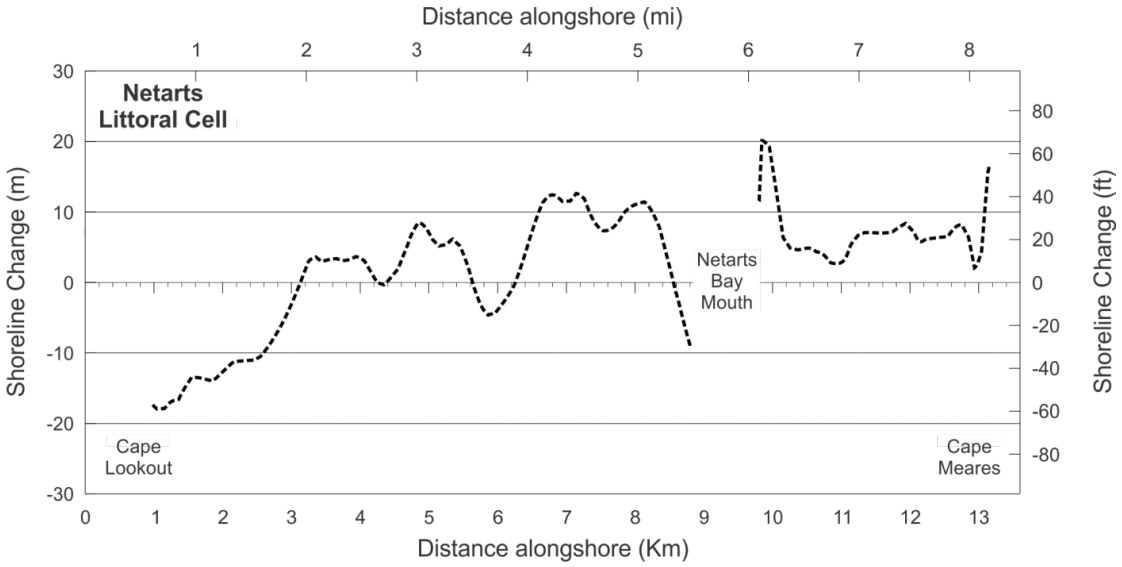

Figure 2-21. De-meaned shoreline changes in the Netarts cell derived by subtracting the 1998 lidar shoreline from the 1997 shoreline (after Allan and others, 2003).

Prior to the 1982-83 El Niño, erosion on Netarts Spit had been minimal (Komar and others, 1989). As a result, significant erosion of CLSP did not begin to occur until the 1982-83 El Niño and was very advanced by the 1987-88 El Niño erosion event. Interestingly, the 1980s era and 1994 shorelines presented in **Figure 2-20** indicate a relatively broad beach in front of the park, suggesting that the beach had reformed somewhat after the 1982-83 El Niño. This is consistent with observations reported by Komar and others (1989). However, they noted further that although some of the sand had returned, the volume of sand contained on the beach was still depleted when compared with the period prior to the 1982-83 El Niño. Extensive areas of gravel exposed on the beach and the presence of rock outcrops in the shallow offshore were evidence for their conclusion. Because the beach was in such a depleted state, its capacity to act as a buffer against storm waves during subsequent winter seasons was severely reduced. This was especially the case during the 1987-88 El Niño event, which eventually caused the destruction of a wooden bulkhead emplaced along the beach foredune during the late 1960s (**Figure 2-22**). By April 1998 the width of the beach in front of CLSP had narrowed significantly, from about 50–91 m (170–300 ft) wide in 1994, to around 12–24 m (40–80 ft) wide in 1998 (**Figure 2-20**). Furthermore, the area affected by the erosion extended about 1.4 km (0.9 mi) north and 1.1 km (0.7 mi) south of the campground. In an effort to mitigate the erosion problems, the Oregon Parks and Recreation Department responded by installing a dynamic revetment structure in the area most affected (**Figure 2-23**). Such structures are a "soft" form of engineering (when compared with basaltic rip rap revetments), because they are less intrusive on the coastal system and are designed to respond dynamically to wave attack.

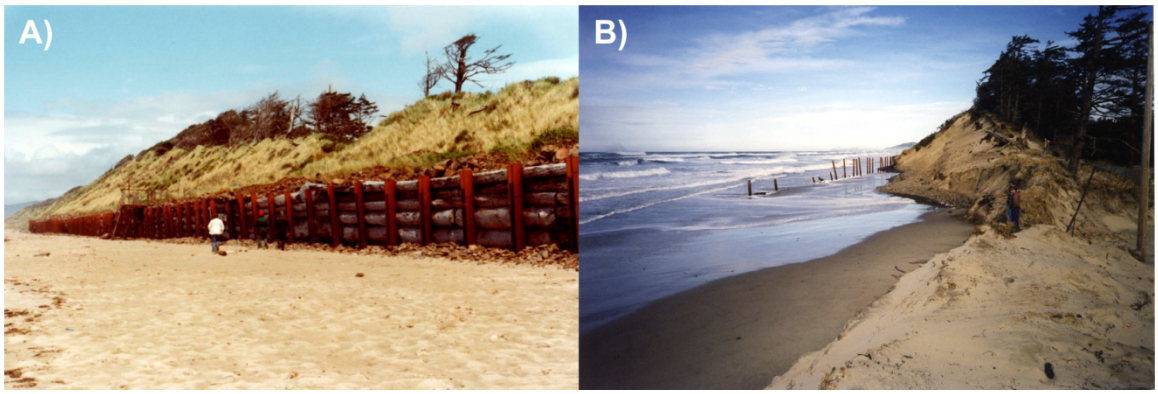

Figure 2-22. Cape Lookout State Park. A) A wooden bulkhead constructed at CLSP [Photo OPRD, June 1978]; B) The same area in February 1998 (photo: P. Komar, February 1998).

Figure 2-23. Dynamic revetment "cobble beach" constructed at Cape Lookout State Park. The cobble beach is backed by an artificial dune, which periodically is overtopped during major storms (photo: J. Allan, DOGAMI, 2008).

Farther north along Netarts Spit (about 2.9 km [1.8 mi] north of CLSP), erosion of the high foredune remains acute. For the most part, the 1980s shoreline shifts landward with progress along the spit, tracking close to the vegetation line and indicating significant erosion along much of the northern end of Netarts Spit (**Figure 2-24**). This is characterized by the position of the 1980s shoreline and by the presence of a prominent erosion scarp. In contrast, the 1994, 1997, and 1998 shorelines shift seaward and track about 60 to 75 m (196 to 246 ft) seaward of the 1980s shoreline (**Figure 2-24**). Such a change is analogous to a pivot point in which one set of processes (erosion), gives way to another (accretion). In other words, the coastal response along Netarts Spit reflects a reorientation of the entire shoreline toward the direction of wave attack, with erosion occurring along the southern end of the cell and accretion in the north (Komar and others, 1989; Revell and others, 2002). Recent measurements by DOGAMI staff using RTK-DGPS to document beach and shoreline changes along Netarts Spit have revealed that the foredune periodically undergoes 10 to 15 m (33 to 49 ft) of dune retreat during single storm events, highlighting the intensity of the erosion processes that dominate much of this coastline.

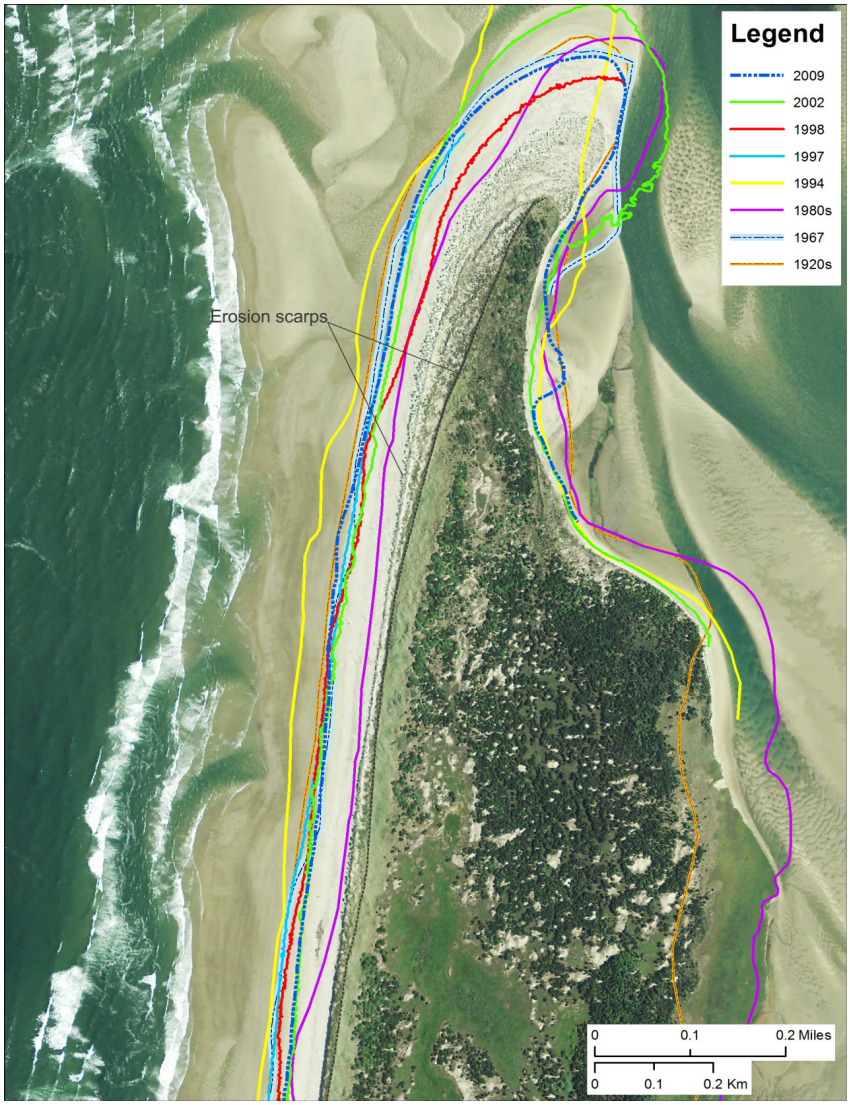

Figure 2-24. Historical and contemporary shoreline positions identified along the northern end of Netarts Spit, adjacent to Cape Lookout State Park. Note: The 1920s (1927/28) shoreline is derived from NOS T-sheets, 1967 and 1994 from orthorectified aerial photographs, 1980s (1985/86) is from U.S. Geological Survey topographic maps, and 1997–2009 are derived from lidar. Black dashed line on the dune denotes an erosion scarp.

Figure 2-25 compares the historical shoreline positions adjacent to the end of Netarts Spit; here we include one additional shoreline (1950s), which was derived from a NOS T-sheet not available south of Netarts Spit. Apart from the 1950s shoreline, which shows the spit end having re-curved into the bay and a much narrower mouth, the morphology of Netarts Spit has remained broadly the same. In keeping with the Nestucca and Sand Lake estuary mouths, the spit tip migrated northward some 122 m (400 ft) between the 1980s and 1994 shorelines. Part of this response is probably related to the prevalence of El Niños throughout the 1980s, which would have helped shift the mouth of Netarts Bay to the north in response to the increase in waves from the southwest typical of El Niño conditions. However, by 1998 the spit tip had returned to the south. These changes again highlight the dynamic nature of spit ends.

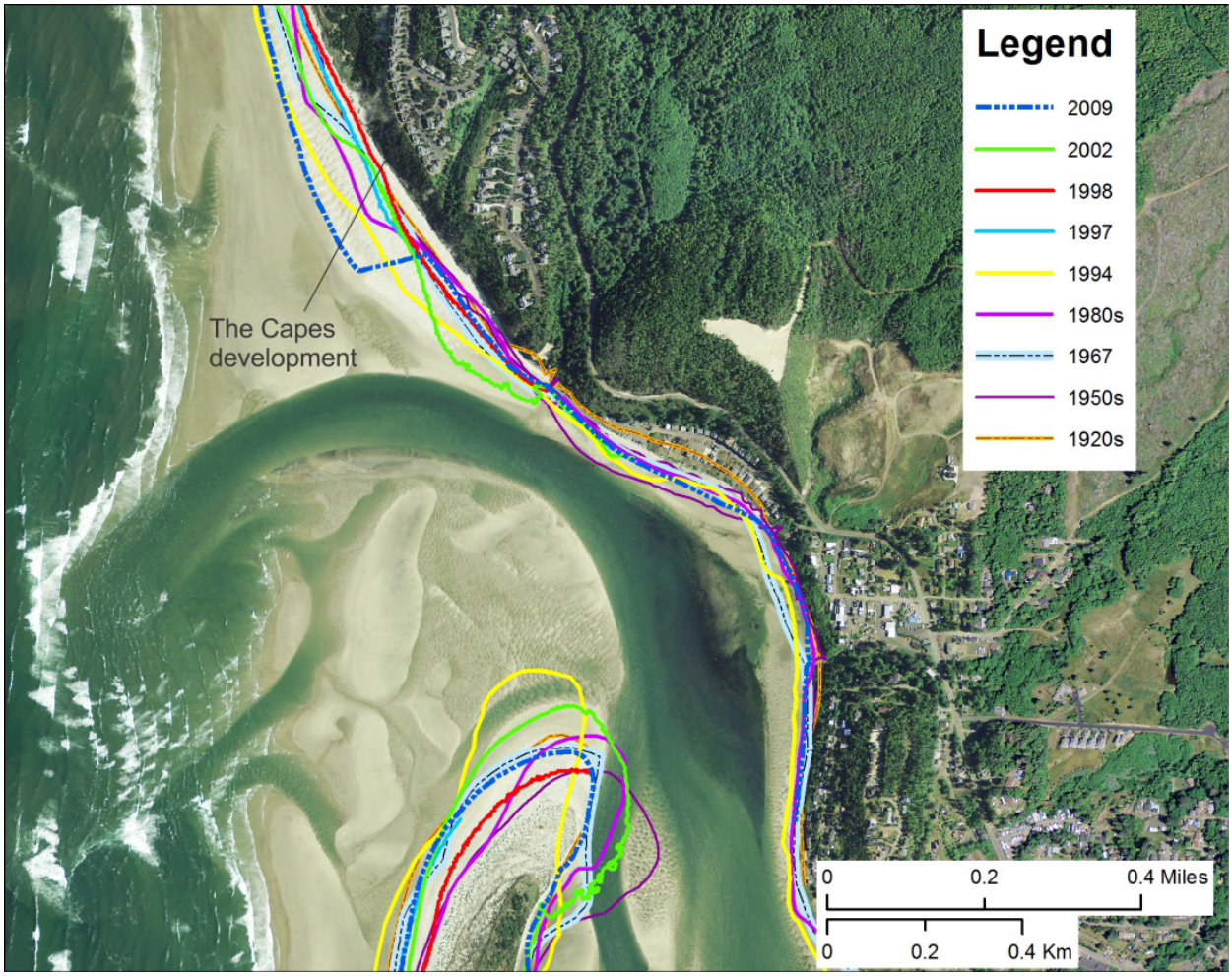

Figure 2-25. Historical shoreline positions identified at the end of Netarts Spit.

On the north side of Netarts Bay is The Capes development, which consists of homes built along the head scarp of a large landslide (**Figure 2-25** and **Figure 2-26**). During the 1997-98 El Niño, homeowners observed movement on the slide immediately seaward of homes built adjacent to the head scarp (**Figure 2-26**). The movement accelerated over the winter, resulting in several cracks opening up landward of a few of the homes. The cause of the movement was attributed to extensive wave erosion along the toe of the landslide, the product of the northward movement of the mouth of the estuary. The erosion essentially removed the toe supporting structure, which effectively enhanced the lateral movement of the landslide material.

Our analyses of shoreline data reveal that the width of the beach in front of The Capes has varied considerably (**Figure 2-25** and **Figure 2-26**). For example, the width of the beach at the toe of the slide in 1994 was some 106 m (350 ft) wide, while small dunes had developed along a 1.1 km (0.6 mi) section of the beach. This suggests the accumulation of a significant volume of sand in the area. However, as a result of the 1997-98 El Niño, the beach eroded back about 98 m (320 ft), eroding into the toe of the slide (**Figure 2-26**). This process has been repeated over the years (e.g., 1950s shoreline) and most recently in the mild 2009-10 El Niño. During this last event, the sand beach in front of The Capes narrowed significantly, almost approaching the position of the shoreline in 1998. **Figure 2-26** shows the magnitude of change characterized by the shift in the shoreline from 2009 and 2011, as the mouth of the bay once again shifted north.

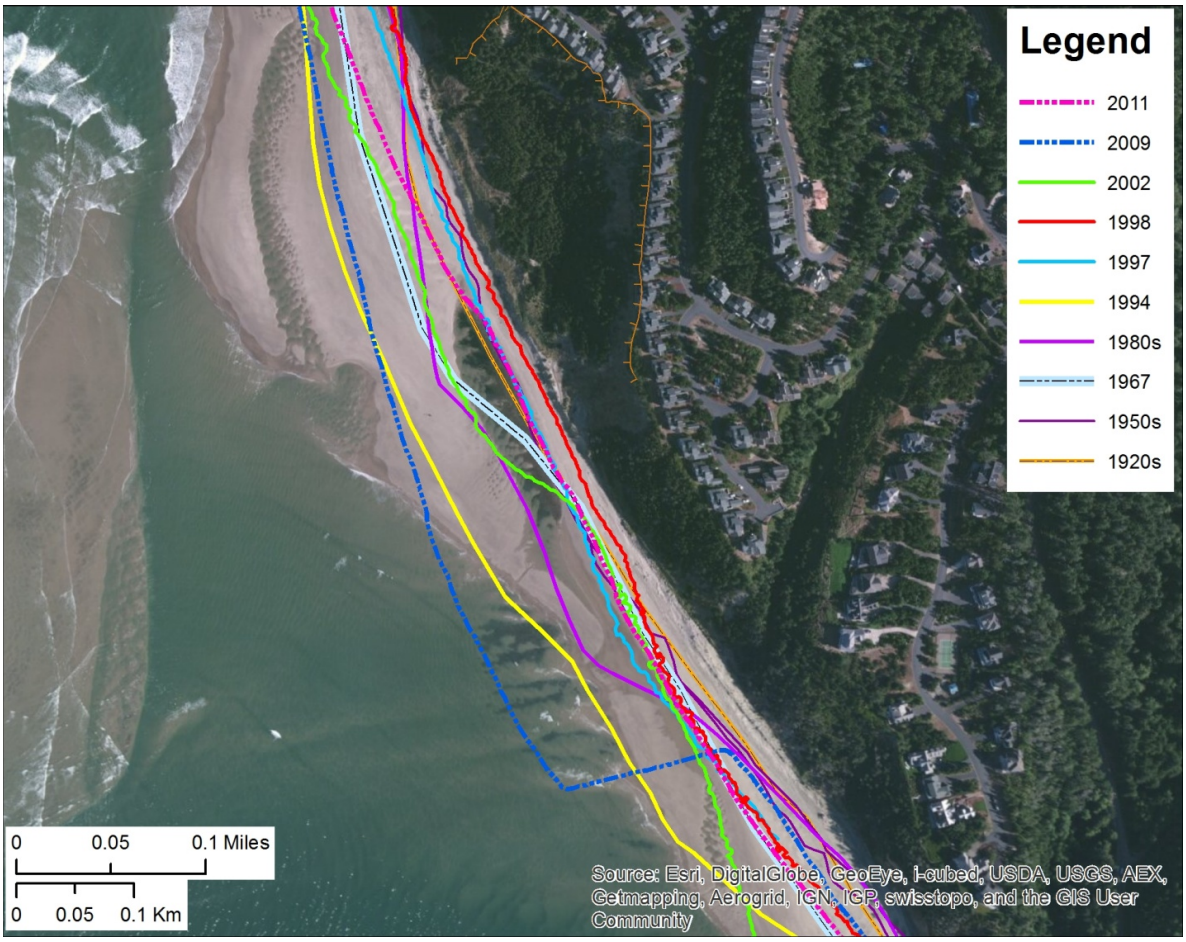

Figure 2-26. Historical shoreline positions identified along the toe of The Capes development near the mouth of Netarts Bay. Here we include one additional shoreline (2011) surveyed using GPS. Brown hashed line depicts the landslide headscarp.

Finally, **Figure 2-27** shows the spread of shorelines adjacent to Oceanside. The 1920s and 1950s shorelines reveal the presence of an extremely narrow beach at Oceanside. This suggests a period of extensive erosion during those years. However, as can be seen from **Figure 2-28**, although the beach may have been narrow the bluff face is covered in vegetation with little sign of erosion. In fact, comparisons between historical and modern photos reinforce the perception that this section of shore is essentially stable.

Of interest also is the 1980s shoreline, which highlights significant differences between Oceanside and Short Sand Beach to the north. At Oceanside, the 1980s shoreline is located in the approximate same location as the 1994, 1997, and 1998 shorelines and indicates a relatively broad beach (**Figure 2-27**). In the two pocket beaches to the north, the 1980s shoreline tracks close to the base of the bluff, indicating a very narrow beach. The latter is not surprising given that this particular beach consists of gravels and as noted previously, the shorelines tend to track much closer to each other on steep beaches. Overall, variations in the shoreline positions along this section of coast may reflect a lag in the transport of sediment around the bluff headlands that bound the smaller pocket beaches. Furthermore, erosion events similar to what occurred at the Capes likely contribute large slugs of sediment that progressively move northwards along the coast, producing the apparent shoreline fluctuations seen at Oceanside and in the smaller pocket beaches to the north. Overall, these findings clearly highlight a very dynamic and complex coastal environment, in which a wide range of different processes are operating over a broad range of spatial and temporal scales.

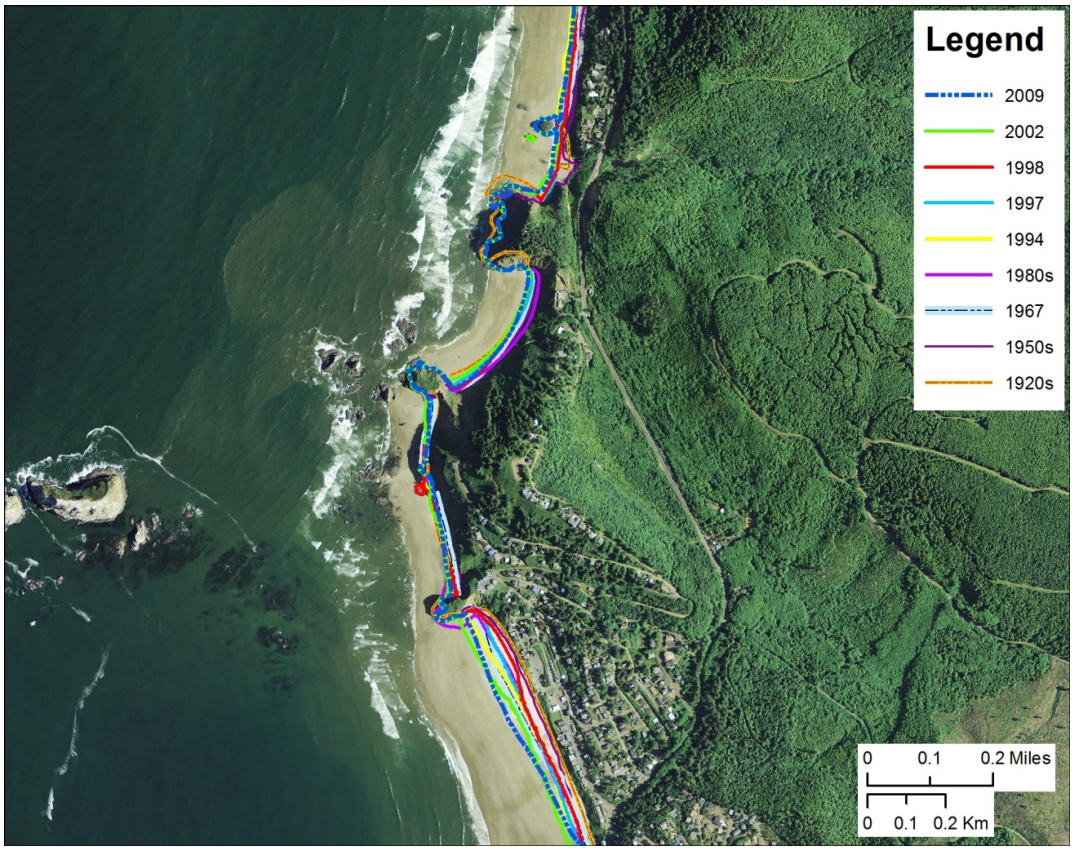

Figure 2-27. Historical shoreline positions identified at the mouth of Netarts Bay, Oceanside and along Short Sand Beach. Note: The 1920s and 1950s (1927/28, 1953/55) shoreline is derived from NOS T-sheets, 1967 and 1994 are from orthorectified aerial photographs, 1980s (1985/86) is from U.S. Geological Survey topographic maps, and 1997–2009 are derived from lidar. Black dashed line on the dune denotes an erosion scarp.

Figure 2-28. Stable shorelines at Neskowin and Oceanside. A) A 1920s era photo of the community of Neskowin looking south toward the entrance to Netarts Bay. Note well vegetated bluffs and the presence of the gravel berm along the toe of the bluffs (photos courtesy of Neskowin community archives); B) Oceanside in March 1998 following the 1997-98 El Niño winter. Note again the well vegetated bluff and gravel berm at the back of the beach (photo courtesy of P. Komar).

2.4.1.4 Rockaway Cell

Some of the most dramatic shoreline changes identified on the Oregon coast have occurred in the Rockaway littoral cell, particularly in response to the construction of the north jetty at the mouth of Tillamook Bay (**Figure 2-29** and **Figure 2-30**). Previous descriptions of the response of Tillamook Bay mouth to jetty construction are given by Terich and Komar (1974), while (Komar, 1997) provides a historical summary of the destruction of Bayocean spit.

Construction of Tillamook's north jetty was completed in October 1917. During the construction phase, changes in the inlet channel and the adjacent shorelines soon became evident (**Figure 2-29**). North of the jetty, sand began to accumulate rapidly and the shoreline advanced seaward at a rate almost equal to the speed at which the jetty was being constructed (Komar, 1997). Between 1914 and 1927, the coastline just north of the jetty advanced seaward by ~1 km (0.62 mi). However, by 1920 the rate of sand accumulation on the north side of the jetty had slowed dramatically, so that the position of the shoreline was much the same as it is today (**Figure 2-30**). According to (Komar and others, 1976), the volume of sand that accumulated north of the jetty caused some to speculate that the predominant net sand transport was to the south. However, Komar and others argued that this was not the case. They observed that if a net southward drift of sediment was occurring, why was there no evidence of an accumulation of sand adjacent to Cape Meares, located at the southern end of the Rockaway littoral cell. Instead, the Cape Meares beach is narrow and is composed mainly of cobbles and gravels.

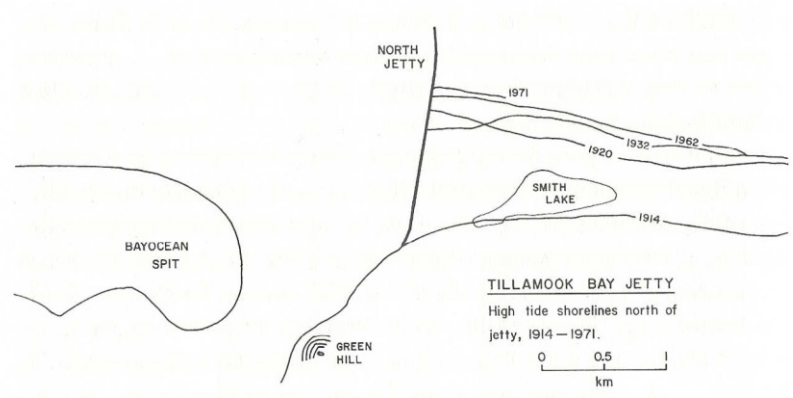

Figure 2-29. Shoreline positions north of Tillamook Bay jetty, 1914-1972 (From Terich 1973 in Komar 1997).

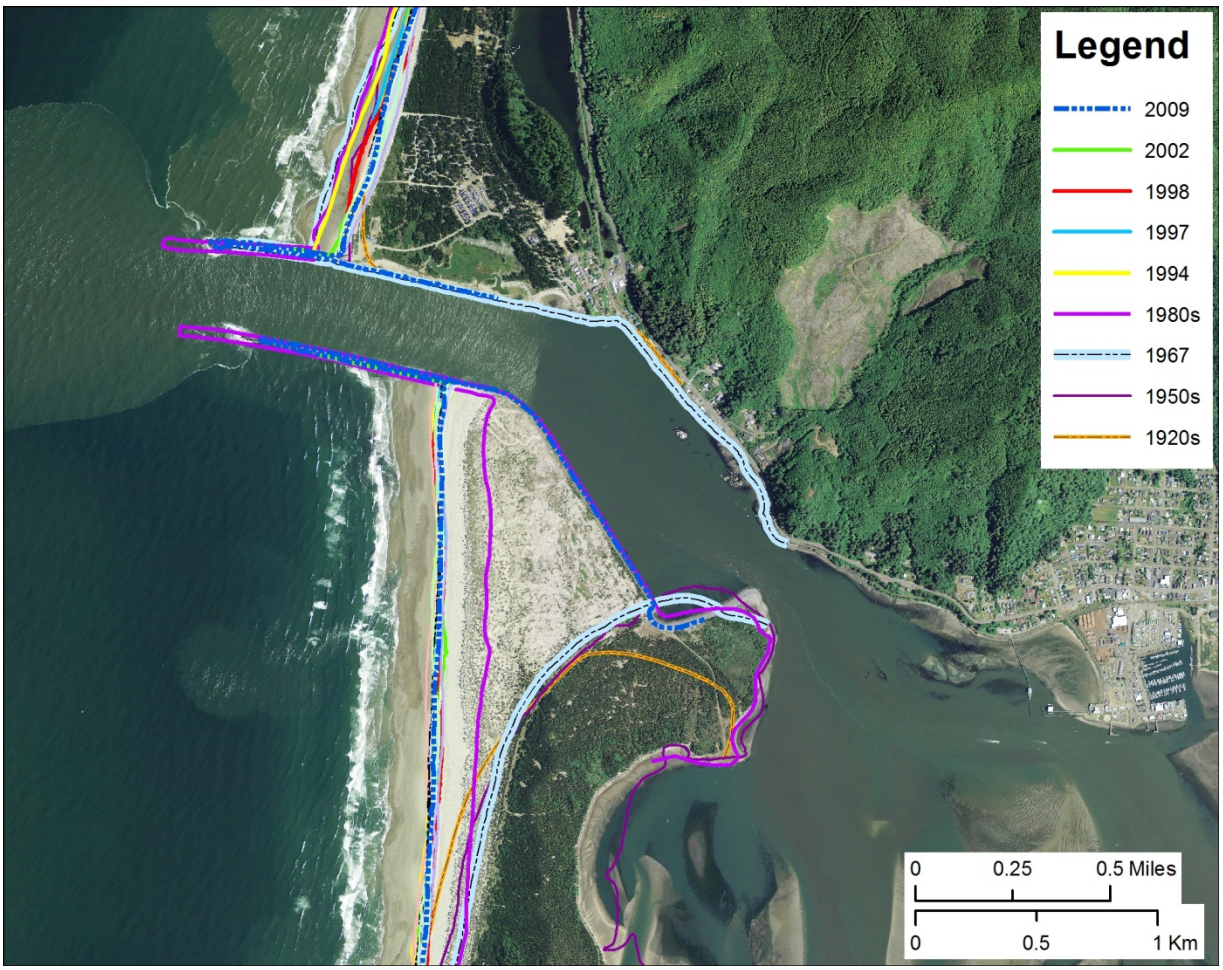

Figure 2-30. Historical shoreline positions identified adjacent to the mouth of Tillamook Bay in the Rockaway littoral cell. Note: The 1920s and 1950s (1927/28, 1953/55) shoreline is derived from NOS T-sheets, 1967 and 1994 are from orthorectified aerial photographs, 1980s (1985/86) is from U.S. Geological Survey topographic maps, and 1997–2009 are derived from lidar.

Although the coastline from Rockaway to Manzanita experienced some erosion (discussed below) due to jetty construction, the most dramatic changes were in fact observed farther south along Bayocean Spit. In particular, significant coastal retreat occurred at the south end of the Rockaway cell in the vicinity of the Cape Meares community (**Figure 2-31**). As shown in the figure, the 1927 shoreline previously extended well seaward (up to 260 m [850 ft]) of the present-day shoreline; when visiting the community of Cape Meares, 3rd Street is the most seaward street with 1st and 2nd Streets having been located out on what is now the beach. Over time the shoreline has progressively retreated landward to its present position. Between 1920s and 1950s the shoreline retreated by about 67 to 85 m (220 to 280 ft) at an average erosion rate of ~2 to 3 m/yr (6 to 10 ft/yr). In particular, significant coastal erosion occurred in the vicinity of the Cape Meares community as a result of a major storm during January 3–6, 1939 (Komar, 1997). Additional large storm wave events during the winter of 1940 continued to erode the spit. This process was repeated throughout the 1940s and culminated with the removal of a 1.2 km (0.75 mi) section of Bayocean spit on November 13, 1952, breaching the spit (**Figure 2-32**).

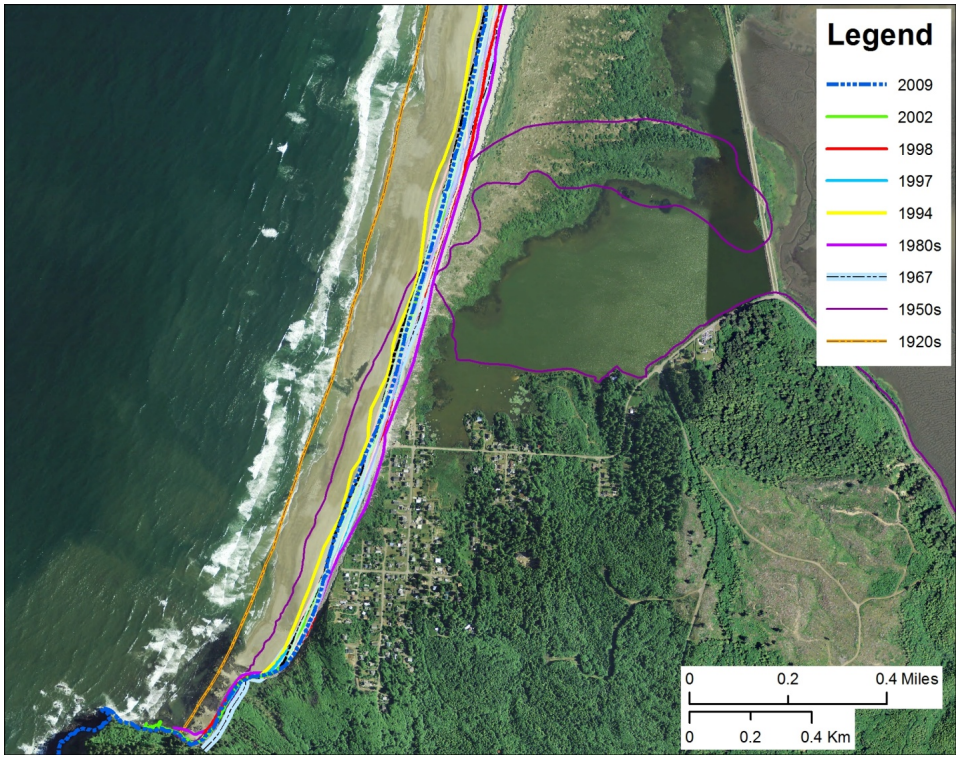

Figure 2-31. Historical shoreline positions identified at the southern end of the Rockaway littoral cell in the vicinity of the Cape Meares community.

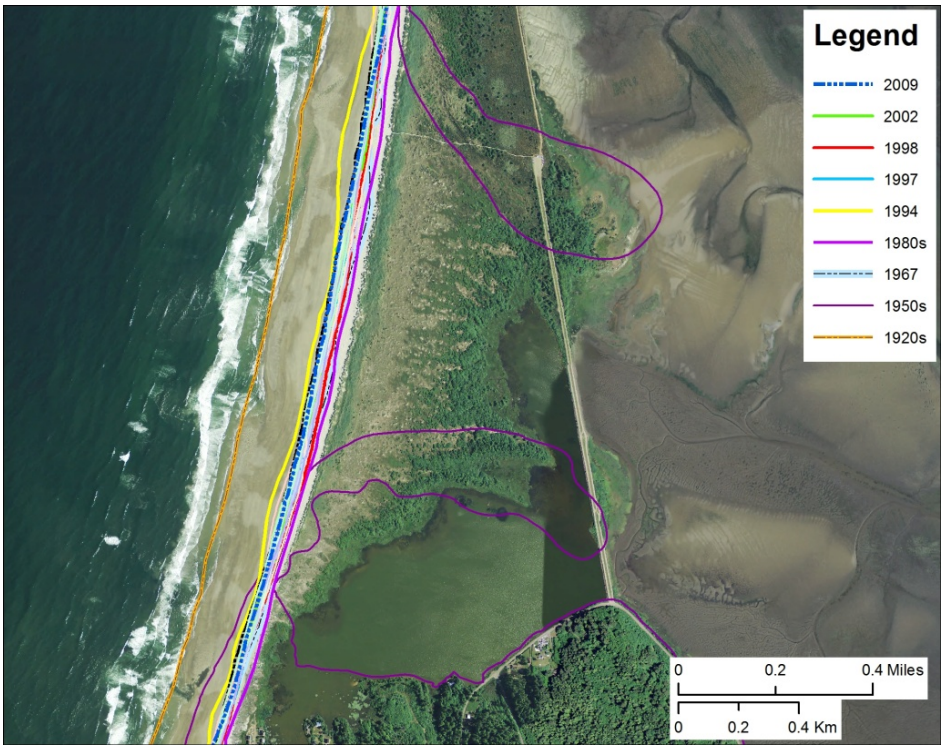

Figure 2-32. The breach of Bayocean Spit on November 13, 1952. Note: The 1920s and 1950s (1927/28, 1953/55) shoreline is derived from NOS T-sheets, 1967 and 1994 are from orthorectified aerial photographs, 1980s (1985/86) is from U.S. Geological Survey topographic maps, and 1997–2009 are derived from lidar.

The estimated erosion rate (~2 to 3 m/yr [6 to 10 ft/yr]) for the area around Cape Meares appears to have been maintained between the 1950s to the 1980s, as the shoreline continued to retreat landward by an additional 91 m (300 ft, **Figure 2-28**). However, since then the lidar and GPS shorelines indicate that the shoreline may have stabilized, because it appears to be oscillating around its present location. The absence of a south jetty at Tillamook Bay prior to 1974 probably enhanced the erosion of Bayocean spit, as a lot of sediment accumulated as shoals at the spit end or was washed into the bay (Komar, 1997). However, with the completion of the south jetty in November 1974, sand quickly began to accumulate at the north end of the spit, causing the shoreline to prograde seaward by some 300 to 760 m (1,000 to 2,500 ft; **Figure 2-27**). Since then, the shoreline along Bayocean Spit has stabilized, so that it now responds in a manner similar to other littoral cells on the Oregon coast (Komar, 1997), with the pair of jetties on the inlet acting more like a headland. Repeat GPS surveys of Bayocean Spit undertaken by DOGAMI staff since 2004 indicate that the southern end of the spit is stable (http://www.oregongeology.org/¬nanoos/data/img/lg/Bay1_6mchange.png), while the northern one third of the spit has been accreting at an average rate of ~+0.7 to +1 m/yr (+2.3 to +3.3 ft/yr) (http://www.oregongeology.org/nanoos/data/img/lg/Bay6_6mchange.png).

Farther north along the Rockaway-Manzanita coastline, the 1920s and 1950s shorelines were positioned well landward of contemporary shorelines (**Figure 2-33** and **Figure 2-34**). This type of pattern is a direct response to construction of the north Tillamook jetty. However, the erosion that occurred along the Rockaway-Manzanita beaches was generally much less then on Bayocean Spit (Komar, 1997). This is because the length of shoreline along the Rockaway-Manzanita coastline is much greater than along Bayocean spit. As a result, only a small amount of sand had to be eroded from those beaches, per unit length of shoreline, to supply sand to the accreting area around the north jetty. Erosion along the Rockaway-Manzanita coastline probably stabilized sometime after the 1950s, enabling the coastline to enter an accretionary phase. As shown in **Figure 2-33** and **Figure 2-34**, the 1994 and 1997 shorelines characterize the seaward extent of this rebuilding phase. This view is also supported from observations of dune growth around Manzanita, culminating with the initiation of a dune management program to control the growth of the foredunes (Dr. J. Marra, personal comm., 2001). While the historical patterns of change suggest overall stability, this is in fact not the case. Commencing in the late 1990s, the beach between the Tillamook and Nehalem jetties have been subject to a number of major storms that have resulted in chronic erosion hazards. This latest response is described in Section 3.3.1.

In summary, this section has presented information on the historical shoreline changes that have occurred along the Tillamook County coastline over the past century. The analyses indicate that for the most part the dune-backed shorelines respond episodically to such processes as the El Niño/La Niña Southern Oscillation, and as a result of rip current embayments that cause highly localized "hotspot erosion" of the coast. Accordingly, the coastline undergoes periods of both localized and widespread erosion, with subsequent intervening periods during which the beaches and dunes slowly rebuild. Perhaps the most significant coastal changes identified in Tillamook County have occurred in response to human activity, particularly as a result of jetty construction during the early part of last century. In particular, jetty construction has had a dramatic influence on the morphology of Bayocean Spit and, to a lesser extent, between the north Tillamook jetty and the Rockaway-Manzanita beaches to the north. Finally, the present analyses have shown that the mouths of the estuaries and the spit ends are extremely dynamic features, migrating over large distances in response to changes in both the sediment supply and the predominant wave conditions, making these areas hazardous for any form of development.

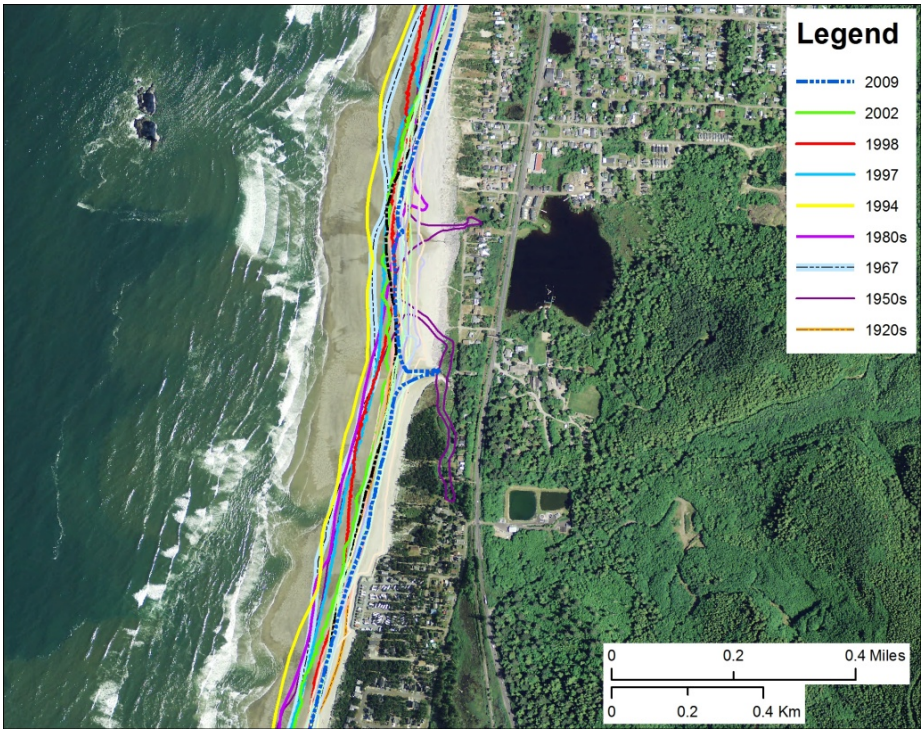

Figure 2-33. Historical shoreline positions identified near Twin Rocks. Note: The 1920s and 1950s (1927/28, 1953/55) shoreline is derived from NOS T-sheets, 1967 and 1994 are from orthorectified aerial photographs, 1980s (1985/86) is from U.S. Geological Survey topographic maps, and 1997–2009 are derived from lidar.

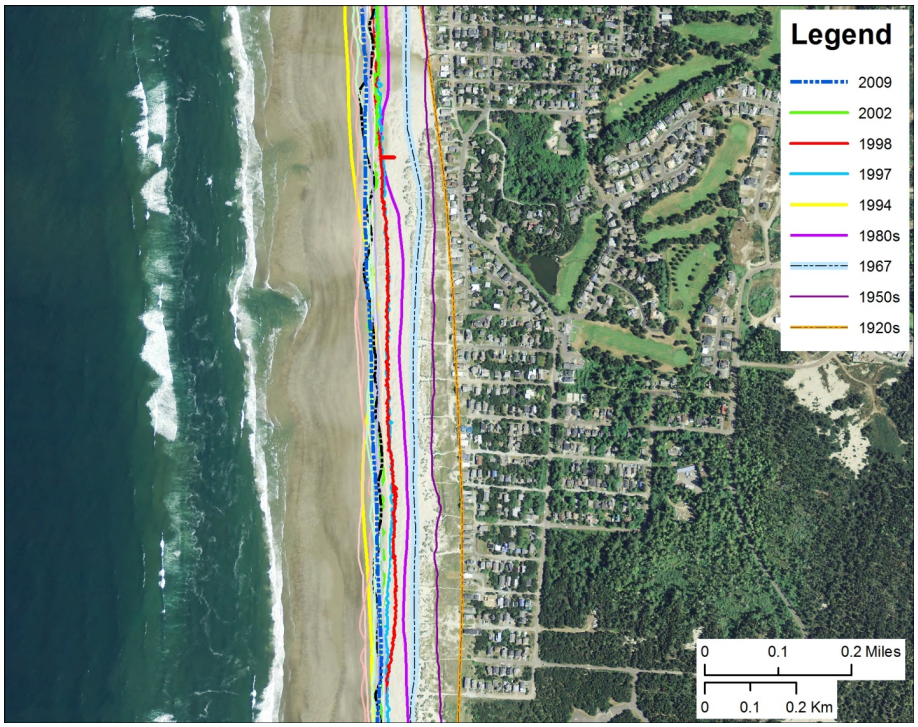

Figure 2-34. Historical shoreline positions at Manzanita. Note: The 1920s and 1950s (1927/28, 1953/55) shoreline is derived from NOS T-sheets, 1967 and 1994 are from orthorectified aerial photographs, 1980s (1985/86) is from U.S. Geological Survey topographic maps, and 1997–2009 are derived from lidar.

3.0 BEACH AND BLUFF MORPHOLOGY ASSESSMENTS

Field surveys were undertaken throughout Tillamook County in summer 2011 and again in winter 2012 in order to better define the seasonal variability. These surveys serve two important objectives:

1. To establish beach profile transects along discrete but representative sections of the shoreline's geomorphology/geology, including sections of coast where coastal engineering structures have been constructed, for the purposes of coastal hydraulic analyses.
2. To provide representative measurements, derived from lidar or GPS data, of the beach in its winter state, in order to define the morphology, elevations, and slope of the beach face for use in subsequent wave runup and overtopping computations.

Surveying along the Tillamook County coast was initially carried out in August and September 2011, and again in February/March 2012. The surveys were completed late in the winter season when Oregon beaches are typically in their most eroded state (Aguilar-Tunon and Komar, 1978; Komar, 1997; Allan and Komar, 2002; Allan and Hart, 2008). A total of 178 beach profile transects were established along the length of Tillamook County (**Figure 3-1** to **3-3**) and can be subdivided according to the following littoral cells:

- Neskowin: 28 sites;
- Nestucca spit/Pacific City: 14 sites;
- Tierra Del Mar/Sand Lake: 32 sites;
- Netarts Spit/Oceanside: 29 sites;
- Short Sand Beach: 3 sites;
- Bayocean Spit: 11 sites;
- Twin Rocks/Rockaway/Nedonna Beach: 40 sites; and
- Nehalem Spit/Manzanita: 21 sites.

Appendix B provides a table that describes the naming conventions used by DOGAMI, which is linked to the transect database in the final DFIRM for Tillamook County.

3.1 Survey Methodology

Beach profiles that are oriented perpendicular to the shoreline can be surveyed using a variety of approaches, including a simple graduated rod and chain, surveying level and staff, total station theodolite and reflective prism, lidar airborne altimetry, and Real-Time Kinematic Differential Global Positioning System (RTK-DGPS) technology. Traditional techniques such as leveling instruments and total stations are capable of providing accurate representations of the morphology of a beach, but are demanding in terms of time and effort. At the other end of the spectrum, high-resolution topographic surveys of the beach derived from lidar are ideal for capturing, within a matter of hours, the three-dimensional state of the beach over an extended length of coast; other forms of lidar technology are now being used to measure nearshore bathymetry out to moderate depths but are dependent on water clarity. However, the lidar technology remains expensive and is impractical along small segments of shore and, more importantly, the high costs effectively limits the temporal resolution of the surveys and hence the ability of the end-user to understand short-term changes in the beach morphology (Bernstein and others, 2003).

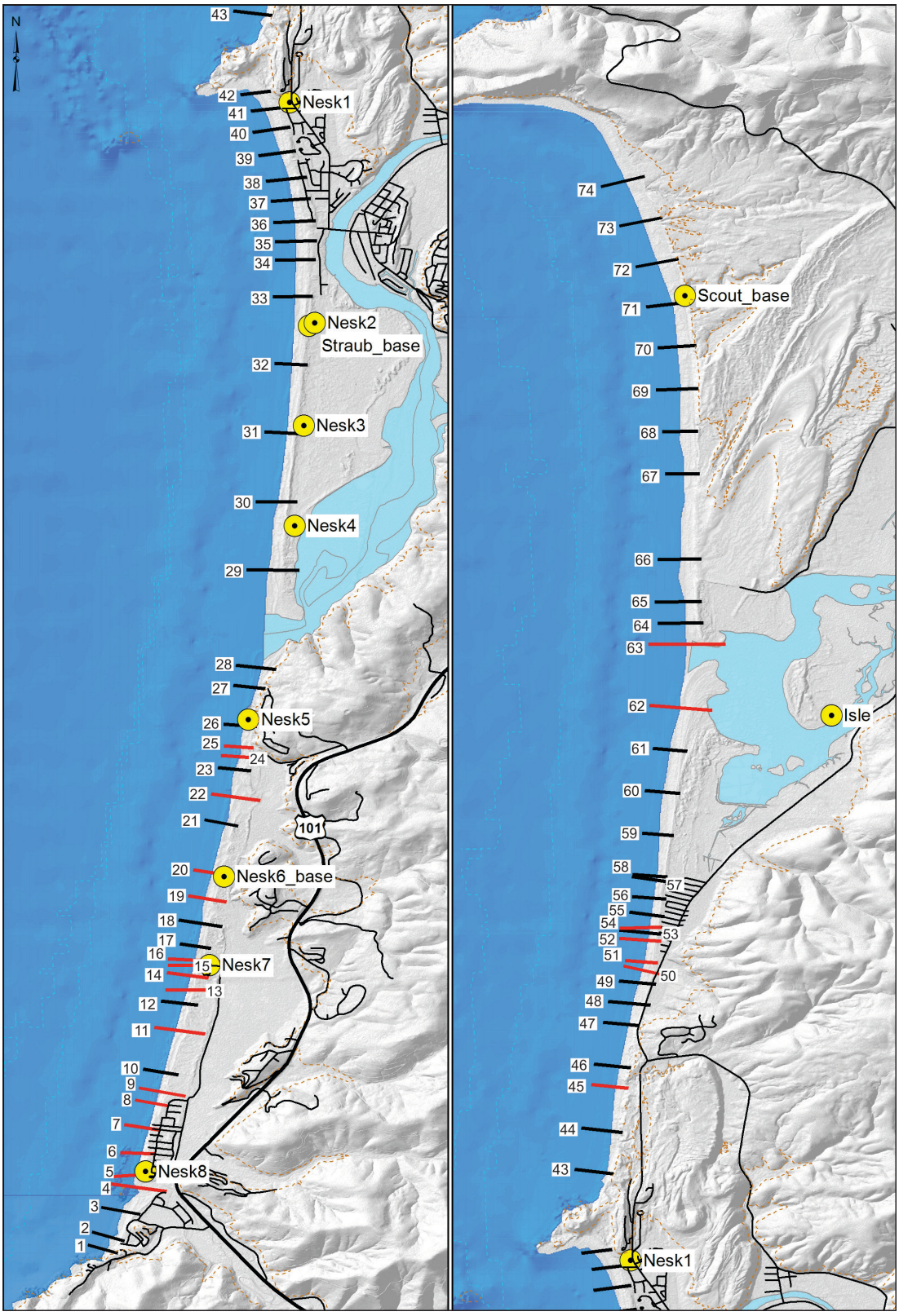

Figure 3-1. Location map of beach profiles in southern Tillamook County. Left) Beach profiles measured along the Neskowin shoreline (transects 1–28), Nestucca spit and adjacent to Pacific City (transects 29–42); Right) and within the Sand Lake littoral cell in Tillamook County (transects 43–74). Red lines denote transects where overtopping has been identified. Yellow circles denote the locations of benchmarks used in local site calibrations.

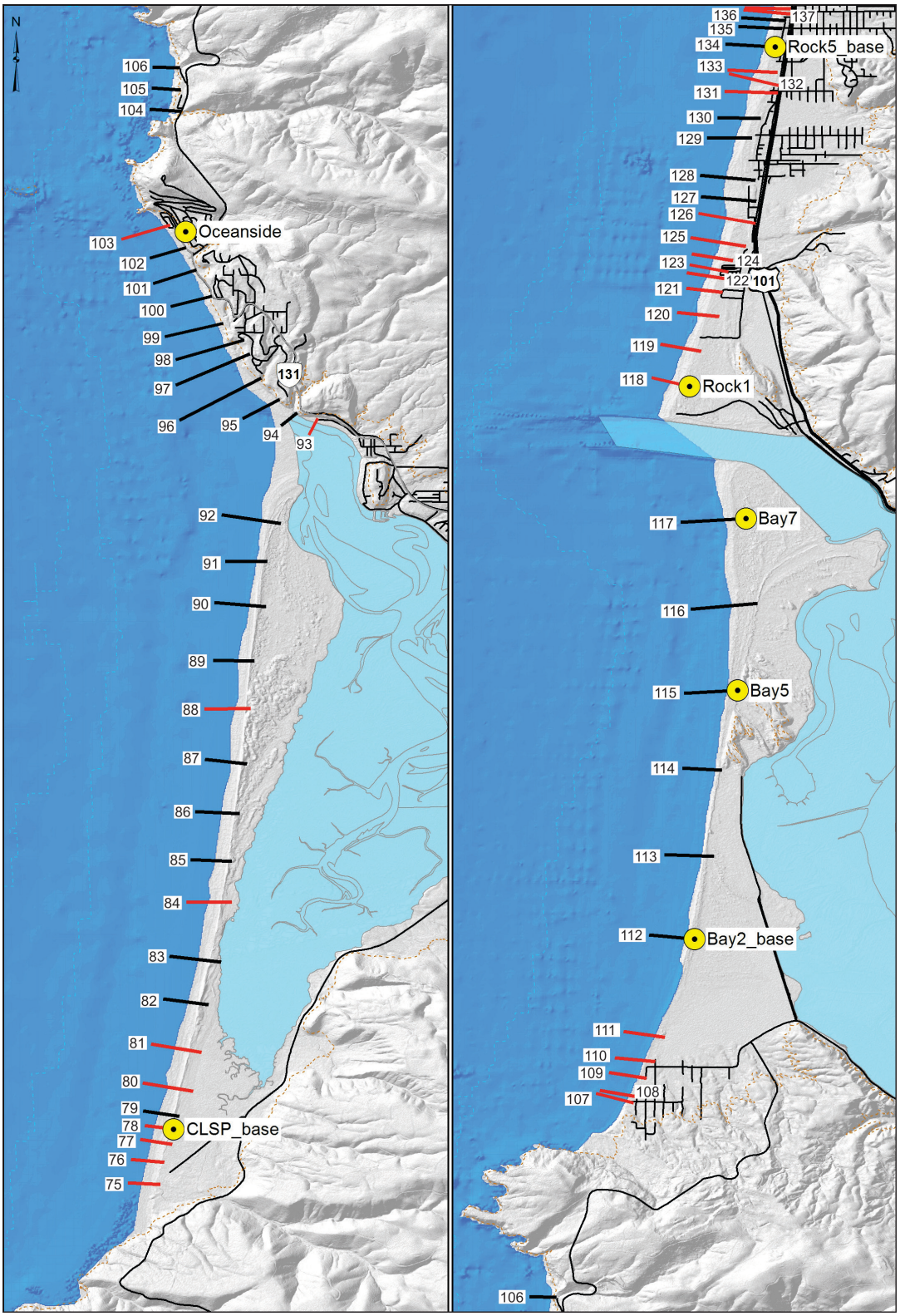

Figure 3-2. Location map of beach profiles in central Tillamook County. Left) Location map of beach profiles measured along Netarts Spit (transects 75–92), at Oceanside (transects 93–103) and at Short Sand Beach (transects 104–106); Right) along Bayocean Spit (transects 107–117), and in the Twin Rocks area (transects 118–137) in Tillamook County. Red lines denote transects where overtopping has been identified. Yellow circles denote the locations of benchmarks used in local site calibrations.

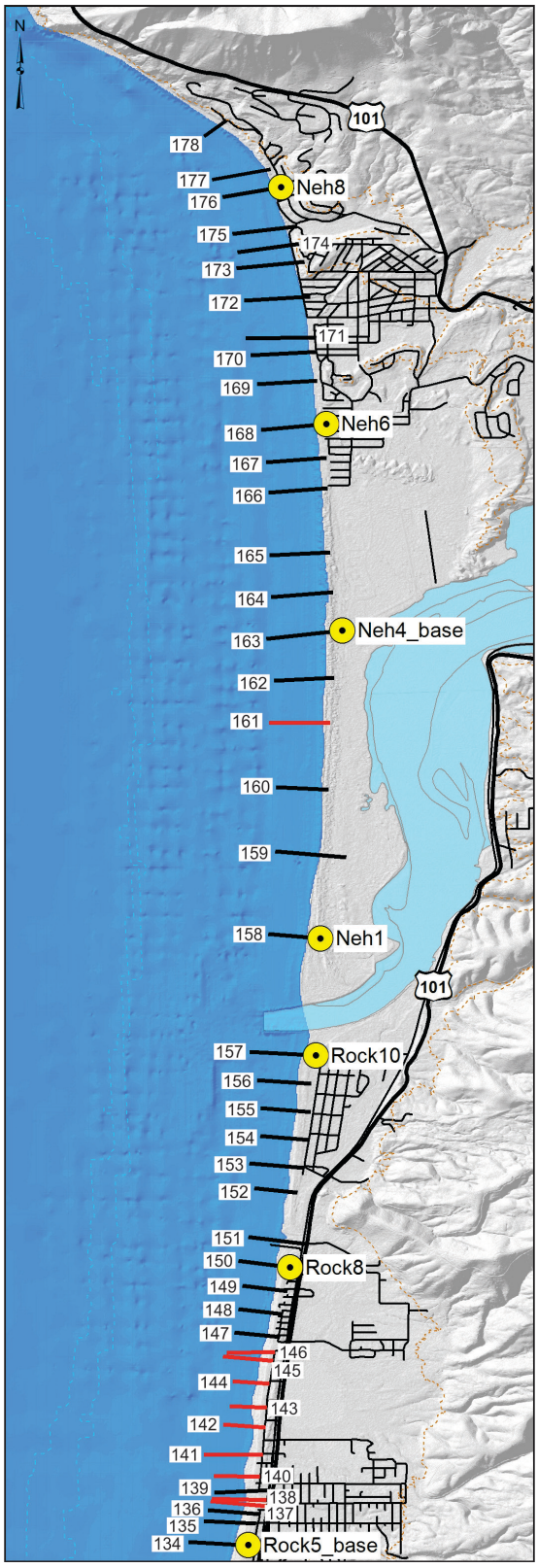

Figure 3-3. Location of map of beach profiles in northern Tillamook County showing profiles measured along Rockaway/Nedonna Beach (transects 134–157), Nehalem Spit (transects 158–166), and in the Manzanita area (transects 167–178) in Tillamook County. Red lines denote transects where overtopping has been identified. Yellow circles denote the locations of benchmarks used in local site calibrations.

Within this range of technologies, the application of RTK-DGPS for surveying the morphology of both the subaerial and subaqueous portions of the beach has effectively become the accepted standard (Morton and others, 1993; Ruggiero and Voigt, 2000; Bernstein and others, 2003; Ruggiero and others, 2005) and is the surveying technique used in this study. The Global Positioning System (GPS) is a worldwide radio-navigation system formed from a constellation of 24 satellites and their ground stations, originally developed by the U.S. Department of Defense; in 2007 the Russian Government made their GLONASS satellite network available increasing the number of satellites to ~46 (as of February 2011).

In its simplest form, GPS can be thought of as triangulation with the GPS satellites acting as reference points, enabling users to calculate their position to within several meters (e.g., using inexpensive off the shelf hand-held units), while survey grade GPS units are capable of providing positional and elevation measurements that are accurate to a centimeter. At least four satellites are needed mathematically to determine an exact position, although more satellites are generally available. The process is complicated because all GPS receivers are subject to error, which can significantly degrade the accuracy of the derived position. These errors include the GPS satellite orbit and clock drift plus signal delays caused by the atmosphere and ionosphere and multipath effects (where the signals bounce off features and create a poor signal). For example, hand-held autonomous receivers have positional accuracies that are typically less than about 10 m (<~30 ft), but can be improved to less than 5 m (<~15 ft) using the Wide Area Augmentation System (WAAS). This latter system is essentially a form of differential correction that accounts for the above errors, which is then broadcast through one of two geostationary satellites to WAAS-enabled GPS receivers.

Greater survey accuracies are achieved with differential GPS (DGPS) using two or more GPS receivers to simultaneously track the same satellites, enabling comparisons to be made between two sets of observations. One receiver is typically located over a known reference point, and the position of an unknown point is determined relative to that reference point. With the more sophisticated 24-channel dual-frequency RTK-DGPS receivers, positional accuracies can be improved to the sub-centimeter level when operating in static mode and to within a few centimeters when in RTK mode (i.e., as the rover GPS is moved about). In this study we used Trimble® 24-channel dual-frequency R7/R8 and 5700/5800 GPS receivers. This system consists of a GPS base station (R7 and/or 5700 unit), Zephyr Geodetic™ antenna (model 2), HPB450 radio modem, and R8 (and/or 5800) "rover" GPS **(Figure 3-4)**. Trimble reports that both the R7/R8 and 5700/5800 GPS systems have horizontal errors of approximately ±1 cm + 1 ppm (parts per million × the baseline length) and ±2 cm in the vertical (Trimble, 2005).

To convert a space-based positioning system to a ground-based local grid coordinate system, a precise mathematical transformation is necessary. While some of these adjustments are accomplished by specifying the map projection, datum, and geoid model prior to commencing a field survey, an additional transformation is necessary whereby the GPS measurements are tied to known ground control points (**Figure 3-5**). This latter step is called a GPS site calibration, such that the GPS measurements are calibrated to ground control points with known vertical and horizontal coordinates using a rigorous least-squares adjustment procedure. Performing the calibration is initially undertaken in the field using the Trimble TSC2 GPS controller and then re-evaluated in the office using Trimble's Business Office software (version 2.5).

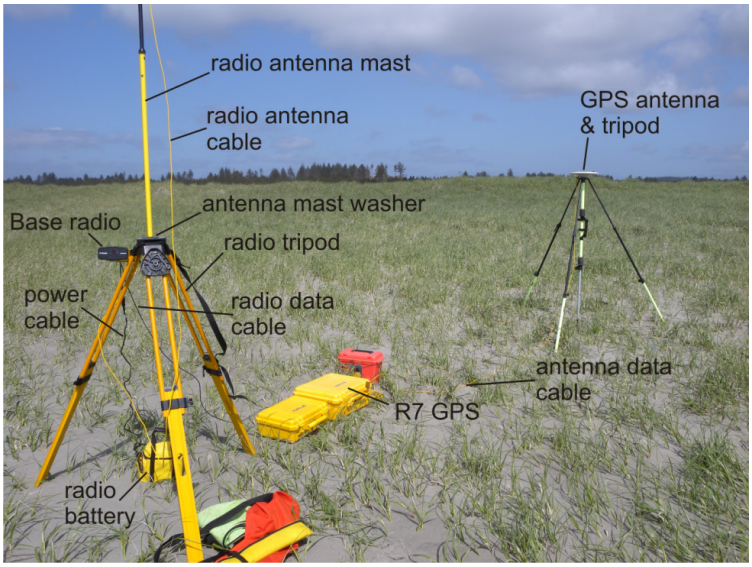

Figure 3-4. The Trimble R7 base station antenna in operation on the Tillamook Plains. Corrected GPS position and elevation information is transmitted by an HPB450 Pacific Crest radio to the R8 GPS rover unit (photo: J. Allan, DOGAMI, 2010).

Figure 3-5. A 180-epoch calibration check is performed on a survey monument (Rock7) established in the Rockaway littoral cell in Tillamook County. This procedure is important for bringing the survey into a local coordinate system and for reducing errors associated with the GPS survey (photo: J. Allan, DOGAMI, 2004).

3.1.1 Tillamook County survey control procedures

Survey control (Table 3-1) along the Tillamook County shore was provided by occupying multiple benchmarks established by the Coastal Field Office of DOGAMI. The approaches used to established the benchmarks are fully described in reports by Allan and Hart (2007, 2008).

Coordinates assigned to the benchmarks (**Table 3-1**), were derived by occupying a Trimble R8 GPS receiver over the established benchmark, which then receives real-time kinematic corrections via the Oregon Real Time GPS Network (ORGN) (http://www.theorgn.net/). The ORGN is a network of permanently installed, continuously operating GPS reference stations established and maintained by ODOT and partners (essentially a CORS network similar to those operated and maintained by the National Geodetic Survey [NGS]) that provide real-time kinematic (RTK) correctors to field GPS users over the internet via cellular phone networks. As a result, GPS users that are properly equipped to take advantage of these correctors, such as the Trimble system used in this study, can survey in the field to the one centimeter horizontal accuracy level in real time. Each benchmark was observed on at least two occasions, at different times of the day or on alternate days; the derived values were reviewed and, if reasonable, were averaged.

Furthermore, additional checking was undertaken for each of the GPS base station sites (**Table 3-1**), by comparing the multi-hour GPS measurements to coordinates and elevations derived using the Online Positioning User Service (OPUS) maintained by the NGS (http://www.ngs.noaa.gov/OPUS/ [Soler and others, 2011]). OPUS provides a simplified way to access high-accuracy National Spatial Reference System (NSRS) coordinates using a network of continuously operating GPS reference stations (CORS, http://www.ngs.noaa.gov/CORS/). In order to use OPUS, static GPS measurements are typically made using a fixed height tripod for periods of 2 hours or greater. OPUS returns a solution report with positional accuracy confidence intervals for adjusted coordinates and elevations for the observed point. In all cases we used the Oregon State Plane coordinate system, northern zone (meters), while the vertical datum is relative to the North American Vertical Datum of 1988 (NAVD88).

For each of the discrete shore reaches, the R7 GPS base station was located on the prescribed base station monument (i.e., NEH4, ROCK5, BAY2, CLSP, SCOUT, STRAUB, NESK6; **Table 3-1**), using a 2.0-m fixed height tripod. Survey control was provided by undertaking 180 GPS epoch measurements (~3 minutes of measurement per calibration site) using the calibration sites indicated in **Table 3-1**, enabling us to perform a GPS site calibration that brought the survey into a local coordinate system. This step is critical in order to eliminate various survey errors that may be compounded by factors such as poor satellite geometry, multipath, and poor atmospheric conditions that in combination increase the total error to several centimeters. **Table 3-2** shows the relative variability identified when comparing the mean derived benchmark coordinate and the original ORGN/OPUS derivations. As can be seen from **Table 3-2**, differences in the horizontal and vertical values at the benchmarks were typically less than 2 cm (i.e., within one standard deviation [σ]).

Table 3-1. Survey benchmarks used to calibrate GPS surveys of the beach along the Tillamook County coastline. Asterisk signifies the location of the GPS base station during each respective survey. NGS denotes National Geodetic survey monument, ORGN signifies Oregon Real Time GPS Network.

Study Area	Primary Identification (PID) Name[1]	Northing (m)	Easting (m)	Elevation (m)
Nehalem Spit	NEH8 - DOGAMI/ORGN	2232106.115	234997.630	9.101
	NEH6 - DOGAMI/ORGN	2232318.132	232654.396	11.201
	NEH4 - DOGAMI/ORGN*	2232342.755	230612.045	8.703
	NEH1 - DOGAMI/ORGN	2232062.218	227586.204	12.828
Rockaway	ROCK10 - DOGAMI/ORGN	2231980.938	226431.232	8.400
	ROCK8 - DOGAMI/ORGN	2231714.373	224350.055	5.276
	ROCK5 - DOGAMI/ORGN*	2231306.182	221626.396	10.046
	ROCK1 - DOGAMI/ORGN	2230430.835	217674.746	6.732
Bayocean Spit	BAY7 - DOGAMI/ORGN	2230194.049	211189.992	9.440
	BAY5 - DOGAMI/ORGN	2230672.493	214089.934	8.155
	BAY2 - DOGAMI/ORGN*	2230827.791	216103.016	8.497
Netarts Spit/ Oceanside	AJ1985 – NGS/ORGN	2228840.68	205112.21	37.609
	RD1459 – NGS/ORGN	2239922.16	200302.4695	4.5265
	CLSP - DOGAMI/ORGN*	2228287.197	194592.782	4.763
Sand Lake/ Tierra Del Mar	SCOUT - DOGAMI/ORGN*	2228476.091	189282.575	8.261
	ISLE - DOGAMI/ORGN	2229478.034	184302.823	4.638
	NESK1 - DOGAMI/ORGN	2227540.749	177975.0305	12.367
Nestucca spit/ Pacific City	NESK1 - DOGAMI/ORGN	2227540.749	177975.0305	12.367
	STRAUB - DOGAMI/ORGN*	2227589.237	175343.511	12.936
	NESK2 - DOGAMI/ORGN	2227636.668	175375.163	7.085
	NESK3 - DOGAMI/ORGN	2227495.199	174174.595	4.437
	NESK4 - DOGAMI/ORGN	2227368.161	173001.673	4.827
Neskowin	NESK5 - DOGAMI/ORGN	2226885.830	170740.992	4.12
	NESK6 - DOGAMI/ORGN*	2226603.997	168908.419	8.215
	NESK7 - DOGAMI/ORGN	2226438.263	167871.992	6.504
	NESK8 - DOGAMI/ORGN	2225802.096	165471.981	9.529

Notes: Coordinates are expressed in the Oregon State Plane Coordinate System, northern zone (meters), and the vertical datum is NAVD88.

[1]Control provided using both horizontal and vertical values derived by averaging multiple separate GPS occupations with survey control provide by the ORGN.

Table 3-2. Comparison of horizontal and vertical coordinates (expressed as a standard deviation) at each of the benchmark locations, compared to the final coordinates referenced in Table 3-1. Asterisk signifies the location of the GPS base station during each respective survey.

Study Area	Primary Identification (PID) Name[1]	Northing (m) σ	Easting (m) σ	Elevation (m) σ
Nehalem Spit	NEH8	0.001	0.016	0.029
	NEH6	0.004	0.001	0.020
	NEH4*	0.012	0.004	0.010
	NEH1	0.010	0.011	0.001
Rockaway	RCK10	0.010	0.049	0.141
	RCK8	—	—	—
	RCK5*	0.012	0.005	0.024
	RCK1	0.020	0.007	0.006
Bayocean Spit	BAY7	0.003	0.011	0.002
	BAY5	0.012	0.000	0.003
	BAY2*	0.010	0.007	0.025
Netarts Spit	AJ1985	0.019	0.011	0.036
	RD1459	0.021	0.013	0.012
	CLSP*	0.015	0.006	0.010
Sand Lake	SCOUT*	0.010	0.005	0.034
	ISLE	0.029	0.000	0.003
	NESK1	0.014	0.006	0.001
Nestucca spit	STRAUB*	0.003	0.001	0.020
	NESK2	0.011	0.003	0.001
	NESK3	0.005	0.004	0.044
	NESK4	0.008	0.021	0.000
Neskowin	NESK5	—	—	—
	NESK6*	0.014	0.007	0.013
	NESK7	0.008	0.023	0.049
	NESK8	0.015	0.037	0.004

After local site calibration (**Figure 3-5),** cross-shore beach profiles were surveyed with the R8 GPS rover unit mounted on a backpack, worn by a surveyor (**Figure 3-6**). This was undertaken during periods of low tide, enabling more of the beach to be surveyed. The approach generally was to walk from the landward edge of the primary dune or bluff edge, down the beach face and out into the ocean to approximately wading depth. A straight line perpendicular to the shore was achieved by navigating along a predetermined line displayed on a hand-held Trimble TSC2 computer controller connected to the R8 receiver. The computer shows the position of the operator relative to the survey line and indicates the deviation of the GPS operator from the line. The horizontal variability during the survey is generally minor, typically less than about ±0.25 m either side of the line (**Figure 3-7**), which results in negligible vertical uncertainties due to the relatively uniform nature of beaches characteristic of much of the Oregon coast (Ruggiero and others, 2005). From our previous research at numerous sites along the Oregon coast, this method of surveying can reliably detect elevation changes on the order of 4-5 cm, that is, well below normal seasonal changes in beach elevation, which typically varies by 1–2 m (3–6 ft) (Ruggiero and others, 2005; Allan and Hart, 2007, 2008).

Analysis of beach survey data involved a number of stages. The data were first imported into the MathWorks® MATLAB® environment (a suite of computer programming languages) by using a customized script. A least-squares linear regression was then fit to the profile data. The purpose of this script is to examine the reduced data and eliminate data point residuals (e.g., **Figure 3-7**) that exceed a ±0.75-m threshold (i.e., the outliers) on either side of the predetermined profile line. The data are then exported into a Microsoft® Excel® database for archiving purposes. A second MATLAB script uses the Excel profile database to plot the survey data (relative to the earlier surveys) and outputs the generated figure as a Portable Network Graphics (png) file. Appendix C shows the reduced beach profile plots for the Tillamook County transects.

Figure 3-6. Surveying the morphology of the beach at Bandon using a Trimble 5800 "rover" GPS (photo: J. Allan, DOGAMI, 2009).

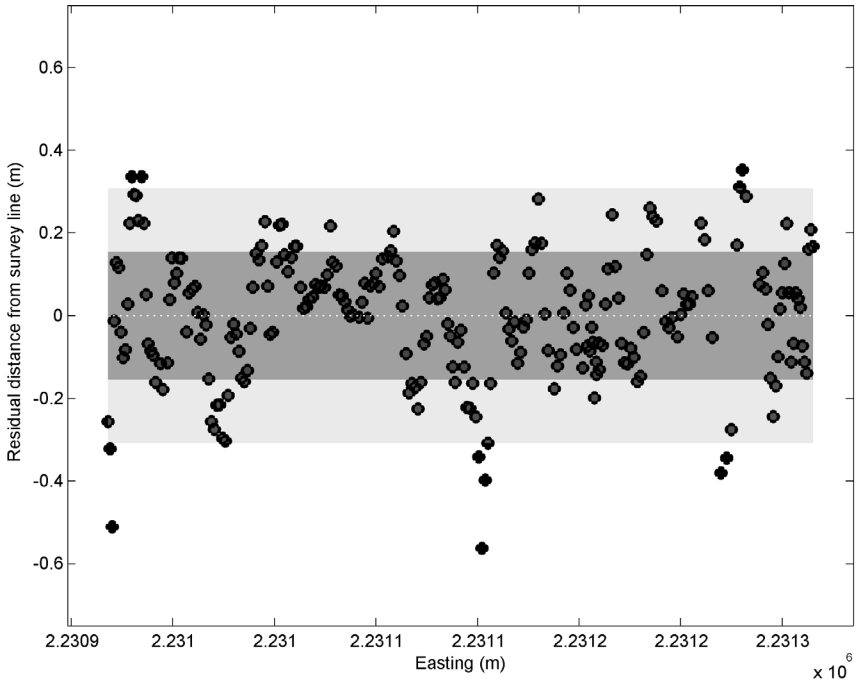

Figure 3-7. Residuals of GPS survey points relative to zero (transect) line. Example reflects the Cannon Beach 10 profile line. Dark grey shading indicates 68.3% of measurements located ±0.15 m (1σ) from the transect line, while 95.5% (2σ) of the measurements are located within ±0.30 m of the profile line (grey shading).

To supplement the GPS beach and bluff data, high-resolution lidar data measured by Watershed Sciences, Inc. (WSI) in 2009 for DOGAMI were also analyzed and integrated into the beach profile data set. This was especially important for backshore areas where it was not possible to easily survey with the GPS gear. In addition, lidar data flown by the U.S. Geological Survey (USGS)/National Aeronautics and Space Administration (NASA)/NOAA in 1997, 1998, and 2002 were used to extend the time series of the beach and bluff profile data. In particular, the 1998 lidar data measured at the end of the major 1997-98 El Niño were analyzed, providing additional measurements of the beach in an eroded state that can be compared with more recent winter surveys of the beach. The 1997, 1998, and 2002 lidar data were downloaded from NOAA's Coastal Service Center (http://coast.noaa.¬gov/dataregistry/search/collection/info/coastallidar) and were gridded in Esri® ArcGIS® by using a triangulated irregular network (TIN) algorithm; distance and elevation data were extracted from the grid lidar digital elevation models (DEMs).

3.2 Beach Characterization

Analyses of the beach profile data were undertaken using additional scripts developed in MATLAB. These scripts require the user to interactively locate the positions of the seaward edge and crest of the *primary frontal dune* (PFD) backing the beach, and then evaluate the beach-dune juncture (E_j) elevations and beach slopes (tan β) for the 1997, 1998, 2002, 2008/2009, 2011 and 2012 surveys along each of the profile sites. Beach slope was determined by fitting a linear regression through the measured profile data. In all cases, the slope of the beach face was determined to be the region of the beach located between mean sea level (~1.4 m, MLLW [mean lower low water]) and the highest observed tide (~3.8 m, MLLW), an approach that is consistent with methodologies adopted by Ruggiero and others, 2005; Stockdon and others (2006). Determination of the location of the beach-dune junctures (E_j) was accomplished interactively using the MATLAB scripts and from local knowledge of the area. In general, the

beach-dune juncture (E_j) reflects a major break in slope between the active part of the beach face and the toe location of the primary dune or bluff. For most sites along the Oregon coast, the beach-dune juncture (E_j) typically occurs at elevations between about 4 and 6 m (NAVD88). **Figure 3-8** provides an example of the identified beach-dune juncture (E_j) for one site, TILL 21, located at the north end of the Neskowin shoreline (**Figure 3-1**) after it has been eroded (described in Section 7). In this example, it is apparent that the dune has experienced considerable erosion during the past two decades, with the dune face retreating landward by 32.6 m (107 ft) since 1997 as measured at the 7 m (23 ft) contour elevation.

Examination of the profile data indicates that the beach-dune juncture (E_j) has varied in elevation, a function of repeated phases of both erosion and accretion events. As of winter 2012, an erosion scarp had formed and the beach-dune juncture reflected the toe of the scarp, located at an elevation of 5.1 m (16.7 ft). **Figure 3-8** also includes the derived beach slope ($\tan \beta = 0.049$), the crest of the primary dune, as well as the landward boundary of the primary frontal dune. These latter data are used later to develop new Zone VE flood hazard zones along the Tillamook County coast. Recall that Zone VE is the flood insurance rate zone that corresponds to areas within the 1% annual chance coastal floodplain where wave erosion, overtopping, and inundation may take place.

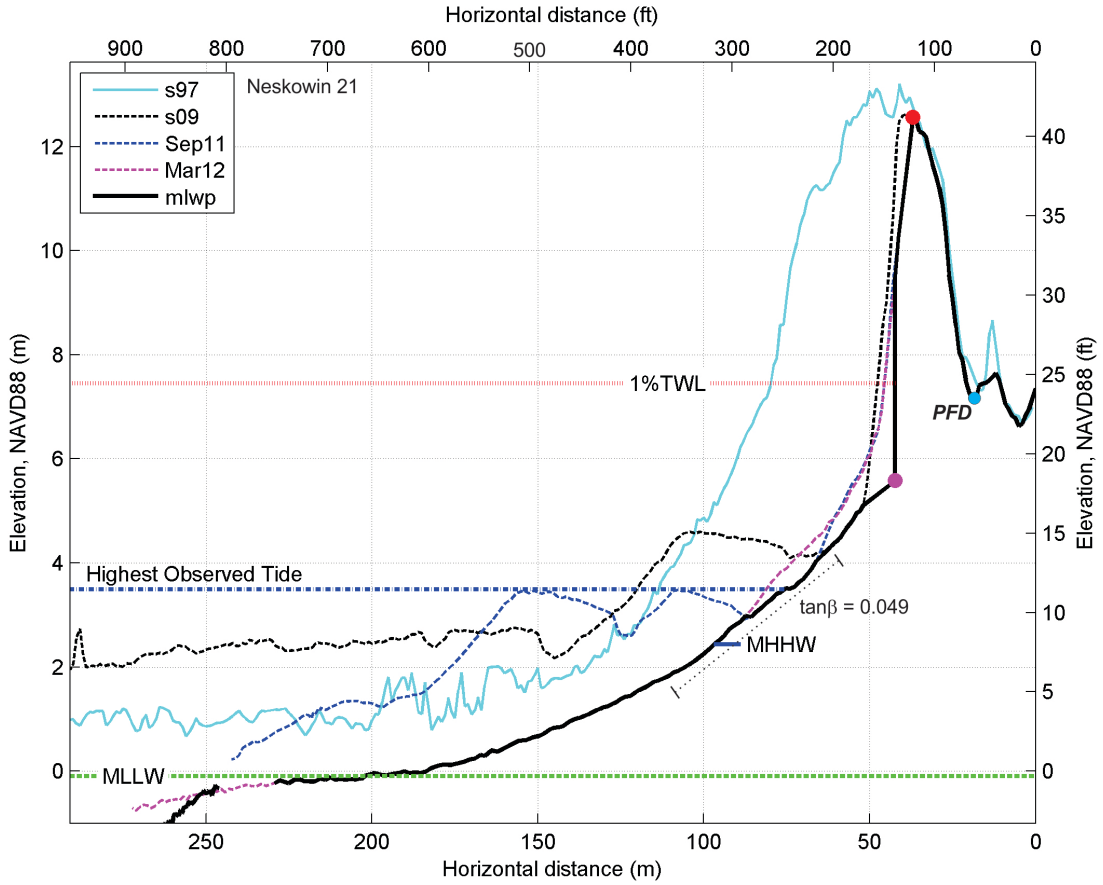

Figure 3-8. Plot showing various beach cross-sections at the TILL 21 (aka Neskowin 21) profile site. In this example, the most likely winter profile (MLWP) is depicted as the heavy black line, the *eroded* beach-dune juncture location, dune crest, and primary frontal dune location (PFD) are characterized by magenta, red, and blue circles, respectively. The plot also provides a dramatic example of the extent of erosion that has taken place along this section of Neskowin beach. MLLW is mean lower low water. MHHW is mean higher high water. TWL is total water level. PFD is primary frontal dune.

To estimate beach erosion and profile changes for a specific coastal setting that occurs during a particular storm, it is essential to first define the initial conditions of the morphology of the beach prior to the actual event of interest (Northwest Hydraulic Consultants, 2005). This initial beach profile is referred to as the *most likely winter profile* (MLWP) condition for that particular coastal setting and is depicted in **Figure 3-8** as the heavy black line. The MLWP was assessed from examination of the combined surveyed profiles and lidar data. In the **Figure 3-8** example, the 2009 lidar survey of the primary dune and backshore was found to best characterize the landward component of the MLWP, while our March 2012 survey best captured the state of the active beach and seaward edge of the foredune. Landward of the dune crest, information on the backshore topography was derived by incorporating the actual measured GPS data because those data provided the best representation of the actual ground surface. Where GPS survey data were not available, we used topographic data derived from the 2009 lidar flown for DOGAMI.

Table 3-3 summarizes the various morphological parameters identified for each transect site along the Tillamook County coastline, including their geomorphic classification.

Table 3-3. Identified beach morphological parameters from the most likely winter profile (MLWP) along the Tillamook County shoreline. Parameters include the beach-dune junction elevation (Ej_MLWP), beach slope (tan β), and a site description.

Reach	Transect	DFIRM Transect	Dune Crest/Bluff Top (m)	*Ej_MLWP* (m)	Beach Slope (tan *β*)	Description
Salmon River Cascade Head	LINC 308	1	6.251	5.058	0.084	dune-backed cliff
	LINC 309	2	48.172	1.609	0.027	plunging cliff
	LINC 310	3	43.56	1.207	0.028	plunging cliff
	LINC 311	4	24.427	0.358	0.022	boulder beach backed by bluffs
	LINC 312	5	93.24	2.125	0.026	plunging cliff
	LINC 313	6	139.103	0	0.023	plunging cliff
Neskowin	TILL 1	7	47.278	0.764	0.025	sandy beach backed by riprap and high cliffs
	TILL 2	8	8.684	3.914	0.045	sand beach backed by riprap
	TILL 3	9	8.452	3.914	0.042	sand beach backed by riprap
	TILL 4	10	5.184	3.448	0.018	sand beach backed by riprap
	TILL 5	11	8.312	2.712	0.049	sand beach backed by riprap
	TILL 6	12	8.447	3.563	0.073	sand beach backed by riprap
	TILL 7	13	8.169	1.904	0.062	sand beach backed by riprap
	TILL 8	14	8.539	2.533	0.062	sand beach backed by riprap
	TILL 9	15	7.075	5.888	0.06	dune-backed
	TILL 10	16	8.897	6.235	0.054	dune-backed
	TILL 11	17	6.679	5.604	0.041	dune-backed
	TILL 12	18	8.374	5.521	0.044	dune-backed
	TILL 13	19	7.126	5.709	0.049	dune-backed
	TILL 14	20	8.118	5.086	0.099	sand beach backed by riprap
	TILL 15	21	7.587	4.642	0.069	sand beach backed by riprap
	TILL 16	22	6.767	6.014	0.052	dune-backed
	TILL 17	23	9.986	4.326	0.039	dune-backed
	TILL 18	24	8.387	5.512	0.074	dune-backed
	TILL 19	25	6.014	6.014	0.059	dune-backed
	TILL 20	26	7.648	7.066	0.098	dune-backed
	TILL 21	27	12.562	5.582	0.049	dune-backed
	TILL 22	28	6.241	4.489	0.034	dune-backed
	TILL 23	29	14.334	6.819	0.088	dune-backed
	TILL 24	30	7.792	7.185	0.06	dune-backed
	TILL 25	31	7.642	5.627	0.061	dune-backed
	TILL 26	32	32.562	3.877	0.059	sandy beach backed by high cliffs
	TILL 27	33	28.194	4.519	0.088	sandy beach backed by high cliffs
	TILL 28	34	39.31	6.292	0.084	sandy beach backed by dunes and high cliffs

Reach	Transect	DFIRM Transect	Dune Crest/Bluff Top (m)	*Ej_MLWP* (m)	Beach Slope (tan *β*)	Description
Nestucca spit/ Pacific City	TILL 29	35	10.245	4.903	0.043	dune-backed
	TILL 30	36	14.485	5.083	0.048	dune-backed
	TILL 31	37	15.49	5.933	0.061	dune-backed
	TILL 32	38	14.358	5.413	0.093	dune-backed
	TILL 33	39	13.16	5.338	0.072	dune-backed
	TILL 34	40	15.877	6.611	0.086	dune-backed
	TILL 35	41	15.147	5.312	0.05	dune-backed
	TILL 36	42	17.709	5.908	0.051	dune-backed
	TILL 37	43	12.932	4.389	0.051	sand beach backed by riprap?
	TILL 38	44	11.283	4.69	0.053	sand beach backed by riprap?
	TILL 39	45	18.954	5.407	0.041	dune-backed
	TILL 40	46	11.314	5.539	0.057	sand beach backed by riprap?
	TILL 41	47	11.06	4.785	0.039	sand beach backed by riprap?
	TILL 42	48	13.304	4.681	0.043	sand beach backed by riprap and high bluffs
Sand Lake/ Tierra Del Mar	TILL 43	49	23.369	5.582	0.046	sandy beach backed by high cliffs
	TILL 44	50	16.741	6.162	0.075	sandy beach backed by high cliffs
	TILL 45	51	6.868	4.232	0.042	sandy beach backed by cobbles - grades into bluff
	TILL 46	52	18.071	4.865	0.055	sandy beach backed by high cliffs
	TILL 47	53	18.396	4.063	0.045	sand beach backed by riprap
	TILL 48	54	7.412	6.555	0.048	dune-backed
	TILL 49	55	8.24	6.197	0.044	dune-backed
	TILL 50	56	6.931	5.891	0.041	dune-backed
	TILL 51	57	6.317	4.554	0.05	sand beach backed by riprap
	TILL 52	58	7.721	4.543	0.055	sand beach backed by riprap
	TILL 53	59	8.141	5.026	0.056	sand beach backed by riprap
	TILL 54	60	7.462	5.055	0.058	sand beach backed by riprap
	TILL 55	61	8.094	5.159	0.045	dune-backed
	TILL 56	62	8.357	4.652	0.046	sand beach backed by riprap
	TILL 57	63	11.383	4.823	0.04	sand beach backed by riprap
	TILL 58	64	10.224	6.18	0.042	dune-backed
	TILL 59	65	12.153	5.72	0.052	dune-backed
	TILL 60	66	9.595	5.355	0.041	dune-backed
	TILL 61	67	9.37	6.193	0.048	dune-backed
	TILL 62	68	6.573	6.26	0.052	dune-backed
	TILL 63	69	3.38	3.324	0.009	dune-backed
	TILL 64	70	18.524	6.915	0.111	dune-backed
	TILL 65	71	18.296	5.556	0.053	dune-backed
	TILL 66	72	15.211	5.34	0.049	dune-backed
	TILL 67	73	19.042	8.385	0.069	sandy beach backed by high cliffs
	TILL 68	74	24.72	6.441	0.044	sandy beach backed by high cliffs
	TILL 69	75	29.519	5.96	0.051	sandy beach backed by high cliffs
	TILL 70	76	30.293	4.588	0.045	sandy beach backed by high cliffs
	TILL 71	77	37.153	4.979	0.055	sandy beach backed by high cliffs
	TILL 72	78	30.575	4.844	0.037	sandy beach backed by high cliffs
	TILL 73	79	28.571	6.625	0.048	sandy beach backed by high cliffs
	TILL 74	80	20.692	5.762	0.038	sandy beach backed by high cliffs

Reach	Transect	DFIRM Transect	Dune Crest/Bluff Top (m)	*Ej_MLWP* (m)	Beach Slope (tan *β*)	Description
Netarts Spit/ Oceanside	TILL 75	81	6.775	2.43	0.029	sandy beach backed by low/high cliffs
	TILL 76	82	7.6	2.937	0.037	sandy beach backed by cobbles/boulders and low cliff
	TILL 77	83	8.447	3.235	0.047	sandy beach backed by dynamic revetment/artificial dune
	TILL 78	84	7.298	3.706	0.051	sandy beach backed by dynamic revetment/artificial dune
	TILL 79	85	10.798	3.976	0.043	dune-backed (+cobbles)
	TILL 80	86	9.131	5.381	0.082	dune-backed (+cobbles)
	TILL 81	87	7.159	4.661	0.067	dune-backed (+cobbles)
	TILL 82	88	11.562	5.04	0.056	dune-backed
	TILL 83	89	12.413	5.492	0.056	dune-backed
	TILL 84	90	7.322	6.012	0.046	dune-backed
	TILL 85	91	11.621	5.37	0.044	dune-backed
	TILL 86	92	11.763	6.361	0.047	dune-backed
	TILL 87	93	19.722	4.114	0.043	dune-backed
	TILL 88	94	6.567	5.72	0.057	dune-backed
	TILL 89	95	10.543	5.754	0.048	dune-backed
	TILL 90	96	12.156	4.768	0.046	dune-backed
	TILL 91	97	9.61	6.516	0.052	dune-backed
	TILL 92	98	8.324	6.36	0.05	dune-backed
	TILL 93	99	4.971	4.855	0.069	Cobble beach backed by low wall (estuary mouth)
	TILL 94	100	14.619	5.554	0.074	sandy beach backed by high cliffs
	TILL 95	101	29.639	4.999	0.032	sandy beach backed by high cliffs
	TILL 96	102	39.082	4.536	0.055	sandy beach backed by high cliffs
	TILL 97	103	55.206	4.631	0.065	sandy beach backed by dune and high cliffs
	TILL 98	104	60.658	5.832	0.073	sandy beach backed by dune and high cliffs
	TILL 99	105	33.925	4.907	0.044	sandy beach backed by high cliffs
	TILL 100	106	36.465	4.585	0.041	sandy beach backed by high cliffs
	TILL 101	107	13.733	5.191	0.045	sandy beach backed by poor riprap and low cliffs
	TILL 102	108	18.353	5.953	0.05	sandy beach backed by moderately high cliffs
	TILL 103	109	8.241	4.068	0.057	sandy beach backed by moderately high cliffs
Short Sand Beach	TILL 104	110	33.582	3.026	0.056	sandy beach backed by gravels and high cliffs
	TILL 105	111	26.461	3.932	0.075	sandy beach backed by gravels and high cliffs
	TILL 106	112	47.152	5.674	0.109	sandy beach backed by gravels and high cliffs

Reach	Transect	DFIRM Transect	Dune Crest/Bluff Top (m)	*Ej_MLWP* (m)	Beach Slope (tan *β*)	Description
Bayocean Spit	TILL 107	113	8.705	3.527	0.072	sandy beach backed by cobble/boulder and low cliffs
	TILL 108	114	7.74	2.981	0.05	sandy beach backed by cobble/boulder and low cliffs
	TILL 109	115	6.34	3	0.036	sandy beach backed by cobble/boulder berm
	TILL 110	116	6.081	2.495	0.026	sandy beach backed by cobble/boulder berm
	TILL 111	117	6.863	3.33	0.04	sandy beach backed by cobble/boulder berm
	TILL 112	118	9.667	6.824	0.041	dune-backed
	TILL 113	119	11.095	6.67	0.043	dune-backed
	TILL 114	120	9.781	6.804	0.04	dune-backed
	TILL 115	121	8.97	4.932	0.043	dune-backed
	TILL 116	122	10.49	5.889	0.04	dune-backed
	TILL 117	123	10.053	6.537	0.043	dune-backed
Rockaway	TILL 118	124	5.932	5.932	0.048	dune-backed
	TILL 119	125	6.332	4.905	0.043	dune-backed
	TILL 120	126	6.72	5.37	0.049	dune-backed
	TILL 121	127	6.749	5.178	0.058	dune-backed
	TILL 122	128	6.518	5.388	0.047	dune-backed
	TILL 123	129	7.242	3.13	0.029	sand beach backed by riprap
	TILL 124	130	6.905	5.82	0.05	dune-backed
	TILL 125	131	5.489	5.489	0.046	dune-backed
	TILL 126	132	5.858	4.586	0.02	dune-backed
	TILL 127	133	7.148	5.709	0.037	dune-backed
	TILL 128	134	7.976	5.327	0.038	dune-backed
	TILL 129	135	7.237	5.136	0.048	dune-backed
	TILL 130	136	7.344	5.839	0.046	dune-backed
	TILL 131	137	7.032	4.682	0.037	dune-backed
	TILL 132	138	5.486	3.77	0.038	sand beach backed by riprap
	TILL 133	139	7.133	5.593	0.038	dune-backed
	TILL 134	140	10.147	5.68	0.043	dune-backed
	TILL 135	141	8.387	7.085	0.052	dune-backed
	TILL 136	142	7.062	5.92	0.032	sand beach backed by low bluff
	TILL 137	143	6.827	4	0.034	sand beach backed by riprap
	TILL 138	144	6.359	3.045	0.013	sand beach backed by riprap
	TILL 139	145	8.67	5.263	0.034	dune-backed
	TILL 140	146	8.923	3.759	0.051	sand beach backed by riprap
	TILL 141	147	7.643	3.759	0.044	sand beach backed by riprap
	TILL 142	148	8.305	3.759	0.057	sand beach backed by riprap
	TILL 143	149	8.196	4.068	0.051	sand beach backed by riprap
	TILL 144	150	8.305	3.312	0.051	sand beach backed by riprap
	TILL 145	151	8.092	4.309	0.054	sand beach backed by riprap
	TILL 146	152	8.176	4.029	0.047	sand beach backed by riprap
	TILL 147	153	7.927	7.16	0.056	dune-backed
	TILL 148	154	8.101	5.982	0.052	dune-backed
	TILL 149	155	8.029	5.997	0.05	dune-backed
	TILL 150	156	8.315	6.325	0.045	dune-backed
	TILL 151	157	6.974	4.176	0.022	sand beach backed by riprap
	TILL 152	158	8.688	6.358	0.068	dune-backed
	TILL 153	159	8.773	4.786	0.037	dune-backed
	TILL 154	160	8.966	6.457	0.051	dune-backed
	TILL 155	161	8.448	6.267	0.042	dune-backed
	TILL 156	162	8.409	6.061	0.04	dune-backed
	TILL 157	163	6.833	5.548	0.031	dune-backed

Reach	Transect	DFIRM Transect	Dune Crest/Bluff Top (m)	*Ej_MLWP* (m)	Beach Slope (tan *β*)	Description
Nehalem Spit/ Manzanita	TILL 158	164	7.752	6.112	0.049	dune-backed
	TILL 159	165	12.218	6.616	0.053	dune-backed
	TILL 160	166	8.676	6.254	0.063	dune-backed
	TILL 161	167	7.828	5.901	0.056	dune-backed
	TILL 162	168	15.433	5.338	0.042	dune-backed
	TILL 163	169	13.023	5.823	0.043	dune-backed
	TILL 164	170	14.069	5.912	0.055	dune-backed
	TILL 165	170	15.75	5.514	0.051	dune-backed
	TILL 166	172	12.088	4.356	0.034	dune-backed
	TILL 167	173	12.772	5.616	0.039	dune-backed
	TILL 168	174	13.313	6.617	0.038	dune-backed
	TILL 169	175	10.635	7.807	0.075	dune-backed
	TILL 170	176	9.226	4.313	0.022	sand beach backed by riprap
	TILL 171	177	8.847	5.064	0.026	dune-backed
	TILL 172	178	9.502	6.107	0.03	dune-backed with road
	TILL 173	179	11.496	5.245	0.028	dune-backed with road
	TILL 174	180	9.609	5.516	0.027	dune-backed with road
	TILL 175	181	11.367	4.73	0.029	dune-backed
	TILL 176	182	9.012	5.504	0.048	sand beach backed by extensive cobble berm
	TILL 177	183	6.996	5.077	0.049	sand beach backed by extensive cobble berm and bluff
	TILL 178	184	7.921	7.894	0.169	sand beach backed by extensive cobble berm and bluff
Falcon Cove	CP 1	185	15.935	7.027	0.167	sand, cobble berm backed by high bluff

Figure 3-9 provides a plot of the alongshore changes in beach slopes (tan β), mean sediment grain sizes (M_z), beach-dune juncture (E_j) elevations, and dune/bluff/structure crest heights. In general, the steepest slopes are confined to those beaches with coarse sediments on the foreshore (e.g., **Figure 2-13**), while sites containing finer sediments are characterized by generally lower beach slopes (e.g., **Figure 2-1**). Mean grain sizes in the Neskowin littoral cell are characterized as medium sand (M_z = 1.3Ø (0.42 mm [Peterson and others, 1994]) and decrease to M_z = 2.5Ø (0.18 mm, or fine sand) along the rest of the Tillamook County coastline. The steepest beach slopes are typically identified adjacent to the headlands, where the beach is composed predominantly of gravels and boulders and the sediment is locally sourced from the headlands as a result of landslides. At several beach study sites, sediment grain sizes vary in both along-shore and cross-shore directions. For example, beaches at Cape Lookout State Park, located at the south end of Netarts Spit, may be characterized as "composite" using the nomenclature of Jennings and Shulmeister (2002), that is, consisting of a wide dissipative sandy beach composed of fine sand (**Figure 3-9**), backed by an extensive gravel beach on the upper foreshore. In contrast, the beach at the north end of Manzanita exhibits a substantial cobble/boulder berm on the beach face that is fronted by a wide dissipative sand beach in the intertidal zone (**Figure 3-10**). The cobble/boulder berm provides significant protection to the backshore (Allan and others, 2005).

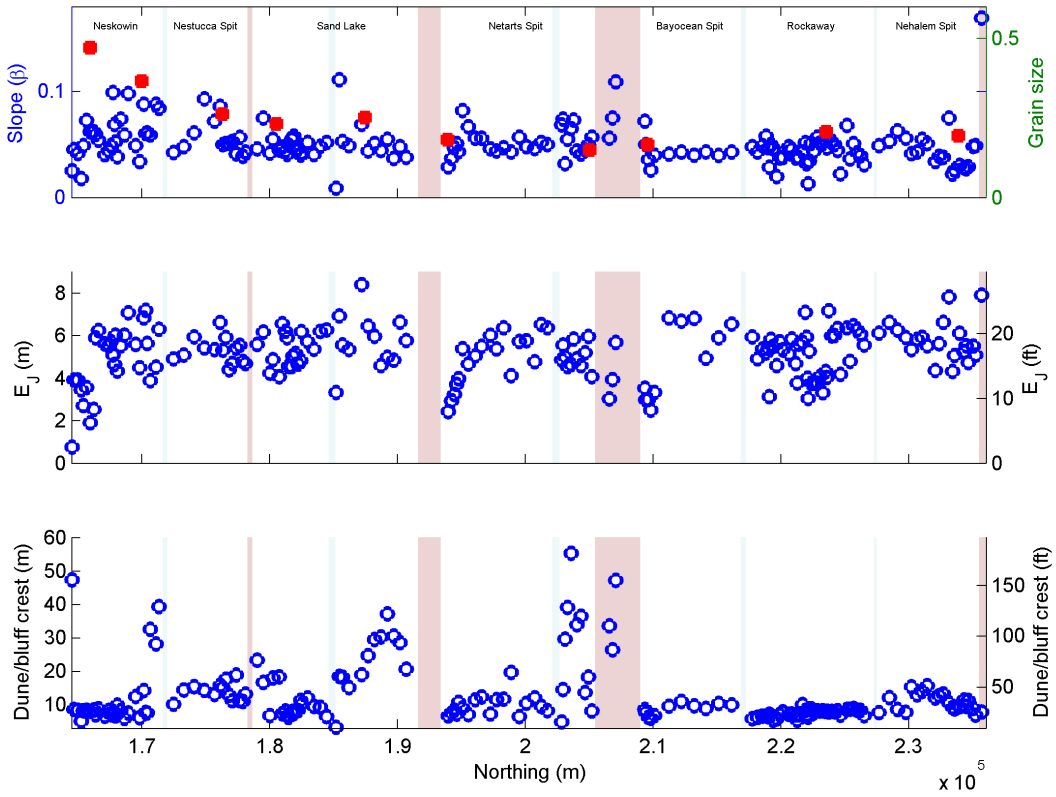

Figure 3-9. Alongshore changes in beach slopes (tan β), beach-dune juncture (Ej) elevations, and dune/bluff crest/tops along Tillamook County. Red squares indicate mean sediment grain sizes measured by Peterson and others (1994). Vertical blue shading denotes the location of estuary mouths, while the red shading denotes the location of headlands.

Figure 3-9 also plots the beach-dune and beach-bluff juncture elevations (Ej) for the various study sites. Values for Ej vary significantly along the length of the Tillamook County coast. The lowest Ej values tend to occur along the toe of coastal engineering structures (e.g., the riprap structures that protect the community of Neskowin) and on beaches backed by gravel and boulders. In general, the highest beach-dune juncture elevations are found along Nehalem and Bayocean Spits, areas that are actively aggrading. In addition, **Figure 3-9** (bottom) indicates the dune/bluff/structure crest elevations. Because these heights are indicative of the potential for flooding, with higher crests generally limiting flood overtopping, it can be seen that the risk from coastal flooding and inundation is likely to be highest along much of the shores in Neskowin, Tierra Del Mar, Cape Meares, and Rockaway beach. Along the remainder of the shore, the beaches are protected by prominent bluffs (e.g., adjacent to the mouth of the Nestucca estuary, adjacent to Oceanside and at Short Sand Beach) and/or dunes (e.g., Nestucca and Nehalem Spit) with crest elevations that range from 10 to 18 m (33–59 ft) that effectively preclude wave overtopping and hence inundation in those areas. Nevertheless, some of these sites are subject to erosion hazards that likely will influence the extent of the flood zones in those areas, after factoring the potential for erosion from storms.

Figure 3-10. Cobble/boulder beach located on the south side of Neahkahnie Mountain, north of Manzanita (photo: J. Allan, DOGAMI, July 2, 2003).

3.3 Recent Coastal Changes in Tillamook County

This section briefly reviews beach profile changes that have occurred during the past decade, as documented by lidar and recent GPS surveys of the shore.

The overall approach used to define the morphology of the beach and dune system, including the location of the PFD along the length of county shoreline, and shoreline changes over the past decade, was based on detailed analyses of lidar data measured by USGS/NASA/NOAA in 1997, 1998, and 2002 and by DOGAMI in 2009. However, because lidar data flown by USGS/NASA/NOAA are of relatively poor resolution (~1 point/m^2) and reflect a single return (i.e., include vegetation where present), while the lidar data flown by DOGAMI have higher resolution (8 points/m^2) and are characterized by multiple returns enabling development of a bare-earth digital elevation model (DEM), our determination of the most critical beach/dune morphological features was based entirely on analysis of the 2009 lidar data.

Lidar data flown in 1997, 1998, and 2002 were downloaded from NOAA's Coastal Service Center and gridded in ArcGIS using a TIN algorithm (Allan and Harris, 2012); a similar approach was undertaken with the 2009 lidar data. Transects spaced 25 m apart were cast for the full length of the county coastline by using the Digital Shoreline Analysis System (DSAS) developed by the USGS (Thieler and others, 2009). For each transect, xyz values for the 1997, 1998, 2002, and 2009 lidar data were extracted at 1-m intervals along each transect line and saved as a text file using a customized ArcGIS script.

Processing of the lidar data was undertaken in MATLAB using a custom beach profile analysis script developed by DOGAMI. This script requires the user to interactively define various morphological features including the dune/bluff crest/top, bluff slope (where applicable), landward edge of the PFD, beach-dune juncture elevations for each year, and the slope of the beach foreshore.

3.3.1 Rockaway littoral cell changes

As a result of the major storms of the late 1990s, the Rockaway littoral cell (Cape Meares to Neahkahnie Mountain) effectively experienced a "one-two punch" with successive winters of extreme erosion, commencing first with the unusually strong 1997-98 El Niño, followed immediately by the even more severe 1998-99 winter (see **Figure 3-11**). **Figure 3-11** was derived by analyzing topographic changes collected using airborne lidar flown in 1997 and 2002. The volume change estimated using this approach is confined to just the subaerial beach and hence excludes the vegetated foredune. The results indicate that the Rockaway subcell lost ~1.4 × 10^6 m^3 (1.86*10^6 yd^3) of sand between 1997 and 2002 (**Figure 3-11**). Sand volume losses can also be seen for Nehalem Spit, which lost an estimated 1.45 × 10^5 m^3 (1.90 × 10^5 yd^3) of sand, while Bayocean Spit gained ~1.3 × 10^5 m^3 (1.7 × 10^5 yd^3) of sand. It is not clear where all the sand went. One hypothesis is that most of the eroded sand was removed offshore into deeper water; another potential sink is the estuaries. However, we speculate that the volume of sand removed into the estuaries is likely to be small compared to that carried offshore. As can be seen from **Figure 3-12**, which is derived from our repeated monitoring of the Rockaway cell beaches up to February 2014, the overall pattern of erosion within the Rockaway subcell has continued. In contrast, the northern half of Bayocean Spit (along with portions of the Nehalem Spit) has essentially recovered from the storms of the late 1990s and has gained significant amounts of sand (**Figure 3-12**). It is highly likely that a significant portion of the accumulated sand may be sediment eroded from Rockaway beach in the late 1990s. However, in all cases, the volume of sand gained along Bayocean and Nehalem Spit remains relatively small when compared to overall losses in the Rockaway subcell.

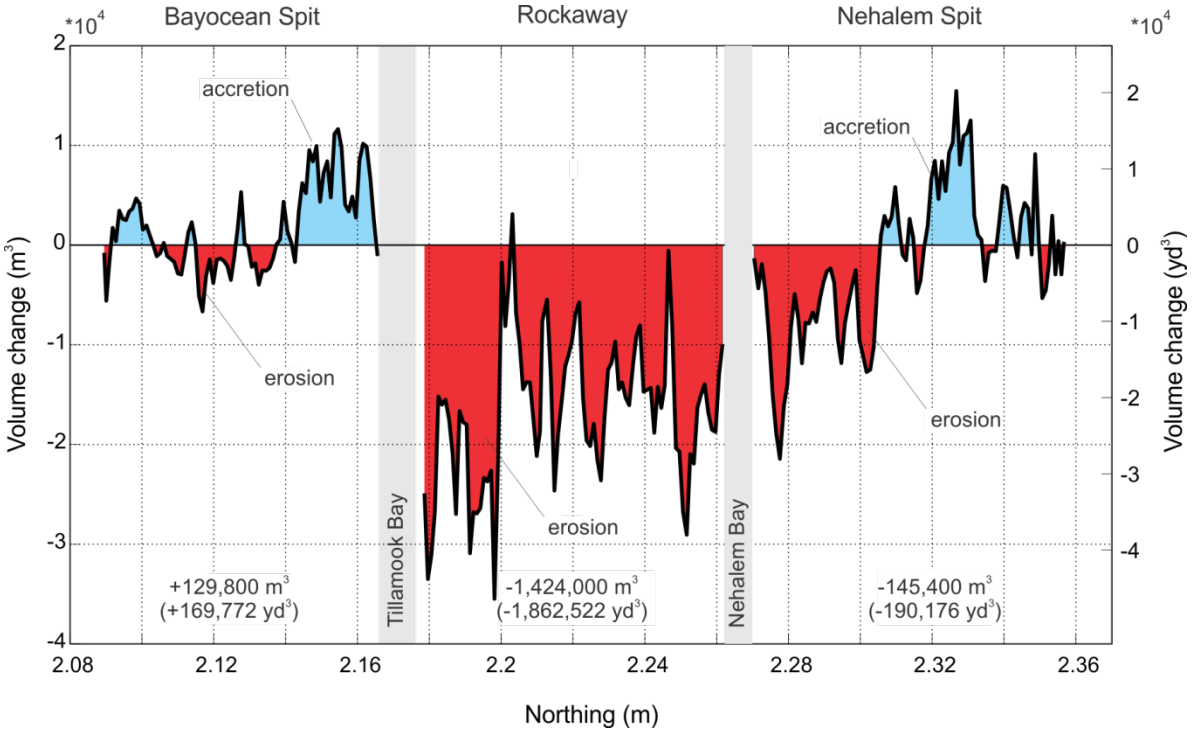

Figure 3-11. Net beach sediment volume changes along the Rockaway littoral cell for the period 1997–2009. Gray bands denote the locations of the Tillamook and Nehalem Bay mouths (after Allan and others, 2009).

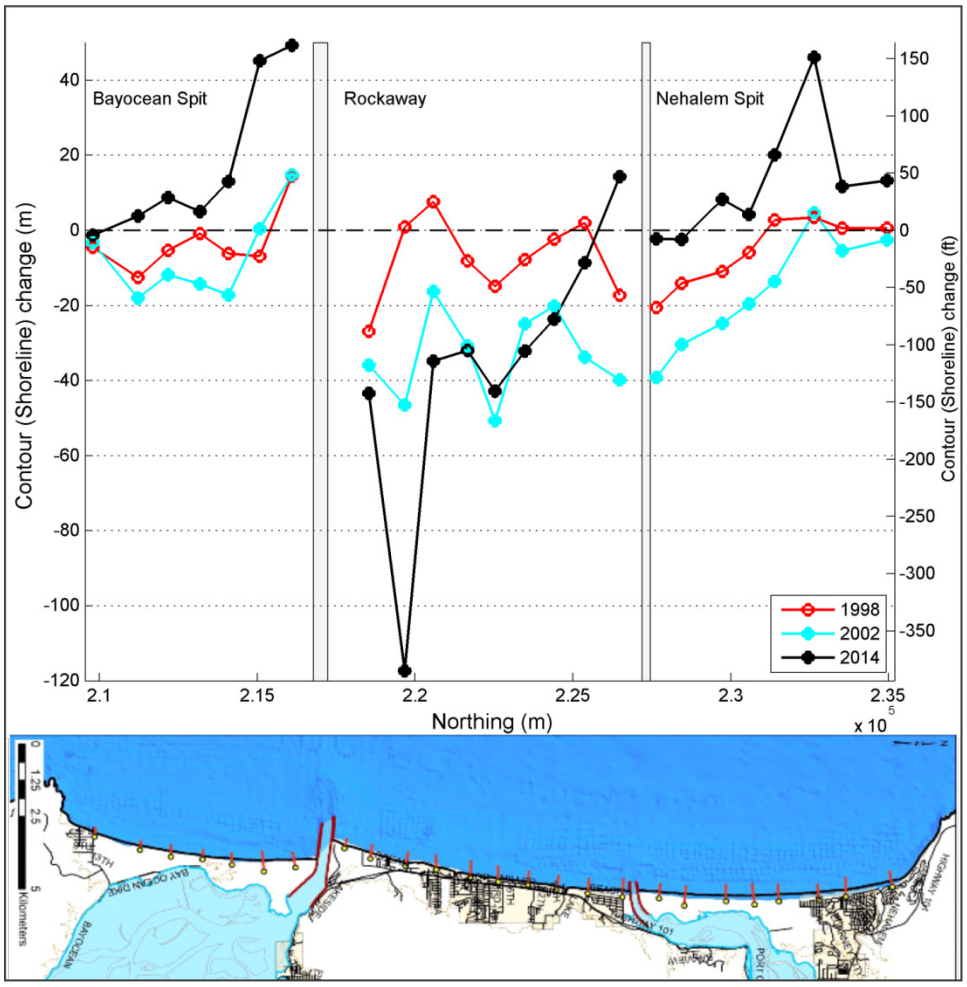

Figure 3-12. The Rockaway cell beach monitoring network maintained by DOGAMI showing the measured changes in the position of the dune toe (6 m [19 ft] elevation) from 1997 to 2014.

Figure 3-13, **Figure 3-14**, and **Figure 3-15** show the profile changes measured at four representative transect sites located along Nehalem Spit, Rockaway beach, and Bayocean Spit, respectively. Beginning in the north on Nehalem Spit, **Figure 3-13** indicates that apart from a brief period between 1997 and 2002, Nehalem Spit has essentially been in an accretional phase. As a result, the frontal foredune has aggraded vertically, and in some cases by several meters since 2002. This response is confined almost entirely to the southern two thirds of the spit (i.e., south of TILL 170, **Figure 3-3**). Erosion of the spit was especially significant between 1997 and 2002 along the southern one third of the spit (**Figure 3-12**), where recovery of the beach has taken some 10–14 years to fully rebuild. Shoreline erosion rates derived from GPS monitoring by DOGAMI staff indicate that the south end of Nehalem Spit is accreting at the fastest rate (~0.95 m/yr [3.1 ft/yr]), decreasing to ~0.2 m/yr (0.7 ft/yr) near Manzanita.

Farther south in the Rockaway subcell, the four transects highlight the contrasting responses observed along this particular subcell (**Figure 3-14**). In general, erosion rates are highest in the south (~-0.4 m/yr [-1.3 ft/yr]), and decrease toward the north. As can be seen in **Figure 3-14**, the TILL 120 transect site has retreated landward by about 40 m (130 ft) since 1997, with erosion dominating most of the transects. In essence, erosion dominates the entire section of coast south of about the TILL150 transect and extends all the way to the mouth of Tillamook Bay, while the beach and dune along Nedonna Beach are either stable or are slowly gaining sand.

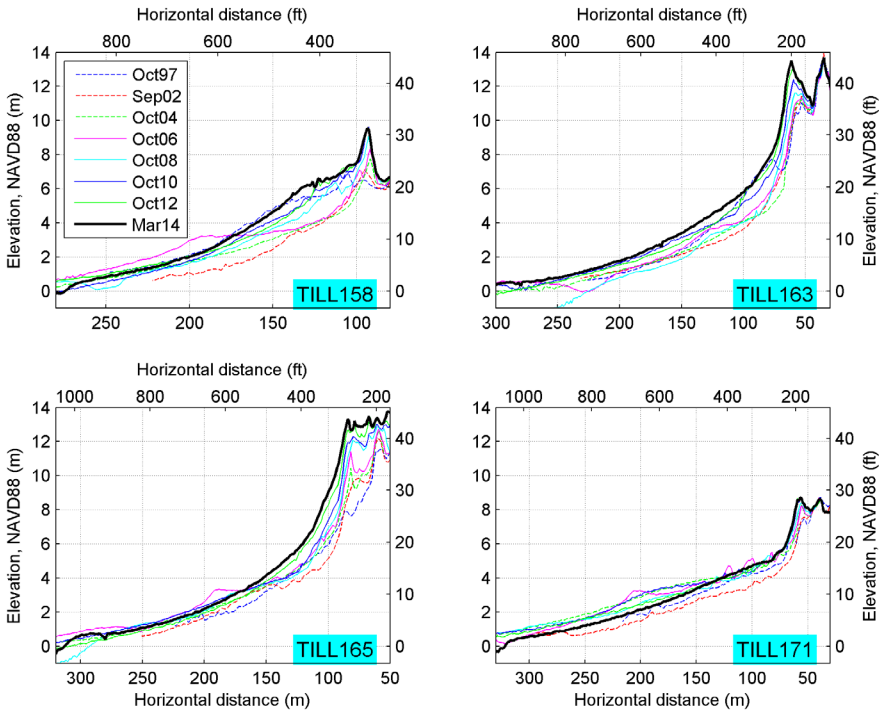

Figure 3-13. Measured beach morphological changes carried out between 1997 and 2014 for selected sites on Nehalem Spit from summer surveys undertaken by DOGAMI.

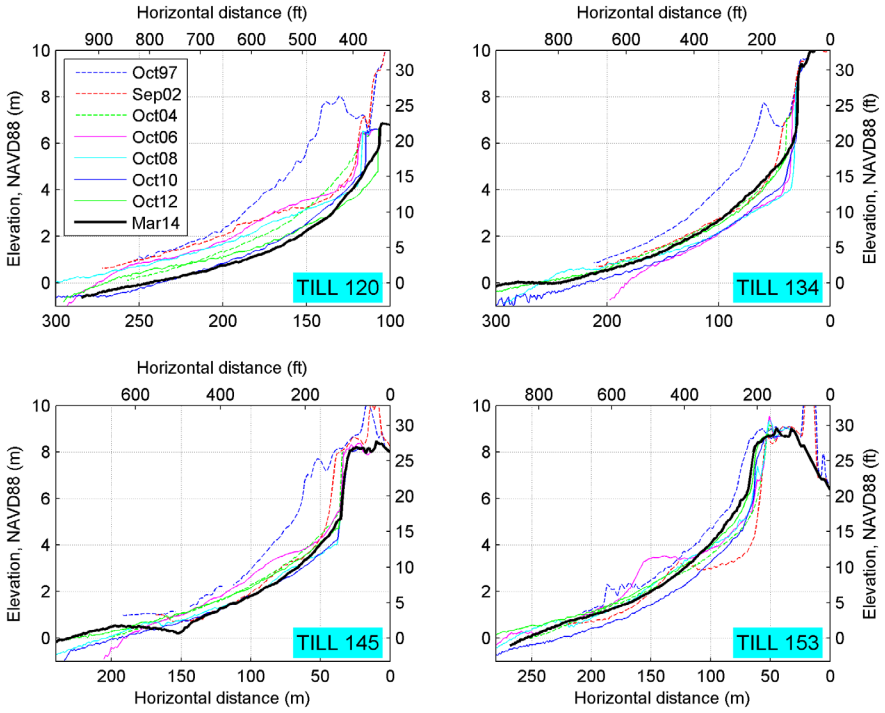

Figure 3-14. Measured beach morphological changes carried out between 1997 and 2014 for selected sites along the Rockaway subcell from summer surveys undertaken by DOGAMI.

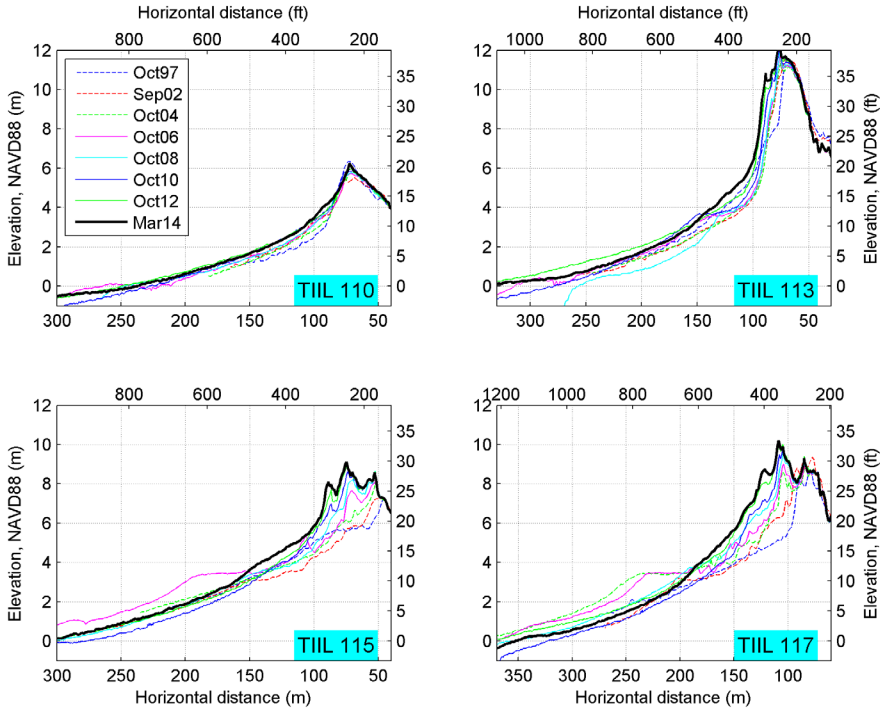

Figure 3-15. Measured beach morphological changes carried out between 1997 and 2014 for selected sites along Bayocean spit from summer surveys undertaken by DOGAMI.

As described previously in Section 2.4.1.4, Bayocean Spit has experienced dramatic change to its shorelines over the past century, much of which is directly a function of construction of the Tillamook Bay jetties. **Figure 3-15** depicts the changes that have taken place over the past 15 years. In the far south, the beach is backed by an extensive gravel beach that provides considerable protection from erosion to the backshore properties. As a result, this section of the beach is essentially stable, oscillating between minor bouts of erosion and accretion. With progress north along the spit, it is apparent that the dunes have fully recovered from the late 1990s winter storms (**Figure 3-12**) and are now actively aggrading along the length of the spit. Accretion rates are highest along the north end of the spit (reaching around +1m/yr [3.3 ft/yr]) and lowest in the south.

3.3.2 Tillamook County

Figure 3-16 summarizes the changes that have taken place along the full length of the county's shoreline since 1997. The analyses reflect the change in position of the 6 m (19.7 ft) contour elevation (essentially the dune/bluff toe) from 1997 (baseline) to 1998 (post El Niño), and from 1997 to 2009; the latter includes the updated lidar flight undertaken by WSI for DOGAMI. Several characteristics are apparent and worth highlighting:

- Erosion has continued along much of the shore to the north of the community of Neskowin;
- Along Nestucca spit, the beaches and dunes appear to have recovered slightly, although much of the remainder of the spit remains in a degraded state;
- Beach recovery is nonexistent in the vicinity of Tierra Del Mar and along the dunes to its immediate north. However, significant accretion has occurred on the south side of the Sand Lake estuary and farther north up to the south side of Cape Lookout;
- Erosion continues unabated on Netarts Spit, although there has been little to no change near Oceanside at the north end of this littoral cell. Considerable accretion has occurred on the south side of Netarts Bay, on the spit tip;
- Beach recovery is prevalent along Bayocean Spit, particularly along the northern half of the

spit where the dune face has clearly advanced (prograded) seaward by tens of meters;

- Erosion continues unabated along the bulk of the Rockaway subcell and, in many locations, is considered to be acute. This contrasts with significant aggradation along Nedonna Beach at the north end of the subcell and adjacent to the Nehalem jetties; and
- Beach recovery is occurring along the bulk of Nehalem Spit, with the area near Manzanita having prograded seaward.

Given these changes, we can conclude that the bulk of the Tillamook coast remains in a degraded or poor state, such that were we to experience storms comparable in magnitude to those experienced in 1998-99, it can be expected that massive erosion would again occur, potentially endangering many homes built adjacent to this coast.

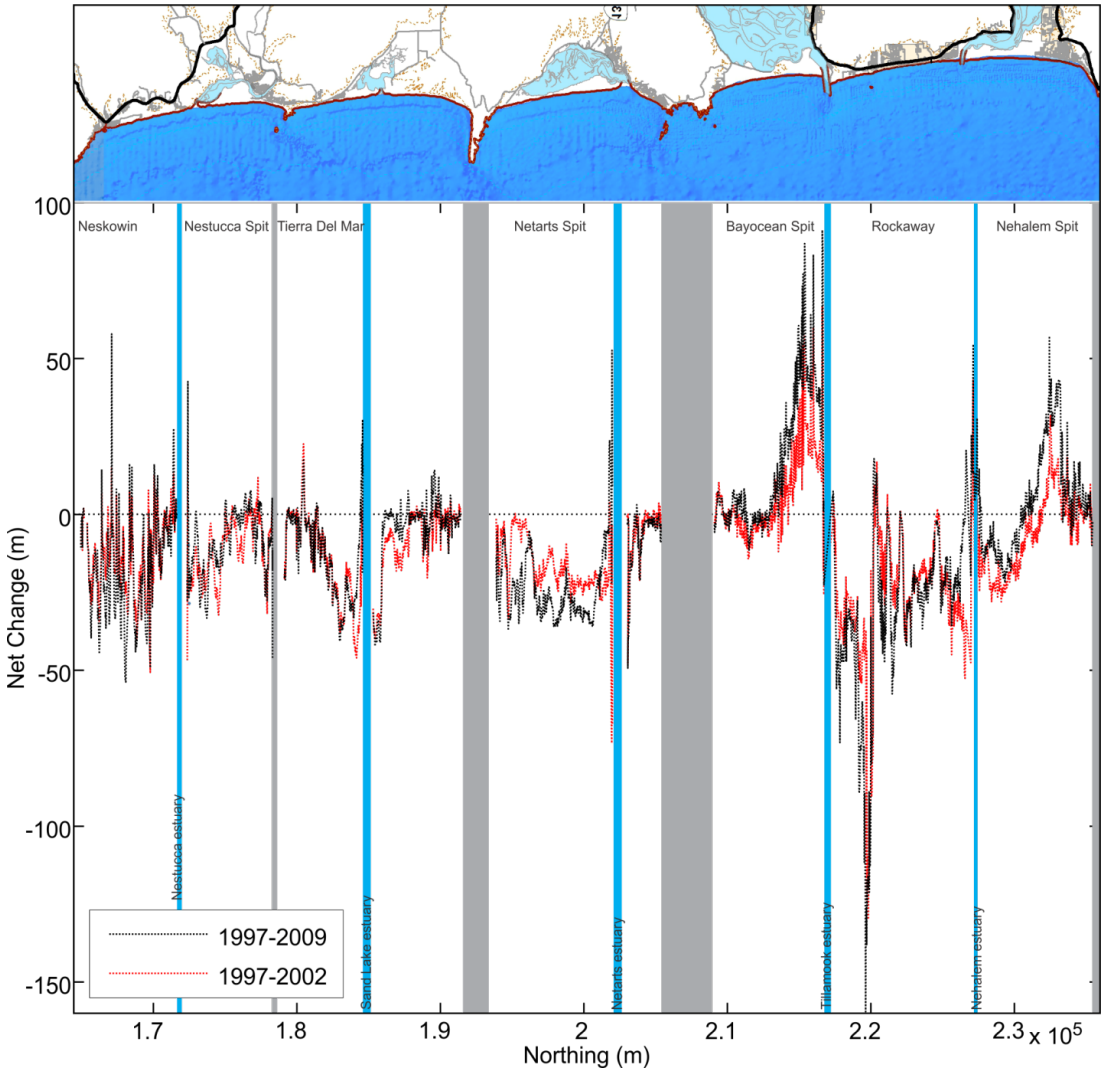

Figure 3-16. Net shoreline response in Tillamook County as measured at the 6-m (19.7 ft) contour elevation for the period 1997–2002 and 1997–2009. Cyan bands denote the locations of estuary mouths; grey bands indicate the positions of headlands.

3.4 Bathymetry

Important for calculating wave transformations and determining nearshore beach slopes is information on the local bathymetry seaward from the Tillamook County coast. For the purposes of this study we have adopted two approaches:

1. For the purposes of SWAN numerical wave modeling, we used bathymetric data compiled by the National Geophysical Data Center (NGDC), an office of NOAA, for the purposes of developing an integrated DEM for tsunami inundation modeling.
2. For erosion assessments and wave runup calculations, we used bathymetric data collected in late summer 2010 with the aid of personal watercrafts (Ozkan-Haller and others, 2009).

To develop an integrated bathymetric-topographic DEM that can be used for tsunami inundation modeling, the NGDC has compiled detailed bathymetric data across the continental shelf from multiple agencies. The synthesized bathymetric-topographic DEM (Astoria [http://www.ngdc.noaa.gov/dem/squareCellGrid/download/454], Garibaldi [http://www.ngdc.noaa.gov/dem/squareCellGrid/download/249], and Central Oregon Coast [http://www.ngdc.noaa.gov/dem/squareCellGrid/download/320]) is a 1/3 arc-second (approximately 10 m [~33 ft]) DEM of the north central Oregon coast that spans all of Tillamook County and includes the offshore rocks, small islands, and reefs that affect wave shoaling. The DEM was generated from a diverse suite of digital data sets that span the region (Carignan and others, 2009a, b, c). A summary of the data sources and methods used to synthesize the data to develop the Astoria and Garibaldi DEMs is described in the reports by Carignan and others. In general, the best available data were obtained by the NGDC and shifted to common horizontal and vertical datums: North America Datum 1983 (NAD 83) and Mean High Water (MHW).

NGDC used shoreline, bathymetric, and topographic digital data sets (**Figure 3-17**) from several U.S. federal, state, and local agencies (e.g., NOAA's National Ocean Service (NOS), Office of Coast Survey (OCS) and Coastal Services Center (CSC); the U.S. Geological Survey (USGS); the U.S. Army Corps of Engineers (USACE); and the Oregon Department of Fish and Wildlife/Marine Resource Program (ODFW). After all the data were converted to a common coordinate system and vertical datum, the grid data were checked for anomalous data and corrected accordingly. Because the data sets, particularly in deep water and near to the coast, were relatively sparse, further manipulation and smoothing was required to create a uniform grid. These products were then compared with the original surveys to ensure grid accuracy. According to Carignan and others (2009a) the final DEM is estimated to have an accuracy of up to 10 m (~33 ft), although some portions of the grid are more accurate (e.g., the coastal strip where high-resolution lidar data were available). The bathymetric portion of the data set is estimated to have an accuracy of between 0.1 m (0.33 ft) and 5% of the water depth, again depending on the type of survey data that was used to calibrate the final grid development.

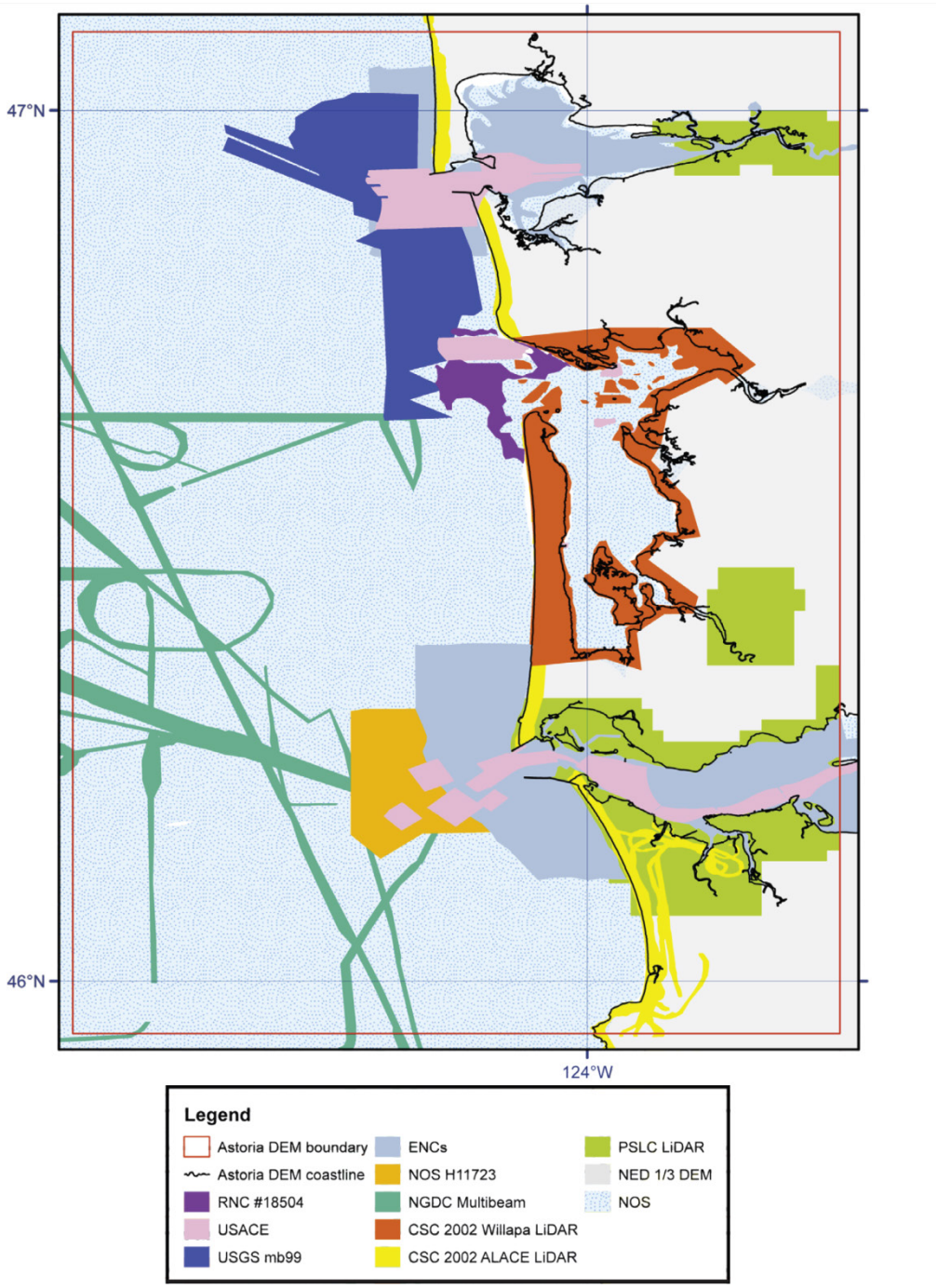

Figure 3-17. U.S. federal, state, and local agency bathymetric data sets used to compile the Astoria digital elevation model (DEM) (Carignan and others, 2009b).

Finally, despite all these efforts it is important to note that a limitation of the DEMs being developed by NGDC is the virtual absence of suitable bathymetric data in the nearshore (effectively landward of the 10 m (33 ft) bathymetry contour), because few survey boats are able to venture into this highly turbulent and dangerous portion of the surf zone. The exception to this is where surveys have been undertaken by the USACE in the entrance channels to estuaries where navigable water depths need to be maintained. Thus, there is some uncertainty about estimating nearshore slopes for the surf zone due to the absence of sufficient data for this region, with the user having to make assumptions based on the best available data that are present outside the surf zone and information at the shore face. This is a recognized problem with all coastal flood analyses. To resolve this problem, we used a Coastal Profiling System (CPS) that developed for nearshore bathymetric surveys by Dr. Peter Ruggiero (Department of Geosciences, Oregon State University [Ruggiero and others, 2005]). The CPS consists of a highly maneuverable personal watercraft equipped with a survey grade GPS receiver and antenna, an echo sounder, and an on board computer. Repeatability tests undertaken by Ruggiero and colleagues indicate sub-decimeter accuracy on the order of 0.15 m (0.5 ft) (Ozkan-Haller and others, 2009). **Figure 3-18** provides an example of the CPS system, while **Figure 3-19** and **Figure 3-20** present the mapped coverage of our bathymetric surveys undertaken in the summer 2009. An example of two of the bathymetric transects undertaken in Tillamook County is presented in **Figure 3-21**.

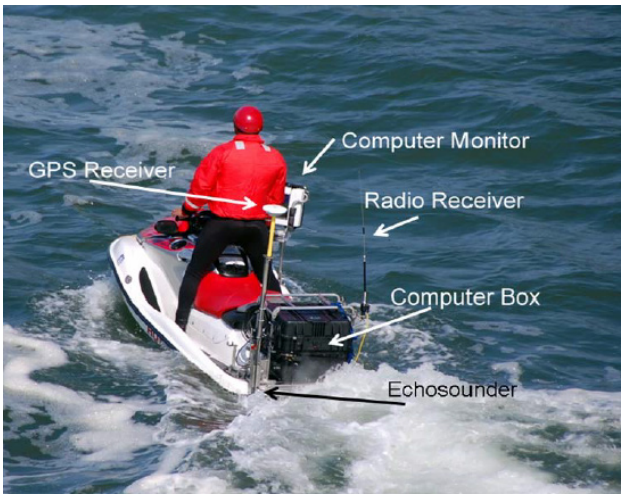

Figure 3-18. Data acquisition boat and onboard equipment (photo: courtesy of P. Ruggiero, OSU).

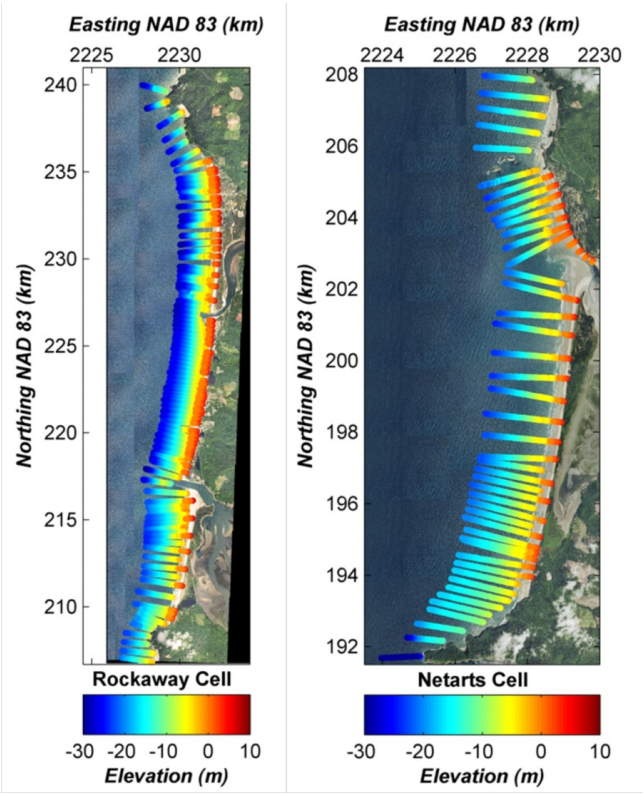

Figure 3-19. Collected bathymetry transects measured offshore the coast of the Rockaway and Netarts littoral cells, Tillamook County, Oregon.

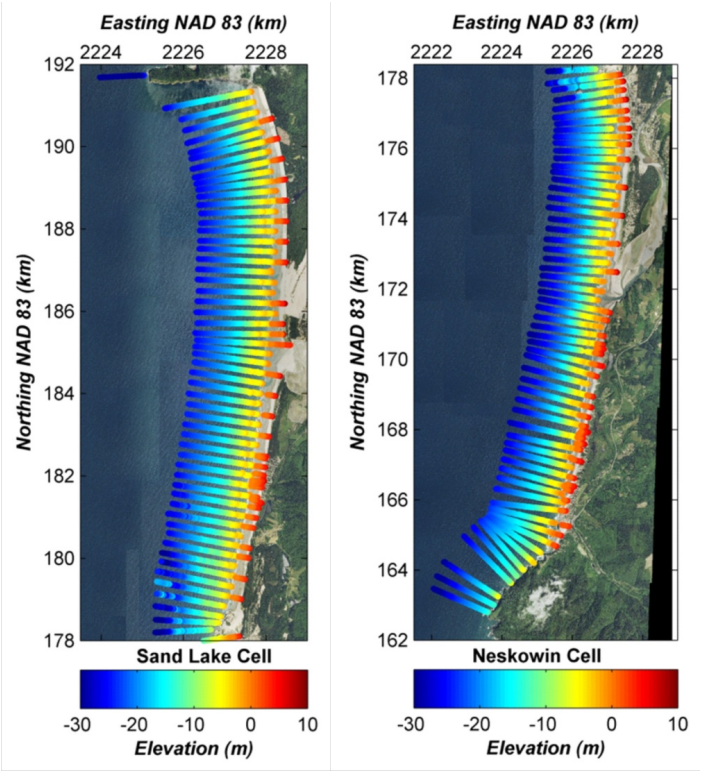

Figure 3-20. Collected bathymetry transects measured offshore the coast of the Rockaway and Netarts littoral cells, Tillamook County, Oregon.

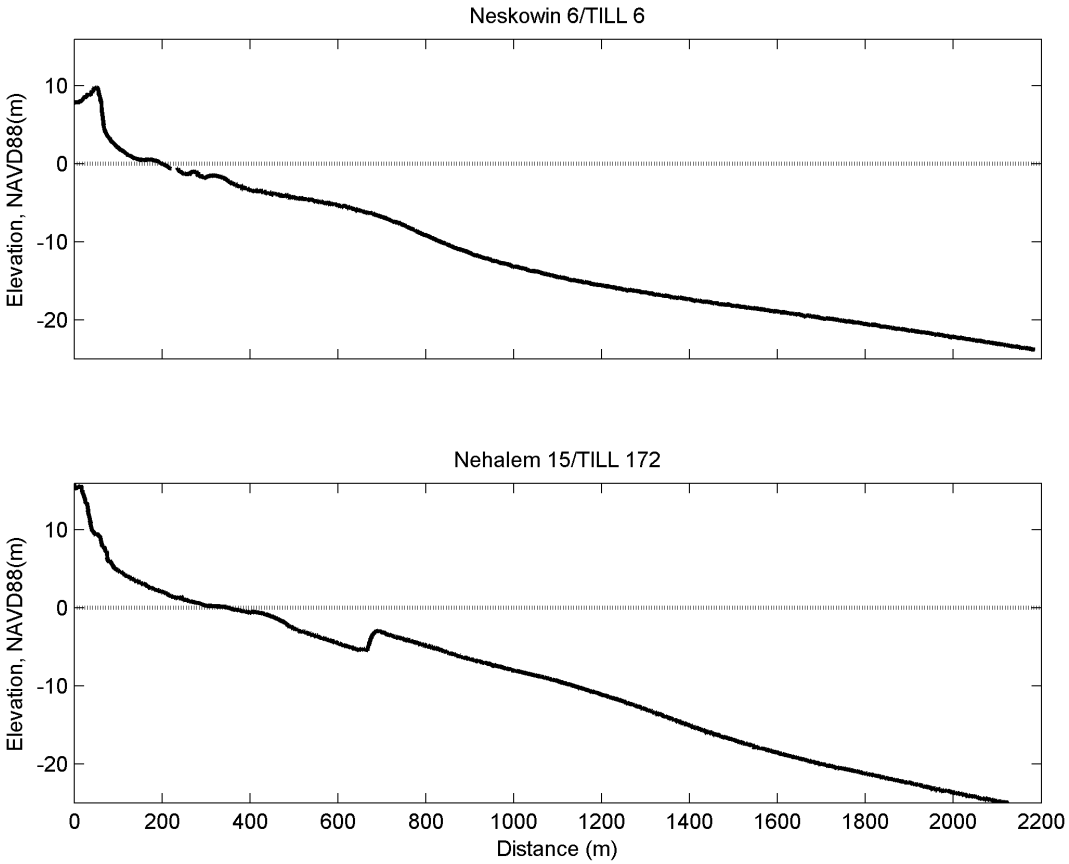

Figure 3-21. Combined topographic and bathymetric cross-shore transects measured offshore from Neskowin and Nehalem Spit near the town of Manzanita (southern and northern Tillamook County, respectively) showing the presence of sand bars. Note the contrasting nearshore slopes between the two sites, with steeper topography observed at Neskowin and wider shallower topography offshore from Manzanita.

4.0 TIDES

Measurements of tides on the Oregon coast are available from various tide gauges (http://www.tidesandcurrents.noaa.gov/map/index.shtml?type=PreliminaryData&region=Oregon) operated by NOS. Hourly tidal records are available from the following coastal sites (**Table 4-1**): Willapa Bay, Washington (Toke Point, #9440910), the Columbia River (Astoria, #9439040), Tillamook Bay (Garibaldi, #9437540), Newport (South Beach, #9435380), Coos Bay (Charleston, #9432780), and Port Orford (#9431647) on the southern Oregon coast. Long-term tidal records are also available from the Crescent City tide gauge (#9419750), located in northern California. The objective of this section is to establish which tide gauge would be most appropriate in applications directed toward FEMA wave and total water level analyses for the Tillamook coastline. Results presented here will also help guide future total water level (TWL) analyses scheduled for Lincoln County.

The tide gauges and their record intervals are listed in **Table 4-1**. **Figure 4-1** maps the locations of the most pertinent tide gauges present on the central to northern Oregon coast, along with the locations of various wave buoys operated by the National Data Buoy Center (NDBC) and the Coastal Data Information Program (CDIP), and Global Reanalysis of Ocean Waves (GROW) Fine Northeast Pacific wave hindcast data. These latter stations are pertinent to discussions of the wave climate and modeling described in Section 5 and, ultimately, in calculations of wave runup and overtopping.

As can be seen in **Table 4-1**, a number of the gauges have long records (30+ years) suitable for coastal flood analyses. The longest tide-gauge records (87 and 80 years, respectively) are from Astoria (AST), located 23.5 km up-channel from the mouth of the Columbia River, and at Crescent City (CC) in northern California. The South Beach (SB) and Toke Point (TP) gauges have moderately long records on the order of 45 and 43 years respectively (**Table 4-1**); the SB gauge is located within Yaquina Bay, ~2 km from the open coast, and the TP gauge is close to the mouth of Willapa Bay. The shortest record (~6 years), is that for Garibaldi (GB), located near the mouth of Tillamook Bay. All hourly tide data were purchased from NOS and were processed using various scripts developed in MATLAB. In addition to the measured tides, hourly tide predictions were calculated for all years using the NOS tide prediction program NTP4 (for NTP4, see the contact information at http://tidesandcurrents.noaa.gov/faq2.html#60).

Table 4-1. Pacific Northwest NOAA tide gauges.

Gauge Site	Gauge Location	Record Interval	Years
Washington			
Toke Point (TP)	Willapa Bay, near the inlet mouth	Oct. 1968 – present	43.6
Oregon			
Astoria (AST)	Astoria	Feb. 1925 – present	87.2
Garibaldi (GB)	Tillamook Bay, near the inlet mouth	July 2005 – present	6.8
South Beach (SB)	Yaquina Bay, near the inlet mouth	Feb. 1967 – present	45.2
Charleston (CH)	Coos Bay, near the inlet mouth	Apr. 1970 – present	42
Port Orford (PO)	Port Orford, open coast harbor	Oct. 1977 – present	34.6
California			
Crescent City (CC)	Crescent City, open coast harbor	Sep. 1933 – present	79.4

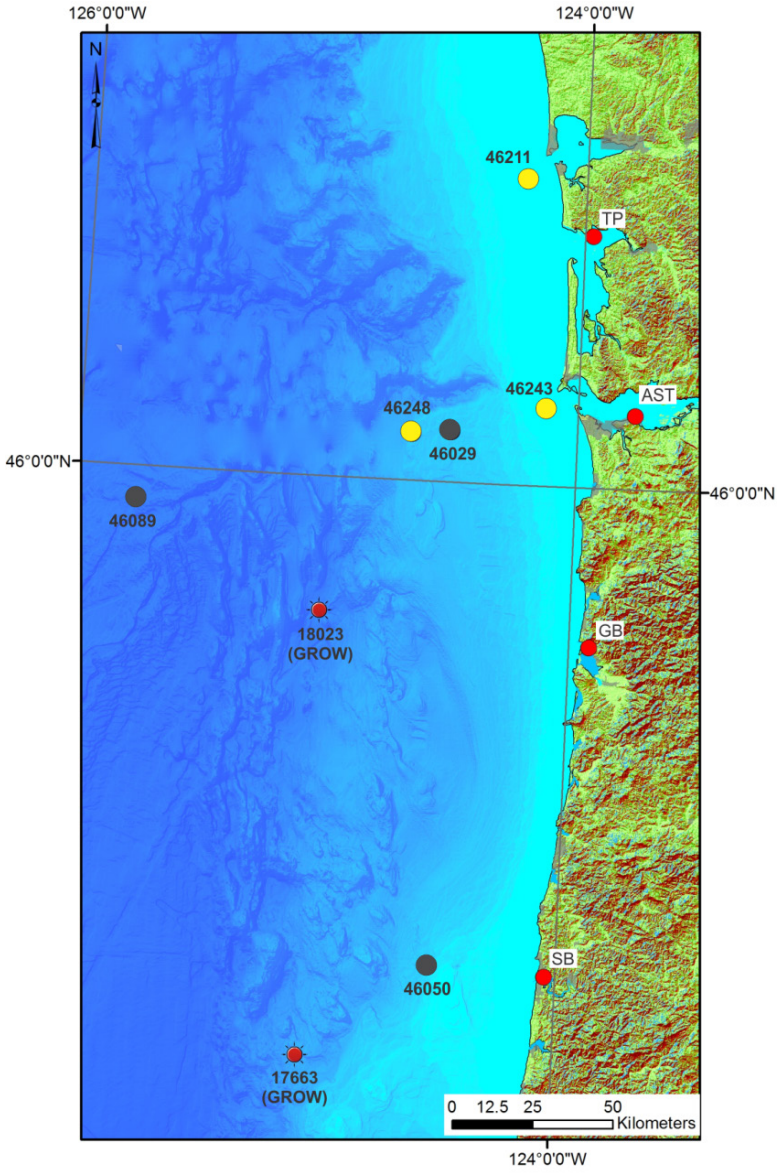

Figure 4-1. Location map of NDBC (black) and CDIP (yellow) wave buoys, tide gauges (red), and GROW wave hindcast stations (red suns). NDBC is National Data Buoy Center of NOAA and CDIP the Coastal Data Information Program (CDIP) of Scripps Institution of Oceanography. Note: NDBC Buoy #46005 referenced in this report is located 540 km (335 mi) west of the Columbia River mouth.

4.1 Tide Characteristics on the Central to Northern Oregon Coast

Tides along the Oregon coast are classified as moderate, with a maximum range of up to 4.3 m (14 ft) and an average range of about 1.8 m (6 ft) (Komar, 1997). There are two highs and two lows each day, with successive highs (or lows) usually having markedly different levels. Tidal elevations are given in reference to the mean of the lower low water levels (MLLW) and can easily be adjusted to the NAVD88 vertical datum. (MLLW to NAVD88 conversions may be performed by using values provided for a specific tide gauge by the NOS or by using the VDATUM (http://vdatum.noaa.gov/) tool developed by NOAA.) As a result, most tidal elevations are positive numbers with only the most extreme lower lows having negative values.

Initial analyses of the measured tides focused on developing empirical probability density function (PDF) plots of the measured tidal elevations for each tide gauge located between Newport, Oregon, and Willapa Bay, Washington. The objective here is to assess the measured tides along the Oregon and southwest Washington coasts in order to identify significant characteristics (including differences) between the gauges. **Figure 4-2** presents a series of PDF plots from each of the gauges. Because the gauges are characterized by varying record lengths, we have initially truncated the analyzed data to the period 2006–2011, when measurements were available from all four gauges.

As seen in the top plot of **Figure 4-2**, the gauges can be broadly characterized into two distinct regions. Those along the central and northern Oregon coast (SB and GB) indicate a slightly higher incidence of water levels between ~1.25 m and 2.25 m (4.1–7.4 ft, i.e., MSL [mean sea level] to MHW). In contrast, the AST and TP gauges, located in the Columbia River and in southern Washington, indicate a lower incidence of water levels in that same range. These differences are probably related to a combination of effects associated with the regional oceanography (upwelling, shelf currents, and Coriolis effects that deflect the currents toward the coast) and effects from the Columbia River plume (Legaard and Thomas, 2006). The lower plot in **Figure 4-2** shows the same PDF, but now clipped to span tidal elevations between 2 and 4 m (6.5–13 ft). In this latter plot, the higher water levels characteristic of TP clearly stand out. In terms of determining ultimately which tide gauge to use as a basis for the still water level time series, these initial results suggest strongly that we can effectively rule out Toke Point as a candidate site as it consistently yields much higher water levels and surges (described later), which are probably a function of its location at the mouth of a broad inlet and the potential for additional wind setup along the length of the bay. At the high water level end of the plot, differences between the three remaining gauges are relatively minor.

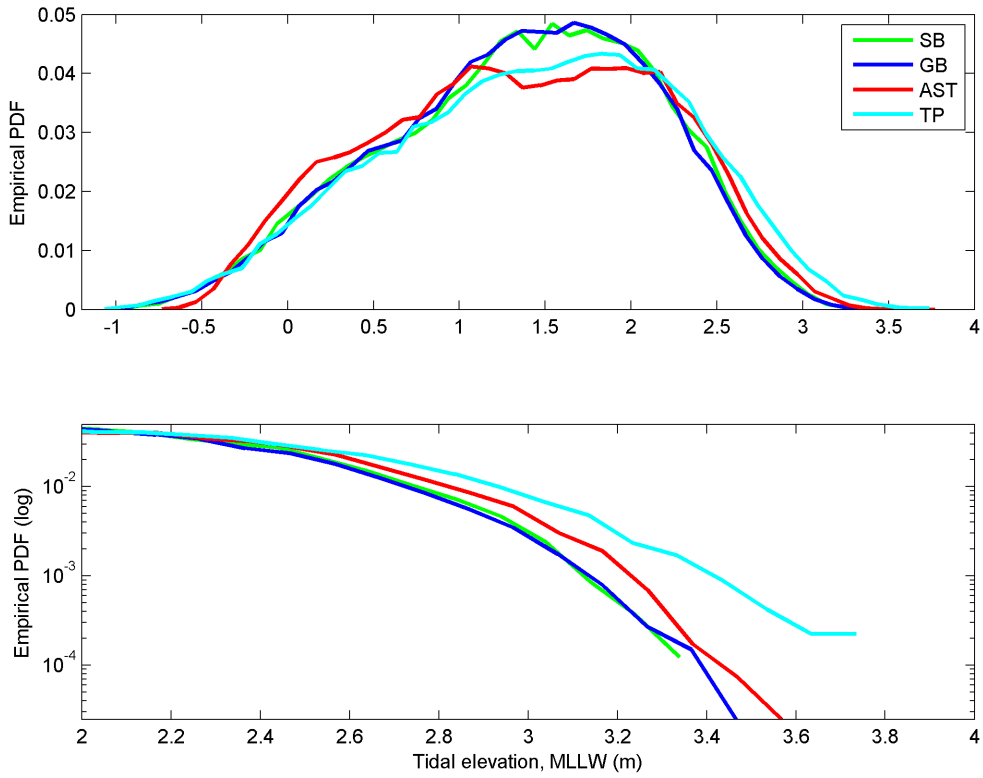

Figure 4-2. Empirical probability density function (PDF) plots for various tide gauges for overlapping years of data (2006 – 2011). Top) PDF plots showing the complete range of tidal elevations, Bottom) truncated to higher water levels.

Figure 4-3 is broadly similar to **Figure 4-2**, with the exception that the PDFs now include the complete time series of data measured by the respective tide gauges. In general, the AST gauge is characterized by a higher incidence of water levels between about -0.18 and 1.0 m (-0.6–3.3 ft), and again between 2.1 and 3.5 m (6.9–11.5 ft). This contrasts with the SB and GB gauges, which show a higher incidence of water levels between ~1.0 and 2.0 m (3.3–6.6 ft). As noted previously, these differences are probably caused by regional oceanographic factors. Detailed examination of the hourly tides indicates that the higher incidence of AST water levels in the wings of the PDF reflect the fact that both the higher highs (HH) and lower highs (LH) are greatest at AST when compared with SB and GB, while the lower lows (LL) and higher lows (HL) are generally lower at AST compared with SB and GB.

At the extreme high end of the complete PDF plots (**Figure 4-3**), the highest water levels measured at AST, GB, and SB are, respectively, 3.76, 3.62, and 3.71 m (12.3, 11.9, and 12.2 ft). These results equate to a difference of 0.05 m (0.16 ft) between AST and SB and 0.14 m (0.46 ft) between AST and GB, while indicating the absence of any real latitudinal trend with the extreme water levels. Furthermore, differences between these values and those reported by NOS for the respective stations differ by no more than 2 cm. The larger difference between the GB and AST gauges when compared with the SB gauge is entirely due to the shortness of the Garibaldi measurement record (~6 years). Overall, the relative consistency in the PDF plots generated for each gauge, particularly at the more extreme end of the measured water levels, is indicative of the areal impact of major North Pacific extratropical storms, which can affect stretches of coast up to 1,500 km (932 mi, i.e., 3 times the length of the Oregon coast) in length (Davis and Dolan, 1993; Allan and Komar, 2002).

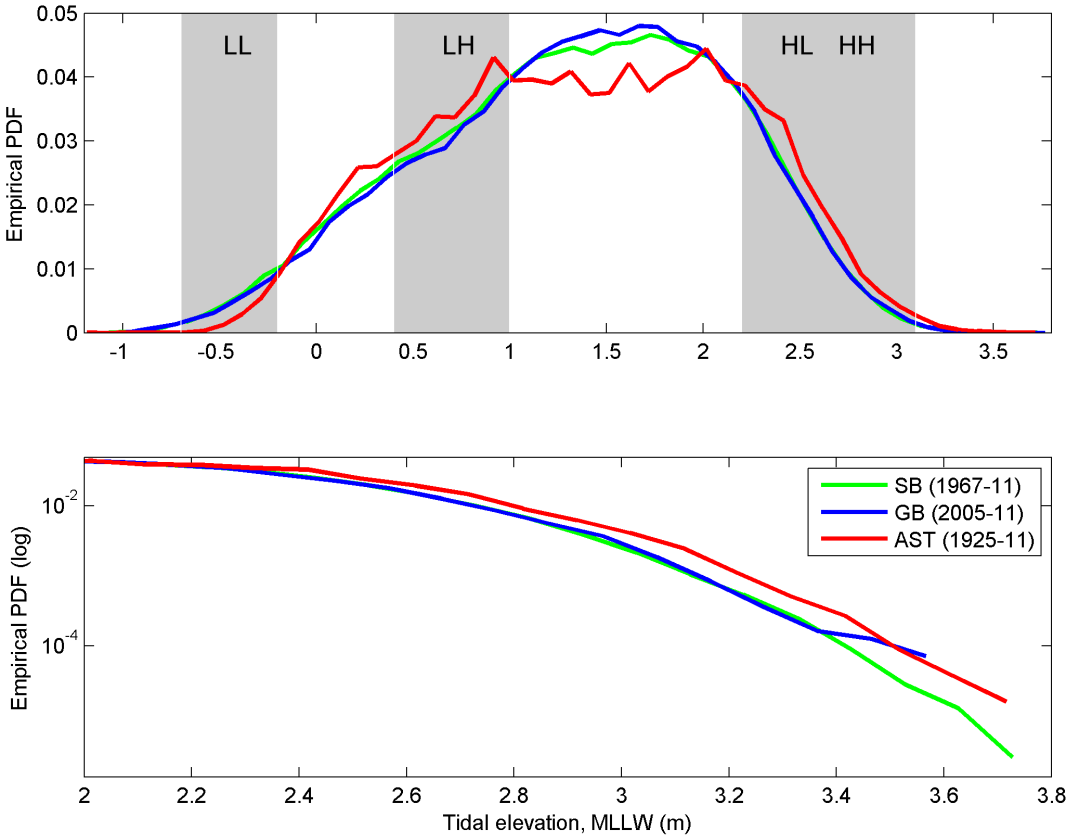

Figure 4-3. Empirical probability density functions (PDFs) for SB, GB, and AST based on all available data. Top) PDF plot showing the complete range of tidal elevations. LL, LH, HL, and HH denote, respectively, the lower lows, lower highs, higher lows, and higher highs in the tide data. Bottom) PDF truncated to higher water levels.

4.2 Seasonal Changes

Figure 4-4 presents a plot of the characteristic seasonal cycles determined for the three gauges, AST, GB, and SB, to further examine their consistencies. All three gauges depict the typical seasonal cycle that reflects the combination of ocean upwelling effects along the coast, and seasonal reversals in the California current system. The Astoria gauge has been divided into two time periods that reflect conditions prior to Columbia River dam control (~mid 1960s, dotted line), and post dam conditions (solid black line). The reason for the latter is that the AST gauge exhibits seasonal characteristics that are not apparent in the other coastal tide gauges (including TP), which are entirely a function of Columbia River discharge flows (Sherwood and others, 1990; Burgette and others, 2009).

Prior to dam and irrigation control on the Columbia River, the seasonal cycle at the AST tide gauge was characterized by generally higher monthly mean sea levels from May through June (Figure 4-4), decreasing to a minimum between August and September. Between September and February, ocean water levels increase, reaching peaks in December and February. The high mean monthly sea levels observed between May and July are entirely due to the occurrence of spring freshets (i.e., high discharge flows due to spring snow melt [Sherwood and others, 1990]).

Following dam control, the incidence of high mean sea levels during spring at the AST tide gauge was clearly reduced (Figure 4-4), while the timing of these events remained essentially unchanged, although the period of higher spring mean sea levels was shortened slightly by about 1 month. In contrast, the seasonal pattern between October and March is essentially the same for AST as it is for SB and GB, with all three sites experiencing peak water levels in January, while the broad shape of the curve is effectively the same. As noted by Sherwood and others (1999), with the introduction of river control on the Columbia River in the mid 1960s for the purposes of flood control and for irrigation use, the incidence of spring freshets were reduced by up to 40% compared with the natural regime. This change is captured in Figure 4-4 by the marked drop in monthly mean sea levels observed from May to July. Interestingly, under conditions today there is essentially little difference in the seasonal water levels between the three gauges during the critical winter period (October to March) when storms are affecting this northern part of the Oregon coast.

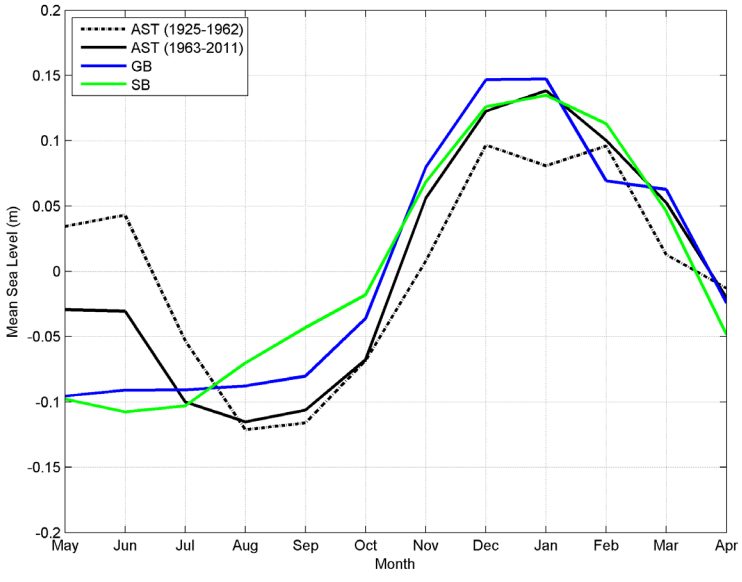

Figure 4-4. Seasonal plot of tides along the central to northern Oregon coast.

Finally, although not shown in **Figure 4-4**, all the tide gauges are strongly influenced by the El Niño Southern Oscillation phenomenon, which periodically causes mean sea levels along the U.S. West Coast to increase (Komar and others, 2011). This response is due to an intensification of the processes, especially enhanced ocean sea surface temperatures offshore from the Oregon coast. This occurred particularly during the unusually strong 1982-83 and 1997-98 El Niños, whereby mean sea levels increased by approximately 20–25 cm (~0.8 ft) above the normal seasonal cycle in mean sea level depicted in **Figure 4-4** (i.e., for a total mean sea level rise of up to 50 cm (1.6 ft) relative to the preceding summer). As a result, under these latter conditions, wave swash processes are able to reach much higher elevations on the beach, potentially eroding dunes and bluffs.

4.3 Oregon Storm Surges

The actual level of the measured tide can be considerably higher than the predicted tides provided in standard tide tables and is a function of a variety of atmospheric and oceanographic forces, which ultimately combine to raise the mean elevation of the sea. These latter processes vary over a wide range of time scales and may have quite different effects on the coastal environment. For example, strong onshore winds coupled with the extremely low atmospheric pressures associated with a major storm can cause the water surface to be locally raised along the shore as a storm surge, and such surges have been found in tide-gauge measurements to be as much as 1.5 m (4.9 ft) along the Pacific Northwest coast (Allan and Komar, 2002). However, during the summer months these processes can be essentially ignored due to the absence of major storm systems.

Analyses have been undertaken to examine the non-tidal residuals and ultimately the storm surges identified at the various tide gauges on the northern Oregon coast. The objective is to provide a better understanding of the spatial and temporal variabilities of storms as they track across the North Pacific, the magnitudes (and frequency) of the surges, and the potential differences in the non-tidal residuals between gauges due to variations in the storm tracks, barometric pressures, and winds. This last point is particularly important in terms of finalizing the tide gauge time series to be used in the Tillamook total water level analyses.

For the PNW, the measured water level (h_t) at a particular tide gauge is given by the following relationship:

$$h_t(t) = z_o + X_{at}(t) + X_{oc}(t) + S(t) \qquad \text{(Eq. 4-1)}$$

where z_o is the mean water level, X_{at} is the predicted astronomical tide, X_{oc} is the altered mean water level due to ocean processes (water temperatures, currents and El Niño "sea-level" waves), and S is the contribution by the storm surge at time t. The predicted astronomical tide for the specific tide gauge is calculated using its harmonic constituents:

$$X_{at} = \sum_{i=1}^{M} H_i \cos(\sigma_i t + \varphi_i) \qquad \text{(Eq. 4-2)}$$

where H_i is the amplitude of the constituent i, σ_i is its frequency, φ_i is the phase of the constituent, and M is the number of tidal constituents included in the analysis.

4.4 Non-Tidal Residual Analyses

The procedures used to analyze the non-tidal residuals and storm surge incidence follow those developed by Allan and others (2011), which used an harmonic analysis method of least squares (HAMELS) approach developed in MATLAB to estimate the amplitude and phase for any set of tidal constituents at each of the tide gauge sites (Boon, 2004). The purpose here is to develop a predicted time series of the water levels produced entirely by astronomic forces that excludes the seasonal component produced by oceanographic processes on the West Coast; the seasonal component can be integrated into tide predictions through the solar annual (Sa) and solar semiannual (Ssa) tide and is integrated as an *average term* in the predicted tides provided by NOS.

HAMELS analyses of tide gauge data have previously been completed for the SB and TP tide gauges (Allan and others, 2011). Thus, similar analyses were undertaken using the AST and GB tide gauges. The specific steps included the following:

1. HAMELS was used to derive an estimate of the amplitude and phase for the tidal constituents. This was initially done using just a spring/summer data set for testing purposes and then expanded to the full year of data;
2. After the tidal constituents were determined, HAMELS was used to derive the astronomic tide predictions for the entire record on a year-by-year basis (eliminating any long-term trend). The non-tidal residuals (NTRs) were calculated by subtracting the astronomic tide from the measured tides;
3. The NTR time series were then filtered using a moving average filter (averaged over ±30 days) with zero phase shift, and the seasonal cycle was removed from the NTRs;
4. The winter standard deviation was calculated, and those events exceeding 2*σ were used to define individual surge events (Zhang and others, 2001).

Figure 4-5 presents a plot of the derived NTRs for the South Beach (SB), Garibaldi (GB), and Astoria (AST) tide gauges. These data reflect the corresponding NTRs associated with the higher highs and higher lows of the diurnal tidal cycle, which were determined using a peak detection algorithm in MATLAB. Analyses here span the period of record for the respective tide gauges. Correlation (R^2) values calculated for the three plots are 0.91, 0.69, and 0.79, respectively, with the strongest correlation found between the SB and GB tide gauges on the open coast, while the weakest correlation was between the SB and the AST tide gauges.

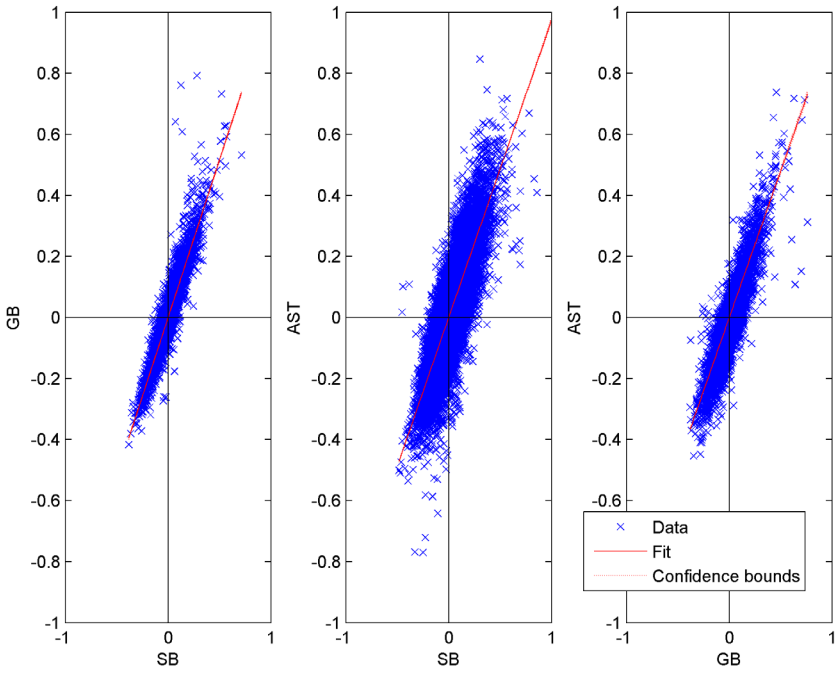

Figure 4-5. Comparison of non-tidal residuals determined for South Beach (SB) versus Garibaldi (GB), SB versus Astoria (AST), and GB versus AST tide gauges. Values plotted here reflect the daily peak values.

Figure 4-6 presents the actual time series of de-seasoned NTRs derived for the SB, GB, and AST tide gauges for the 2005-06 winter. In this example, the NTRs have been time adjusted to a single station. As can be seen in this example, the SB and GB tide gauges tend to track very closely to each other, consistently capturing the same peaks and troughs. In contrast, the AST gauge shows larger fluctuations, when compared to the other tide gauges. These differences are further highlighted in the anomaly plot (**Figure 4-6** bottom), which indicates more subtle differences between SB and GB tide gauges, with both gauges characterized by anomalies that reach as much as 0.2 m (0.65 ft). In contrast, anomalies between the GB and AST tide gauges reveal much larger differences. While differences here to a large degree reflect differences in the position of the storms relative to the tide-gauges, the storm's barometric pressures, winds, and the associated wave forcing along the coast, the fluctuations shown for the AST gauge suggest that other factors (e.g., Columbia River discharge) may be exerting a strong influence on the observed patterns between GB and AST. Overall, differences between the SB and GB tide gauges probably reflect mostly subtle shifts in the timing of the events as they impact the coast, reinforcing our confidence that the effects of North Pacific extratropical storms are indeed widespread, affecting large tracts of the coast at similar times.

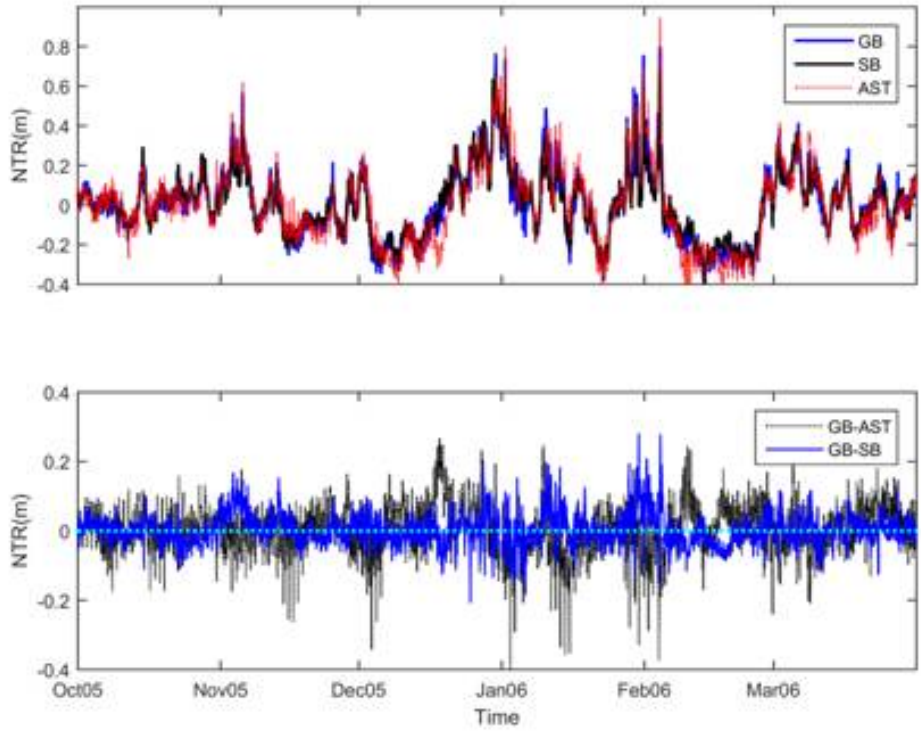

Figure 4-6. Comparison of non-tidal residuals (NTRs, top), and their differences (bottom) between the South Beach (SB), Garibaldi (GB), and Astoria (AST) tide gauges for the 2005-06 winter.

After NTRs for each of the tide gauges had been identified, individual storm surge events were identified following the procedures of Zhang and others (2001) and Allan and others (2011). **Figure 4-7** (left) presents a log number plot of all surge events for SB, GB, and AST gauges; here we include similar analyses performed on the TP tide gauge. The plot indicates that for the most part the four gauges are showing relatively similar patterns in terms of the storm surge magnitudes. In general, the mean storm surges increase northward (0.45 m [1.5 ft] at SB to 0.66 m [2.2 ft] at TP), while the highest surges have occurred at TP (1.62 m [5.3 ft]) and SB (1.42 m [4.7 ft]); despite its significantly longer record, the highest surge observed at AST reached 1.1 m (3.6 ft). **Figure 4-7** (right) presents the empirical cumulative distribution function (CDF) calculated for the four gauges, further highlighting the progressive shift in the surge magnitudes to the north. Again, the TP gauge stands out as an exception, further confirming why this site should be excluded as the time series of water levels for the Tillamook coast.

Taken together, these analyses confirm that the two open coast tide gauges located at South Beach in Newport on the central Oregon coast and at Garibaldi in Tillamook Bay provide, overall, the best measure of the open-coast still water levels, important in FEMA total water level and overtopping analyses. The main distinction between these two stations is the length of available measurements, with the Newport site having the longest record (~45 years) and Garibaldi having the shortest. Furthermore, from our analyses, we believe that the measured tides at Astoria (located 23 km upriver from the coast) are so significantly influenced by Columbia River flows that this gauge should not be used in FEMA flood analyses for the Tillamook County open coast.

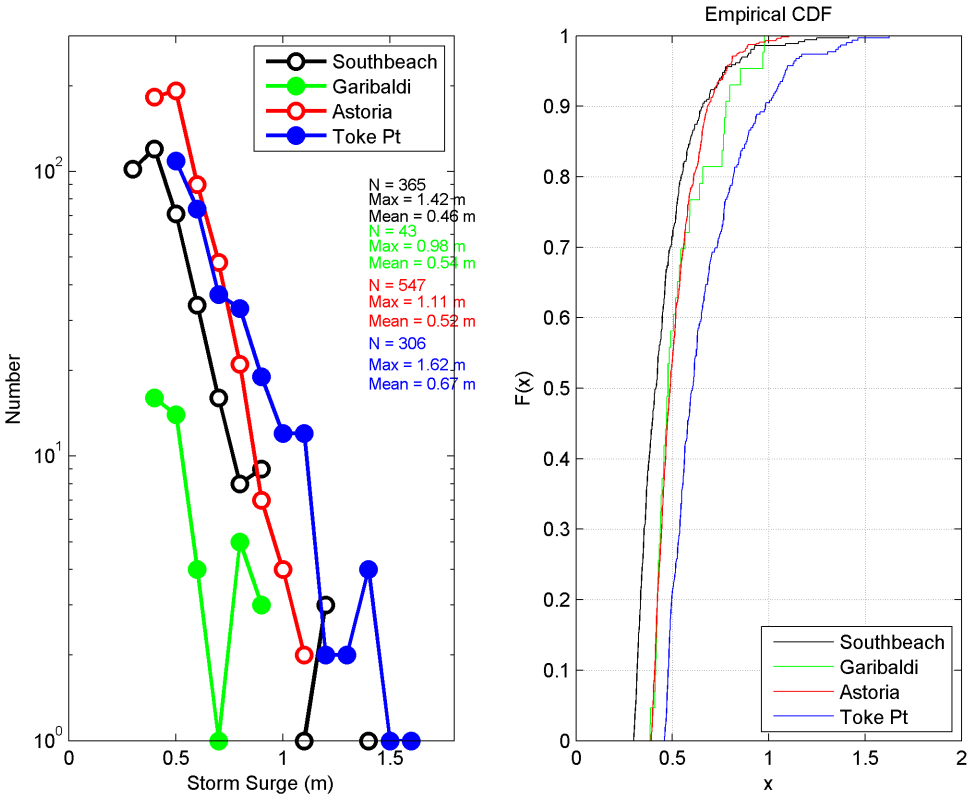

Figure 4-7. (Left) Histogram of surge magnitudes determined for selected tide gauge stations. (Right) Cumulative distribution plot of storms surge magnitudes.

4.5 Tillamook County Tides

For the purposes of this study, we have based our *still water level* (SWL) and *wave runup* calculations on a combined time series (1967–2011) that encompasses tides measured at the South Beach gauge (#9435380) in Yaquina Bay (1967–2005) and from the Garibaldi tide gauge (#9437540) in Tillamook Bay (2005–present). **Figure 4-8** shows the tidal elevation statistics derived from the South Beach tide gauge (the longest temporal record), with a mean range of 1.91 m (6.3 ft) and a diurnal range of 2.54 m (8.3 ft). The highest tide measured from this record reached 3.73 m (12.2 ft), recorded in December 1969 during a major storm. These values are comparable to those measured at the Garibaldi site (mean = 1.9 m, diurnal = 2.53 m), with the only real difference that this latter gauge recorded a peak water level of 3.64 m (11.9 ft) in December 2005 due to its shorter record.

As noted previously, tides on the Oregon coast tend to be enhanced during the winter months due to warmer water temperatures and the presence of northward flowing ocean currents that raise water levels along the shore. These enhanced tides persist throughout the winter rather than lasting for only a couple of days as is the case for a storm surge. This effect can be seen in the monthly averaged water levels derived from the combined time series (**Figure 4-9**), but where the averaging process has removed the water-level variations of the tides, yielding a mean water level for the entire month. Based on 45 years of data, the results in **Figure 4-9** show that on average monthly-mean water levels during the winter are nearly 25 cm (0.8 ft) higher than in the summer. Water levels are most extreme during El Niño events, due to an intensification of the processes, largely enhanced ocean sea surface temperatures offshore from the Oregon coast. This occurred particularly during the unusually strong 1982-83 and 1997-98 El Niños. As seen in **Figure 4-9**, water levels during those climate events were approximately 25–30 cm (0.8–1 ft) higher than the seasonal peak, and as much as 56 cm (1.8 ft) higher than during the preceding summer, enabling wave swash processes to reach much higher elevations on the beach during the winter months, with storm surges potentially raising the water levels even more.

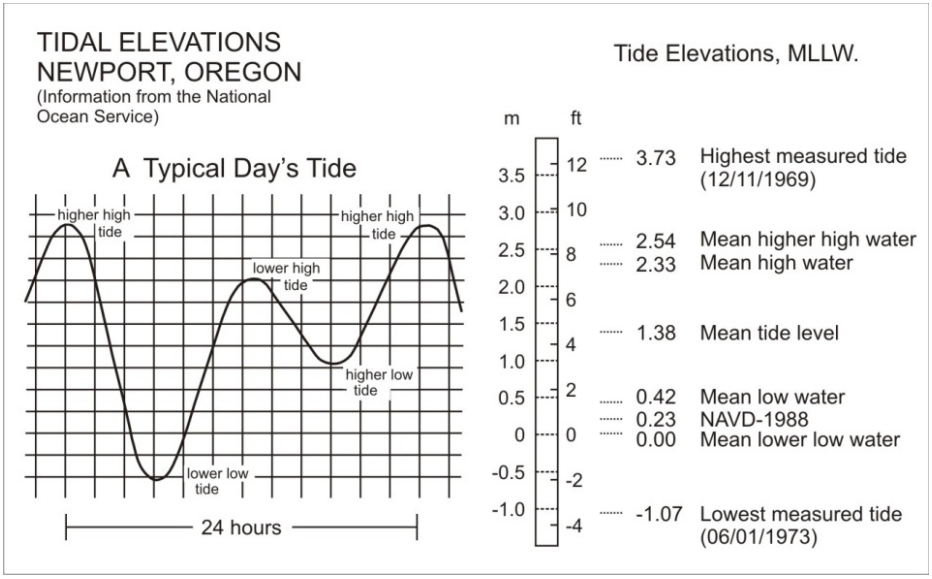

Figure 4-8. Daily tidal elevations measured at South Beach, Newport on the central Oregon coast. Data from the NOS (http://www.co-ops.nos.noaa.gov/waterlevels.html?id=9435380). MLLW is mean lower low water.

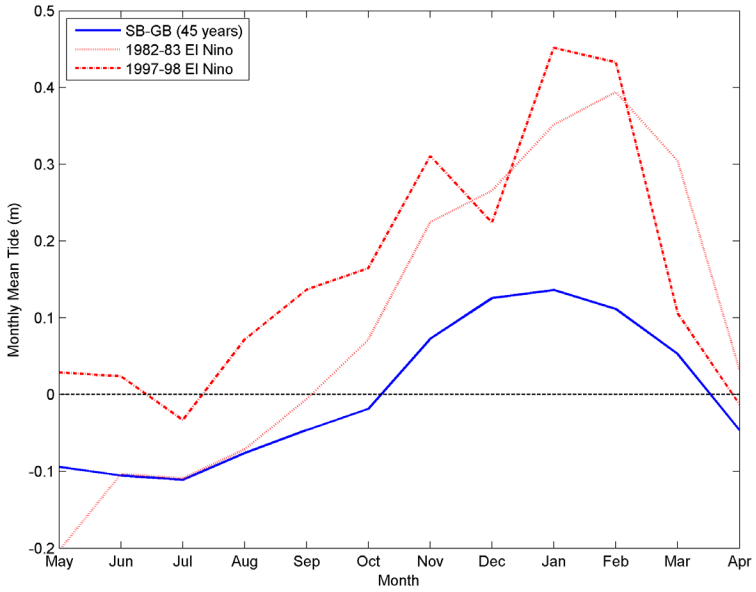

Figure 4-9. Seasonal cycles in monthly-mean water levels based on data from the combined South Beach-Garibaldi (SB-GB) measured tides.

Aside from seasonal to interannual effects of climate events on ocean water levels, of interest are long-term trends associated with relative sea level changes due to climate change along the Tillamook County coastline. **Figure 4-10** shows results from an analysis of the combined SB-GB time series based on a separate analysis of the summer and winter tide levels. For our purposes, "winter" is defined as the combined average tide level measured over a three-month period around the peak of the seasonal maximum in winter water levels, typically the months of December through February. Similarly, "summer" water levels reflect the combined average tide level measured over a three-month period around the seasonal minimum, typically the months of May through July when water levels also tend to be less variable (Komar and others, 2011).

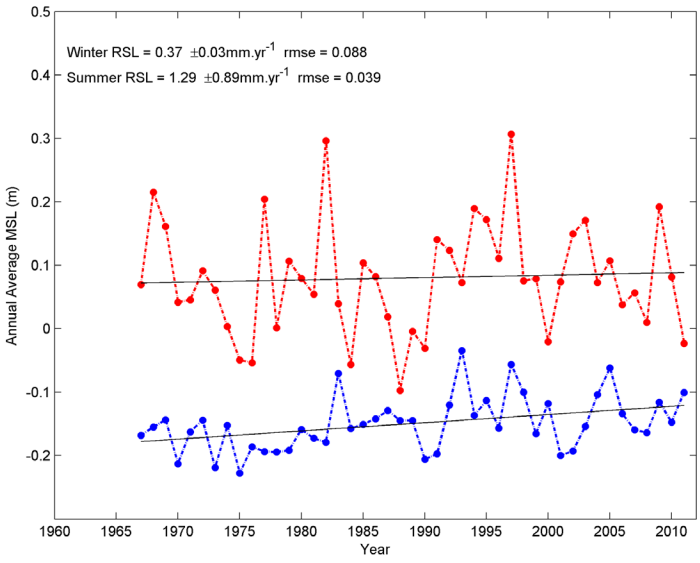

Figure 4-10. Trends of "winter" (red) and "summer" (blue) mean sea levels measured by the SB-GB tide gauges. Results for the summer regression are statistically significant, while the estimated winter rate is not significant at the 95% confidence level.

As observed previously in **Figure 4-9**, the winter tidal elevations are systematically displaced upward by about 25 cm (0.8 ft) above the summer elevations, with the difference between the regression lines reflecting the seasonal change in ocean water levels from summer to winter. **Figure 4-10** also emphasizes the extremes associated with major El Niños; the peaks between the 1983 and 1997 major events have systematically shifted upward over the years due to relative sea level changes along this particular section of the coast. In contrast, the summer regression line is characterized by significantly less scatter in the residuals, as it effectively excludes the influence of storms and El Niños that are dominant during the winter. Using this approach, it can be seen that the central Oregon coast is slowly being transgressed at a rate of ~1.29 ± 0.89 mm/yr, which is slightly lower than that reported by NOS (~2.18 ± 0.85 mm/yr). This difference is due to the SB tide gauge having been affected by localized subsidence, particularly in the late 1960s and early 1970s, that continued to decrease over time up until the mid 1990s (Burgette and others, 2009). Since then, repeat surveys of NGS benchmark indicate that the land now appears to be stable.

Finally, it is important to appreciate that the trends shown in **Figure 4-10** reflect relative sea level changes due to the PNW coast of Oregon and Washington being locally influenced by changes in the elevation of the land due to regional tectonics as well as by the global rise in sea level, with the net change important to both coastal erosion and flood hazards. **Figure 4-11** presents a synthesis of both tectonic land elevation changes and sea level trends derived for multiple stations along the PNW coast (Komar and others, 2011), correlated against differential surveys of first-order NGS benchmarks (e.g., Burgette and others, 2009) and GPS CORS stations. Results here indicate that, in general, the southern Oregon coast is an emergent coast with tectonic uplift of the land outpacing sea level rise. In contrast, the central to northern Oregon coast (i.e., Tillamook County) is slowly being transgressed by sea level.

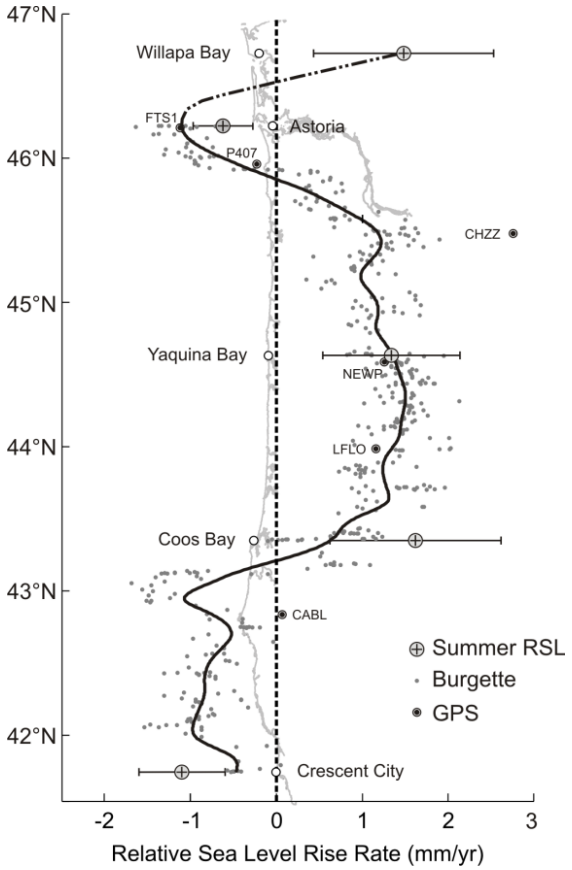

Figure 4-11. Assessments of changes in relative sea level (RSL) based on tide-gauge records compared with NGS benchmark (Burgette) and GPS measurements of land-elevation changes, with their corresponding RSL rates obtained by adding the 2.28 mm/yr PNW eustatic rise in sea level.

4.6 Still Water Level (SWL)

The still water level (SWL) is the sum of the predicted astronomical tide listed in Tide Tables plus the effects of processes such as an El Niño or storm surge that can elevate the measured tide above the predicted tide (Northwest Hydraulic Consultants, 2005). Of importance to erosion and flooding hazards are the extremes of the measured tides. In conventional analyses of extreme values, the general assumption is that the data being analyzed (e.g., the annual maxima) represent independent and identically distributed (stationary) sequences of random variables. The generalized extreme value (GEV) family of distributions is the cornerstone of extreme value theory, in which the cumulative distribution function is given as:

$$G(z, \mu, \sigma, \xi) = \exp\left\{-\left[1+\xi\left(\frac{z-\mu}{\sigma}\right)\right]^{-1/\xi}\right\} \qquad \text{(Eq. 4.3)}$$

defined on $\left\{z: 1+\frac{\xi(z-\mu)}{\sigma} > 0\right\}$,

where the parameters satisfy $-\infty < \mu < \infty$, $\sigma > 0$, $-\infty < \xi < \infty$ (Coles, 2001). The model has three parameters; μ is a location parameter, σ is a scale parameter, and ξ is a shape parameter. The EV-II (Frechet) and EV-III (Weibull) classes of extreme value distributions correspond, respectively, to the cases of $\xi > 0$ and $\xi < 0$. When $\xi = 0$, equation 4.3 collapses to the Gumbel or EV-I type extreme value distribution. By inferring the shape parameter ξ (estimated here, along with the other parameters, by maximizing the log-likelihood function), the data themselves determine the most appropriate type of tail behavior and it is not necessary to make an a priori assumption about which individual extreme family to adopt, as in a classical Weibull-type extreme wave height analysis (Coles, 2001).

The GEV is often applied to annual maxima data in an approach referred to as the annual maximum method (AMM). However, one of the primary shortcomings of fitting an extreme-value distribution with annual maximum data is that useful information about the extremes is inherently discarded, particularly when data are sampled on either a daily or hourly basis (as in the case of the measured tides and deep-water significant wave heights measured by Oregon tide gauges and NDBC wave buoys). Two well-known approaches exist for characterizing extremes by using data other than simply annual (block) maxima. The first is based on the behavior of the r largest-order statistics within a block, for low r, and the second is based on exceedances above a high threshold value. For the purposes of this study, we use the peak-over-threshold (POT) approach for determining extreme SWL and wave heights.

In the peak-over-threshold (POT) method, a high threshold, u, is chosen in which the statistical properties of all exceedances over u and the amounts by which the threshold is exceeded are analyzed. It is assumed that the number of exceedances in a given year follows a Poisson distribution with annual mean νT, where ν is the event rate and T = 1 year, and that the threshold excesses $y > 0$ are modeled using the Generalized Pareto Distribution (GPD) given by:

$$H(y, \sigma, \xi) = 1-\left(1+\frac{\xi y}{\sigma}\right)^{-1/\xi} \qquad \text{(Eq. 4-4)}$$

where ξ is the shape parameter of the GEV distribution and σ is a scale parameter related to GEV parameters by $\sigma = \sigma + \xi(u - \mu)$. The event rate can also be expressed in a form compatible with the GEV distribution provided that

$$\nu = (1+\frac{\xi(u-\mu)}{\sigma})^{-1/\xi}$$

Estimates of extreme quantiles of the distributions are obtained by inverting the distributions in equation 4.4. For GPD-Poisson analyses the N-year return level, y_N, is given as:

$$y_N = \mu + \frac{\sigma}{\xi}\left[(N n_y \zeta_u)^{\xi} - 1\right] \qquad \text{(Eq. 4-5)}$$

where n_y is the number of observations per year and ζ_u is the probability of an individual observation exceeding the threshold u.

Figure 4-12 presents results of the GEV analyses for the combined SB-GB measured tides. In constructing this plot, we used a threshold of 3.06 m (10 ft). Included in the figure are the calculated 1- through 500-year SWLs. As can be seen in **Figure 4-12**, the 1% SWL calculated for the combined time series is 3.71 m (12.2 ft, relative to MLLW). When adjusted to the NAVD88 vertical datum, this value becomes 3.60 m (11.8 ft, NAVD88); note the adjustment from NAVD88 to MLLW is calculated to be 0.108 m (0.35 ft) at the GB site. The NAVD88 to MLLW adjustment at the GB site was calculated using the VDATUM tool developed by NOAA (http://vdatum.noaa.gov/). The 500-year SWL is estimated to be 3.68 m (12.1 ft) relative to the NAVD88 vertical datum. As observed previously, the highest tide measured in the combined time series reached 3.62 m (11.9 ft, relative to NAVD88).

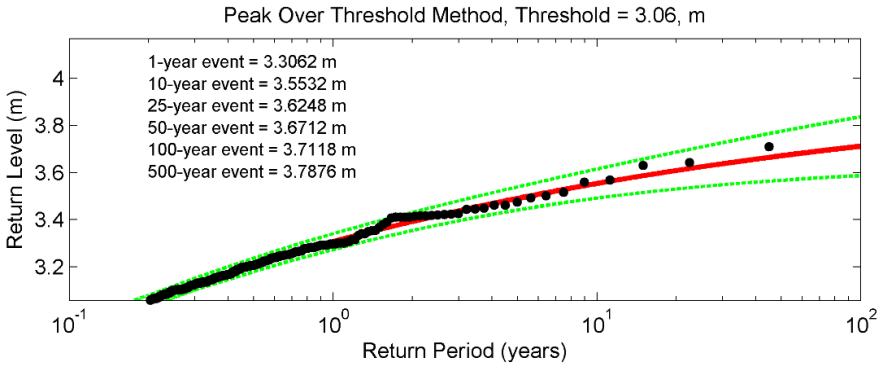

Figure 4-12. Extreme-value analyses of the still water level (SWL) determined for the combined South Beach-Garibaldi tide gauge time series. These data are relative to the MLLW vertical datum. Black dots reflect the discrete peak tidal events and the red line is the extreme value distribution fit to those data. Green dashed line reflects the 95% confidence boundary.

5.0 PACIFIC NORTHWEST WAVE CLIMATE

The wave climate offshore from the Oregon coast is one of the most extreme in the world, with winter storm waves regularly reaching heights in excess of several meters. This is because the storm systems emanating from the North Pacific travel over fetches that are typically a few thousand miles in length and are also characterized by strong winds, the two main factors that account for the development of large wave heights and long wave periods (Tillotson and Komar, 1997). These storm systems originate near Japan or off the Kamchatka Peninsula in Russia and typically travel in a southeasterly direction across the North Pacific toward the Gulf of Alaska, eventually crossing the coasts of Oregon and Washington or along the shores of British Columbia in Canada (Allan and Komar, 2002).

Wave statistics (heights and periods and, more recently, wave direction) have been measured in the Eastern North Pacific using wave buoys and sensor arrays since the mid 1970s. These data have been collected by the National Data Buoy Center (NDBC) of NOAA and by the Coastal Data Information Program (CDIP) of Scripps Institution of Oceanography (**Figure 4-1**). The buoys cover the region between the Gulf of Alaska and Southern California and are located in both deep and intermediate to shallow water over the continental shelf. The NDBC operates some 30 stations along the West Coast of North America, while CDIP has at various times carried out wave measurements at 80 stations. Presently, there are two CDIP buoys operating offshore from the mouth of the Columbia River (#46243 and #46248) and three NDBC buoys (Washington [#46005], Tillamook [#46089], and Columbia River Bar [#46029]); Note buoy #46005 is located ~540 km (335 mi) directly west of the Columbia River mouth. Wave measurements by NDBC are obtained hourly (CDIP provides measurements every 30 minutes), and are transmitted via satellite to the laboratory for analysis of the wave energy spectra, significant wave heights and peak spectral wave periods. These data can be obtained directly from the NDBC through their website[1].

An alternate source of wave data appropriate for FEMA flood modeling is hindcast wave data such as the Global Reanalysis of Ocean Waves Fine Northeast Pacific Hindcast (GROW-FINE NEPAC), purchased through Oceanweather, Inc., and Wave Information Studies (WIS)[2] hindcasts developed by the USACE (Baird, 2005). GROW is a global wave model, while GROW Fine Northeast Pacific extends the original model by incorporating a higher-resolution analysis (4 times as many data nodes), basin-specific wind adjustments based on QUIKSCAT scatterometry, enhancements due to Southern Ocean swells, and inclusion of shallow water physics (Oceanweather, Inc., 2010). These data can ultimately be applied to offshore structure design, tow-analysis, operability, and other applications where wind and wave data are required. Standard products from GROW include time series of wind and wave parameters (including sea/swell partitions), extreme criteria, operability statistics, and wave spectra (Oceanweather, Inc., 2010). The advantage of GROW as opposed to measured data is that it provides a continuous time series of wave and wind data suitable for FEMA flood modeling. In contrast, measured data obtained from wave buoys may be characterized by significant data gaps due to the instruments having come off their mooring or from instrument failure. The main disadvantage of GROW Fine Northeast Pacific data is that it is modeled basin-scale wind models and data, and the data time series is 3 hourly as opposed to hourly as provided by the buoys. For the purposes of this study, we have explored both data sets in order to define the most appropriate time series of wave data. To that end, GROW Fine Northeast Pacific data were purchased for three nodes offshore the Oregon coast. **Figure 4-1** identifies the locations of two of the GROW sites, station #18023 located offshore from southern Clatsop / northern Tillamook County and #17663 offshore from Lincoln County. Besides the hourly measured wave buoy data, we also obtained wave hindcast information on the deepwater wave climate determined through comparisons with the WIS station located adjacent to NDBC buoy 46005.

[1] http://www.ndbc.noaa.gov/maps/Northwest.shtml

[2] http://wis.usace.army.mil/wis.shtml

Analyses of the wave climate offshore from Tillamook County were undertaken by DOGAMI staff, and as a subcontract to Dr. Peter Ruggiero, College of Earth, Ocean, and Atmospheric Sciences (CEOAS), OSU, and included numerical analyses of the 1% or 100-year extreme total water levels, which reflect the calculated wave runup superimposed on the tidal level (i.e., the still water level [SWL]) to help determine the degree of coastal flood risk along the coast of Tillamook County.

OSU performed a series of tests and analyses including wave transformations, empirical wave runup modeling, and total water level modeling. For the purposes of this study, OSU used the SWAN (Simulating Waves Nearshore) wave model to transform deepwater waves to the nearshore (typically the 20 m [65.6 ft] contour). The transformed waves were then linearly shoaled back into deep water to derive a *refracted deepwater equivalent wave parameterization* (wave height and peak period) that can be used to calculate runup levels, which combined with tides, are used to estimate the flood risk along the county's shoreline.

In our Coos County FEMA study (Allan and others, 2012b), the approach we developed involved several stages:

1. We first defined a time series of deepwater wave heights and periods for a particular location offshore of the shelf break, which we used to calculate an initial wave runup and total water level time series based on two representative beach slopes characteristic of beaches in the Coos County detailed study areas.
2. Using the above approach we defined ~135 discrete storm events for the two different slope types. We transformed the deepwater wave statistics associated with these events into the nearshore (20-m water depth) to account for wave refraction and shoaling effects. Depth-limited breaking, wind growth, quadruplets, and triad interactions were all turned off in the SWAN runs. The derived nearshore wave statistics were then converted back to their adjusted deepwater equivalent wave heights in order to perform the wave runup analyses and ultimately compute the 1% total water levels.

The main limitations associated with this approach were:

1. Only a very limited number of model runs were performed, ~135 per representative beach slope.
2. Because we used only two representative beach slopes, we may have missed a particular wave condition (wave height [H_s], period [T_P], direction [D_d]) and beach slope (tan β) combination that resulted in a higher total water level (TWL) at the shoreline.
3. The structural function approach used to generate the initial extreme TWLs and therefore to pick the offshore wave conditions input in SWAN is fundamentally limited. Nature gave us only one combination of waves and water levels during the 30 years we used to generate input conditions, which is not necessarily a statistically robust sample.

For the purposes of the Tillamook County study, including other detailed FEMA coastal studies underway for Oregon, we have adopted a more refined approach that reflects the following enhancements.

1. Rather than steps 1 and 2 as described for our Coos County study, modeling will be carried out based on analyses of the full range of wave and tide combinations observed over the historical period. This approach will ultimately provide a more robust measure of the 1% (and other desired return periods) total water levels.
2. We have developed a lookup table approach for analyzing thousands of possible storm combinations rather than only a few hundred as performed in Coos County. The general idea is that a "lookup table" can be developed by transforming all combinations of wave quadruplets (H_S, T_P, D_d, and water levels). We used SWAN to compute the transformed wave characteristics of these waves up to wave breaking.
3. Our approach still suffers from the third limitation listed above for the Coos County study.

The area over which the SWAN grid was set up is shown in **Figure 5-1**. In general, our analyses proceeded in the following order:

1. Develop a long time series of both measured (NDBC) and modeled (WIS) wave conditions (~30 years long) at approximately the shelf edge offshore of the study area;
2. Run the SWAN model with a full range of input conditions, using constant offshore boundary conditions, to compute bathymetric induced wave transformations up to wave breaking.
3. Develop "lookup tables" from the suite of SWAN simulations.
4. Transform the long time series through the "lookup tables" such that we generate alongshore varying long time series at approximately the 20-m depth contour throughout the study area.
5. Use the deepwater equivalent alongshore varying wave conditions and the appropriate measured tides from the combined Yaquina Bay-Garibaldi time series, to compute time series of TWLs for 178 beach profiles along the Tillamook County coast. These include transects established on Nehalem Spit-Manzanita (21 sites), Twin Rocks-Rockaway-Nedonna Beach (40 sites), Bayocean Spit (11 sites), Short Sand Beach (3 sites), Netarts Spit-Oceanside (29 sites), Tierra Del Mar – Sand Lake (32 sites), Nestucca spit – Pacific City (14 sites), and Neskowin (28 sites).
6. Using a Poisson-generalized Pareto distribution, compute the 1-, 10-, 25-, 50-, 100-, and 500-year TWL elevations using a peak-over-threshold (POT) approach.
7. Compare extreme TWLs with topographic elevations of various beach backing features to determine the potential extent of coastal flooding during extreme events.

The following sections describe in more detail the various procedures used in each of the aforementioned steps in this analysis.

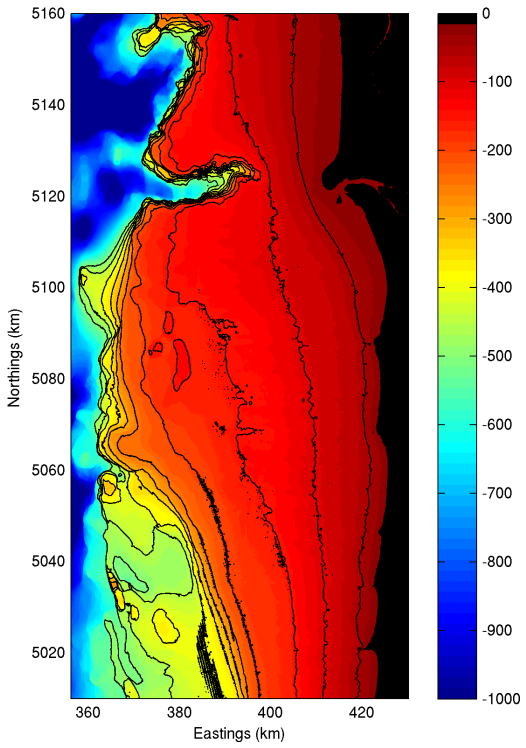

Figure 5-1. The SWAN model domain developed for the Tillamook County coast. The model bathymetry was developed using 1/3 arc-second (~10 m) DEMs downloaded from the NOAA's NGDC. Color scale reflects depth in meters.

5.1 Development of a Synthesized Wave Climate for Input into SWAN

Our primary goal was to use existing measured and hindcast wave time series to generate as long a record of the deepwater wave climate as possible for the offshore boundary of the SWAN model, approximately the edge of the continental shelf break. To this end, we downloaded all available National Data Buoy Center (NDBC, http://www.ndbc.noaa.gov/) and Coastal Data Information Program (CDIP, http://cdip.ucsd.edu/) hourly wave buoy data in the region for several wave buoys. **Figure 5-2** shows the various buoys used to derive a synthesized northern Oregon coast wave data set (data availability shown in **Figure 5-3**). In addition to the hourly measured wave buoy data, we obtained wave hindcast information on the deepwater wave climate determined through the Wave Information Studies (WIS, http://wis.usace.army.mil/) (Baird & Associates, 2005).

For the purposes of this study, we used wave hindcast data determined for station 81067 (**Figure 5-2**), which is located adjacent to NDBC buoy #46005. While NDBC #46005 has a high quality, long record of data (1975–2012), it is located in 2,981 m (9,780 ft) of water and is over 400–500 km (250–310 miles) from the shelf edge. Therefore NDBC #46089, a shelf edge, deepwater buoy, was selected as the priority buoy to be used in the SWAN analyses. A buoy (Columbia River #46029) located on the shelf was also included in this analysis, reverse shoaled to deep water to account for wave height changes in intermediate depths. Because of the variation in locations and water depths of the buoys, we needed to develop a methodology to transform these "off-shelf" and "on-shelf" waves to the "shelf-edge" offshore boundary condition of the SWAN model. This was necessary as the wave climates observed at 46005 and 46029 are significantly different than the climate observed at the Tillamook offshore buoy (**Figure 5-4**).

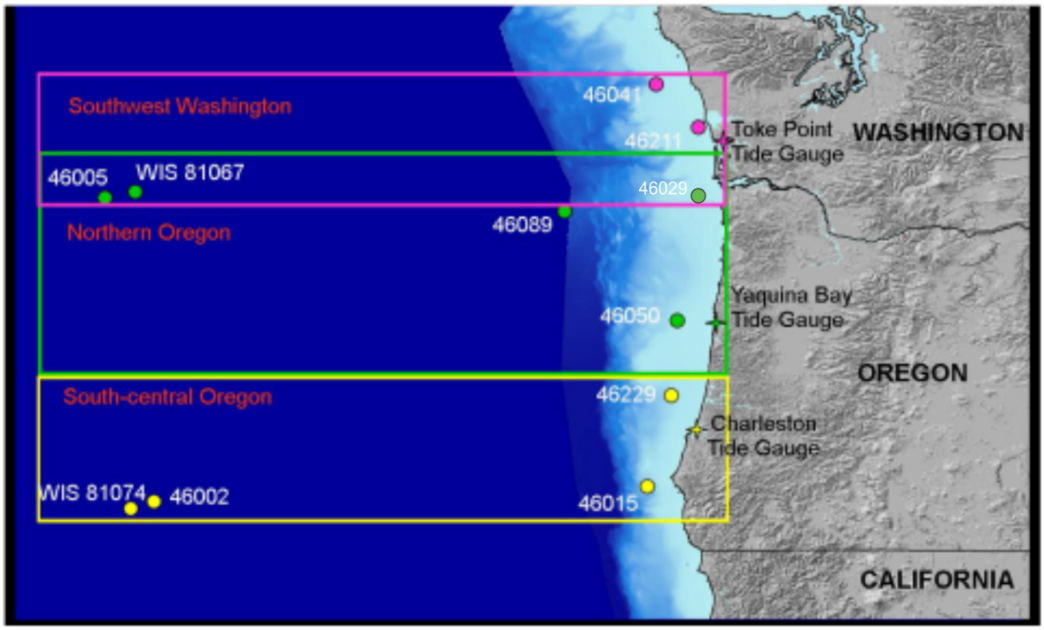

Figure 5-2. Map showing the regional divisions from which synthesized wave climates have been developed.

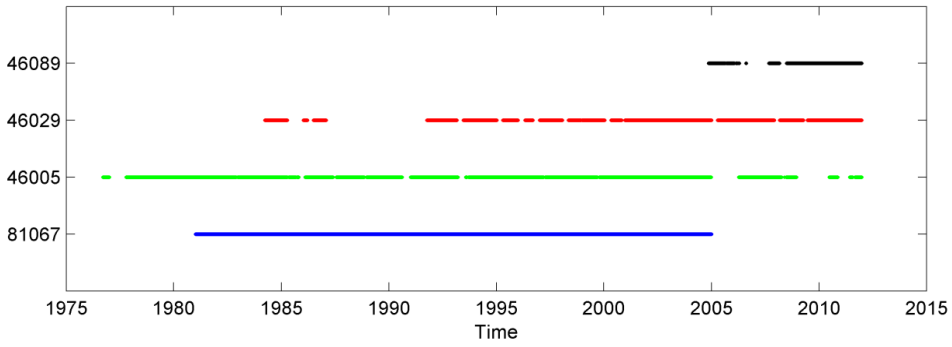

Figure 5-3. Available wave data sets timeline (after Harris, 2011).

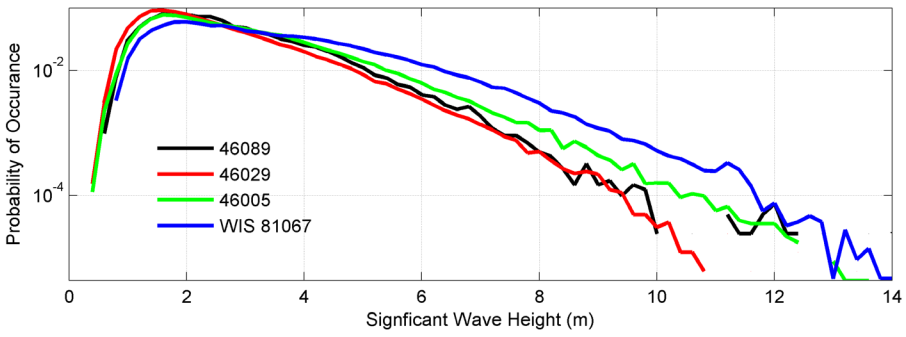

Figure 5-4. Differences in the empirical probability distribution functions of the on shore and off shore buoys.

To transform the 46005 and 46029 waves to the shelf edge, we created wave period bins (0–6, 6–8, 8–10, 10–12, 12–14, 14–16, 16–21, and 21–30 s) to evaluate if there has been a wave period dependent difference in wave heights observed at Washington 46005 and Columbia River 46029 compared with the Tillamook buoy. (Note that the NDBC wave buoys only relatively coarsely resolve long-period waves. Between 21 and 30 s only a wave period of 25 s is populated in the data set. There are no 30-s waves in the time series. Of the waves with periods between 16 s and 20 s, over 80 percent are at approximately 16 s. Only a relatively few waves in the record have recorded periods of 17, 18, and 19 s. This coarse resolution in the raw data determined our choice of period bin widths.) For our comparisons, the time stamps associated with waves measured at either 46005 or 46029 were adjusted based on the group celerity (for the appropriate wave period bin) and travel time it takes the wave energy to propagate to the wave gauge locations. For example, for waves in the period range 10–12 s the group celerity is about 8.3 m/s, and therefore it takes 13 hours for the energy to propagate from 46005 to the Tillamook buoy (**Figure 5-5**).

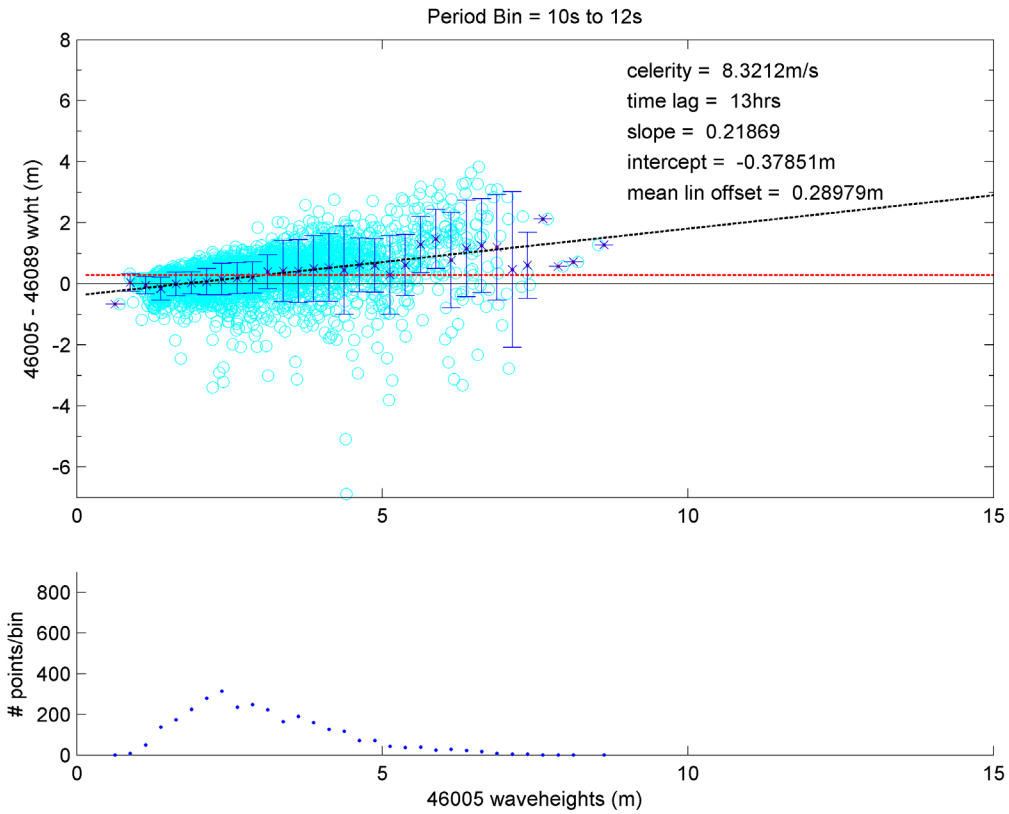

Figure 5-5. Example development of transformation parameters between the Washington buoy (#46005) and the Tillamook (#46089) buoy for period range 10 s to 12 s. In the top panel the dashed black line is the linear regression and the dashed red line is the constant offset. Blue error bars represent the standard deviation of the wave height differences in each period bin (Harris, 2011).

After correcting for the time of wave energy propagation, the differences in wave heights between the two buoys, for each wave period bin, were examined in two ways as illustrated in **Figure 5-5**:

1. A best fit linear regression through the wave height differences was computed for each wave period bin; and
2. A constant offset was computed for the wave height differences for each period bin.

Upon examination of the empirical probability density functions (PDF) of the buoys' raw time series (using only the years where overlap between the buoys being compared occurred) and after applying both transformation methods (**Figure 5-6**), it was determined that the constant offset method did a superior job of matching the PDFs, particularly for the high wave heights. Therefore, a constant offset adjustment dependent on the wave period was applied to the wave heights from the Washington 46005 and Columbia River 46029 buoys. Because the WIS hindcast data used in this study were also located well beyond the boundary of the SWAN model (basically at the location of 46005), the same series of steps comparing WIS wave heights to the Tillamook buoy was carried out, with a new set of constant offsets having been calculated and applied.

After applying the wave height offsets to the necessary buoys, gaps in the time series of Tillamook 46089 were filled in respectively with the Columbia River and Washington buoys. Where there were still gaps following this procedure, we filled in the time series with the corrected WIS data. Because wave transformations (particularly refraction) computed by SWAN are significantly dependent on wave direction, when this information was missing in the buoy records it was replaced with WIS data for the same date in the time series (but the wave height and period remained buoy observations where applicable).

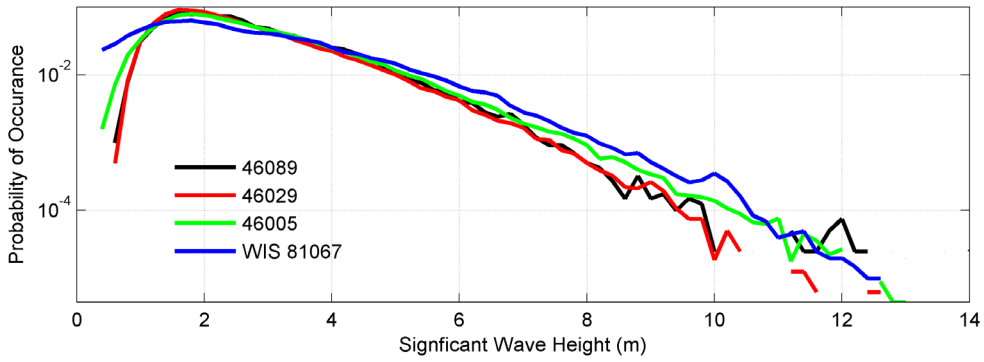

Figure 5-6. Adjusted probability density functions (corrected using the constant offset approach) for buoy 46005 (green line), buoy 46029 (red line), and WIS station 81067 (blue line) as compared to the raw probability density function for buoy 46089 (black line).

The final synthesized wave time series developed for Tillamook County extends from June 1980 through December 31, 2011, and consists of approximately ~31 years of data (measurements including at least wave height and periods) (**Figure 5-7**). Forty-two percent of the synthesized wave climate is from NDBC 46050, 36% from NDBC 4605, 15% from NDBC 46089, and ~7% from WIS station 81067. As can be seen from **Figure 5-7A**, the wave climate offshore from the northern Oregon coast is episodically characterized by large wave events (> 8 m [26 ft]), with some storms having generated deepwater extreme waves on the order of 14.5 m (48 ft). The average wave height offshore from Tillamook County is 2.6 m (8.5 ft), while the average peak spectral wave period is 10.9 s, although periods of 20–25 s are not uncommon (**Figure 5-7B**).

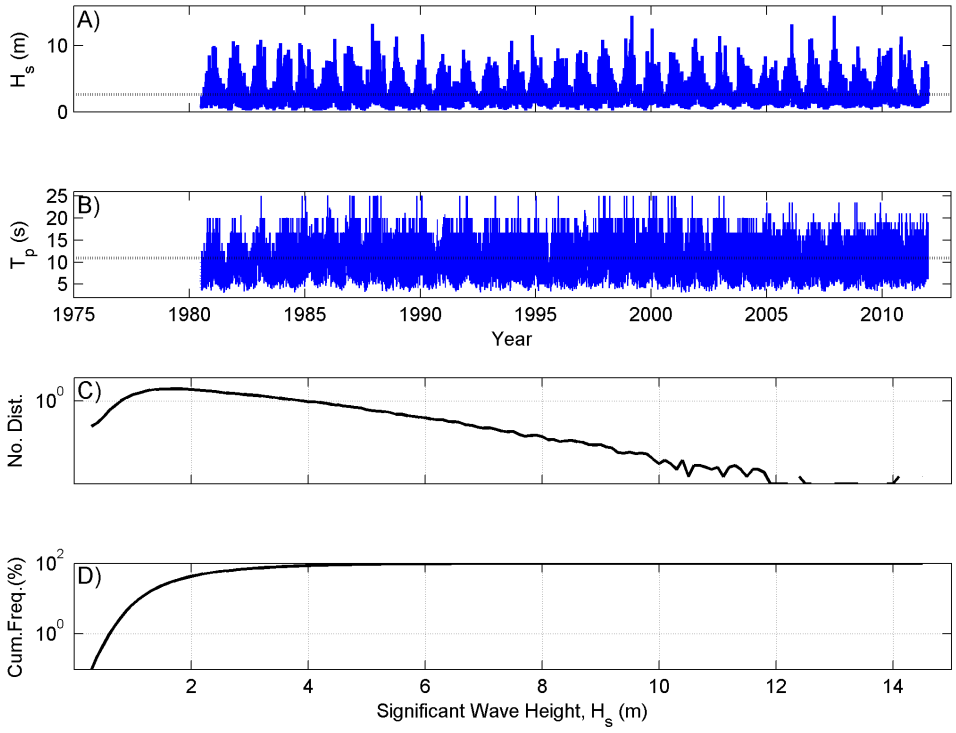

Figure 5-7. Synthesized wave climate developed for Tillamook County. A) Significant wave height with mean wave height denoted (dashed line), B) Peak spectral wave period with mean period denoted (dashed line), C) Probability distribution of wave heights plotted on a semi-log scale, and D) Significant wave height cumulative frequency curve plotted on a semi-log scale.

The PNW wave climate is characterized by a distinct seasonal cycle that can be seen in **Figure 5-8** by the variability in wave heights and peak periods between summer and winter. (The groupings evident in the peak periods (**Figure 5-7B**) are directly from the data and are a product of the data processing methods used by the NDBC to establish the wave frequencies and hence periods. It is for this reason that we chose coarse wave period bins for long-period waves [i.e., > 16 s].) Monthly mean significant wave heights are typically highest in December and January (**Figure 5-8**), although large wave events (>12 m [39.4 ft]) have occurred in all of the winter months except October. The highest significant wave height observed in the wave climate record is 14.5 m (48 ft). In general, the smallest waves occur during late spring and in summer, with wave heights typically averaging ~1.5 m during the peak of the summer (July/August). These findings are consistent with other studies that have examined the PNW wave climate (Tillotson and Komar, 1997; Allan and Komar, 2006; Ruggiero and others, 2010b). **Figure 5-7C** shows a probability density function determined for the complete time series, while **Figure 5-7D** is a cumulative frequency curve. The latter indicates that for 50% of the time waves are typically less than 2.2 m (7.2 ft), and less than 4.4 m (14.4 ft) for 90% of the time. Wave heights exceed 6.9 m (22.6 ft) for 1% of the time. However, although rare in occurrence it is these large wave events that typically produce the most significant erosion and flooding along the Oregon coast.

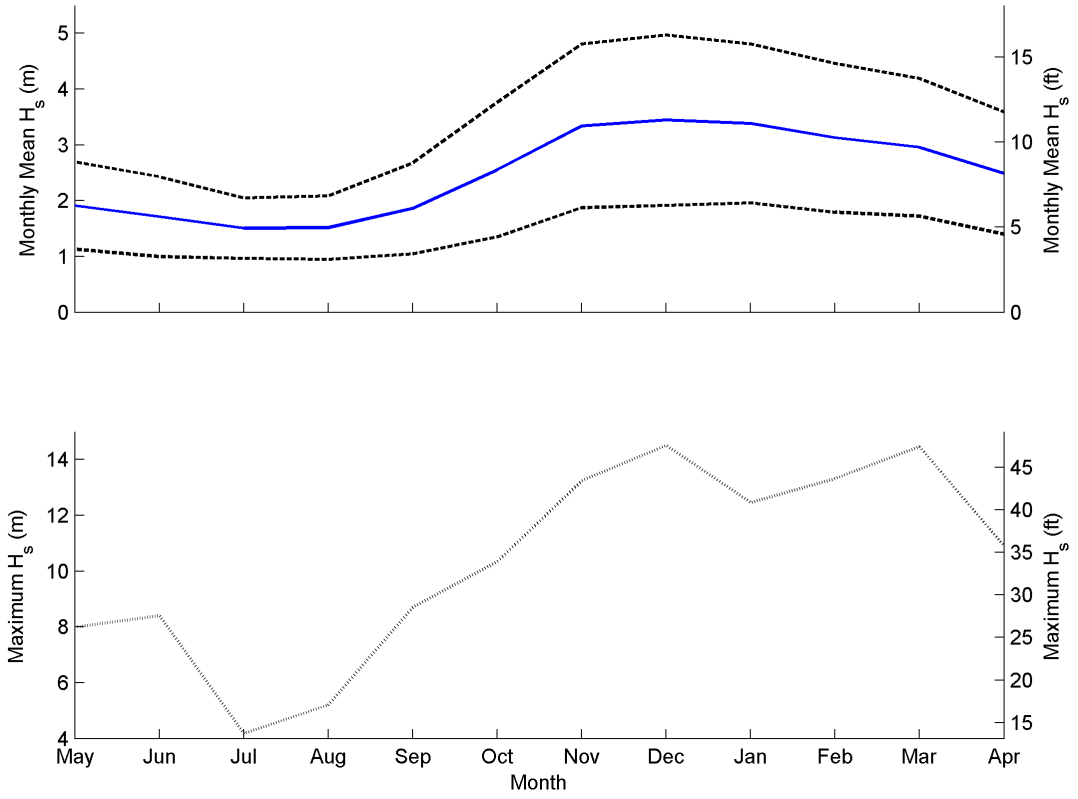

Figure 5-8. Seasonal variability in the deepwater wave climate offshore from the northern Oregon coast. (Top) The monthly average wave height (blue line) and standard deviation (dashed line); (Bottom) The maximum monthly significant wave height.

Finally, **Figure 5-9** provides a wave rose of the significant wave height versus direction developed for the northern Oregon coast. In general, the summer is characterized by waves arriving from the northwest, while winter waves typically arrive from the west or southwest (Komar, 1997). This pattern is shown in **Figure 5-9**, which is based on separate analyses of the summer and winter directional data developed from the synthesized time series. As can be seen in **Figure 5-9**, summer months are characterized by waves arriving from mainly the west-northwest (~48%) to northwesterly quadrant (~42%), with few waves out of the southwest. The bulk of these reflect waves with amplitudes that are predominantly less than 3 m (9.8 ft). In contrast, the winter months are dominated by much larger wave heights out of the west (~23%) and to a lesser extent the northwest (~5.8%), while waves from the southwest account for ~21% of the waves.

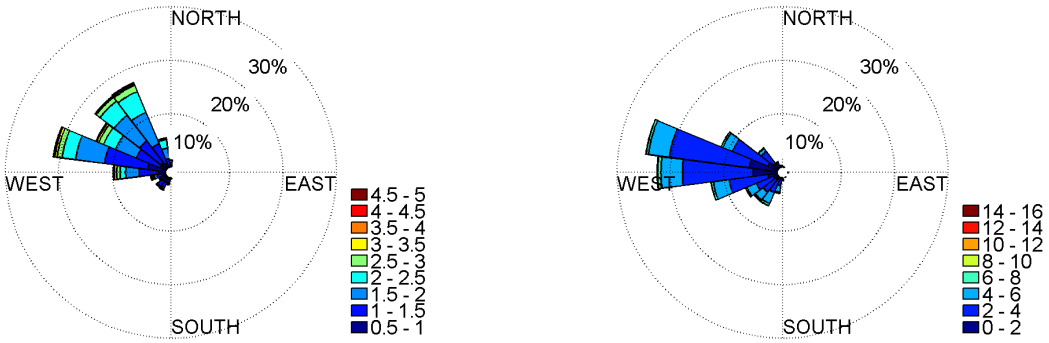

Figure 5-9. (Left) Predominant wave directions for the summer months (June-August), and (Right) winter (December-February). Colored scales indicate the significant wave height in meters.

5.2 Comparison of GROW versus Measured Waves

This section presents a more detailed analysis of GROW Fine Northeast Pacific wave hindcast data compared with measured waves obtained from selected wave buoys offshore from the Oregon coast. The objective here is to better define the degree of congruence between these two contrasting data sets in order to assess their relative strengths and weaknesses. The approach used here is similar to the tide analyses presented in Section 4, using empirical probability density functions (PDFs) to assess the shapes of the distributions. For the purposes of this analysis, PDF plots were derived for the GROW station (#18023) and for NDBC wave buoys 46089, located 66 km (41 mi) northwest of 18023 (**Figure 4-1**), and 46005 (not shown on map), located 540 km (335 mi) west of the Columbia River mouth.

The first plot (**Figure 5-10**) presents a series of significant wave height empirical PDFs for all measured data from NDBC buoys 46005 and 46089 as well as the GROW hindcast data from site 18023. Data from the stations span the following time frames: NDBC 46005 from 1976 through 2010; NDBC 46089 from 2004 through 2010; GROW 18023 from 1980 through 2009. Based on these PDFs, it is immediately apparent that the GROW data contain a larger number of smaller wave heights (in the 2-3 m range) than those measured by the buoys.

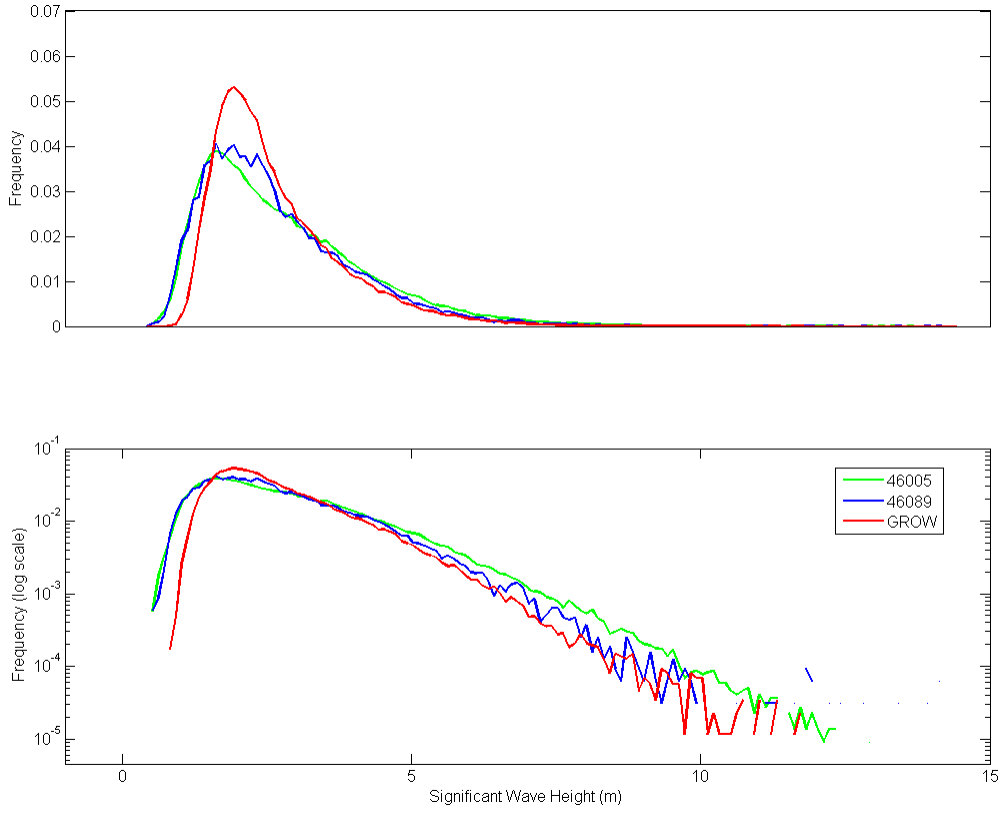

Figure 5-10. Probability density function (PDF) plots of significant wave heights plotted on a normal (top) and log (bottom) scale. Plots include all existing data from these stations.

Additionally, examination of the log-scale plot (bottom of **Figure 5-10**) indicates that the GROW hindcast at 18023 tends to underestimate the more extreme wave heights (waves >7 m), which are the most important for inundation and erosion vulnerability studies. **Table 5-1** lists general statistics of the various data sets where the maximum wave height modeled by GROW is shown to be nearly 3 m lower than that measured by the 46089 buoy. In contrast, GROW indicates on average slightly higher peak periods when compared with the NDBC stations. While differences between NDBC 46005 and NDBC 46089 may simply reflect buoy locations relative to the tracks of the storms, differences between 46089 and GROW 18023 are almost certainly entirely due to the ability of the numerical model to hindcast the waves. Because NDBC station 46089 spans a much shorter measurement period compared with 46005 and the GROW site, the results from the full PDFs may be construed to be misleading. To better assess this potential bias, we again performed analyses of the truncated time series, which revealed nearly identical results to those presented in **Figure 5-10**. Summary statistics for the truncated time series are included in **Table 5-1**. **Figure 5-11** shows a PDF of the peak periods for 46005, 46089, and GROW for the time period 2004–2009. This last plot clearly indicates that GROW is tending to overestimate the higher peak periods when compared with the measured data.

Table 5-1. General statistics of the NDBC buoy and GROW data sets based on the complete time series of data and on truncated time series. Note: *H* denotes the significant wave height and *T* is the wave period.

	46005	46089	GROW
Data availability	1976–present	2004–present	1980–2009
Mean *H*	2.8 m	2.7 m	2.6 m
Max *H*	13.6 m	14.5 m	11.7 m
Min *H*	0.2 m	0.4 m	0.72 m
H standard dev.	1.4 m	1.3 m	1.1 m
Mean *T*	10.8 s	11.1 s	12.6 s
Data availability	2004–2009	2004–2009	2004–2009
Mean *H*	2.8 m	2.6 m	2.6 m
Max *H*	12.7 m	14.5 m	11.7 m
Min *H*	0.5 m	0.4 m	0.9 m
H standard dev.	1.4 m	1.3 m	1.1
Mean *T*	10.6 s	11.1 s	12.7 s

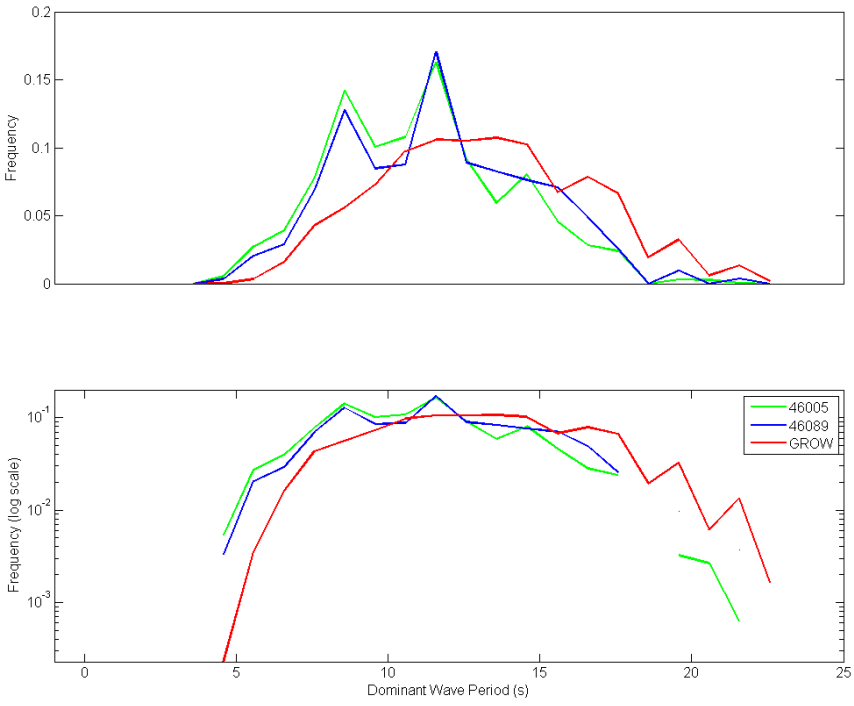

Figure 5-11. Probability density function (PDF) plots of peak wave periods from 2004 through 2009 on a normal (top) and log (bottom) plot.

After examination of PDFs of the various data sets, additional analyses were carried out for selected individual storms in order to better assess how well GROW is performing. The approach adopted was to select the five largest storms measured by the NDBC 46089. The storm events were selected by using a 3-day filter to ensure the selection of independent storm events. Once the peak of the storm was identified, the data (±2 days) were plotted with the GROW data. **Figure 5-12** presents results from two of the five selected storms. In general, our results indicate that while the timing of the events seems to be accurately determined by the GROW model, the magnitude is often lower than that measured by the wave gauges. This result may be due to the GROW approach of only estimating model results every 3 hours as opposed to NDBC's hourly buoy measurements. As a result, sampling at 3 hourly intervals has the potential to miss the peak of the storms. In fairness to GROW, the 3 hourly sampling probably reflects the fact that modeling waves on an hourly basis is dependent on having temporally and spatially suitable meteorological information, which remains a challenge for large-scale regional models.

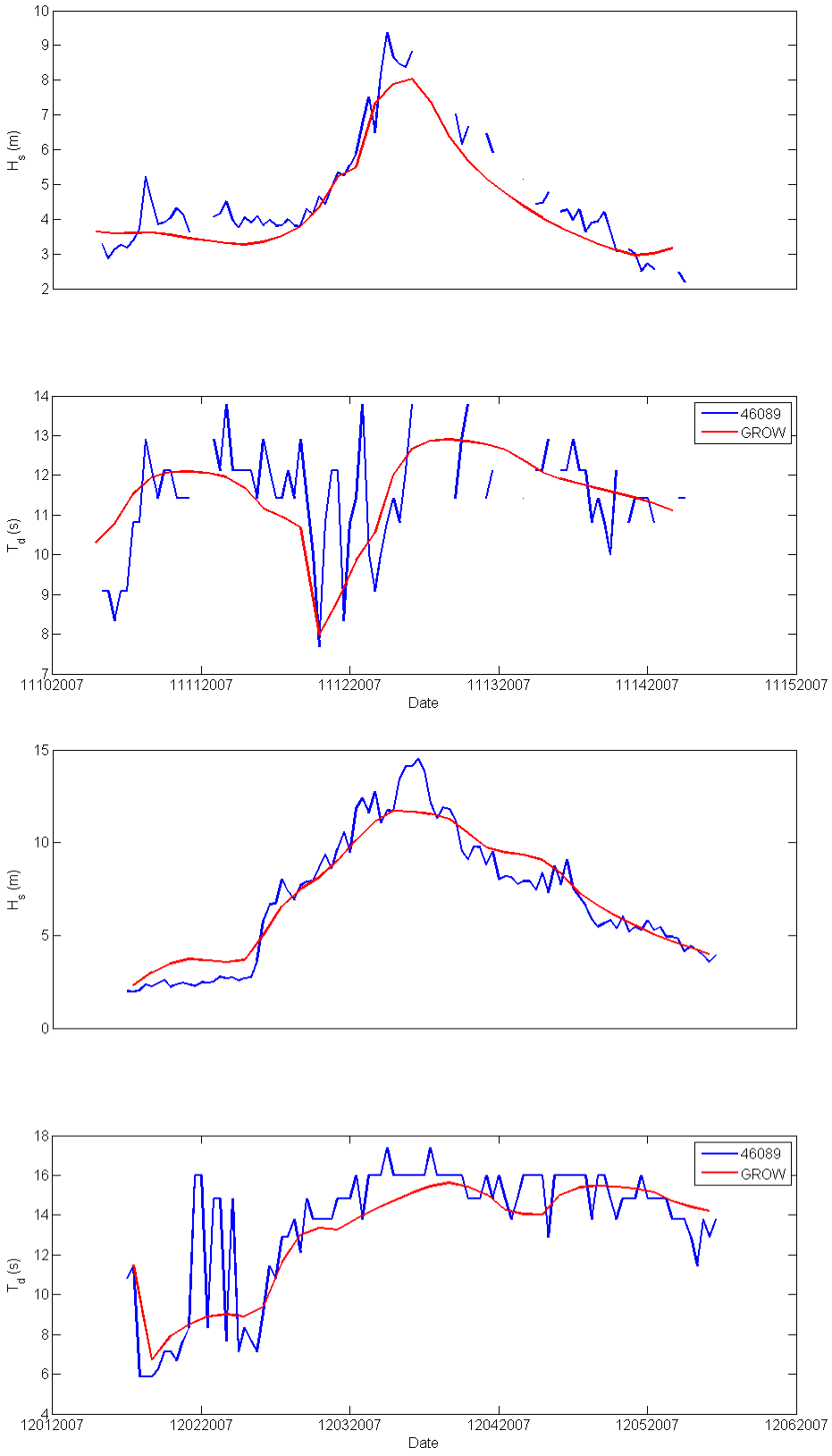

Figure 5-12. Two examples of storms where measured and modeled waves are compared. Top) Storm on November 12, 2007, and Bottom) Major storm event on December 3, 2007.

Finally, we also compared 2% exceedance extreme runup values estimated using the Stockdon and others (2006) approach and waves from the buoys and the GROW station. These results are presented in **Figure 5-13** and were calculated using a representative beach slope (tan β) of 0.04, which is typical for Oregon beaches. Only data from 2004 through 2009 were included in these calculations to provide a standard time frame for the comparison. Results indicate that, just as with the significant wave height PDFs, the extreme runup levels (>2.5 m [8.2 ft]) are underestimated by the GROW model, while the highest calculated runup differs by about 0.4 m (1.3 ft). Although the difference in the calculated runup between GROW and our measured time series is not as large as expected, the shape of the PDF plot would potentially reduce the number of storms available for defining the 100-year wave runup and total water level, as well as in overtopping, inundation, and erosion analyses as required for FEMA detailed coastal studies. From these findings we have concluded that all subsequent modeling of waves should be based, as much as possible, on the measured wave time series as opposed to using GROW hindcast data.

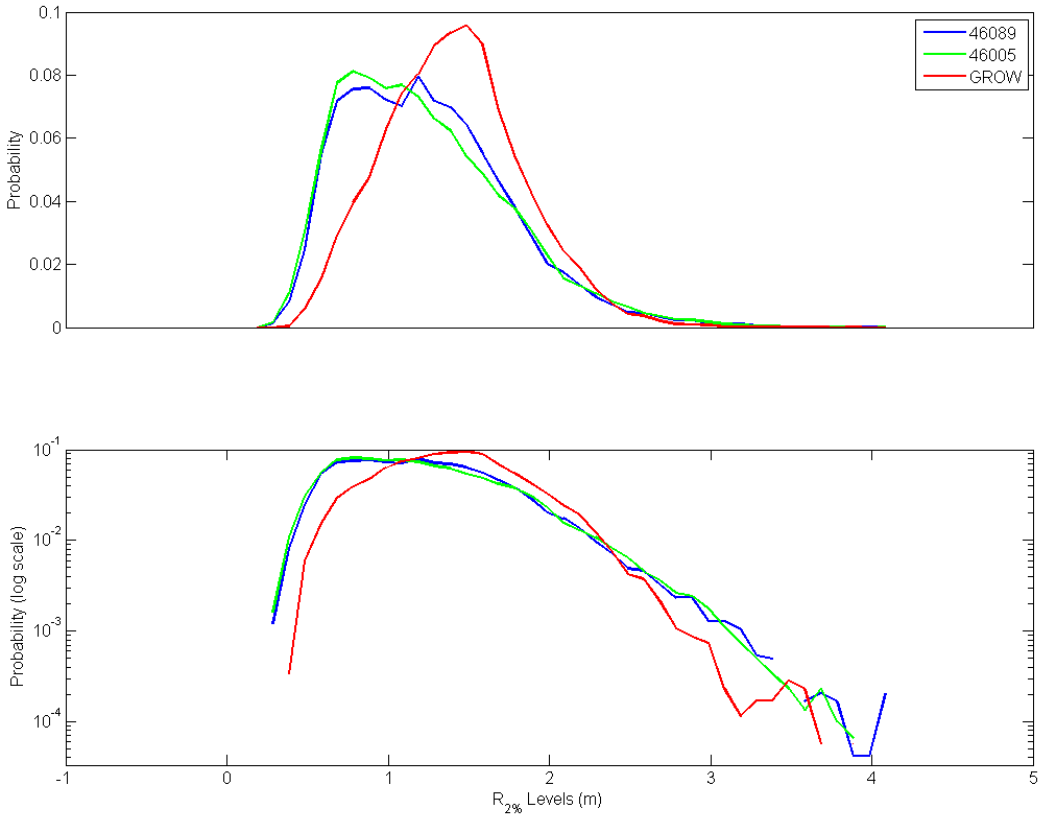

Figure 5-13. Probability density function (PDF) plots of 2 percent extreme runup elevations ($R_{2\%}$) for NDBC 46005, 46089, and GROW hindcast results. An average beach slope of 0.04 was used for runup calculations. The bottom plot is the same as the top, but with the y-axis having been plotted using with a logarithmic scale in order to emphasize the higher wave runup characteristics.

5.3 SWAN Model Development and Parameter Settings

We used the historical bathymetry assembled by the National Geological Data Center (NGDC) (described in Section 3.4) and created a model grid that covers a large portion of the northern Oregon coast (**Figure 5-1**).

SWAN (Simulating WAves Nearshore) version 40.81, a third-generation wave model developed at the Technical University of Delft in the Netherlands (Booij and others, 1999; Ris and others, 1999), was used in this study. The model solves the spectral action balance equation using finite differences for a spectral or parametric input (as in our case) specified along the boundaries. For the Tillamook County study, the cross-shore and alongshore resolution of the model grid used is 100*100 m. The total grid area is 72 km by 139 km in length, which yields 716*1,390 computational nodes. The SWAN runs were executed in stationary mode and included physics that account for shoaling, refraction, and breaking, while model settings varying from the default values are discussed in more detail below.

The north, south, and west boundaries of the model were specified using grid coordinates and forced using a parameterized JONSWAP spectrum. The functions for spectral peakedness parameters γ and *nn* in the JONSWAP directional spectra are given as:

$$\gamma = \begin{cases} 3.3 \; if \; Tp < 11s \\ 0.5Tp - 1.5 \; if \; Tp \geq 11s \end{cases}$$

$$nn = \begin{cases} 4 \; if \; Tp < 11s \\ 2.5Tp - 20 \; if \; Tp \geq 11s \end{cases} \qquad (5.1)$$

Thus, the directional distribution is generated by multiplying the standard JONSWAP frequency spectrum by $cos^{nn}(\theta - \theta_{peak})$ (Smith and others, 2001). Wind wave spectra are broad (low γ and *nn* values) while swell typically have narrow distributions (high γ and *nn* values). The values used in the SWAN wave modeling were based on the input peak periods which ranged 4.055 ≤ γ ≤ 11.03 and 7.775 ≤ nn ≤ 42.65. To ensure that the wave directional spread is sufficiently resolved by the model, we specified directional bins giving a 4-degree directional resolution. The spectrum was discretized in frequency space with 29 bins from 0.032 to 1 Hz. Wind was not included in the SWAN simulations and therefore no energy growth due to wind or quadruplet wave-wave interactions occur in the simulations. Triad interactions, diffraction, and wave setup also were not activated in the model. We used the Janssen frictional dissipation option, which has a default friction coefficient of 0.067 m^2/s^3. No model calibration was performed in this study, although several numerical experiments were implemented to test various assumptions in the wave modeling (e.g., not to use winds).

5.3.1 Wind effects

The decision not to model the effect of winds on wave growth over the continental shelf in our original Coos County study (Allan and others, 2012) was based on two observations:

- To develop our combined wave time series described previously, we performed a "statistical" wave transformation between buoy 46002 and the buoys at the edge of the continental shelf and found that, in general, the wave heights during storm events decreased even with hundreds of kilometers of additional fetch. Without understanding the details of this phenomenon (e.g., white capping versus wind wave growth) and with no data for calibration we felt that attempting to model wind growth would add to the uncertainty of our input wave conditions.
- We also have previous experience with SWAN wave modeling in the region (U.S. Pacific Northwest) in which sensitivity runs including wind were performed with only minor impact on results (Ruggiero and others, 2010a).

To test the validity of the assumptions made in our Coos County study, several wave modeling experiments were performed in order to specifically examine the role of additional wind wave development over the shelf. The basic question that was addressed is: How much do wind fields result in wave growth between the location of the GROW stations that were purchased (an off-shelf location roughly equivalent to the offshore extent of the Tillamook (46089) buoy shown in **Figure 4-1**) and the inner shelf. The latter was defined as the 100 m (300 ft) isobath. To address

this question, hindcast waves were modeled for the months of January and February (i.e., peak of the winter season) and for two representative years (2006 and 2010). The wave modeling was accomplished by running a regional Eastern North Pacific (ENP) model and a 3 arc-min grid for the Oregon coast, with the outer boundary coinciding with the Tillamook buoy station (**Figure 5-14**). The model runs were forced by analyzed Global Forecast System winds with a temporal resolution of 6 hours and a spatial resolution of 1 arc-degree. A similar run was undertaken without winds over the same 3 arc-min grid, just propagating the boundary conditions. Hindcast wave data were obtained from selected points across the shelf at contour depths of 500, 400, 300, 200, and 100 m along a cross-shore transects from the offshore GROW station (A and B in **Figure 5-14**).

Results from the model runs (with and without winds) are presented in **Figure 5-15** and **Figure 5-16**. Modeled and measured waves for two NDBC buoys (46089 and 46029) are included for comparative purposes (**Figure 5-17** and **Figure 5-18**). In general, our experiments indicated that although the addition of wind sometimes changed the timing of the large wave events, producing at times a relatively large percentage error for part of the "wave hydrograph," the peaks of the wave events showed very little difference between cases where wind was included or excluded (**Figure 5-15** and **Figure 5-16**). Furthermore, in the majority of cases, the differences in the derived wave heights between model runs including (excluding) wind (no wind) were on the whole minor. This finding was also observed in the derived peak wave periods, which appear to be virtually identical in all the plots. Of greater concern in these model tests are the occasional large differences between the modeled runs (irrespective of whether wind/no wind is applied) and the actual measurements derived from NDBC wave buoys (**Figure 5-17** and **Figure 5-18**), as well as the GROW data derived for station 18023. These latter findings will be explored in more detail later in this section.

These experiments support our decision to not include wind growth in our model runs, and therefore quadruplet wave-wave interactions were also not incorporated in the simulations. Further, wave setup is not included in the simulations because we extract the transformed wave parameters at the 20-m depth contour and use the Stockdon and others (2006) empirical model to compute wave runup (which incorporates setup) along the coast.

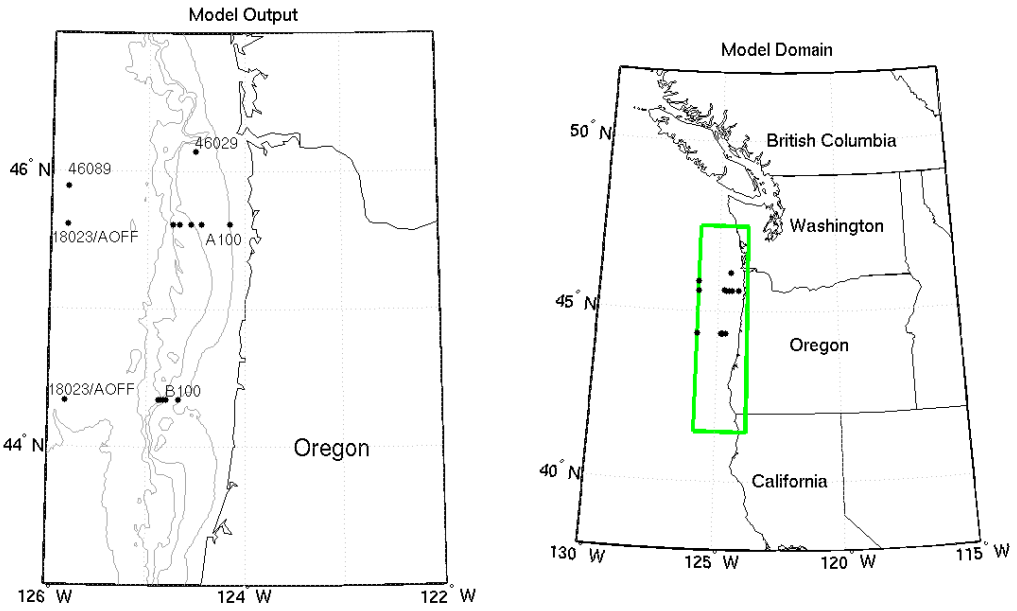

Figure 5-14. Left) Map showing the locations of the northern Oregon coast buoys, and transect lines (A and B), and Right) model domain.

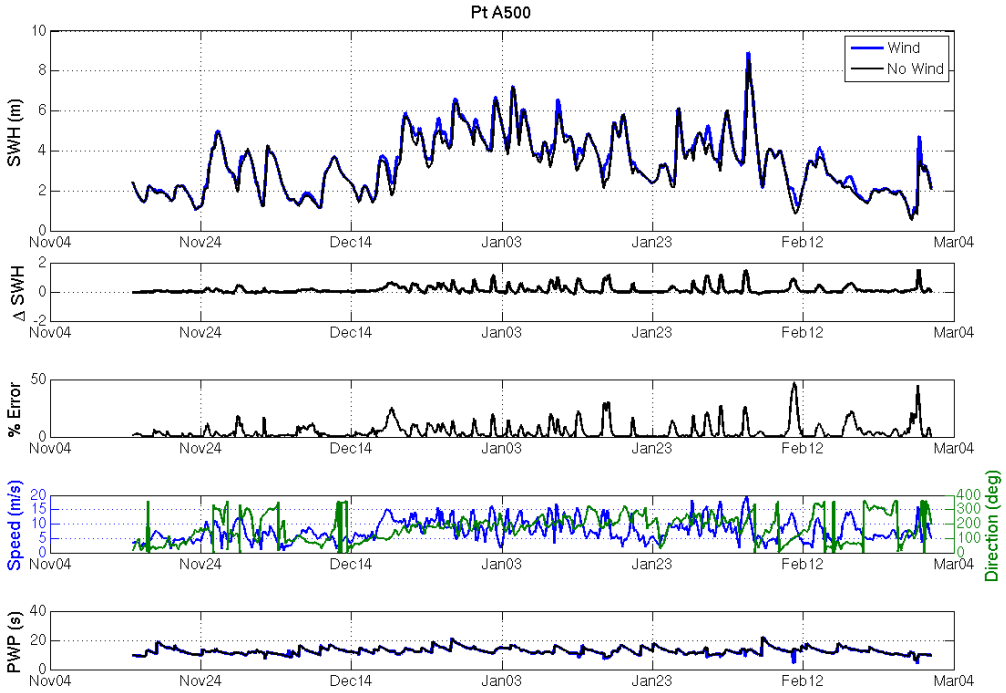

Figure 5-15. Model-model comparison at 500-m depth on transect A for the 2006 simulation.

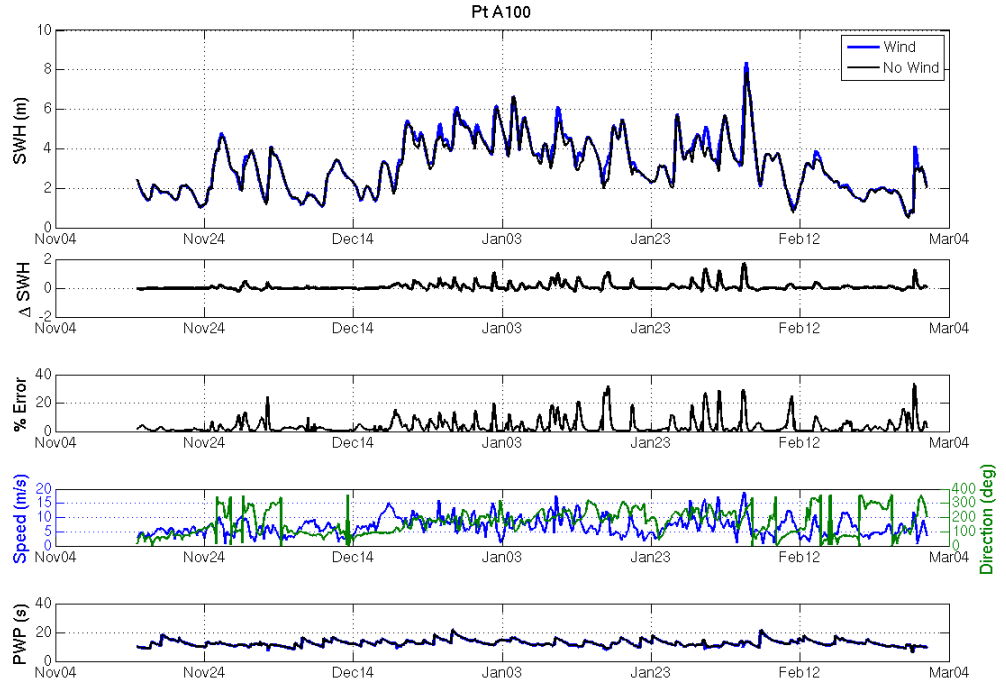

Figure 5-16. Model-model comparison at 100-m depth on transect A for the 2006 simulation.

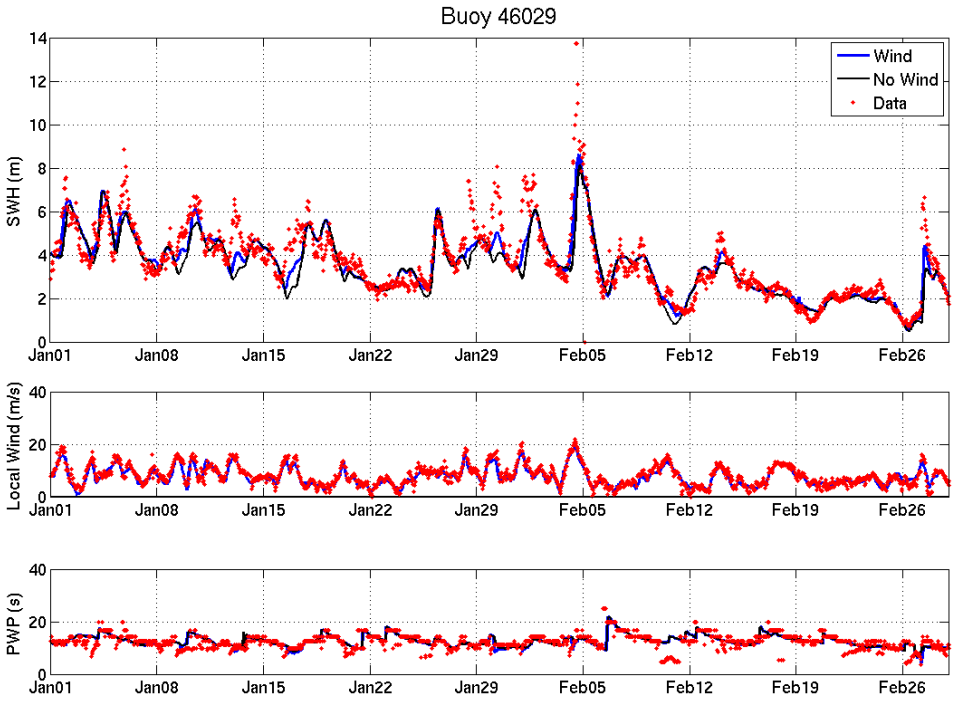

Figure 5-17. Model data comparison at NDBC buoy #46029 for the 2006 simulations.

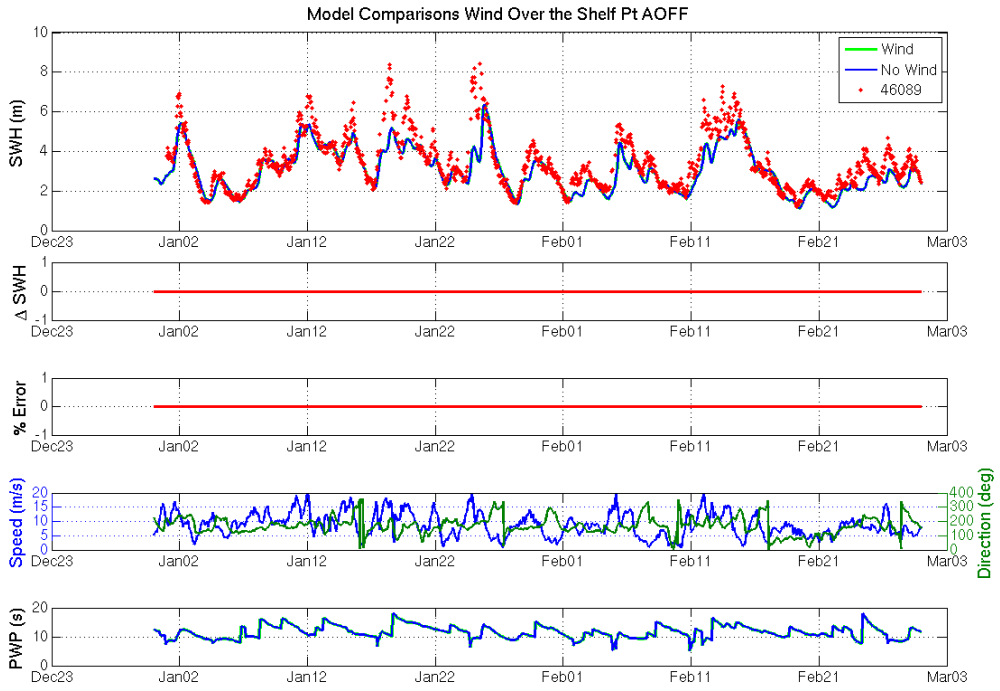

Figure 5-18. Model data comparison at Station Aoff (GROW station location) versus NDBC buoy #46089 for the 2010 simulations.

5.3.2 Frictional and Whitecapping Dissipation of the Wave Energies

Additional testing was undertaken to explore the effect of not including friction and whitecapping. **Figure 5-19** and **Figure 5-20** provide two test case conditions associated with a significant wave height of 10 m and peak period of 20 s, with the waves approaching from a direction of 285 degrees (NW), while the second case is for a significant wave height of 14 m, peak period of 14 s, with the waves approaching from a direction of 270 degrees (W). **Figure 5-19** indicates that for this particular condition, the modeled results are relatively similar until immediately prior to wave breaking, where significant differences arise. However, as the significant wave height increases (**Figure 5-20**) the effect of excluding bottom friction and whitecapping becomes considerably larger. The exclusion of these processes results in an overestimation of wave heights prior to breaking. Therefore, we have chosen to include frictional dissipation and dissipation due to whitecapping in our modeling.

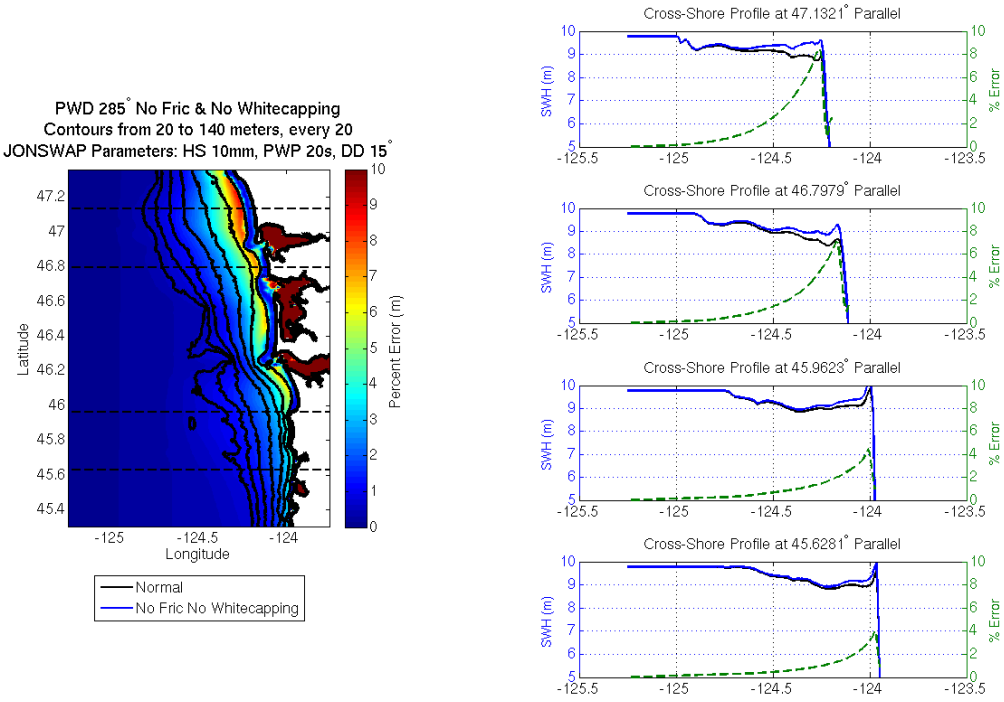

Figure 5-19. The impact of ignoring bottom frictional dissipation and dissipation due to whitecapping for a 10-m significant wave height with a peak period of 20 s approaching from a direction of 285 degrees.

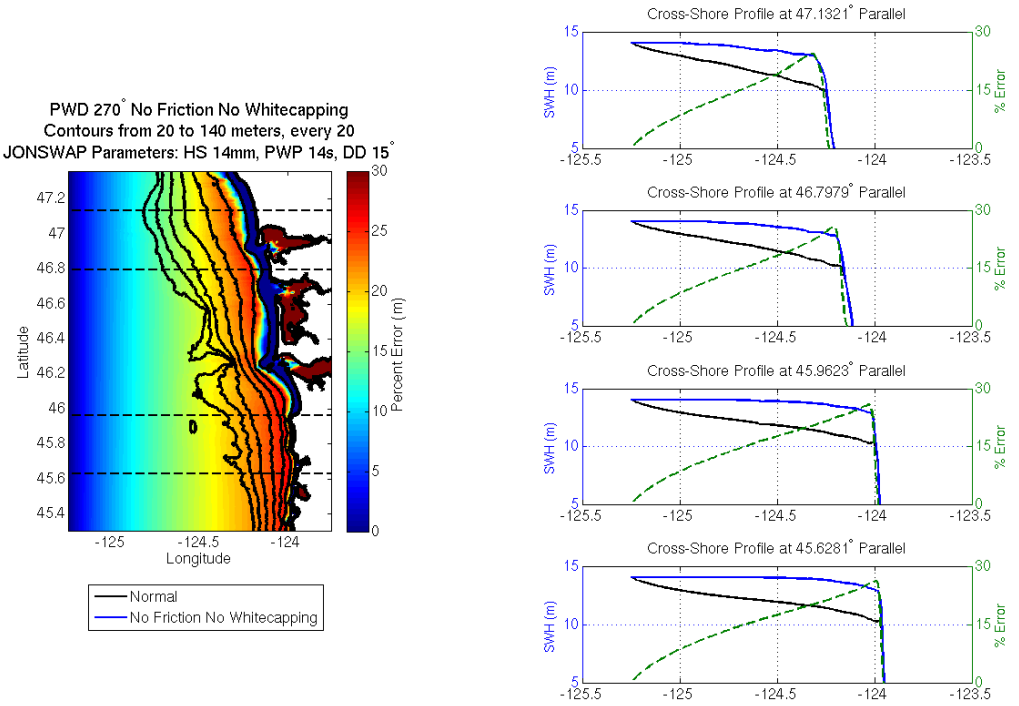

Figure 5-20. The impact of ignoring bottom frictional dissipation and dissipation due to whitecapping for a 14-m significant wave height with a peak period of 14 s approaching from a direction of 270 degrees.

5.3.3 Lookup table development

Having demonstrated that winds have little impact in terms of additional wave development across the continental shelf of Oregon, our next goal was to develop an efficient methodology that could be used to minimize the total number of SWAN runs needed to perform the actual wave modeling and transformations, while ensuring that we resolve the influence of varying parameters on the wave transformations. To do this, we discretized the significant wave height (H_s), peak period (T_p), wave direction (D_p), and water level (WL) time series.

For the direction bins (D_p), the bin widths were made approximately proportional to the probability distribution function of the GROW time series (and the synthesized wave climate time series). In application of this approach in our Clatsop County study, 11 directional bins were created that have approximately an equal probability of occurrence (**Figure 5-21**). As defined, the bin edges are: D_p = [170, 225, 240, 251, 260, 268, 277, 288, 304, 331, 370] and were subsequently refined in SWAN to D_p = [170, 225, 240, 250, 260, 270, 280, 290, 305, 330, 370], resulting in 11 direction cases for our SWAN runs. At the bin edges, linear interpolation is used to derive the wave parameters. Using initial sensitivity runs undertaken as part of our Clatsop County study, we have determined that these bin widths are more than adequate. **Figure 5-22** shows the result of interpolating over a 20-degree bin spacing.

For the purposes of the Tillamook County work, we further refined our original approach to include an additional two directional bins. This was accomplished by refining the spread of the bins to better reflect the observed conditions offshore Tillamook and Lincoln Counties. The final bin edges are defined as: D_p = [175, 205, 225, 240, 250, 260, 270, 280, 290, 300, 315, 335, 365].

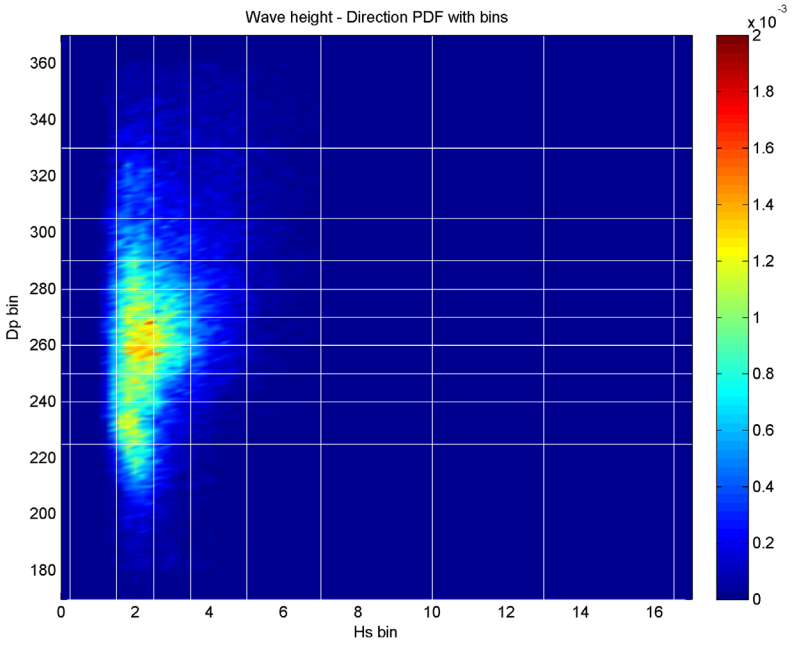

Figure 5-21. Joint probability of wave height and dominant direction derived from the GROW time series. Overlaid in white are the wave height and direction bins for use in the wave modeling on the Clatsop coast.

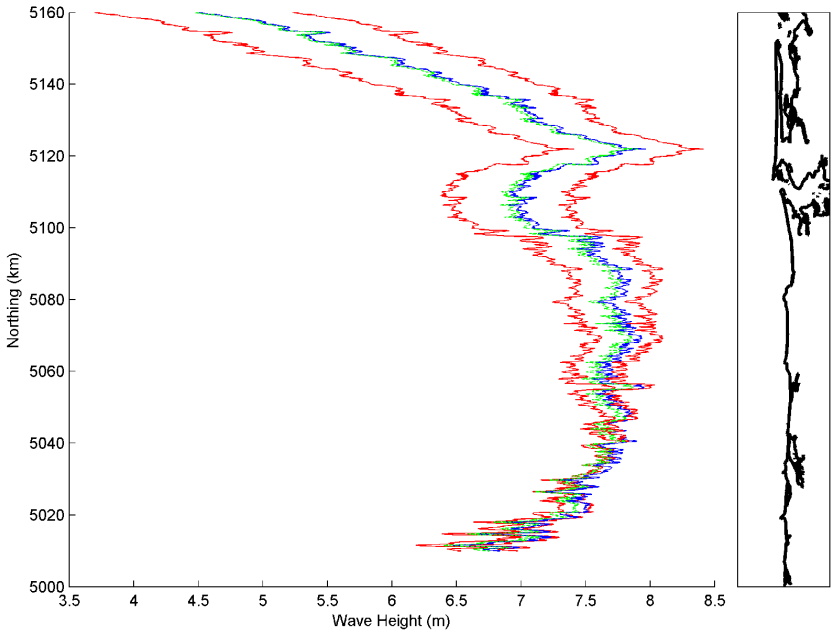

Figure 5-22. SWAN wave modeling and calculated alongshore wave variability using the look-up table approach. The left red line represents the alongshore variable wave height at the 20-m depth contour for an incident angle of 240 degrees (H_s = 10, T_p = 15 s) and the right red line is for an angle of 260 degrees. The blue line is the wave height for an angle of 250 degrees as modeled in SWAN, while the green line represents the linearly interpolated wave heights using the look-up table. Note that this is a preliminary SWAN model run, meant for testing the interpolation scheme, and the lateral boundary conditions are not dealt with in the same manner as in our production SWAN runs.

For the significant wave heights bins, we identified the following deepwater significant wave heights for inclusion in SWAN: H_s = [0.25, 1.5, 2.5, 3.5, 5, 7, 10, 13, 16.5], which gives us nine cases. From our sensitivity tests, we found that a bin width of 3 m for large waves is sufficient for resolving the linearly interpolated wave conditions (**Figure 5-23**). In the case of the deepwater peak periods, our analyses identified the following period bins for inclusion in SWAN: T_p = [2, 4, 6, 9, 11, 13, 15, 17, 20, 23, 26], which provides a total of 11 additional cases. From our sensitivity tests, we found that the linear interpolation approach for wave period is not quite as good as for direction and wave height. Because wave period affects breaking, shoaling, and whitecapping, there is significant variability in the wave transformations as a function of wave period. For our sensitivity run of H_s = 10 m, and D_p = 260 degrees, **Figure 5-24** illustrates the impact of linear interpolation. However, for the most part in our parameter space we will have interpolation errors only around 10%. In this particular example the maximum error is only approximately 4 percent.

Figure 5-25 presents the joint probability of wave height and peak period from the GROW time series. The white dots represent bin centers, from a much smaller mesh, in which this combination of H_s and T_p does not exist in the GROW time series. The red line represents the theoretical wave steepness limit below which waves are nonphysical. We can use this information to reduce the overall matrix of model runs.

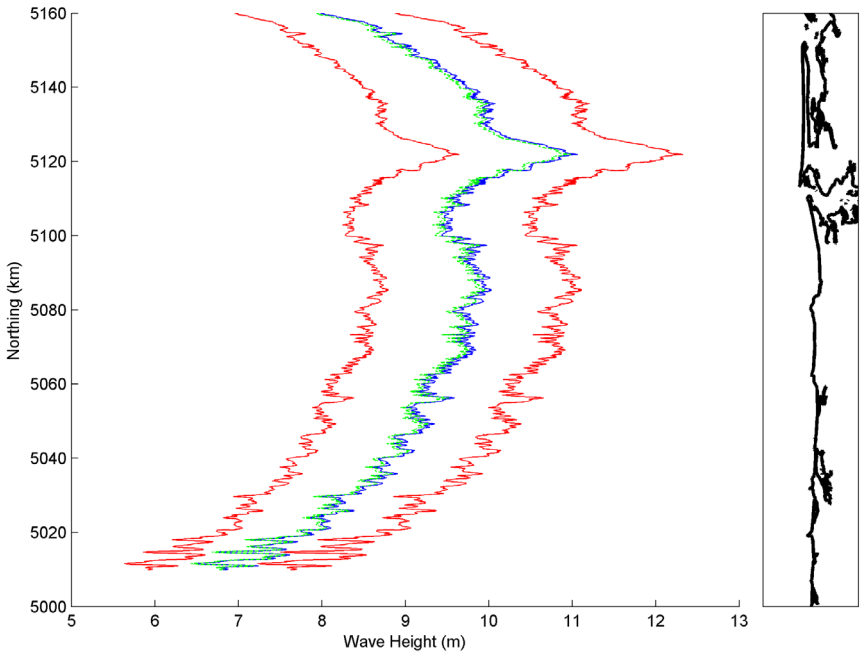

Figure 5-23. SWAN wave modeling and calculated alongshore wave variability using the look-up table approach for an 11-m and 15-m wave. In this example the red lines are the alongshore varying wave height for an 11-m and 15-m incident wave height in 20 m. The blue line is the modeled transformed 13-m wave height, while the green represents a linear interpolation between the 11- and 15-m results.

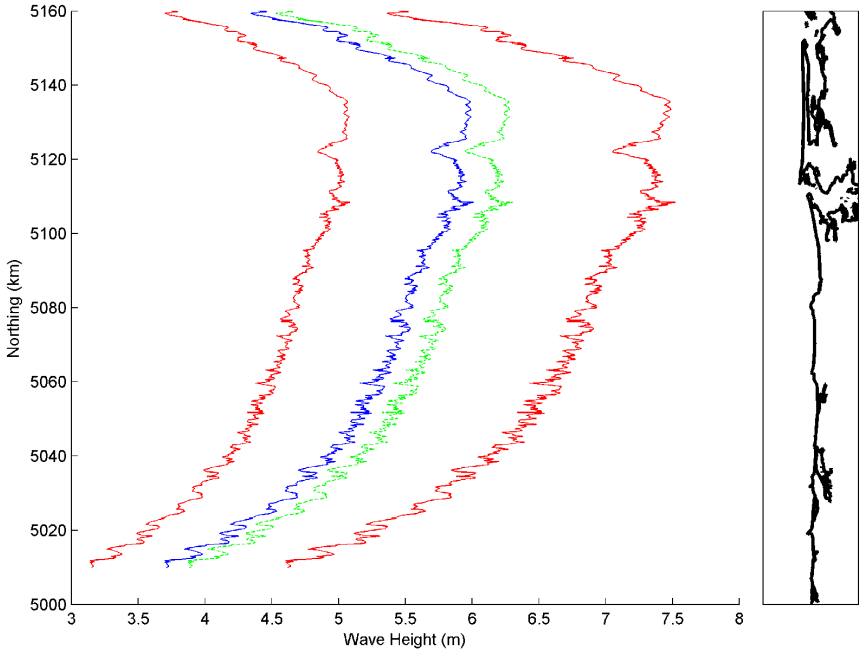

Figure 5-24. SWAN wave modeling and calculated alongshore wave variability using the look-up table approach for a 10-m wave. In this example the red lines are the alongshore varying wave height for a 10-m wave arriving from 260 degrees for 20 s and 24 s. The blue line is the modeled wave height for 22 s, and the green line represents a linear interpolation.

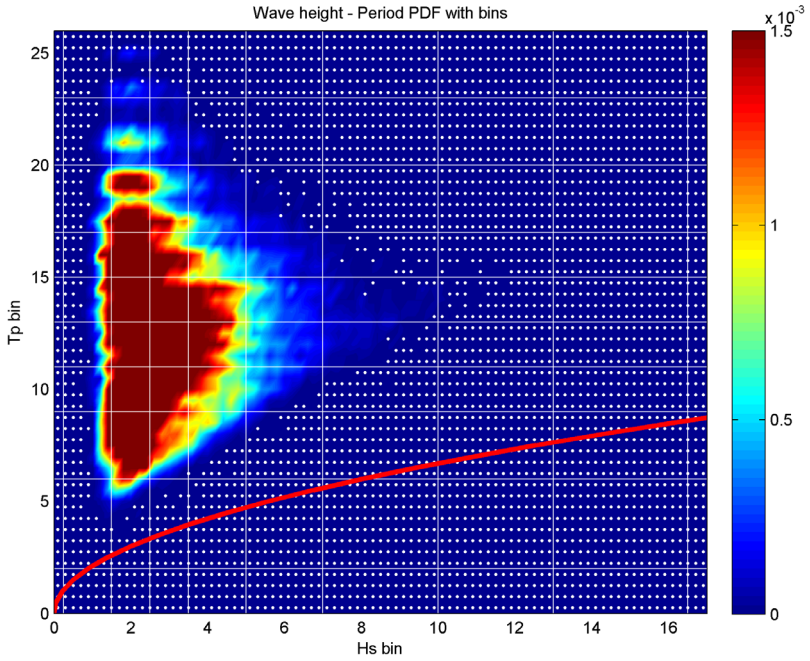

Figure 5-25. Joint probability of wave height and peak period from the GROW time series. The white dots represent bin centers, from a much smaller mesh, in which this combination of Hs and Tp does not exist in the GROW time series. The red line represents the theoretical wave steepness limit below which waves are nonphysical.

Figure 5-26 is the joint probability of peak period and dominant wave height shown here for completeness. Finally, we illustrate our bin choice on the individual parameter PDFs in **Figure 5-27** (buoy data).

In summary, the lookup tables were generated using all wave parameter cases and two contrasting water levels. Our sensitivity tests indicated that varying water levels have a negligible impact on the model and linearly transformed waves. The following matrix of SWAN runs is considered for lookup table development for transforming waves offshore from Tillamook County:

D_p = [175, 205, 225, 240, 250, 260, 270, 280, 290, 300, 315, 335, 365] — 13 cases
H_s = [0.25, 1.5, 2.5, 3.5, 5, 7, 10, 13, 16.5] — 9 cases
T_p = [2, 4, 6, 9, 11, 13, 15, 17, 20, 23, 26] — 11 cases
WL = [-1.5, 4.5] — 2 cases

In total, this equates to 2,574 model cases that can be used for linearly interpolating the waves from a time series of data. However, **Figure 5-25** indicates that several H_s–T_p combinations are physically not realistic. Multiplying these bins by the D_p and WL bins means that we can eliminate 390 bins for a new total of only 2,184 model runs.

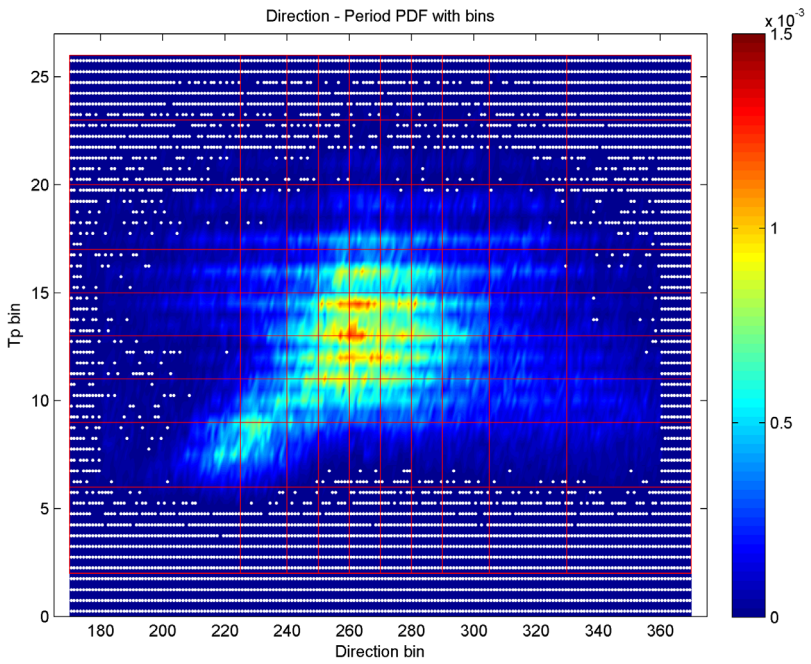

Figure 5-26. Joint probability of dominant direction and peak period from the GROW time series. The white dots represent bin centers, from a much smaller mesh, in which this combination of D_p and T_p does not exist in the GROW time series. The red lines depict the boundaries of the binning.

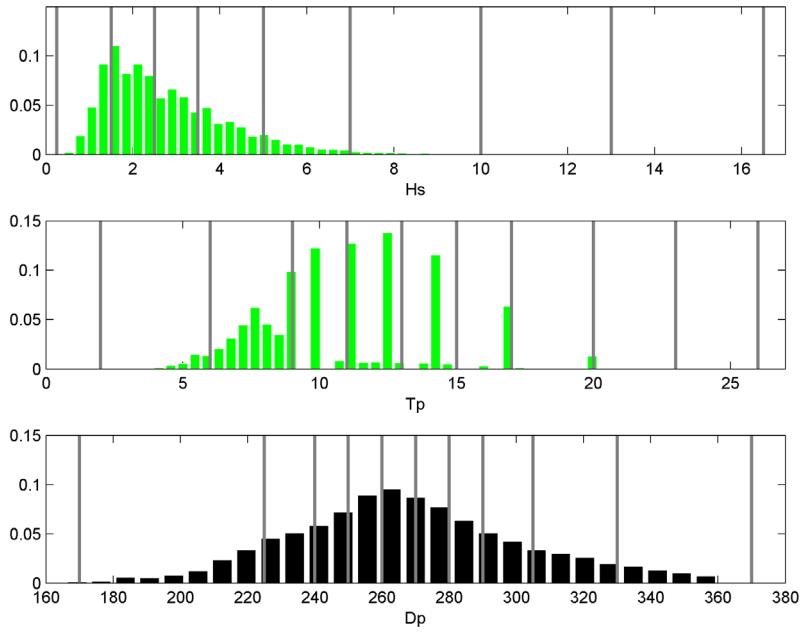

Figure 5-27. Individual parameter probability density function plots and bin edges using the combined buoy wave time series.

5.4 Summary of SWAN Results

Significant alongshore variability is apparent in many of the conditions examined with SWAN (**Figure 5-28**). Differences on the order of 3 m in significant wave height along the 20-m isobaths are not uncommon in Tillamook County. To calculate the wave runup along the County's shoreline, we subsequently extracted the wave characteristics along the 20-m contour, or the seawardmost location where the wave breaking parameter equaled 0.4, throughout the model domain (**Figure 5-28**, right panel). Because all of the parametric runup models used in this study rely on information on the deepwater equivalent wave height and peak periods as inputs, we then computed the linear wave theory shoaling coefficient and back shoaled our transformed waves to deep water. These transformed deepwater equivalent waves were then used to calculate the wave runup and generate the TWL conditions used in the subsequent extreme value analysis.

To confirm that our approach of interpolating wave transformations using lookup tables yields acceptable results, we ran several additional SWAN runs that were not part of our original matrix. These additional runs extended across a range of conditions, including extreme events capable of forcing high water levels at the coast. We then compared the results from using the lookup tables to these additional direct SWAN computations at the 20-m contour location. **Figure 5-29**, **Figure 5-30**, and **Figure 5-31** show a sample of these results for wave heights, peak periods, and directions, respectively, for a SWAN run driven with an offshore boundary condition of H_s = 11.5, T_p = 18.5, D_p = 320, and a water level of 4.5 m NAVD88. In all cases, the percentage error between the lookup table and direct computation is low, averaging well less than 5 percent. In only a few locations, near model boundaries or inlets, are the errors significant. None of the transects analyzed in detail for extreme flooding later in this report are near those problem locations.

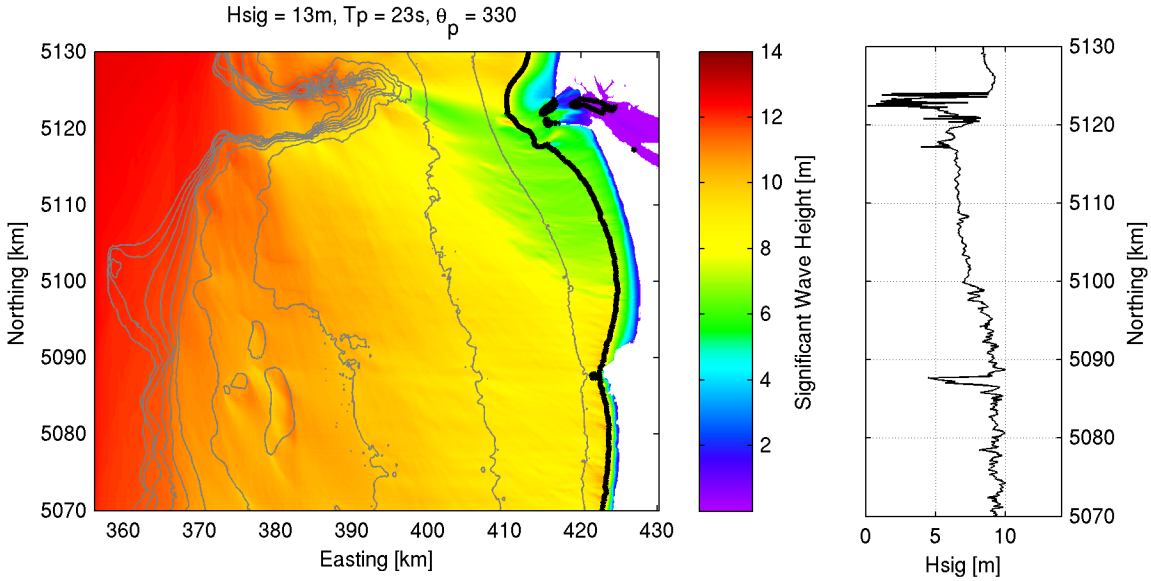

Figure 5-28. Example SWAN simulation, for an offshore significant wave height 13 m, peak wave period 23 s, and peak wave direction of 330°. Left) Significant wave height in the modeling domain is shown in colors. Dissipation processes result in reduced wave height. Contour lines are drawn from 50 to 500 m every 50 m in grey and every 20 m in black. Right) Modeled significant wave height extracted at 20-m water depth.

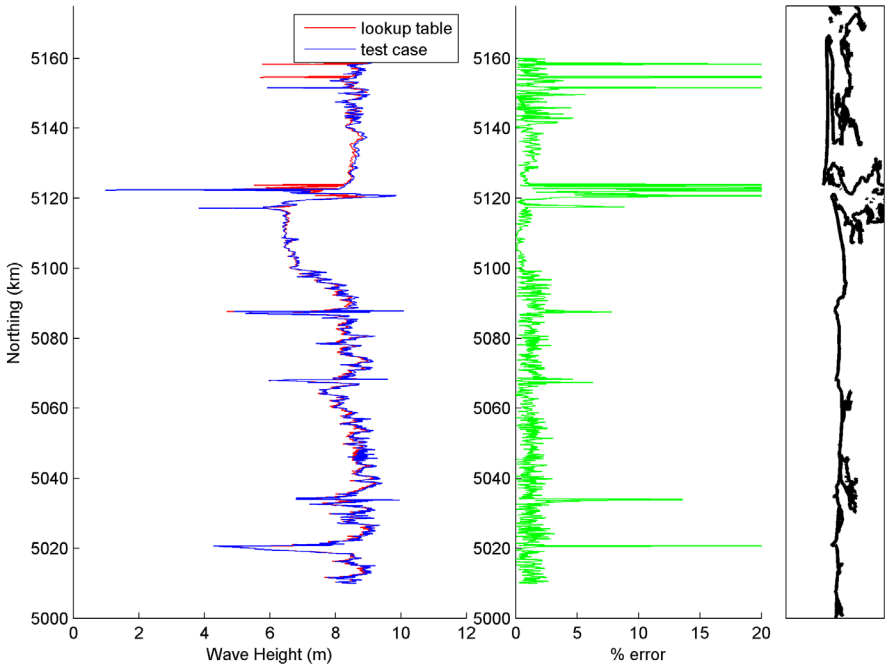

Figure 5-29. Comparison of alongshore varying wave height at the 20-m contour extracted from the lookup tables (red line) and from a direct SWAN computation (blue line) with an offshore boundary condition characterized as H_s = 11.5, T_p = 18.5, D_p = 320, and a water level of 4.5 m NAVD88.

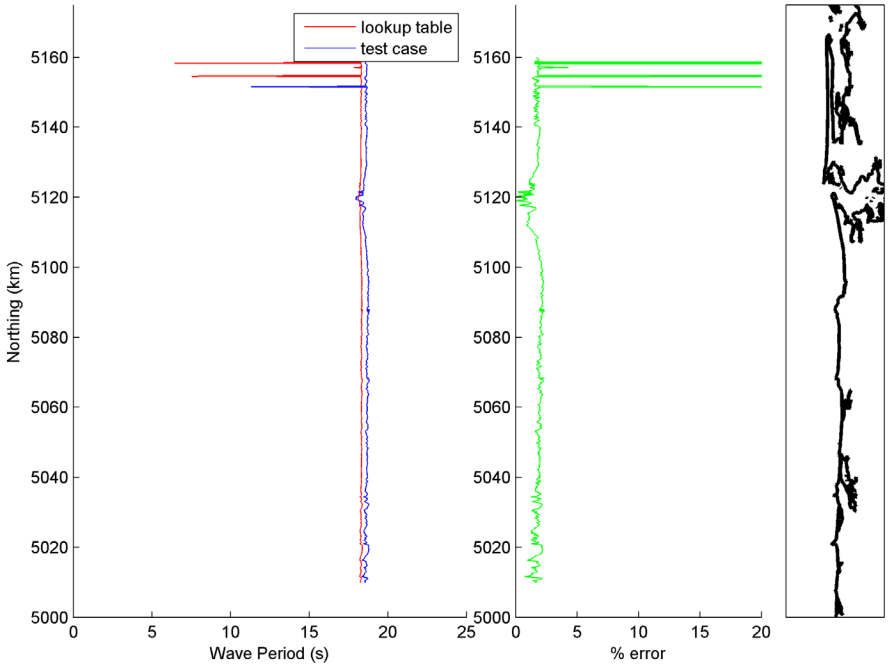

Figure 5-30. Comparison of alongshore varying wave period at the 20-m contour extracted from the lookup tables (red line) and from a direct SWAN computation (blue line) with an offshore boundary condition characterized as H_s = 11.5, T_p = 18.5, D_p = 320, and a water level of 4.5 m NAVD88.

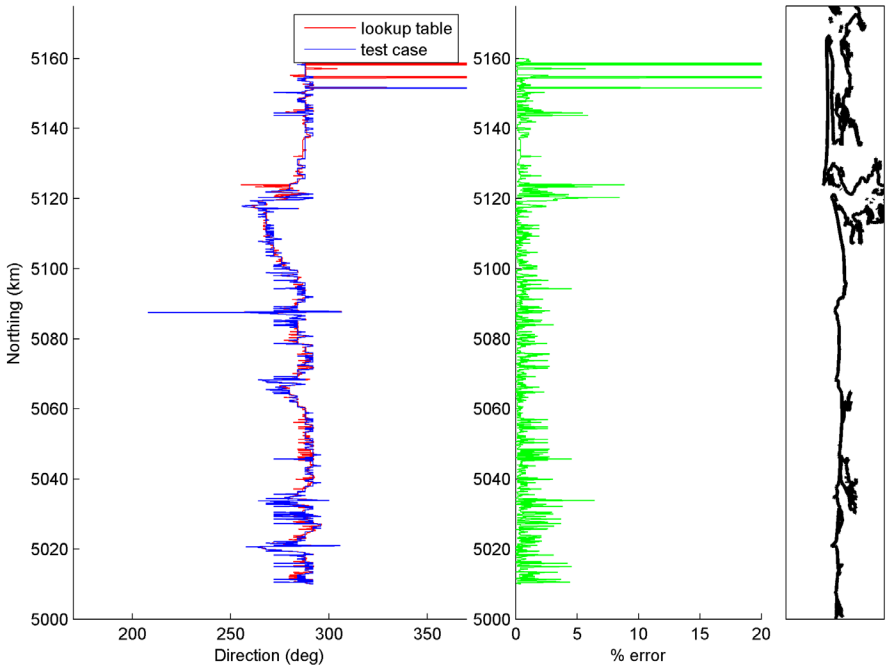

Figure 5-31. Comparison of alongshore varying wave direction at the 20-m contour extracted from the lookup tables (red line) and from a direct SWAN computation (blue line) with an offshore boundary condition characterized as H_s = 11.5, T_p = 18.5, D_p = 320, and a water level of 4.5 m NAVD88.

6.0 WAVE RUNUP AND OVERTOPPING

Wave runup is the culmination of the wave breaking process whereby the swash of the wave above the still water level is able to run up the beach face, where it may encounter a dune, structure, or bluff, potentially resulting in the erosion or in overtopping and flooding of adjacent land (**Figure 6-1**). Runup, *R*, or wave setup plus swash, is generally defined as the time-varying location of the intersection between the ocean and the beach and, as summarized, is a function of several key parameters. These include the deepwater wave height (H_o or H_s), peak spectral wave period (T_p) and the wave length (L_o) (specifically the wave steepness, H_o/L_o), and through a surf similarity parameter called the Iribarren number,

$$\xi_o = \frac{\beta}{\sqrt{H_o/L_o}},$$

which accounts for the slope (β) of a beach or an engineering structure, as well as the steepness of the wave.

The total runup, *R*, produced by waves includes three main components:

- wave setup, $\overline{\eta}$;
- a dynamic component to the still water level, $\hat{\eta}$; and
- incident wave swash, S_{inc}

$$R = \overline{\eta} + \hat{\eta} + S_{inc} \qquad (6.1)$$

Along the Pacific Northwest Coast of Oregon and Washington, the dynamic component of still water level, $\hat{\eta}$, has been demonstrated to be a major component of the total wave runup due to relatively high contributions from infragravity energy (Ruggiero and others, 2004). This process occurs due to a transfer of energy from the incident wind-generated waves to the longer-period infragravity wave energy, the division being placed at ~20-s periods. On the dissipative beaches of the Oregon coast, it is the infragravity energy that increases swash runup levels during major storms that is ultimately responsible for erosion and overwash events. The combination of these processes produces "sneaker waves," yielding the most extreme swash runup levels.

A variety of models have been proposed for calculating wave runup on beaches (Ruggiero and others, 2001; Hedges and Mase, 2004; Northwest Hydraulic Consultants, 2005; Stockdon and others, 2006). Here we explore two approaches available for runup calculations along Tillamook County, Oregon. These included the runup model developed by Stockdon and others (2006) and the direct integration method (DIM) described in NHC (2005).

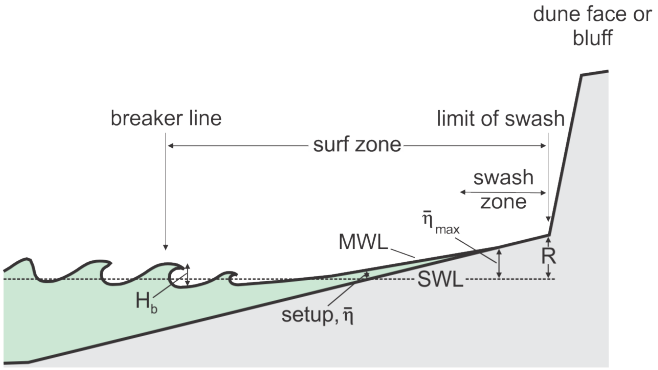

Figure 6-1. Conceptual model showing the components of wave runup associated with incident waves (modified from Hedges and Mase, 2004).

6.1 Runup Models for Beaches

6.1.1 Stockdon Runup Model

For sandy beaches, Stockdon and others (2006) developed an empirical model based on analyses of 10 experimental runup data sets obtained from a wide variety of beach and wave conditions, including data from Oregon (Ruggiero and others, 2004), and by separately parameterizing the individual runup processes: setup and swash. Stockdon and others (2006) proposed the following general relationship for the elevation of the 2% exceedance elevation of swash maxima, R_2, for any data run:

$$R_2 = 1.1[\overline{\eta} + \frac{S}{2}] \quad (6.2)$$

where:

$$S = \sqrt{(S_{inc})^2 + (\widehat{\eta})^2} \quad (6.3)$$

and:

$$\overline{\eta}, S_{inc}, \widehat{\eta} = f(H_o, T_o, \beta_f)$$

where β_f is the slope of the beach face, and S reflects both the dynamic, $\widehat{\eta}$, and incident swash, S_{inc}, components. The 1.1 coefficient value was determined because the swash level assumes a slightly non-Gaussian distribution. The final parameterized runup equation is:

$$R_{2\%} = 1.1\left(0.35\tan\beta\,(H_o L_o)^{\frac{1}{2}} + \frac{[H_o L_o(0.563\tan\beta^2 + 0.004)]^{\frac{1}{2}}}{2}\right) \quad (6.4)$$

which may be applied to natural sandy beaches over a wide range of morphodynamic conditions. In developing equation 6.4, Stockdon and others (2006) defined the slope of the beach as the average slope over a region ±2σ around the wave setup, $\overline{\eta}$, where σ is the standard deviation of the continuous water level record, η(t). Simply put, the setup reflects the height of the mean-water level (MWL) excursion above the SWL, such that the slope is determined to span the region around this MWL. For Tillamook County, the slope of the beach was determined by fitting a linear regression through those data points spanning the region located between 2 and 4 m.

Combining equation 6.4 with the measured water level at tide gauges produces the total water level (TWL) at the shore, important for determining the erosion or flood risk potential. Given that equation 6.4 has been derived from quantitative runup measurements spanning a range of beach slopes (beach slopes ranged from 0.01 to 0.11 and Iribarren numbers [ξ] ranged from 0.1 [fully dissipative conditions] to ~2.2 [reflective conditions], Table 1 of Stockdon and others [2006]), the model is valid for the range of slopes and conditions observed along the Tillamook County coastline and elsewhere on the Oregon coast.

6.1.2 Direct integration method—beaches

The FEMA coastal flood mapping guidelines (NHC, 2005) for the U.S. West Coast presents an alternative method for calculating runup. According to NHC (2005), the direct integration method (DIM) approach allows for the wave and bathymetric characteristics to be taken into consideration; specifically, the spectral shape of the waves and the actual bathymetry can be represented. Here we review the parameterized set of runup equations that may be used to calculate runup on beaches. The equations are based on a parameterized JONSWAP spectra and uniform beach slopes.

Similar to equation 6.1, the runup of waves using DIM can be defined according to its three components: the wave setup, $\overline{\eta}$, a dynamic component, $\widehat{\eta}$, and the incident band swash, S_{inc}. Wave setup can be calculated using:

$$\overline{\eta} = 4.0\, F_H F_T F_{Gamma} F_{slope} \tag{6.5}$$

while the root mean square (rms) of the dynamic component, $\widehat{\eta}_{rms}$, may be estimated using:

$$\widehat{\eta}_{rms} = 2.7\, G_H G_T G_{Gamma} G_{slope} \tag{6.6}$$

where the units of $\overline{\eta}$ and $\widehat{\eta}_{rms}$ are in *feet* and the factors (F) are for the wave height (F_H and G_H), wave period (F_T and G_T), JONSWAP spectrum narrowness (F_{Gamma} and G_{Gamma}), and the nearshore slope (F_{slope} and G_{slope}). These factors are summarized as a series of simple equations in Table D.4.5-1 (NHC, 2005). For the purposes of defining an average slope, NHC recommended that the nearshore slope be based on the region between the runup limit and twice the wave breaking depth, h_b, where:

$$h_b = H_b / k \tag{6.7}$$

and

$$H_b = 0.39 g^{0.2} \left(T_p H_o^2\right)^{0.4} \tag{6.8}$$

where H_b is the breaker height calculated using equation 6.8 (Komar, 1998b), g is acceleration due to gravity (9.81 m/s), and for the purposes here k (breaker depth index) can be taken to be 0.78. Thus, one important distinction between the DIM and Stockdon methods for calculating runup is the method used to define the beach slope; the former accounts for a larger portion of the nearshore slope, while the latter is based on the slope calculated around the mid beach-face.

To derive the statistics of the oscillating wave setup and the incident swash components, the recommended approach is to base the calculations on the standard deviations (σ) of each component. The standard deviation of the incident wave oscillation (σ_2) on natural beaches may be calculated from:

$$\sigma_2 = 0.3 \xi_o H_o \tag{6.9}$$

Because the standard deviation of the wave setup fluctuations (σ_1) is proportional to equation 6.6, the total oscillating component of the dynamic portion of the wave runup can be derived from:

$$\widehat{\eta_T} = 2.0 \sqrt{\sigma_1^2 + \sigma_2^2} \tag{6.10}$$

Combining the results of equations 6.10 and 6.5 yields the 2% wave runup, and when combined with the tidal component results in the TWL.

6.1.3 Comparison between the Stockdon and DIM runup calculations

Fundamentally, the wave runup model proposed by Stockdon and others (2006) and the DIM method described in NHC (2005) are similar, because both models account for the three components of runup described in equation 6.1. Here we examine the runup results derived from both models based on a range of conditions characteristic of the Clatsop shore (**Figure 6-2** and **Figure 6-3**). We focus on our results from Clatsop, because this is where we first tested both approaches, before settling on one approach for calculating all subsequent runup for the Oregon coast.

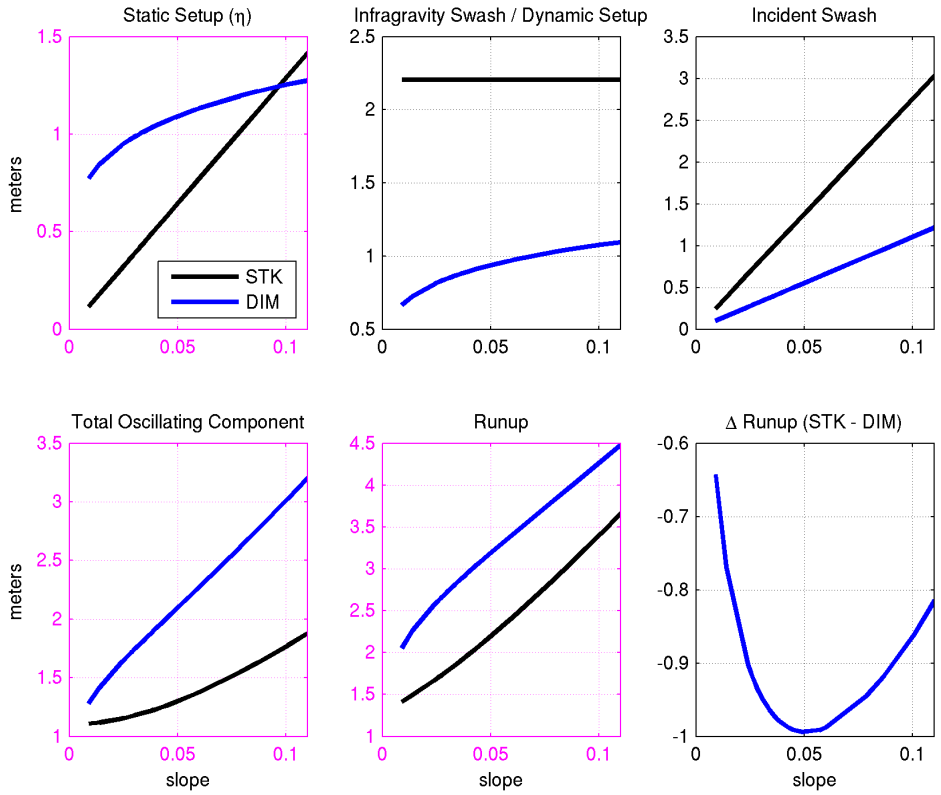

Figure 6-2. Calculated setup, swash and runup using the Stockdon and DIM runup equations. In this example, slope values are defined similarly for both methods, at a mid-beach elevation range of 2–4 m (6.6–13 ft). A 6-m (19.7 ft) significant wave height, 12-s peak wave period, and 270° wave direction were used to drive the models. Due to the semi-empirical nature of the equations, only the magnitudes of the subplots outlined in magenta are directly comparable (the two panels showing swash results are not directly comparable). The total oscillating component compares the results from equation 6.3 (S/2) with equation 6.10.

Figure 6-2 provides a comparison of the various calculated parameters (setup, infragravity swash, incident swash, total oscillating component, and runup) determined using the Stockdon and DIM approaches. In this example, we use the same slope defined for the mid-beach region in order to provide a direct comparison between DIM and Stockdon. Upper estimates have been truncated to tan β = 0.11, which reflects the slope limit on which Stockdon has been tested. In contrast, it is unclear the range of slope conditions on which DIM may be applied as there is no quantitative field testing of this particular formulation. As can be seen in **Figure 6-2**, although there are notable differences in the various parameterizations, the derived runup (bottom, middle plot) is similar. Nevertheless, as can be seen from the ΔR plot (bottom

right), the DIM approach tends to estimate a slightly higher runup when compared to Stockdon, which in this example reaches a maximum of ~1 m (3.3 ft) for a beach slope of 0.04 to 0.05. Thus, overall, we can conclude that the two approaches are performing in a similar fashion when tested using the same slope.

Figure 6-3 presents a similar suite of comparisons under the same hydrodynamic conditions. Therefore the Stockdon and others (2006) results are identical to **Figure 6-2** in all panels. However, in this example we now account for the appropriate nearshore slope in the DIM runup calculations as defined above in Section 6.1.2. This was originally done by computing the DIM runup components for this hydrodynamic condition using the full nearshore slope at 85 transects spread along the Clatsop County coastline (Allan and others, 2014). The DIM values are, however, plotted against the foreshore beach slopes defined for all 85 transects in order to make the comparisons with Stockdon meaningful. As can be seen in **Figure 6-3**, application of the nearshore slope significantly changes the magnitudes of all the runup components and, in particular, reduces the calculated runup when compared to Stockdon for most foreshore slopes. In general, at lower slopes (tan β < 0.05) runup calculated by DIM is slightly higher than Stockdon, which reverses at steeper slopes (tan β > 0.05). This pattern is consistent with analyses performed by Allan and others (2012) in Coos County.

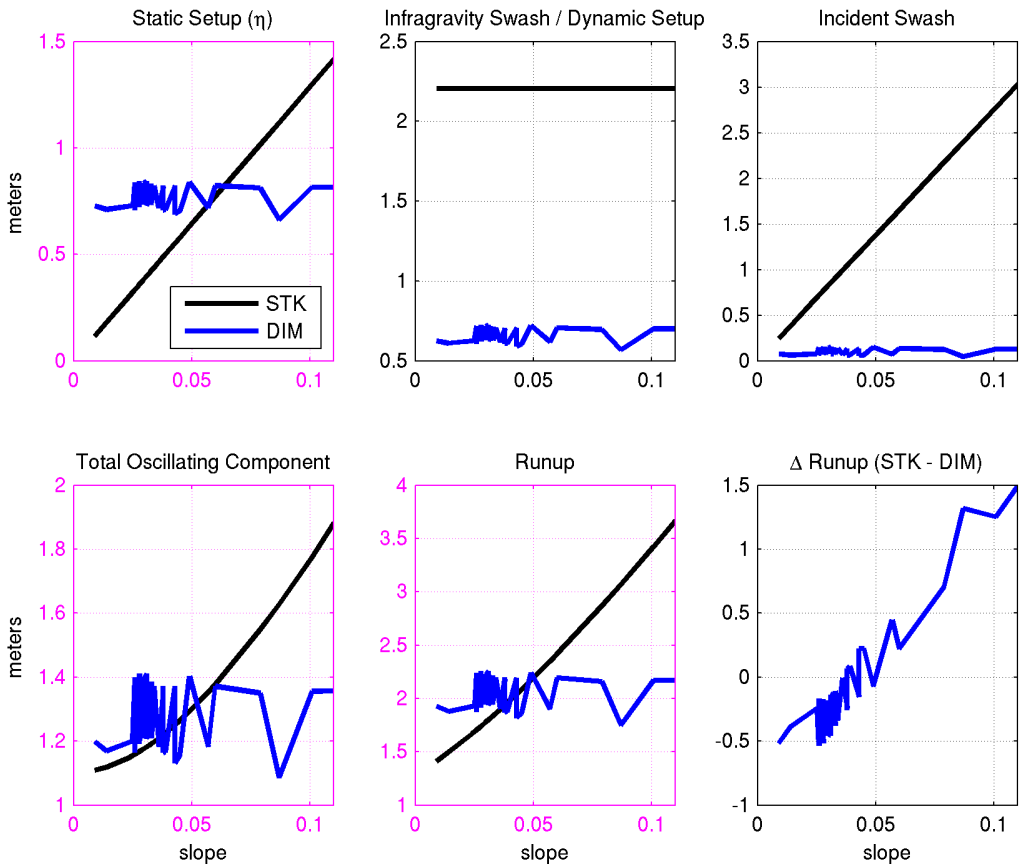

Figure 6-3. Total water level calculations using the Stockdon (foreshore slope) and DIM runup equations (nearshore slope). A 6-m (19.7-ft) significant wave height, 12-s peak wave period, and 270° wave direction were used to drive the models. Due to the semi-empirical nature of these equations only the magnitudes of the subplots outlined in magenta are directly comparable. The results for DIM are sorted in ascending order as a function of foreshore beach slope.

Most interesting in the comparisons shown in **Figure 6-3**, is that the DIM runup components actually do not vary as a function of the foreshore slope. The total runup **Figure 6-3**, bottom center) produced by DIM is relatively constant, oscillating between 1.7 and 2.3 m (5.6 and 7.5 ft). The oscillations are due primarily to the variability in the nearshore slopes, which are a function of wave height (equations 6.7 and 6.8). Because waves in the PNW are relatively large and upper shoreface slopes are relatively shallow, the DIM runup values are controlled by the nearshore slope with little influence from the upper beach. This lack of dependence on the foreshore is in contrast to field measurements made in Oregon (Ruggiero and others, 2004) in which runup is clearly a function of the foreshore slope. Because the Stockdon model has been extensively validated against measured runup data, including measurements on the Oregon coast (e.g., Ruggiero and others, 2001; Ruggiero and others, 2004) together with qualitative observations of runup during storms by DOGAMI staff at multiple sites along the coast, 1% extreme values of TWLs calculated for sandy beaches along the Tillamook County coast will be based primarily on the Stockdon and others (2006) model.

6.2 "Barrier" Runup Calculations

6.2.1 Introduction

According to NHC (2005) an alternate approach is recommended for use in calculating runup on steep barriers. By definition, *barriers include "steep dune features and coastal armoring structures such as revetments"* (NHC, 2005, p. D.45-10), although little guidance is offered in terms of the range of slopes to which this alternate approach would apply. Throughout this document we use the generic term *barrier* to define the range of morphological and engineering conditions where barrier runup calculations may apply. In general, runup on barriers depends not only on the height and steepness of the incident waves defined through the Iribarren number or breaker parameter ($\xi_{m\text{-}1,0}$) but also on the geometry (e.g., the slope of the barrier and/or if a berm is present), design characteristics of the structure, and its permeability.

The recommended approach for calculating runup on barriers is to use the TAW (Technical Advisory Committee for Water Retaining Structures) method, which provides a mechanism for calculating the runup, adjusted for various reduction factors that include the surface roughness, the influence of a berm (if present), and effects associated with the angle of wave approach (van der Meer, 2002; Northwest Hydraulic Consultants, 2005; Pullen and others, 2007). According to NHC (2005) the TAW method is useful as it includes a wide range of conditions for calculating the wave runup (e.g., both smooth and rough slopes) and because it agrees well with both small- and large-scale experiments.

Figure 6-4 is a conceptual model of the various components required to determine the extent of runup on barriers. Of importance is first determining the 2% dynamic water level ($DWL_{2\%}$) at the barrier, which includes the combined effects of the measured still water level (SWL), the wave setup ($\bar{\eta}$) and the dynamic portion ($\hat{\eta}$) of the runup (**Figure 6-4**), which is then used to establish the spectral significant wave height (H_{mo}) at the toe of the "barrier" (NHC, 2005).

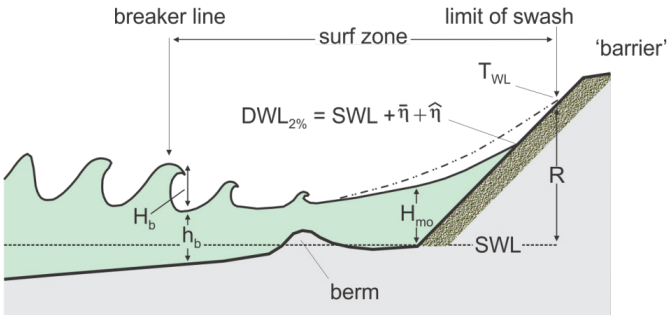

Figure 6-4. Wave runup on a beach backed by a structure or bluff (modified from NHC, 2005).

The general formula for calculating the 2% wave runup height on barriers is given in a non-dimensional form by equation 6.11:

$$\frac{R_{2\%}}{H_{mo}} = c_1 . \gamma_b . \gamma_f . \gamma_\beta . \xi_{m-1,0} \qquad (6.11)$$

with a maximum of:

$$\frac{R_{2\%}}{H_{mo}} = \gamma_f . \gamma_\beta \left(c_2 - \frac{c_3}{\sqrt{\xi_{m-1,0}}} \right)$$

where:

$R_{2\%}$ = wave runup height exceeded by 2% of the incoming waves

H_{mo} = spectral significant wave height at the structure toe

c_1, c_2, and c_3 = empirical coefficients with:

γ_b = influence factor for a berm (if present),

γ_f = influence factor for roughness element of slope,

γ_β = influence factor for oblique wave attack,

$\xi_{m-1,0}$ = breaker parameter

$$\left(\tan\beta / \left(\frac{H_{mo}}{L_{m-1,0}} \right)^{0.5} \right),$$

$\tan\beta$ = slope of the "barrier,"

$L_{m-1,0}$ = the deepwater wave length $\left(gT_{m-1,0}^2 / 2\pi \right)$, and

$T_{m-1,0}$ can be calculated from $T_p/1.1$, where T_p is the peak spectral wave period.

Substituting the empirical coefficients derived from wave tank experiments and incorporating a 5% upper exceedance limit into the general equations of 6.11 (van der Meer, 2002; Pullen and others, 2007), runup on barriers may be calculated by using:

$$R_{2\%} = H_{mo}\left(1.75 . \gamma_b . \gamma_f . \gamma_\beta . \xi_{m-1,0}\right), \quad \text{where } 0 < \gamma_b . \xi_{m-1,0} < 1.8 \qquad (6.12)$$

with a maximum of:

$$R_{2\%} = H_{mo}\left(1.0 . \gamma_f . \gamma_\beta \left(4.3 - \frac{1.6}{\sqrt{\xi_{m-1,0}}} \right) \right), where\ \gamma_b . \xi_{m-1,0} \geq 1.8$$

There are, however, notable differences between equation 6.12 originally described by van der Meer (2002) and Pullen and others (2007) from that presented in equation D.4.5-19 in the FEMA West Coast methodology (NHC, 2005). For example, equation D.4.5-19 in the NHC report contains a higher coefficient value (1.77), along with one additional reduction factor (porosity) for calculating runup when the breaker parameter is less than 1.8. Similarly, for conditions where the breaker parameter exceeds 1.8 and the maximum runup equation is used, equation D.4.5-19 in the NHC report contains two extra reduction factors (berm and porosity reduction factors) that are not included in the original solution, which potentially could have a very significant effect on the calculated runup. Based on these differences, we have used the original solution presented as equation 6.12 in van der Meer (2002) and Pullen and others (2007).

6.2.2 Specific procedure for calculating "barrier" runup

For those cases where the TAW method is used for determining runup on barriers (i.e., beaches backed by structures, cobble berms, and/or bluffs), we have followed the general approach laid out in section D.4.5.1.5.2 in NHC (2005), with the exception that we use Stockdon to define the $DWL_{2\%}$ (instead of DIM) at the structure toe, and TAW to calculate the incident swash on the barrier (i.e., equation 6-12). Because waves are depth limited at the barrier toe, H_{mo} may be estimated from $DWL_{2\%}$ using a breaker index of 0.78 (i.e., $H_{mo} = DWL_{2\%} * 0.78$). In performing these various derivations, $DWL_{2\%}$ was first determined using equation 6.13:

$$DWL_{2\%} = SWL + 1.1 * \left(\overline{\eta} + \frac{\widehat{\eta}}{2}\right) - D_{low} \qquad (6.13)$$

where:

SWL = measured tide

$\overline{\eta} = 0.35 * \tan\beta\sqrt{H_s * L}$ *Eqn. 10 in Stockdon and others (2006)*

$\widehat{\eta} = 0.06 * \sqrt{H_s * L}$ *Eqn. 12 in Stockdon and others (2006)*

D_{low} = the toe of the structure or bluff

$\tan\beta$ = the beach slope defined for the region between 2 and 4 m.

Having calculated $DWL_{2\%}$ and H_{mo}, the TAW runup calculation can be implemented. Equation 6.12 requires information on the slope of the barrier, used in the breaker parameter ($\xi_{m\text{-}1,0}$) calculation, which can be somewhat challenging to define. This is especially the case if the morphology of the barrier exhibits a composite morphology characterized by different slopes, such that errors in estimating the slope will translate to either significant underestimation or overestimation of the runup. According to van der Meer (2002) and Pullen and others (2007), because the runup process is influenced by the change in slope from the breaking point to the maximum wave runup, the characteristic slope should be specified for this same region. On the Oregon coast, the most common composite slope example is the case where a broad, dissipative sand beach fronts a structure or bluff that is perched relatively high on the back of the beach (structure toe > ~4-5 m). In this example, the wave runup is first influenced by the sandy beach slope and finally by the slope of the structure itself. To address this type of situation, we define a "local barrier slope" as the portion of the barrier that ranges from the calculated storm TWL (calculated initially using equation 6.4) down to a lower limit defined by the wave setup plus the SWL [i.e., $(1.1 * \overline{\eta}) + SWL$]). In a few cases, the TWL was found to exceed the barrier crest; in those cases we used the structure crest as the upper limit for defining the local slope. This process is repeated for every storm condition. Having determined the barrier slope, the TAW runup is calculated using equation 6.12 and reduced based on the appropriate site specific reduction factors.

Under certain conditions, we identified events that generated extreme runup that made little physical sense. For these (rare) cases, we calculated the TAW runup using an iterative approach based on procedures outlined in the Eurotop (2007) manual. Because the maximum wave runup is the desired outcome and is unknown when initially defining the slope, the process is iterative requiring two steps. First, the breaking limit is defined as $1.5H_{mo}$ *below* the SWL, while $1.5H_{mo}$ *above* the SWL defines the upper limit of the first slope estimate (**Figure 6-5**). Having determined the first slope estimate, the TAW runup is calculated using equation 6.12 and reduced based on the appropriate reduction factors. A second slope estimate is then performed based on the initial runup calculation, while a third iteration is not necessary based on our tests because this method converges quickly. The breaking limit is again defined as $1.5H_{mo}$ *below* the SWL, while $R_{2\%}$ *above* the SWL defines the upper limit, and the final barrier runup estimate is again calculated using equation 6.12 and reduced based on the appropriate reduction factors.

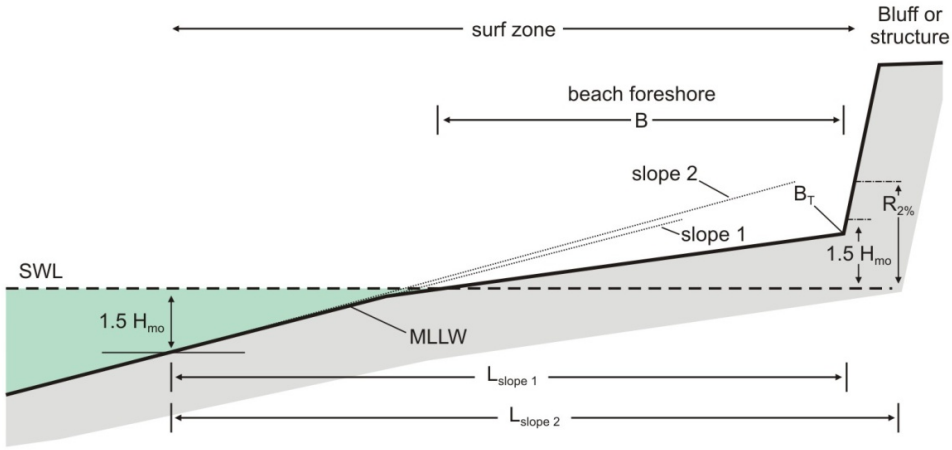

Figure 6-5. Determination of an average slope based on an iterative approach. The first estimate is initially based on 1.5H_{mo} ±SWL, while the second estimate is based on 1.5H_{mo} below the SWL and the calculated $R_{2\%}$ above the SWL that is based on the first slope estimate.

Finally, it is important to note that the runup estimates based on the "barrier" runup calculations is sensitive to the slope. Similar to our study in Coos and Clatsop counties, we identified several sites (primarily beaches backed by bluffs) along the Tillamook coast where the final TWLs calculated using TAW was unreasonably low. These few cases are entirely due to there being a very wide dissipative surf zone at these transect locations that results in very low slopes being defined. For these sites where the calculated TWL_S seemed unreasonably low (relative to the morphology of the beach and observations of storm wave runup along this shore and elsewhere), we have defaulted to the TWLs calculated using the Stockdon and others model.

6.2.3 "Barrier" runup reduction factors

Table 6-1 below presents information pertaining to the suite of parameters used to define wave runup (R) and ultimately the 1% TWLs along the Tillamook County coast. In the case of bluff roughness along the Tillamook shore, we used a value of 0.6 for those situations where a bluff face was highly vegetated. These bluffs are typically located at or near their stable angle of repose and are covered with Salal plants (*Gaultheria shallon*), forming a deep, nearly impenetrable thicket. The decision to use 0.6 was based on discussions with Dr. W. G. McDougal (Coastal Engineer, OSU, and Technical Coordinator of the North Pacific FEMA West Coast Guidelines, pers. comm., April 2010). At the Tillamook transects 26–28, 43–44, 46, 67–74, 94–96, and 104 (**Table 6-1**), the reduction factor was set to 1 due to the fact that these beaches were backed by a near-vertical bluff face that was essentially akin to a seawall situation. For those beaches backed by a significant riprap structure, we used a reduction factor of 0.55. In other cases, this was increased to 0.6 to 0.8, depending on whether the beach was backed by gravels/cobbles, a vegetated bluff face, or poor quality riprap. Wave direction (γ_β) reduction factors were determined based on the shoreline orientation at every transect site and the actual wave directions measured during each storm condition. The reduction factor was calculated using equation D.4.5-22 of NHC (2005, p. D.4.5-13). Finally, because none of the transects where structures are present contained a protective berm, no berm reduction factor was adopted for Tillamook County.

Table 6-1. Parameters used to define runup (*R*) and total water levels (TWLs) on beaches backed by dunes, structures, and bluffs.

Reach	Transect	DFIRM Transect	D_{HIGH} (m)	D_{LOW} (m)	Beach Slope (tan β)	Wave Dir. (γ_β)	Rough-ness (γ_r)	Approach	Description
Salmon River	LINC 308	1	6.251	5.058	0.084	272.2	1.0	3	dune-backed cliff
Cascade Head	LINC 309	2	48.172	1.609	0.027	268.8	0.95	1	plunging cliff
	LINC 310	3	43.56	1.207	0.028	274.1	0.95	1	plunging cliff
	LINC 311	4	24.427	0.358	0.022	270.3	0.8	1	boulder beach backed by bluffs
	LINC 312	5	93.24	2.125	0.026	271.8	0.95	1	plunging cliff
	LINC 313	6	139.1	0	0.023	273.7	0.95	1	plunging cliff
Neskowin	TILL 1	7	47.278	0.764	0.025	294.5	0.55	1	sandy beach backed by riprap and high cliffs
	TILL 2	8	8.684	3.914	0.045	294	0.55	1	sand beach backed by riprap
	TILL 3	9	8.452	3.914	0.042	287.1	0.55	1	sand beach backed by riprap
	TILL 4	10	5.184	3.448	0.018	283.3	0.55	1	sand beach backed by riprap
	TILL 5	11	8.312	2.712	0.049	267.3	0.55	1	sand beach backed by riprap
	TILL 6	12	8.447	3.563	0.073	275.6	0.55	1	sand beach backed by riprap
	TILL 7	13	8.169	1.904	0.062	284.3	0.55	1	sand beach backed by riprap
	TILL 8	14	8.539	2.533	0.062	286.8	0.55	1	sand beach backed by riprap
	TILL 9	15	7.075	5.888	0.06	286.7	1.0	3	dune-backed
	TILL 10	16	8.897	6.235	0.054	285.1	1.0	3	dune-backed
	TILL 11	17	6.679	5.604	0.041	282.9	1.0	3	dune-backed
	TILL 12	18	8.374	5.521	0.044	281	1.0	3	dune-backed
	TILL 13	19	7.126	5.709	0.049	273.3	1.0	3	dune-backed
	TILL 14	20	8.118	5.086	0.099	282.3	0.55	1	sand beach backed by riprap
	TILL 15	21	7.587	4.642	0.069	272.4	0.55	1	sand beach backed by riprap
	TILL 16	22	6.767	6.014	0.052	277	1.0	3	dune-backed
	TILL 17	23	9.986	4.326	0.039	283.7	1.0	3	dune-backed
	TILL 18	24	8.387	5.512	0.074	284.4	1.0	3	dune-backed
	TILL 19	25	6.014	6.014	0.059	285.4	1.0	3	dune-backed
	TILL 20	26	7.648	7.066	0.098	284.5	1.0	3	dune-backed
	TILL 21	27	12.562	5.582	0.049	287.1	1.0	3	dune-backed
	TILL 22	28	6.241	4.489	0.034	283.2	1.0	3	dune-backed
	TILL 23	29	14.334	6.819	0.088	280.2	1.0	3	dune-backed
	TILL 24	30	7.792	7.185	0.06	278	1.0	3	dune-backed
	TILL 25	31	7.642	5.627	0.061	278.3	1.0	3	dune-backed
	TILL 26	**32**	**32.562**	**3.877**	**0.059**	**278.6**	**1.0**	**2**	**sandy beach backed by high cliffs**
	TILL 27	**33**	**28.194**	**4.519**	**0.088**	**281.5**	**1.0**	**2**	**sandy beach backed by high cliffs**
	TILL 28	**34**	**39.31**	**6.292**	**0.084**	**281.1**	**1.0**	**2**	**sandy beach backed by dunes and high cliffs**
Nestucca spit/ Pacific City	TILL 29	35	10.245	4.903	0.043	273.2	1.0	3	dune-backed
	TILL 30	36	14.485	5.083	0.048	273.8	1.0	3	dune-backed
	TILL 31	37	15.49	5.933	0.061	276.6	1.0	3	dune-backed
	TILL 32	38	14.358	5.413	0.093	277	1.0	3	dune-backed
	TILL 33	39	13.16	5.338	0.072	270.9	1.0	3	dune-backed
	TILL 34	40	15.877	6.611	0.086	271.1	1.0	3	dune-backed
	TILL 35	41	15.147	5.312	0.05	270	1.0	3	dune-backed
	TILL 36	42	17.709	5.908	0.051	268.7	1.0	3	dune-backed
	TILL 37	43	12.932	4.389	0.051	266.5	0.55	1	sand beach backed by riprap?
	TILL 38	44	11.283	4.69	0.053	264	0.55	1	sand beach backed by riprap?
	TILL 39	45	18.954	5.407	0.041	262.2	1.0	3	dune-backed
	TILL 40	46	11.314	5.539	0.057	261.1	0.55	3	sand beach backed by riprap?
	TILL 41	47	11.06	4.785	0.039	262.9	0.55	3	sand beach backed by riprap?
	TILL 42	48	13.304	4.681	0.043	262.8	0.6	1	sand beach backed by riprap and high bluffs

Reach	Transect	DFIRM Transect	D_{HIGH} (m)	D_{LOW} (m)	Beach Slope (tan β)	Wave Dir. (γ_θ)	Rough-ness (γ_r)	Approach	Description
Sand Lake/ Tierra Del Mar	**TILL 43**	**49**	**23.369**	**5.582**	**0.046**	**281.8**	**1.0**	**1**	**sandy beach backed by high cliffs**
	TILL 44	**50**	**16.741**	**6.162**	**0.075**	**281.3**	**1.0**	**1**	**sandy beach backed by high cliffs**
	TILL 45	51	6.868	4.232	0.042	280.2	0.6	1	sandy beach backed by cobbles - grades into bluff
	TILL 46	**52**	**18.071**	**4.865**	**0.055**	**280.8**	**1.0**	**1**	**sandy beach backed by high cliffs**
	TILL 47	53	18.396	4.063	0.045	279.7	0.55	1	sand beach backed by riprap
	TILL 48	54	7.412	6.555	0.048	279.8	1.0	3	dune-backed
	TILL 49	55	8.24	6.197	0.044	279.7	1.0	3	dune-backed
	TILL 50	56	6.931	5.891	0.041	290.1	1.0	3	dune-backed
	TILL 51	57	6.317	4.554	0.05	278.7	0.8	1	sand beach backed by riprap
	TILL 52	58	7.721	4.543	0.055	278.8	0.8	1	sand beach backed by riprap
	TILL 53	59	8.141	5.026	0.056	280.3	0.6	1	sand beach backed by riprap
	TILL 54	60	7.462	5.055	0.058	269.7	0.6	1	sand beach backed by riprap
	TILL 55	61	8.094	5.159	0.045	283.1	1.0	3	dune-backed
	TILL 56	62	8.357	4.652	0.046	278.7	0.55	1	sand beach backed by riprap
	TILL 57	63	11.383	4.823	0.04	284.8	0.55	3	sand beach backed by riprap
	TILL 58	64	10.224	6.18	0.042	278.7	1.0	3	dune-backed
	TILL 59	65	12.153	5.72	0.052	278.4	1.0	3	dune-backed
	TILL 60	66	9.595	5.355	0.041	278.4	1.0	3	dune-backed
	TILL 61	67	9.37	6.193	0.048	279.3	1.0	3	dune-backed
	TILL 62	68	6.573	6.26	0.052	279.1	1.0	3	dune-backed
	TILL 63	69	3.38	3.324	0.009	273.1	1.0	3	dune-backed
	TILL 64	70	18.524	6.915	0.111	270.7	1.0	3	dune-backed
	TILL 65	71	18.296	5.556	0.053	270.7	1.0	3	dune-backed
	TILL 66	72	15.211	5.34	0.049	271.5	1.0	3	dune-backed
	TILL 67	**73**	**19.042**	**8.385**	**0.069**	**272.4**	**1.0**	**3**	**sandy beach backed by high cliffs**
	TILL 68	**74**	**24.72**	**6.441**	**0.044**	**270.6**	**1.0**	**3**	**sandy beach backed by high cliffs**
	TILL 69	**75**	**29.519**	**5.96**	**0.051**	**268.7**	**1.0**	**3**	**sandy beach backed by high cliffs**
	TILL 70	**76**	**30.293**	**4.588**	**0.045**	**266.9**	**1.0**	**1**	**sandy beach backed by high cliffs**
	TILL 71	**77**	**37.153**	**4.979**	**0.055**	**263.4**	**1.0**	**1**	**sandy beach backed by high cliffs**
	TILL 72	**78**	**30.575**	**4.844**	**0.037**	**257.8**	**1.0**	**1**	**sandy beach backed by high cliffs**
	TILL 73	**79**	**28.571**	**6.625**	**0.048**	**256.8**	**1.0**	**3**	**sandy beach backed by high cliffs**
	TILL 74	**80**	**20.692**	**5.762**	**0.038**	**253.8**	**1.0**	**3**	**sandy beach backed by high cliffs**

Reach	Transect	DFIRM Transect	D_{HIGH} (m)	D_{LOW} (m)	Beach Slope (tan β)	Wave Dir. (γ_θ)	Rough-ness (γ_r)	Approach	Description
Netarts Spit/ Oceanside	TILL 75	81	6.775	2.43	0.029	276.8	0.6	1	sandy beach backed by low/high cliffs
	TILL 76	82	7.6	2.937	0.037	279.7	0.6	1	sandy beach backed by cobbles/boulders and low cliff
	TILL 77	83	8.447	3.235	0.047	285.7	0.6	1	sandy beach backed by dynamic revetment/artificial dune
	TILL 78	84	7.298	3.706	0.051	281.8	0.6	1	sandy beach backed by dynamic revetment/artificial dune
	TILL 79	85	10.798	3.976	0.043	284.6	0.6	1	dune-backed (+cobbles)
	TILL 80	86	9.131	5.381	0.082	285.4	1.0	3	dune-backed (+cobbles)
	TILL 81	87	7.159	4.661	0.067	285.8	1.0	3	dune-backed (+cobbles)
	TILL 82	88	11.562	5.04	0.056	283.3	1.0	3	dune-backed
	TILL 83	89	12.413	5.492	0.056	281.9	1.0	3	dune-backed
	TILL 84	90	7.322	6.012	0.046	271.7	1.0	3	dune-backed
	TILL 85	91	11.621	5.37	0.044	275.8	1.0	3	dune-backed
	TILL 86	92	11.763	6.361	0.047	276	1.0	3	dune-backed
	TILL 87	93	19.722	4.114	0.043	281.1	1.0	3	dune-backed
	TILL 88	94	6.567	5.72	0.057	271.2	1.0	3	dune-backed
	TILL 89	95	10.543	5.754	0.048	274	1.0	3	dune-backed
	TILL 90	96	12.156	4.768	0.046	278.7	1.0	3	dune-backed
	TILL 91	97	9.61	6.516	0.052	272.5	1.0	3	dune-backed
	TILL 92	98	8.324	6.36	0.05	284.5	1.0	3	dune-backed
	TILL 93	99	4.971	4.855	0.069	202.6	0.6	3	Cobble beach backed by low wall (estuary mouth)
	TILL 94	**100**	**14.619**	**5.554**	**0.074**	**223.7**	**1.0**	**2**	**sandy beach backed by high cliffs**
	TILL 95	**101**	**29.639**	**4.999**	**0.032**	**235.6**	**1.0**	**1**	**sandy beach backed by high cliffs**
	TILL 96	**102**	**39.082**	**4.536**	**0.055**	**236.2**	**1.0**	**2**	**sandy beach backed by high cliffs**
	TILL 97	103	55.206	4.631	0.065	241.7	1.0	3	sandy beach backed by dune and high cliffs
	TILL 98	104	60.658	5.832	0.073	250.3	1.0	3	sandy beach backed by dune and high cliffs
	TILL 99	105	33.925	4.907	0.044	254.1	0.6	3	sandy beach backed by high cliffs
	TILL 100	106	36.465	4.585	0.041	252.2	0.6	1	sandy beach backed by high cliffs
	TILL 101	107	13.733	5.191	0.045	248.4	0.7	3	sandy beach backed by poor riprap and low cliffs
	TILL 102	108	18.353	5.953	0.05	250	0.6	3	sandy beach backed by moderately high cliffs
	TILL 103	109	8.241	4.068	0.057	250.4	0.7	1	sandy beach backed by moderately high cliffs
Short Sand Beach	**TILL 104**	**110**	**33.582**	**3.026**	**0.056**	**277.7**	**1.0**	**1**	**sandy beach backed by gravels and high cliffs**
	TILL 105	111	26.461	3.932	0.075	277.9	0.8	1	sandy beach backed by gravels and high cliffs
	TILL 106	112	47.152	5.674	0.109	275.7	0.8	1	sandy beach backed by gravels and high cliffs

Reach	Transect	DFIRM Transect	D_{HIGH} (m)	D_{LOW} (m)	Beach Slope (tan β)	Wave Dir. (γ_θ)	Rough-ness (γ_r)	Approach	Description
Bayocean Spit	TILL 107	113	8.705	3.527	0.072	292	0.6	1	sandy beach backed by cobble/boulder and low cliffs
	TILL 108	114	7.74	2.981	0.05	286.2	0.6	1	sandy beach backed by cobble/boulder and low cliffs
	TILL 109	115	6.34	3	0.036	284.8	0.8	1	sandy beach backed by cobble/boulder berm
	TILL 110	116	6.081	2.495	0.026	280	0.8	1	sandy beach backed by cobble/boulder berm
	TILL 111	117	6.863	3.33	0.04	283.7	0.8	1	sandy beach backed by cobble/boulder berm
	TILL 112	118	9.667	6.824	0.041	279.7	1.0	3	dune-backed
	TILL 113	119	11.095	6.67	0.043	274.8	1.0	3	dune-backed
	TILL 114	120	9.781	6.804	0.04	276.6	1.0	3	dune-backed
	TILL 115	121	8.97	4.932	0.043	268.4	1.0	3	dune-backed
	TILL 116	122	10.49	5.889	0.04	265.4	1.0	3	dune-backed
	TILL 117	123	10.053	6.537	0.043	268.1	1.0	3	dune-backed
Rockaway	TILL 118	124	5.932	5.932	0.048	290.2	1.0	3	dune-backed
	TILL 119	125	6.332	4.905	0.043	285.6	1.0	3	dune-backed
	TILL 120	126	6.72	5.37	0.049	280.7	1.0	3	dune-backed
	TILL 121	127	6.749	5.178	0.058	282.2	1.0	3	dune-backed
	TILL 122	128	6.518	5.388	0.047	284.7	1.0	3	dune-backed
	TILL 123	129	7.242	3.13	0.029	286.4	0.55	1	sand beach backed by riprap
	TILL 124	130	6.905	5.82	0.05	285.9	1.0	3	dune-backed
	TILL 125	131	5.489	5.489	0.046	285.1	1.0	3	dune-backed
	TILL 126	132	5.858	4.586	0.02	286.4	1.0	3	dune-backed
	TILL 127	133	7.148	5.709	0.037	279.2	1.0	3	dune-backed
	TILL 128	134	7.976	5.327	0.038	279.6	1.0	3	dune-backed
	TILL 129	135	7.237	5.136	0.048	272.7	1.0	3	dune-backed
	TILL 130	136	7.344	5.839	0.046	274.4	1.0	3	dune-backed
	TILL 131	137	7.032	4.682	0.037	274.8	1.0	3	dune-backed
	TILL 132	138	5.486	3.77	0.038	290.9	0.8	3	sand beach backed by riprap
	TILL 133	139	7.133	5.593	0.038	276.7	1.0	3	dune-backed
	TILL 134	140	10.147	5.68	0.043	277.1	1.0	3	dune-backed
	TILL 135	141	8.387	7.085	0.052	276.2	1.0	3	dune-backed
	TILL 136	142	7.062	5.92	0.032	278.5	1.0	3	sand beach backed by low bluff
	TILL 137	143	6.827	4	0.034	279.7	0.55	1	sand beach backed by riprap
	TILL 138	144	6.359	3.045	0.013	274.8	0.55	1	sand beach backed by riprap
	TILL 139	145	8.67	5.263	0.034	268.9	1.0	3	dune-backed
	TILL 140	146	8.923	3.759	0.051	273.9	0.55	1	sand beach backed by riprap
	TILL 141	147	7.643	3.759	0.044	272.4	0.55	1	sand beach backed by riprap
	TILL 142	148	8.305	3.759	0.057	277.7	0.55	1	sand beach backed by riprap
	TILL 143	149	8.196	4.068	0.051	276	0.55	1	sand beach backed by riprap
	TILL 144	150	8.305	3.312	0.051	277.6	0.55	1	sand beach backed by riprap
	TILL 145	151	8.092	4.309	0.054	279.9	0.55	1	sand beach backed by riprap
	TILL 146	152	8.176	4.029	0.047	270.8	0.64	1	sand beach backed by riprap
	TILL 147	153	7.927	7.16	0.056	280.1	1.0	3	dune-backed
	TILL 148	154	8.101	5.982	0.052	281.5	1.0	3	dune-backed
	TILL 149	155	8.029	5.997	0.05	282	1.0	3	dune-backed
	TILL 150	156	8.315	6.325	0.045	283.3	1.0	3	dune-backed
	TILL 151	157	6.974	4.176	0.022	282.2	0.55	1	sand beach backed by riprap
	TILL 152	158	8.688	6.358	0.068	280.3	1.0	3	dune-backed
	TILL 153	159	8.773	4.786	0.037	279.4	1.0	3	dune-backed
	TILL 154	160	8.966	6.457	0.051	278.8	1.0	3	dune-backed
	TILL 155	161	8.448	6.267	0.042	278.2	1.0	3	dune-backed
	TILL 156	162	8.409	6.061	0.04	277.6	1.0	3	dune-backed
	TILL 157	163	6.833	5.548	0.031	277	1.0	3	dune-backed

Reach	Transect	DFIRM Transect	D_{HIGH} (m)	D_{LOW} (m)	Beach Slope (tan β)	Wave Dir. (γ_β)	Rough-ness (γ_r)	Approach	Description
Nehalem Spit/ Manzanita	TILL 158	164	7.752	6.112	0.049	279.2	1.0	3	dune-backed
	TILL 159	165	12.218	6.616	0.053	279.7	1.0	3	dune-backed
	TILL 160	166	8.676	6.254	0.063	276.6	1.0	3	dune-backed
	TILL 161	167	7.828	5.901	0.056	273.6	1.0	3	dune-backed
	TILL 162	168	15.433	5.338	0.042	268.4	1.0	3	dune-backed
	TILL 163	169	13.023	5.823	0.043	263.4	1.0	3	dune-backed
	TILL 164	170	14.069	5.912	0.055	265.7	1.0	3	dune-backed
	TILL 165	170	15.75	5.514	0.051	268.4	1.0	3	dune-backed
	TILL 166	172	12.088	4.356	0.034	266.4	1.0	3	dune-backed
	TILL 167	173	12.772	5.616	0.039	266.2	1.0	3	dune-backed
	TILL 168	174	13.313	6.617	0.038	264.6	1.0	3	dune-backed
	TILL 169	175	10.635	7.807	0.075	267.9	1.0	3	dune-backed
	TILL 170	176	9.226	4.313	0.022	268.1	0.7	1	sand beach backed by riprap
	TILL 171	177	8.847	5.064	0.026	271.3	1.0	3	dune-backed
	TILL 172	178	9.502	6.107	0.03	267.6	1.0	3	dune-backed with road
	TILL 173	179	11.496	5.245	0.028	265	1.0	3	dune-backed with road
	TILL 174	180	9.609	5.516	0.027	261.3	1.0	3	dune-backed with road
	TILL 175	181	11.367	4.73	0.029	263	1.0	3	dune-backed
	TILL 176	182	9.012	5.504	0.048	258.9	0.7	3	sand beach backed by extensive cobble berm
	TILL 177	183	6.996	5.077	0.049	257.8	0.55	3	sand beach backed by extensive cobble berm and bluff
	TILL 178	184	7.921	7.894	0.169	227.4	0.55	1	sand beach backed by extensive cobble berm and bluff
Falcon Cove	CP 1	185	15.935	7.027	0.167	278	0.8	1	sand, cobble berm backed by high bluff

Notes:

D_{HIGH} denotes the crest of the dune, bluff, or structure;

D_{LOW} denotes the toe of the dune (i.e., E_j), bluff, or structure;

Beach slope reflects the calculated slope spanning the region between 2- and 4-m elevation;

Wave direction denotes the shoreline orientation used to calculate the wave reduction (γ_β) factor used in TAW runup calculations;

Roughness (γ_r) defines the backshore roughness used in TAW runup calculations. Bold values indicate sites where the local slope goes to 1 due to the presence of a vertical bluff; and

Approach defines the final runup approach used to calculate the wave runup, where STK = Stockdon, Snsh/TAW = nearshore slope and TAW, and LocSlp/TAW = the local barrier slope and TAW.

6.3 Tillamook County Wave Runup and Total Water Level Calculations

The complete hourly combined time series is run through the lookup tables to derive alongshore varying transformed wave time series. Using the transformed wave conditions, and the measured alongshore varying beach and barrier slopes, initial TWL time series based on the Stockdon approach are developed at all transect locations. From these time series we identify the ~150 highest independent TWLs at each transect over the length of the record. Wave runup is then computed for each of these storm input conditions (about 5 events per year) at every profile site shown in **Figure 3-1**, **Figure 3-2**, and **Figure 3-3** using a combination of the Stockdon and others (2006) runup equation for dune-backed beaches (equation 6.4) and TAW (equation 6-12) for wave runup on a barrier. The specific approaches used in our calculations are defined above in **Table 6-1.** For both models, the calculated runup is combined with the SWL (measured tides) to develop the TWL conditions used to generate the 10, 50, and 100-year return level event as well as the 500-year return event. The input wave conditions from the SWAN modeling used in the various calculations were determined for each transect location by extending the shore-perpendicular transects from the backshore to where they intersected the 20-m contour, or the seaward most location of H_{mo}/depth = 0.4, whichever was farther offshore (but almost always shallower than 30 m). This ensured that only minor dissipation due to wave breaking influenced the model results. These intersections are where wave statistics from the SWAN output were extracted.

Having calculated the storm-induced TWLs, we used the generalized extreme value (GEV) family of distributions (specifically the peak over threshold (POT) approach) to estimate the 100-year and 500-year Total Water Levels for each of the beach profile sites. Specific information about the extreme value techniques used to estimate these TWL_S is described in Section 4.6. **Figure 6-6** gives an example of the extreme value (GPD-Poisson) model for the TILL 6 profile site in which the 100-year event is calculated to be 11.6 m (38 ft) and the 500-year event is estimated to be 12.6 m (41 ft). The results for all of the profiles can be found in **Table 6-2**.

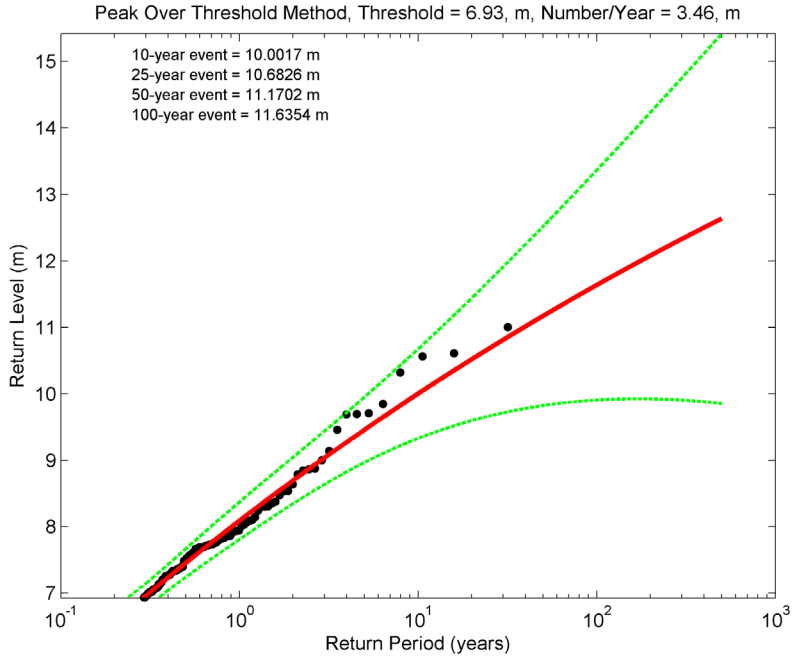

Figure 6-6. Example peak over threshold (POT) extreme value theory results for the Tillamook 6 transect site (with 95% confidence levels) located in the Neskowin littoral cell. Note that the y-axis vertical datum is relative to the NAVD88 vertical datum. Black dots reflect the discrete peak total water level events and the red line is the extreme value distribution fit to those data. Green dashed line reflects the 95% confidence boundary.

Table 6-2. 100-year (1%) and 500-year (0.2%) total water levels calculated for the Tillamook County transect sites.

Reach	Transect	DFIRM Transect	D_{HIGH} (m)	D_{LOW} (m)	100-year (m)	500-year (m)	Description
Salmon River	LINC 308	1	6.251	5.058	9.29	10.62	dune-backed cliff
Cascade Head	LINC 309	2	48.172	1.609	14.13	14.28	plunging cliff
	LINC 310	3	43.56	1.207	13.83	14.01	plunging cliff
	LINC 311	4	24.427	0.358	12.91	13.46	boulder beach backed by bluffs
	LINC 312	5	93.24	2.125	12.4	12.68	plunging cliff
	LINC 313	6	139.103	0	17.29	17.49	plunging cliff
Neskowin	TILL 1	7	47.278	0.764	9.97	10.04	sandy beach backed by riprap and high cliffs
	TILL 2	8	8.684	3.914	8.32	8.91	sand beach backed by riprap
	TILL 3	9	8.452	3.914	8.05	9.23	sand beach backed by riprap
	TILL 4	10	5.184	3.448	7.84	9.18	sand beach backed by riprap
	TILL 5	11	8.312	2.712	10.98	11.53	sand beach backed by riprap
	TILL 6	12	8.447	3.563	11.64	12.64	sand beach backed by riprap
	TILL 7	13	8.169	1.904	12.57	13.09	sand beach backed by riprap
	TILL 8	14	8.539	2.533	11.56	12.24	sand beach backed by riprap
	TILL 9	15	7.075	5.888	7.77	8.02	dune-backed
	TILL 10	16	8.897	6.235	7.79	8.27	dune-backed
	TILL 11	17	6.679	5.604	7.11	7.51	dune-backed
	TILL 12	18	8.374	5.521	7.22	7.60	dune-backed
	TILL 13	19	7.126	5.709	7.34	7.62	dune-backed
	TILL 14	20	8.118	5.086	11.24	12.59	sand beach backed by riprap
	TILL 15	21	7.587	4.642	9.13	9.41	sand beach backed by riprap
	TILL 16	22	6.767	6.014	7.47	7.73	dune-backed
	TILL 17	23	9.986	4.326	6.94	7.25	dune-backed
	TILL 18	24	8.387	5.512	8.66	9.25	dune-backed
	TILL 19	25	6.014	6.014	7.98	8.48	dune-backed
	TILL 20	26	7.648	7.066	10.08	10.68	dune-backed
	TILL 21	27	12.562	5.582	7.46	7.84	dune-backed
	TILL 22	28	6.241	4.489	6.77	7.07	dune-backed
	TILL 23	29	14.334	6.819	10.11	10.95	dune-backed
	TILL 24	30	7.792	7.185	7.95	8.16	dune-backed
	TILL 25	31	7.642	5.627	8.29	8.77	dune-backed
	TILL 26	32	32.562	3.877	9.35	10.11	sandy beach backed by high cliffs
	TILL 27	33	28.194	4.519	9.63	10.07	sandy beach backed by high cliffs
	TILL 28	34	39.310	6.292	8.76	9.08	sandy beach backed by dunes and high cliffs
Nestucca spit/ Pacific City	TILL 29	35	10.245	4.903	7.15	7.49	dune-backed
	TILL 30	36	14.485	5.083	7.31	7.66	dune-backed
	TILL 31	37	15.490	5.933	7.96	8.37	dune-backed
	TILL 32	38	14.358	5.413	9.76	10.32	dune-backed
	TILL 33	39	13.160	5.338	8.74	9.28	dune-backed
	TILL 34	40	15.877	6.611	9.45	10.03	dune-backed
	TILL 35	41	15.147	5.312	7.42	7.84	dune-backed
	TILL 36	42	17.709	5.908	7.58	8.01	dune-backed
	TILL 37	43	12.932	4.389	8.27	8.51	sand beach backed by riprap?
	TILL 38	44	11.283	4.690	7.68	8.12	sand beach backed by riprap?
	TILL 39	45	18.954	5.407	7.12	7.50	dune-backed
	TILL 40	46	11.314	5.539	8.06	8.66	sand beach backed by riprap?
	TILL 41	47	11.060	4.785	7.12	7.55	sand beach backed by riprap?
	TILL 42	48	13.304	4.681	7.81	8.67	sand beach backed by riprap and high bluffs

Reach	Transect	DFIRM Transect	D_{HIGH} (m)	D_{LOW} (m)	100-year (m)	500-year (m)	Description
Sand Lake/ Tierra Del Mar	TILL 43	49	23.369	5.582	7.30	7.67	sandy beach backed by high cliffs
	TILL 44	50	16.741	6.162	8.57	9.02	sandy beach backed by high cliffs
	TILL 45	51	6.868	4.232	10.93	12.05	sandy beach backed by cobbles - grades into bluff
	TILL 46	52	18.071	4.865	10.43	11.18	sandy beach backed by high cliffs
	TILL 47	53	18.396	4.063	9.01	10.64	sand beach backed by riprap
	TILL 48	54	7.412	6.555	7.36	7.71	dune-backed
	TILL 49	55	8.240	6.197	7.19	7.58	dune-backed
	TILL 50	56	6.931	5.891	7.13	7.46	dune-backed
	TILL 51	57	6.317	4.554	9.83	11.96	sand beach backed by riprap
	TILL 52	58	7.721	4.543	10.03	11.37	sand beach backed by riprap
	TILL 53	59	8.141	5.026	7.59	7.96	sand beach backed by riprap
	TILL 54	60	7.462	5.055	8.03	8.52	sand beach backed by riprap
	TILL 55	61	8.094	5.159	7.33	7.85	dune-backed
	TILL 56	62	8.357	4.652	7.29	7.68	sand beach backed by riprap
	TILL 57	63	11.383	4.823	7.00	7.36	sand beach backed by riprap
	TILL 58	64	10.224	6.180	7.11	7.51	dune-backed
	TILL 59	65	12.153	5.720	7.51	7.80	dune-backed
	TILL 60	66	9.595	5.355	7.22	7.63	dune-backed
	TILL 61	67	9.370	6.193	7.37	7.73	dune-backed
	TILL 62	68	6.573	6.260	7.64	8.09	dune-backed
	TILL 63	69	3.380	3.324	5.79	6.04	dune-backed
	TILL 64	70	18.524	6.915	10.87	11.59	dune-backed
	TILL 65	71	18.296	5.556	7.86	8.40	dune-backed
	TILL 66	72	15.211	5.340	7.66	8.14	dune-backed
	TILL 67	73	19.042	8.385	8.70	9.33	sandy beach backed by high cliffs
	TILL 68	74	24.720	6.441	7.08	7.40	sandy beach backed by high cliffs
	TILL 69	75	29.519	5.960	7.65	8.12	sandy beach backed by high cliffs
	TILL 70	76	30.293	4.588	9.71	10.22	sandy beach backed by high cliffs
	TILL 71	77	37.153	4.979	10.25	10.89	sandy beach backed by high cliffs
	TILL 72	78	30.575	4.844	7.30	7.95	sandy beach backed by high cliffs
	TILL 73	79	28.571	6.625	7.57	8.13	sandy beach backed by high cliffs
	TILL 74	80	20.692	5.762	6.82	7.17	sandy beach backed by high cliffs

Reach	Transect	DFIRM Transect	D_{HIGH} (m)	D_{LOW} (m)	100-year (m)	500-year (m)	Description
Netarts Spit/ Oceanside	TILL 75	81	6.775	2.430	9.63	9.99	sandy beach backed by low/high cliffs
	TILL 76	82	7.600	2.937	10.40	11.58	sandy beach backed by cobbles/boulders and low cliff
	TILL 77	83	8.447	3.235	10.38	11.11	sandy beach backed by dynamic revetment/artificial dune
	TILL 78	84	7.298	3.706	10.06	10.97	sandy beach backed by dynamic revetment/artificial dune
	TILL 79	85	10.798	3.976	9.84	11.42	dune-backed (+cobbles)
	TILL 80	86	9.131	5.381	9.15	9.59	dune-backed (+cobbles)
	TILL 81	87	7.159	4.661	8.58	9.13	dune-backed (+cobbles)
	TILL 82	88	11.562	5.040	7.87	8.34	dune-backed
	TILL 83	89	12.413	5.492	7.55	7.86	dune-backed
	TILL 84	90	7.322	6.012	7.34	7.77	dune-backed
	TILL 85	91	11.621	5.370	7.43	7.88	dune-backed
	TILL 86	92	11.763	6.361	7.40	7.83	dune-backed
	TILL 87	93	19.722	4.114	7.36	7.85	dune-backed
	TILL 88	94	6.567	5.720	8.17	8.84	dune-backed
	TILL 89	95	10.543	5.754	7.58	8.04	dune-backed
	TILL 90	96	12.156	4.768	7.33	7.63	dune-backed
	TILL 91	97	9.610	6.516	7.76	8.26	dune-backed
	TILL 92	98	8.324	6.360	7.70	8.20	dune-backed
	TILL 93	99	4.971	4.855	8.52	9.12	Cobble beach backed by low wall (estuary mouth)
	TILL 94	100	14.619	5.554	8.89	9.79	sandy beach backed by high cliffs
	TILL 95	101	29.639	4.999	7.30	8.08	sandy beach backed by high cliffs
	TILL 96	102	39.082	4.536	8.29	9.13	sandy beach backed by high cliffs
	TILL 97	103	55.206	4.631	8.30	8.80	sandy beach backed by dune and high cliffs
	TILL 98	104	60.658	5.832	8.71	9.15	sandy beach backed by dune and high cliffs
	TILL 99	105	33.925	4.907	7.21	7.56	sandy beach backed by high cliffs
	TILL 100	106	36.465	4.585	7.08	7.44	sandy beach backed by high cliffs
	TILL 101	107	13.733	5.191	7.05	7.36	sandy beach backed by poor riprap and low cliffs
	TILL 102	108	18.353	5.953	7.57	8.01	sandy beach backed by moderately high cliffs
	TILL 103	109	8.241	4.068	9.77	10.24	sandy beach backed by moderately high cliffs
Short Sand Beach	TILL 104	110	33.582	3.026	11.00	11.60	sandy beach backed by gravels and high cliffs
	TILL 105	111	26.461	3.932	11.99	12.89	sandy beach backed by gravels and high cliffs
	TILL 106	112	47.152	5.674	14.39	18.27	sandy beach backed by gravels and high cliffs

Reach	Transect	DFIRM Transect	D_{HIGH} (m)	D_{LOW} (m)	100-year (m)	500-year (m)	Description
Bayocean Spit	TILL 107	113	8.705	3.527	11.43	12.49	sandy beach backed by cobble/boulder and low cliffs
	TILL 108	114	7.740	2.981	10.15	10.57	sandy beach backed by cobble/boulder and low cliffs
	TILL 109	115	6.340	3.000	10.39	10.83	sandy beach backed by cobble/boulder berm
	TILL 110	116	6.081	2.495	10.44	10.69	sandy beach backed by cobble/boulder berm
	TILL 111	117	6.863	3.330	10.84	11.71	sandy beach backed by cobble/boulder berm
	TILL 112	118	9.667	6.824	7.34	7.76	dune-backed
	TILL 113	119	11.095	6.670	7.50	7.99	dune-backed
	TILL 114	120	9.781	6.804	7.12	7.50	dune-backed
	TILL 115	121	8.970	4.932	7.22	7.59	dune-backed
	TILL 116	122	10.490	5.889	6.74	6.97	dune-backed
	TILL 117	123	10.053	6.537	7.36	7.89	dune-backed
Rockaway	TILL 118	124	5.932	5.932	7.52	7.99	dune-backed
	TILL 119	125	6.332	4.905	6.93	7.19	dune-backed
	TILL 120	126	6.720	5.370	7.23	7.60	dune-backed
	TILL 121	127	6.749	5.178	7.79	8.18	dune-backed
	TILL 122	128	6.518	5.388	7.29	7.74	dune-backed
	TILL 123	129	7.242	3.130	8.32	8.52	sand beach backed by riprap
	TILL 124	130	6.905	5.820	7.13	7.44	dune-backed
	TILL 125	131	5.489	5.489	6.94	7.20	dune-backed
	TILL 126	132	5.858	4.586	6.06	6.28	dune-backed
	TILL 127	133	7.148	5.709	6.79	7.07	dune-backed
	TILL 128	134	7.976	5.327	7.05	7.42	dune-backed
	TILL 129	135	7.237	5.136	7.07	7.63	dune-backed
	TILL 130	136	7.344	5.839	7.30	7.78	dune-backed
	TILL 131	137	7.032	4.682	7.10	7.60	dune-backed
	TILL 132	138	5.486	3.770	7.34	7.81	sand beach backed by riprap
	TILL 133	139	7.133	5.593	7.26	7.70	dune-backed
	TILL 134	140	10.147	5.680	7.25	7.61	dune-backed
	TILL 135	141	8.387	7.085	7.60	7.89	dune-backed
	TILL 136	142	7.062	5.920	6.85	7.20	sand beach backed by low bluff
	TILL 137	143	6.827	4.000	7.44	8.20	sand beach backed by riprap
	TILL 138	144	6.359	3.045	7.82	8.27	sand beach backed by riprap
	TILL 139	145	8.670	5.263	6.93	7.25	dune-backed
	TILL 140	146	8.923	3.759	9.71	10.57	sand beach backed by riprap
	TILL 141	147	7.643	3.759	10.71	13.99	sand beach backed by riprap
	TILL 142	148	8.305	3.759	10.34	11.71	sand beach backed by riprap
	TILL 143	149	8.196	4.068	9.55	10.34	sand beach backed by riprap
	TILL 144	150	8.305	3.312	10.35	10.88	sand beach backed by riprap
	TILL 145	151	8.092	4.309	8.80	9.77	sand beach backed by riprap
	TILL 146	152	8.176	4.029	8.93	9.79	sand beach backed by riprap
	TILL 147	153	7.927	7.160	7.73	8.15	dune-backed
	TILL 148	154	8.101	5.982	7.80	8.27	dune-backed
	TILL 149	155	8.029	5.997	7.44	7.88	dune-backed
	TILL 150	156	8.315	6.325	7.08	7.37	dune-backed
	TILL 151	157	6.974	4.176	6.17	6.41	sand beach backed by riprap
	TILL 152	158	8.688	6.358	8.24	8.76	dune-backed
	TILL 153	159	8.773	4.786	6.71	7.03	dune-backed
	TILL 154	160	8.966	6.457	7.74	8.35	dune-backed
	TILL 155	161	8.448	6.267	7.21	7.69	dune-backed
	TILL 156	162	8.409	6.061	6.98	7.39	dune-backed
	TILL 157	163	6.833	5.548	6.39	6.67	dune-backed

Reach	Transect	DFIRM Transect	D_{HIGH} (m)	D_{LOW} (m)	100-year (m)	500-year (m)	Description
Nehalem Spit/ Manzanita	TILL 158	164	7.752	6.112	7.62	8.13	dune-backed
	TILL 159	165	12.218	6.616	7.83	8.33	dune-backed
	TILL 160	166	8.676	6.254	8.62	9.40	dune-backed
	TILL 161	167	7.828	5.901	8.13	8.73	dune-backed
	TILL 162	168	15.433	5.338	7.01	7.36	dune-backed
	TILL 163	169	13.023	5.823	6.89	7.17	dune-backed
	TILL 164	170	14.069	5.912	7.66	8.19	dune-backed
	TILL 165	170	15.750	5.514	7.57	8.05	dune-backed
	TILL 166	172	12.088	4.356	6.89	7.27	dune-backed
	TILL 167	173	12.772	5.616	7.05	7.49	dune-backed
	TILL 168	174	13.313	6.617	6.94	7.33	dune-backed
	TILL 169	175	10.635	7.807	8.93	9.58	dune-backed
	TILL 170	176	9.226	4.313	6.35	6.67	sand beach backed by riprap
	TILL 171	177	8.847	5.064	6.48	6.81	dune-backed
	TILL 172	178	9.502	6.107	6.51	6.78	dune-backed with road
	TILL 173	179	11.496	5.245	6.61	6.94	dune-backed with road
	TILL 174	180	9.609	5.516	6.54	6.86	dune-backed with road
	TILL 175	181	11.367	4.730	6.65	7.04	dune-backed
	TILL 176	182	9.012	5.504	7.81	8.51	sand beach backed by extensive cobble berm
	TILL 177	183	6.996	5.077	7.60	8.03	sand beach backed by extensive cobble berm and bluff
	TILL 178	184	7.921	7.894	14.26	15.29	sand beach backed by extensive cobble berm and bluff
Falcon Cove	CP 1	185	15.935	7.027	9.93	10.33	sand, cobble berm backed by high bluff

Notes:

100-year and 500-year total water level (TWL) values relative to NAVD88 vertical datum.

D_{HIGH} is the crest of the dune, bluff, or barrier determined for the eroded profile. *Red text denotes that the crest is overtopped.*

6.4 Overtopping Calculations

Overtopping of natural features such as foredunes, spits, and coastal engineering structures and barriers occurs when the wave runup superimposed on the tide exceeds the crest of the foredune or structure (**Figure 6-7**). Hazards associated with wave overtopping can be linked to a number of simple direct flow parameters including (Pullen and others, 2007):

- mean overtopping discharge, *q*;
- overtopping velocities over the crest and farther landward, *V*;
- landward extent of green water and splash overtopping $y_{G,\,outer}$; and
- overtopping flow depth, *h* at a distance *y* landward of the foredune crest or "barrier."

NHC (2005) notes that there are three physical types of wave overtopping:

1. *Green water or bore overtopping* occurs when waves break onto or over the foredune or barrier and the overtopping volume is relatively continuous;
2. *Splash overtopping* occurs when the waves break seaward of the foredune or barrier, or where the foredune or barrier is high relative to the wave height and overtopping consists of a stream of droplets. Splash overtopping can be a function of its momentum due to the runup swashing up the barrier and/or may be enhanced due to onshore direct winds; and,
3. *Spray overtopping* is generated by the effects of wind blowing droplets and spray that are derived from the wave crests.

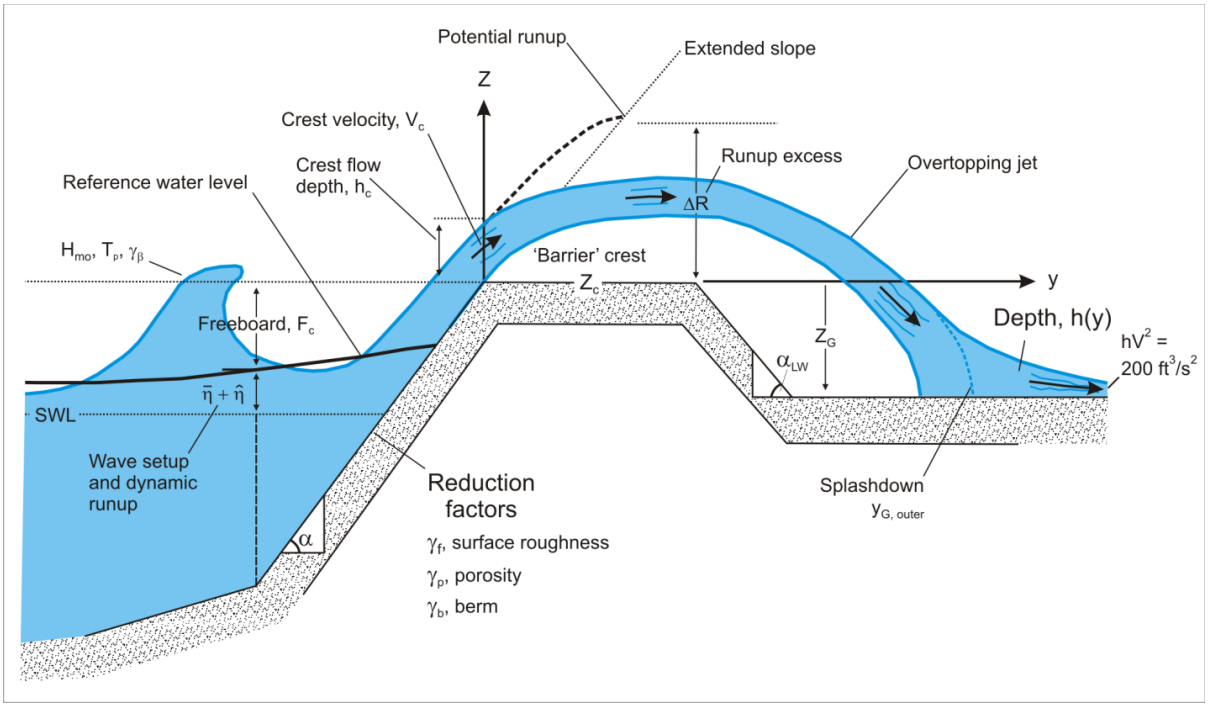

Figure 6-7. Nomenclature of overtopping parameters available for mapping base flood elevations (BFEs) and flood hazard zones (after NHC, 2005).

Mapping these respective flood inundation zones requires an estimate of the velocity, *V*, the overtopping discharge, *q*, of the water that is carried over the crest, the inland extent of green water and splash overtopping, and the envelope of the water surface that is defined by the water depth, *h*, landward of the barrier crest. According to NHC (2005) these hazard zones are ultimately defined from following two derivations:

- Base flood elevations (BFEs) are determined based on the water surface envelope landward of the barrier crest; and
- Hazard zones are determined based on the landward extent of green water and splash overtopping, and on the depth and flow velocity in any sheet flow areas beyond that, defined as $hV^2 = 5.7\ m^3/s^2$ *or* $200\ ft^3/s^2$.

A distinction can be made between whether green water (or bore) or splash overtopping predominates at a particular location that is dependent on the ratio of the calculated wave runup height relative to the barrier crest elevation, R/Z_c. When $1 < R/Z_c < 2$, splash overtopping dominates; when $R/Z_c > 2$, bore propagation occurs. In both cases, R and Z_c are relative to the 2% dynamic water level ($DWL_{2\%}$) at the barrier (Figure D.4.5-12 in NHC [2005, p. D.4.5-22]).

6.4.1 Mean overtopping rate at the "barrier" crest

Wave overtopping of dunes and barrier is a function of both hydraulic and barrier structure parameters whereby:

$$q = f(H_{mo}, T_p, \beta, F_c, DWL_{2\%}, geometry) \qquad (6.14)$$

where q is the overtopping discharge (expressed as cubic meters per second per meter, $m^3/s/m$ [$ft^3/s/ft$]), H_{mo} is the significant wave height at the toe of the structure, T_p is the peak period, β is the angle of wave attack, F_c is the freeboard, and $DWL_{2\%}$ is 2% dynamic water level at the toe of the structure (**Figure 6-7**).

Prior to calculating the mean overtopping rate at the barrier crest it is necessary to distinguish between four contrasting types of wave breaking situations that may impact a particular barrier or dune overtopping situation. There four conditions include *non-breaking* or *breaking* on a normally sloped barrier (where $0.067 < \tan\alpha < 0.67$), and *reflecting* or *impacting* on steeply sloping or vertical barriers (where $\tan\alpha \geq 0.67$). Of these, the breaking wave situation is the dominant condition in Tillamook County, where the waves have already broken across the surf zone and are reforming as bores prior to swashing up the beach face or barrier.

For beaches and normally sloping barriers (where $0.067 < \tan\alpha < 0.67$), a distinction can be made between situations where waves break directly on the barrier versus those conditions where the waves have not yet broken. These conditions can be determined using the surf similarity parameter (Iribarren number) defined here in terms of the beach or structure slope ($\tan\alpha$), and the wave steepness ($S_{op} = H_{mo}/L_o$):

$$\xi_{op} = \frac{\tan\alpha}{\sqrt{\frac{H_{mo}}{L_o}}} = \frac{\tan\alpha}{\sqrt{S_{op}}} \qquad (6.15)$$

Breaking on normally sloping surfaces generally occurs where the surf similarity number, $\xi_{op} \leq 1.8$, while non-breaking conditions occur when $\xi_{op} > 1.8$. As noted above, for the Tillamook County coastline the identified Iribarren numbers almost always fell below the 1.8 criteria, indicating that the incident waves are always broken prior to reaching the beach or the barrier face.

At the beach or barrier crest, the relative freeboard (F_c/H_{mo}), **Figure 6-7,** is a particularly important because changing these two parameters controls the volume of water that flows over the barrier crest. For example, increasing the wave height or period increases the overtopping discharge, as does reducing the beach or barrier crest height or raising the water level.

A variety of prediction methods are available for calculating the overtopping discharge and are almost entirely based on laboratory experiments using a range of structure slopes (slopes between 1:1 and 1:8, with occasional tests at slopes around 1:15 or lower). Factors that will serve to reduce the potential overtopping discharge include the barrier *surface roughness* (γ_f), the presence of a *berm* (γ_b), *wave approach directions* (γ_β), and the *porosity* of the barrier (γ_p) (**Figure 6-7**). In terms of porosity, increasing this variable effectively reduces the wave runup and overtopping discharge because more of the water is able to be taken up by the voids between the clasts

and particles. As noted in NHC (2005), the effect of the *porosity* factor makes it convenient to distinguish between impermeable and permeable structures. Methods for determining the various reduction factors are described in Table D.4.5-3 in NHC (2005, p. D.4.5-13), with one difference whereby the approach recommended for determining the wave approach (γ_β) reduction factor for wave overtopping calculations is based on the following equation:

$$\gamma_\beta = \begin{Bmatrix} 1 - 0.0033|\beta|, (0 \le |\beta| \le 80°) \\ 1 - 0.0033|80|, (|\beta| \ge 80°) \end{Bmatrix} \quad (6.16)$$

Table D.4.5-3 in NHC (2005, p. D.4.5-13) identifies four general categories of overtopping applications: overtopping on a normally sloping barrier (e.g., riprap structure), steep sloping or vertical barrier (e.g., seawall or bluff where some waves broken); steep sloping or vertical barrier (all waves broken); and shallow foreshore slopes subject to large Iribarren numbers.

For a normally sloping barrier, where 0.05 < tan α < 0.67 and the Iribarren number (ξ_{op}) ≤ 1.8 (breaking wave condition), the following formulation can be used to determine the mean overtopping discharge (both dimensional [q] and non-dimensional [Q] forms) at the barrier crest:

$$q = Q\sqrt{\frac{gH_{mo}\tan\alpha}{S_{op}}} \text{ where:} \quad (6.17)$$

$$Q = 0.06e^{-4.7F'}, \text{ and}$$

$$F' = \frac{F_c}{H_{mo}} \frac{\sqrt{S_{op}}}{\tan\alpha} \frac{1}{\gamma_f\gamma_b\gamma_\beta\gamma_p}$$

For non-breaking conditions (Iribarren number (ξ_{op}) > 1.8):

$$q = Q\sqrt{gH_{mo}^3} \text{ where:} \quad (6.18)$$

$$Q = 0.2e^{-2.3F'}, \text{ and}$$

$$F' = \frac{F_c}{H_{mo}} \frac{1}{\gamma_f\gamma_\beta}$$

For steep sloping or vertical barrier, where tan α > 0.67 and $h_* \ge 0.3$ (reflecting conditions where

$$h_* = \frac{h}{H_{mo}}\left(\frac{2\pi h}{gT_m^2}\right)$$

and h is the water depth at the structure toe), the following formulation can be used:

$$q = Q\sqrt{gH_{mo}^3} \text{ where:} \quad (6.19)$$

$$Q = 0.05e^{-2.78F_c/H_{mo}}$$

For impacting conditions (h_* < 0.3):

$$q = Q\sqrt{gh^3}\, h_*^2 \text{ where:} \quad (6.20)$$

$$Q = 1.37 * 10^{-4}(F')^{-3.24}, \text{ and}$$

$$F' = \frac{F_c}{H_{mo}} h_*$$

For steep sloping or vertical barrier (all waves are broken) where the structure toe < $DWL_{2\%}$ water level and where $(F_c/H_{mo})^* h_* \le 0.03$:

$$q = Q\sqrt{gh^3}\, h_*^2 \text{ where:} \quad (6.21)$$

$$Q = 0.27 * 10^{-4}e^{-3.24\,(F_c/H_{mo})h_*}$$

For steep sloping or vertical barrier (all waves are broken) where the structure toe > $DWL_{2\%}$ water level:

$$q = Q\sqrt{gh^3}\, h_*^2 \text{ where:} \quad (6.22)$$

$$Q = 0.06e^{-4.7\,F_c S_{op}^{-0.17}}$$

We have implemented two additional overtopping calculations following discussions with Dr. W. G. McDougal, which may be applied to beaches subject to gently sloping (tan β < 0.4), dissipative foreshores:

$$q = Q\sqrt{gh^3}h_*^2 \text{ where:} \quad (6.23)$$

$$Q = 0.21\sqrt{gH_{mo}^3}e^{-F'}, \text{ and}$$

$$F' = \frac{F_c}{\gamma_f \gamma_\beta H_{mo}(0.33 + 0.022\xi_{op})}$$

and cases where there is negative freeboard. The latter occurs when the dynamic water level (DWL2%) is higher than the barrier crest, which produces a negative freeboard (i.e., $-F_c$). In this situation we apply the well-known weir type formula to define the volume of water that is overflowing the crest (Eurotop, 2007). The formulation used is:

$$q = Q_s + q_w \text{ where:} \quad (6.24)$$

$$Q_s = 0.4583(-F_C)\sqrt{-F_C g},$$

$$Q_w = 0.21\sqrt{gH_{mo}^3}, \text{ and}$$

$$q_w = Q_w\sqrt{gh^3}h_*^2$$

6.4.2 Overtopping limits and flood hazard zones landward of the "barrier" crest

Estimates of the landward limit of the splashdown distance associated with wave overtopping and the landward limit of the hazard zone require several calculation steps. These include:

1. The following three initial parameters are first calculated:
   a. excess potential runup: $\Delta R = R\text{-}Z_c$;
   b. crest flow rate, $V_c \cos\alpha$ (where $V_c = 1.1\sqrt{g\Delta R}$ for cases where splash overtopping, and $V_c = 1.8\sqrt{g\Delta R}$ for bore overtopping); and
   c. initial flow depth, h_c (where $h_c = 0.38\Delta R$).

2. The associated onshore wind component, *Wy*, is determined from available wind data. For the purposes of this study, we used *Wy* = 19.6 m/s (64.3 ft/s), which was determined from an analysis of winds (mean from a select number of storms) measured at the Cape Arago C-MAN station operated by the NDBC. In the absence of wind data, NHC (2005) recommends a wind speed of 13.4 m/s (44 ft/s).
3. The enhanced onshore water velocity component $(V_c \cos\alpha)'$ is then calculated using equation 6.25:

For vertical bluffs and seawalls;

$$(V_c \cos\alpha)' = 0.3 * W_y \quad (6.25)$$

All other cases: $(V_c \cos\alpha)' = V_c \cos\alpha + 0.3(W_y - V_c \cos\alpha)$

4. The effective angle, α_{eff}, is calculated from:

$$\tan\alpha_{eff} = \frac{V_c \sin\alpha}{(V_c \cos\alpha)'}.$$

5. Having determined the above parameters, the outer limit of the splash region, $y_{G\ outer}$ is calculated using equation 6.26. Here we have used an algorithm developed by Dr. W. G. McDougal (Coastal Engineer, OSU and Technical Coordinator of the North Pacific FEMA West Coast Guidelines) of the form:

$$y_{G\ outer} = \frac{(V_c \cos\ \alpha)'}{g} * V_c\ \sin\ \alpha - mBackshore * (V_c \cos\ \alpha)' * \left(1 + \sqrt{1 - \frac{2g * bBackshore}{(V_c\ \sin\ \alpha - mBackshore * (V_c\ \cos\ \alpha)'^2)}}\right) \quad (6.26)$$

and

$$Z_G = bBackshore + (mBackshore * y_{G\ outer}) \quad (6.27)$$

where *bBackshore* is the intercept for the backshore slope adjacent to the barrier crest and mBackshore is the slope of the backshore. equation 6.26 is ultimately based on Figure D.4.5-15 in NHC (2005, p. D.4.5-30).

6. The total energy, *E*, of the splashdown is calculated from $E = \Delta R\text{-}Z_G$.
7. Finally, the initial splashdown velocity, V_o (where $V_o = 1.1\sqrt{gE}$), and depth, h_o (where $h_o = 0.19E$) are calculated. In the case of green water or bore overtopping, the splashdown velocity, V_o, can be calculated from $V_o = 1.1\sqrt{g\Delta R}$, while the flow depth is determined as $h_o = 0.38E$.

Having determined the initial splashdown velocity, V_o, and flow depth, h_o, the landward extent of the overland flow is calculated using an approach modified from that originally proposed by Cox and Machemehl (1986). The version presented by NHC (2005) effectively calculates the flow depth, *h*, with distance, *y*, from the barrier crest, such that the flow depth decays asymptotically as y-distance increases away from the barrier crest, eventually approaching zero. The NHC (2005) equation is shown as equation 6.28:

$$h(y) = \left[\sqrt{h_o} - \frac{5(y - y_o)}{A\sqrt{gT^2}}\right]^2 \quad (6.28)$$

where h_o is determined from step 7 above and for an initial approximation the nondimensional *A* parameter may be taken as unity. For sloping backshores, the *A* parameter in equation 6.28 can be modified such that $A_m = A(1 - 2 * \tan\alpha_{LW})$, and the value in parentheses is limited to the range 0.5 to 2. According to NHC (2005) if the maximum distance of splash or bore propagation calculated using equation 6.28 does not appear reasonable or match field observations, the *A* parameter can be adjusted in order to increase or decrease the landward wave propagation distance. In addition, for green water or bore propagation the *A* parameter value is taken initially to be 1.8.

For the purposes of this study we have adopted a modified version of equation 6.28 developed by Dr. W. G. McDougal of the form:

$$h(y) = \left[h_o^{1/2} - \frac{y - y_o}{2\alpha(\alpha+1)^{\frac{3}{2}}(1-2m)\,g^{0.5}T} \right]^2 \qquad (6.29)$$

where m is the slope of the backshore and α is a constant that can be varied in order to increase or decrease the landward wave propagation distance.

Finally, the landward limit of the hazard zone defined as hV^2 = 5.7 m^3/s^2 (or 200 ft^3/s^2) is determined, whereby h is the water depth given by the modified Cox and Machemehl (1986) method (equation 6.29) and $V = V_o$ calculated from step 7 above.

6.4.3 Initial testing of the landward limit of wave overtopping

Our initial computations of the landward extent of wave overtopping using the steps outlined above yielded narrow hazard zones for our original coastal FIRM study in Coos County. To calibrate equation 6.29, we performed wave overtopping calculations and inundation for a site on the northern Oregon coast where there are field observations of wave overtopping: Cape Lookout State Park in Tillamook County (Allan and others, 2006; Allan and Komar, 2002a; Komar and others, 2003). The southern portion of Cape Lookout State Park is characterized by a wide, gently sloping, dissipative sand beach, backed by a moderately steep gravel berm and ultimately by a low foredune that has undergone significant erosion since the early 1980s (Komar and others, 2000).

On March 2-3, 1999, the crest of the cobble berm/dune at Cape Lookout State Park was overtopped during a major storm; the significant wave heights reached 14.1 m (46.3 ft), while the peak periods were 14.3 s measured by a deepwater NDBC wave buoy (Allan and Komar, 2002b). Wave overtopping of the dune and flooding extended ~70 m (230 ft) into the park (Dr. P. Komar, Emeritus Professor, College of Oceanic and Atmospheric Sciences, pers. comm., 2010), evidence for which included photos and field evidence including pockmarks at the bases of tree trunks located in the park. These pockmarks were caused by cobbles having been carried into the park from the beach by the overtopping waves, where the cobbles eventually slammed into the bases of the trees as ballistics. Because the average beach slopes at Cape Lookout State Park are analogous to those observed elsewhere along the Tillamook County coastline and because large wave events associated with extratropical storms affect significant stretches (100s to 1000 kilometers) of the coast at any single point in time, we believe these data provide a reasonable means in which to investigate a range of alpha (α) values that may be used to determine the landward extent of wave inundation in the park.

Using beach morphology data (slope (tan β) = 0.089, barrier crest = 5.5 m [18 ft]) from Cape Lookout State Park and deepwater wave statistics from a nearby NDBC wave buoy (#46050), we experimented with a range of alpha values in order to replicate the landward extent of the inundation. As can be seen in **Figure 6-8**, in order to emulate the landward extent of flooding observed at Cape Lookout our analyses yielded an alpha of 0.58. Using alpha = 0.58, we in turn calculated the extent of the hazard zone where $h(y)$ = 200 ft^3/s^2, which was found to be ~34 m from the crest of the cobble berm/dune, consistent with damage to park facilities.

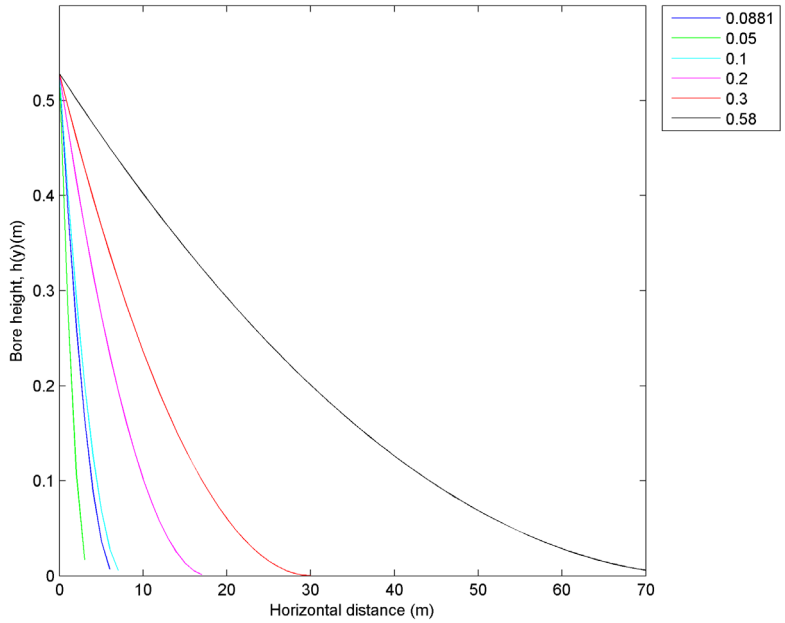

Figure 6-8. Calculations of bore height decay from wave overtopping at Cape Lookout State Park at the peak of the March 2-3, 1999, storm based on a range of alpha (α) values (shown in small box).

6.4.4 Wave overtopping and hazard zone limits calculated for Tillamook County

Table 6-3 presents the results of the calculated splashdown distances ($y_{G\,outer}$) and the landward extent of the flow (hV^2) where the flows approach 5.7 m^3/s^2 (or 200 ft^3/s^2). **Table 6-3** includes a more conservative splashdown distance, based on an enhanced wind velocity of 19.6 m/s (64.3 ft/s); this contrasts with the default wind speed of 13.4 m/s (44 ft/s) suggested by NHC (2005). This enhanced wind velocity was determined from an analysis of wind speeds measured by the Cape Arago C-MAN (http://www.ndbc.noaa.gov/station_page.php?¬station=CARO3) station located adjacent to the mouth of Coos Bay (Allan and others 2012b). Essentially, Allan and others examined the wind speeds identified at Cape Arago for a range of storm events and identified a wide range of values, with a maximum mean wind speed of 19.6 m/s (64.3 ft/s). Because the measured wind speeds reflect a 2-min average such that higher wind speeds have been measured throughout the entire record (e.g., the maximum 2-minute average wind speed is 29.3 m/s [96 ft/s], while the maximum 5-s wind gust reached 38.1 m/s [125.0 ft/s]), we believe it is justified to use the more conservative enhanced wind velocity of 19.6 m/s (64.3 ft/s). Furthermore, comparisons by Allan and others (2012b) indicated that the relative difference between the value suggested by NHC (2005) and the enhanced wind used here differs by about 30%. As can be seen from the **Table 6-3**, the calculated splash-down distances ($y_{G\,outer}$) indicate splash distances that range from as little as 0.9 m (3 ft) to a maximum of 5.9 m (19.4 ft); the mean splash distance is 2.9 m (9.6 ft), while the standard deviation is 1.6 m (5.2 ft). Thus, adopting the reduced wind velocity would cause the zones to narrow by ~1.8 m for the highest splash distance and 0.3 m for the smallest. Overall, these differences are negligible given the tremendous uncertainties in calculating splash and overtopping (NHC, 2005).

Table 6-3. Splashdown and hazard zone limits calculated for Tillamook County detailed coastal sites. Values reported in the table reflect the maximum values derived from all the storm runup and overtopping calculations. Note: Dist_3, Dist_2, and Dist_1 reflect the landward extent at which the calculated bore height decreases from 0.9 m (3 ft), to 0.6 m (2 ft) and, finally, to 0.3 m (1 ft). In all cases, the hazard zones are ultimately defined relative to the location of the dune/structure crest.

Profiles	Transect	DFIRM Transect	Splashdown $y_{G\ outer}$ (m)	Bore Ht (m)	Dist_3 (≥0.91 m)	Dist_2 (>0.61 <0.91 m)	Dist_1 (≤0.31 m)	$hV^2 > 5.7 m^3/s^2$ (m)
Salmon River	LINC 308	1	1.4	0.57			2.66	36.24
Neskowin	TILL 4	10	4.64	0.48			19.79	36.33
	TILL 5	11	6.54	0.50			21.97	39.86
	TILL 6	12	2.30	0.53			17.37	31.08
	TILL 7	13	7.69	0.82		14.24	39.89	64.60
	TILL 8	14	4.29	0.54			24.21	43.10
	TILL 9	15	1.29	0.15				
	TILL 11	17	0.33	0.04				
	TILL 13	19	1.15	0.05				
	TILL 14	20	2.73	0.55			26.58	47.15
	TILL 15	21	5.62	0.51			22.03	39.86
	TILL 16	22	1.59	0.16				
	TILL 18	24	3.74	0.29				
	TILL 19	25	2.55	0.42			14.05	26.84
	TILL 20	26	1.77	0.45			17.56	32.79
	TILL 22	28	1.30	0.11				
	TILL 24	30	0.77	0.04				
	TILL 25	31	0.69	0.08				
Sand Lake	TILL 45	51	1.00	0.68		7.52	47.53	80.16
	TILL 50	56	2.33	0.13				
	TILL 51	57	5.49	0.76		10.30	36.60	60.29
	TILL 52	58	4.71	0.51			18.23	32.88
	TILL 54	60	2.03	0.16				
	TILL 62	68	0.37	0.19				
	TILL 63	69	0.19	0.44			15.82	29.75
Netarts	TILL 75	81	2.24	0.52			30.63	54.94
	TILL 76	82	5	0.6			39.42	68.39
	TILL 77	83	10.79	1.33	27.1	51.41	83.07	123.33
	TILL 78	84	11.97	1.57	43.8	69.78	103.84	150.1
	TILL 80	86						
	TILL 81	87	1.1	0.24				
	TILL 88	94	4.53	0.48			20.98	38.47
	TILL 93	99	1.27	0.66		4.84	37.22	63.07
	TILL 103	109	3.78	0.37			7.02	14.21
Bayocean Spit	TILL 107	113	2.40	0.46			15.18	28.24
	TILL 108	114	1.51	0.44			14.67	27.56
	TILL 109	115	0.74	0.76		13.67	48.34	79.62
	TILL 110	116	2.21	0.81		18.46	53.68	87.21
	TILL 111	117	6.14	0.94	1.76	27.24	60.44	95.45

Profiles	Transect	DFIRM Transect	Splashdown $y_{G\ outer}$ (m)	Bore Ht (m)	Dist_3 (≥0.91 m)	Dist_2 (>0.61 <0.91 m)	Dist_1 (≤0.31 m)	$hV^2 > 5.7 m^3/s^2$ (m)
Rockaway	TILL 118	124	1.83	0.33			2.95	6.84
	TILL 119	125	1.23	0.12				
	TILL 120	126	0.81	0.10				
	TILL 121	127	1.72	0.21				
	TILL 122	128	0.86	0.15				
	TILL 123	129	9.34	1.06	8.87	30.77	59.32	91.65
	TILL 124	130	0.22	0.05				
	TILL 125	131	1.99	0.31			0.56	2.10
	TILL 126	132	0.77	0.04				
	TILL 131	137	2.03	0.10				
	TILL 132	138	0.77	0.34			4.69	10.02
	TILL 137	143	0.58	0.02				
	TILL 138	144	1.55	0.27				
	TILL 140	146	1.71	0.15				
	TILL 141	147	2.84	0.52			24.25	43.49
	TILL 142	148	5.79	0.57			26.12	45.86
	TILL 143	149	6.12	0.49			18.26	33.29
	TILL 144	150	3.93	0.32			1.34	3.48
	TILL 145	151	1.58	0.12				
	TILL 146	152	0.92	0.14				

Hazard zone calculations shown in **Table 6-3** indicate a similarly broad range of values that vary from negligible (i.e., effectively where the 1% TWL intersects with the backshore, plus the width of the splash zone where applicable) to as much as 73 m (240 ft) wide, with the widest zones having occurred where overtopping significantly exceeds the eroded beach crest elevations such as at Falcon Cove and at the south end of Seaside. Qualitative field observations of past storm wave overtopping events at all sites subject to overtopping calculated in this study confirm that this is indeed the case. Hence, field-based observations appear to be consistent with the calibrated results identified in **Table 6-3**. Overtopping for supplemental transects can be found in Appendix D. The depth of flooding at each mapped overtopping zone is indicated in **Table 6-4**.

Table 6-4. The depth of flooding at the overtopping zones landward of the structure crest.

Profiles	Transect	DFIRM Transect	Dist_3 (≥0.91 m)	Dist_2 (>0.61 <0.91 m)	Dist_1 (≤0.31 m)	hV^2 > 5.7m^3/s^2 (m)	Comment
Neskowin	TILL 4	10			0.3	0.3	
	TILL 5	11			0.3	0.3	
	TILL 6	12			0.3	0.3	
	TILL 7	13		0.61	0.3	0.3	
	TILL 8	14			0.3	0.3	
	TILL 14	20			0.3	0.3	
	TILL 15	21			0.3	0.3	
	TILL 20	26			0.3	0.3	hV^2 zone added to VE zone
Sand Lake	TILL 45	51		0.61	0.3	0.3	hV^2 zone not mapped due to topo barrier
	TILL 51	57		0.61	0.3	0.3	
	TILL 52	58			0.3	0.3	
Netarts	TILL 75	81			0.3	0.3	overtopping stopped by topo barrier
	TILL 76	82			0.3	0.3	
	TILL 77	83	0.91	0.61	0.3	0.3	
	TILL 78	84	0.91	0.61	0.3	0.3	
	TILL 88	94			0.3	0.3	
	TILL 93	99		0.61	0.3	0.3	hV^2 zone cut short by topo barrier
	TILL 103	109			0.3	0.3	
Bayocean Spit	TILL 107	113			0.3	0.3	
	TILL 108	114			0.3	0.3	
	TILL 109	115		0.61	0.3	0.3	
	TILL 110	116		0.61	0.3	0.3	
	TILL 111	117	0.91	0.61	0.3	0.3	
Rockaway	TILL 118	124			0.3	0.3	narrow overtopping added to VE zone
	TILL 123	129	0.91	0.61	0.3	0.3	
	TILL 141	147			0.3	0.3	
	TILL 142	148			0.3	0.3	
	TILL 143	149			0.3	0.3	
	TILL 144	150			0.3	0.3	narrow overtopping added to VE zone

7.0 COASTAL EROSION CAUSED BY INDIVIDUAL STORM EVENTS

In order to estimate beach (or bluff) erosion and the resulting profile changes that occur during a particular storm, it is important to first establish the initial profile conditions that existed prior to that storm. As outlined in Section 3.2, this initial profile morphology is represented by the most likely winter profile (MLWP), which forms the basis for determining profile changes that could eventuate as a result of a particularly severe storm(s). Having established the MLWP for a site, the profile is then modified according to the amount of erosion estimated to occur during a specified storm as a result of the increased water levels (tide + surge + ENSO) as well as from wave processes, specifically the wave runup. This section explores two approaches described in the revised FEMA guidelines, which may be used to establish the eroded profiles along the Tillamook County coastline. The second half of the section describes the specific approach adopted for Tillamook County and the results from our erosion analyses.

7.1 Models of Foredune Erosion

7.1.1 The Komar and others (1999) model

The erosion potential of sandy beaches and foredunes along the Pacific Northwest coast of Oregon and Washington is a function of the total water level produced by the combined effect of the wave runup plus the tidal elevation (E_T), exceeding some critical elevation of the fronting beach, typically the elevation of the beach-dune junction (E_J). This basic concept is depicted in **Figure 7-1A** based on the model developed by Ruggiero and others (1996), and in the case of the erosion of a foredune backing the beach the application of a geometric model (**Figure 7-1B**) formulated by Komar and others (1999). Clearly, the more extreme the total water level elevation, the greater the resulting erosion that occurs along both dunes and bluffs.

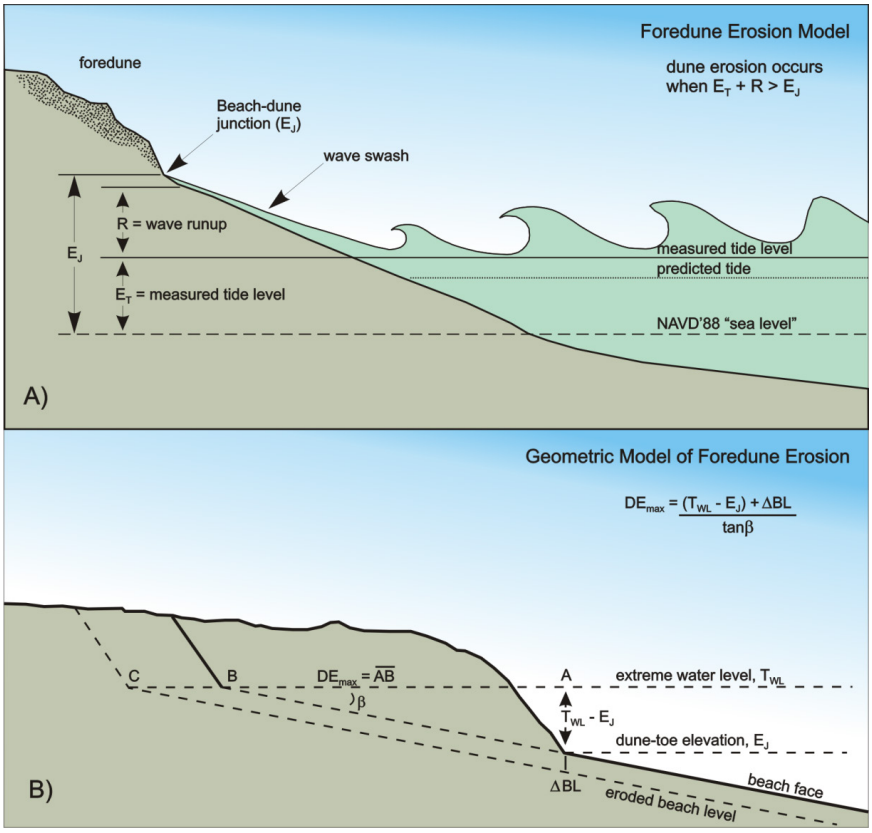

Figure 7-1. A) The foredune erosion model. B) The geometric model used to assess the maximum potential beach erosion in response to an extreme storm (Komar and others, 1999).

As can be seen **from Figure 7-1B**, estimating the maximum potential dune erosion (DE_{max}) is dependent on first determining the total water level (TWL) elevation diagrammed in **Figure 7-1A**, which includes the combined effects of extreme high tides plus storm surge plus wave runup, relative to the elevation of the beach-dune junction (E_J). Therefore, when the TWL > E_J, the foredune retreats landward by some distance, until a new beach-dune junction is established, the elevation of which approximately equals the extreme water level. Because beaches along the high-energy Oregon coast are typically wide and have a nearly uniform slope (tan β), the model assumes that this slope is maintained, and the dunes are eroded landward until the dune face reaches point B in **Figure 7-1B**. As a result, the model is geometric in that it assumes an upward and landward shift of a triangle, one side of which corresponds to the elevated water levels, and then the upward and landward translation of that triangle and beach profile to account for the total possible retreat of the dune (Komar and others, 1999).

An additional feature of the geometric model is its ability to accommodate further lowering of the beach face due to the presence of a rip current, which has been shown to be important to occurrences on the Oregon coast of localized "hot spot" erosion and property impacts (Komar, 1997). This feature of the model is represented by the beach-level change ΔBL shown in **Figure 7-1B**, which causes the dune to retreat some additional distance landward until it reaches point C. As can be seen from **Figure 7-1B**, the distance from point A to point C depicts the total retreat, DE_{max}, expected during a particularly severe storm event (or series of storms) that includes the localized effect enhancement by a rip current. Critical then in applying the model to evaluate the susceptibility of coastal properties to erosion, is an evaluation of the occurrence of extreme tides (E_T), the runup of waves, and the joint probabilities of these processes along the coast (Ruggiero and others, 2001), this having been the focus of Section 6, above.

The geometric model gives the maximum potential equilibrium cross-shore change in the shoreline position landward of the MLWP resulting from a storm. However, in reality it is unlikely that this extreme degree of response is ever fully realized, because of the assumptions that had been made in deriving the geometric model with the intent of evaluating the maximum potential dune erosion. As noted by Komar and others (1999), in the first instance the geometric model projects a mean linear beach slope. As a result, if the beach is more concave, it is probable that the amount of erosion would be less, though not by much. Perhaps of greater significance is that the geometric model assumes an instantaneous erosional response, with the dunes retreating landward as a result of direct wave attack. However, the reality of coastal change is that it is far more complex, there in fact being a lag in the erosional response behind the forcing processes. As noted by Komar and others (1999), the extreme high runup elevations typically occur for only a relatively short period of time (e.g., the period of time in which the high wave runup elevations coincide with high tides). Because tide elevation varies with time (e.g., hourly), the amount of erosion can be expected to be much less when the water levels are lower. Thus, it is probable that several storms during a winter may be required to fully realize the degree of erosion estimated by the geometric model; this did occur, for example, during the winter of 1998-99, with the last five storms the most extreme and erosive (Allan and Komar, 2002). In addition, as beaches erode, the sediment is removed offshore (or farther along the shore) into the surf zone where it accumulates in near shore sand bars. This process helps to mitigate the incoming wave energy by causing the waves to break farther offshore, dissipating some of the wave energy and forming the wide surf zones that are characteristic of the Oregon coast. In turn, this process helps to reduce the rate of beach erosion that occurs. In summary, the actual amount of beach erosion and dune recession is dependent on many factors, the most important of which include the incident wave conditions, the TWL, and the duration of the storm event(s).

7.1.2 The Kriebel and Dean (1993) model

Kriebel and Dean (1993), hereafter known as K&D, developed a dune erosion model that is broadly similar to the Komar and others (1999) geometric model. At its core is the assumption that the beach is in statistical equilibrium with respect to the prevailing wave climate and mean water levels (Bruun, 1962). As water levels increase, the beach profile is shifted upward by an amount equal to the change in water level (S) and landward by an amount R_∞ until the volume of sand eroded from the subaerial beach matches the volume deposited offshore in deeper water (**Figure 7-2**); *note that DE_{MAX} and R_∞ are essentially synonymous with each other*.

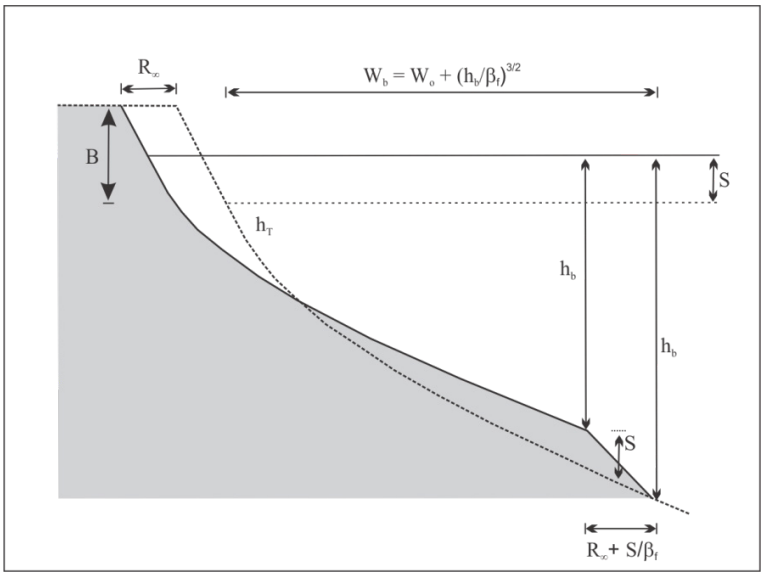

Figure 7-2. Maximum potential erosion (R_∞) due to a change in water levels (after Kriebel and Dean, 1993).

One important distinguishing feature in the K&D model relative to Bruun (1962) is that it relies on the equilibrium beach profile theory proposed by Dean (1977) to account for the erosion following an increase in the water level. The Dean model is a simplified equilibrium form for open-coast beach profiles expressed as a power-law curve of the form:

$$h = Ax^{2/3} \text{ or equivalently as } x = \left(\frac{h}{A}\right)^{3/2} \qquad (7.1)$$

where h is the water depth at a distance x offshore from the still water level and A is a parameter that governs the overall steepness (and slope) of the profile and is a function of the beach grain size. Thus, incorporating the assumed components of Bruun (1962) and Dean (1977), the maximum erosion potential, R_∞, was determined by K&D to be a function of the increase in mean water level (S) caused by a storm, the breaking wave water depth (h_b), surf zone width (W_b), berm or dune height (B or D), and the slope (β_f) of the upper foreshore beach face. The breaking wave depth (h_b) may be calculated from the wave breaker height (equation 6.8) multiplied by 0.78 (the breaker index).

As a result of the above concepts, K&D developed two approaches for determining the maximum erosion potential. These include:

- A beach backed by a low sand berm

$$R_\infty = \frac{S\left(W_b - h_b/\beta_f\right)}{B + h_b - S/2} \qquad (7.2)$$

- A beach backed by high sand dune

$$R_\infty = \frac{S\left(W_b - h_b/\beta_f\right)}{D + h_b - S/2} \qquad (7.3)$$

Like the Komar and others (1999) model, the Kriebel and Dean (1993) dune erosion model estimates the *maximum potential erosion* (DE_{MAX}) associated with a major storm and assumes that a particular storm will last sufficiently long enough to fully erode the dune. In reality, DE_{MAX} is almost never fully realized because storms rarely last long enough to fully erode the dune to the extent of the model predictions. Because the duration of a storm is a major factor controlling beach and dune erosion, K&D developed an approach to account for the duration effects of storms with respect to the response time scale required to fully erode a beach profile. The time scale for the erosion of a dune to the extent R given by equation (7.2) can be estimated using equation 7.4:

$$T_S = C_1 \frac{H_b^{3/2}}{g^{1/2} A^3} \left(1 + \frac{h_b}{B} + \frac{\beta_f W_b}{h_b}\right)^{-1} \qquad (7.4)$$

where T_S is the time scale of response, C_1 is an empirical constant (320), H_b is the breaker height, h_b is the breaker depth, g is acceleration due to gravity, B is the berm elevation, β_f is the slope of the foreshore, W_b is the surf zone width, and A is the beach profile parameter that defines an equilibrium profile. Using equation 7.4 yields typical response times for complete profile erosion that are on the order of 10 to 100 hours (NHC, 2005). In general, as the surf zone width increases due to larger wave heights, smaller grain sizes or gentler slopes, the response time increases. In addition, the response time will also increase as the height of the berm increases.

The beach profile response is determined by a convolution integral. According to NHC (2005), the time dependency of the storm hydrograph may be approximated by:

$$f(t) = \sin^2\left(\pi \frac{t}{T_D}\right) \; for \; 0 < t < T_D \qquad (7.5)$$

where t is time from the start of the storm and T_D is the storm duration. The convolution integral is:

$$DE(t) = \frac{DE_{MAX}}{T_S} \int_0^t f(\tau) e^{-(t-\tau)/T_S} \, d\tau \qquad (7.6)$$

which integrates to:

$$\frac{DE(t)}{DE_{MAX}} = 0.5 \left\{ 1 - \frac{\beta^2}{1+\beta^2} \exp\left(-\frac{t}{T_S}\right) - \frac{1}{1+\beta^2} \left[\cos\left(\frac{2\pi t}{T_D}\right) + \beta \sin\left(\frac{2\pi t}{T_D}\right) \right] \right\} \qquad (7.7)$$

where $\beta = 2\pi T_S / T_D$ and DE_{MAX} is the maximum potential recession that would occur if the storm duration was infinite. Thus, if the storm duration, T_D, is long relative to the time scale of profile response, T_S, then a significant portion of the estimated erosion determined by the K&D or geometric model will occur. As the ratio of these two values decreases, the amount of erosion will also decrease. The time required for maximum beach and dune recession is determined by setting the derivative of equation 7.7 to zero and solving for time. This yields:

$$exp\left(-\frac{t_m}{T_D}\right) = \cos\left(\frac{2\pi t_m}{T_S}\right) - \frac{T_D}{2\pi T_S} \sin\left(\frac{2\pi t_m}{T_S}\right) \qquad (7.8)$$

in which t_m is the time that the maximum erosion occurs with respect to the beginning of the storm. Unfortunately, this equation can only be solved by approximation or numerically. Thus the maximum recession associated with a duration limited storm can be calculated by:

$$\alpha = \frac{DE_m}{DE_{MAX}} = 0.5 \left[1 - \cos\left(2\pi \frac{t_m}{T_D}\right) \right] \qquad (7.9)$$

where α is the duration reduction factor and DE_m is the maximum recession that occurs for a given storm duration that occurs at time t_m. As a result, the duration limited recession is:

$$DE_m = \alpha DE_{MAX} \qquad (7.10)$$

7.1.3 Erosion modeling on Tillamook County beaches

In order to determine the duration reduction factor, α, the duration of each storm event first has to be identified. The approach used here involved an analysis of the number of hours a specific TWL event was found to exceed a particular beach profile's beach-dune junction elevation, applying the Ruggiero and others (2001) analysis approach. **Figure 7-3** is an example of the approach we used, which is based on a script developed in MATLAB. In essence, the blue line is the TWL time series for a particular profile, ±3 days from the event. The script moves backward and forward in time from the identified event until the TWL falls below the critical threshold shown as the black line in **Figure 7-3**, which reflects the beach-dune junction elevation. The duration of the storm was then determined as the period where the TWL exceeds the threshold and includes the shoulders of the event (i.e., when the TWL first falls below the critical threshold). This process was undertaken for every storm and for each of the profile sites. One limitation of this approach that was encountered is that it is possible for the duration to be underestimated if the TWL dips below the threshold for an hour or more and then rises again above the threshold, as seen in the example in **Figure 7-3**.

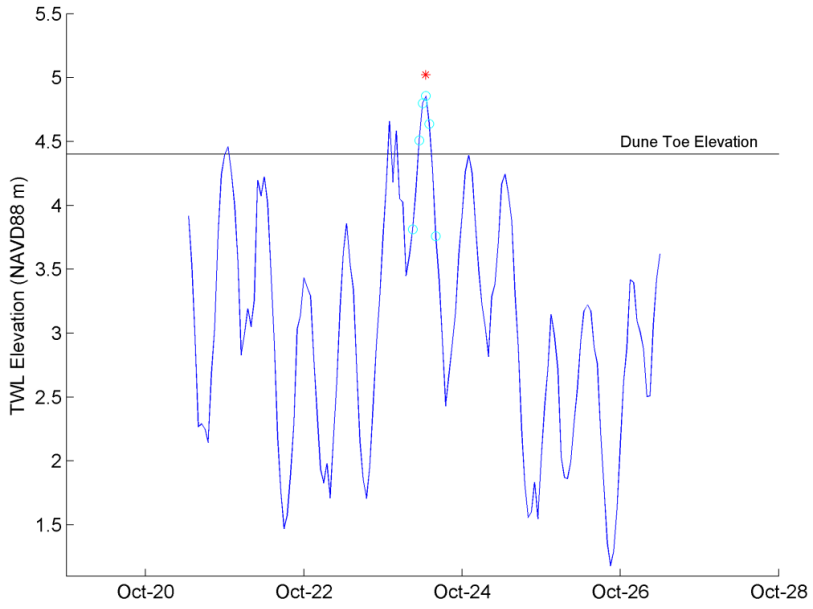

Figure 7-3. Example plot of the approach used to define storm duration along the Coos County shoreline. Note: The red asterisk denotes the location of the storm peak. The light blue circles denote the hours when the event exceeded the critical beach-dune junction toe elevation (including the shoulders) that are used to define the "duration" of the event.

As described previously, the breaker height, H_b, was calculated using equation 6.8 and the breaker depth, h_b, was calculated using a breaker index of 0.78. The berm elevation was established at 3 m (typical for PNW beaches), while the surf zone width, W_b, was determined for each breaker depth value by interpolating along a profile line of interest (**Figure 7-4**). Although we have grain size information available that could have been used to define the A parameter for Tillamook County, the approach we took was to iteritively determine an equilibrium A value based on the actual beach profile data. Here we used the profile data seaward to the 8 m (26.3 ft) water depth, and a range of A values were fit to the data until a value was found that best matched the profile morphology. This approach was adopted for all the profile sites. **Figure 7-5** presents the alongshore varying dune erosion parameters (beach slope, A, surfzone width, and breaker depth) calculated for each transect site and averaged over every storm. These data are also summarized in **Table 7-1**.

Figure 7-6 presents the alongshore varying time scale for the erosion of a dune (T_S), storm duration (T_D), and duration reduction factor (α) values determined for those transect sites characterized as "dune-backed" in Tillamook County. In all cases, we used the surf zone width, breaking depth, and water levels determined at the respective transect site (along with information pertaining to the site's beach/dune morphology) to calculate T_S, and T_D for each storm, while the final parameter, Tm, was solved numerically using equation 7.8 in order to define the duration reduction factor (α). These data have subsequently been averaged for each of the transect locations and are included in **Table 7-1** and presented in **Figure 7-5** and **Figure 7-6**.

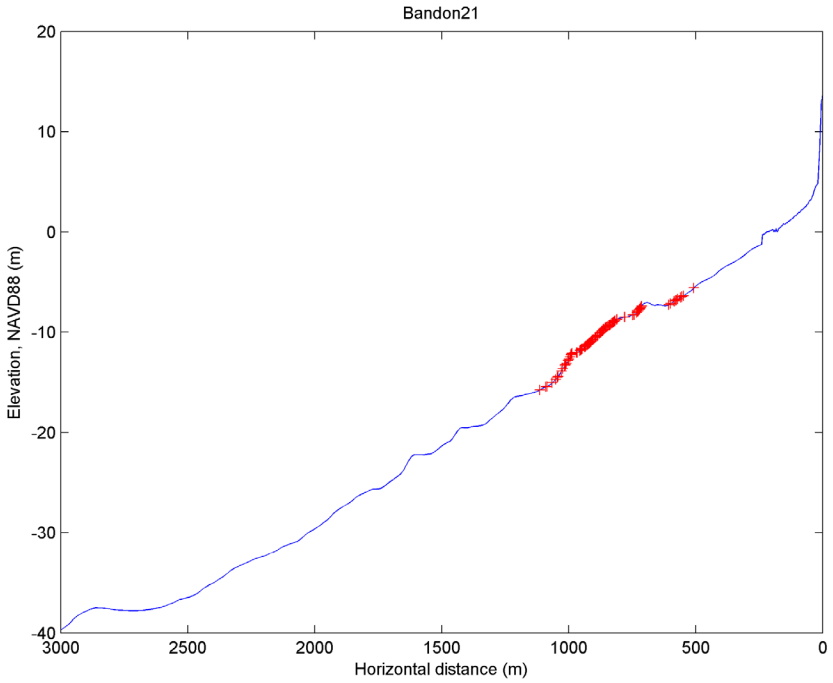

Figure 7-4. Example transect from Coos County showing the locations of h_b (red crosses), used to define the cross-shore width (W_b) of the surf zone.

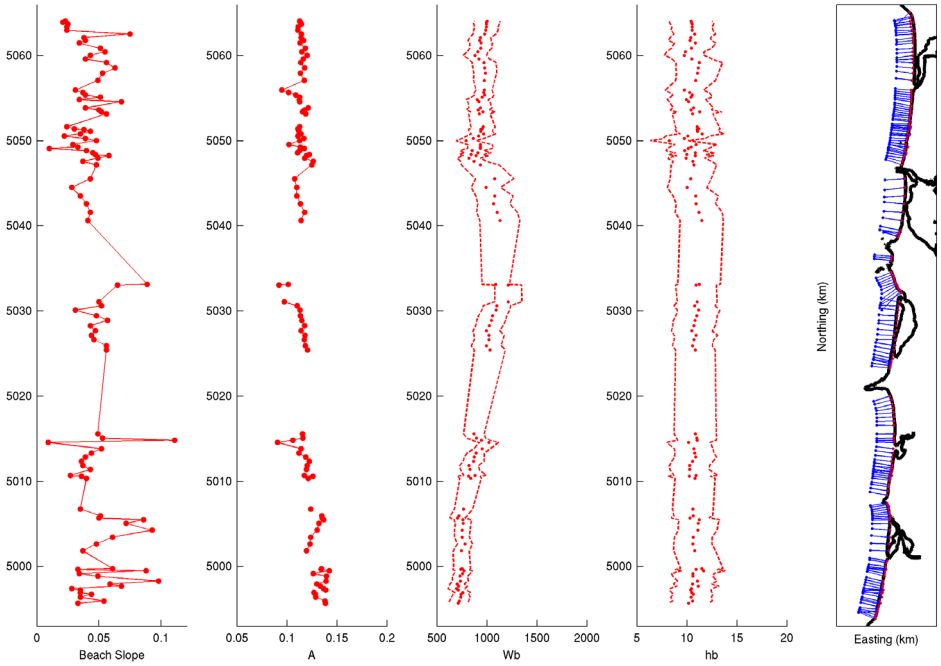

Figure 7-5. Plot showing the dune erosion parameters (tan β, A, W_b, and h_b) used to calculate the profile responses (T_S), storm durations (T_D), alpha, and the storm induced dune erosion. For W_b and h_b we show the mean value and ±1 standard deviation computed using all of the storms.

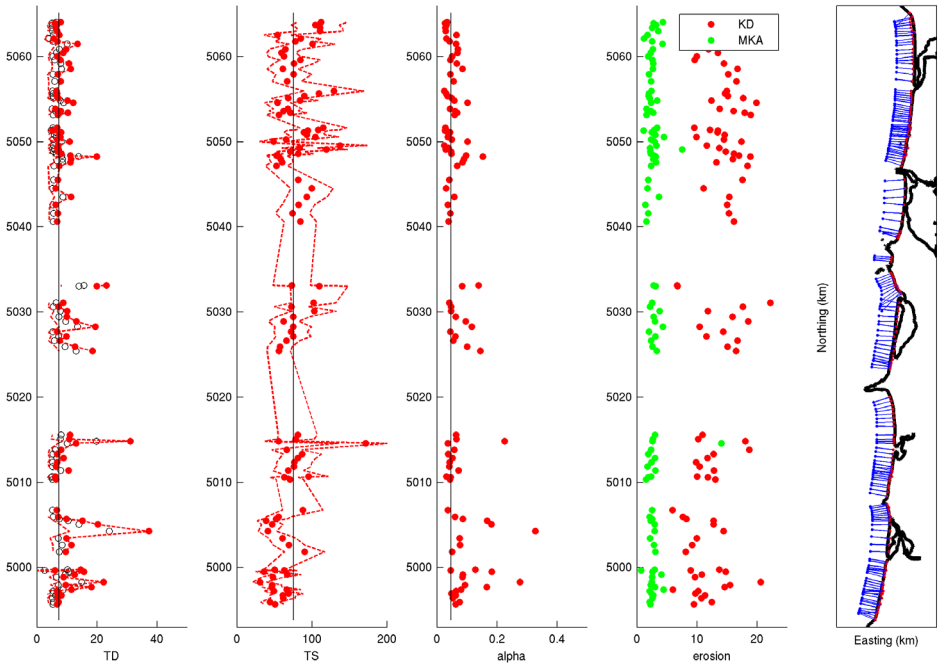

Figure 7-6. Plot showing the storm duration hours (T_D), the calculated time scale of profile response hours (T_S), alpha, and the storm induced K&D and geometric model erosion adjusted using equation 7.10 for the dune-backed profiles along the Tillamook County shore.

Having defined the duration reduction factor (α) for each transect location, the storm-induced erosion was calculated using equation 7.10. As can be seen in **Table 7-1**, calculations of the maximum potential dune erosion (DE_{MAX}) using the Komar and others (1999) geometric model yielded results that are considerably smaller than those derived using the Kriebel and Dean (1993) approach. These differences are largely due to the effect of the surf zone width parameter and the low nearshore slopes used in the K&D calculations. Our initial calculations of storm-induced erosion based on the K&D approach indicated several sites with anomalously large estimates of dune erosion (>20 m [65.6 ft]), when compared with actual field observations by DOGAMI staff over the past two decades. In contrast, storm-induced erosion estimates based on the maximum potential dune erosion (DE_{MAX}) calculated using the geometric model produced very negligible erosion responses that made little physical sense. As a result, our final calculation of the storm-induced erosion (DE_m) is based on the K&D approach. To reduce the large erosion responses observed at several of the transect sites, we ultimately defined an alongshore averaged duration reduction factor (α) of 0.047 (**Table 7-1**), which was used to calculate the storm-induced erosion (DE_m) at each of the dune-backed transect sites present along Tillamook County. As can be seen from **Table 7-1**, this resulted in erosion responses that range from a minimum of 5.9 m (19.4 ft) to as much as 22.3 m (73 ft), while the mean storm-induced erosion response is calculated to be 13 m (42.7 ft). These results are entirely consistent with actual field observations derived from both GPS beach surveys and from previous analyses of topographic change data measured using lidar (Allan and Harris, 2012; Allan and Stimely, 2013).

Table 7-1. Calculated storm-induced erosion parameters for dune-backed beaches in Tillamook County. Note: MKA denotes the geometric model and K&D is the Kriebel and Dean model.

Profiles	Transect	DFIRM Transect	A	W_b	T_D	T_S	α	MKA (DE_{MAX})	MKA (DE_m)	K&D (DE_{MAX})	K&D (DE_m)
Salmon R.	LINC 308	1	0.11	798.42	24.87	69.19	0.16	76.35	3.66	368.05	17.64
Neskowin	TILL 9	15	0.14	712.64	6.68	50.64	0.06	48.09	2.25	203.18	9.5
	TILL 10	16	0.14	722.37	7.17	44	0.08	45.48	2.13	266.33	12.45
	TILL 11	17	0.13	739.27	6.81	61.46	0.05	55.37	2.59	229.76	10.74
	TILL 12	18	0.13	741.74	8.14	60.99	0.06	57.5	2.69	242.34	11.33
	TILL 13	19	0.13	760.19	6.86	68.65	0.05	52.02	2.43	208.52	9.75
	TILL 16	22	0.14	714.18	6.73	49.48	0.06	45.52	2.13	218	10.19
	TILL 17	23	0.14	695.49	11.52	66.27	0.08	95.44	4.46	128.02	5.98
	TILL 18	24	0.13	716.27	18.21	46.66	0.17	63.8	2.98	312.9	14.62
	TILL 19	25	0.13	701.34	9.62	46.86	0.09	49.07	2.29	331.62	15.5
	TILL 20	26	0.14	734.73	22.22	30.54	0.28	53.06	2.48	441.15	20.62
	TILL 21	27	0.14	731.12	8.86	48.09	0.09	53.55	2.5	206.44	9.65
	TILL 22	28	0.13	753.94	12.55	66.68	0.09	87.63	4.1	231.5	10.82
	TILL 23	29	0.14	768.35	15.66	36.01	0.18	55.04	2.57	316.45	14.79
	TILL 24	30	0.13	738.81	6.04	63.03	0.05	14.69	0.69	191.74	8.96
	TILL 25	31	0.13	751.14	14.6	50.47	0.13	62.92	2.94	293.27	13.71
Pacific City	TILL 29	35	0.12	744.43	9.53	90.47	0.05	66.07	3.09	173.33	8.1
	TILL 30	36	0.12	779.31	11.45	69.47	0.08	60.19	2.81	197.34	9.22
	TILL 31	37	0.12	750.86	9.82	60.61	0.08	46.26	2.16	212.93	9.95
	TILL 32	38	0.13	753.17	37.35	41.04	0.33	63.53	2.97	309.26	14.45
	TILL 33	39	0.13	761.88	20.25	47.08	0.18	62.73	2.93	273.59	12.79
	TILL 34	40	0.14	760.24	15.17	38.79	0.17	48.52	2.27	273.82	12.8
	TILL 35	41	0.14	706.32	9.81	52.08	0.09	54.29	2.54	175.78	8.21
	TILL 36	42	0.13	719.24	7.07	55.64	0.06	45.15	2.11	163.42	7.64
	TILL 39	45	0.12	767.5	6.62	87.75	0.04	54.66	2.55	126.49	5.91
Sand Lake	TILL 48	54	0.12	836.71	6.38	70.5	0.04	32.67	1.53	279.25	13.05
	TILL 49	55	0.13	817.5	6.07	63.05	0.05	39.9	1.86	253.02	11.82
	TILL 50	56	0.12	880.96	6.13	95.32	0.03	50.64	2.37	215.19	10.06
	TILL 55	61	0.12	829.65	10.48	68.43	0.07	66.1	3.09	274.64	12.84
	TILL 58	64	0.12	821.41	6.41	75.77	0.04	38.16	1.78	223.87	10.46
	TILL 59	65	0.12	867.33	6.7	76.52	0.04	52.08	2.43	211.22	9.87
	TILL 60	66	0.12	874.61	8.89	81.32	0.05	64.06	2.99	251.35	11.75
	TILL 61	67	0.11	889.38	6.76	87.03	0.04	40.4	1.89	272.73	12.75
	TILL 62	68	0.11	953.4	8.04	66.54	0.06	50.17	2.34	400.8	18.73
	TILL 63	69	0.11	953.4	8.04	66.54	0.06	50.17	2.34	400.8	18.73
	TILL 64	70	0.11	944.48	31.08	55.33	0.23	54.78	2.56	386.3	18.05
	TILL 65	71	0.12	893.19	10.81	78.47	0.06	57.05	2.67	218.31	10.2
	TILL 66	72	0.12	869.49	11.02	81.1	0.06	64.25	3	233.68	10.92
Netarts	TILL 82	88	0.12	1029.92	18.55	55.93	0.14	70.86	3.31	353.98	16.54
	TILL 83	89	0.12	993.78	12.62	57.29	0.1	54.84	2.56	323.33	15.11
	TILL 84	90	0.12	1017.88	7.53	66.01	0.05	50.07	2.34	357.96	16.73
	TILL 85	91	0.12	1021.41	9.84	75.2	0.06	65.12	3.04	247.47	11.57
	TILL 86	92	0.11	994.98	6.78	71.99	0.05	42.1	1.97	307.03	14.35
	TILL 87	93	0.12	1023.68	19.44	75.08	0.12	92.71	4.33	222.97	10.42
	TILL 88	94	0.11	1043.23	13.12	62.3	0.1	64.85	3.03	397.13	18.56
	TILL 89	95	0.11	1056.53	9.91	75.08	0.06	58.65	2.74	340.41	15.91
	TILL 90	96	0.11	1089.76	10.05	103.28	0.05	80.54	3.76	253.07	11.83
	TILL 91	97	0.11	1099.97	7.16	72.44	0.05	46.47	2.17	378.14	17.67
	TILL 92	98	0.1	1214.09	8.74	102.14	0.04	54.7	2.56	476.14	22.25
	TILL 97	103	0.09	1213.67	19.94	109.98	0.08	66.55	3.11	143.97	6.73
	TILL 98	104	0.1	1088.69	23.13	73.19	0.14	59.13	2.76	143.92	6.73

Profiles	Transect	DFIRM Transect	A	W_b	T_D	T_S	α	MKA (DE_{MAX})	MKA (DE_m)	K&D (DE_{MAX})	K&D (DE_m)
Bayocean	TILL 112	118	0.11	1129.98	6.77	84.29	0.04	33.25	1.55	346.07	16.17
	TILL 113	119	0.12	1102.1	6.96	74.17	0.04	40.27	1.88	327.78	15.32
	TILL 114	120	0.11	1067.45	6.25	82.08	0.04	29.5	1.38	321.71	15.04
	TILL 115	121	0.11	1076.73	11.41	93.32	0.06	78.67	3.68	329.28	15.39
	TILL 116	122	0.11	990.11	6.25	99.92	0.03	36.98	1.73	237.39	11.09
	TILL 117	123	0.11	1076.77	7	81.62	0.04	40.57	1.9	376.63	17.6
Rockaway	TILL 118	124	0.12	933.68	7.5	52.59	0.07	49.99	2.34	393.64	18.4
	TILL 119	125	0.13	868.41	11.19	60.25	0.09	68.29	3.19	283.03	13.23
	TILL 120	126	0.12	817.94	11.39	58.5	0.09	57.74	2.7	341.79	15.97
	TILL 121	127	0.12	891.38	19.95	56.18	0.15	67.22	3.14	404.81	18.92
	TILL 122	128	0.12	841.92	11.13	52.38	0.1	60.72	2.84	363.07	16.97
	TILL 124	130	0.11	908.63	8.16	81.79	0.05	48.71	2.28	345.46	16.15
	TILL 125	131	0.11	851.29	7.02	71.19	0.05	47.96	2.24	316.45	14.79
	TILL 126	132	0.11	851.29	7.02	71.19	0.05	47.96	2.24	316.45	14.79
	TILL 127	133	0.11	934.31	6.71	83.48	0.04	46.17	2.16	293.92	13.74
	TILL 128	134	0.1	933.36	7.04	137.41	0.02	69.61	3.25	249.27	11.65
	TILL 129	135	0.11	792.57	10.94	48.9	0.1	63.12	2.95	372.44	17.41
	TILL 130	136	0.12	863.23	6.72	65.56	0.05	50.22	2.35	309.97	14.49
	TILL 131	137	0.11	917.13	7.83	104.66	0.04	96.74	4.52	212.33	9.92
	TILL 133	139	0.11	967.17	7.59	93.12	0.04	65.91	3.08	312.76	14.62
	TILL 134	140	0.11	937.96	8.03	89.33	0.04	52.74	2.47	286.76	13.4
	TILL 135	141	0.11	938.06	5.18	94.63	0.03	23.48	1.1	288.86	13.5
	TILL 139	145	0.11	961.29	6.71	115.22	0.03	72.28	3.38	204.31	9.55
	TILL 147	153	0.12	924.87	7.01	55.98	0.06	33.36	1.56	405.44	18.95
	TILL 148	154	0.12	960.23	10.27	71.21	0.07	57.41	2.68	383.87	17.94
	TILL 149	155	0.12	912.02	7.97	62.23	0.06	49.47	2.31	344.69	16.11
	TILL 150	156	0.12	934.25	6.17	67.82	0.04	33.35	1.56	294.76	13.78
	TILL 152	158	0.11	919.41	12.08	54.08	0.1	50.89	2.38	426.31	19.92
	TILL 153	159	0.11	902.13	10.16	84	0.06	72.24	3.38	265.94	12.43
	TILL 154	160	0.11	951.31	7.08	68.27	0.05	45.71	2.14	379.01	17.71
	TILL 155	161	0.11	975.26	6.57	89.8	0.04	41.23	1.93	324.63	15.17
	TILL 156	162	0.1	967.48	6.68	109.06	0.03	43.22	2.02	313.58	14.66
	TILL 157	163	0.09	972.43	6.46	129.39	0.02	52.1	2.44	320.55	14.98
Nehalem	TILL 158	164	0.12	972.19	7.87	66.9	0.06	50.89	2.38	354.31	16.56
	TILL 159	165	0.11	982.77	7.01	75.71	0.04	42.75	2	324.99	15.19
	TILL 160	166	0.12	978.15	11.29	60.98	0.09	57.12	2.67	358.29	16.74
	TILL 161	167	0.11	971.16	10.68	75.97	0.07	58.15	2.72	310.33	14.5
	TILL 162	168	0.12	919.97	7.84	84.33	0.04	55.25	2.58	206.23	9.64
	TILL 163	169	0.12	880.48	6.69	62.76	0.05	40.35	1.89	213.27	9.97
	TILL 164	170	0.11	908.82	8.75	59.44	0.07	49.56	2.32	288.63	13.49
	TILL 165	171	0.12	939.04	9.71	64.73	0.07	56.26	2.63	255.72	11.95
	TILL 166	172	0.11	941.75	13.53	100.69	0.06	91.68	4.28	228.42	10.68
	TILL 167	173	0.12	927.17	6.86	77.74	0.04	53.61	2.51	247.47	11.57
	TILL 168	174	0.11	933.89	5.58	84.99	0.03	25.2	1.18	235.56	11.01
	TILL 169	175	0.11	976.6	7.42	54.01	0.06	37.11	1.73	411.96	19.25
	TILL 171	177	0.11	989	6.69	110.48	0.03	75.24	3.52	225.95	10.56
	TILL 172	178	0.11	995.61	6.29	110.49	0.03	53.95	2.52	213.52	9.98
	TILL 173	179	0.11	995.27	6.67	104.42	0.03	67.56	3.16	204.89	9.58
	TILL 174	180	0.11	995.85	6.04	111.34	0.03	58.71	2.74	192.45	8.99
	TILL 175	181	0.11	1002.39	7.96	111.91	0.03	92.54	4.32	195.85	9.15
Mean			**0.12**	**905.16**	**10.11**	**75.39**	**0.047**	**58.85**	**2.75**	**277.17**	**12.96**

Note: A is the beach profile parameter that defines an equilibrium profile; W_b is the surf zone width; T_D is the storm duration; T_S is the time scale of response; α is the duration reduction factor.

Figure 7-7 and **Figure 7-8** provide two examples where the most eroded winter profile is eroded to reflect the storm-induced erosion values identified in **Table 7-1**. The first example is the Clatsop Plains 1 profile site where the beach is backed by a prominent foredune. In this example, the calculated duration reduced recession is ~16.9 m (55 ft). The location of the beach-dune junction is depicted in **Figure 7-7** by the brown circle, while the most eroded winter profile is shown as the black line. Because the underlying principle of the K&D and geometric models is for the slope to remain constant, the dune is eroded landward by shifting the location of the beach/dune junction landward by 16.9 m (55 ft) and upward to its new location where it forms an erosion scarp (**Figure 7-7**). Due to the high dune crest, overtopping does not occur at this location. **Figure 7-8** provides an example where dune breaching and overtopping occurs in response to the calculated 1% TWL for the Clatsop Plains 14 profile site. The calculated dune erosion for Clatsop Plains 14 is ~17.9 m (59 ft). The location of the beach-dune junction is depicted in **Figure 7-8** by the shaded black circle, while the *MLWP* is shown as the black line. As noted by NHC (2005), when dunes are subject to major overtopping events, breaching of the dune typically results in significant lowering of the dune morphology and the development of an over-wash fan on the lee side of the dune. Because the present methodologies are unable to account for such responses, NHC recommends that the dune profile be adjusted by extending the *MLWP* slope to the backside of the dune. This type of adjustment is demonstrated in **Figure 7-8** where the entire foredune is assumed to be eroded and removed as a result of a major storm.

Unfortunately, there are no measured examples of the type of response depicted in **Figure 7-8** for the Tillamook County area that can be used to make comparisons against. However, monitoring of beaches by DOGAMI on the Oregon coast provides some suggestion that this approach is probably reasonable. **Figure 7-9** is an example of beach profile changes measured along a barrier beach adjacent to Garrison Lake, Port Orford, located to the south of Bandon. In this example, the barrier beach, which has a crest elevation of 8-9 m NAVD88 (26–29 ft), is known to have been overtopped during several major storms in February/March 1999 (**Figure 7-10**) (Allan and others, 2003). Analyses of the mean shoreline position at this site indicate that changes in the morphology of the beach is controlled primarily by the occurrence of these major storms as well as by El Niño climate events that result in hotspot erosion. Examination of the beach profile changes along the Garrison Lake shore indicate that during major events characterized by overtopping, the crest of the barrier beach is lowered, with some of the eroded sand having been carried landward where they form washover fans, while the bulk is removed seaward to form sand bars. Ultimately though, any dune located at the back of the profile is removed entirely, as the barrier rolls landward, consistent with the response depicted in **Figure 7-7**.

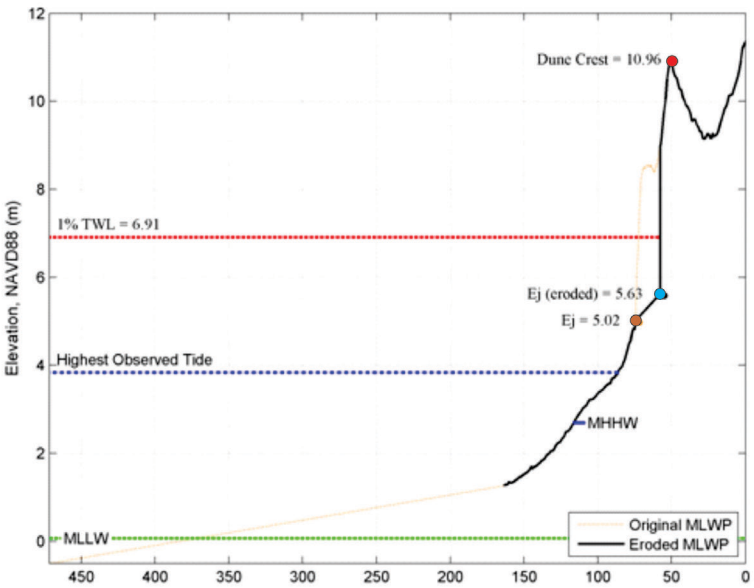

Figure 7-7. Application of the duration reduced erosion estimate to the most likely winter profile *(MLWP)* at Clatsop Plains 1. Brown (cyan) dot depicts the original (eroded) beach/dune juncture, and red dot depicts the dune crest (Dhigh).

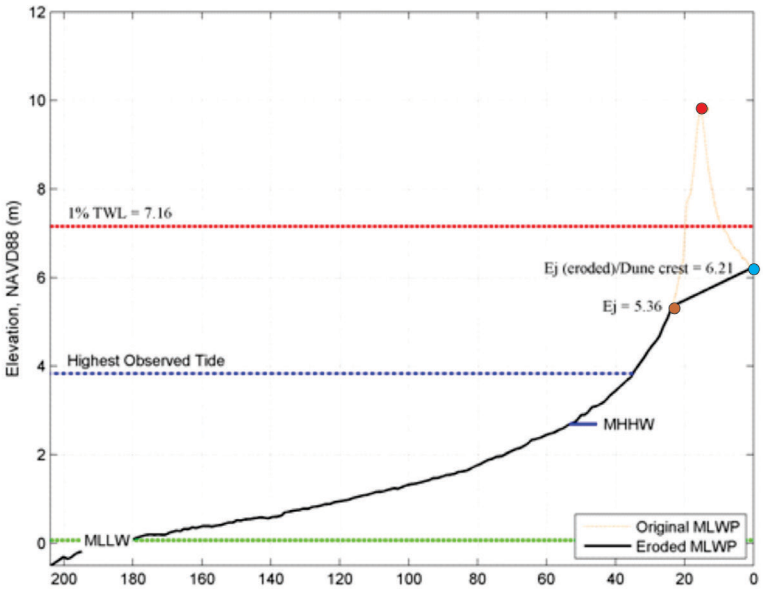

Figure 7-8. Application of the duration reduced erosion estimate to the most likely winter profile *(MLWP)* at Clatsop Plains 14 where overtopping and breaching occurs. Brown (cyan) dot depicts the original (eroded) beach/dune juncture, and red dot depicts the dune crest (Dhigh).

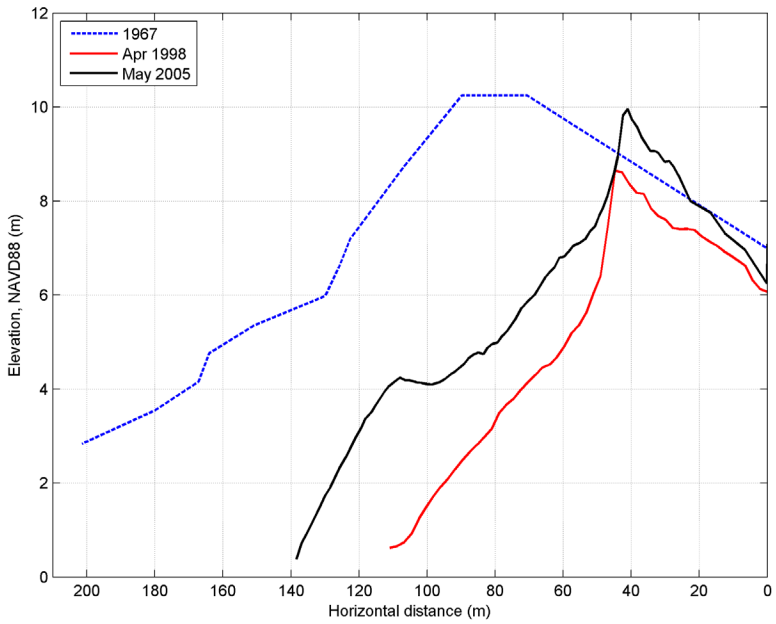

Figure 7-9. Example profile where a barrier beach is overtopped and eroded. This example is based on measured beach profile changes at Garrison Lake, Port Orford on the southern Oregon coast. The 1967 morphology was derived from Oregon Department of Transportation surveys of the beach on September 25, 1967, used to define the Oregon statutory vegetation line.

Figure 7-10. Overtopping of the barrier beach adjacent to Garrison Lake during a major storm on February 16, 1999 (photo courtesy of a resident at Port Orford).

8.0 FLOOD MAPPING

8.1 Detailed Coastal Zone VE Flood Zone Mapping

Detailed mapping of the 1% chance flood event within selected areas of Tillamook County was performed using two contrasting approaches, controlled ultimately by the geomorphology of the beach and backshore. In all cases we followed the methods described in section D.4.9 in the final draft guidelines of the Coastal Flood Hazard Analysis and Mapping for the Pacific Coast of the United States (NHC, 2005). Due to the complexities of each mapping approach for the 0.1% chance flood event, it was not possible to reasonably map the 0.2% chance event. The reasons for this are described in more detail in the following sections.

8.1.1 Bluff-backed beaches

For bluff-backed beaches the total water level (*TWL*) values calculated in Section 6.3 were extended into the bluff. The first step involved identifying specific contours of interest, which were extracted from the 1-m resolution bare-earth lidar grid DEM (surveyed in 2009). For the bluff-backed beaches the landward extent of the coastal Zone VE is defined by the contour representing the TWL elevation calculated for each of the represented detailed surveyed transects (e.g., **Figure 8-1** and **Table 6-2**. FEMA Operating Guidance 9-13 (2013) dictates that areas near the landward extent of Zone VE, where the difference between the TWL and ground elevation is less than 3 feet, be designated as Zone AE. However, due to the steepness of the shoreline along bluff-backed beaches, such areas are too thin in Tillamook County (with one exception at the TILL 177 transect located north of Manzanita) to be visible at the prescribed map scale, and therefore Zone AE was not designated in these environments.

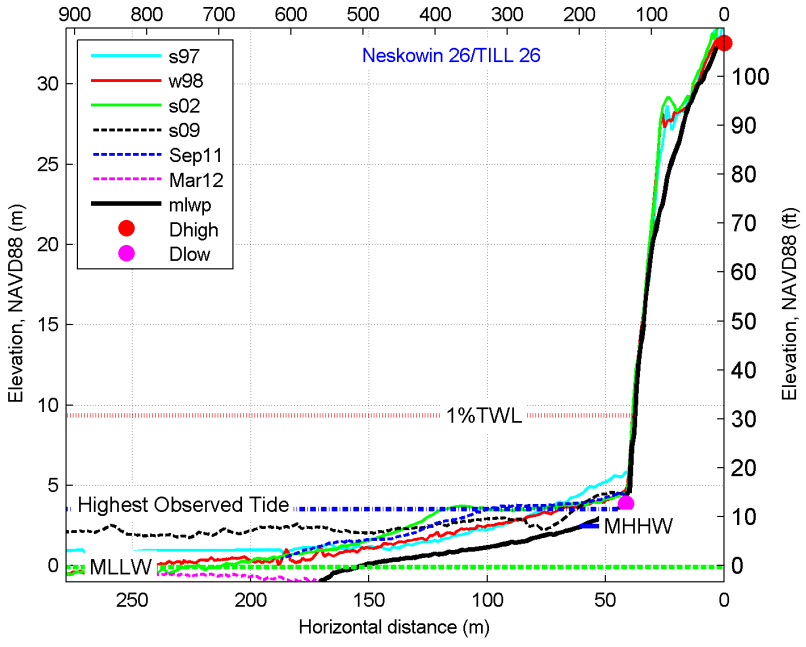

Figure 8-1. Example of a bluff-backed beach (TILL 26) where the calculated total water level and defined velocity (VE) zone extends into the bluff.

To define the velocity zones between transects, we used professional judgment to establish appropriate zone breaks between the various transects. For example, along-shore geomorphic barriers were identified within which the transect TWL value is valid (**Figure 8-2**). Slope and hillshade derivatives of the lidar DEM, as well as 1-m orthophotos (acquired in 2009), provided the base reference. An effort was made to orient zone breaks perpendicular to the beach at the location of the geomorphic barrier. The seaward extents for the majority of Zone VE were inherited from the preliminary DFIRM (2011). In some cases adopting the effective extent produced inconsistent zone widths (too thin), and the boundaries were subsequently extended seaward.

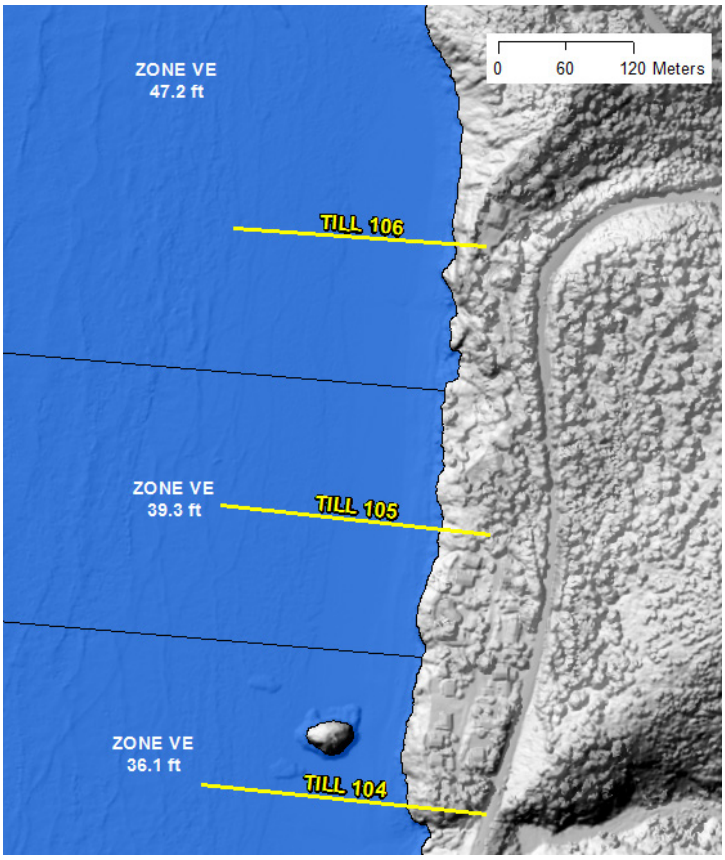

Figure 8-2. Example of along-shore zone breaks and their relationship to geomorphic barriers and surveyed transects. Surveyed transects are symbolized as yellow lines; zone breaks are solid black lines.

8.1.2 Dune-backed beaches

For dune-backed beaches, the VE flood zone was determined according to one or more criteria specified in the NHC (2005) guidelines. These are:

1. The ***wave runup zone***, which occurs where the TWL exceeds the (eroded) ground profile by ≥ 0.91 m (3 ft);
2. The ***wave overtopping splash zone*** is the area landward of the dune/bluff/structure crest where splashover occurs. The landward limit of the splash zone is mapped only in cases where the wave runup exceeds the crest elevation by ≥ 0.91 m (3 ft);
3. The ***high-velocity flow zone*** occurs landward of the overtopping splash zone, where the product of flow times the flow velocity squared (hV^2) is ≥ 5.7 m^3/s^2 (or 200 ft^3/s^2);
4. The ***breaking wave height zone*** occurs where wave heights ≥ 0.91 m (3 ft) could occur and is mapped when the wave crest profile is 0.64 m (2.1 ft) or more above the static water elevation; and
5. The ***primary frontal dune (PFD) zone*** as defined in Part 44 of the U.S. Code of Federal Regulations, Section 59.1; FEMA Coastal Hazard Bulletin, No. 15.

Table 6-3 lists the overtopping calculations for those transects where overtopping occurs, including the calculated splashdown distances ($Y_{G\ outer}$), bore height associated with wave overtopping (h_o), and the landward extent of the high-velocity flow (hV^2) where the flows approach 5.7 m^3/s^2 (or 200 ft^3/s^2). As noted above, hV^2 reflects the farthest point landward of the dune/bluff/structure crest that experiences coastal flooding due to overtopping and is ultimately controlled by the extent of the landward flow where it approaches 5.7 m^3/s^2 (or 200 ft^3/s^2); values greater than 5.7 m^3/s^2 (or 200 ft^3/s^2) are located within the high-velocity flow (VE) zone while lower values are located within the passive overland flooding (AE) zone. Included in **Table 6-3** are the transition zones in which the calculated bore decreases in height, which have been defined accordingly:

- Dist_3 identifies the landward extent of flood zones where the bore height (h_o) was determined to be ≥ 0.91 m (3 ft) and were ultimately rounded up to the nearest whole foot (i.e., having an elevation of 0.91 m (3 ft) above the land surface);
- Dist_2 identifies the landward extent of flood zones where the bore height (h_o) was determined to be between 0.61 and 0.91 m (2 and 3 ft high) and were ultimately rounded up to the nearest whole foot above the ground surface; and
- "Dist_1" marks the seaward extent of flood zones where the bore height falls below 0.3 m (1 ft) above the ground surface; these values were again rounded up to the nearest whole foot.

Areas where flood zones exhibited bore height elevations of 0.61 m (2 ft) above the land surface were inferred as existing in the area between the two previously described regions (i.e., between "Distance from 'x' Where Bore >2 <3 ft" and "Distance from 'x' Where Bore <1").

As with bluff-backed beaches, we used professional judgment to establish appropriate zone breaks between the detailed transects. This was achieved through a combination of having detailed topographic information of the backshore and from knowledge of the local geomorphology. Some interpretation was required to produce flood zones appropriate for the printed map scale. Elevations were identified from the 1-m resolution bare-earth lidar DEM to aid in establishing zone breaks due to changes in flood depth landward of the dune crest (**Figure 8-3**). Slope and hillshade derivatives of the lidar DEM, as well as 1-m orthophotos, provided base reference.

In overtopping splash situations, the flood zone was determined by adding the splashdown distances ($Y_{G\,outer}$) to the D_{high} distance. For all overtopping splash situations on the Tillamook coast, the splash distance was very short and not distinguishable at a mapping scale. Therefore, it was added to the VE zone extent (**Figure 8-4**).

For flood zones seaward of the dune crest, the calculated TWL values were used. As with bluff-backed beaches, along-shore geomorphic barriers were identified within which the transect TWL value is valid. In all cases, an effort was made to orient zone breaks perpendicular to the beach at the location of the geomorphic barrier. The seaward extent of the flood zones were inherited from the preliminary DFIRM (2011).

The PFD is defined as "a continuous or nearly continuous mound or ridge of sand with relatively steep seaward and landward slopes immediately landward and adjacent to the beach and subject to erosion and overtopping from high tides and waves during major coastal storms. The landward limit of the primary frontal dune, also known as the toe or heel of the dune, occurs at a point where there is a distinct change from a relatively steep slope to a relatively mild slope. The primary frontal dune toe represents the landward extension of the Zone VE coastal high hazard velocity zone" (Part 44 of the U.S. Code of Federal Regulations, Section 59.1, as modified in FEMA Coastal Hazard Bulletin, No. 15, https://www.¬floodmaps.fema.gov/listserv/ch_jul02.shtml).

The approach developed by DOGAMI to define the morphology of the beach and dune system, including the location of the PFD, follows procedures developed in our Coos Bay study (Allan and others, 2012) and was based on detailed analyses of lidar data measured by the USGS/NASA/NOAA in 1997, 1998, and 2002 and by DOGAMI in 2009. However, because the lidar data flown by the USGS/NASA/NOAA is of relatively poor resolution (~1 point/m^2) and reflects a single return (i.e., includes vegetation where present), while the lidar data flown by DOGAMI has a higher resolution (8 points/m^2) and is characterized by multiple returns enabling the development of a bare-earth DEM, determination of the PFD was based entirely on analysis of the 2009 lidar data.

Lidar data flown in 1997, 1998, and 2002 were downloaded from NOAA's Coastal Service Center, (http://coast.noaa.gov/dataregistry/search/collection/info/coastallidar) and were gridded in ArcGIS using a triangulated irregular network (TIN) algorithm (Allan and Harris, 2012). Transects spaced 25 m apart were cast for the full length of the county coastline using the Digital Shoreline Analysis System (DSAS) developed by USGS (Thieler and others, 2009); this process yielded 3,628 individual transects in Tillamook County. For each transect, *x*,*y*,*z* values for the 1997, 1998, 2002, and 2009 lidar data were extracted at 1-m intervals along each transect line and saved as a text file using a customized ArcGIS script.

Processing of the lidar data was undertaken in MATLAB using a beach profile analysis script developed by DOGAMI. This script requires the user to interactively define various morphological features including the dune/bluff/structure crest/top, bluff/structure slope, landward edge of the PFD(s), beach-dune juncture elevations for various years, and the slopes of the beach foreshore (Allan and Harris, 2012). Although we evaluated all 3,628 transects, not all morphological features were applicable and therefore the PFD could be defined for only a subset of transects. **Figure 8-5** provides an example from Tillamook #1997 located near the south end of Netarts Spit. In this example, the dune crest in 2009 is located at 10.59 m (34.7 ft); prior to 2009, the dune crest was as high as 11.3 m (37 ft). As can be seen from the figure, the seaward face of the dune eroded landward by ~17 m (56 ft) between 1997 and 2009; shoreline change (erosion/accretion) was determined based on the change in position of the 6 m (19.7 ft) contour elevation, which is an excellent proxy for determining the effects of storm erosion (Allan and others, 2003). **Figure 3-12** and **Figure 3-16** depict changes in the position of the 6-m (19.6 ft) contour along the length of the Tillamook County shoreline. As can be seen from the figures, erosion is acute along much of the county shoreline, especially in the areas of Neskowin, north of Tierra Del Mar, Netarts Spit, and along much of the Rockaway cell (**Figure 3-16**). In contrast, accretion dominates the northern half of Bayocean and Nehalem Spits (**Figure 3-12** and **Figure 3-16**).

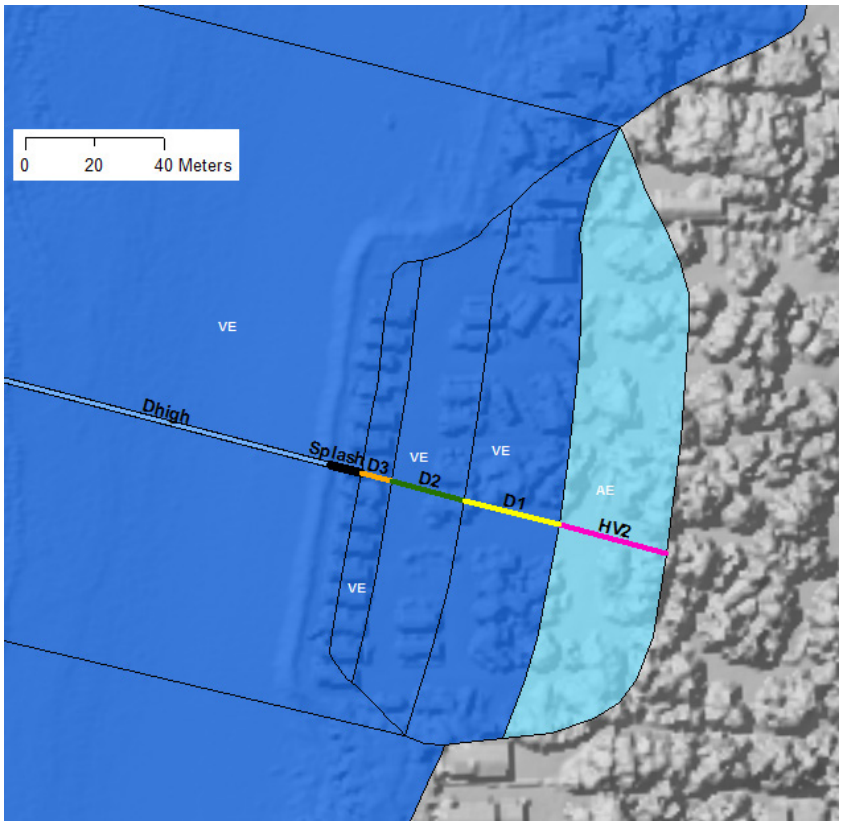

Figure 8-3. Overtopping along the TILL 123 transect (near Twin Rocks), where Dhigh is the area seaward of Dhigh distance, Splash is the splashdown distance, D3 is depth > 3 ft, D2 is depth > 2 and < 3 ft, D1 is depth ≤0.31 m, HV2 is flow < 5.7 m^3/s^2 (or 200 ft^3/s^2). Zone breaks are solid black lines. Dark blue flood zones are VE zones; light blue are AE zones.

Figure 8-4. TILL 144 transect at Rockaway with overtopping splash zone. The short splash zone distance (black) was added to the extent of the VE zone.

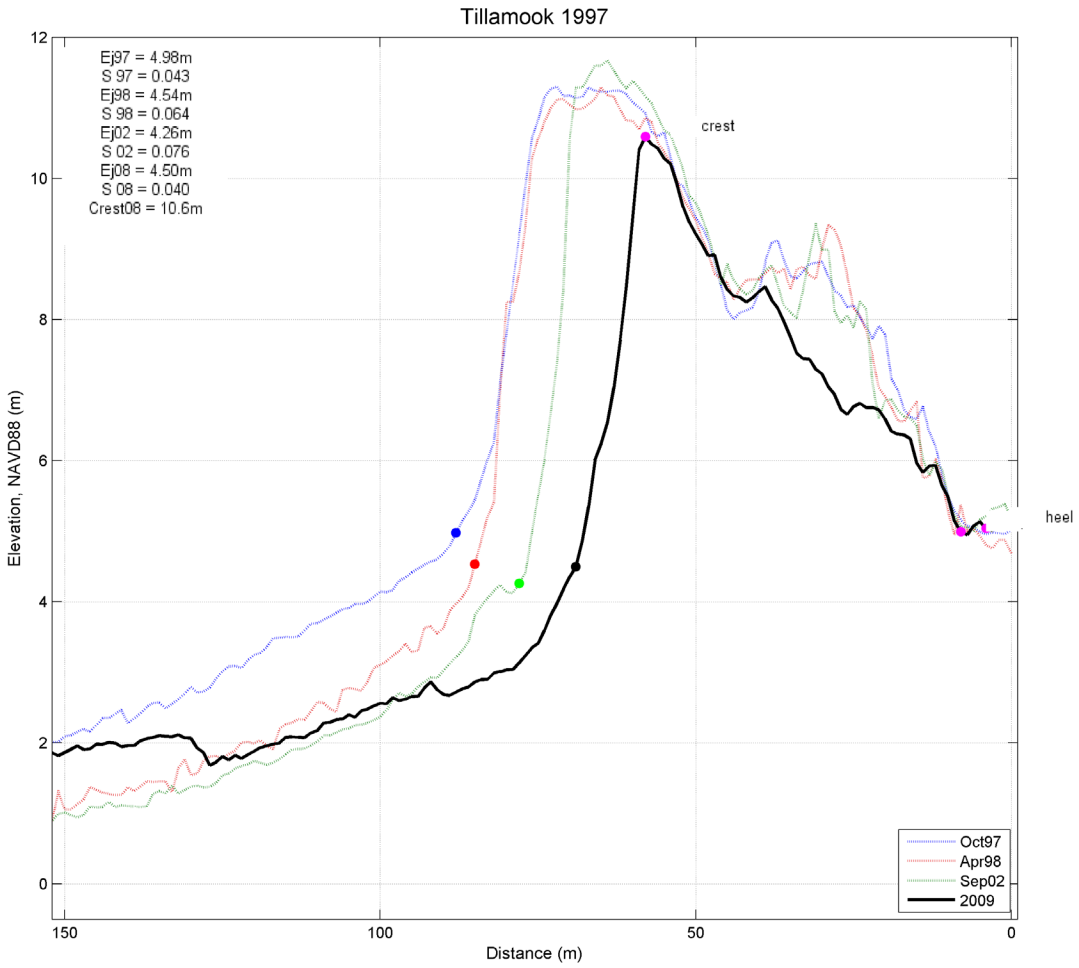

Figure 8-5. Example beach profile (#1997) located near the south end of Netarts Spit and derived from 1997, 1998, 2002, and 2009 lidar data (Allan and Harris, 2012).

After the lidar transect data had been interpolated to define the various morphological parameters, the actual locations of the PFDs[3] were plotted in ArcGIS and overlaid on both current and historical aerial photos of the county and on shaded relief imagery derived from the 2009 lidar. In a number of locations the PFD was found to be located either farther landward or seaward relative to adjacent PFD locations. This response is entirely a function of the degree to which the morphology of foredunes varies along a coast, and further the ambiguity of defining the PFD. Our observations of the PFD approach highlighted a number of uncertainties, including:

1. There were numerous examples of smaller dune features that have begun to develop in front of a main dune (or are the product of erosion of the dune) but have not yet attained dimensions and volumes where they would be considered an established dune; they may continue to erode and could disappear entirely. However, the PFD approach does not adequately account for such features. In this example, the smaller dunes are almost certainly subject to erosion and periodic overtopping and have morphologies that resemble the FEMA PFD definition. However, because they are subject to short-term erosion responses they are more ephemeral in nature, and thus it is debatable whether they should be defined as PFDs. Furthermore, over the life of a typical map (~10 years) these dunes could be

[3] In many cases, multiple PFD locations were defined along a single transect.

eroded and removed entirely leaving a "gap" between the original polygon boundary and the eroding dune. For example, from repeated observations of beach profile transects on the northern Oregon coast, single storm events have been documented to remove as much as 9 to 25 m (30–82 ft) of the dune (Allan and Hart, 2007, 2008);

2. The PFD does not adequately account for a large established foredune, where the dune may have attained heights of 10 to 15 m (33–49 ft), with cross-shore widths on the order of 100 to 200 m (328–656 ft) due to prolonged aggradation and progradation of the beach. In this example, although there may be a clear landward heel located well inland away from the beach (e.g., profile #840 in **Figure 8-6**, which was derived from our Clatsop County study), the PFD is clearly not subject to "frequent" wave overtopping due to its height and erosion (because of its large volume of sand). Defining the PFD at the location of the heel is consistent within the definition provided by FEMA but would almost certainly generate a very conservative V zone.
3. Although numerous transects exhibited clear examples of single PFD locations, many others were characterized by more than one PFD. Profile #1929 (**Figure 8-7**) is an example where, multiple potential PFDs could be defined.

To account for these variations and uncertainties, the PFDs shown on the profile plots (e.g., **Figure 8-5**, **Figure 8-6**, and **Figure 8-7**) were re-examined, and adjustments were made where necessary in order to define a single PFD line. For example, in a few locations along the Clatsop Plains, the PFD extent for a particular transect was physically moved in ArcGIS so that it was more in keeping with the adjacent PFD locations to its immediate north and south. As can be seen in **Figure 8-8**, the final PFD designation was invariably some distance inland, often representing the clearest signal determined from all available data and adhering best to the FEMA definition.

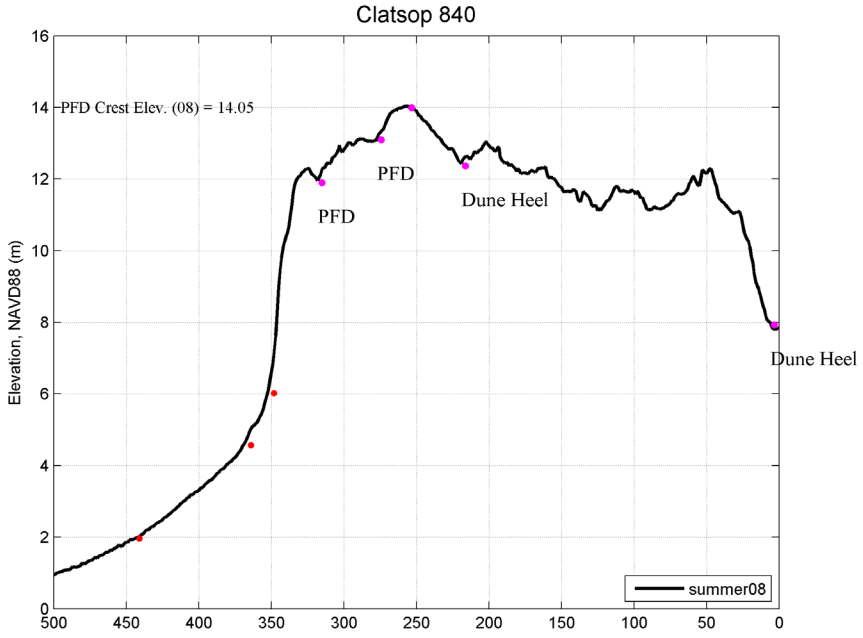

Figure 8-6. Example profile from the Clatsop Plains where considerable aggradation and progradation of the dune has occurred. In this example, the PFD could conceivably be drawn at a variety of locations and meet the FEMA definition.

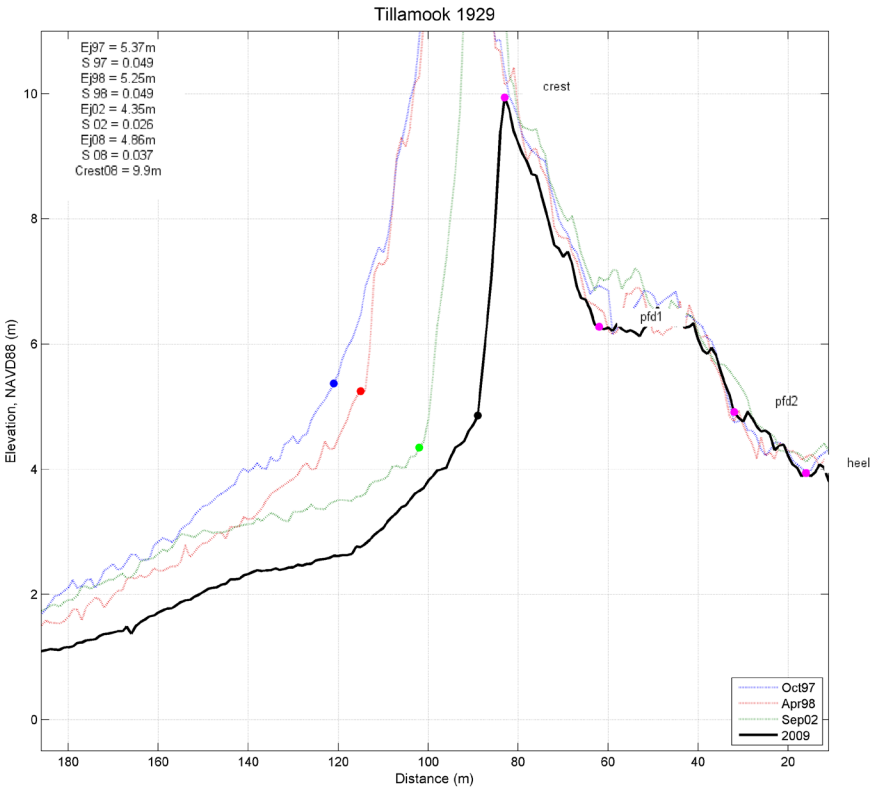

Figure 8-7. Example profile (#1929) from Netarts Spit showing the presence of at least two PFD locations.

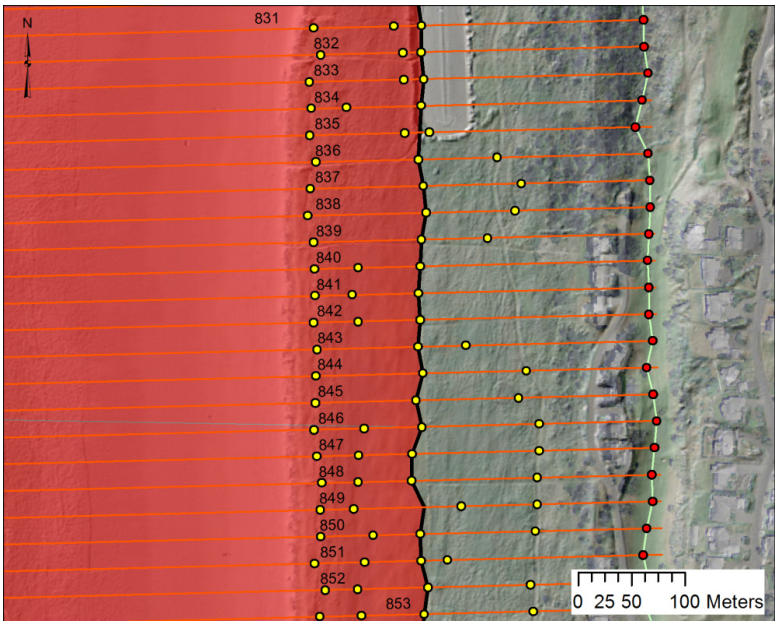

Figure 8-8. Plot showing identified PFD locations (yellow dots) along each transect, landward most dune heel (red dots), and derived PFD line (black line). Red zone depicts the VE zone having accounted for all possible criteria. Red lines depict the locations of the lidar transects, which were spaced 25 m (82 ft) apart.

The PFD was defined at a number of locations where significant human modification has occurred on the dune. In these areas, the natural dune system has been severely impacted and the PFD line does not represent a natural dune system. **Table 8-1** lists the transect locations where this situation occurs and also provides the VE zone extent used in place of the PFD.

Table 8-1. Transect locations where the PFD was not used for mapping due to significant human modification of the dune.

Transect	DFIRM Transect	VE Zone Extent	Transect	DFIRM Transect	VE Zone Extent
TILL 2	8	runup	TILL 54	60	runup
TILL 3	9	runup	TILL 55	61	runup
TILL 4	10	high velocity flow	TILL 56	62	runup
TILL 5	11	high velocity flow	TILL 57	63	runup
TILL 6	12	high velocity flow	TILL 135	141	runup
TILL 7	13	high velocity flow	TILL 136	142	runup
TILL 8	14	high velocity flow	TILL 137	143	runup
TILL 14	20	high velocity flow	TILL 138	144	wave overtopping splash zone
TILL 15	21	high velocity flow	TILL 139	145	runup
TILL 37	43	runup	TILL 140	146	runup
TILL 38	44	runup	TILL 141	147	high velocity flow
TILL 40	46	runup	TILL 142	148	high velocity flow
TILL 41	47	runup	TILL 143	149	high velocity flow
TILL 42	48	runup	TILL 144	150	high velocity flow
TILL 51	57	high velocity flow	TILL 145	151	runup
TILL 52	58	high velocity flow	TILL 146	152	runup
TILL 53	59	runup	TILL 170	176	runup

8.1.3 Mapping of estuarine flooding

Tillamook County includes a number of large estuarine features. Due to their complexity, the following river mouths were redelineated using previously effective BFEs: Kiwanda and Neskowin Creeks, Nestucca Bay, Netarts Bay, Barview Jetty and the Nehalem River (**Figure 8-9**). No new studies were performed at these locations, and the adjacent open coast detailed coastal analysis could not reasonably be used for mapping these estuaries. Open water was mapped in northern part of Tillamook Bay and the southern part of Netarts Bay. These open water areas are digitized water bodies that represent unstudied portions of the bays.

Sand Lake is one estuary that had not previously been subjected to detailed coastal or riverine analyses. This particular estuary is periodically influenced by coastal backwater flooding due to extreme coastal water levels. For the purposes of establishing a new BFE in the estuary, we used the still water level (SWL) to map the coastal backwater effect of the 1% and 0.2% flood events into Sand Lake (**Figure 8-10**). Procedures for developing the SWL are described in Section 4.6. The 1% SWL value for the Tillamook County coast is 3.60 m (11.8 ft, NAVD88), and 0.2% SWL is estimated to be 3.68 m (12.1 ft, NAVD88).

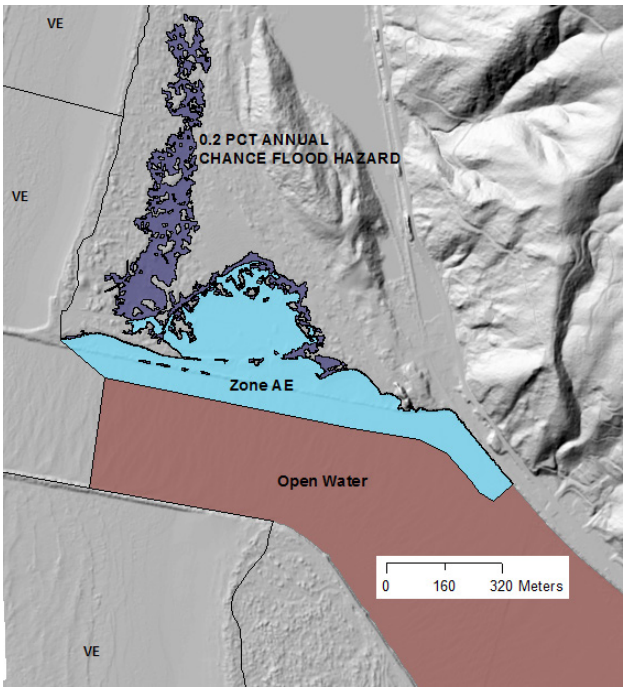

Figure 8-9. Redelineation at Barview Jetty (Zone AE and 0.2 percent annual chance flood hazard) and the open water section of Tillamook Bay.

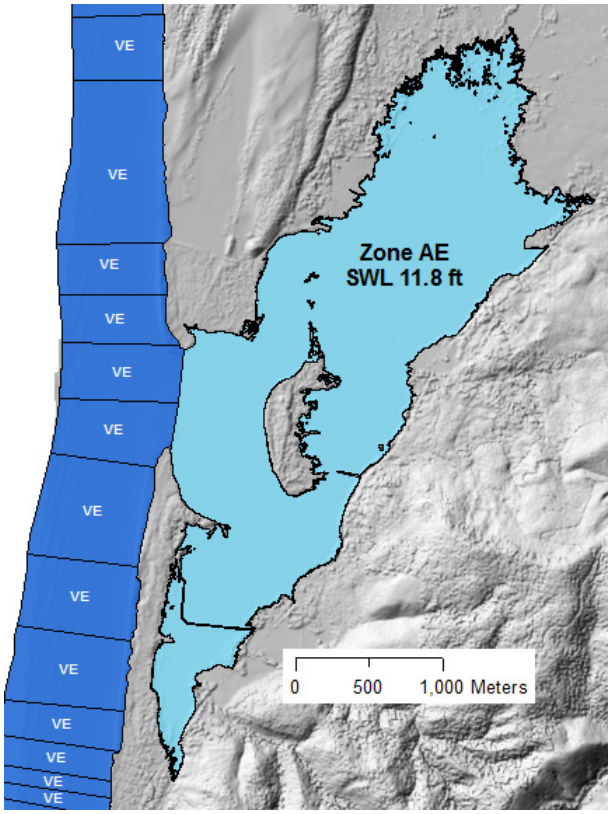

Figure 8-10. Coastal backwater flooding mapped from still water levels (SWLs) for Sand Lake. The 0.2% chance flooding is too small to be visible at this scale.

8.2 Coastal V-Zone Mapping along the Tillamook County Shoreline

8.2.1 Dune-backed beaches

The FEMA guidelines provide little direct guidance for mapping approximate coastal velocity zones (Zone V) in areas where no detailed studies have occurred, other than by defining the location of the PFD, using the methodology described above. In the case of Tillamook County, we have endeavored to undertake detailed mapping in all areas backed by dunes.

8.2.2 V-zone mapping on coastal bluffs and headlands

Several sections of the Tillamook County coastline are characterized by coastal bluffs and cliffs of varying heights. For these areas, the approach adopted by DOGAMI was to map the top of the active bluff (**Figure 8-11**) that is most likely subject to wave erosion, which is a readily identifiable feature that can be used to constrain the landward extent of the Zone V. **Figure 8-11** provides an example of a lidar transect established at the seaward end of Cape Lookout in Tillamook County, where the top of the active bluff face is located at ~65 m (213 ft). **Figure 8-12** depicts the derived bluff top line based on a synthesis of all available information, including the lidar transect data, analyses of lidar contours, and hillshades. This approach was used primarily for the headlands (e.g., Neahkahnie Mountain, Cape Meares, Cape Lookout, Cape Kiwanda, and Cascade Head).

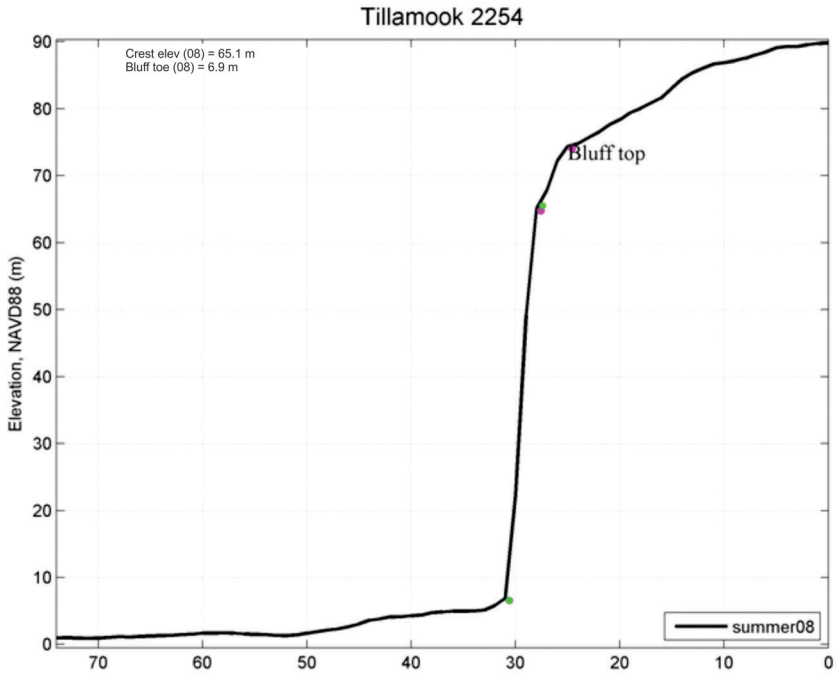

Figure 8-11. Zone V mapping morphology designation along coastal bluffs and cliffs. Example is from the western end of Cape Lookout (Tillamook profile #2254). Magenta dots denote the locations of the bluff/cliff top, while the green dot reflects the bluff toe.

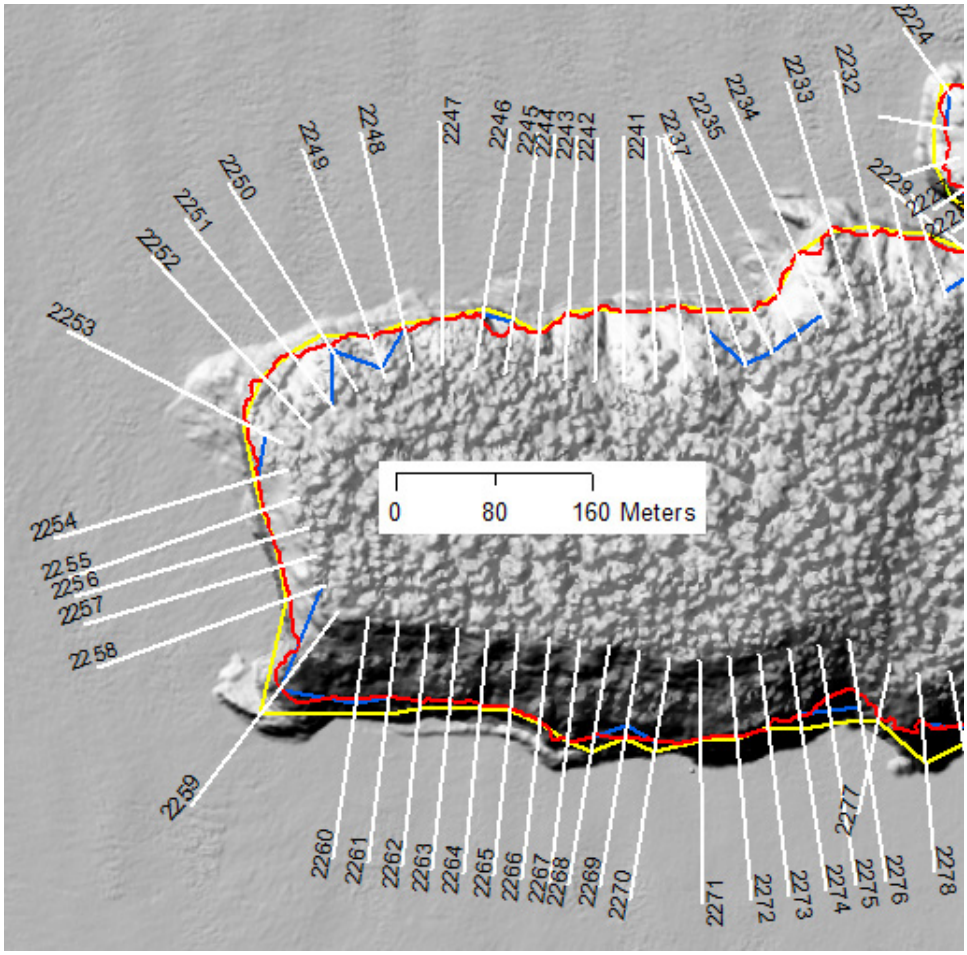

Figure 8-12. Zone V mapping example showing the locations of the individual transects (white lines), bluff top 1 (yellow line) and bluff top 2 (blue line) derived from analyses of the lidar transects, and the final derived bluff line (red line), which incorporates all available data (transects, contours, hillshade, and orthophotos).

9.0 ACKNOWLEDGMENTS

Funding for this study was provided by the Federal Emergency Management Agency as part of the Flood Map Modernization program under Cooperating Technical Partner award EMS-2010-GR-0014. We are grateful to Dr. Bill McDougal for his technical advice throughout this project. We would especially like to acknowledge Nicole Walker from Atkins Global and Dr. Paul Komar for their insightful reviews of the report.

10.0 REFERENCES

Aguilar-Tunon, N.A., and Komar, P.D., 1978, The annual cycle of profile changes of two Oregon beaches: Ore Bin, v. 40, no. 2, p. 25-39.

Allan, J.C., and Komar, P.D., 2000, Are ocean wave heights increasing in the eastern North Pacific?: Eos, Transactions of the American Geophysical Union, v. 81, no. 47, p. 561 and 566-567.

Allan, J.C., and Priest, G.R., 2001, Evaluation of coastal erosion hazard zones along dune and bluff backed shorelines in Tillamook County, Oregon: Cascade Head to Cape Falcon: Oregon Department of Geology and Mineral Industries Open-File Report O-01-03, 126 p.

Allan, J.C., and Komar, P.D., 2002, Extreme storms on the Pacific Northwest Coast during the 1997-98 El Niño and 1998-99 La Niña: Journal of Coastal Research, v. 18, no. 1, p. 175-193.

Allan, J.C., Komar, P.D., and Priest, G.R., 2003, Shoreline variability on the high-energy Oregon coast and its usefulness in erosion-hazard assessments, *in* Byrnes, M.R., Crowell, M., and Fowler, C., eds., Shoreline mapping and change analysis: Technical considerations and management implications: Journal of Coastal Research, Special Issue No. 38, p. 83-105.

Allan, J.C., Hart, R., and Geitgey, R., 2005, Dynamic revetments for coastal erosion stabilization: A feasibility analysis for application on the Oregon Coast: Oregon Department of Geology and Mineral Industries Special Paper 37, 71 p.

Allan, J.C., and Komar, P.D., 2006, Climate controls on U.S. West Coast erosion processes: Journal of Coastal Research, v. 22, no. 3, p. 511-529.

Allan, J.C., and Hart, R., 2007, Assessing the temporal and spatial variability of coastal change in the Neskowin littoral cell: Developing a comprehensive monitoring program for Oregon beaches: Oregon Department of Geology and Mineral Industries Open-File Report O-07-01, 27 p.

Allan, J.C., and Hart, R., 2008, Oregon beach and shoreline mapping and analysis program: 2007-2008 beach monitoring report: Oregon Department of Geology and Mineral Industries Open-File Report O-08-15, 60 p.

Allan, J.C., Komar, P.D., and Ruggiero, P., 2011, Storm surge magnitudes and frequenciy on the central Oregon coast, *in* Solutions to Coastal Disasters 2011, Anchorage, Alaska, American Society of Civil Engineers, p. 53-64.

Allan, J.C., and Harris, E.L., 2012, An "expanded" geospatial database of beach and bluff morphology determined from LIDAR data collected on the northern Oregon coast; Tillamook to Clatsop County: Oregon Department of Geology and Mineral Industries Open-File Report O-12-08, 23 p.

Allan, J.C., Komar, P.D., Ruggiero, P., and Witter, R.C., 2012a, The March 2011 Tōhoku tsunami and its impacts along the U.S. West Coast: Journal of Coastal Research, v. 28, no. 5, p. 1142-1153.

Allan, J.C., Ruggiero, P., and Roberts, J.T., 2012b, Coastal flood insurance study, Coos County, Oregon: Oregon Department of Geology and Mineral Industries Special Paper 44, 132 p.

Allan, J.C., and Stimely, L., 2013, Oregon Beach Shoreline Mapping and Analysis Program: Quantifying short to long-term beach and shoreline changes in the Gold Beach, Nesika, and Netarts littoral cells: Oregon Department of Geology and Mineral Industries Open-File Report O-13-07, 46 p.

Atwater, B.F., Satoko, M.-R., Satake, K., Yoshinobu, T., Kazue, U., and Yamaguchi, D.K., 2005, The orphan tsunami of 1700—Japanese clues to a parent earthquake in North America: U.S. Geological Survey Professional Paper 1707, 144 p.

Baird & Associates, 2005, Pacific Ocean wave information study: Validation of wave model results against satellite altimeter data. Prepared for U.S. Army Corp of Engineers, Engineering Research and Development Center, Vicksburg, Miss.: Madison, Wisconsin, 13 p.

Beaulieu, J.D., 1973, Environmental geology of inland Tillamook and Clatsop Counties, Oregon: Oregon Department of Geology and Mineral Industries Bulletin 79, 65 p.

Bernstein, D.J., Freeman, C., Forte, M.F., Park, J.-Y., Gayes, P.T., and Mitasova, H., 2003, Survey design analysis for three-dimensional mapping of beach and nearshore morphology, *in* Fifth International Symposium on Coastal Engineering and Science of Coastal Sediment Processes (Coastal Sediments '03), Clearwater Beach, Fla., American Society of Civil Engineers, p. 12.

Booij, N., Ris, R.C., and Holthuijsen, L.H., 1999, A third-generation wave model for coastal regions, Part I: Model description and validation: Journal of Geophysical Research, v. 104, no. C4, p. 7649-7666.

Boon, J.D., 2004, Secrets of the tide: Tide and tidal current analysis and predictions, storm surges and sea level trends: Cambridge, U.K., Woodhead Publishing, 224 p.

Bruun, P., 1962, Sea level rise as a cause of shore erosion: Journal of Waterways, Harbors Division, Amer. Soc. Civil Engrs., v. 88, p. 117-130.

Burgette, R.J., Weldon, R.E., III, and Schmidt, D.A., 2009, Interseismic uplift rates for western Oregon and along-strike variation in locking on the Cascadia subduction zone: Journal of Geophysical Research, v. 114, no. B01408, p. 24.

Carignan, K.S., Taylor, L.A., Eakins, B.W., Warnken, R.R., Lim, E., and Grothe, P.R., 2009a, Digital elevation model of central Oregon coast: Procedures, data sources and analysis: National Geophysical Data Center, Marine Geology and Geophysics Division NOAA Technical Memorandum NESDIS NGDC-25, 38 p.

Carignan, K.S., Taylor, L.A., Eakins, B.W., Warnken, R.R., Sazonova, T., and Schoolcraft, D.C., 2009b, Digital elevation model of Garibaldi, Oregon: Procedures, data sources and analysis: National Geophysical Data Center NOAA Technical Memorandum NESDIS NGDC-16, 28 p.

Carignan, K.S., Taylor, L.A., Eakins, B.W., Warnken, R.R., Sazonova, T., and Schoolcraft, D.C., 2009c, Digital elevation model of Astoria, Oregon: Procedures, data sources and analysis: National Geophysical Data Center, Marine Geology and Geophysics Division NOAA Technical Memorandum NESDIS NGDC-22, 43 p.

Clemens, K.E., and Komar, P.D., 1988, Oregon beach-sands compositions produced by the mixing of sediments under a transgressing sea: Journal of Sedimentary Petrology, v. 58, no. 3, p. 519-529.

Coles, S., 2001, An introduction to statistical modeling of extreme values: London, Springer-Verlag, 208 p.

Cooper, W.S., 1958, Coastal sand dunes of Oregon and Washington: Geological Society of America Memoir 72, 169 p.

Davis, R.E., and Dolan, R., 1993, Nor'easters: American Scientist, v. 81, p. 428-439.

Dean, R.G., 1977, Equilibrium beach profiles: U.S. Atlantic and Gulf Coasts; Ocean Engineering Technical Report No. 12: Newark, Del., University of Delaware, Department of Civil Engineering and College of Marine Studies, 45 p.

Goldfinger, C., Nelson, C.H., and Johnson, J.G., 2003, Holocene earthquake records from the Cascadia Subduction Zone and Northern San Andreas fault based on precise dating of offshore turbidites: Annual Review of Earth and Planetary Sciences, v. 31, p. 555-577.

Goldfinger, C., 2009, Paleoseismically derived probabilities for Cascadia great earthquakes [abs.]: Geological Society of America Abstracts with Programs, v. 41, no. 7, p. 520.

Goldfinger, C., and others, 2012, Turbidite event history—Methods and implications for Holocene paleoseismicity of the Cascadia subduction zone: U.S. Geological Survey Professional Paper 1661-F, 170 p.

Hedges, T.S., and Mase, H., 2004, Modified Hunt's equation incorporating wave setup: Journal of Waterway, Port, Coastal, and Ocean Engineering, v. 130, no. 3, p. 109-113.

Jennings, R., and Shulmeister, J., 2002, A field based classification scheme for gravel beaches: Marine Geology, v. 186, p. 211-228.

Kelsey, H.M., Nelson, A.R., Hemphill-Haley, E., and Witter, R.C., 2005, Tsunami history of an Oregon coastal lake reveals a 4600 yr record of great earthquakes on the Cascadia subduction zone: Geological Society of America Bulletin, v. 117, no. 7/8, p. 1009-1032.

Komar, P.D., Terich, T.A., and Lizarraga-Arciniega, J.R., 1976, Oregon coast shoreline changes due to jetties: Journal of the Waterways Harbors and Coastal Engineering Division, American Society of Civil Engineers, v. 102, no. 1, p. 13-30.

Komar, P.D., Good, J.W., and Shih, S.M., 1989, Erosion of Netarts Spit, Oregon: continued impacts of the 1982-83 El Niño: Shore & Beach, v. 57, no. 1, p. 11-19.

Komar, P.D., Torstenson, R.W., and Shih, S.-M., 1991, Bandon, Oregon: Coastal development and the potential for extreme ocean hazards: Shore & Beach, v. 59, no. 4, p. 14-22.

Komar, P.D., 1997, The Pacific Northwest Coast: Living with the shores of Oregon and Washington: Durham and London, Duke University Press, 195 p.

Komar, P.D., 1998a, The 1997-98 El Niño and erosion on the Oregon coast: Shore & Beach, v. 66, no. 3, p. 33-41.

Komar, P.D., 1998b, Beach processes and sedimentation (2nd ed.): Englewood Cliffs, New Jersey, Prentice Hall, Inc., 544 p.

Komar, P.D., McDougal, W.G., Marra, J.J., and Ruggiero, P., 1999, The rational analysis of setback distances: Applications to the Oregon coast: Shore & Beach, v. 67, p. 41-49.

Komar, P.D., McManus, J., and Styllas, M., 2004, Sediment Accumulation in Tillamook Bay, Oregon: Natural Processes versus Human Impacts: Journal of Geology, v. 112, p. 455-469.

Komar, P.D., Allan, J.C., and Ruggiero, P., 2011, Sea level variations along the U.S. Pacific Northwest Coast: Tectonic and climate controls: Journal of Coastal Research, v. 27, no. 5, p. 808-823.

Legaard, K.R., and Thomas, A.C., 2006, Spatial patterns in seasonal and interannual variability of chlorophyll and sea surface temperature in the California Current: Journal of Geophysical Research, v. 111, no. C06032.

Mori, N., Takahashi, T., Yasuda, T., and Yanagisawa, H., 2011, Survey of 2011 Tohoku Earthquake Tsunami Inundation and Run-up: Geophysical Research Letters, v. 38, no. L00G14, p. 6.

Morton, R.A., Leach, M.P., Paine, J.G., and Cardoza, M.A., 1993, Monitoring beach changes using GPS surveying techniques: Journal of Coastal Research, v. 9, no. 3, p. 702-720.

Northwest Hydraulic Consultants, Inc. (NHC), 2005, Final draft guidelines for coastal flood hazard analysis and mapping for the Pacific Coast of the United States, report prepared for FEMA: West Sacramento, Calif., Northwest Hydraulic Consultants, Inc., 344 p.

Oceanweather, Inc., 2010, Global Reanalysis of Ocean Waves Fine Northeast Pacific Hindcast (GROW-FINE NEPAC): Oceanweather Inc., 39 p.

Ozkan-Haller, H.T., Allan, J.C., Barth, J.A., Haller, M.C., Holman, R.A., and Ruggiero, P., 2009, Baseline observations and modeling for the Reedsport wave energy site: Oregon State University and the Oregon Department of Geology and Mineral Industries on behalf of Oregon Wave Energy Trust, 35 p.

Peterson, C., Scheidegger, K., Komar, P.D., and Niem, W., 1984, Sediment composition and hydrography in six high-gradient estuaries of the northwestern United States: Journal of Sedimentary Petrology, v. 54, no. 1, p. 86-97.

Peterson, C.D., Darienzo, M.E., Hamilton, D., Pettit, D.J., Yeager, R.K., Jackson, P.L., Rosenfeld, C.L., and Terich, T.A., 1994, Beach-shoreline database, Pacific Northwest Region, USA: Oregon Department of Geology and Mineral Industries Open-File Report O-94-2, 29 p.

Priest, G.R., Saul, I., and Diebenow, J., 1993, Pilot erosion rate data study of the central Oregon coast, Lincoln County: Final technical report to the Federal Emergency Management Agency: Oregon Department of Geology and Mineral Industries Open-File Report O-93-10, 228 p.

Priest, G.R., Goldfinger, C., Wang, K., Witter, R.C., Zhang, Y., and Baptista, A.M., 2010, Confidence levels for tsunami-inundation limits in northern Oregon inferred from a 10,000-year history of great earthquakes at the Cascadia subduction zone: Natural Hazards, v. 54, p. 27-73.

Pullen, T.A., Allsop, N.W.H., Bruce, T., Kortenhaus, A., Schuttrümpf, H., and van der Meer, J.W., 2007, EurOtop - wave overtopping of sea defences and related structures: Assessment manual, 193 p.

Revell, D.L., Komar, P.D., and Sallenger, Jr., A.H., 2002, An application of LIDAR to analyses of El Niño erosion in the Netarts littoral cell, Oregon: Journal of Coastal Research, v. 18, no. 4, p. 792-801.

Ris, R.C., Booij, N., and Holthuijsen, L.H., 1999, A third-generation wave model for coastal regions, Part II: Verification: Journal of Geophysical Research, v. 104, no. C4, p. 7667-7681.

Ruggiero, P., Komar, P.D., McDougal, W.G., and Beach, R.A., 1996, Extreme water levels, wave runup and coastal erosion, *in* Proceedings of the 25th International Conference on Coastal Engineering, Sept. 2-6, 1996, Orlando, Fla., American Society of Civil Engineers, p. 2793-2805.

Ruggiero, P., and Voigt, B., 2000, Beach monitoring in the Columbia River littoral cell, 1997-2000: Coastal Monitoring & Analysis Program, Washington Department of Ecology Publication No. 00-06-026, 113 p.

Ruggiero, P., Komar, P.D., McDougal, W.G., Marra, J.J., and Beach, R.A., 2001, Wave runup, extreme water levels and the erosion of properties backing beaches: Journal of Coastal Research, v. 17, no. 2, p. 407-419.

Ruggiero, P., Holman, R.A., and Beach, R.A., 2004, Wave run-up on a high-energy dissipative beach: Journal of Geophysical Research, v. 109, p. C06025.

Ruggiero, P., Kaminsky, G.M., Gelfenbaum, G., and Voight, B., 2005, Seasonal to interannual morphodynamics along a high-energy dissipative littoral cell: Journal of Coastal Research, v. 21, no. 3, p. 553-578.

Ruggiero, P., Buijsman, M.C., Kaminsky, G.M., and Gelfenbaum, G., 2010a, Modeling the effects of wave climate and sediment supply variability on large-scale shoreline change: Marine Geology, v. 273, p. 127-140.

Ruggiero, P., Komar, P.D., and Allan, J.C., 2010b, Increasing wave heights and extreme value projections: The wave climate of the U.S. Pacific Northwest: Coastal Engineering, v. 57, no. 5, p. 539-552.

Ruggiero, P., Kratzmann, M.G., Himmelstoss, E.A., Reid, D., Allan, J., and Kaminsky, G., 2013, National Assessment of Shoreline Change: Historical Shoreline Change along the Pacific Northwest coast (Oregon and Washington): U.S. Geological Survey Open-File Report 2012-1007, 62 p.

Satake, K., Shemazaki, K., Yoshinobu, T., and Ueda, K., 1996, Time and size of a giant earthquake in Cascadia inferred from Japanese tsunami records of January 1700: Nature, v. 379, no. 6562, p. 246-249.

Schlicker, H.G., Deacon, R.J., Beaulieu, J.D., and Olcott, G.W., 1972, Environmental geology of the coastal region of Tillamook and Clatsop Counties, Oregon: Oregon Department of Geology and Mineral Industries Bulletin 74, 164 p.

Sherwood, C.R., Jay, D.A., Harvey, R.B., Hamilton, P., and Simenstad, C.A., 1990, Historical changes in the Columbia River Estuary: Progress in Oceanography, v. 25, p. 299-352.

Smith, J.M., Sherlock, A.R., and Resio, D.T., 2001, STWAVE: Steady-state spectral wave model user's manual for STWAVE, Version 3.0: U.S. Army Engineer Research and Development Center, Coastal and Hydraulics Laboratory Technical Report ERDC/CHL SR-01-1, 81 p.

Soler, T., Weston, N.D., and Foote, R.H., 2011, The "Online Positioning User Service" suite (OPUS-S, OPUS-RS, OPUS-DB), *in* Soler, T., ed., CORS and OPUS for Engineers: Tools for Surveying and Mapping Applications Reston, Va., American Society of Civil Engineers, p. 17-26.

Stockdon, H.F., Holman, R.A., Howd, P.A., and Sallenger, A.H., 2006, Empirical parameterization of setup, swash, and runup: Coastal Engineering, v. 53, no. 7, p. 573-588.

Terich, T.A., and Komar, P.D., 1974, Bayocean Spit, Oregon: History of development and erosional destruction: Shore & Beach, v. 42, no. 2, p. 3-10.

Thieler, E.R., Himmelstoss, E.A., Zichichi, J.L., and Ayhan, E., 2009, Digital Shoreline Analysis System (DSAS) version 4.0—An ArcGIS extension for calculating shoreline change: U.S. Geological Survey Open-File Report 2008-1278.

Tillotson, K., and Komar, P.D., 1997, The wave climate of the Pacific Northwest (Oregon and Washington): A comparison of data sources: Journal of Coastal Research, v. 13, no. 2, p. 440-452.

Trimble, 2005, Trimble 5700 GPS system datasheet: Dayton, Ohio, Trimble Navigation Limited, Engineering & Construction Group, p. 2.

van der Meer, J.W., 2002, Technical report wave run-up and wave overtopping at dikes: Deflt, Netherlands, Technical Advisory Committee on Flood Defence, Road and Hydraulic Engineering Institute, 50 p.

Witter, R.C., Kelsey, H.M., and Hemphill-Haley, E., 2003, Great Cascadia earthquakes and tsunamis of the past 6700 years, Coquille River estuary, southern coastal Oregon: Geological Society of America Bulletin, v. 115, p. 1289-1306.

Witter, R.C., 2008, Prehistoric Cascadia tsunami inundation and runup at Cannon Beach, Clatsop County, Oregon: Oregon Department of Geology and Mineral Industries Open-File Report O-08-12, 36 p.

Witter, R.C., Zhang, Y.J., Goldfinger, C., Priest, G.R., and Wang, K., 2010, Validating numerical tsunami simulations in southern Oregon using late Holocene records of great Cascadia earthquakes and tsunamis [abs.]: Seismological Research Letters, v. 81, no. 2, p. 290.

Yamamoto, M., 2011, Tōhoku Tsunami March 11, 2011 as of 30 March 2011: United Nations Educational, Scientific and Cultural Organization, Intergovernmental Oceanographic Comission IOC/UNESCO Bulletin No. 13.

Zhang, K., Douglas, B.C., and Leatherman, S., 2001, Beach erosion potential for severe nor'easters: Journal of Coastal Research, v. 17, no. 2, p. 309-321.

11.0 APPENDICES

- Appendix A: Ground Survey Accuracy Assessment Protocols
- Appendix B: Tillamook County DFIRM/DOGAMI Naming Convention
- Appendix C: Tillamook County Beach and Bluff Profiles
- Appendix D: Supplemental Transect Overtopping Table

11.1 Appendix A: Ground Survey Accuracy Assessment Protocols

See report by Watershed Sciences, Inc., dated December 21, 2009.

11.3 Appendix B: Tillamook County DFIRM/DOGAMI Naming Conventions

Reach	Transect Order	DFIRM Transect	DOGAMI Transect	Transect Type	Site	Lidar Transect	Description
Salmon River	1	1	LINC 308	main	Salmon 6		dune-backed beach
Cascade Head	2	2	LINC 309	main	Cascade 1		plunging cliff
	3	3	LINC 310	main	Cascade 2		plunging cliff
	4	4	LINC 311	main	Cascade 3		boulder beach backed by bluffs
	5	5	LINC 312	main	Cascade 4		plunging cliff
	6	6	LINC 313	main	Cascade 5		plunging cliff
Neskowin	7	7	TILL1	main	Neskowin 1		sandy beach backed by riprap and high cliffs
	8			lidar	Neskowin 2	2_3524	
	9	8	TILL2	main	Neskowin 2		sand beach backed by riprap
	10			lidar	Neskowin 2	2_3521	
	11			lidar	Neskowin 2	2_3517	
	12			lidar	Neskowin 3	3_3514	
	13	9	TILL3	main	Neskowin 3		sand beach backed by riprap
	14			lidar	Neskowin 3	3_3508	
	15			lidar	Neskowin 3	3_3506	
	16			lidar	Neskowin 3	3_3504	
	17			lidar	Neskowin 3	3_3502	
	18	10	TILL4	main	Neskowin 4		sand beach backed by riprap
	19	11	TILL5	main	Neskowin 5		sand beach backed by riprap
	20	12	TILL6	main	Neskowin 6		sand beach backed by riprap
	21	13	TILL7	main	Neskowin 7		sand beach backed by riprap
	22	14	TILL8	main	Neskowin 8		sand beach backed by riprap
	23	15	TILL9	main	Neskowin 9		dune-backed
	24	16	TILL10	main	Neskowin 10		dune-backed
	25	17	TILL11	main	Neskowin 11		dune-backed
	26	18	TILL12	main	Neskowin 12		dune-backed
	27	19	TILL13	main	Neskowin 13		dune-backed
	28	20	TILL14	main	Neskowin 14		sand beach backed by riprap
	29	21	TILL15	main	Neskowin 15		sand beach backed by riprap
	30	22	TILL16	main	Neskowin 16		dune-backed
	31	23	TILL17	main	Neskowin 17		dune-backed
	32	24	TILL18	main	Neskowin 18		dune-backed
	33	25	TILL19	main	Neskowin 19		dune-backed
	34	26	TILL20	main	Neskowin 20		dune-backed
	35	27	TILL21	main	Neskowin 21		dune-backed
	36	28	TILL22	main	Neskowin 22		dune-backed
	37	29	TILL23	main	Neskowin 23		dune-backed
	38	30	TILL24	main	Neskowin 24		dune-backed
	39	31	TILL25	main	Neskowin 25		dune-backed
	40	32	TILL26	main	Neskowin 26		sandy beach backed by high cliffs
	41	33	TILL27	main	Neskowin 27		sandy beach backed by high cliffs
	42	34	TILL28	main	Neskowin 28		sandy beach backed by dunes and high cliffs

Reach	Transect Order	DFIRM Transect	DOGAMI Transect	Transect Type	Site	Lidar Transect	Description
Nestucca Spit/Pacific City	43	35	TILL29	main	PacificC 1		dune-backed
	44	36	TILL30	main	PacificC 2		dune-backed
	45	37	TILL31	main	PacificC 3		dune-backed
	46	38	TILL32	main	PacificC 4		dune-backed
	47	39	TILL33	main	PacificC 5		dune-backed
	48	40	TILL34	main	PacificC 6		dune-backed
	49	41	TILL35	main	PacificC 7		dune-backed
	50	42	TILL36	main	PacificC 8		dune-backed
	51	43	TILL37	main	PacificC 9		sand beach backed by riprap?
	52	44	TILL38	main	PacificC 10		sand beach backed by riprap?
	53	45	TILL39	main	PacificC 11		dune-backed
	54	46	TILL40	main	PacificC 12		sand beach backed by riprap?
	55	47	TILL41	main	PacificC 13		sand beach backed by riprap?
	56	48	TILL42	main	PacificC 14		sand beach backed by riprap and high bluffs
Sand Lake / Tierra Del Mar	57	49	TILL43	main	Sand Lake 1		sandy beach backed by high cliffs
	58	50	TILL44	main	Sand Lake 2		sandy beach backed by high cliffs
	59	51	TILL45	main	Sand Lake 3		sandy beach backed by cobbles - grades into bluff
	60	52	TILL46	main	Sand Lake 4		sandy beach backed by high cliffs
	61	53	TILL47	main	Sand Lake 5		sand beach backed by riprap
	62	54	TILL48	main	Sand Lake 6		dune-backed
	63	55	TILL49	main	Sand Lake 7		dune-backed
	64	56	TILL50	main	Sand Lake 8		dune-backed
	65	57	TILL51	main	Sand Lake 9		sand beach backed by riprap
	66	58	TILL52	main	Sand Lake 10		sand beach backed by riprap
	67	59	TILL53	main	Sand Lake 11		sand beach backed by riprap
	68	60	TILL54	main	Sand Lake 12		sand beach backed by riprap
	69	61	TILL55	main	Sand Lake 13		dune-backed
	70	62	TILL56	main	Sand Lake 14		sand beach backed by riprap
	71	63	TILL57	main	Sand Lake 15		sand beach backed by riprap
	72	64	TILL58	main	Sand Lake 16		dune-backed
	73	65	TILL59	main	Sand Lake 17		dune-backed
	74	66	TILL60	main	Sand Lake 18		dune-backed
	75	67	TILL61	main	Sand Lake 19		dune-backed
	76	68	TILL62	main	Sand Lake 20		dune-backed
	77	69	TILL63	main	Sand Lake 21		dune-backed
	78	70	TILL64	main	Sand Lake 22		dune-backed
	79	71	TILL65	main	Sand Lake 23		dune-backed
	80	72	TILL66	main	Sand Lake 24		dune-backed
	81	73	TILL67	main	Sand Lake 25		sandy beach backed by high cliffs
	82	74	TILL68	main	Sand Lake 26		sandy beach backed by high cliffs
	83	75	TILL69	main	Sand Lake 27		sandy beach backed by high cliffs
	84	76	TILL70	main	Sand Lake 28		sandy beach backed by high cliffs
	85	77	TILL71	main	Sand Lake 29		sandy beach backed by high cliffs
	86	78	TILL72	main	Sand Lake 30		sandy beach backed by high cliffs
	87	79	TILL73	main	Sand Lake 31		sandy beach backed by high cliffs
	88	80	TILL74	main	Sand Lake 32		sandy beach backed by high cliffs

Reach	Transect Order	DFIRM Transect	DOGAMI Transect	Transect Type	Site	Lidar Transect	Description
Netarts Spit/ Oceanside	89	81	TILL75	main	Netarts 1		sandy beach backed by low/high cliffs
	90	82	TILL76	main	Netarts 2		sandy beach backed by cobbles/boulders and low cliff
	91	83	TILL77	main	Netarts 3		sandy beach backed by dynamic revetment/artificial dune
	92	84	TILL78	main	Netarts 4		sandy beach backed by dynamic revetment/artificial dune
	93			lidar	Netarts 5	79_2035	
	94			lidar	Netarts 5	79_2033	
	95	85	TILL79	main	Netarts 5		dune-backed (+cobbles)
	96	86	TILL80	main	Netarts 6		dune-backed (+cobbles)
	97	87	TILL81	main	Netarts 7		dune-backed (+cobbles)
	98	88	TILL82	main	Netarts 8		dune-backed
	99	89	TILL83	main	Netarts 9		dune-backed
	100	90	TILL84	main	Netarts 10		dune-backed
	101	91	TILL85	main	Netarts 11		dune-backed
	102	92	TILL86	main	Netarts 12		dune-backed
	103	93	TILL87	main	Netarts 13		dune-backed
	104	94	TILL88	main	Netarts 14		dune-backed
	105	95	TILL89	main	Netarts 15		dune-backed
	106	96	TILL90	main	Netarts 16		dune-backed
	107	97	TILL91	main	Netarts 17		dune-backed
	108	98	TILL92	main	Netarts 18		dune-backed
	109	99	TILL93	main	Netarts 19		Cobble beach backed by low wall (estuary mouth)
	110	100	TILL94	main	Netarts 20		sandy beach backed by high cliffs
	111	101	TILL95	main	Netarts 21		sandy beach backed by high cliffs
	112	102	TILL96	main	Netarts 22		sandy beach backed by high cliffs
	113	103	TILL97	main	Netarts 23		sandy beach backed by dune and high cliffs
	114	104	TILL98	main	Netarts 24		sandy beach backed by dune and high cliffs
	115	105	TILL99	main	Netarts 25		sandy beach backed by high cliffs
	116	106	TILL100	main	Netarts 26		sandy beach backed by high cliffs
	117	107	TILL101	main	Netarts 27		sandy beach backed by poor riprap and low cliffs
	118	108	TILL102	main	Netarts 28		sandy beach backed by moderately high cliffs
	119	109	TILL103	main	Netarts 29		sandy beach backed by moderately high cliffs
Short Sand Beach	120	110	TILL104	main	Short Sand 1		sandy beach backed by gravels and high cliffs
	121	111	TILL105	main	Short Sand 2		sandy beach backed by gravels and high cliffs
	122	112	TILL106	main	Short Sand 3		sandy beach backed by gravels and high cliffs
Bayocean Spit	123	113	TILL107	main	Bayocean 1		sandy beach backed by cobble/boulder and low cliffs
	124	114	TILL108	main	Bayocean 2		sandy beach backed by cobble/boulder and low cliffs
	125	115	TILL109	main	Bayocean 3		sandy beach backed by cobble/boulder berm
	126	116	TILL110	main	Bayocean 4		sandy beach backed by cobble/boulder berm
	127	117	TILL111	main	Bayocean 5		sandy beach backed by cobble/boulder berm
	128	118	TILL112	main	Bayocean 6		dune-backed
	129	119	TILL113	main	Bayocean 7		dune-backed
	130	120	TILL114	main	Bayocean 8		dune-backed
	131	121	TILL115	main	Bayocean 9		dune-backed
	132	122	TILL116	main	Bayocean 10		dune-backed
	133	123	TILL117	main	Bayocean 11		dune-backed

Reach	Transect Order	DFIRM Transect	DOGAMI Transect	Transect Type	Site	Lidar Transect	Description
Rockaway	134	124	TILL118	main	Rockaway 1		dune-backed
	135	125	TILL119	main	Rockaway 2		dune-backed
	136	126	TILL120	main	Rockaway 3		dune-backed
	137	127	TILL121	main	Rockaway 4		dune-backed
	138	128	TILL122	main	Rockaway 5		dune-backed
	139	129	TILL123	main	Rockaway 6		sand beach backed by riprap
	140	130	TILL124	main	Rockaway 7		dune-backed
	141	131	TILL125	main	Rockaway 8		dune-backed
	142	132	TILL126	main	Rockaway 9		dune-backed
	143	133	TILL127	main	Rockaway 10		dune-backed
	144	134	TILL128	main	Rockaway 11		dune-backed
	145	135	TILL129	main	Rockaway 12		dune-backed
	146	136	TILL130	main	Rockaway 13		dune-backed
	147	137	TILL131	main	Rockaway 14		dune-backed
	148	138	TILL132	main	Rockaway 15		sand beach backed by riprap
	149	139	TILL133	main	Rockaway 16		dune-backed
	150	140	TILL134	main	Rockaway 17		dune-backed
	151			lidar	Rockaway 18	135_857	
	152			lidar	Rockaway 18	135_856	
	153	141	TILL135	main	Rockaway 18		dune-backed
	154	142	TILL136	main	Rockaway 19		sand beach backed by low bluff
	155	143	TILL137	main	Rockaway 20		sand beach backed by riprap
	156	144	TILL138	main	Rockaway 21		sand beach backed by riprap
	157	145	TILL139	main	Rockaway 22		dune-backed
	158	146	TILL140	main	Rockaway 23		sand beach backed by riprap
	159	147	TILL141	main	Rockaway 24		sand beach backed by riprap
	160	148	TILL142	main	Rockaway 25		sand beach backed by riprap
	161	149	TILL143	main	Rockaway 26		sand beach backed by riprap
	162	150	TILL144	main	Rockaway 27		sand beach backed by riprap
	163	151	TILL145	main	Rockaway 28		sand beach backed by riprap
	164	152	TILL146	main	Rockaway 29		sand beach backed by riprap
	165			lidar	Rockaway 30	147_783	
	166	153	TILL147	main	Rockaway 30		dune-backed
	167			lidar	Rockaway 30	147_778	
	168	154	TILL148	main	Rockaway 31		dune-backed
	169	155	TILL149	main	Rockaway 32		dune-backed
	170	156	TILL150	main	Rockaway 33		dune-backed
	171	157	TILL151	main	Rockaway 34		sand beach backed by riprap
	172	158	TILL152	main	Rockaway 35		dune-backed
	173	159	TILL153	main	Rockaway 36		dune-backed
	174	160	TILL154	main	Rockaway 37		dune-backed
	175	161	TILL155	main	Rockaway 38		dune-backed
	176	162	TILL156	main	Rockaway 39		dune-backed
	177	163	TILL157	main	Rockaway 40		dune-backed

Reach	Transect Order	DFIRM Transect	DOGAMI Transect	Transect Type	Site	Lidar Transect	Description
Nehalem Spit / Manzanita	178	164	TILL158	main	Manzanita 1		dune-backed
	179	165	TILL159	main	Manzanita 2		dune-backed
	180	166	TILL160	main	Manzanita 3		dune-backed
	181	167	TILL161	main	Manzanita 4		dune-backed
	182	168	TILL162	main	Manzanita 5		dune-backed
	183	169	TILL163	main	Manzanita 6		dune-backed
	184	170	TILL164	main	Manzanita 7		dune-backed
	185	171	TILL165	main	Manzanita 8		dune-backed
	186	172	TILL166	main	Manzanita 9		dune-backed
	187	173	TILL167	main	Manzanita 10		dune-backed
	188	174	TILL168	main	Manzanita 11		dune-backed
	189	175	TILL169	main	Manzanita 12		dune-backed
	190	176	TILL170	main	Manzanita 13		sand beach backed by riprap
	191	177	TILL171	main	Manzanita 14		dune-backed
	192	178	TILL172	main	Manzanita 15		dune-backed with road
	192	178	TILL172	main	Manzanita 15		dune-backed with road
	193	179	TILL173	main	Manzanita 16		dune-backed with road
	194	180	TILL174	main	Manzanita 17		dune-backed with road
	195	181	TILL175	main	Manzanita 18		dune-backed
	196	182	TILL176	main	Manzanita 19		sand beach backed by extensive cobble berm
	197	183	TILL177	main	Manzanita 20		sand beach backed by extensive cobble berm and bluff
	198	184	TILL178	main	Manzanita 21		sand beach backed by extensive cobble berm and bluff
Falcon Cove	199	185	CP 1	main	CP 1		sand, cobble berm backed by high bluff

11.4 Appendix C: Tillamook County Beach and Bluff Profiles

11.4.1 Neskowin

fm_nesk 1

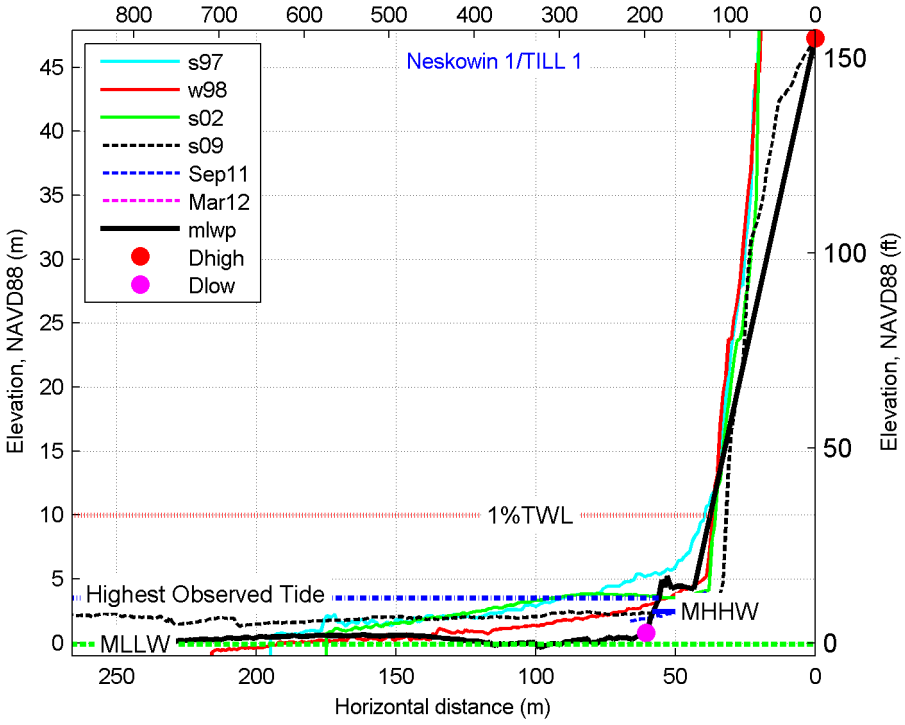

fm_nesk 2

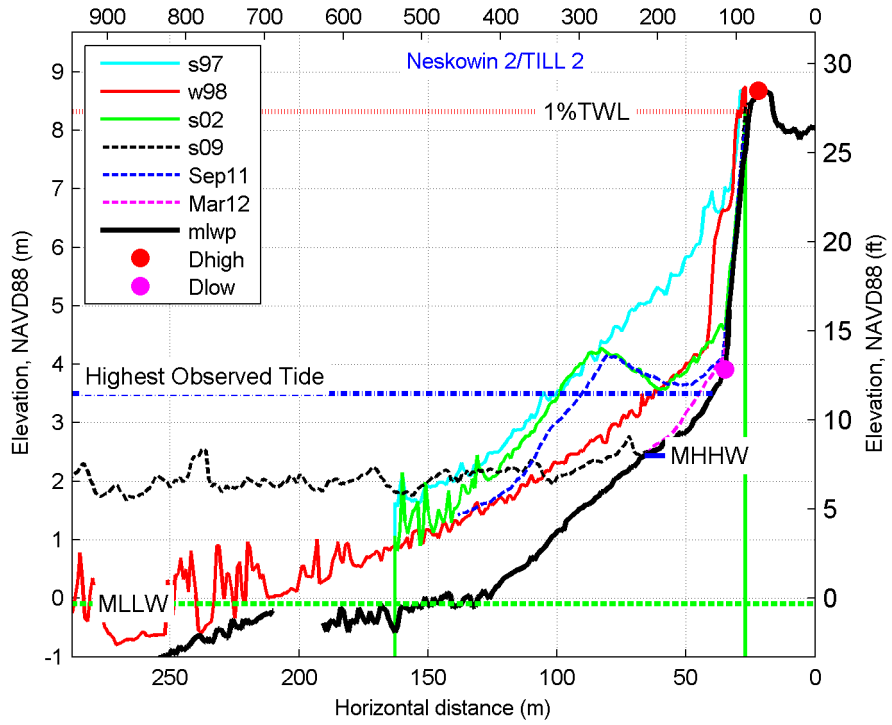

fm_nesk 3

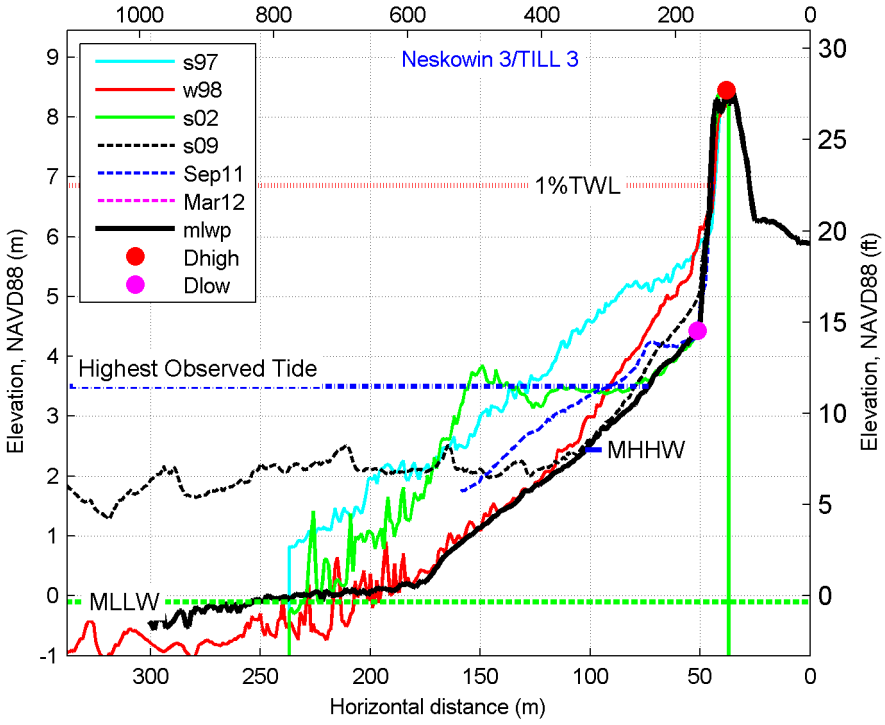

fm_nesk 4

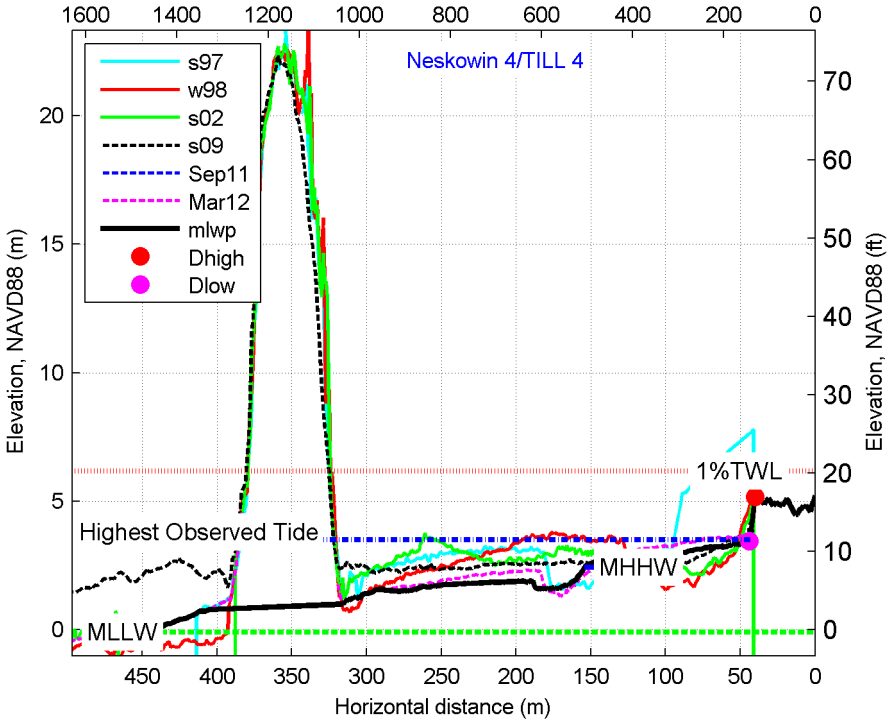

fm_nesk 5

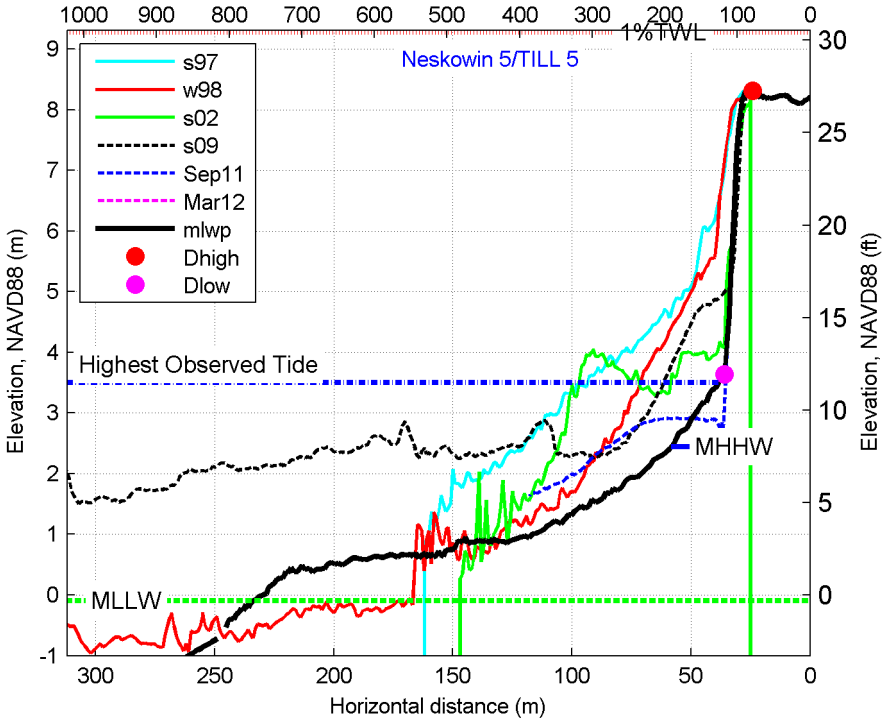

fm_nesk 6

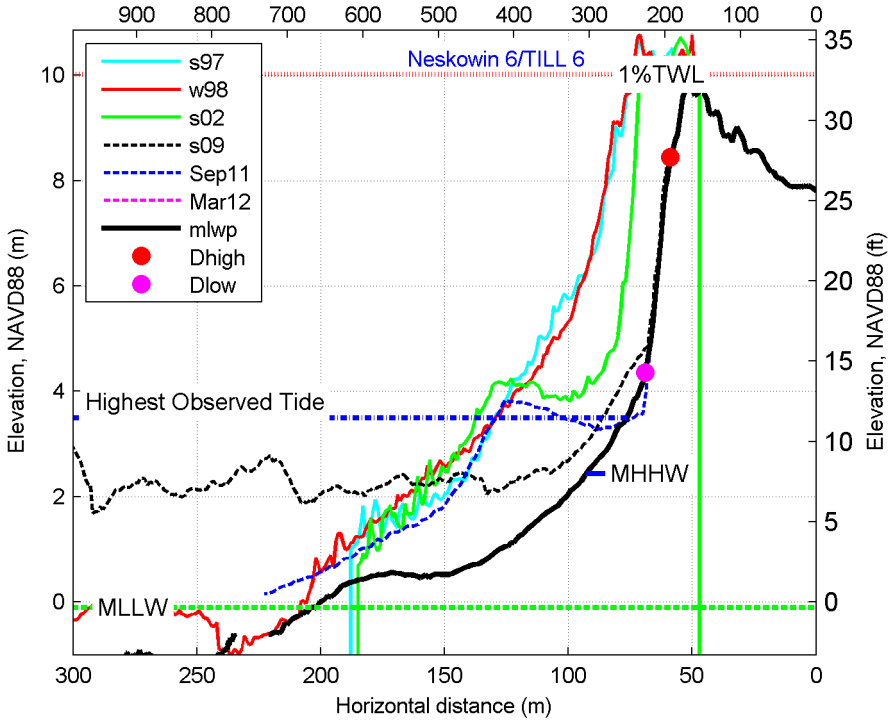

fm_nesk 7

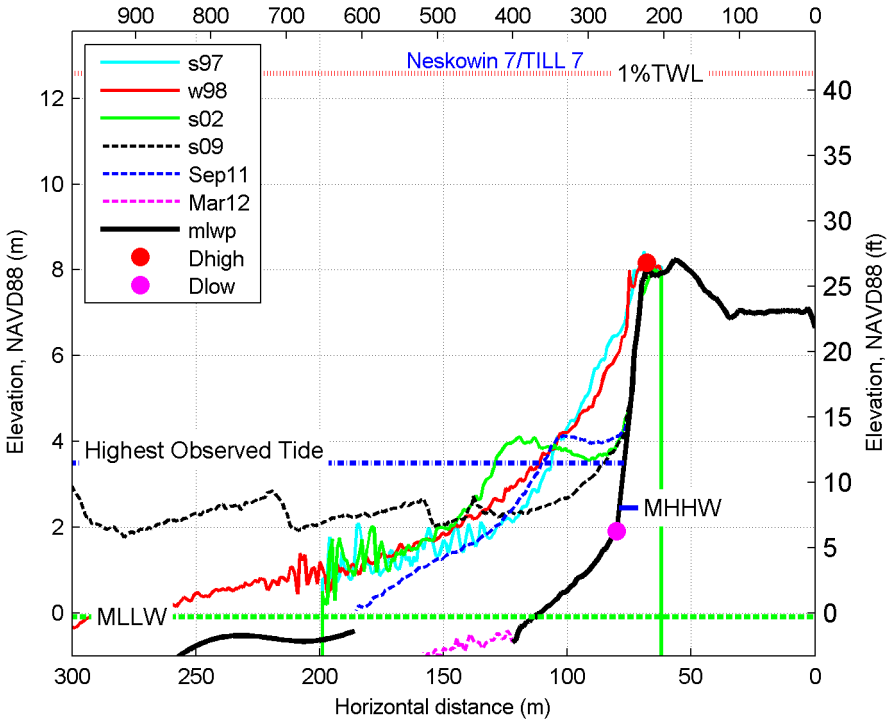

fm_nesk 8

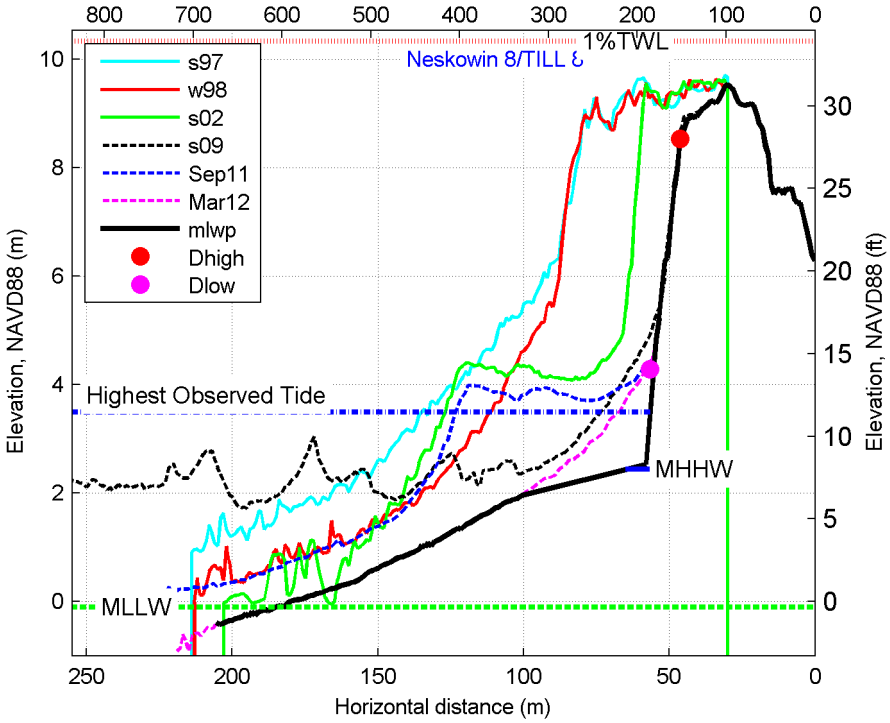

fm_nesk 9

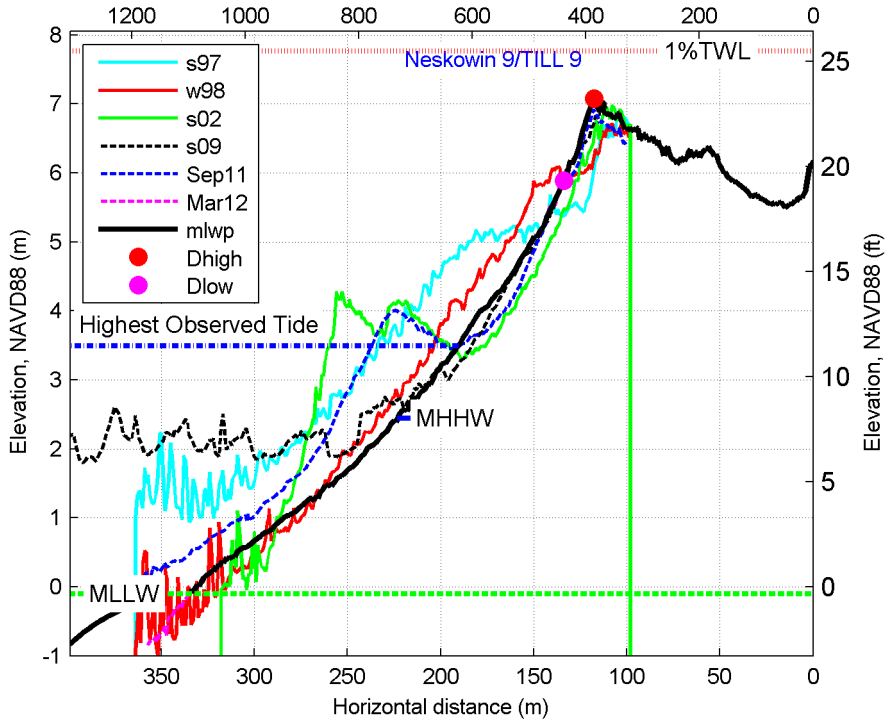

fm_nesk 10

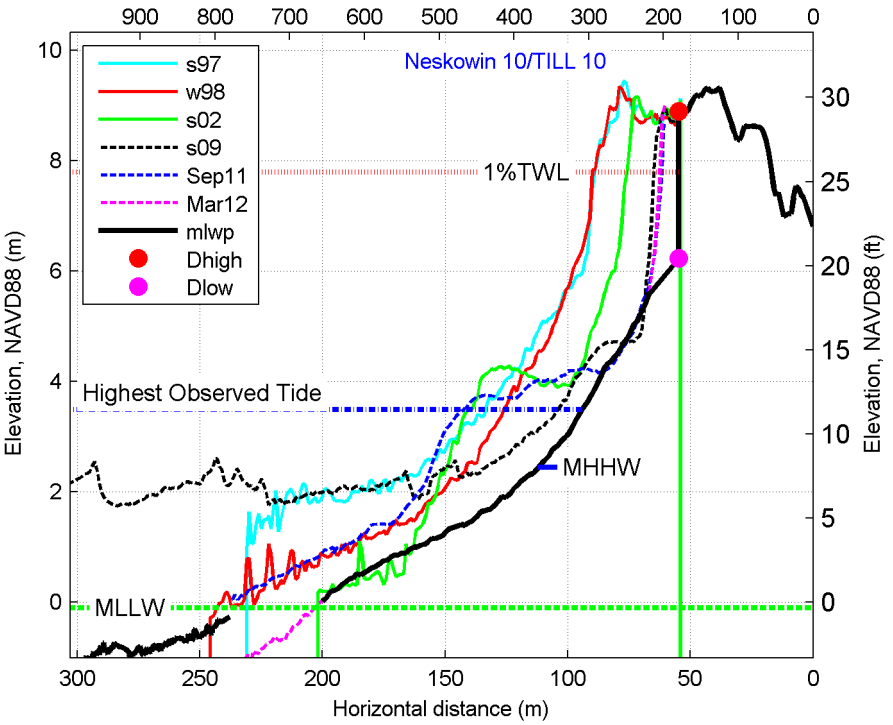

fm_nesk 11

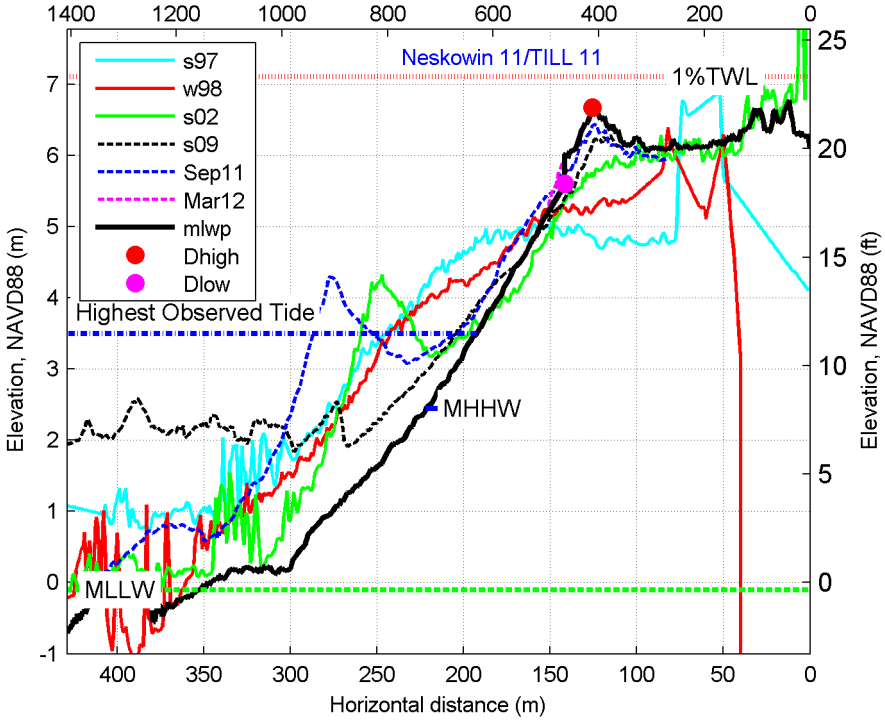

fm_nesk 12

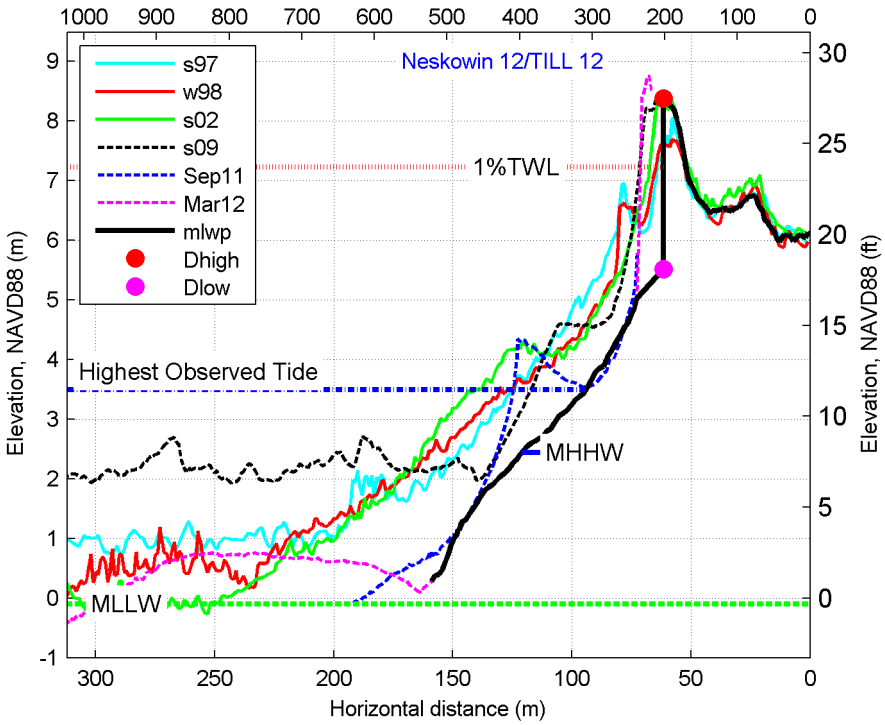

fm_nesk 13

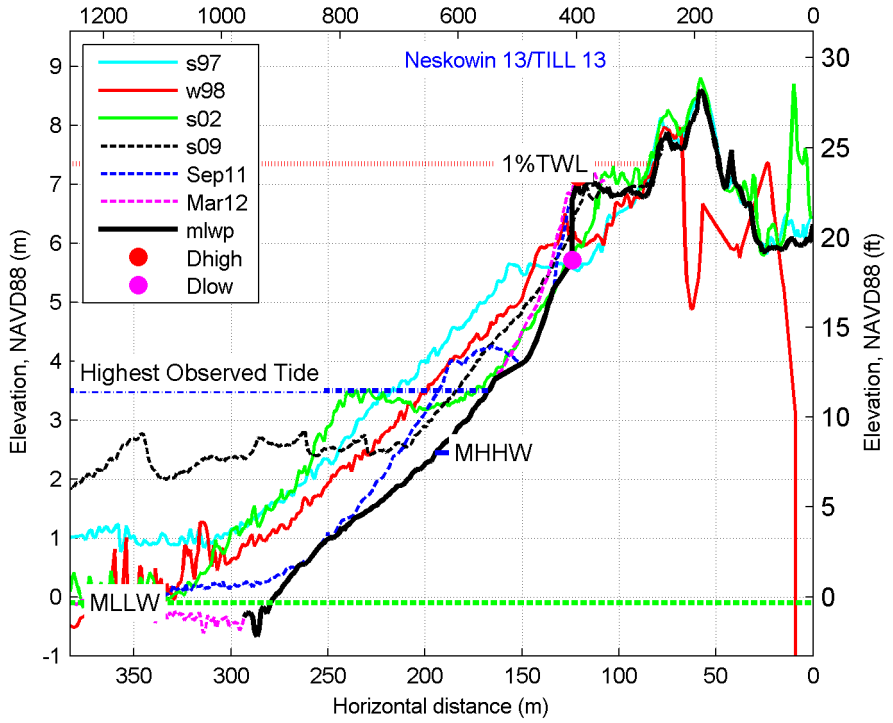

fm_nesk 14

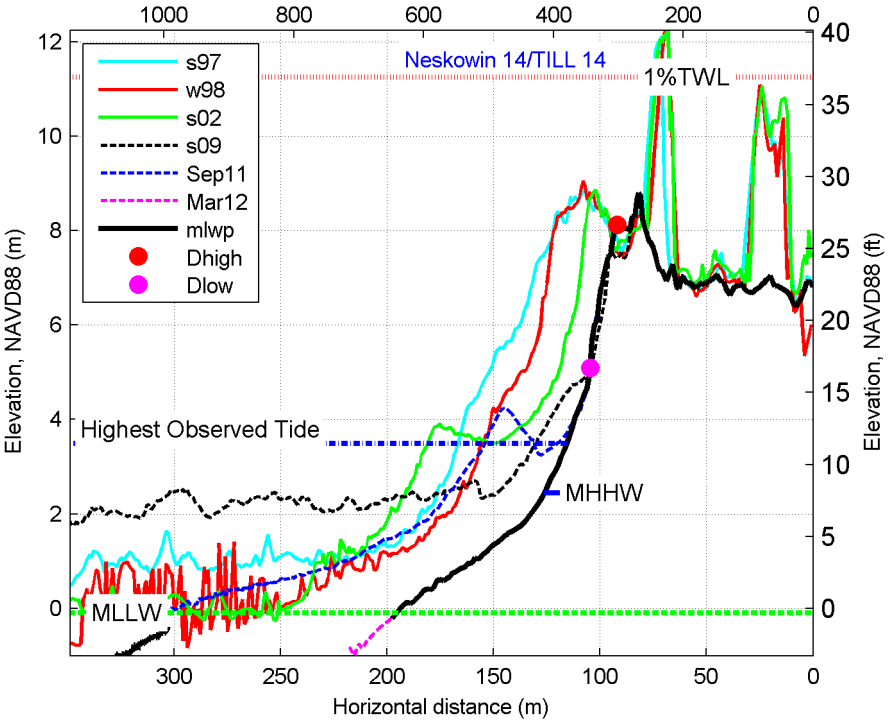

fm_nesk 15

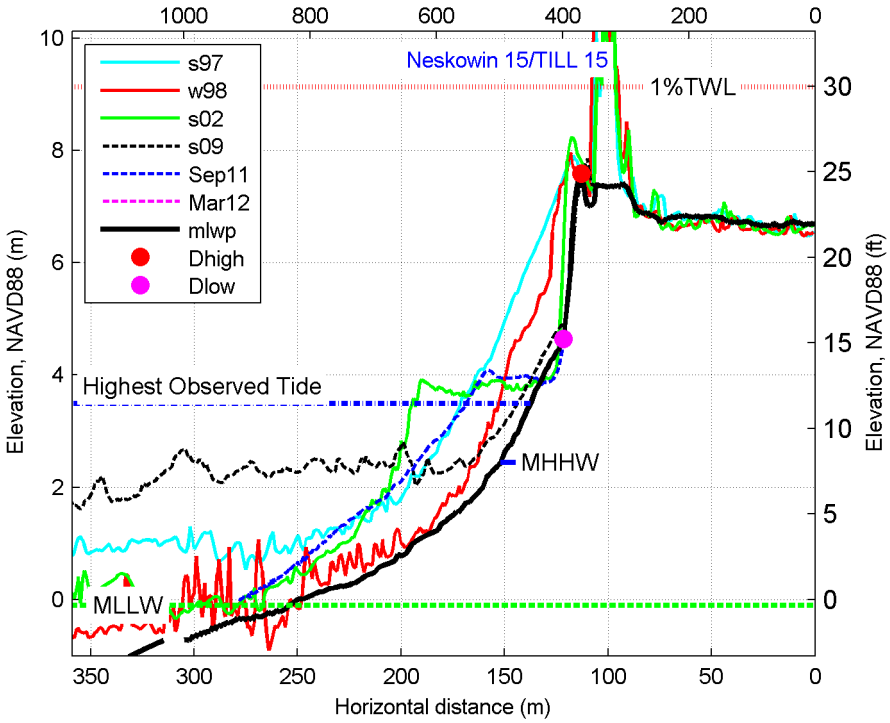

fm_nesk 16

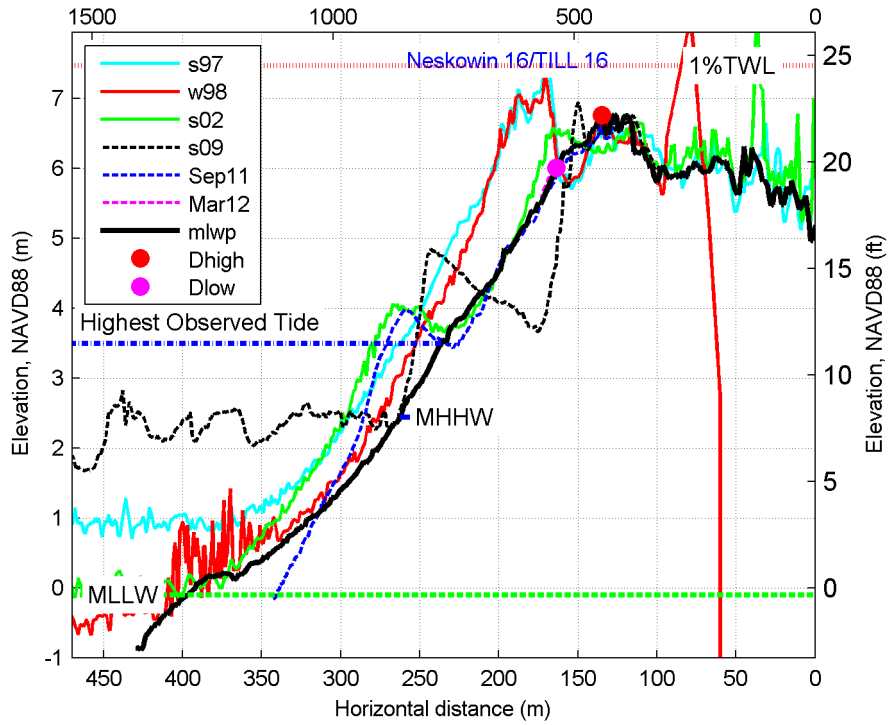

fm_nesk 17

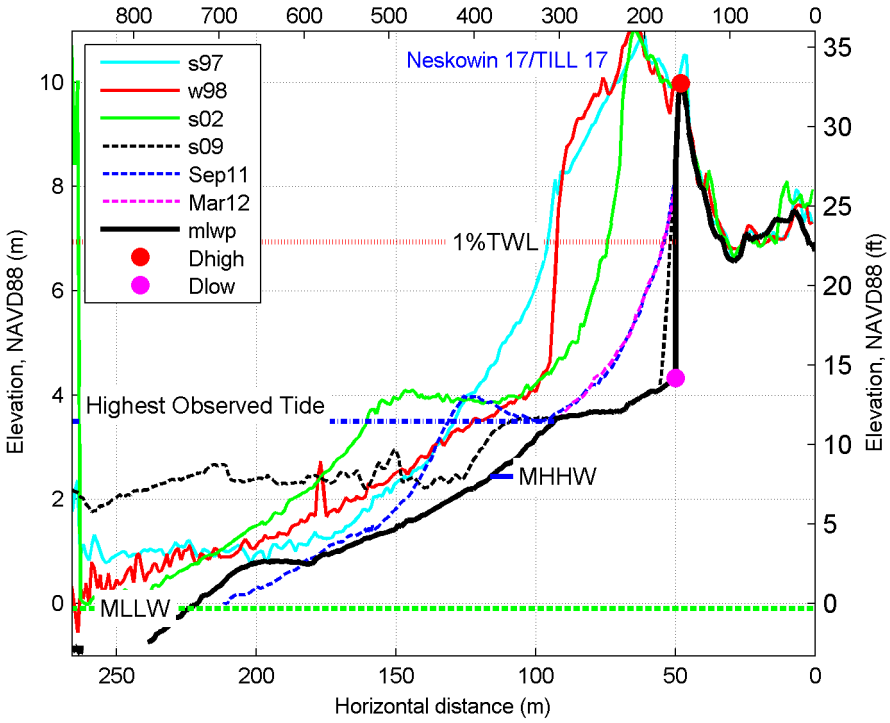

fm_nesk 18

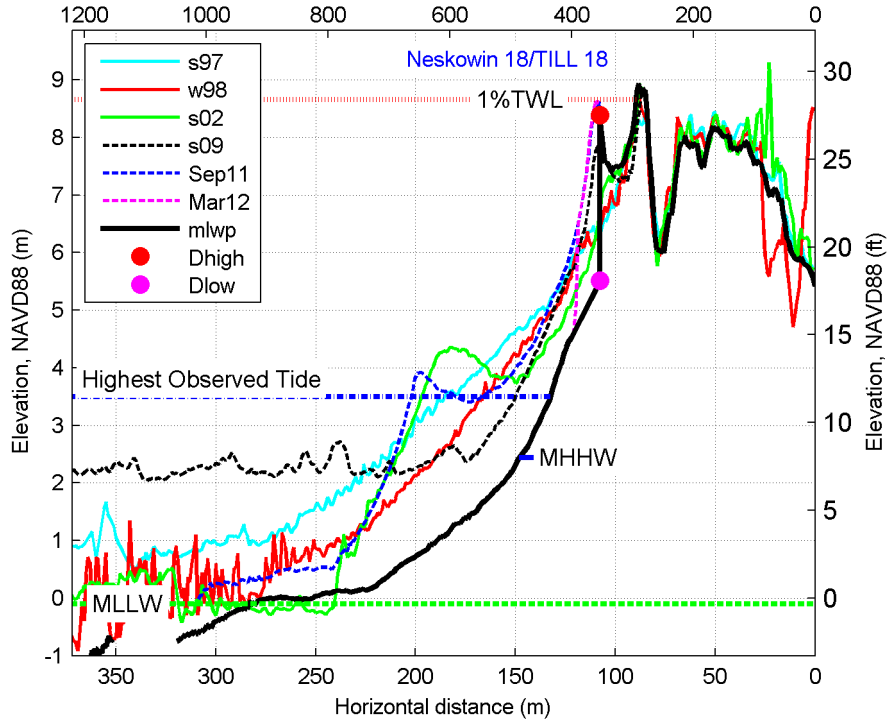

fm_nesk 19

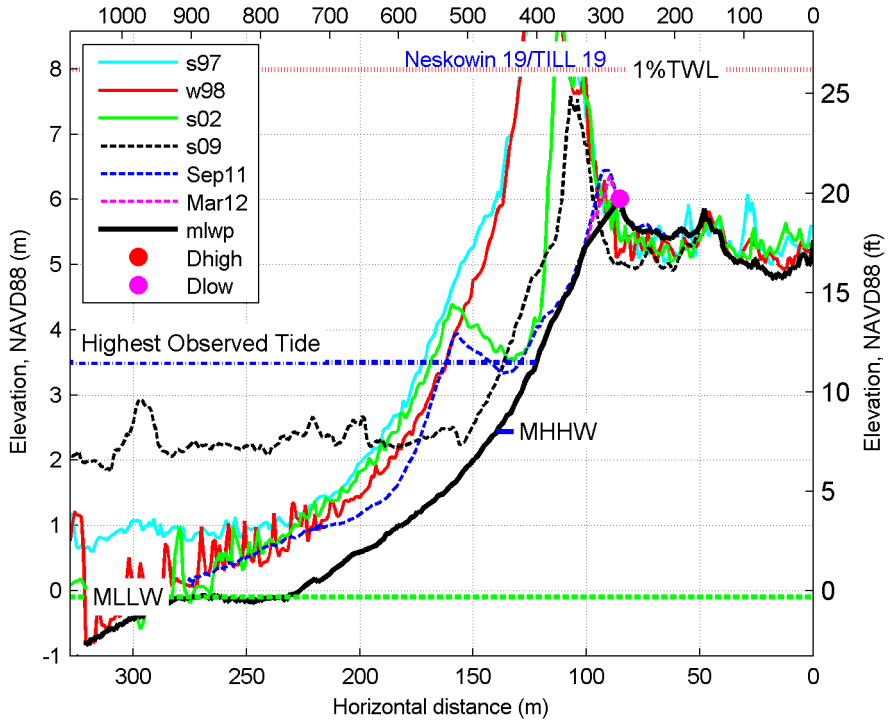

fm_nesk 20

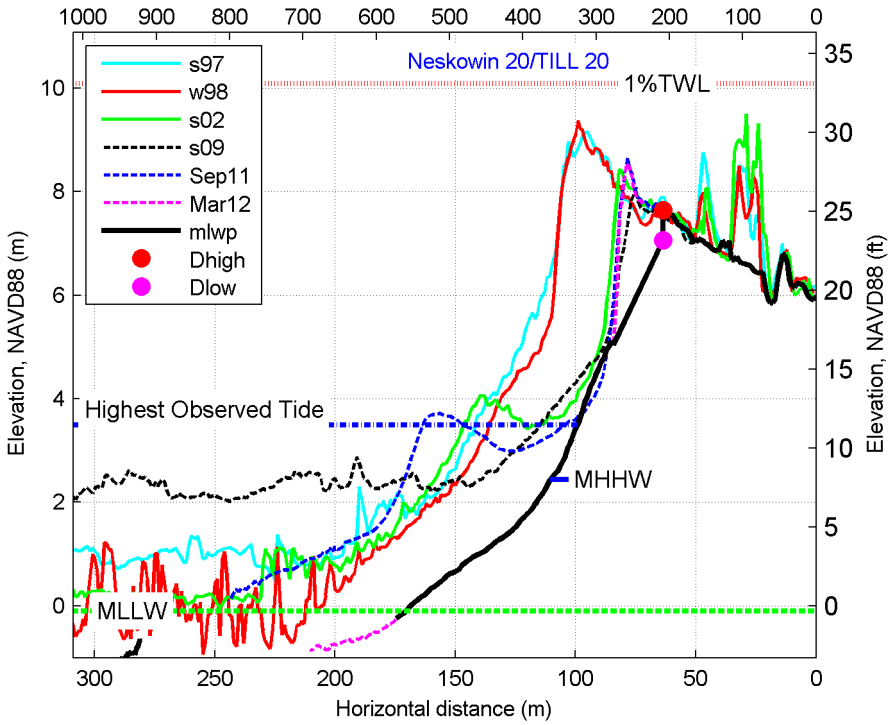

fm_nesk 21

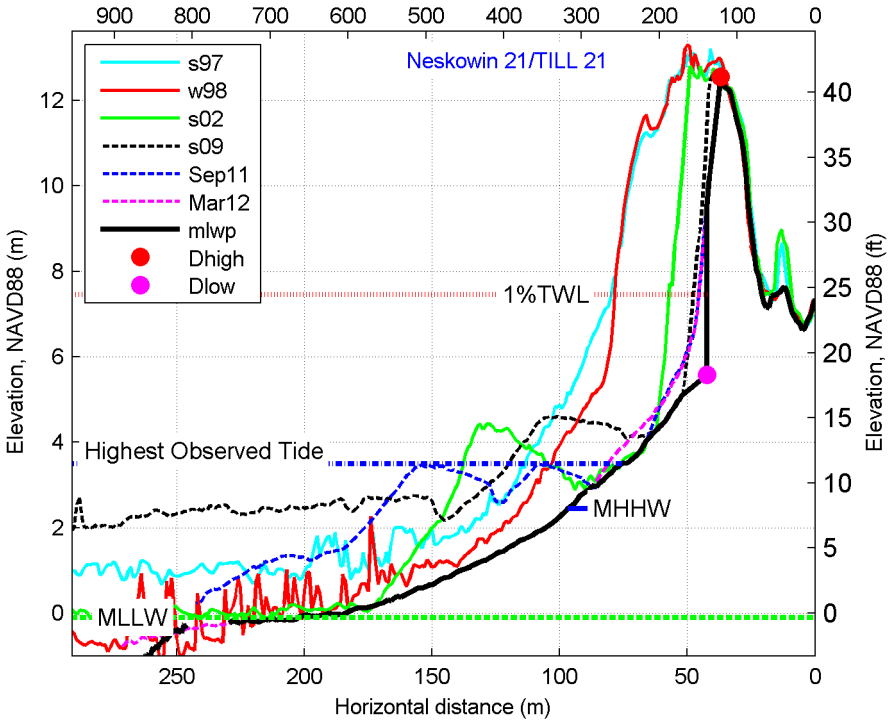

fm_nesk 22

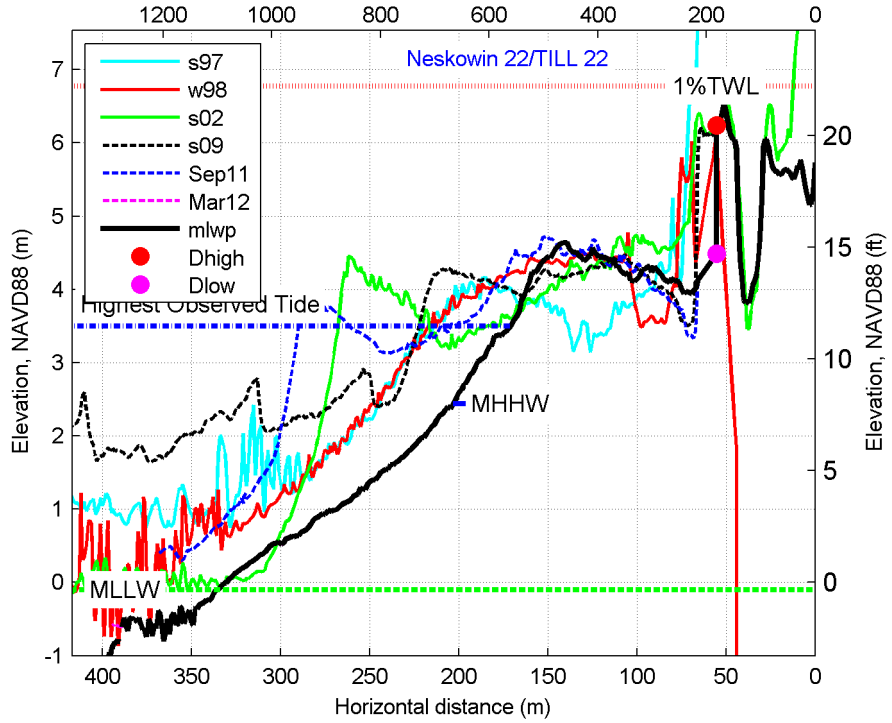

fm_nesk 23

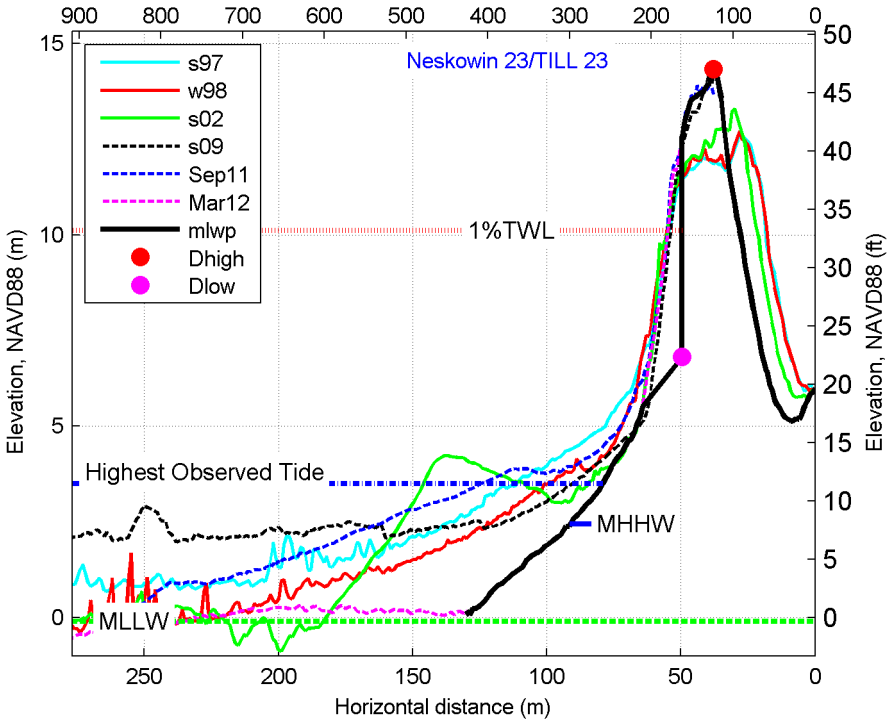

fm_nesk 24

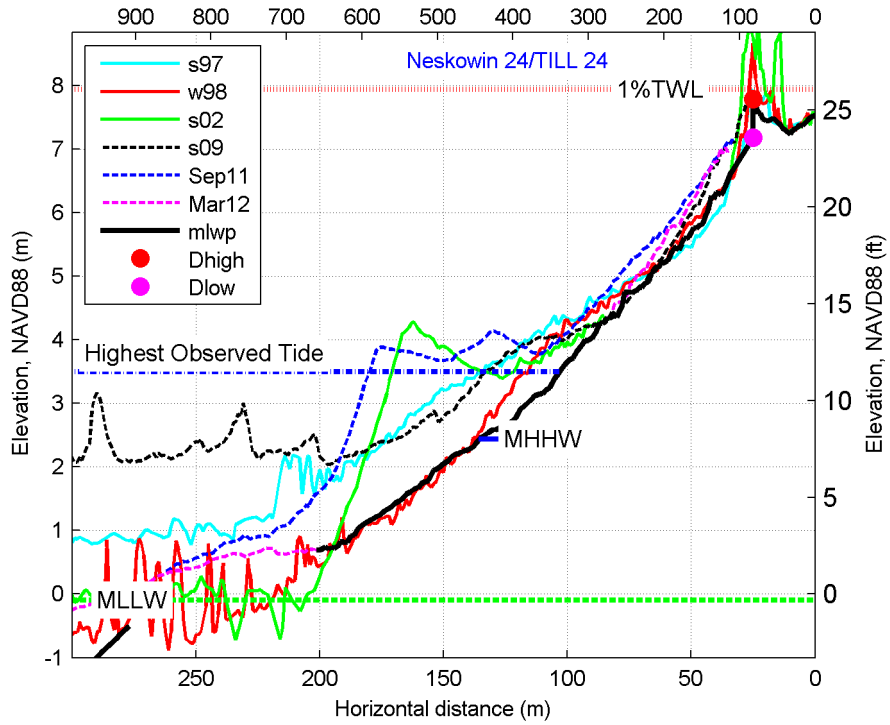

fm_nesk 25

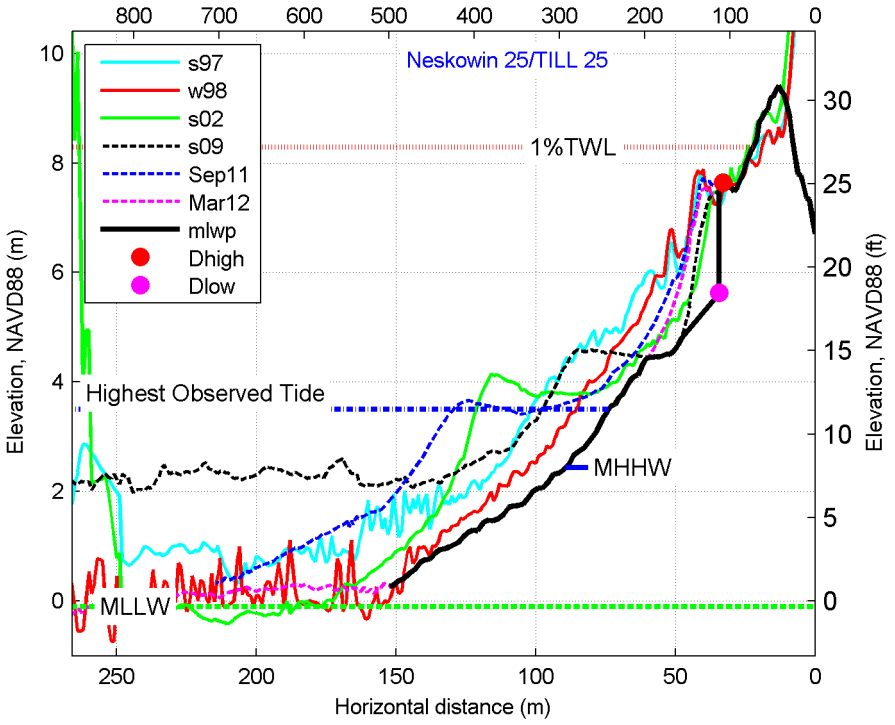

fm_nesk 26

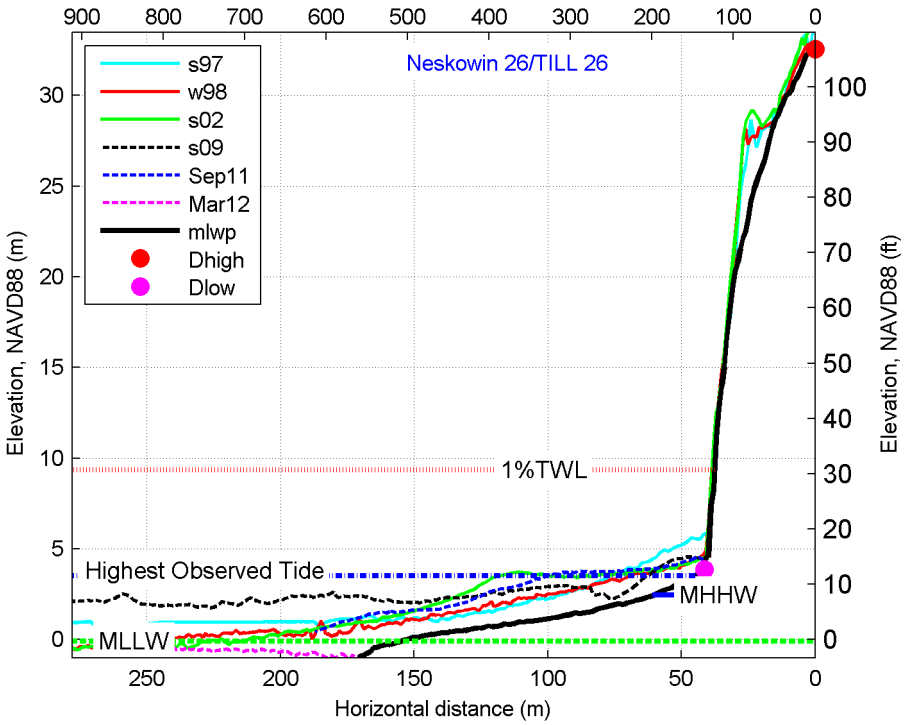

fm_nesk 27

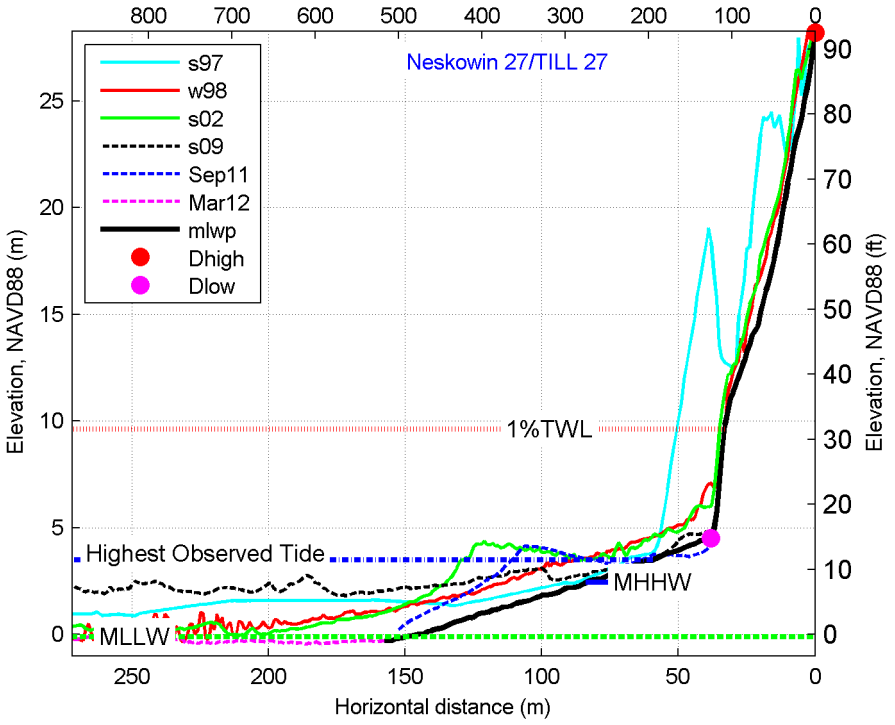

fm_nesk 28

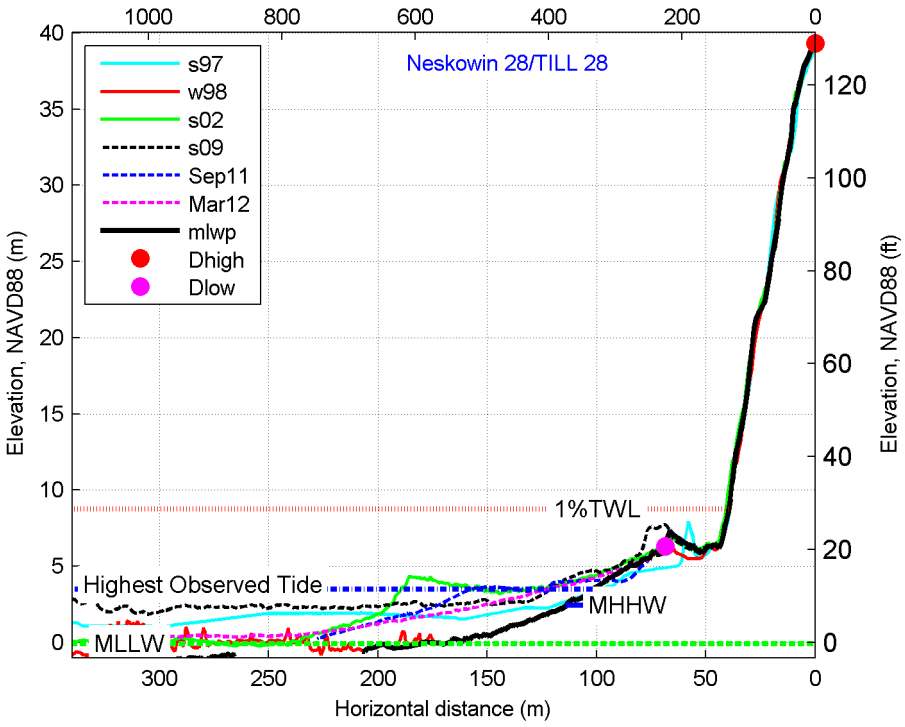

11.4.2 Pacific City

fm_pc 1

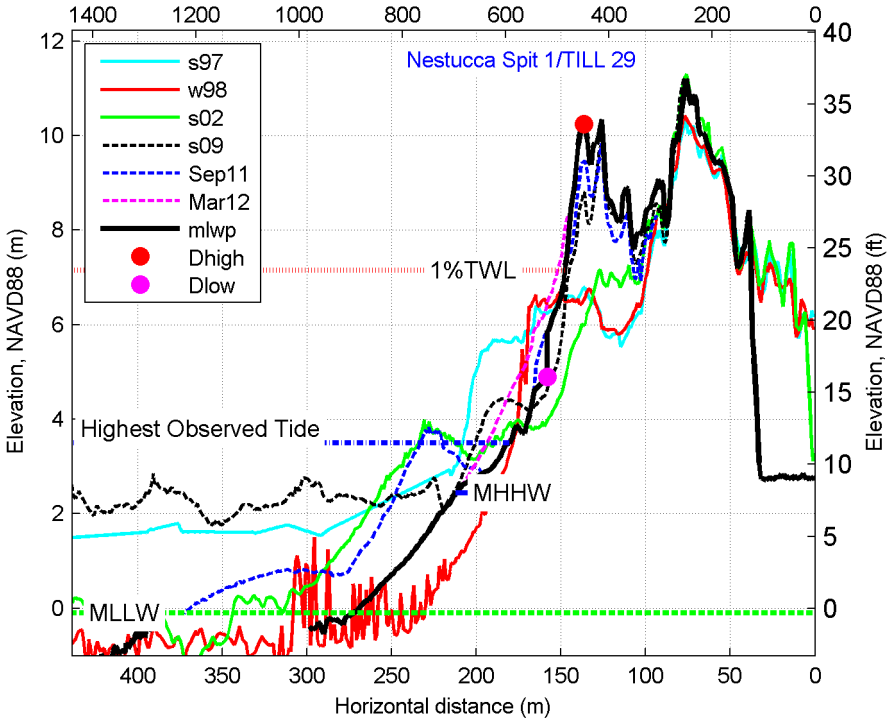

fm_pc 2

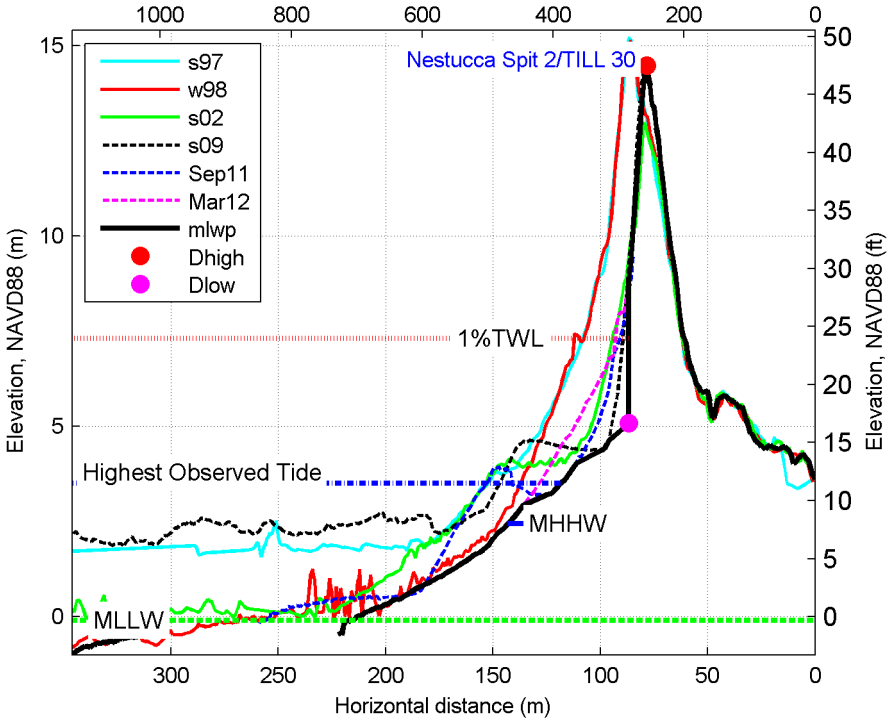

fm_pc 3

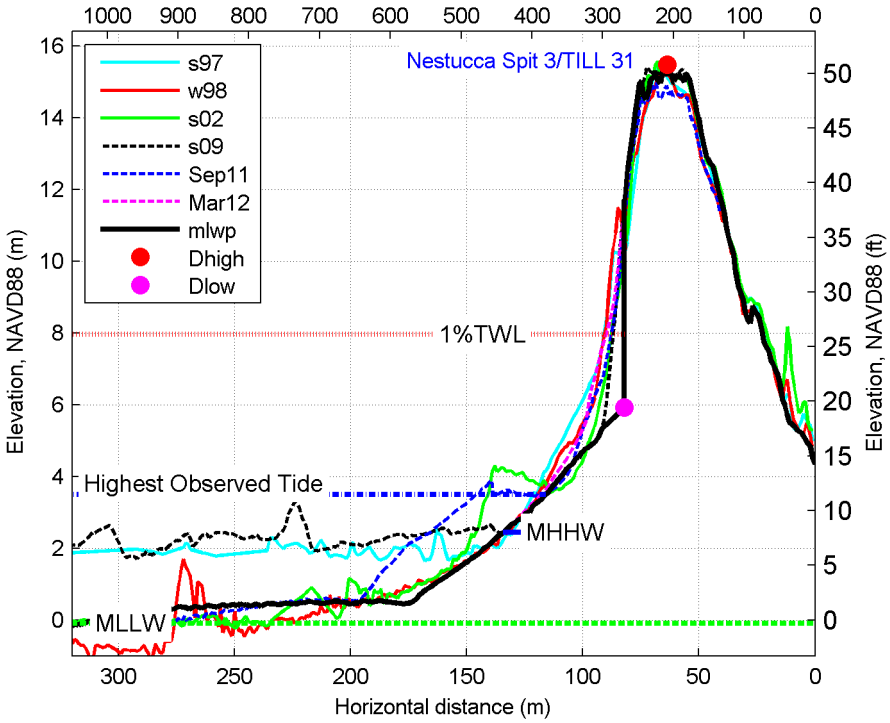
Nestucca Spit 3/TILL 31
s97
w98
s02
s09
Sep11
Mar12
mlwp
Dhigh
Dlow
1%TWL
Highest Observed Tide
MHHW
MLLW
Elevation, NAVD88 (m)
Elevation, NAVD88 (ft)
Horizontal distance (m)

fm_pc 4

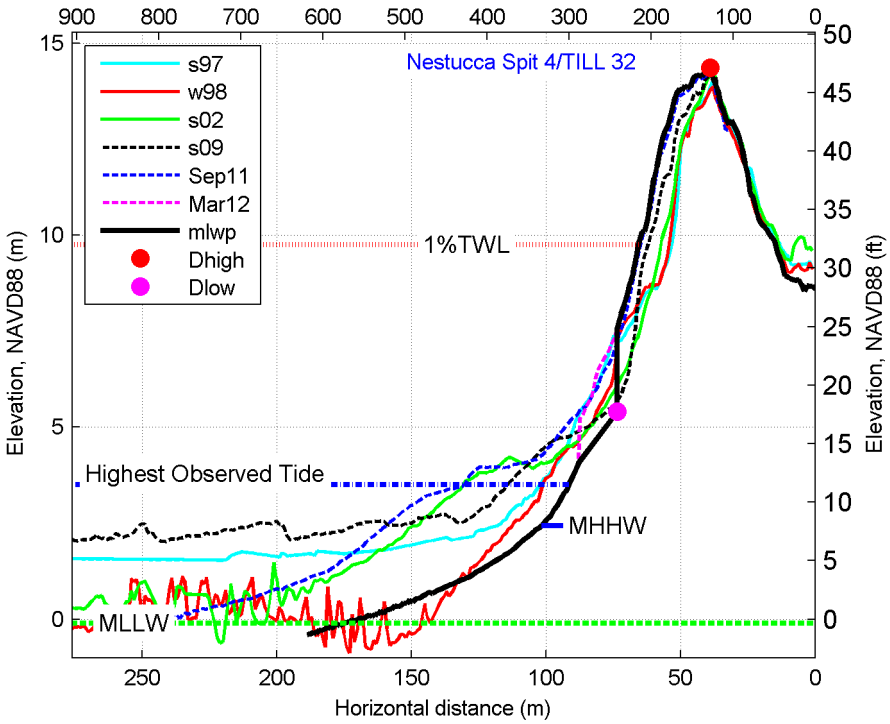
Nestucca Spit 4/TILL 32
s97
w98
s02
s09
Sep11
Mar12
mlwp
Dhigh
Dlow
1%TWL
Highest Observed Tide
MHHW
MLLW
Elevation, NAVD88 (m)
Elevation, NAVD88 (ft)
Horizontal distance (m)

fm_pc 5

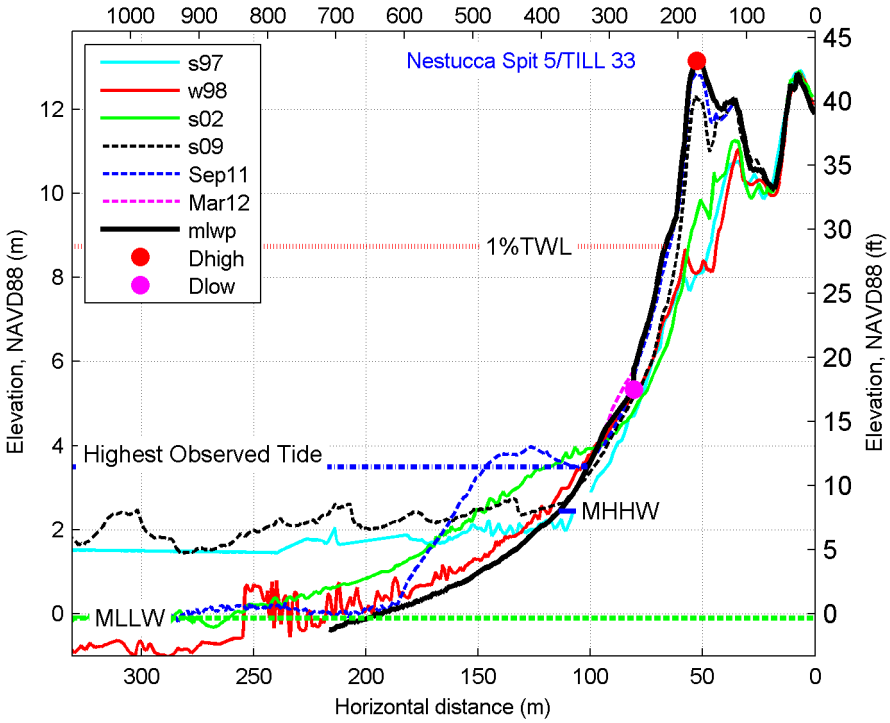
Nestucca Spit 5/TILL 33
s97
w98
s02
s09
Sep11
Mar12
mlwp
Dhigh
Dlow
1%TWL
Highest Observed Tide
MHHW
MLLW
Elevation, NAVD88 (m)
Elevation, NAVD88 (ft)
Horizontal distance (m)

fm_pc 6

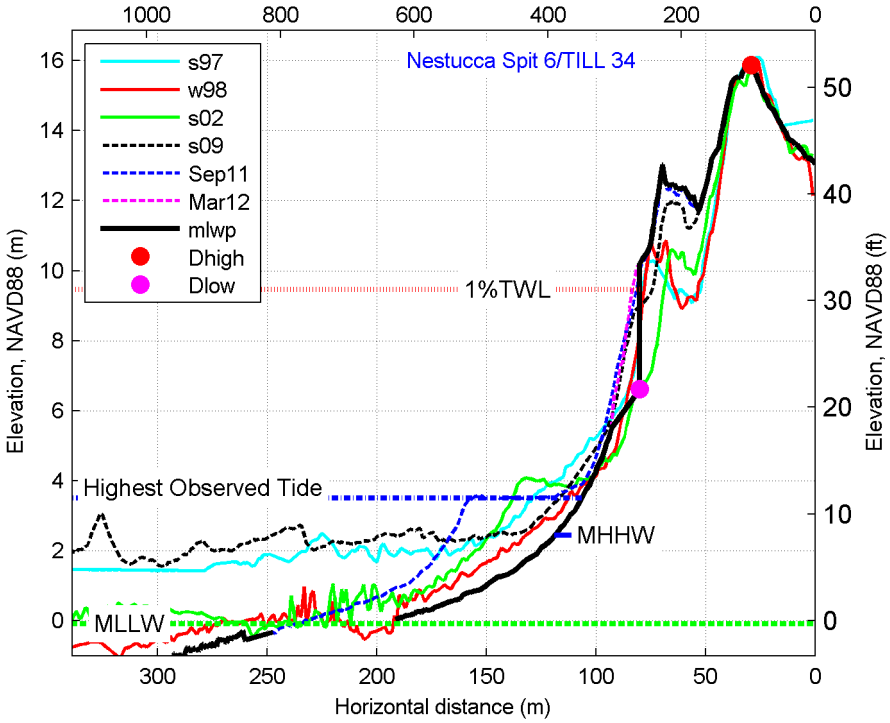
Nestucca Spit 6/TILL 34
s97
w98
s02
s09
Sep11
Mar12
mlwp
Dhigh
Dlow
1%TWL
Highest Observed Tide
MHHW
MLLW
Elevation, NAVD88 (m)
Elevation, NAVD88 (ft)
Horizontal distance (m)

fm_pc 7

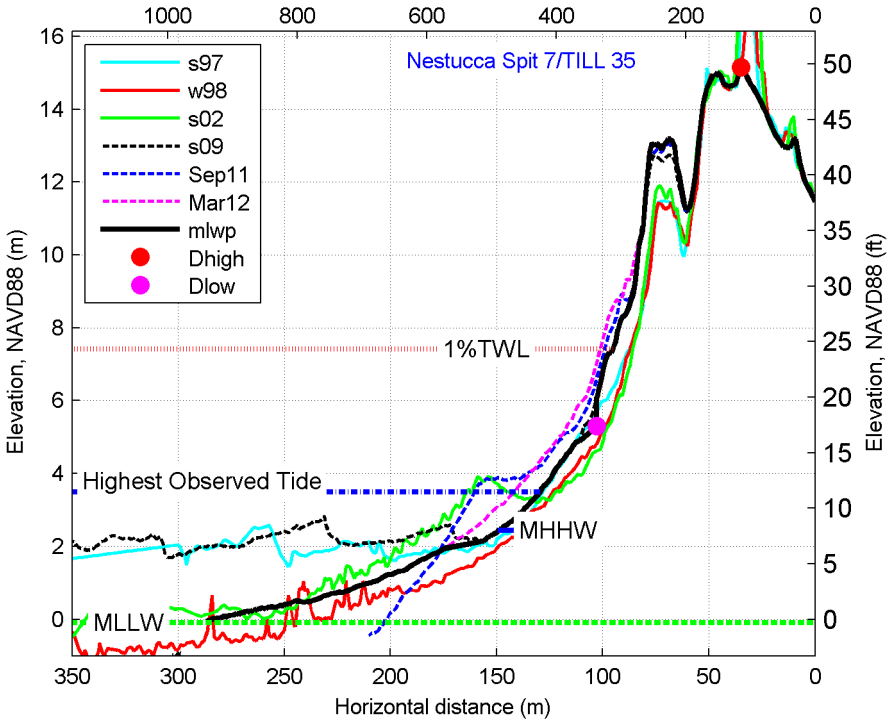
Nestucca Spit 7/TILL 35
s97
w98
s02
s09
Sep11
Mar12
mlwp
Dhigh
Dlow
1%TWL
Highest Observed Tide
MHHW
MLLW
Elevation, NAVD88 (m)
Elevation, NAVD88 (ft)
Horizontal distance (m)

fm_pc 8

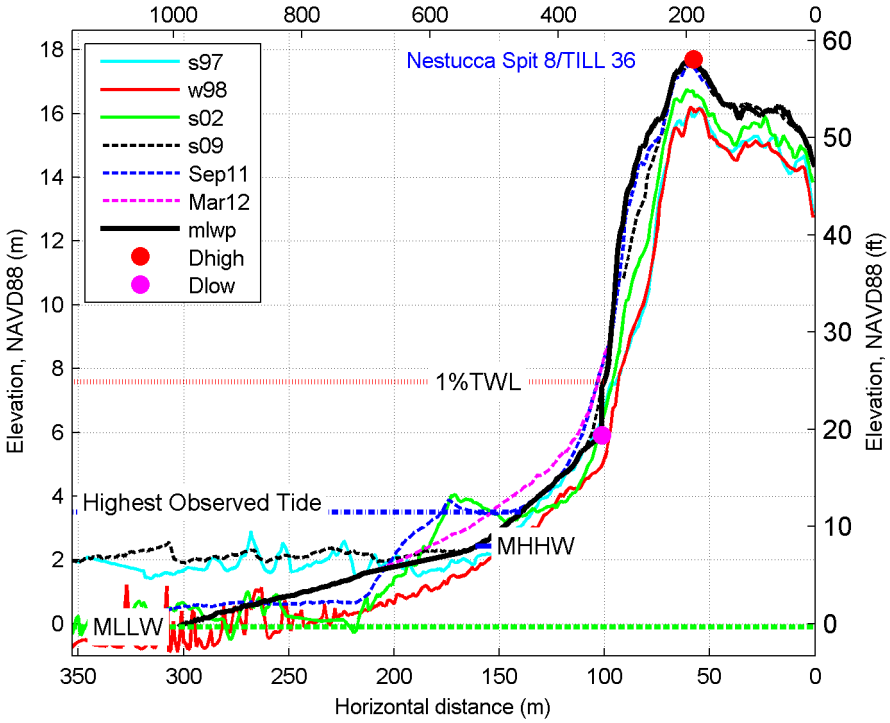
Nestucca Spit 8/TILL 36
s97
w98
s02
s09
Sep11
Mar12
mlwp
Dhigh
Dlow
1%TWL
Highest Observed Tide
MHHW
MLLW
Elevation, NAVD88 (m)
Elevation, NAVD88 (ft)
Horizontal distance (m)

fm_pc 9

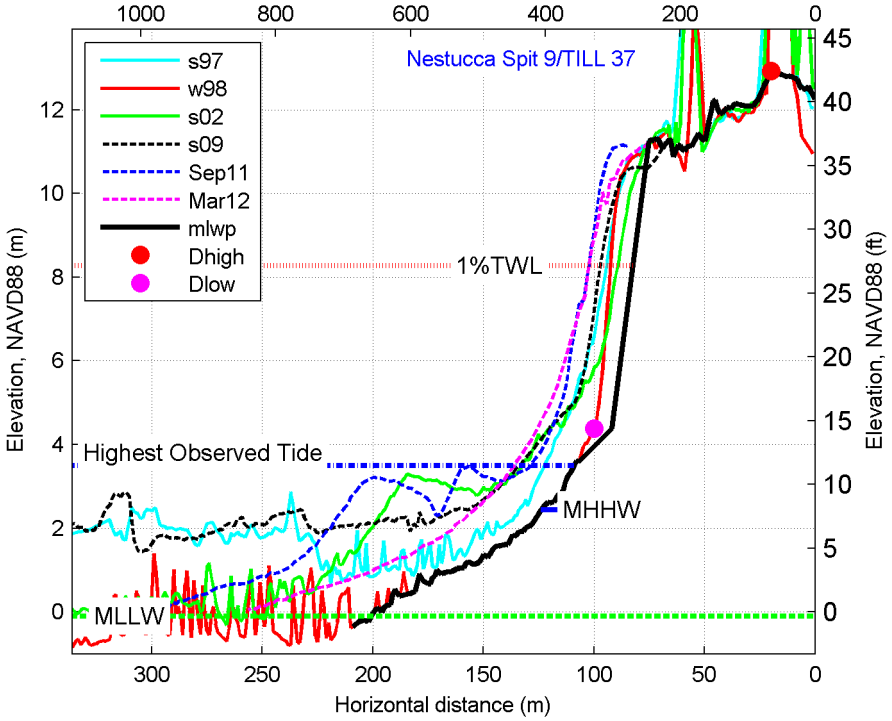

fm_pc 10

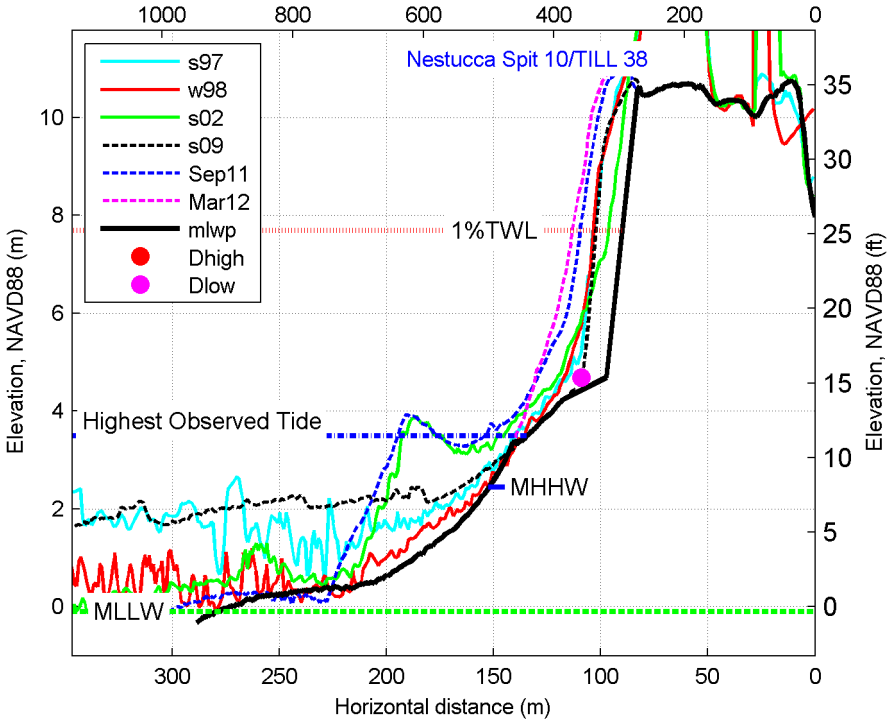

fm_pc 11

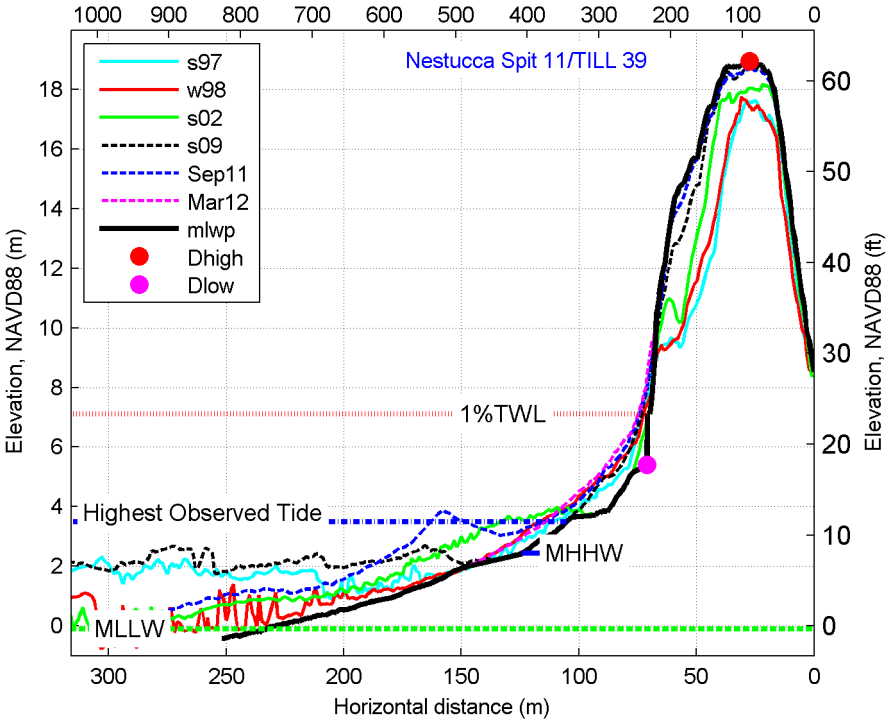

fm_pc 12

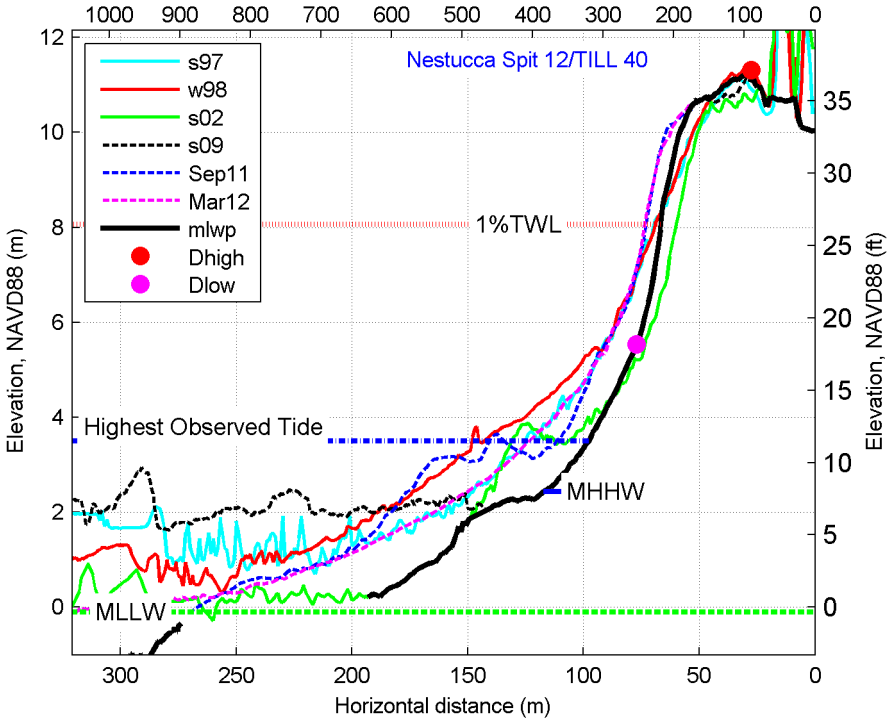

fm_pc 13

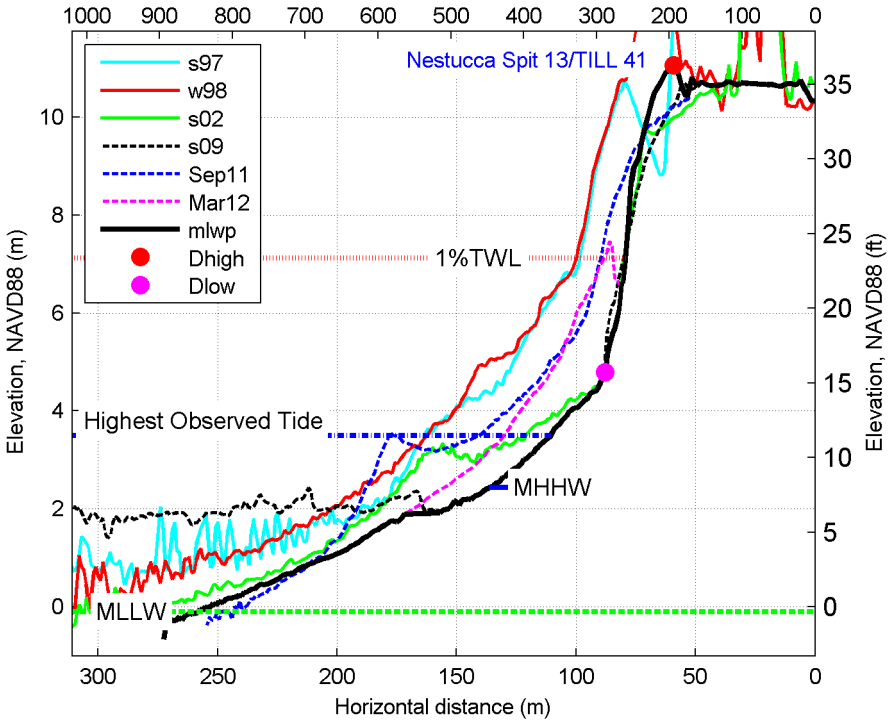

fm_pc 14

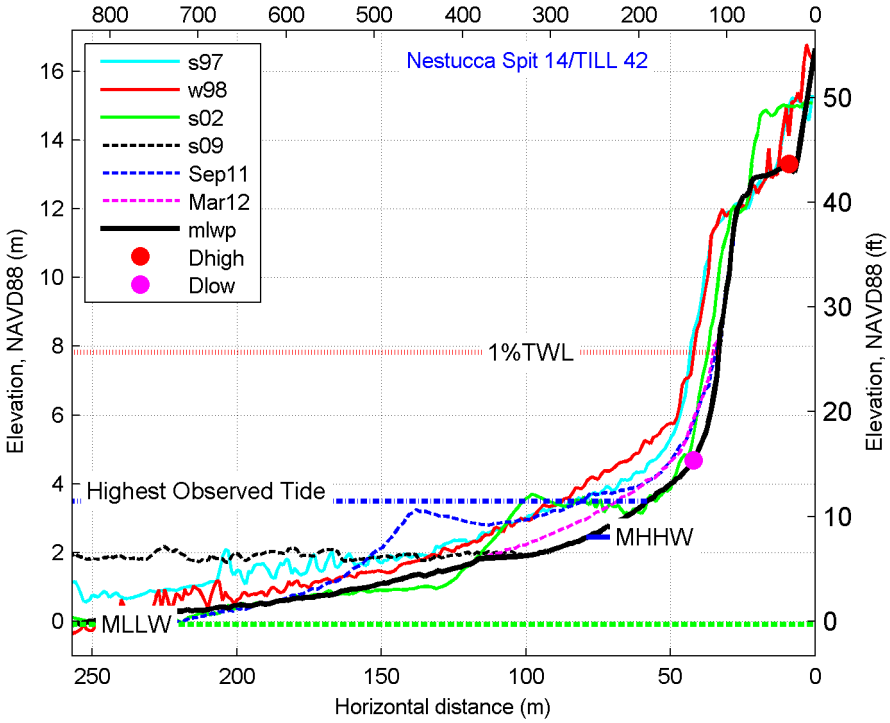

11.4.3 Sand Lake

fm_slk 1

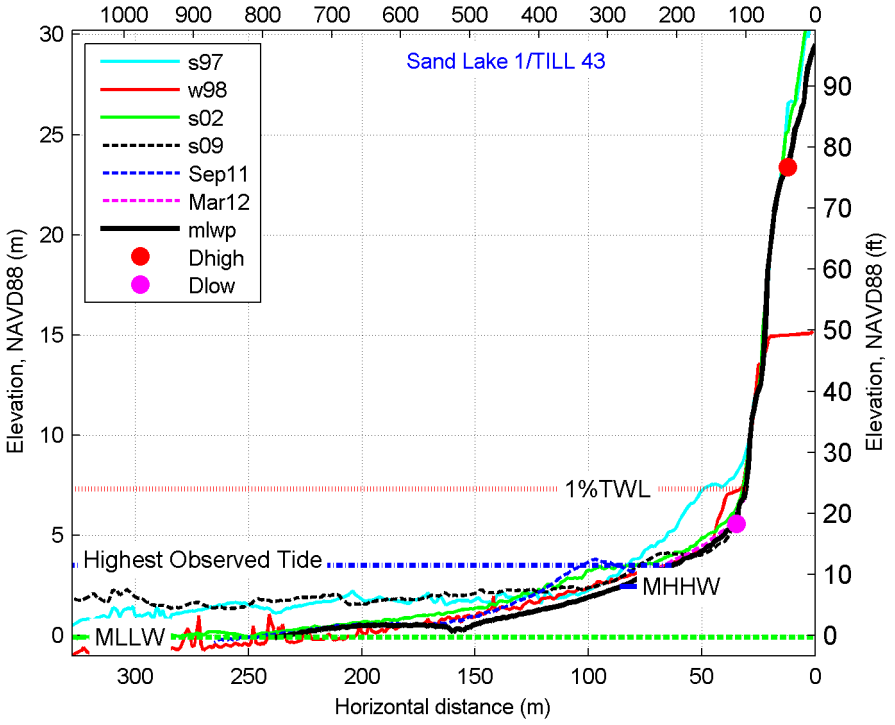

fm_slk 2

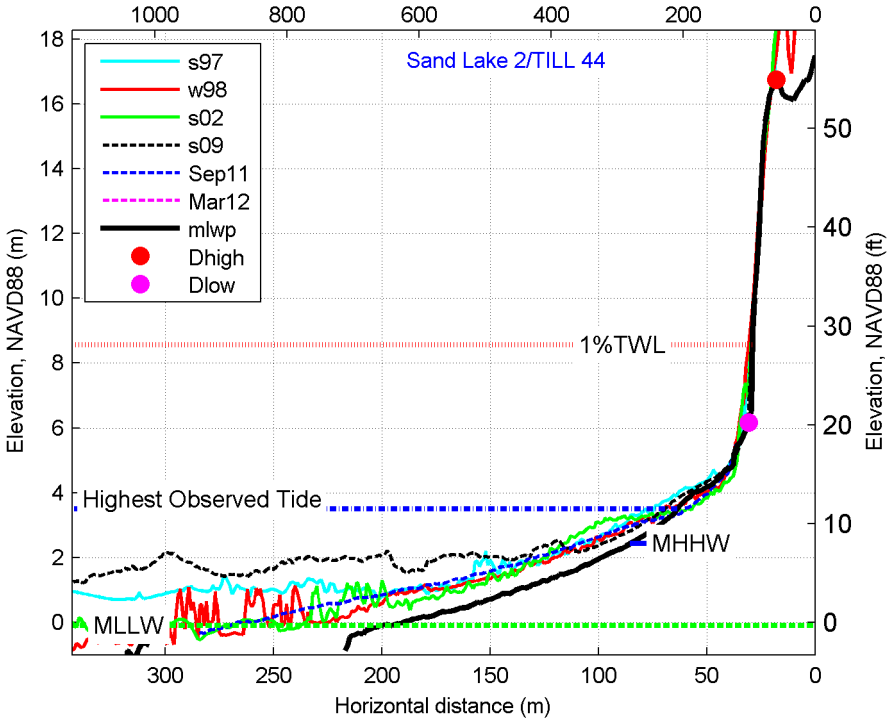

fm_slk 3

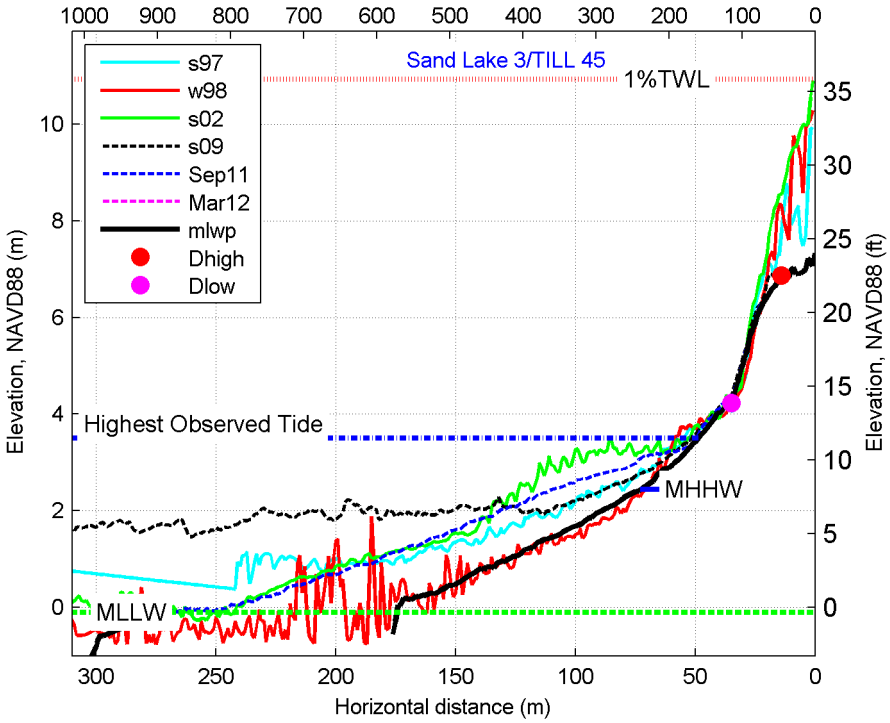

fm_slk 4

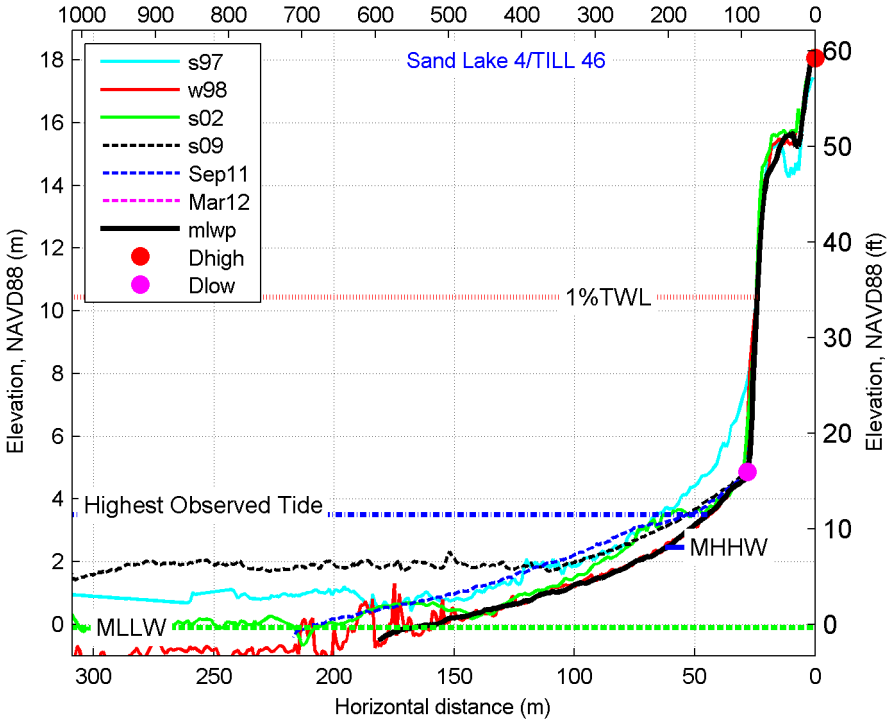

fm_slk 5

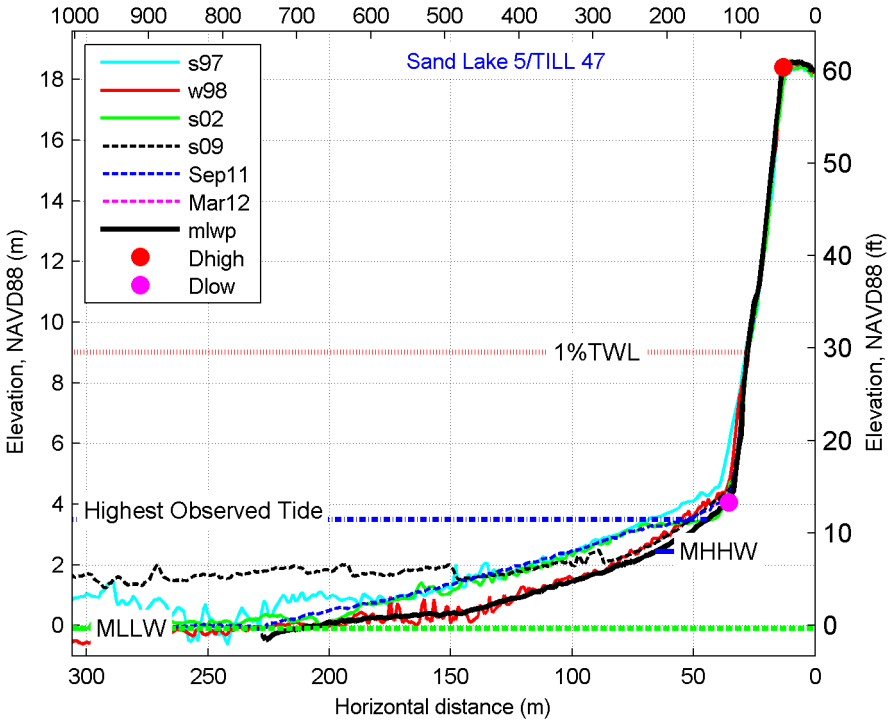

fm_slk 6

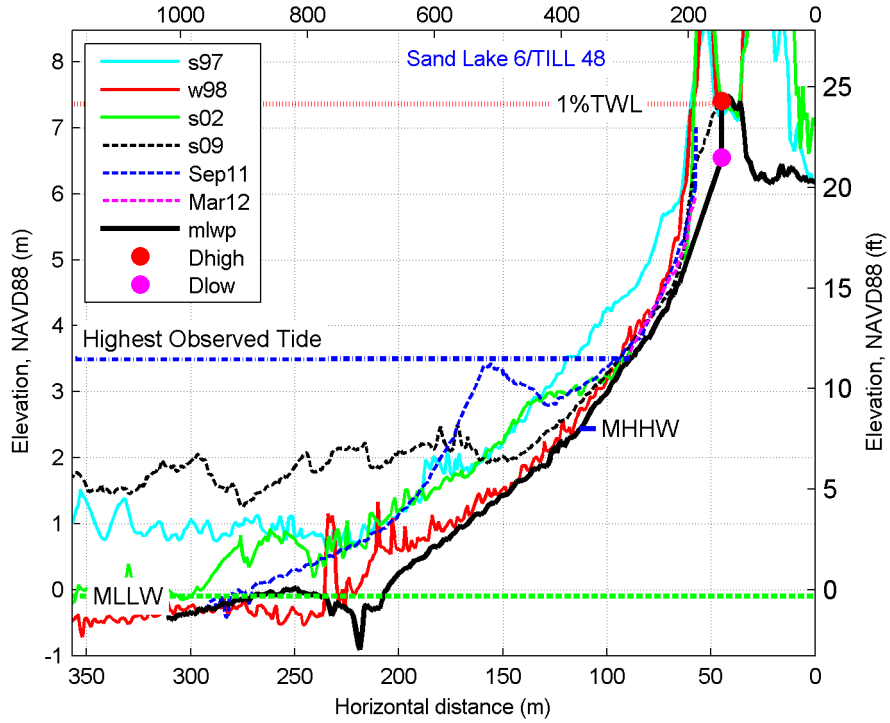

fm_slk 7

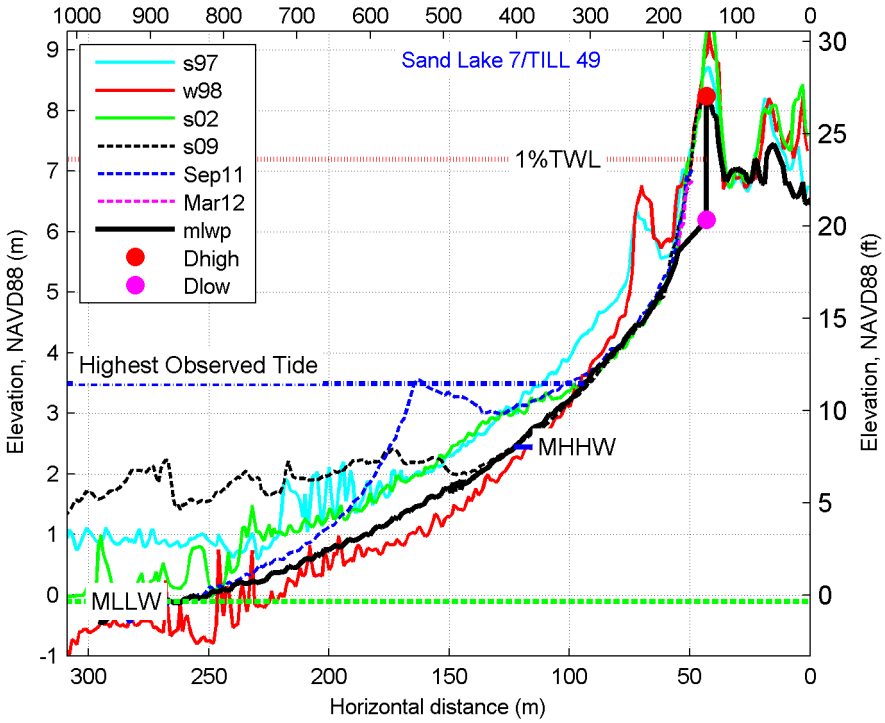

fm_slk 8

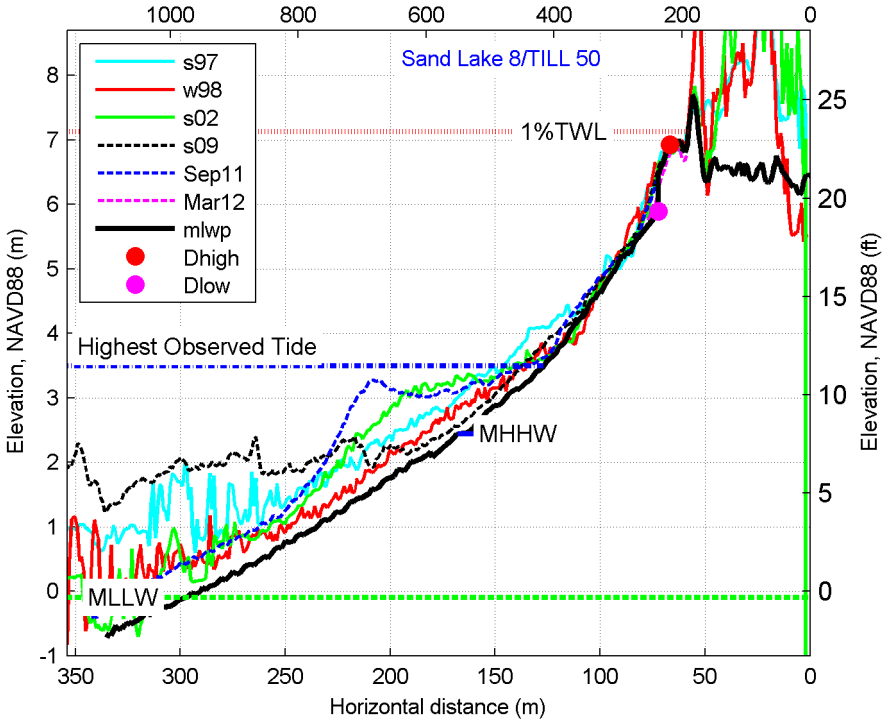

fm_slk 9

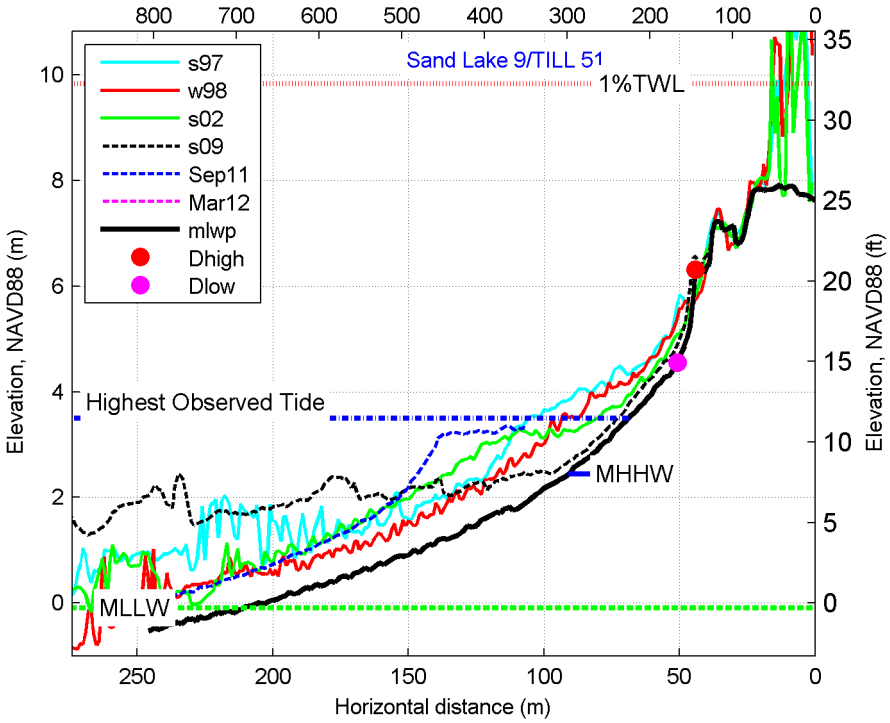

fm_slk 10

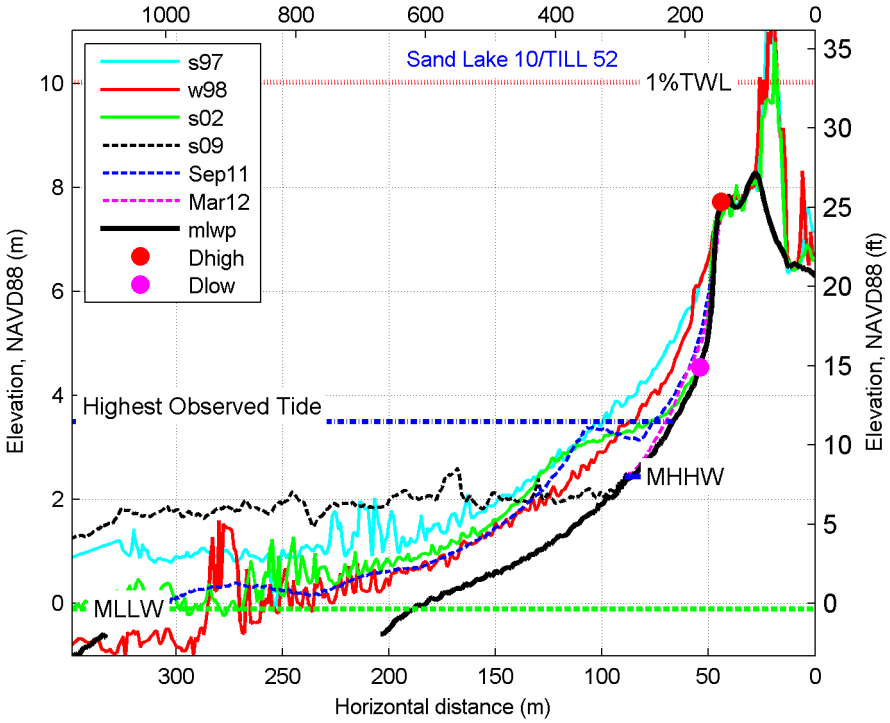

fm_slk 11

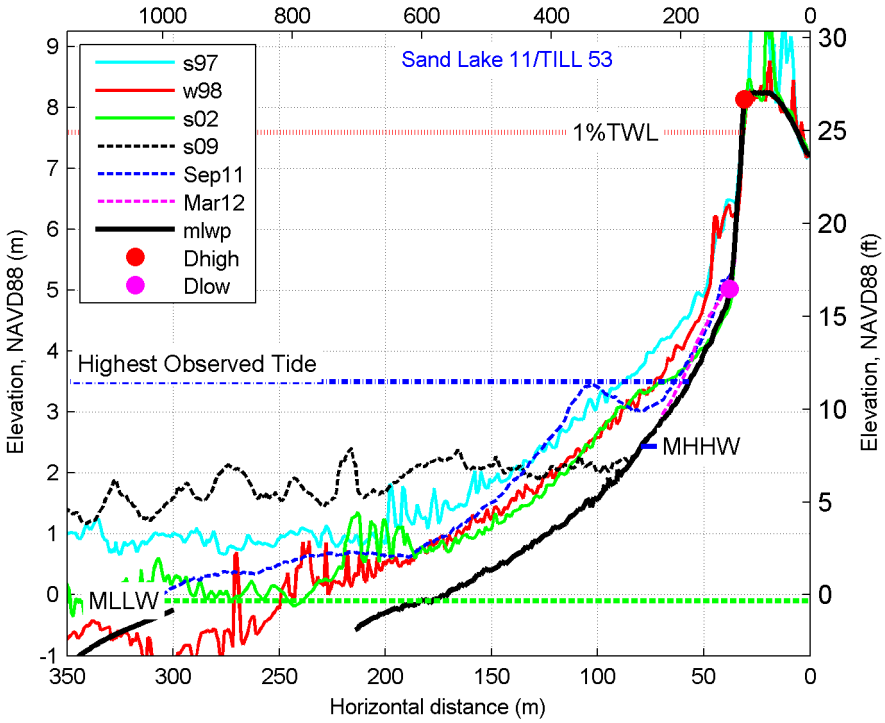

fm_slk 12

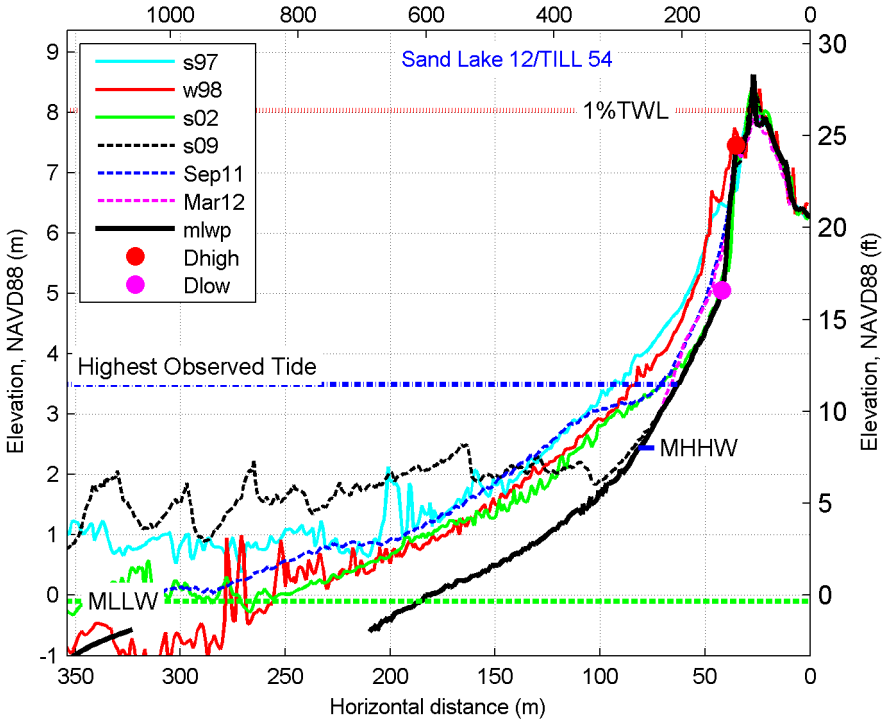

fm_slk 13

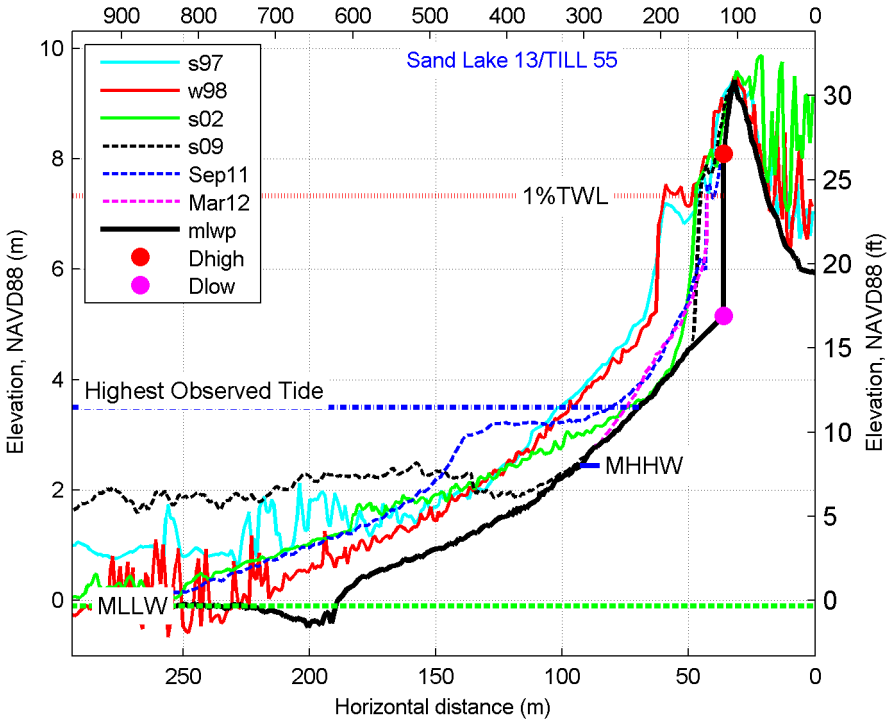

fm_slk 14

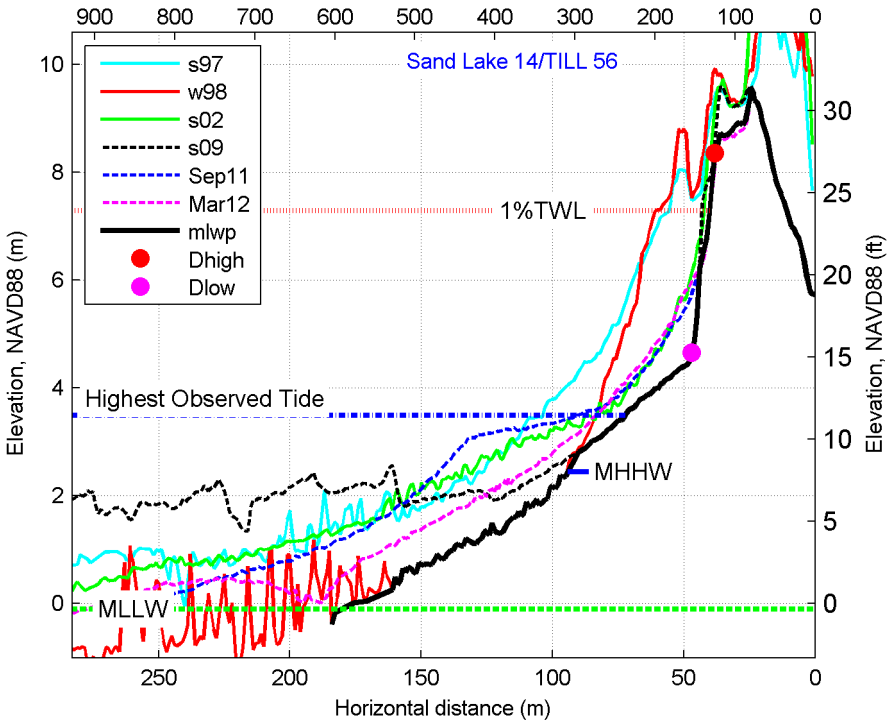

fm_slk 15

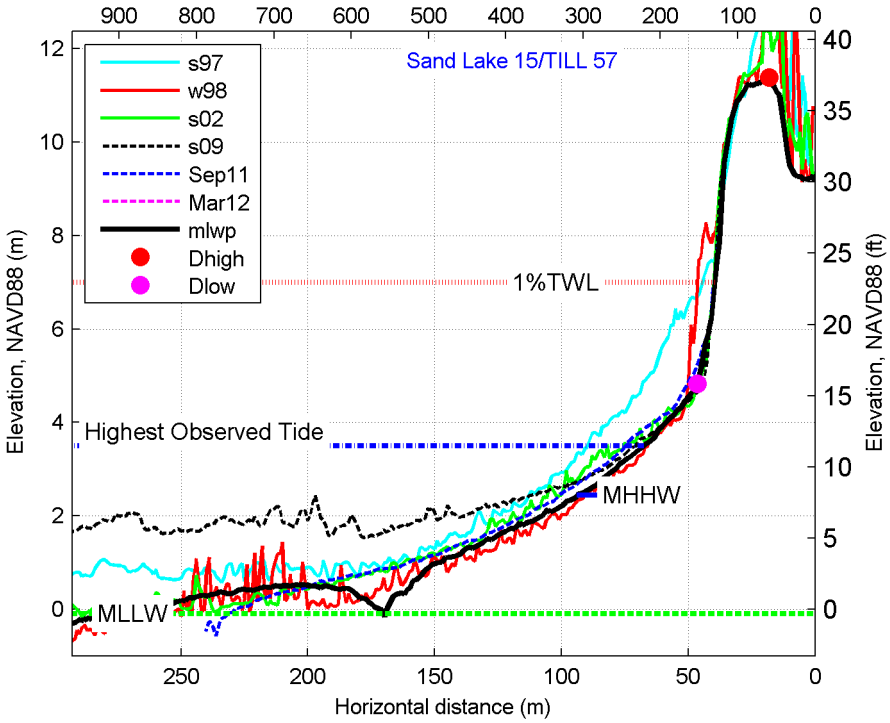

fm_slk 16

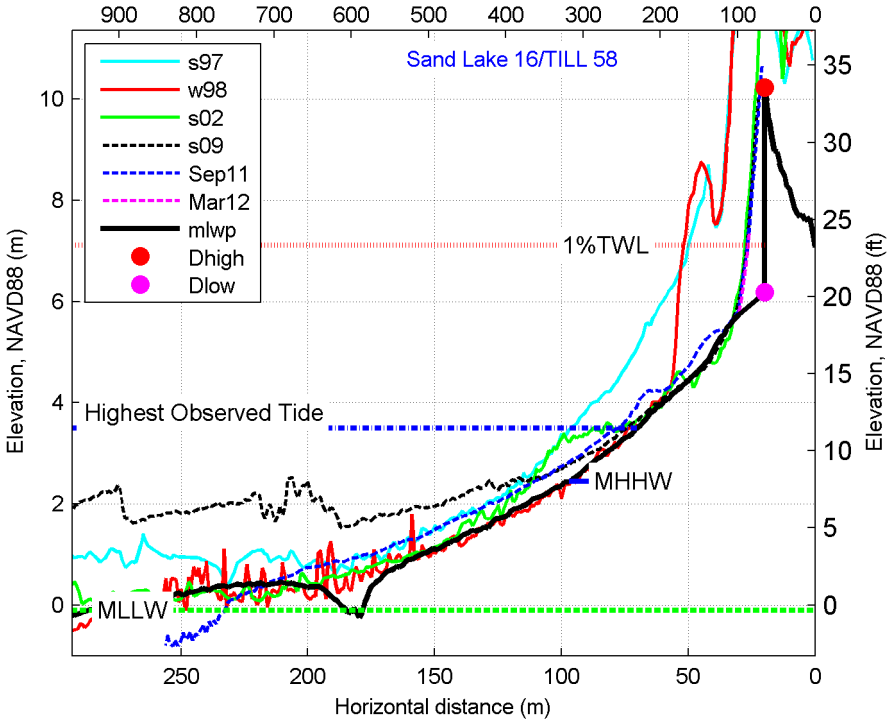

fm_slk 17

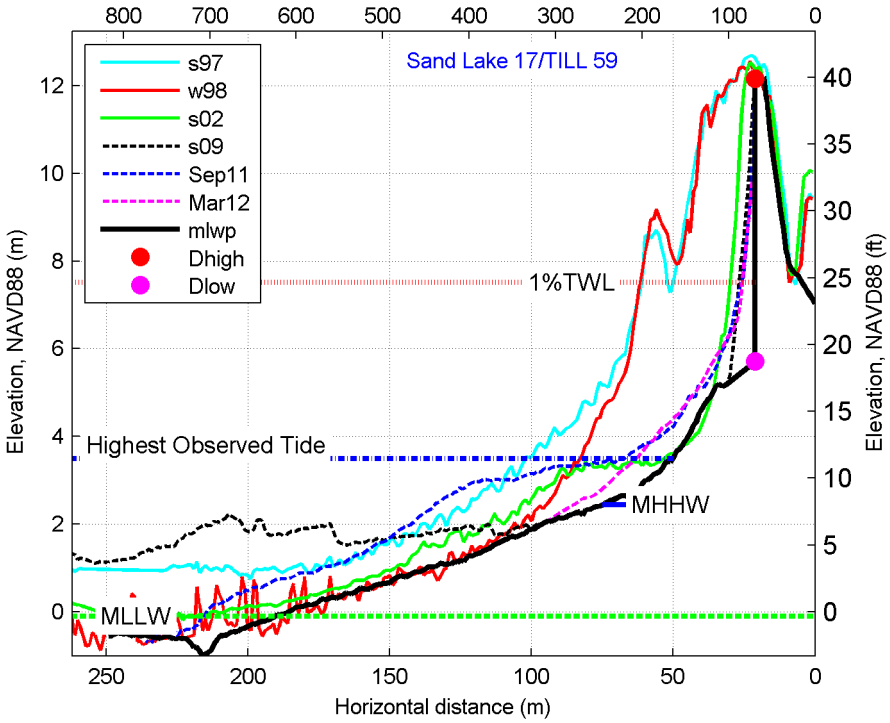

fm_slk 18

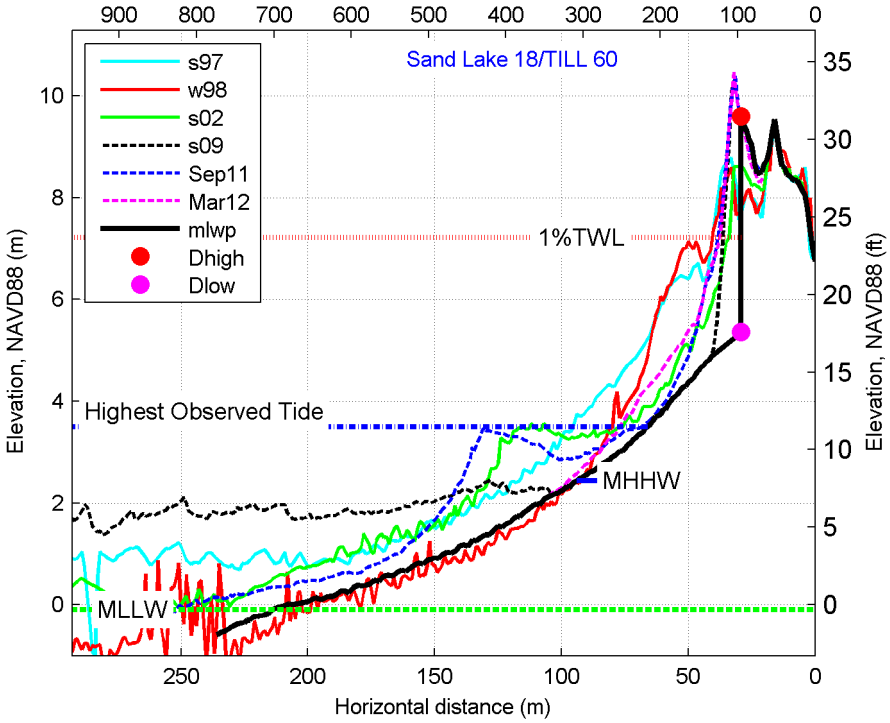

fm_slk 19

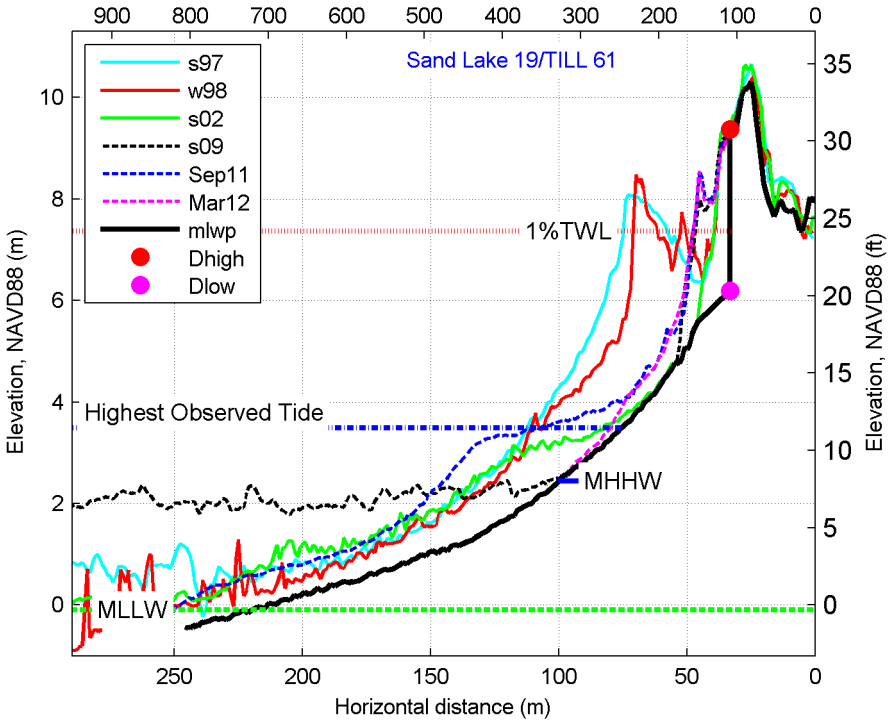

fm_slk 20

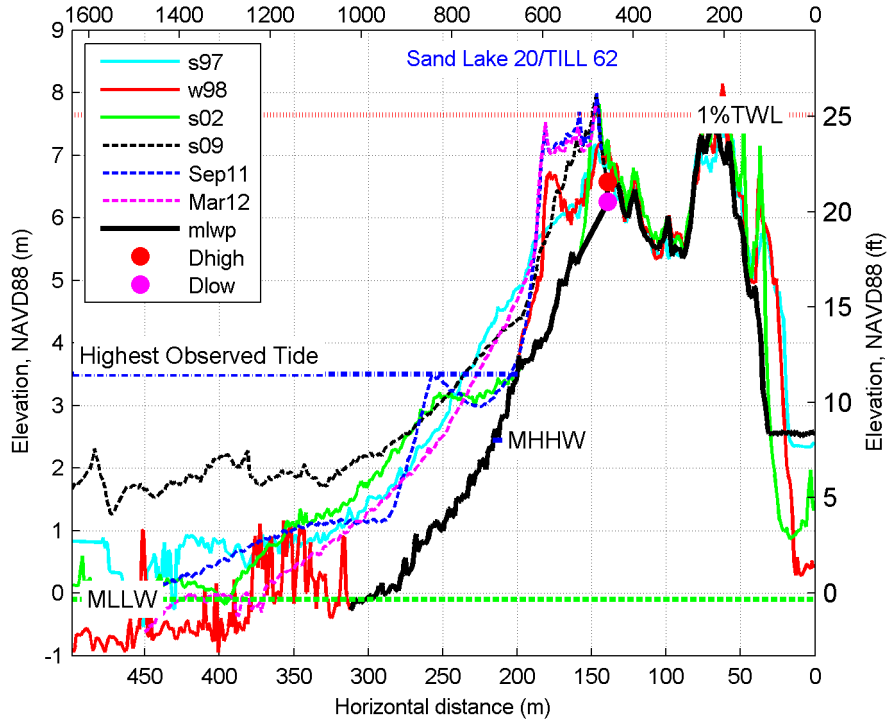

fm_slk 21

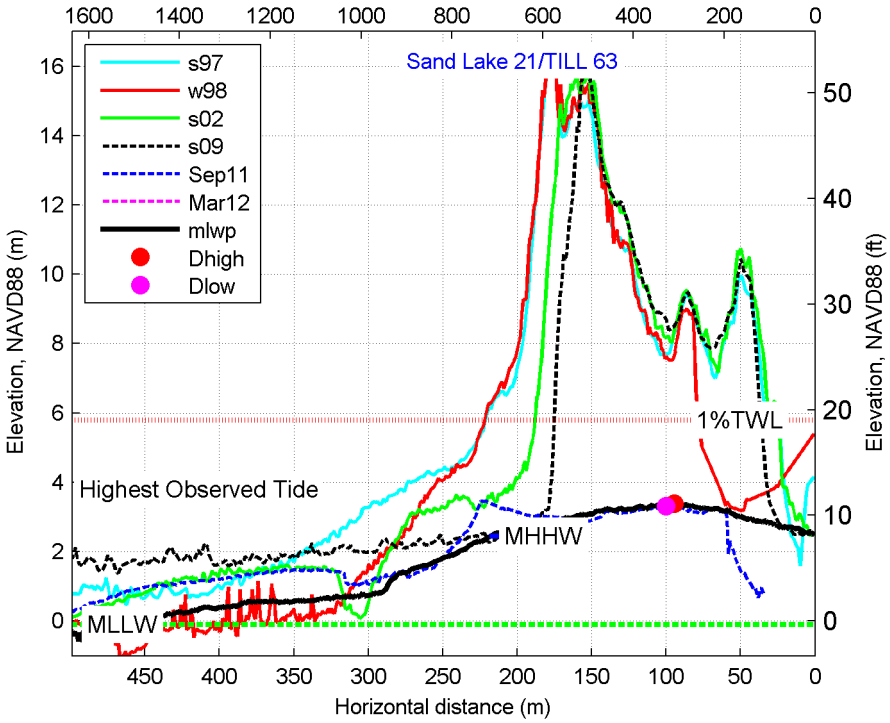

fm_slk 22

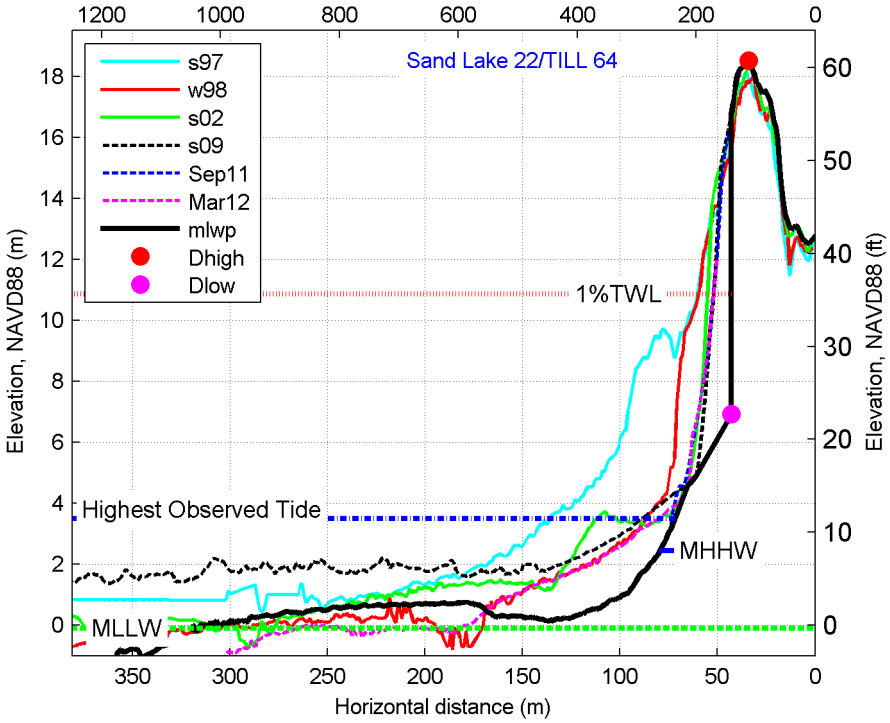

fm_slk 23

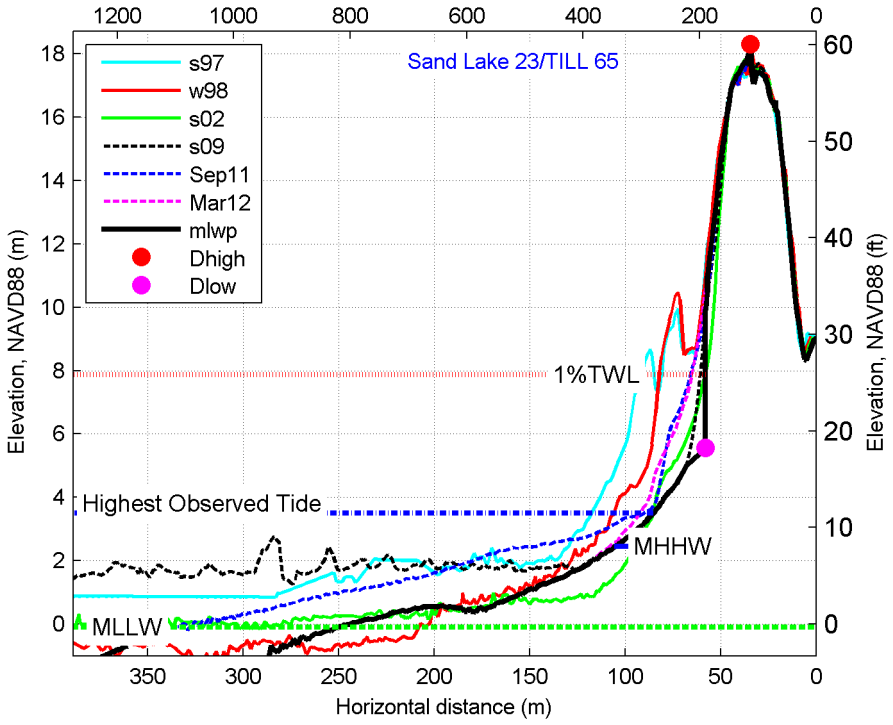

fm_slk 24

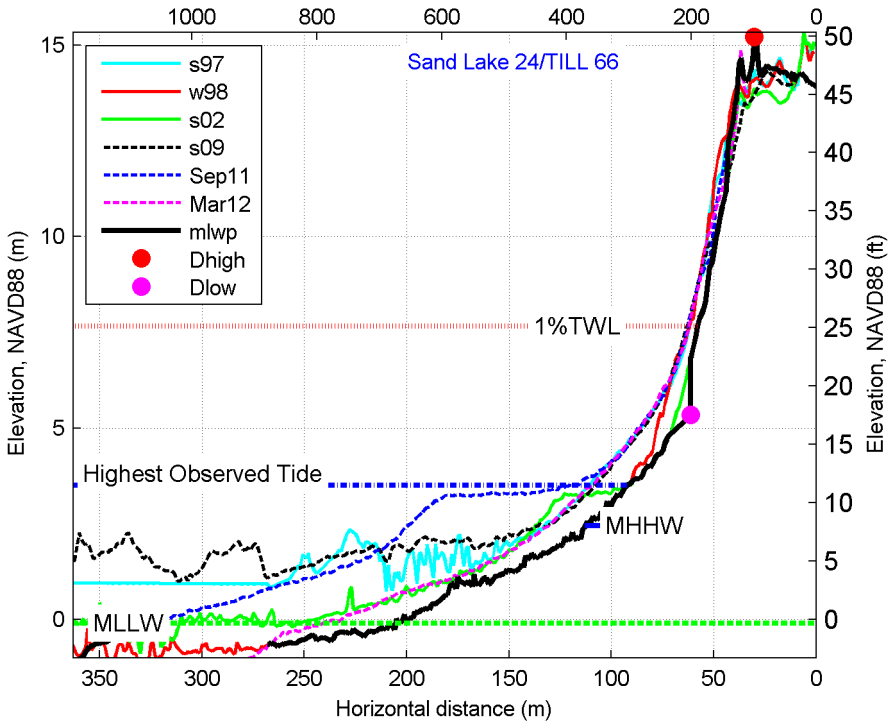

fm_slk 25

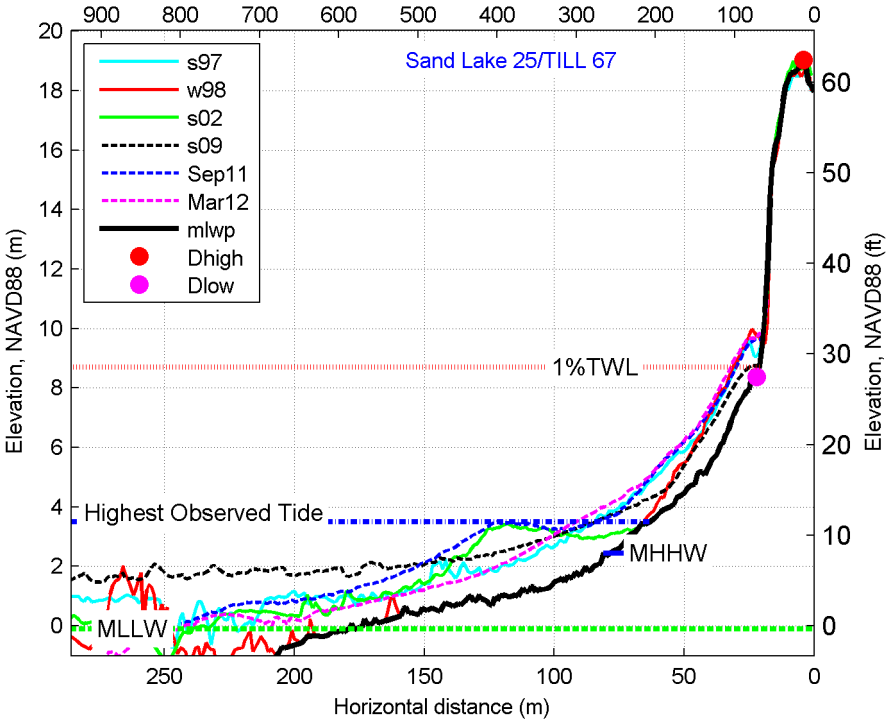

fm_slk 26

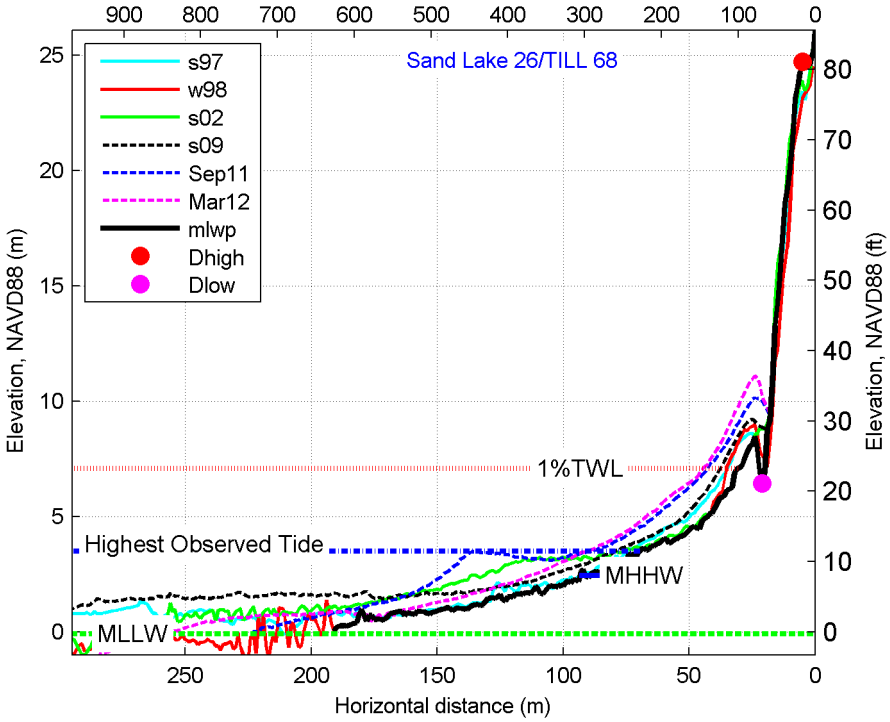

fm_slk 27

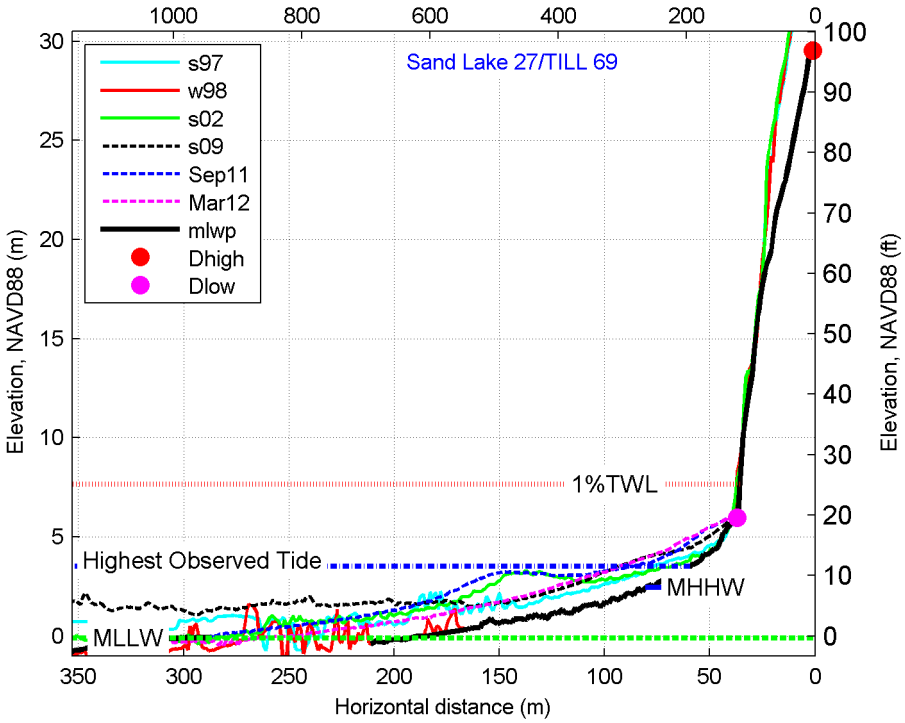

fm_slk 28

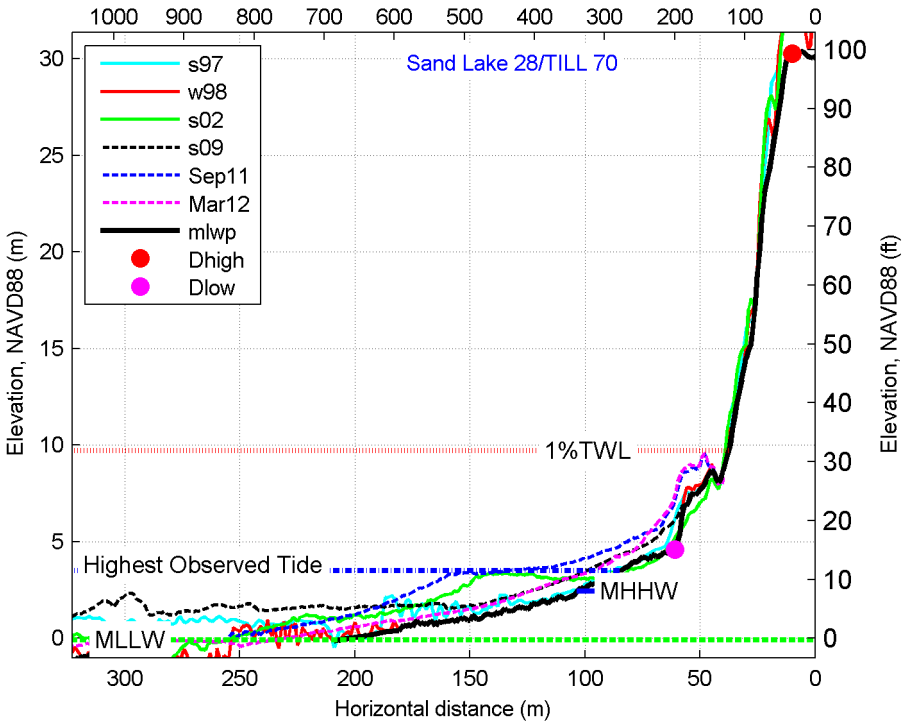

fm_slk 29

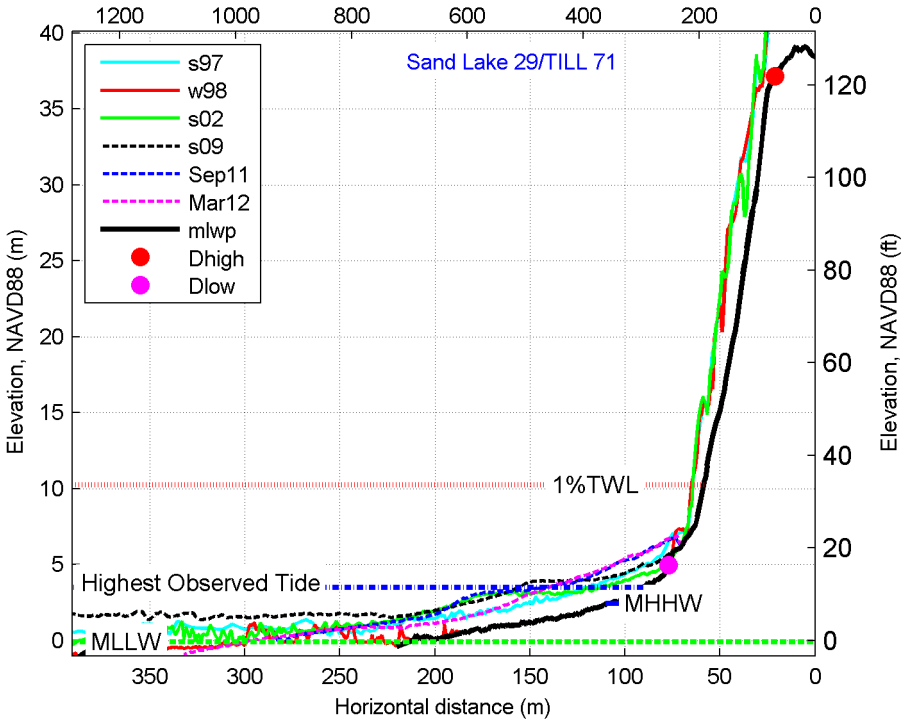

fm_slk 30

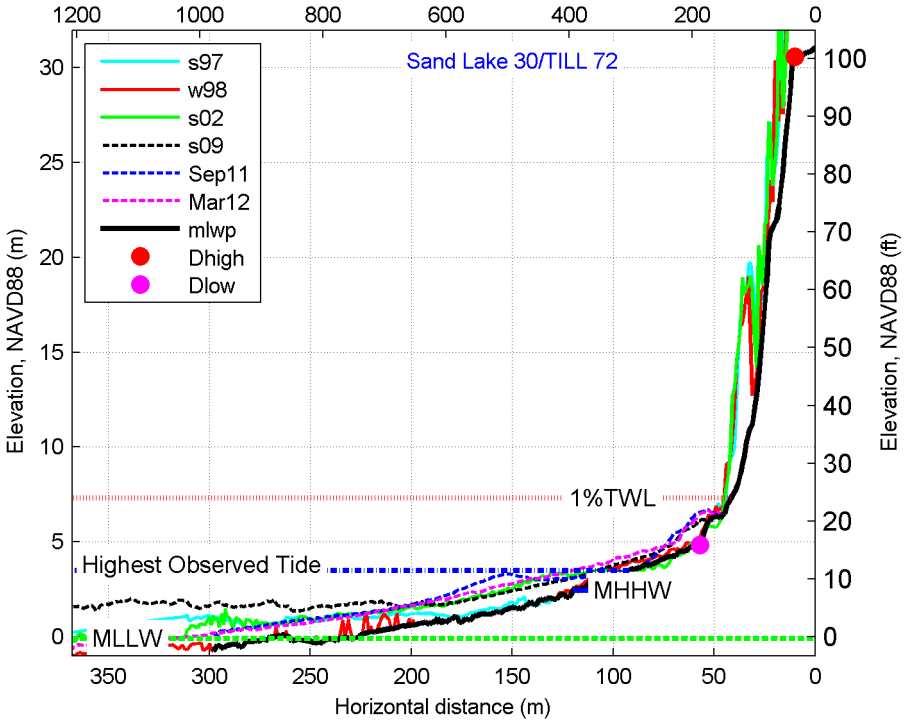

fm_slk 31

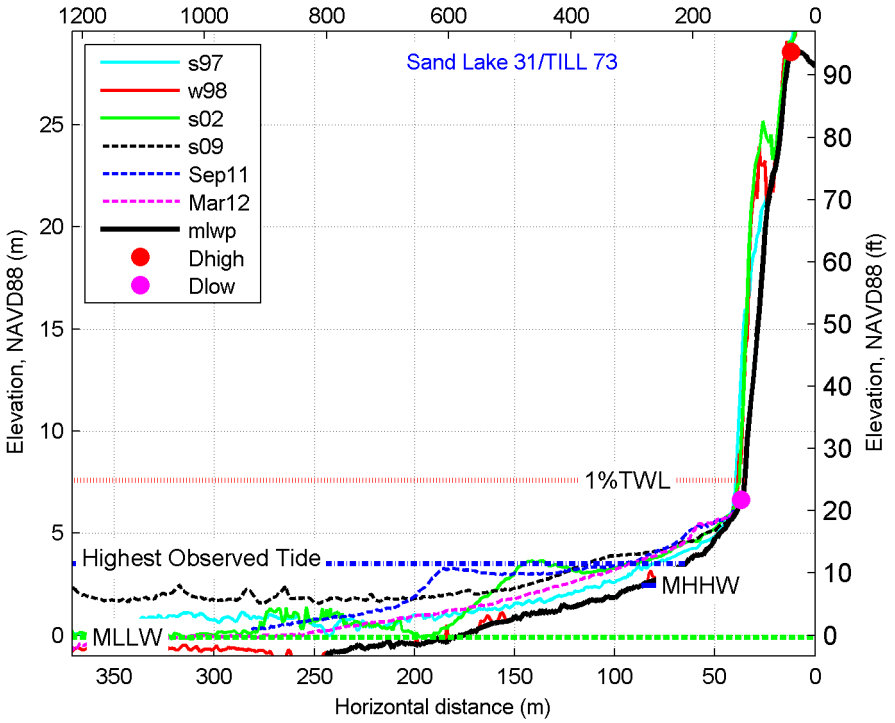

fm_slk 32

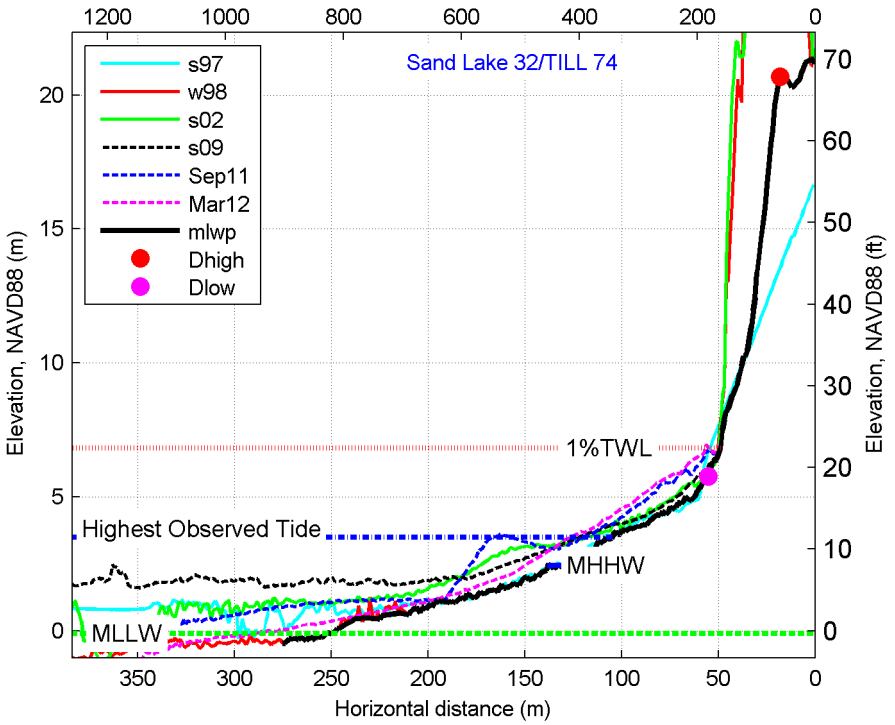

11.4.4 Netarts Spit

fm_netarts 1

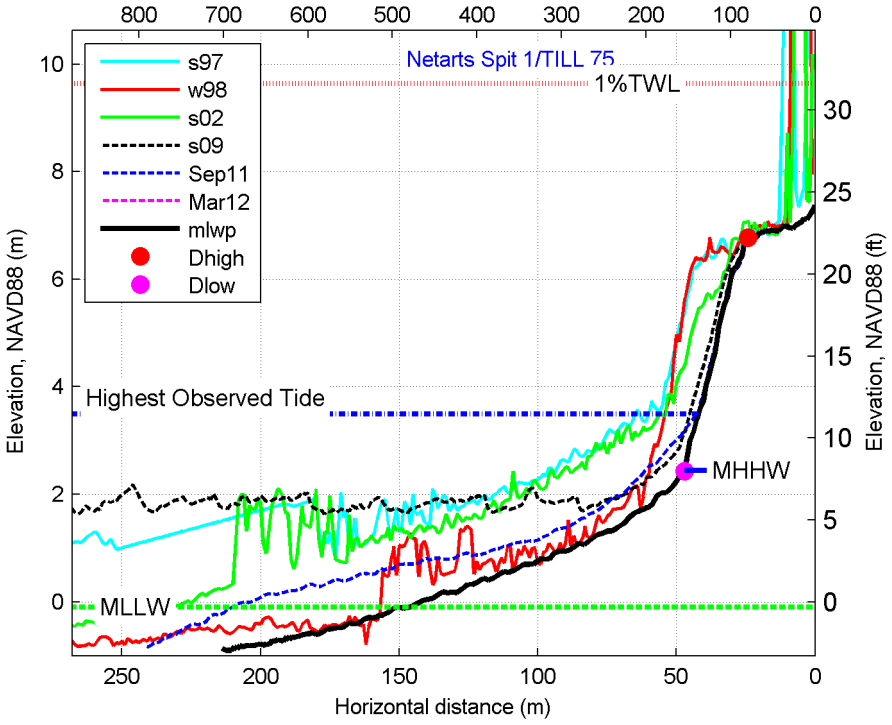

fm_netarts 2

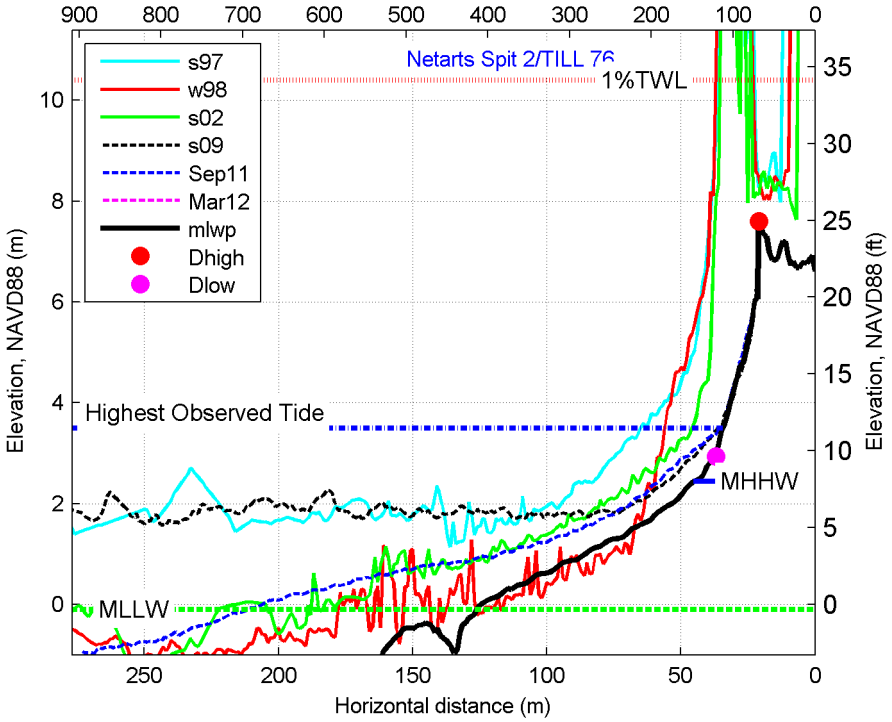

fm_netarts 3

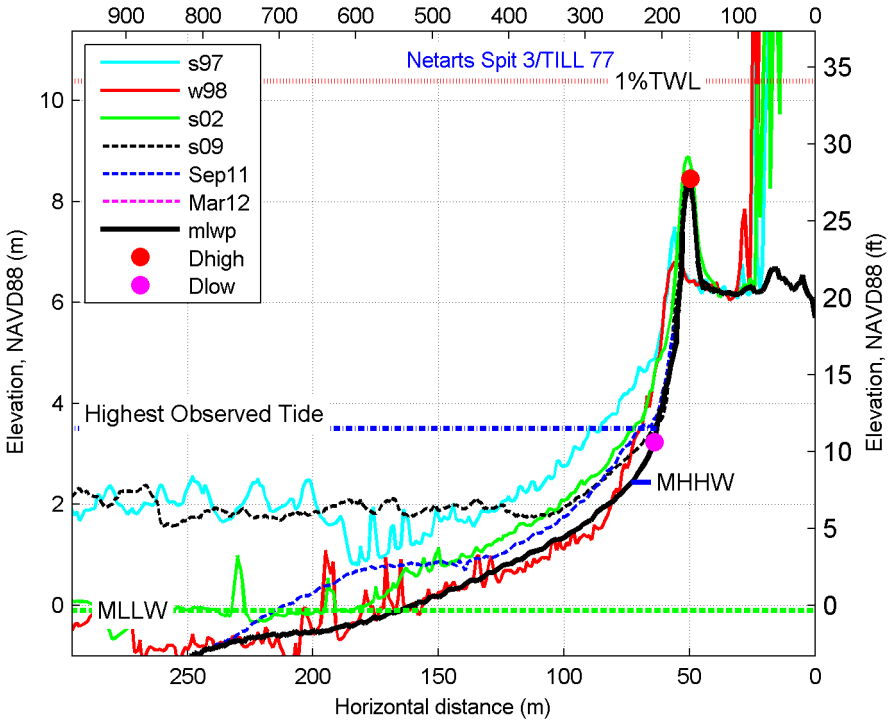

fm_netarts 4

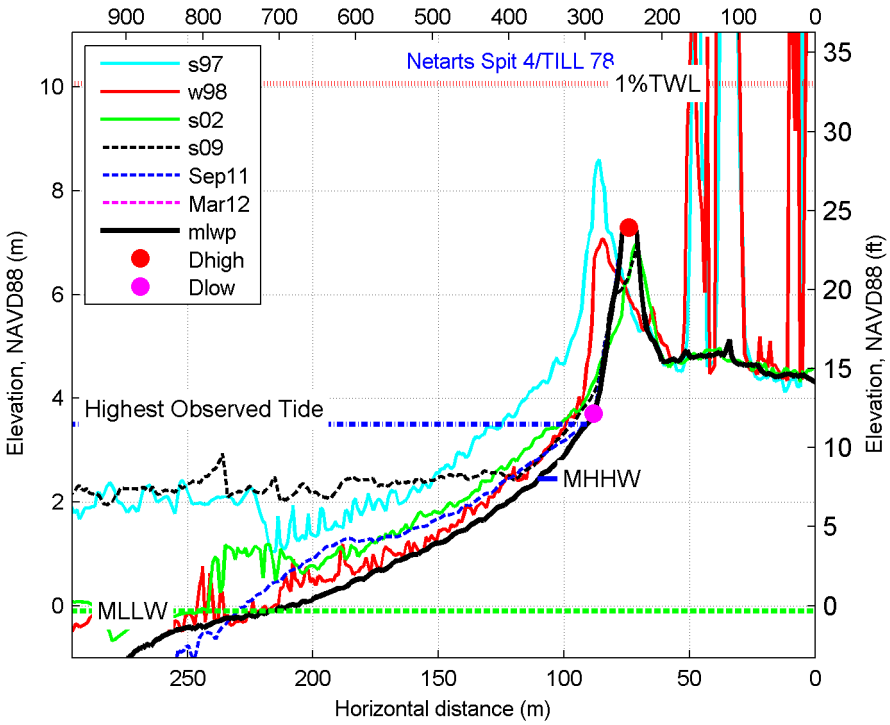

fm_netarts 5

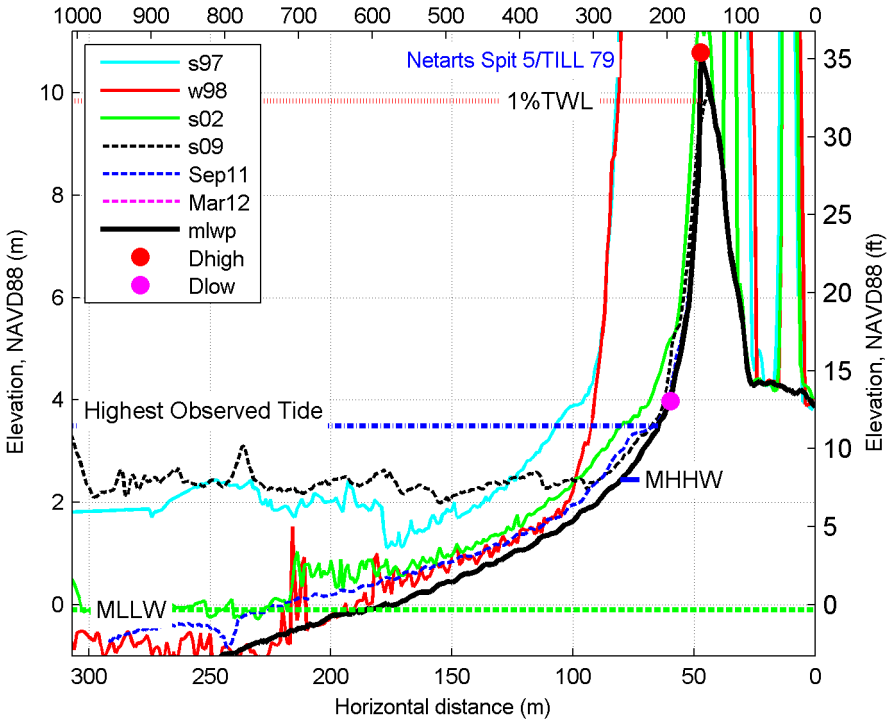

fm_netarts 6

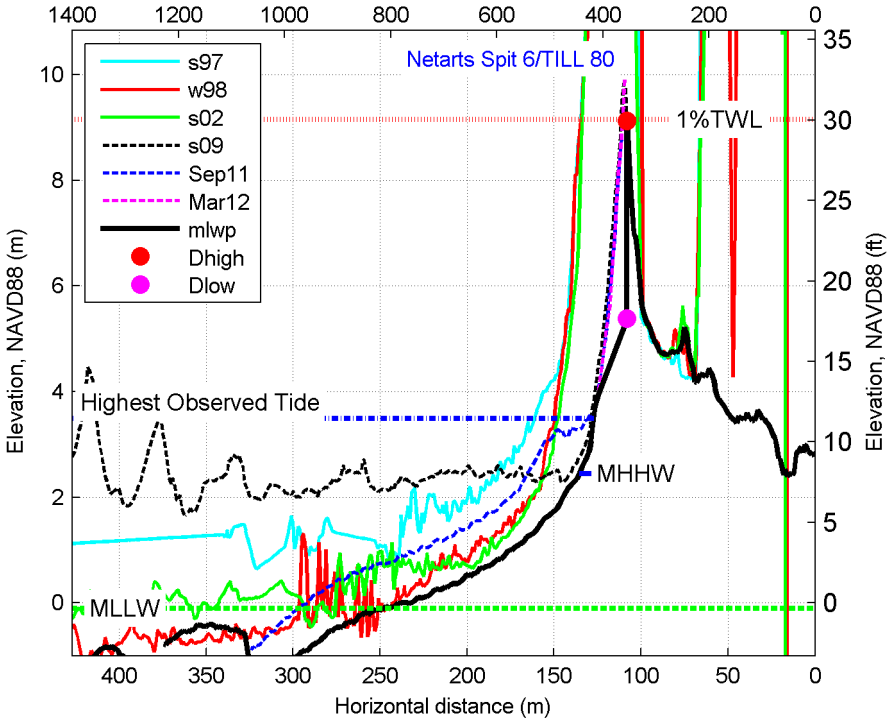

fm_netarts 7

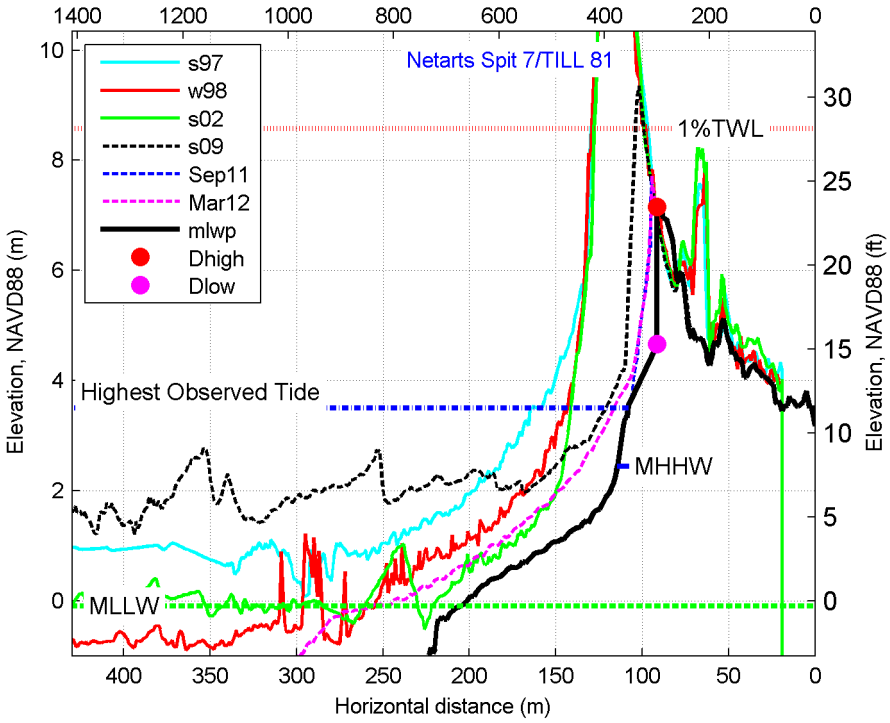

fm_netarts 8

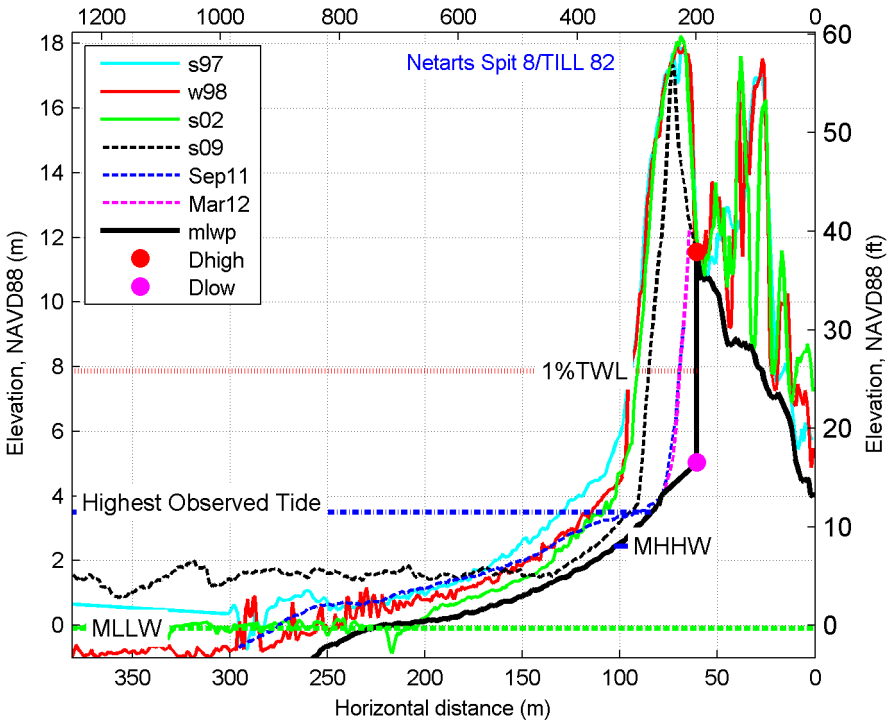

fm_netarts 9

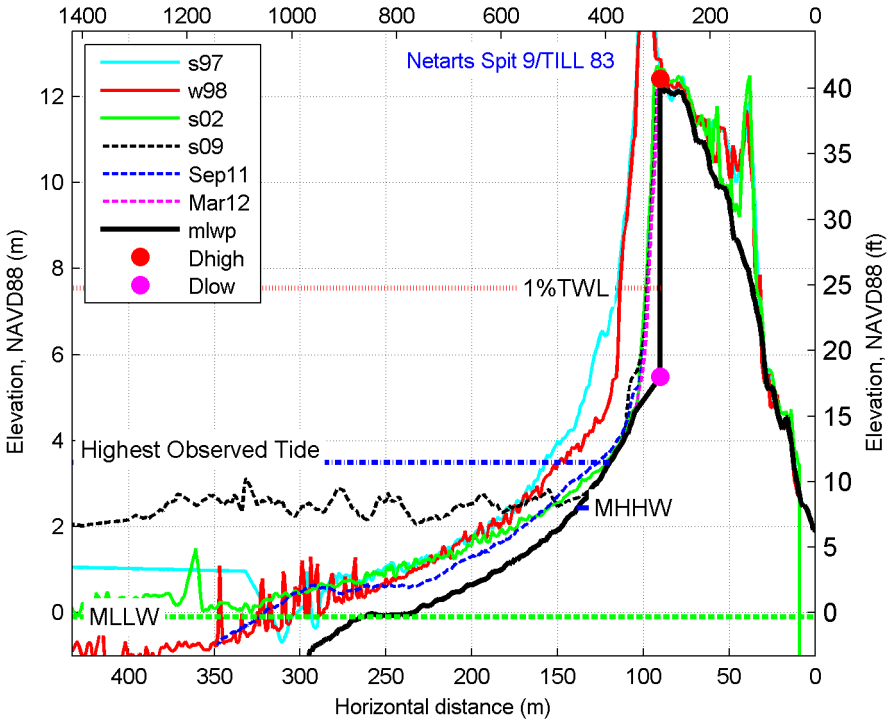

fm_netarts 10

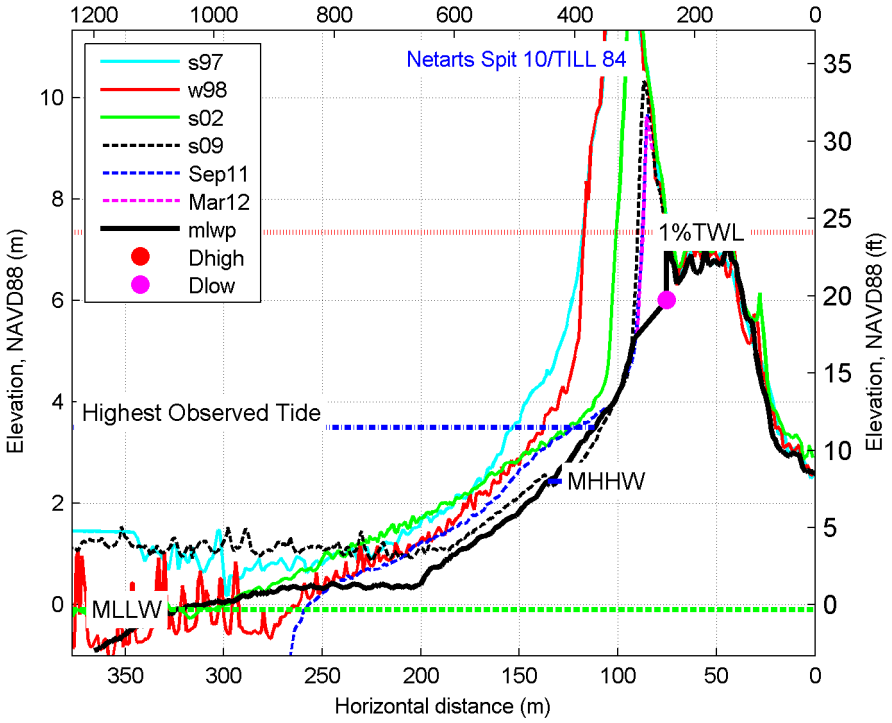

fm_netarts 11

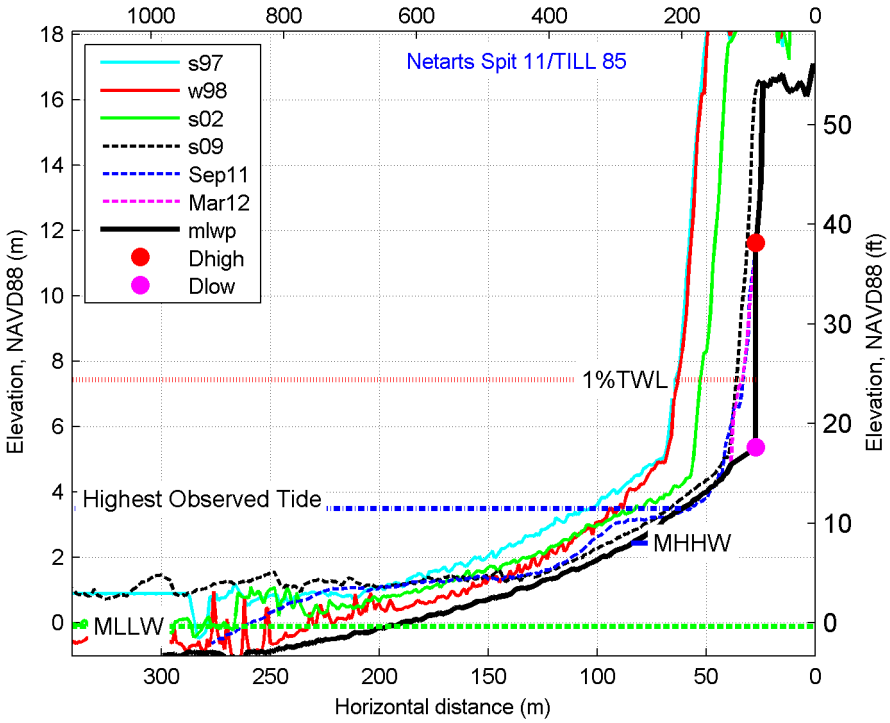

fm_netarts 12

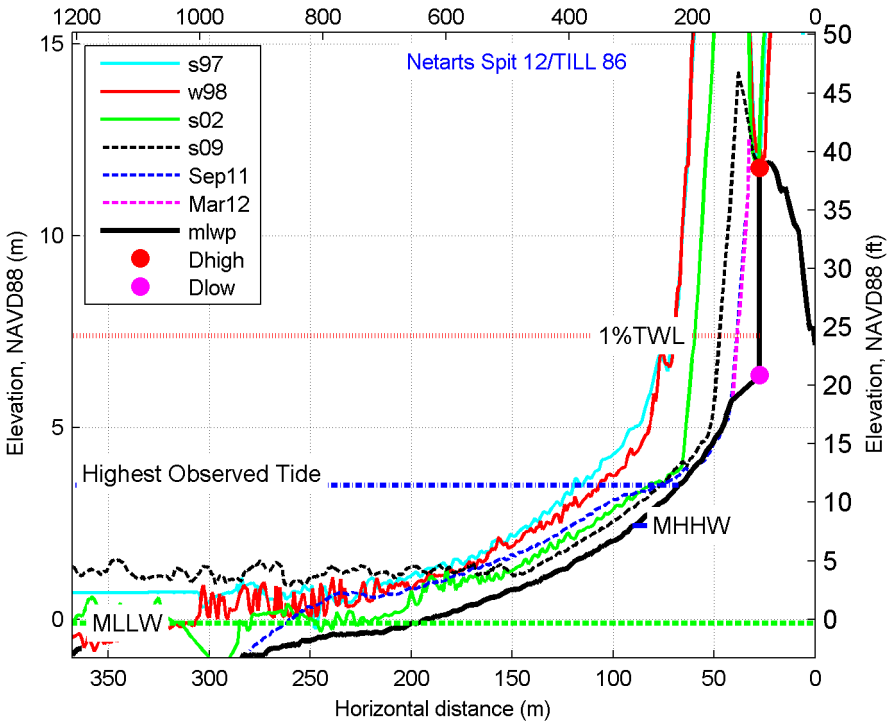

fm_netarts
13

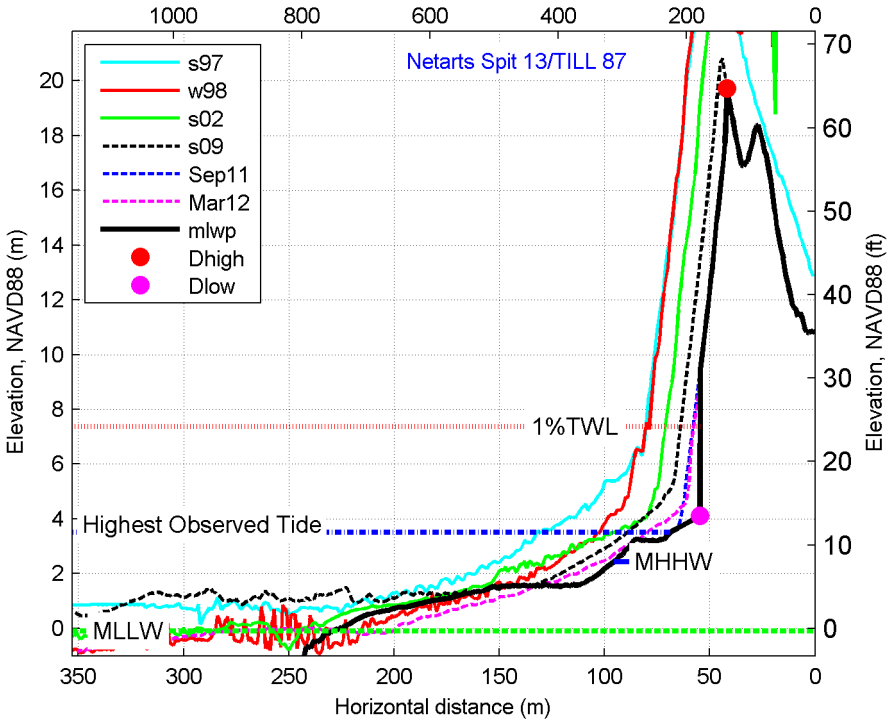

fm_netarts
14

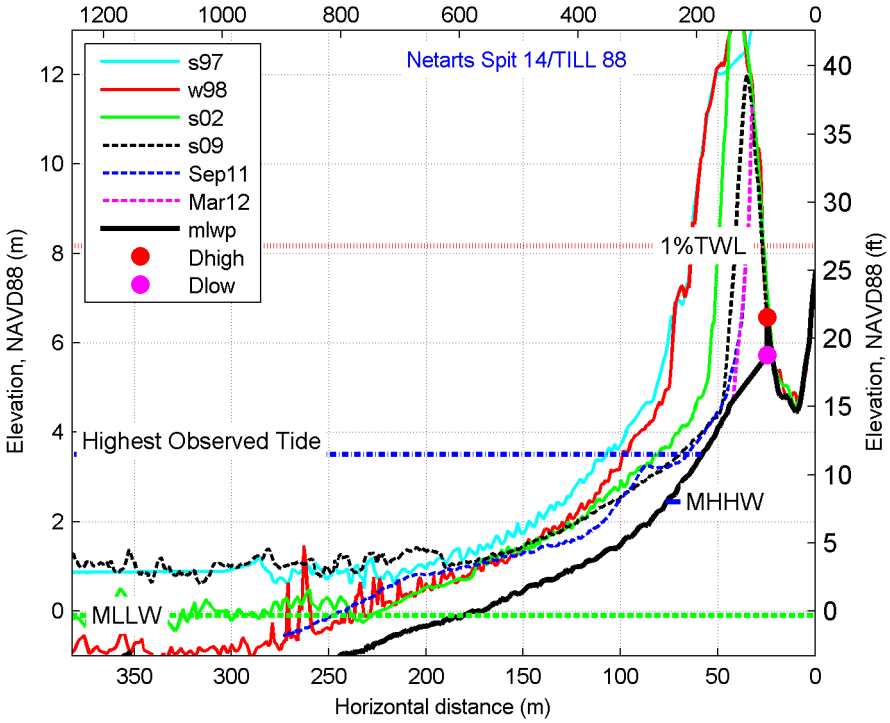

fm_netarts
15

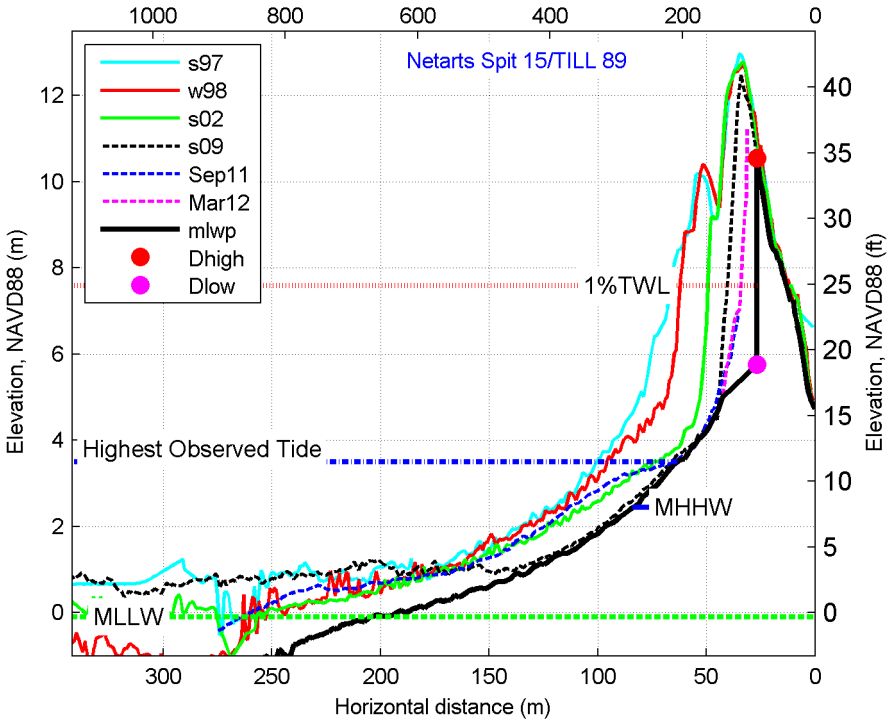

fm_netarts
16

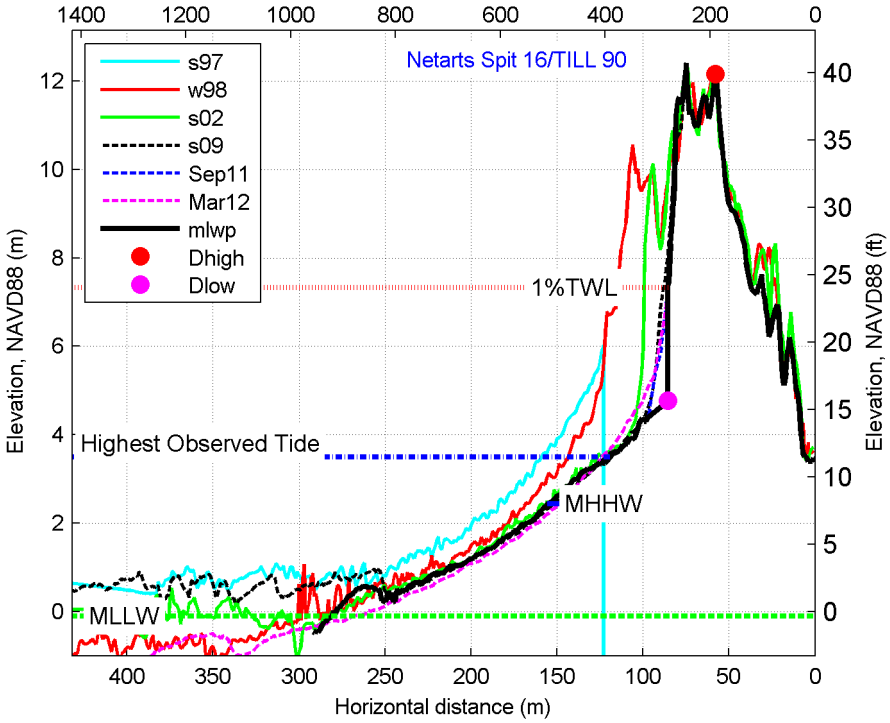

fm_netarts
17

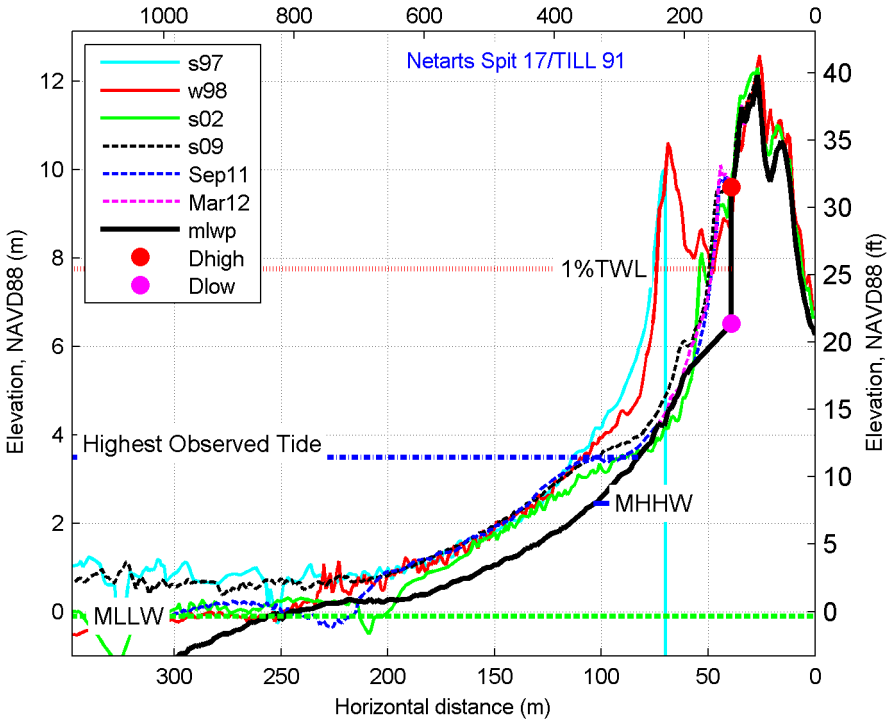

fm_netarts
18

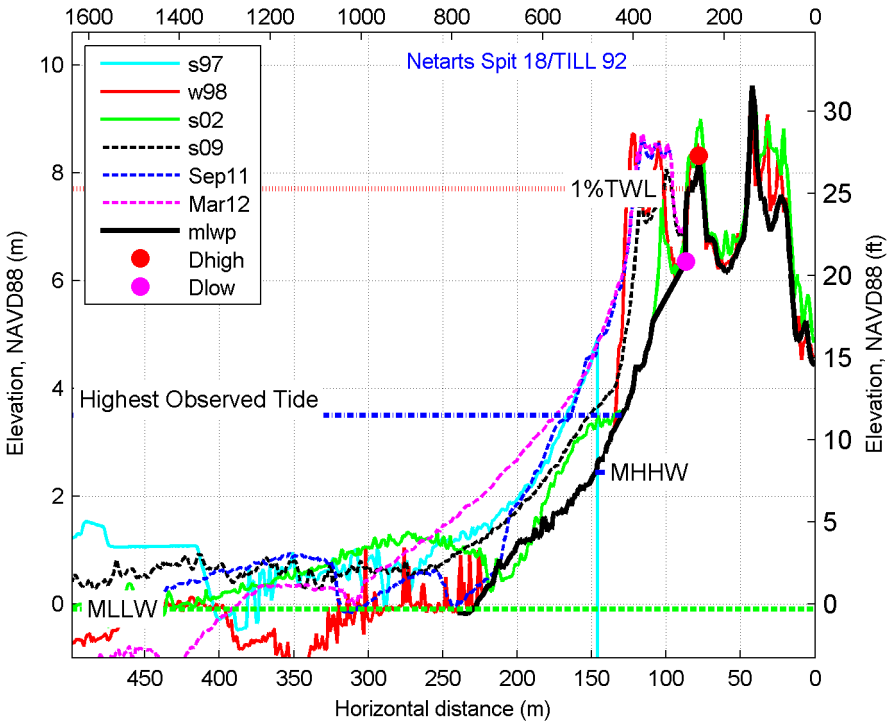

fm_netarts
19

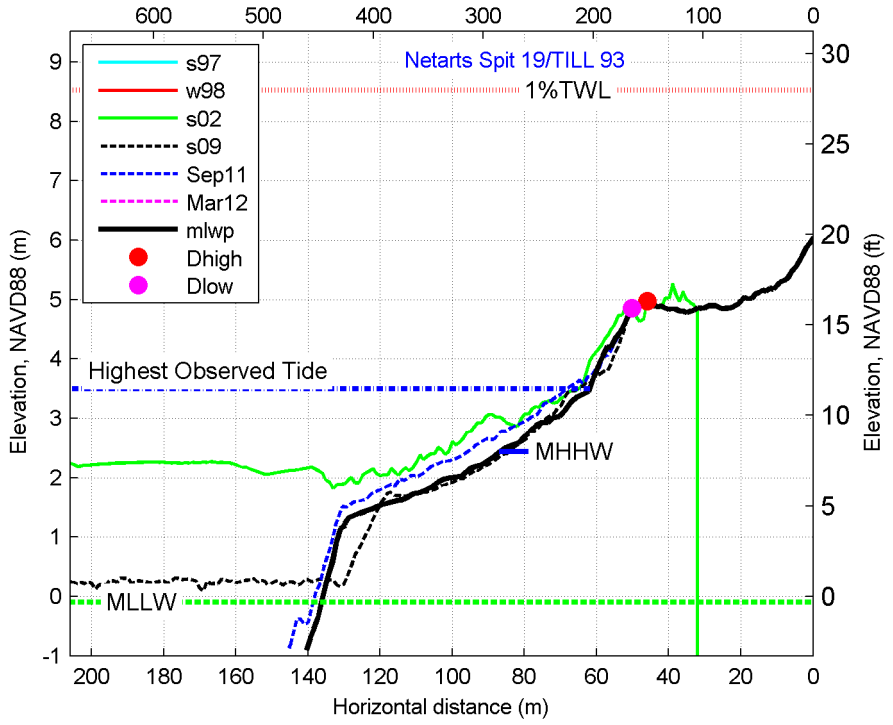

fm_netarts
20

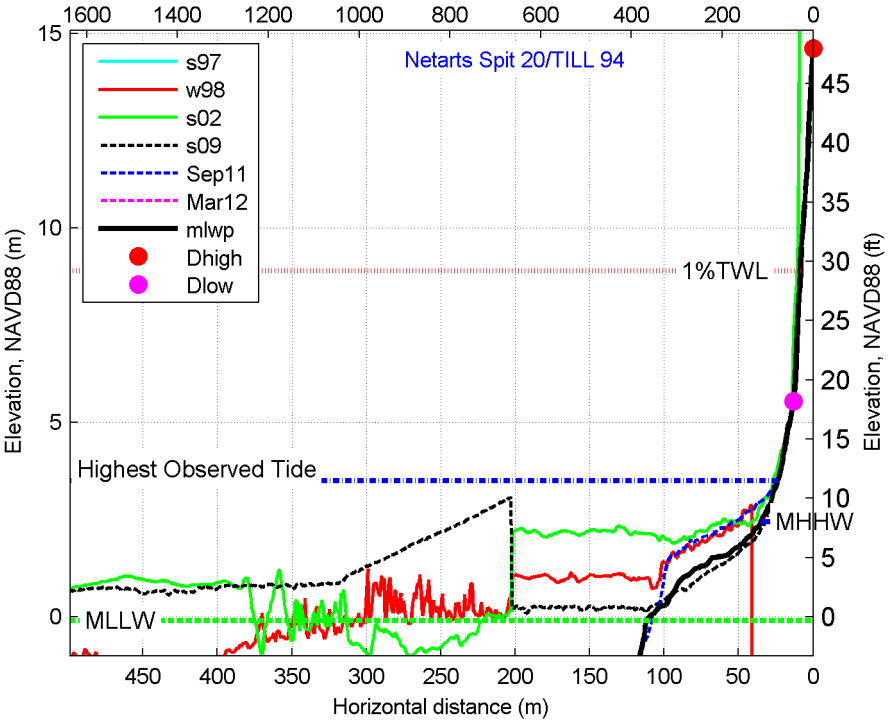

fm_netarts
21

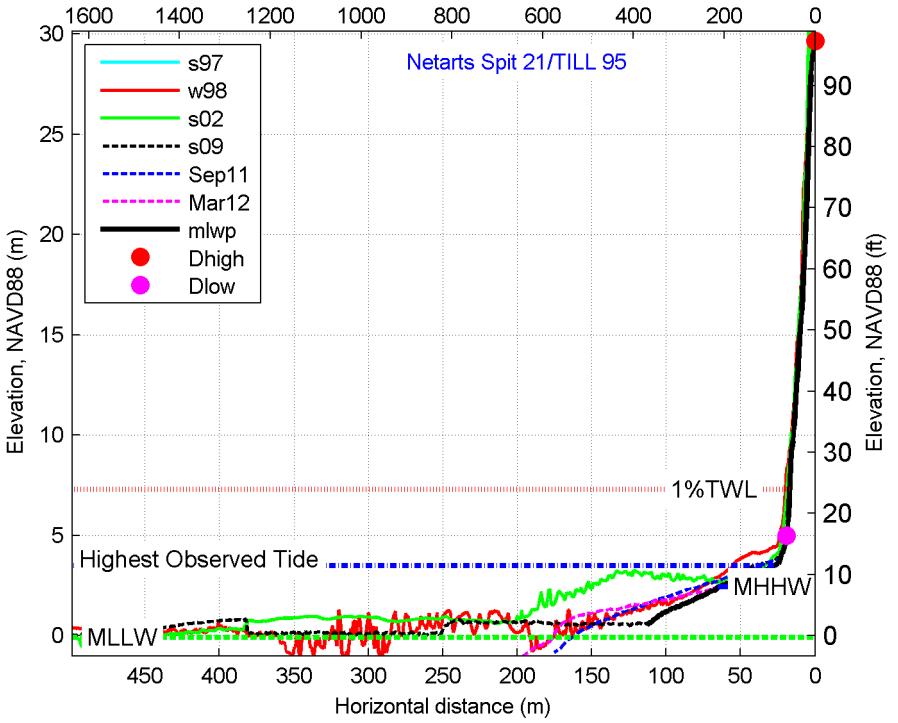

fm_netarts
22

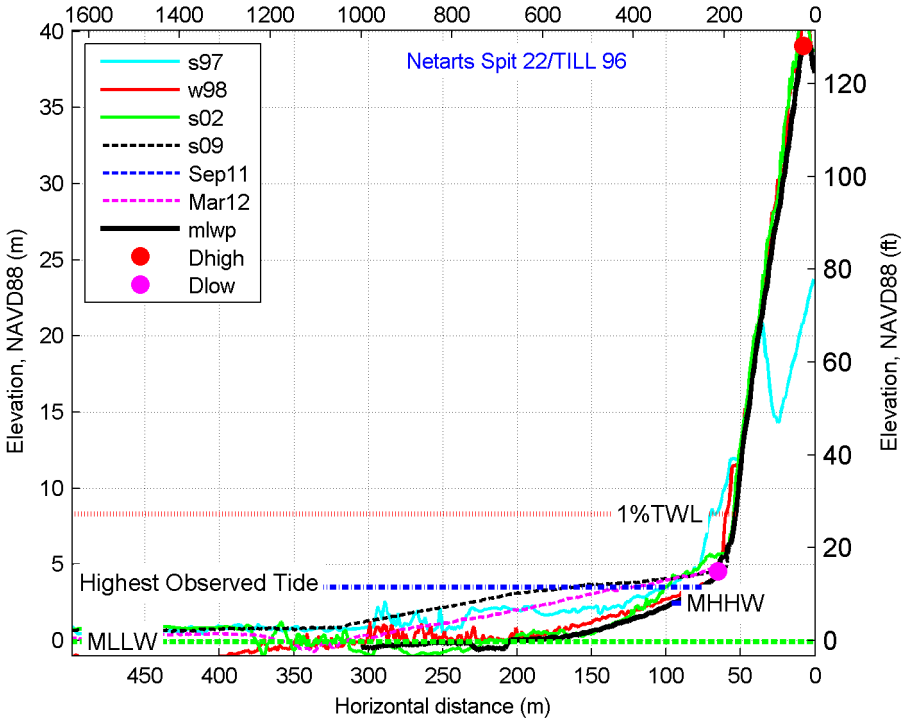

fm_netarts
23

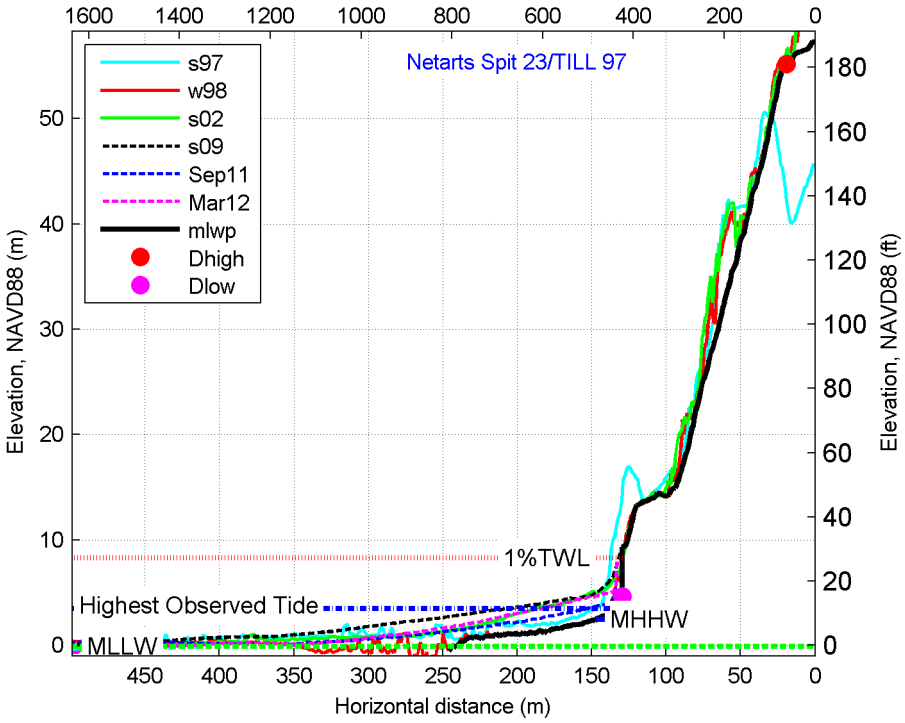

fm_netarts
24

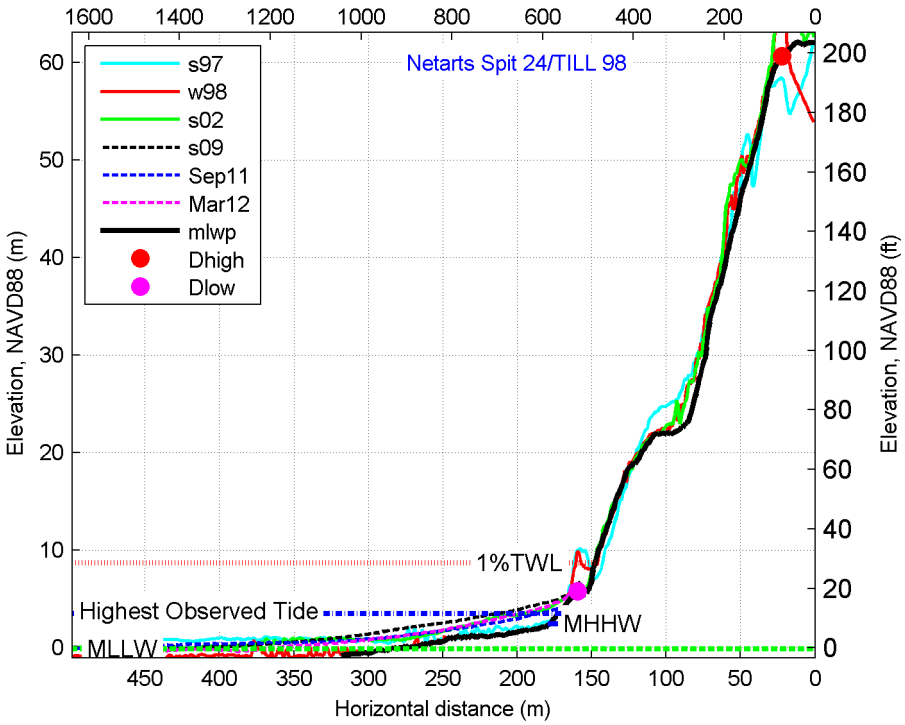

fm_netarts 25

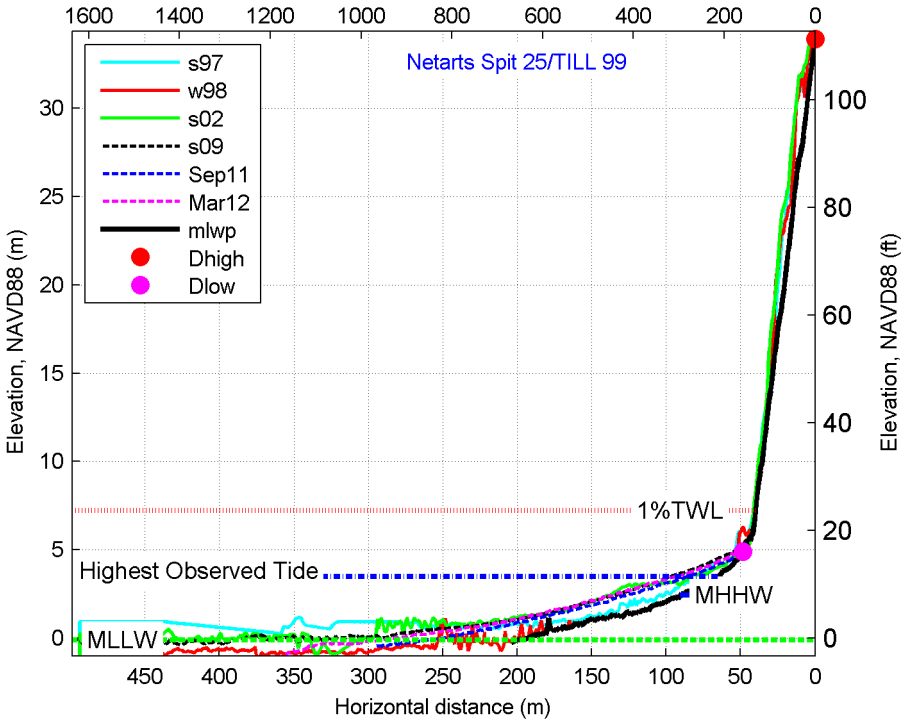

fm_netarts 26

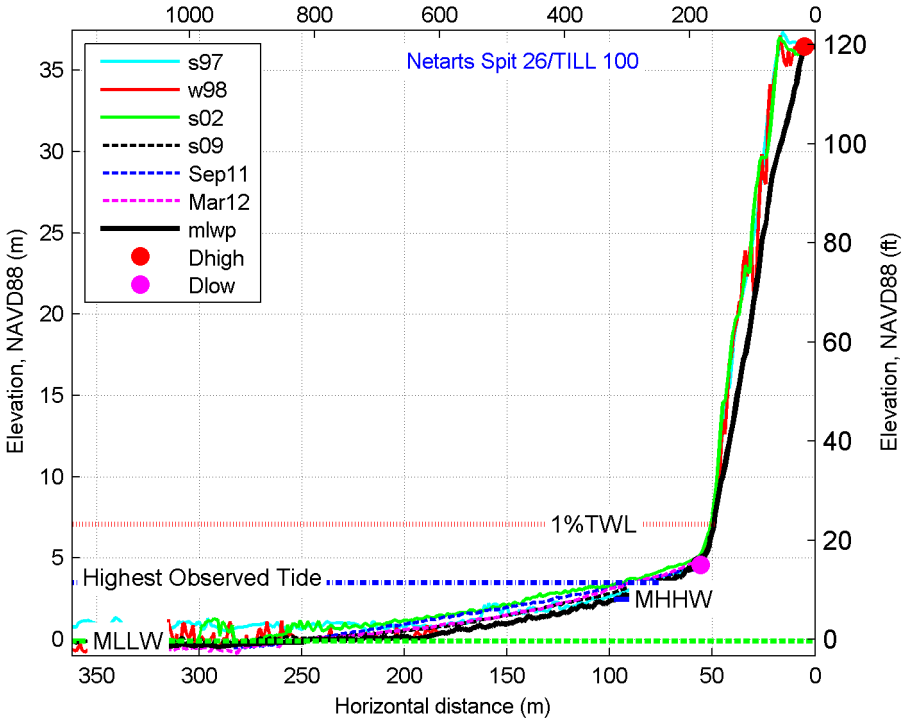

fm_netarts
27

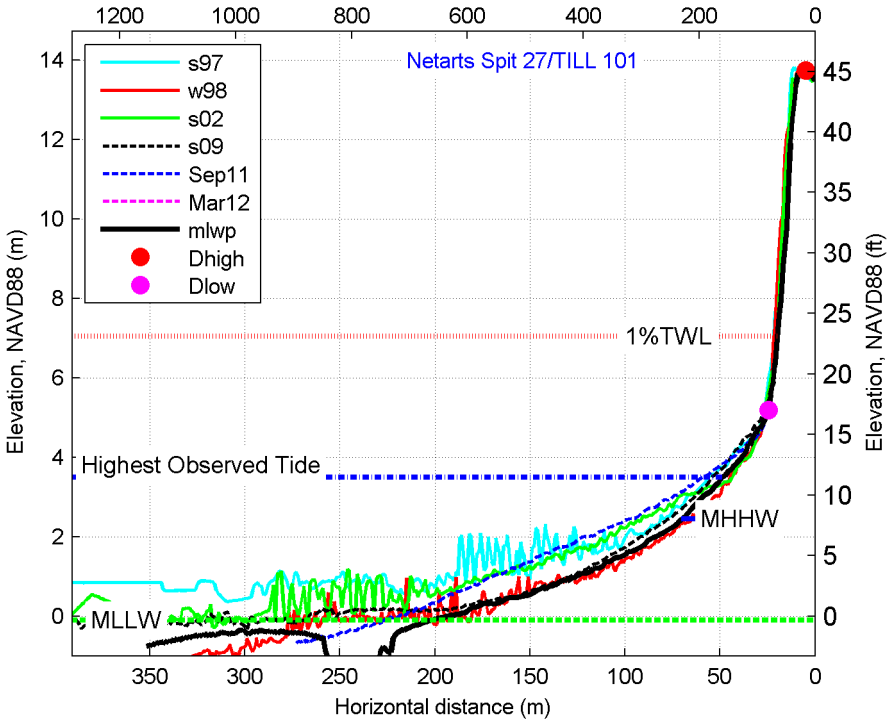

fm_netarts
28

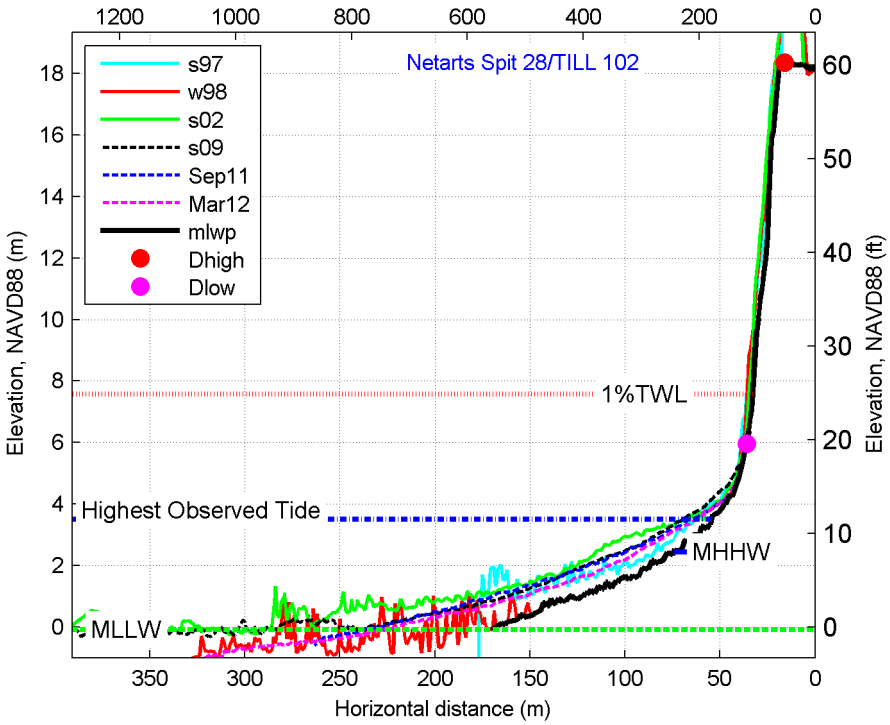

fm_netarts
29

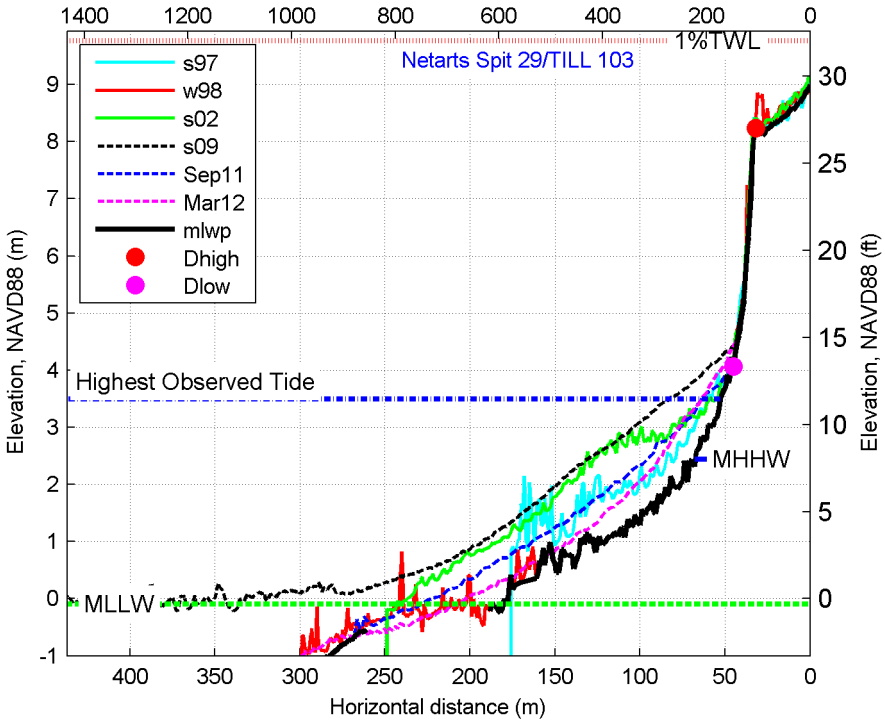

11.4.5 Short Sand Beach

fm_ss 1

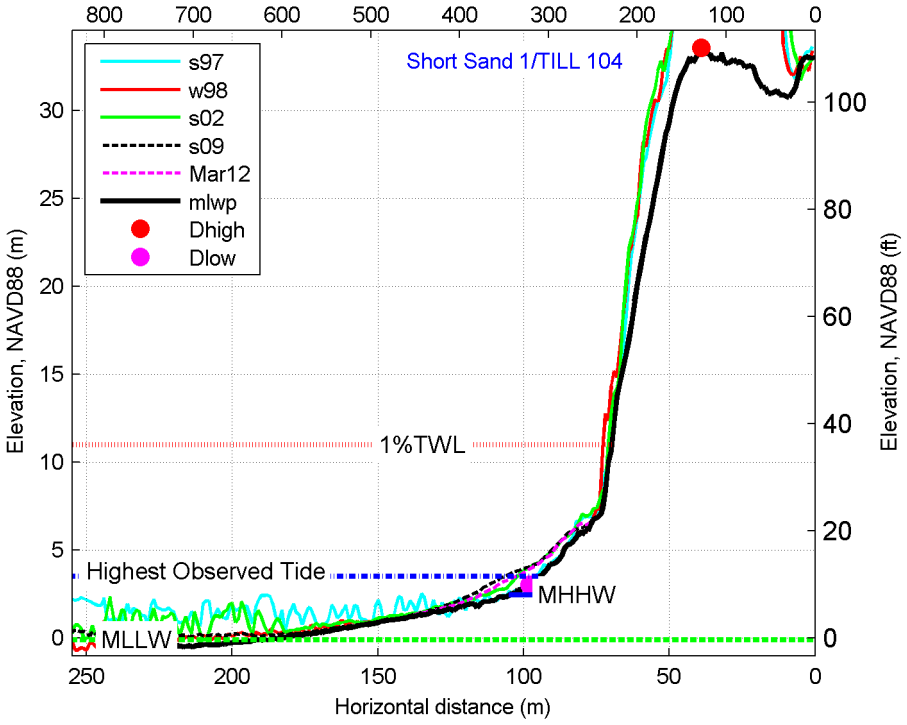

fm_ss 2

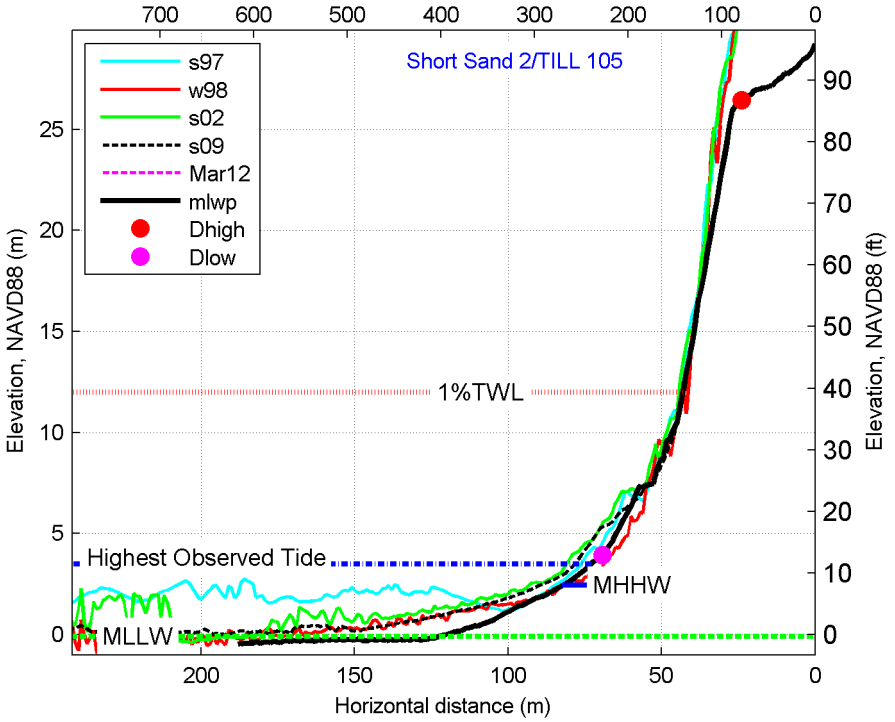

fm_ss 3

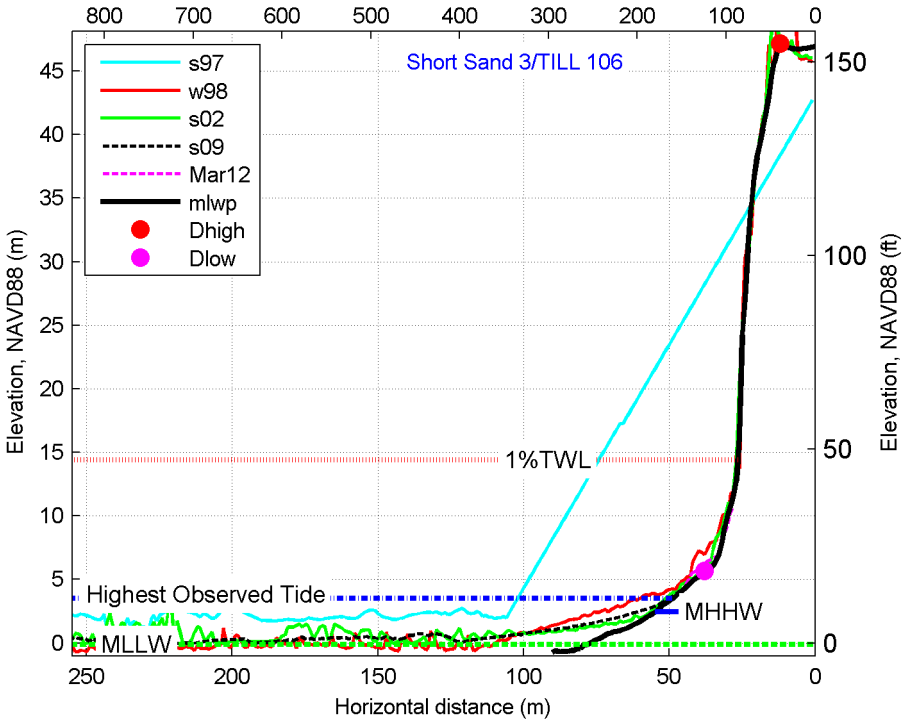
Short Sand 3/TILL 106
s97
w98
s02
s09
Mar12
mlwp
Dhigh
Dlow
1%TWL
Highest Observed Tide
MHHW
MLLW
Elevation, NAVD88 (m)
Elevation, NAVD88 (ft)
Horizontal distance (m)
800
700
600
500
400
300
200
100
0
45
40
35
30
25
20
15
10
5
0
150
100
50
0
250
200
150
100
50
0

11.4.6 Bayocean Spit

fm_bay 1

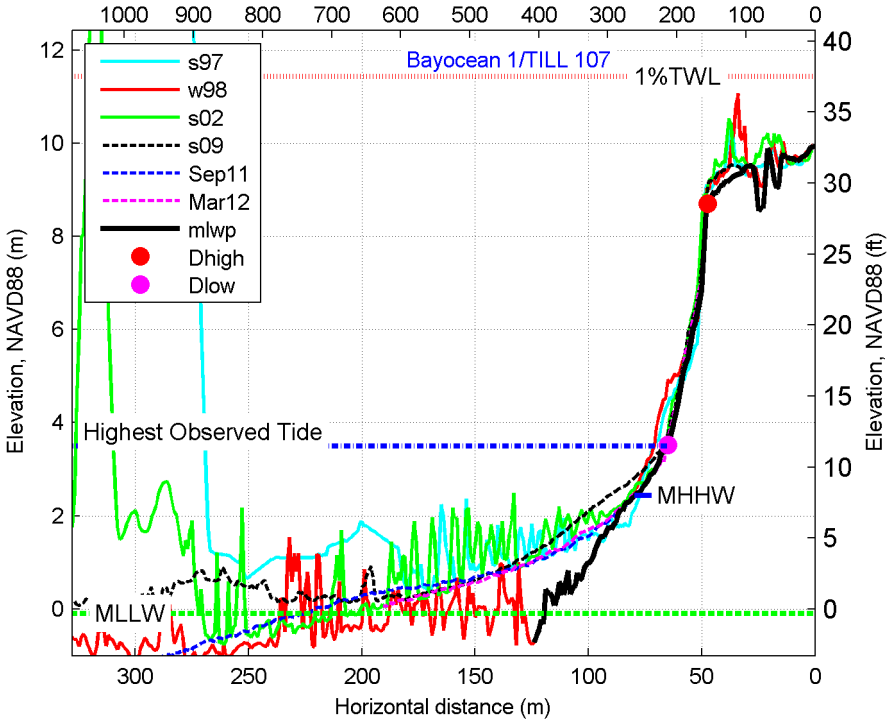

fm_bay 2

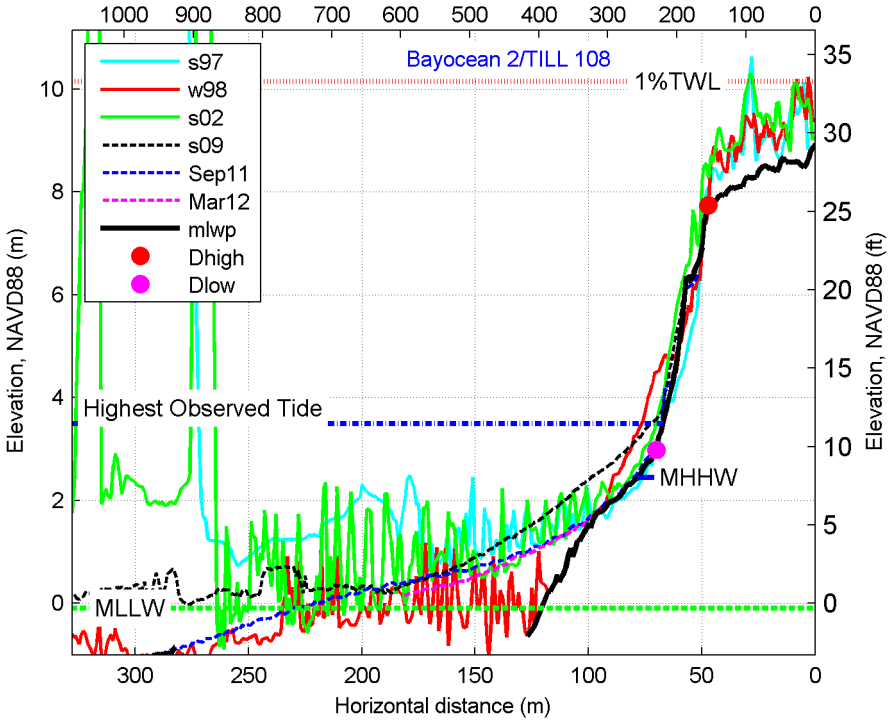

fm_bay 3

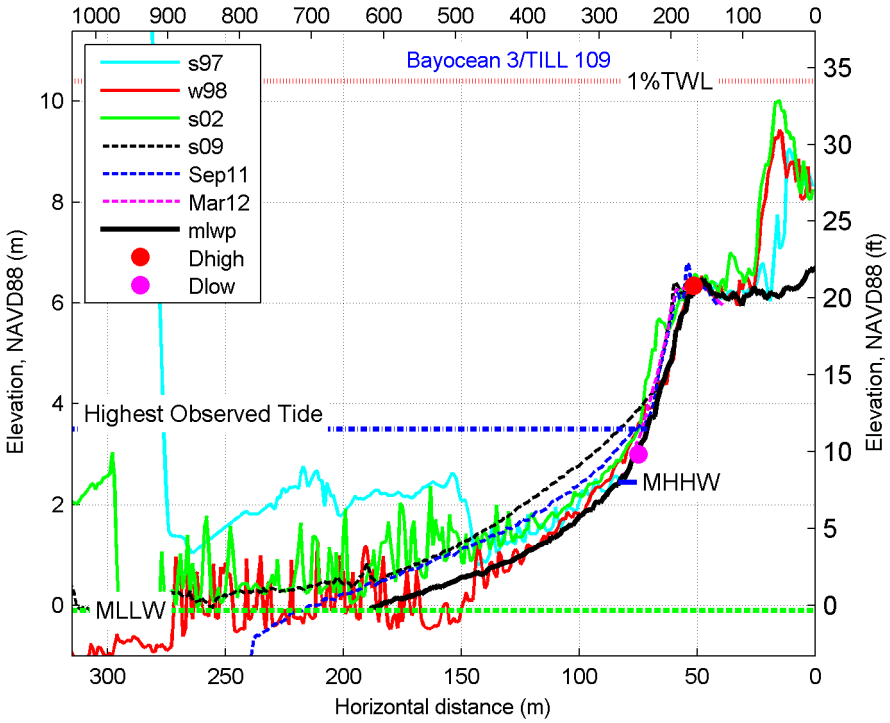

fm_bay 4

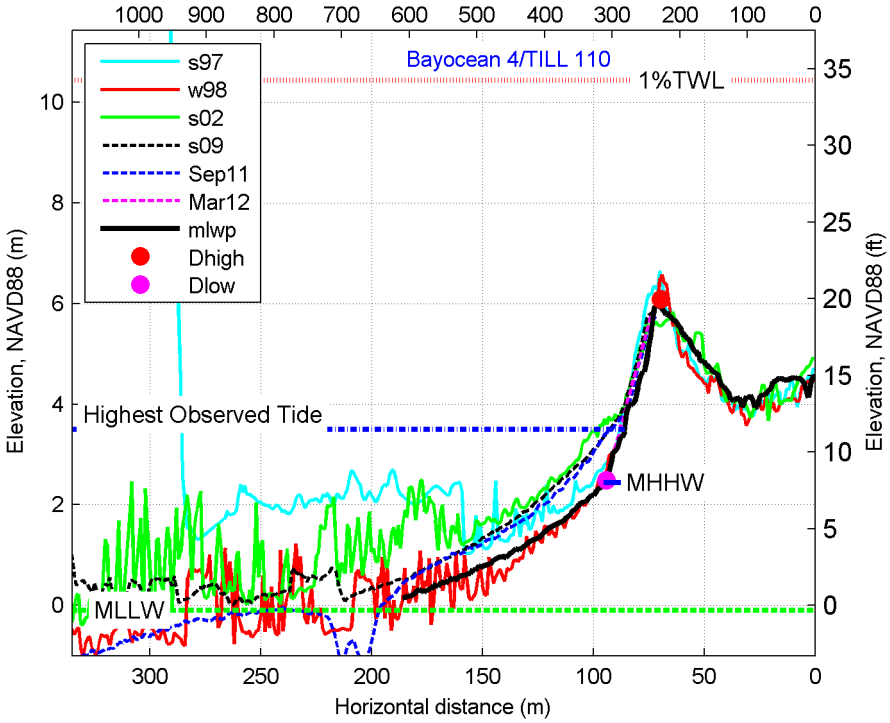

fm_bay 5

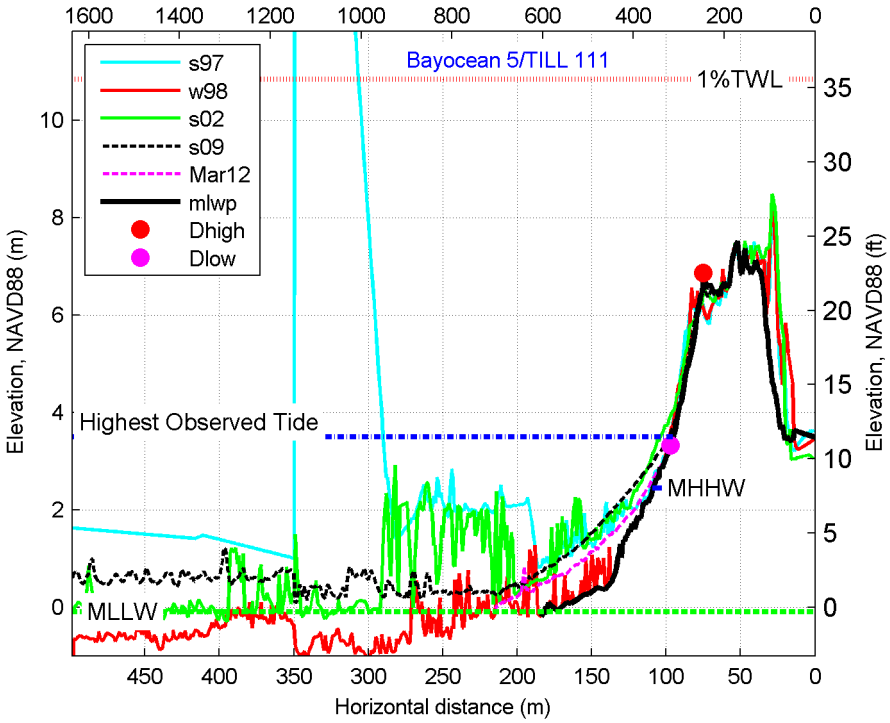

fm_bay 6

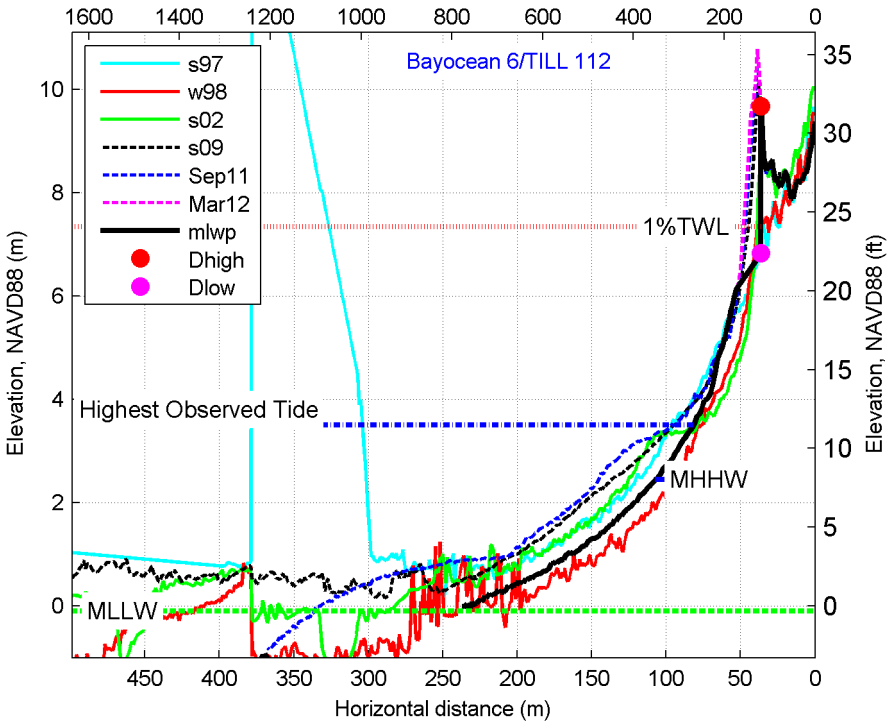

fm_bay 7

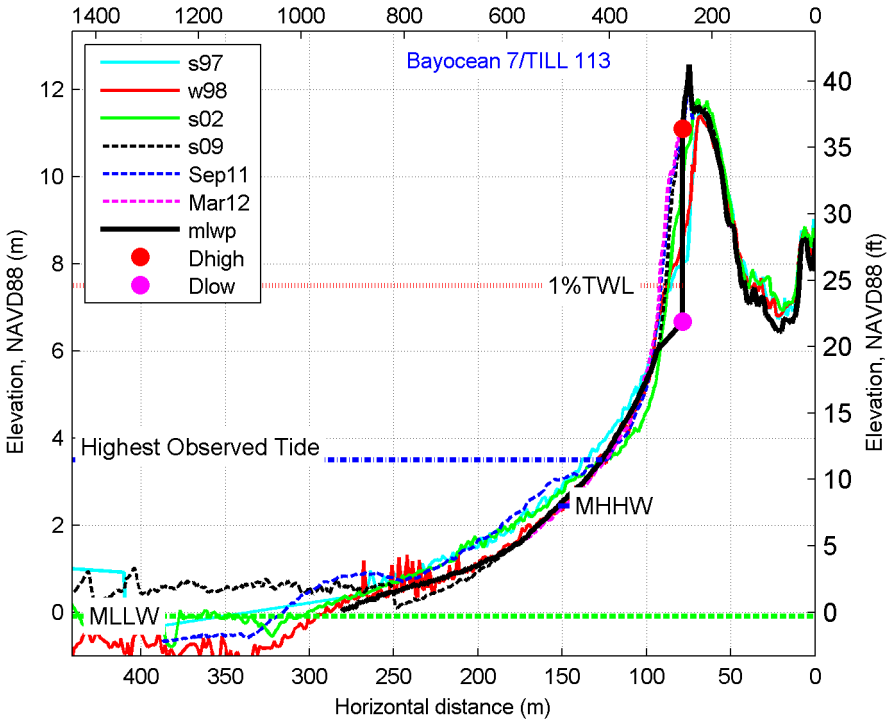

fm_bay 8

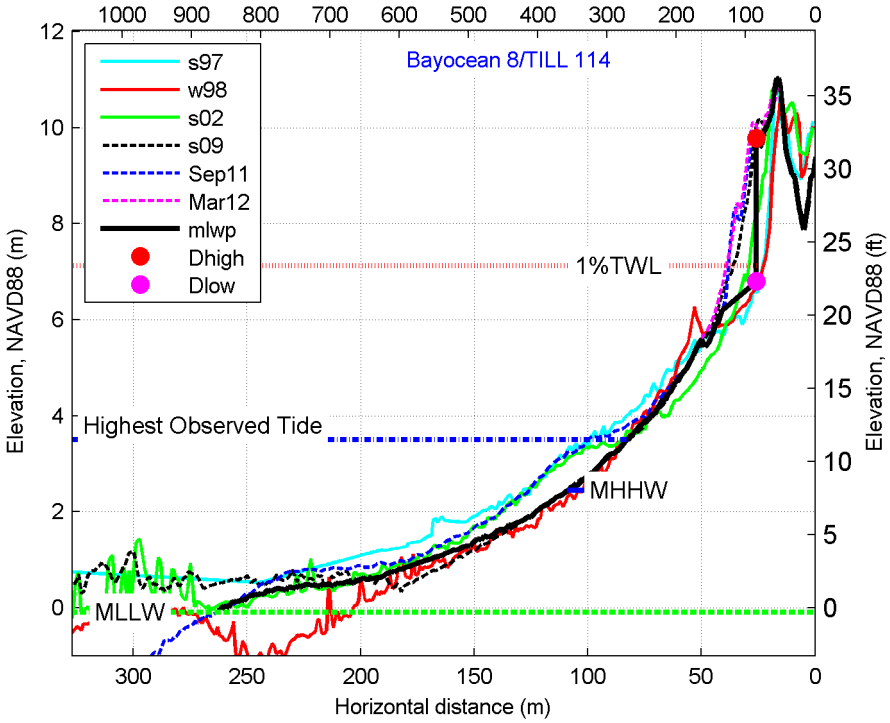

fm_bay 9

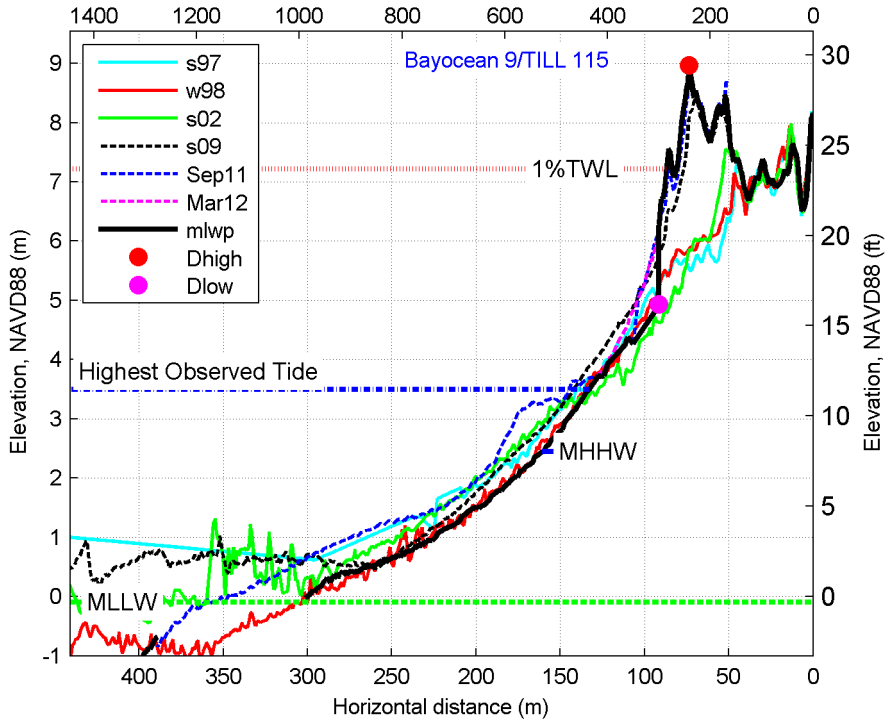

fm_bay 10

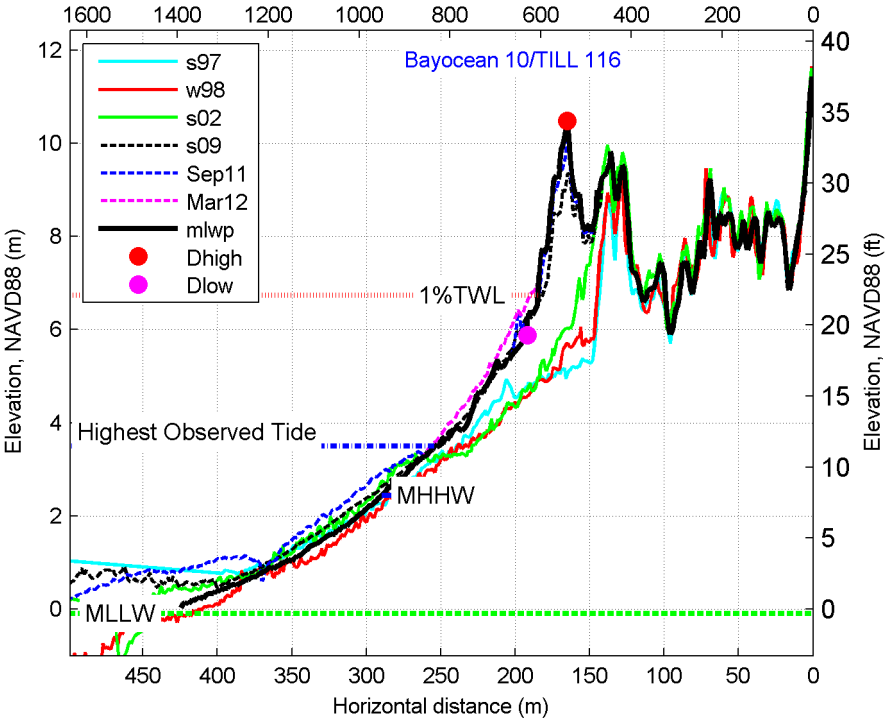

fm_bay 11

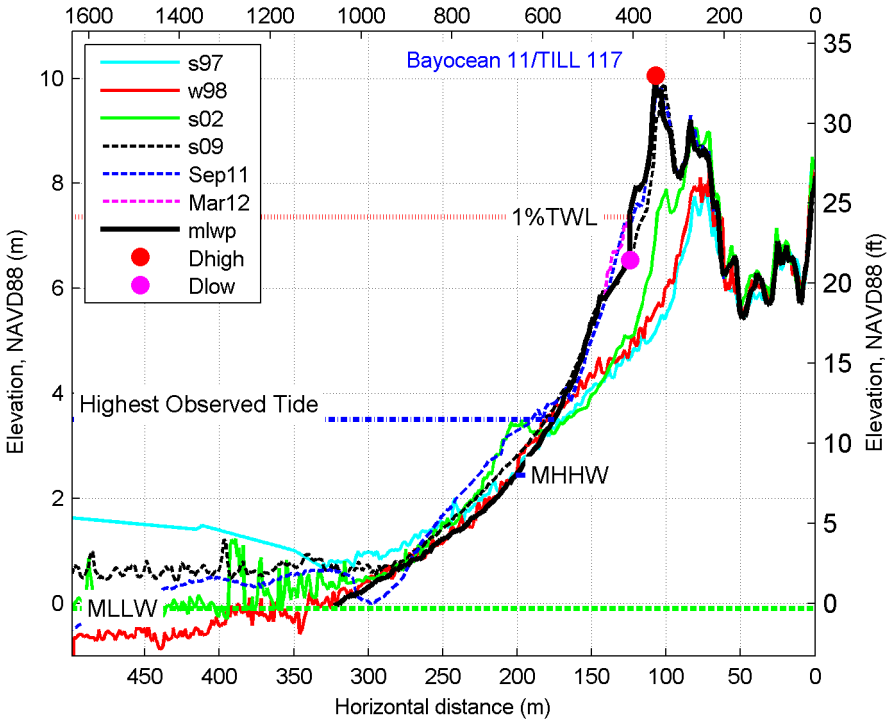
Bayocean 11/TILL 117
s97
w98
s02
s09
Sep11
Mar12
mlwp
Dhigh
Dlow
1%TWL
Highest Observed Tide
MHHW
MLLW
Elevation, NAVD88 (m)
Elevation, NAVD88 (ft)
Horizontal distance (m)
1600
1400
1200
1000
800
600
400
200
0
450
400
350
300
250
200
150
100
50
0
10
8
6
4
2
0
35
30
25
20
15
10
5
0

11.4.7 Rockaway

fm_rck 1

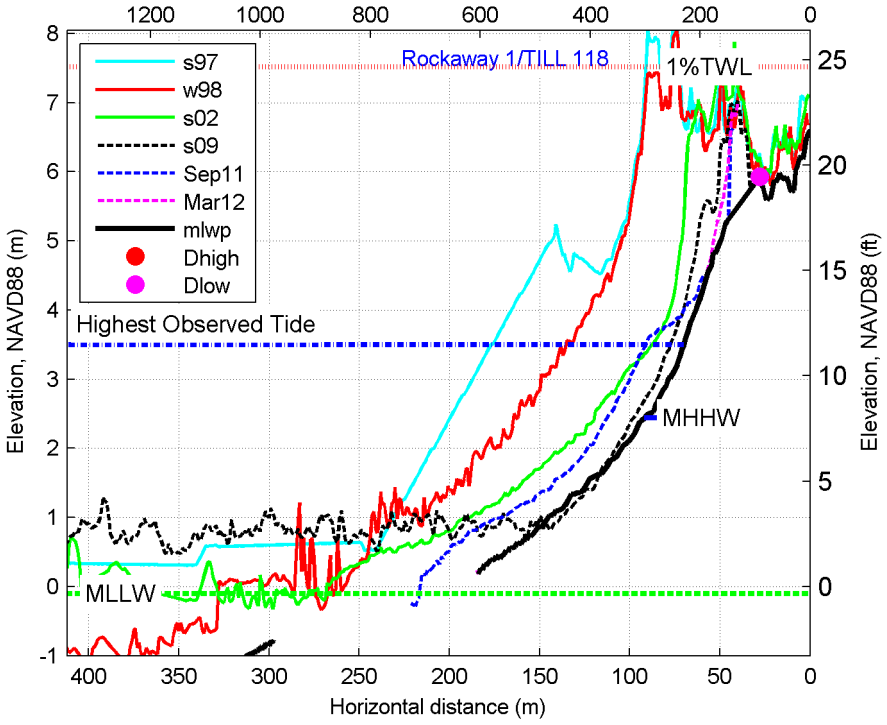

fm_rck 2

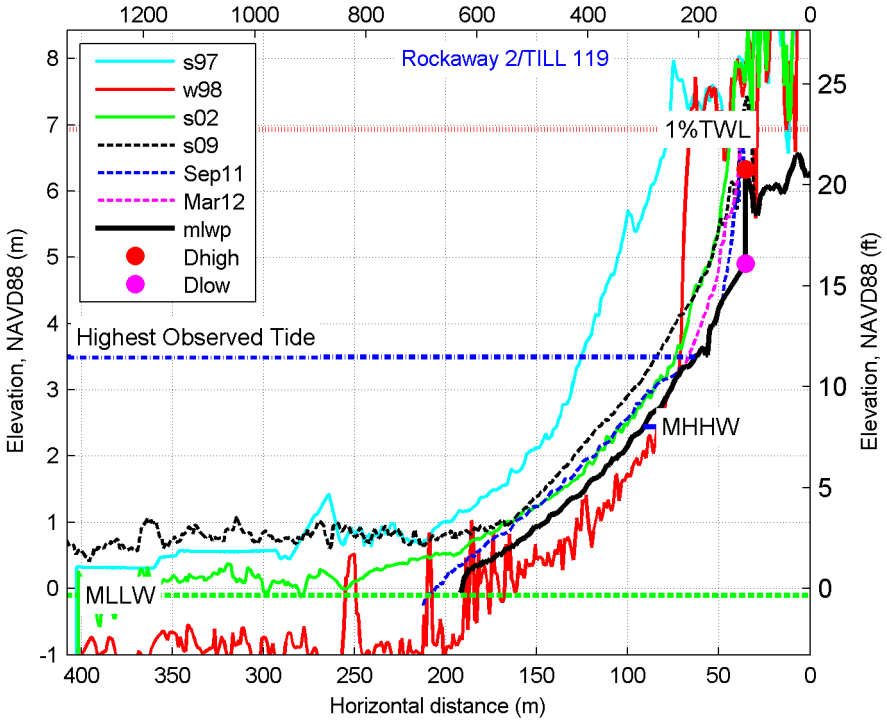

fm_rck 3

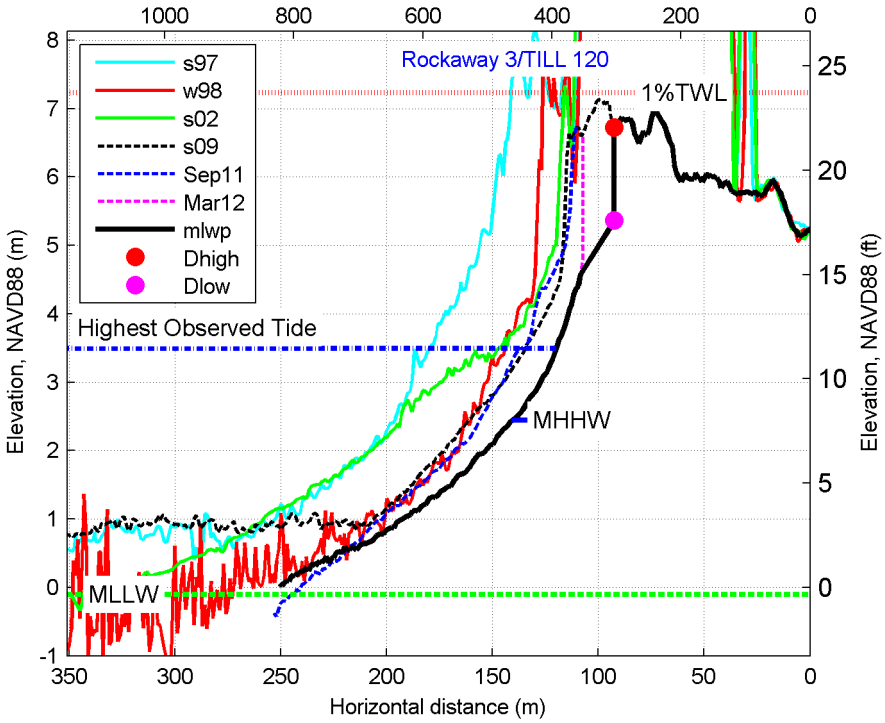

fm_rck 4

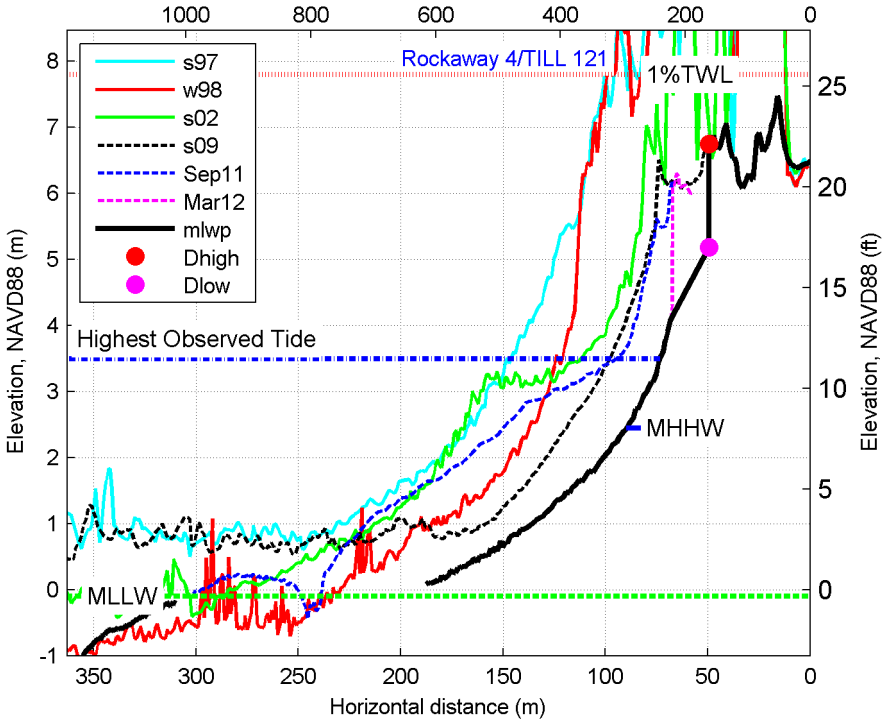

fm_rck 5

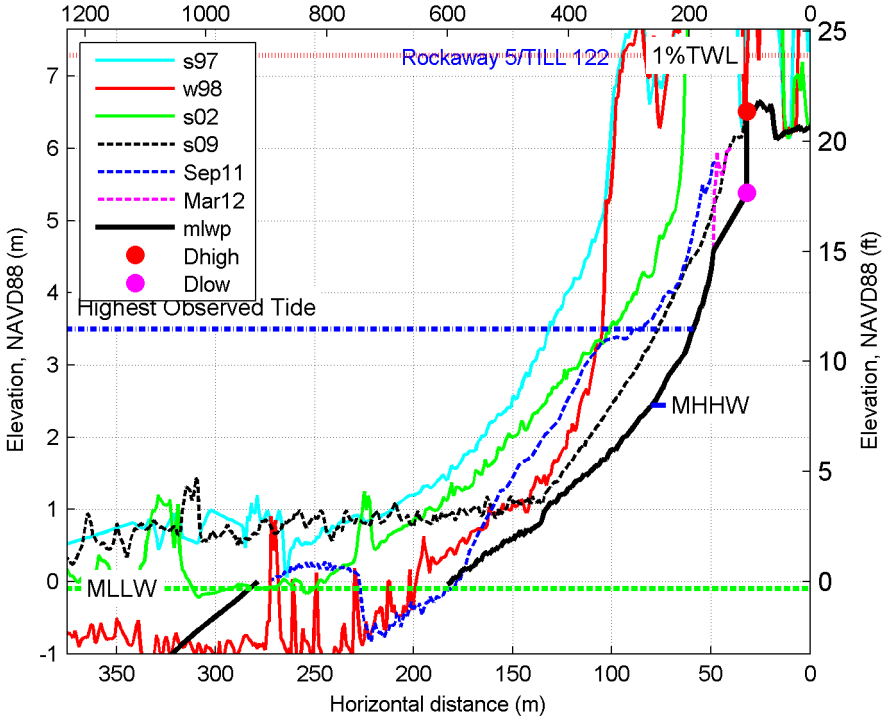

fm_rck 6

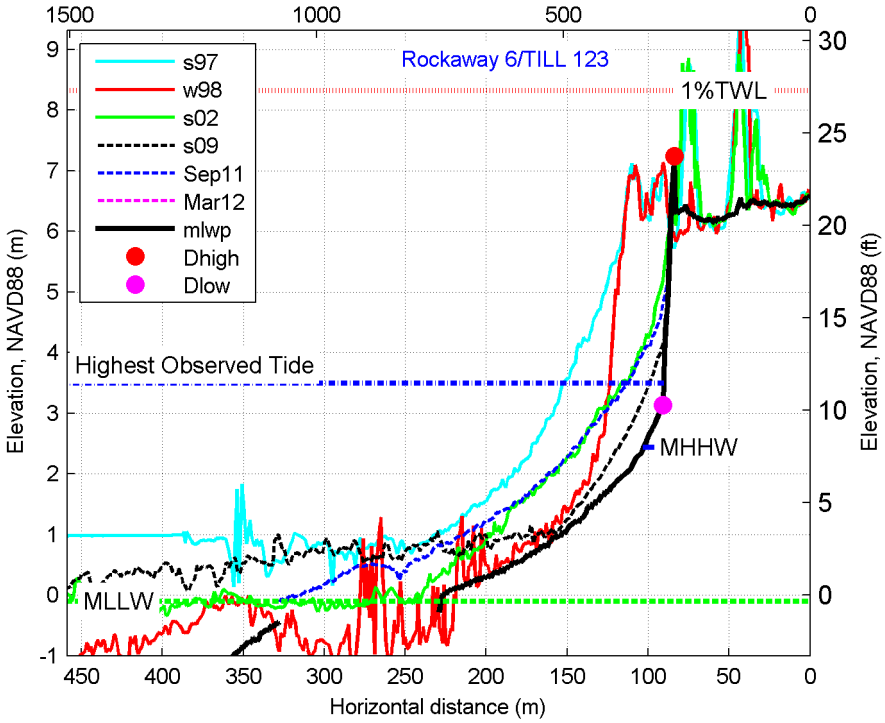

fm_rck 7

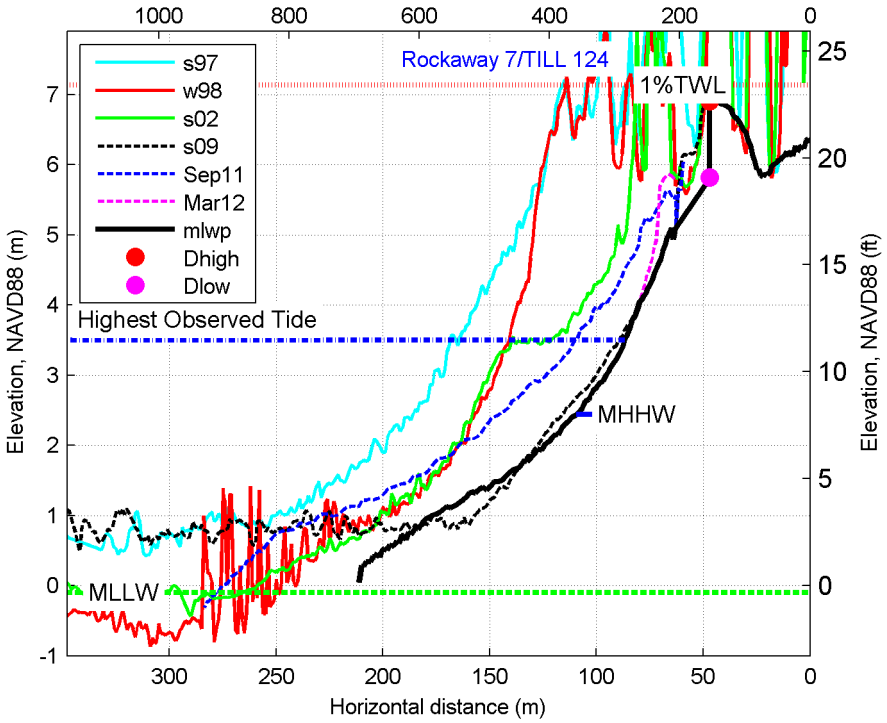

fm_rck 8

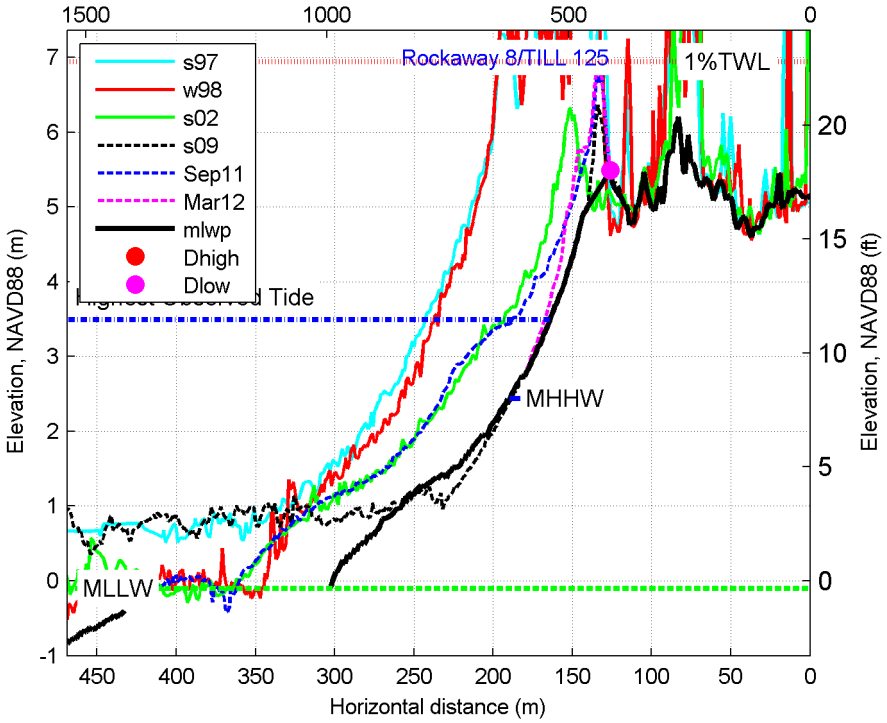

fm_rck 9

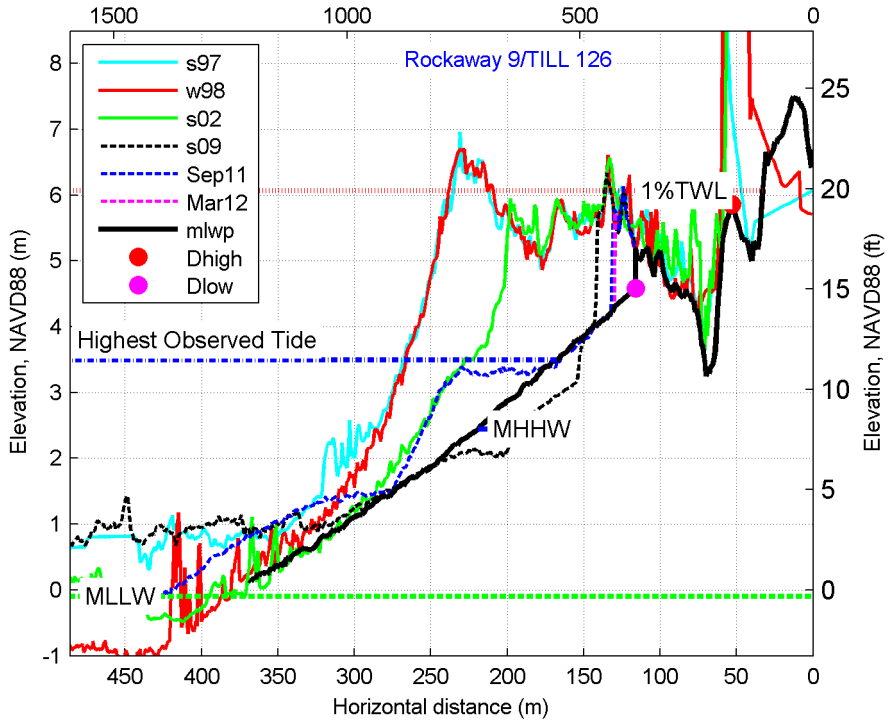

fm_rck 10

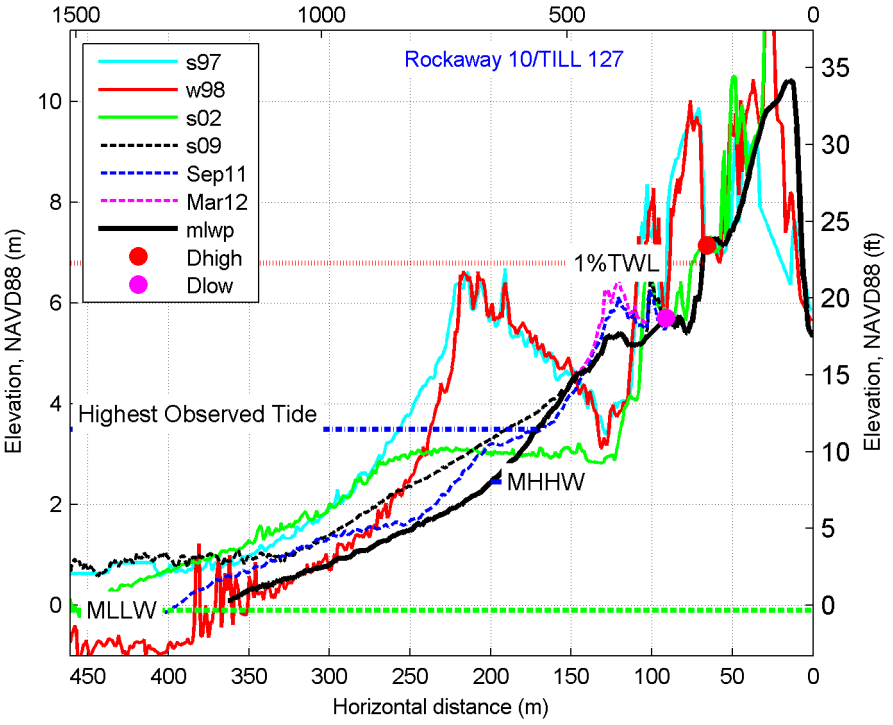

fm_rck 11

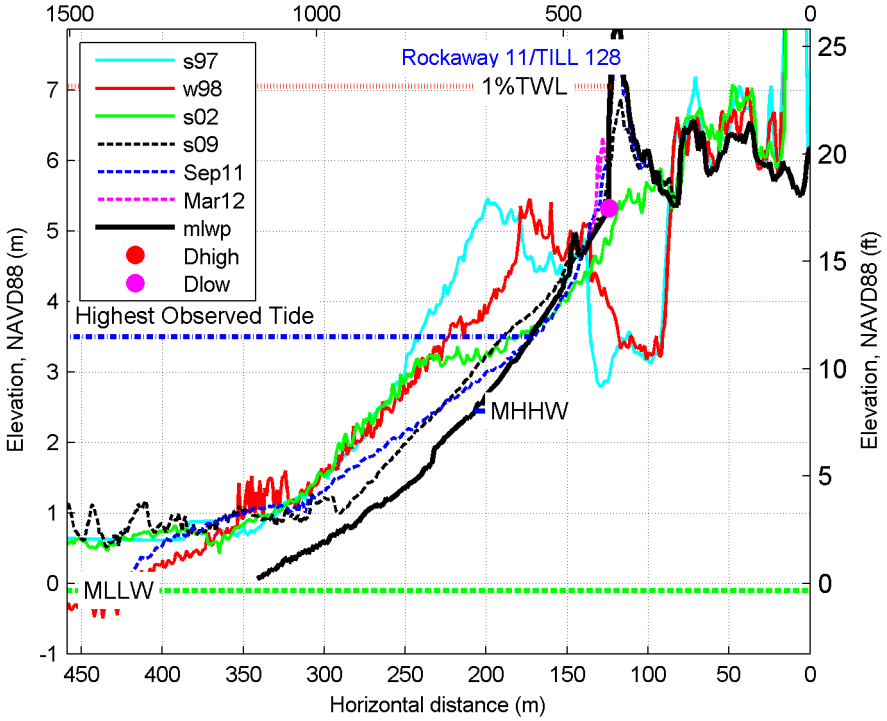

fm_rck 12

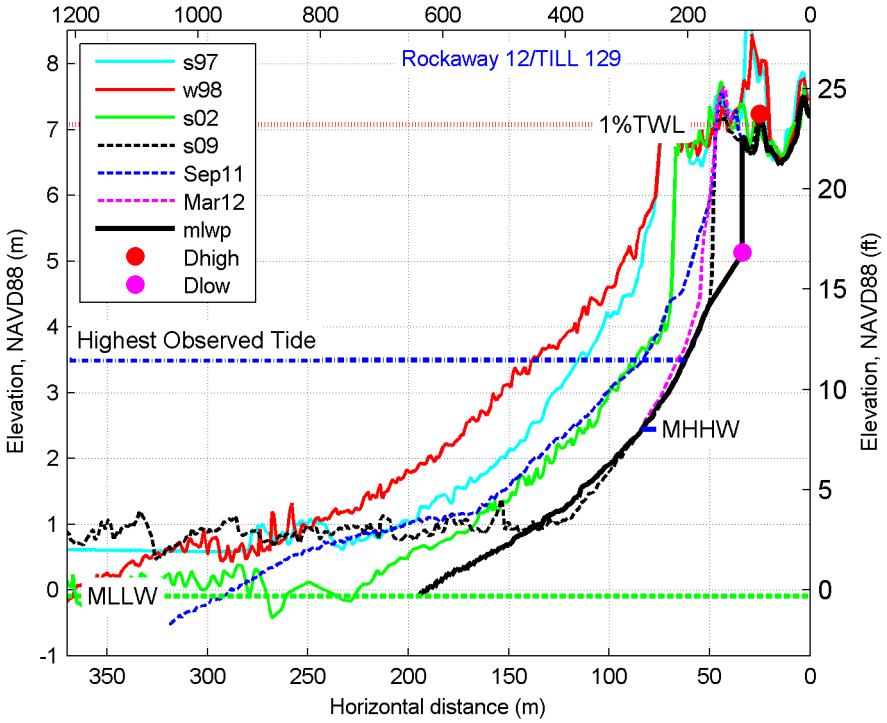

fm_rck 13

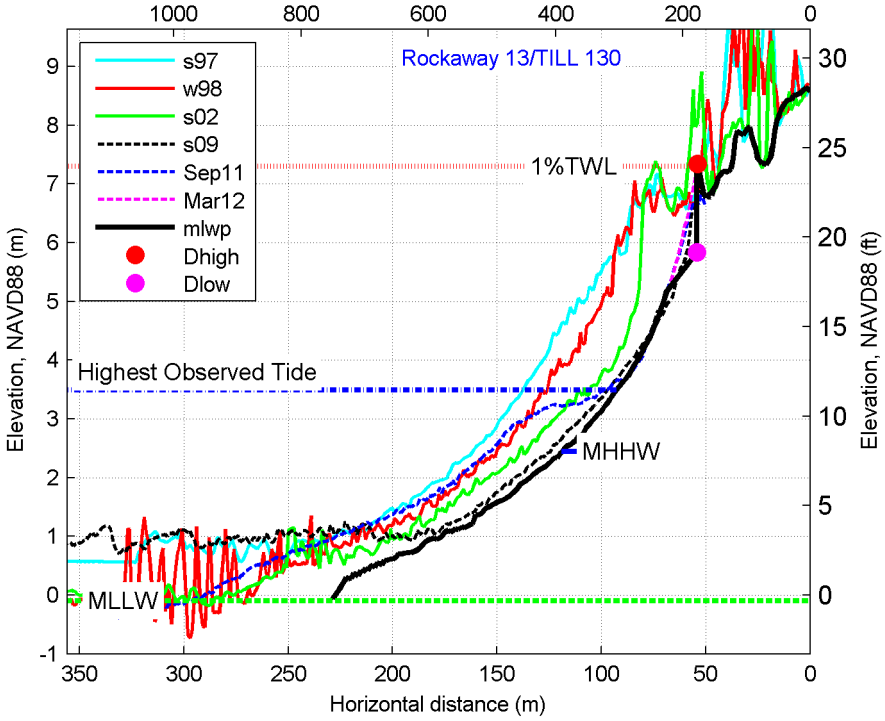

fm_rck 14

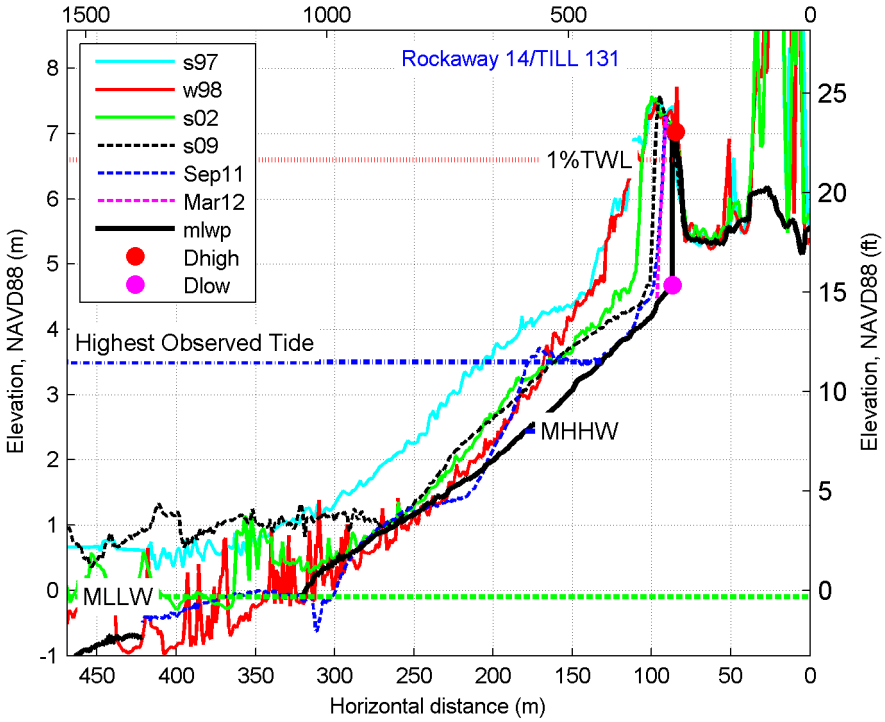

fm_rck 15

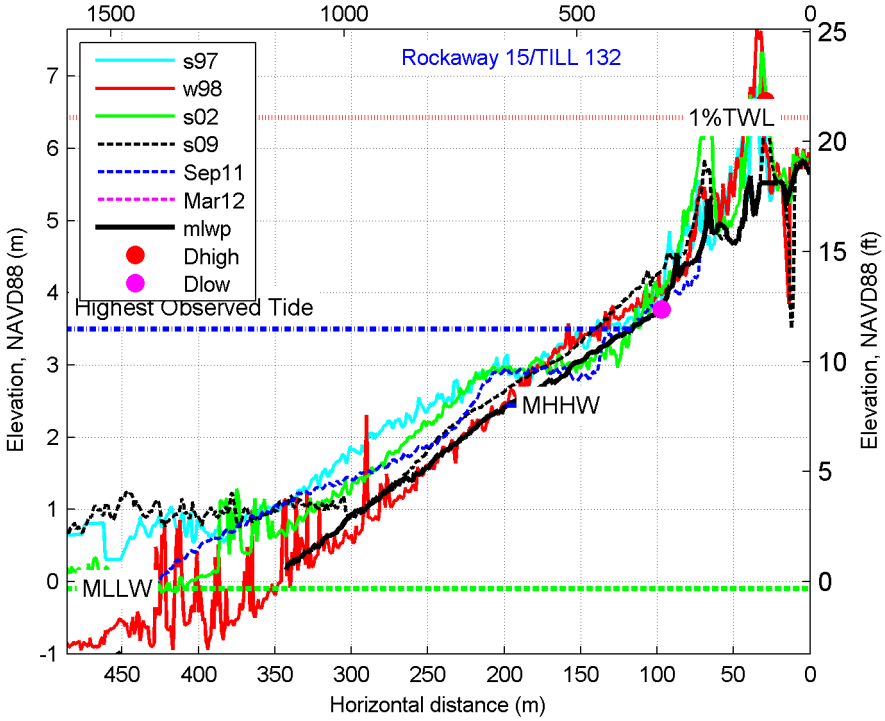

fm_rck 16

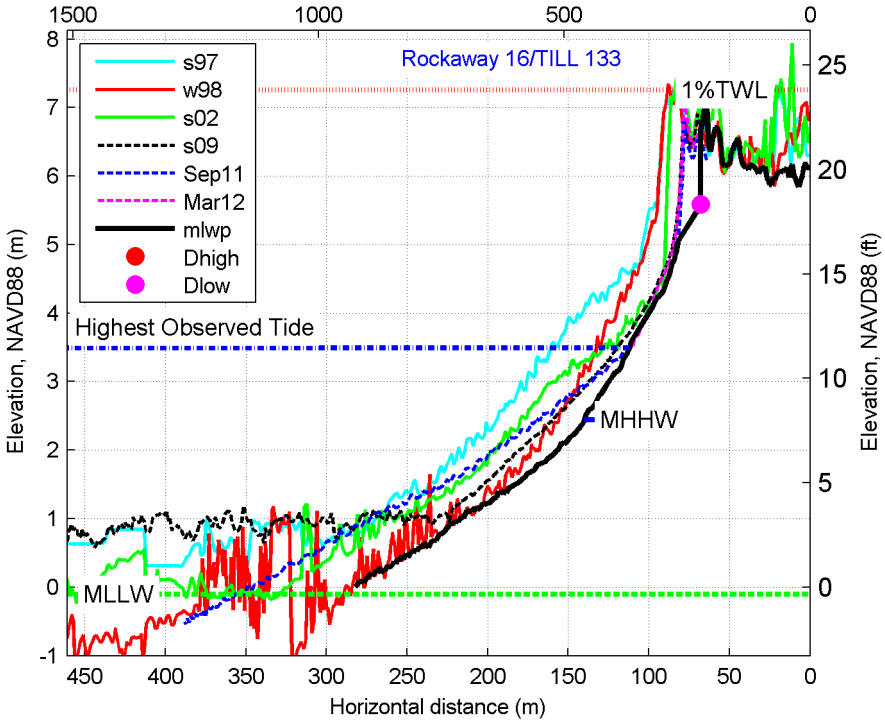

fm_rck 17

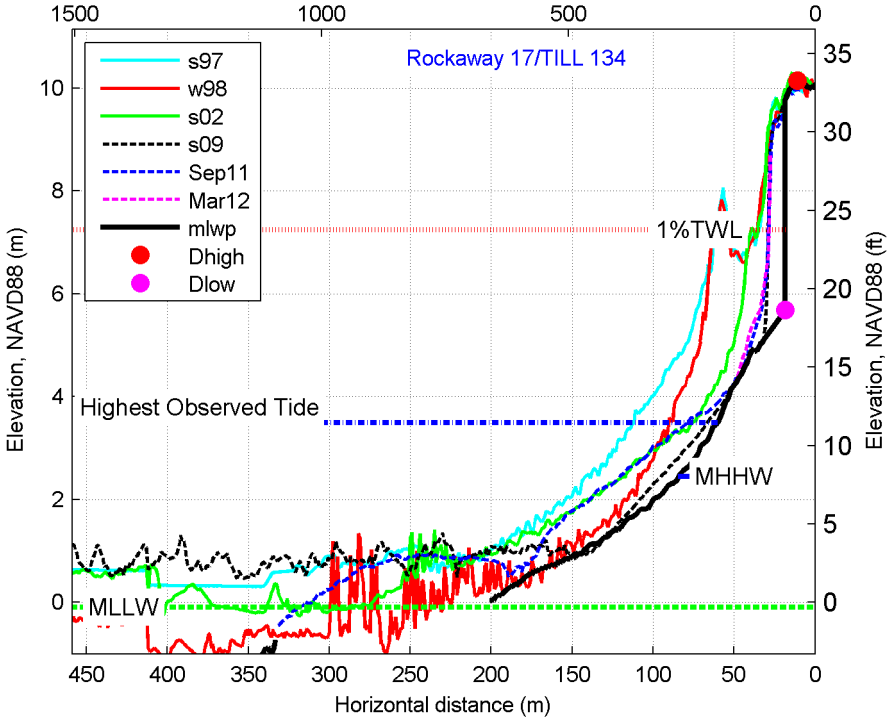

fm_rck 18

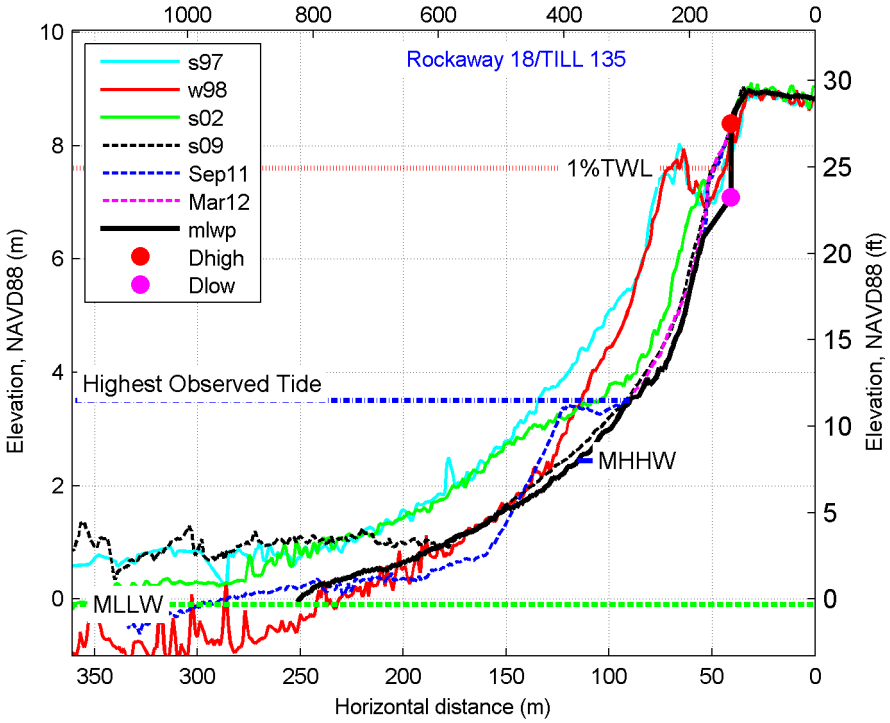

fm_rck 19

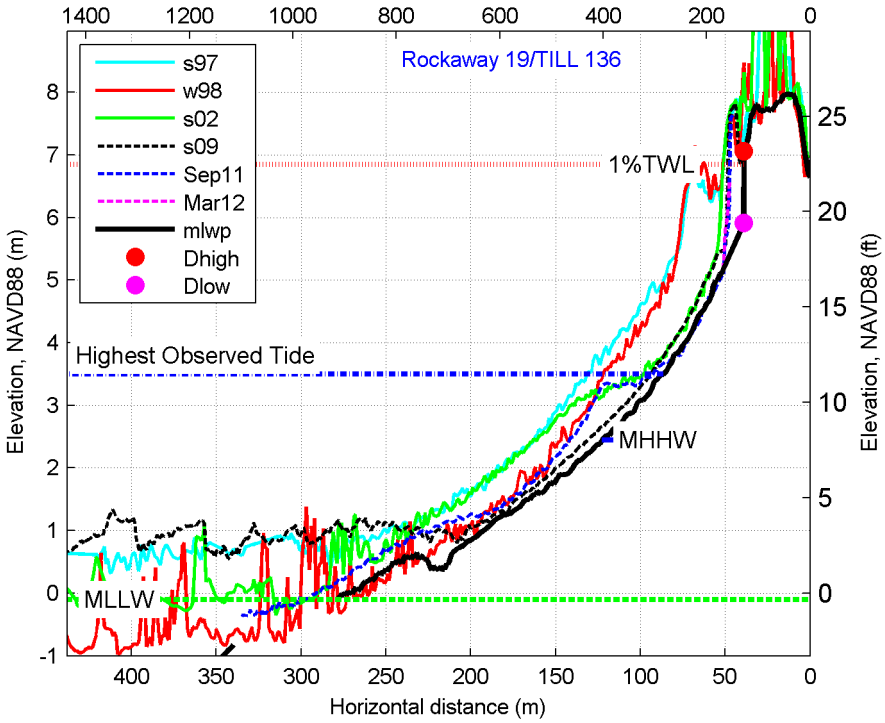

fm_rck 20

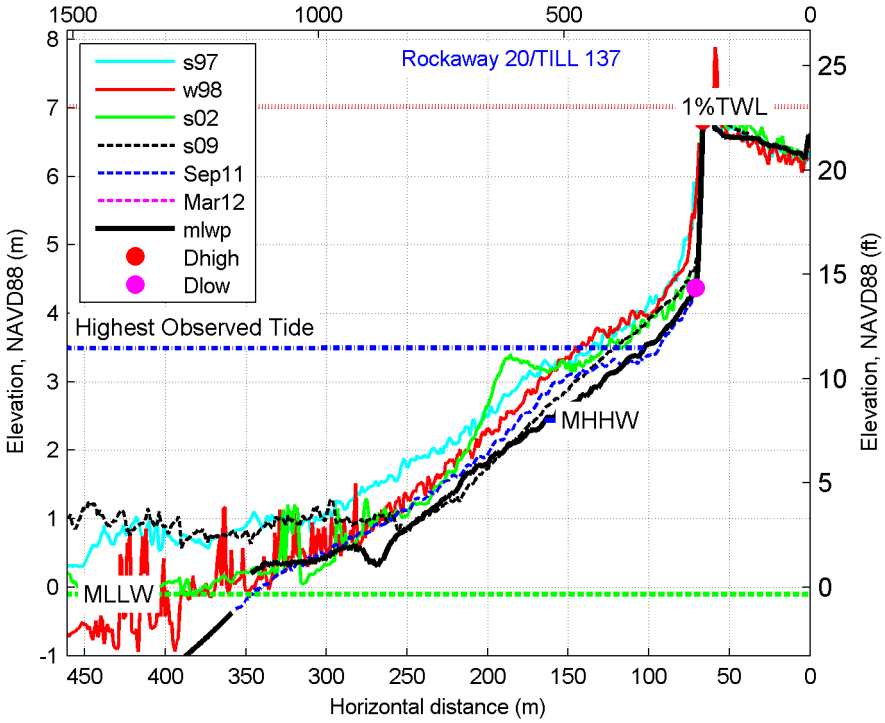

fm_rck 21

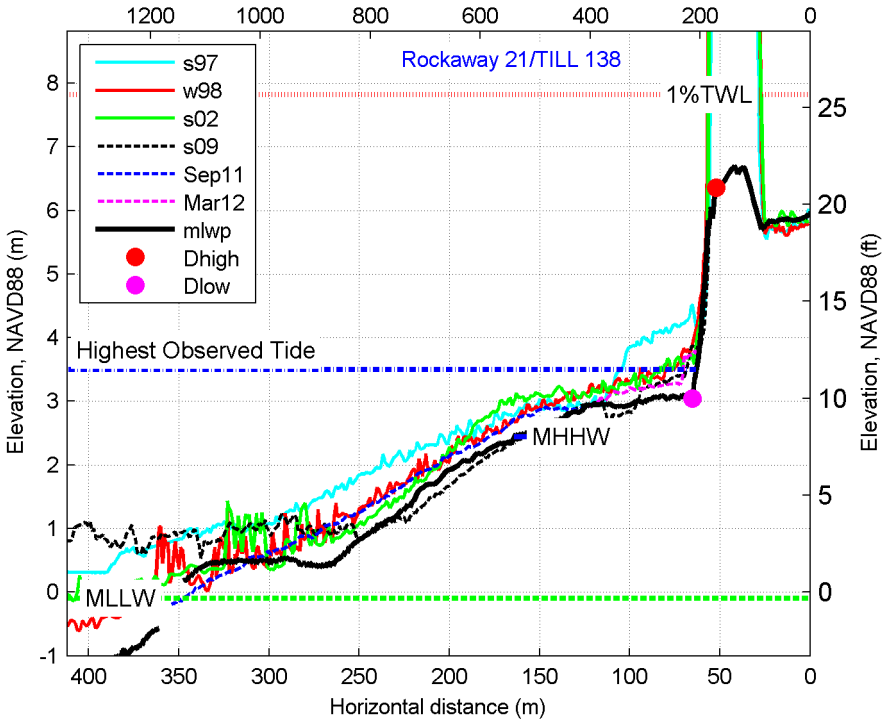

fm_rck 22

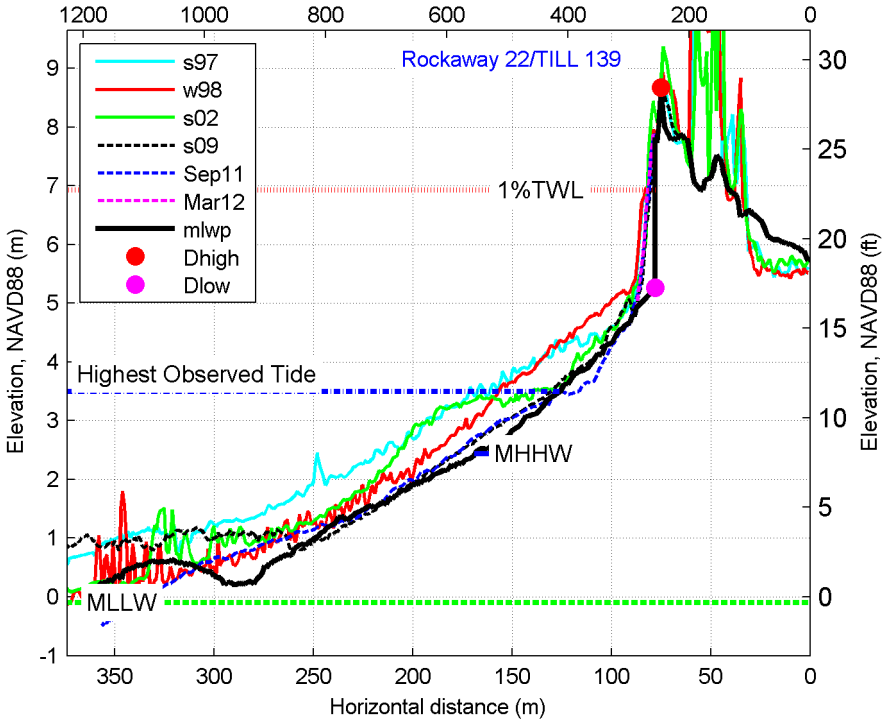

fm_rck 23

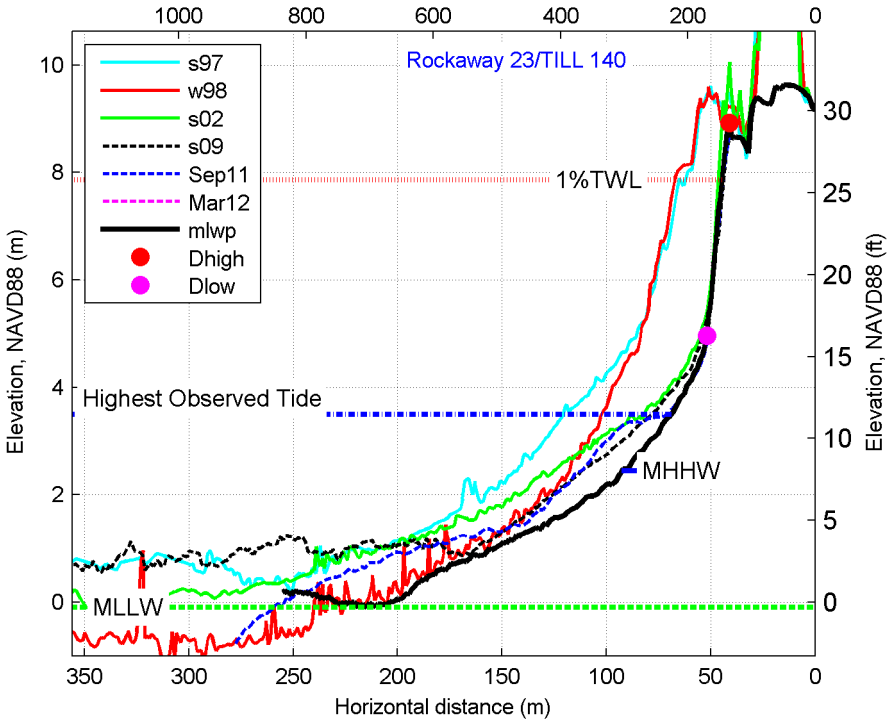

fm_rck 24

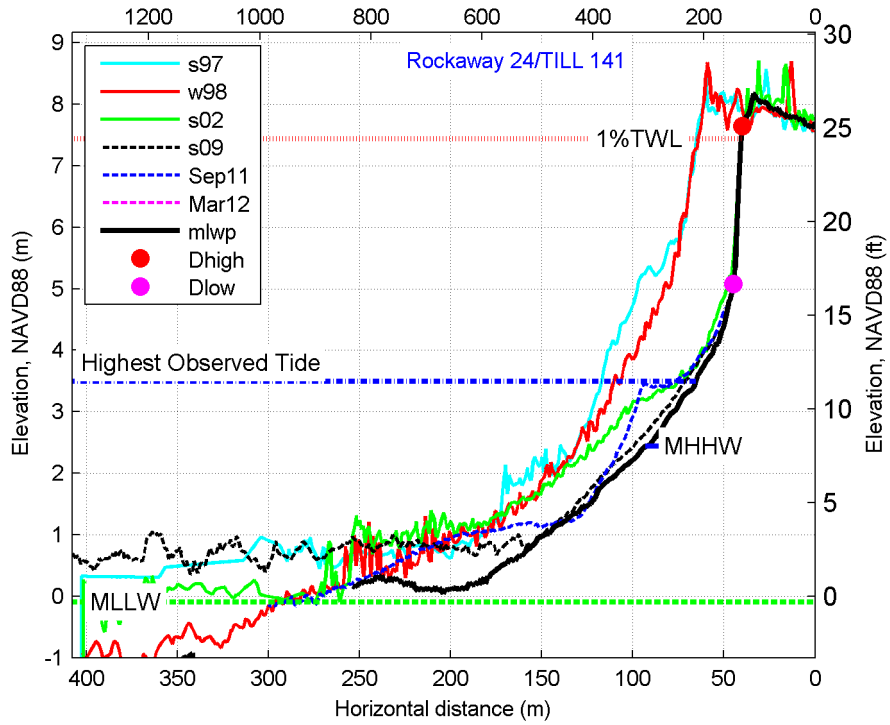

fm_rck 25

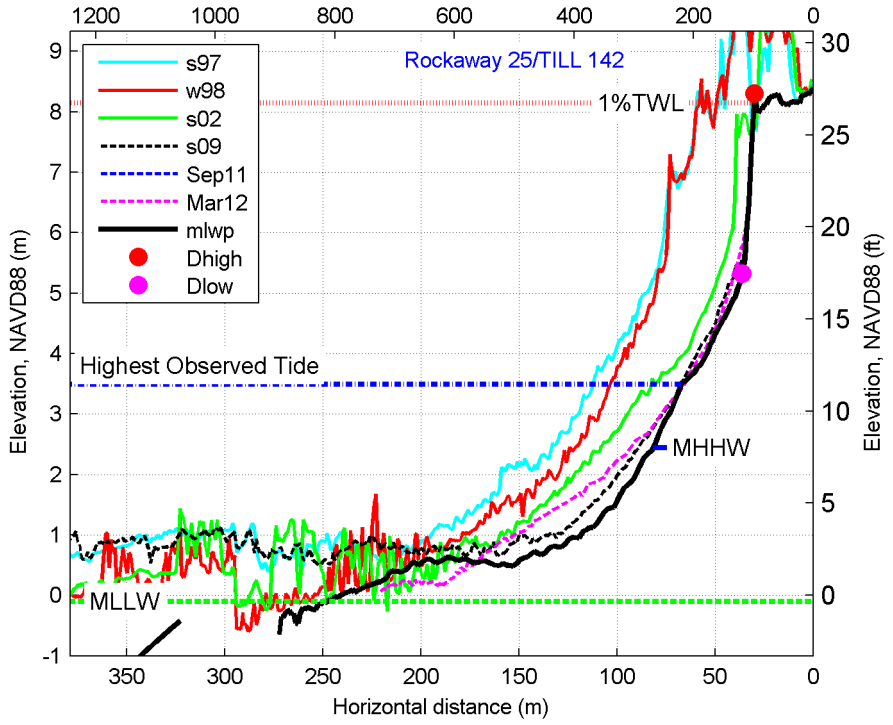

fm_rck 26

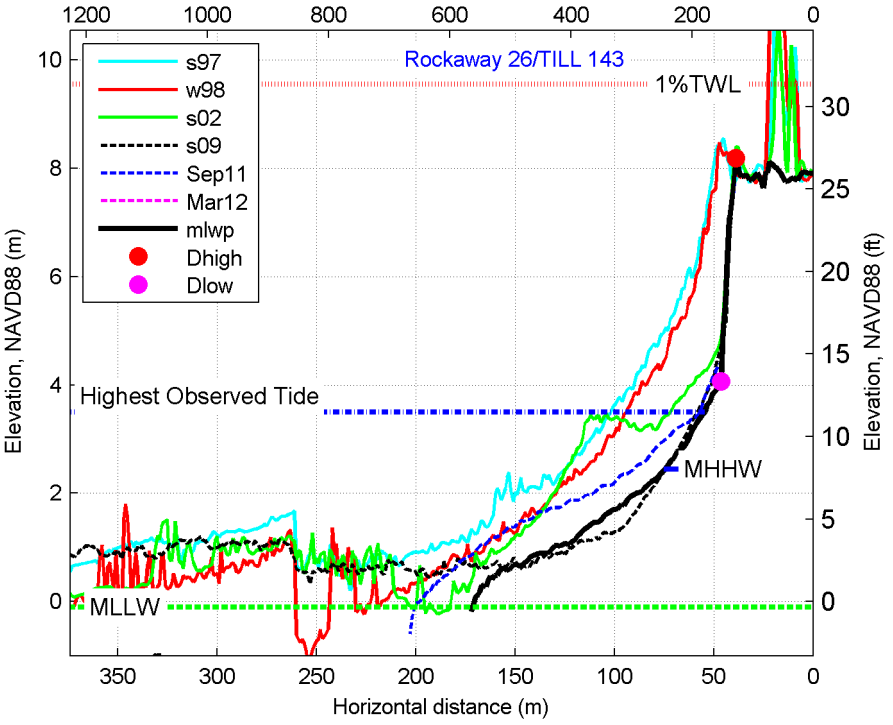

fm_rck 27

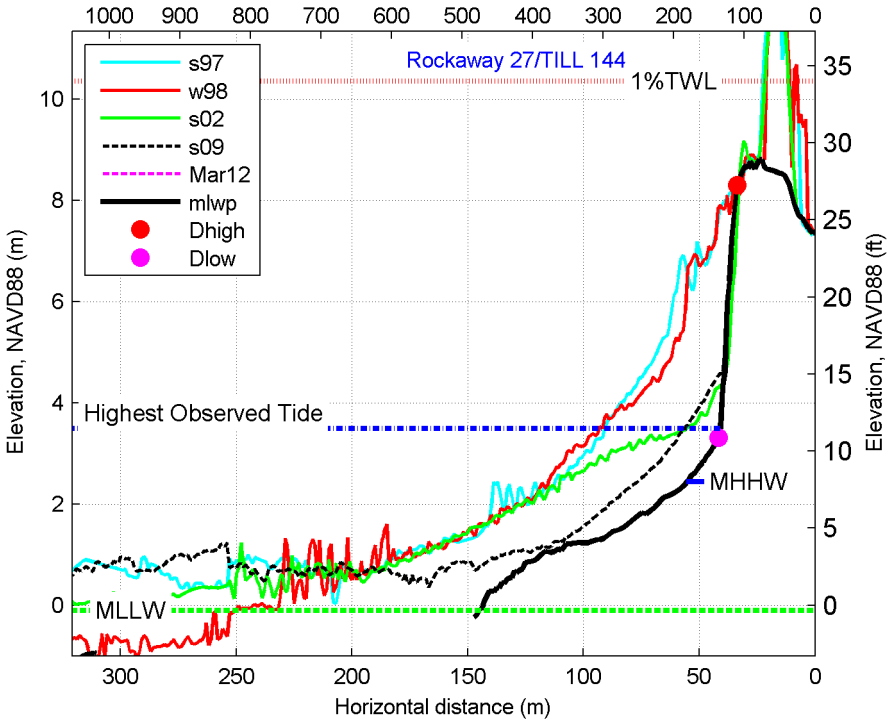

fm_rck 28

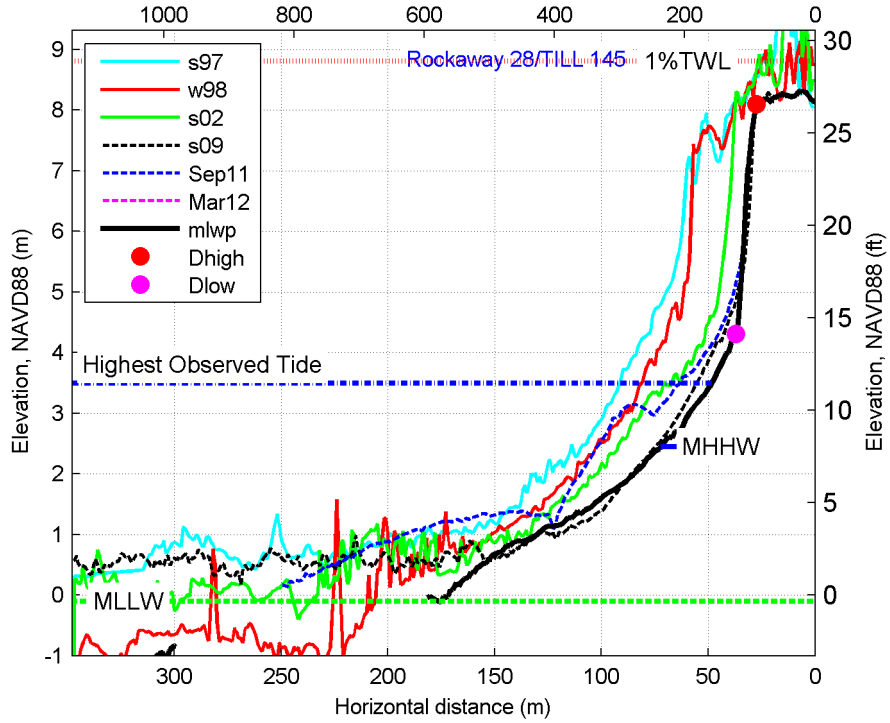

fm_rck 29

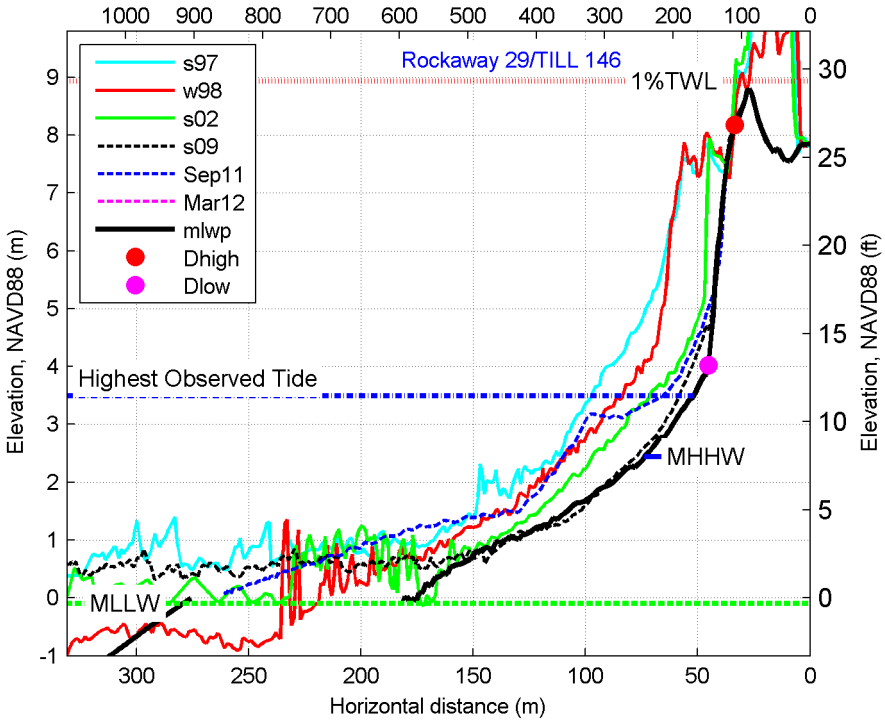

fm_rck 30

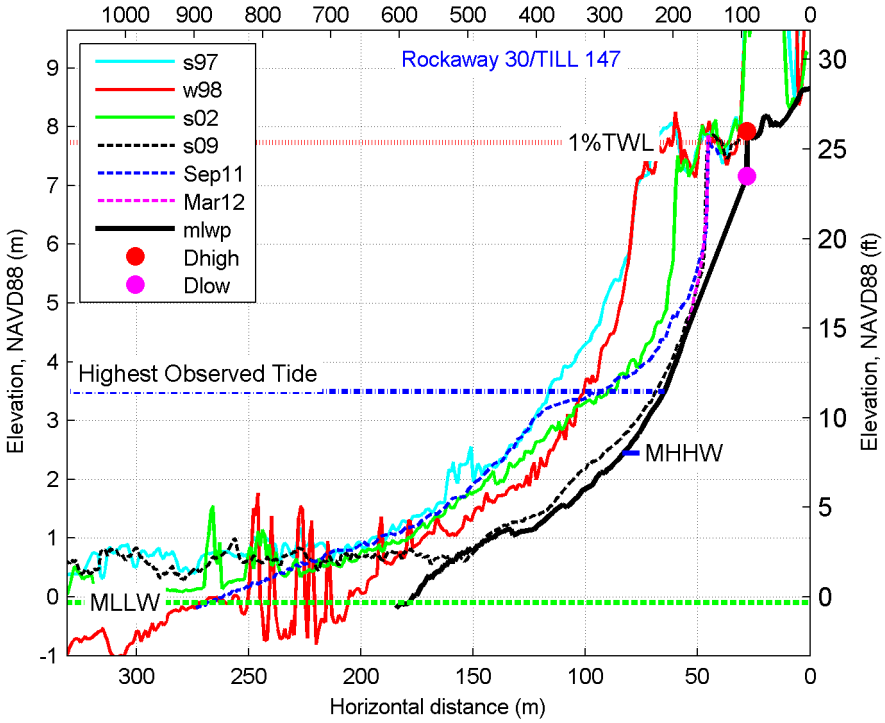

fm_rck 31

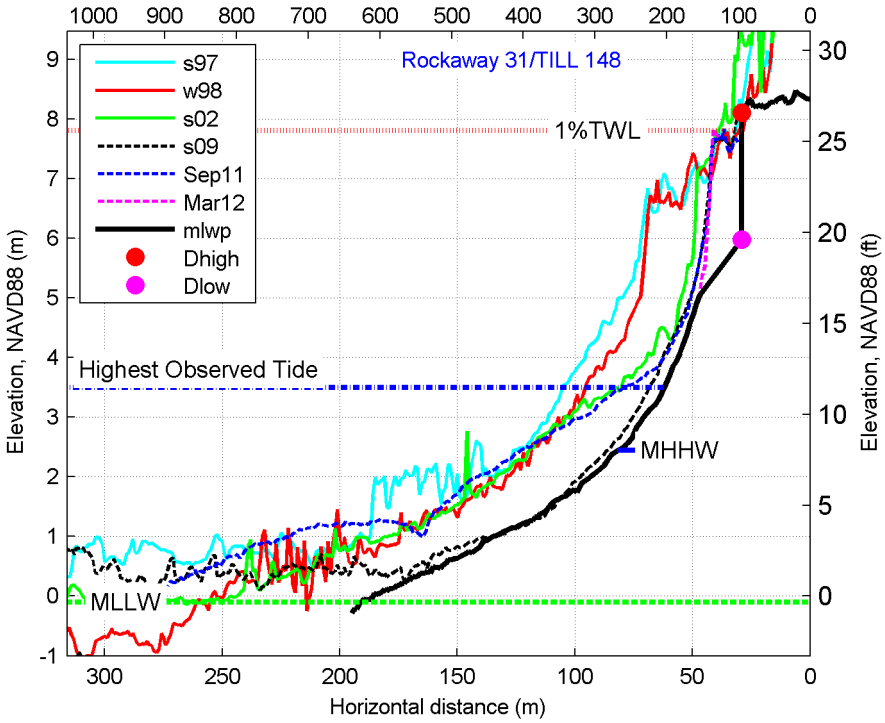

fm_rck 32

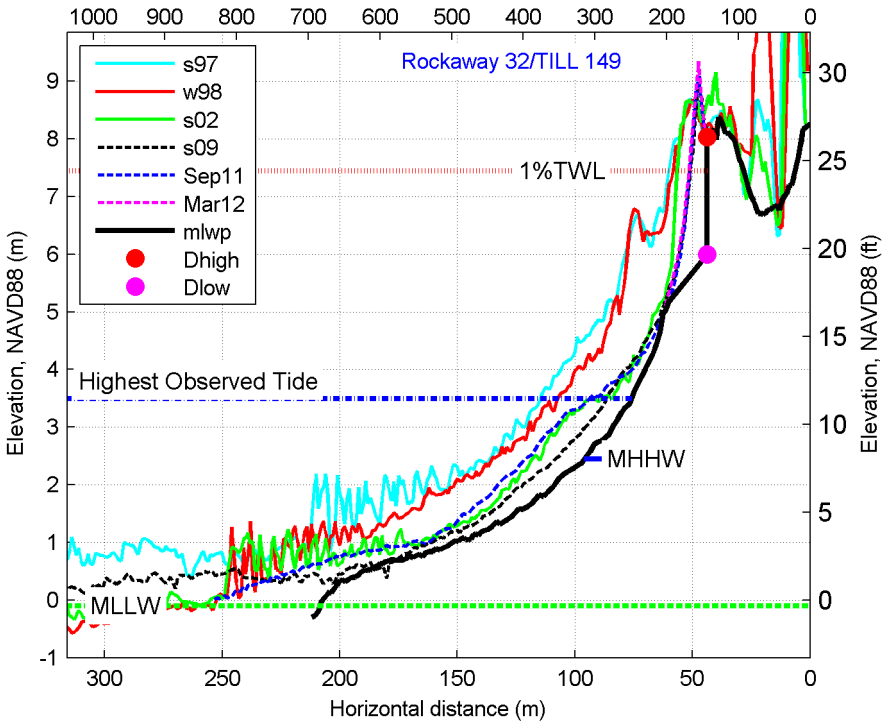

fm_rck 33

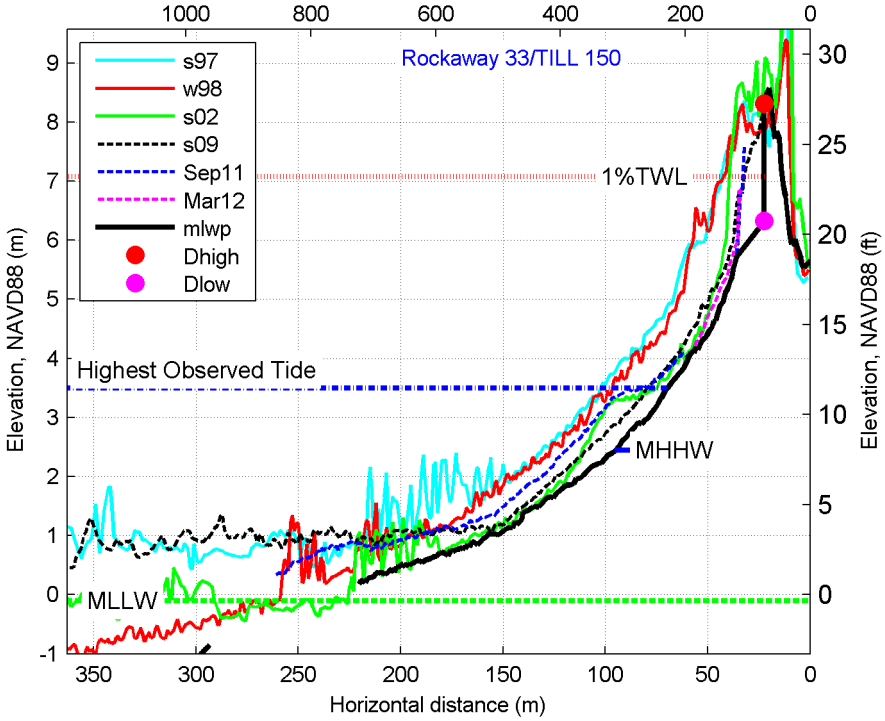

fm_rck 34

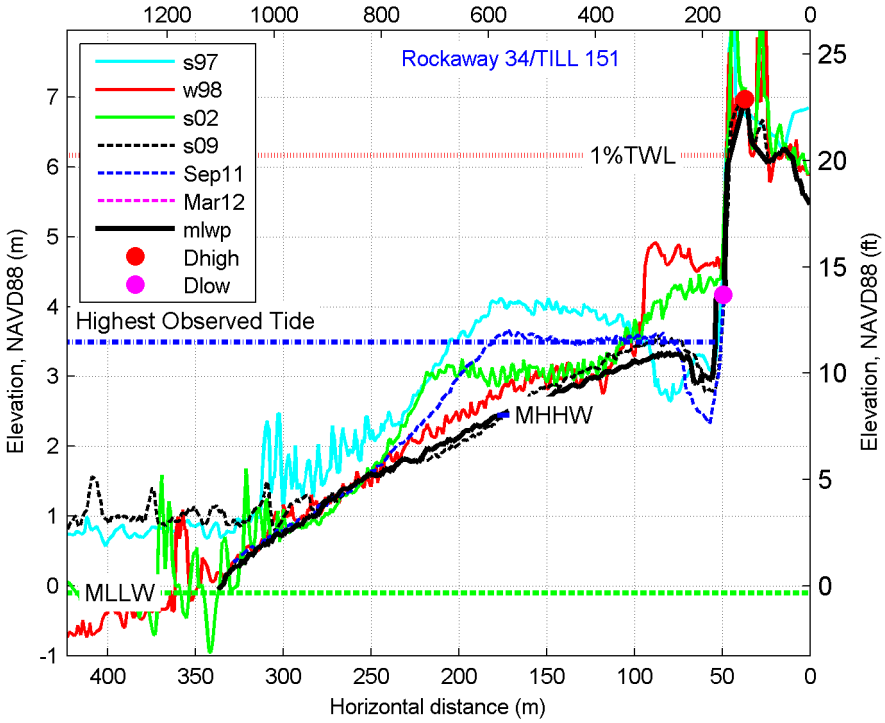

fm_rck 35

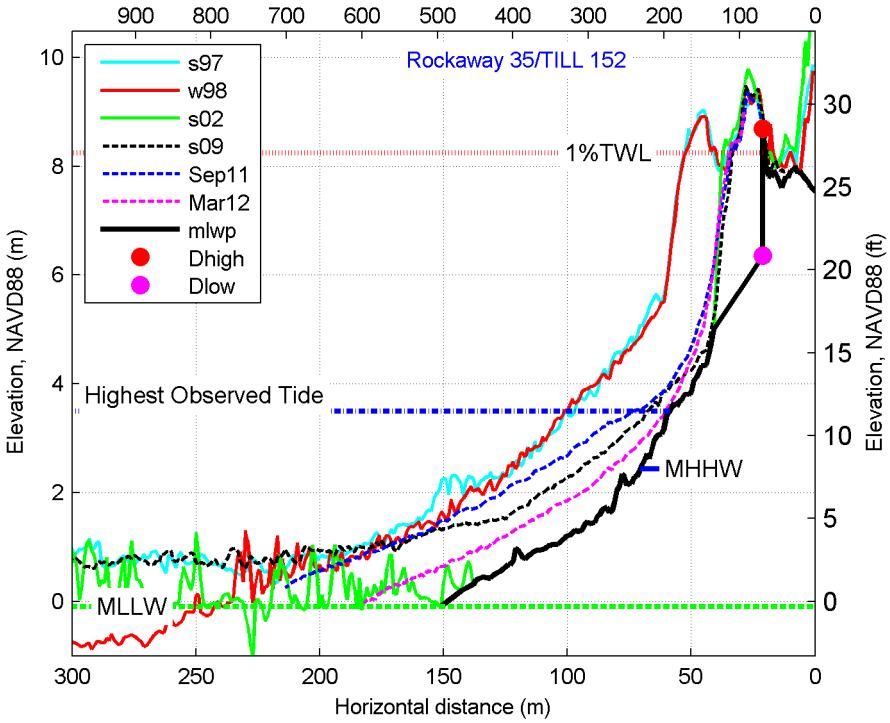

fm_rck 36

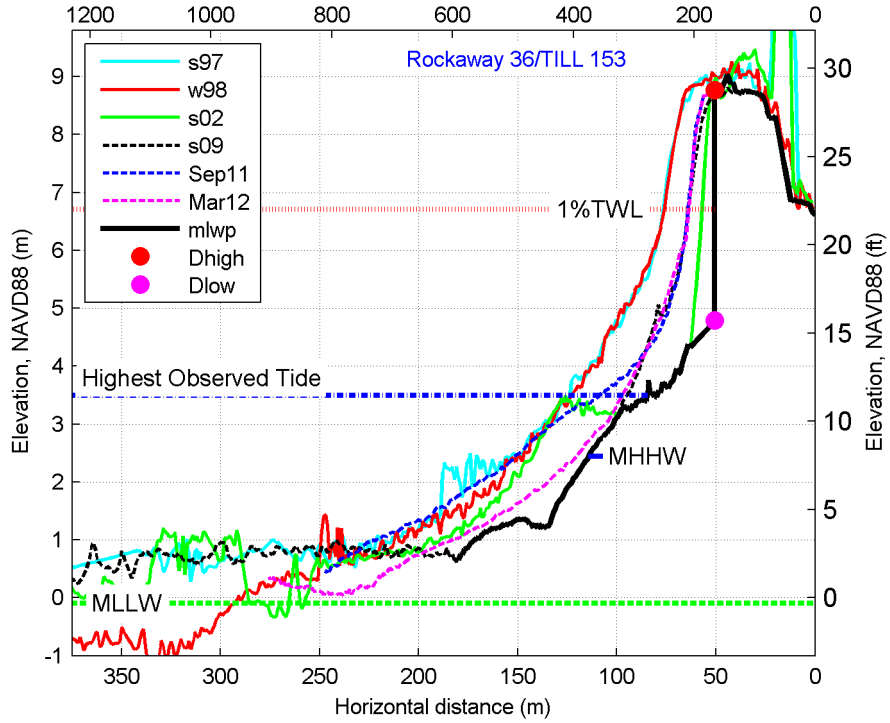

fm_rck 37

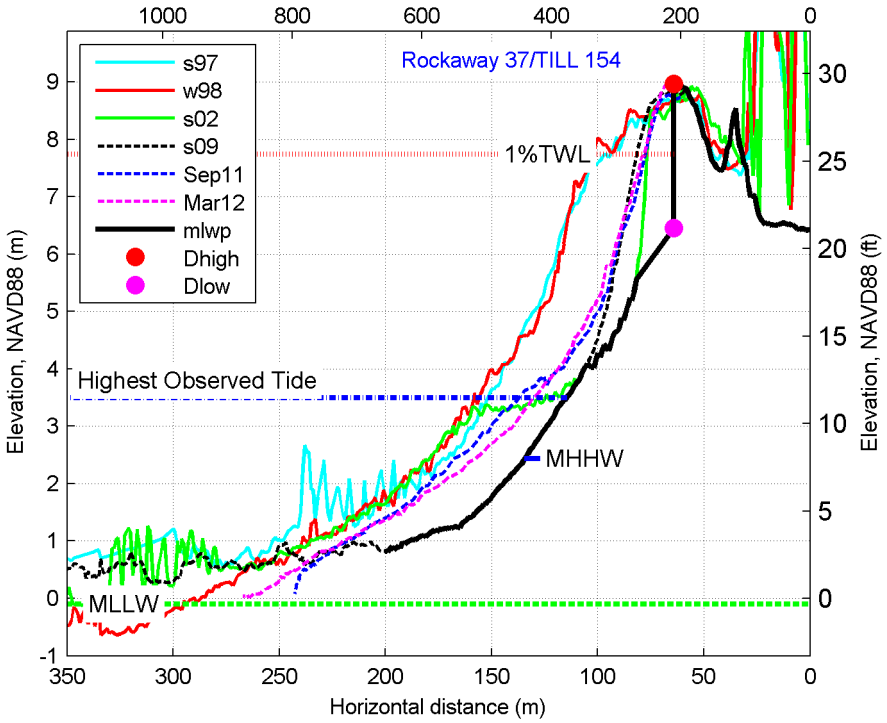

fm_rck 38

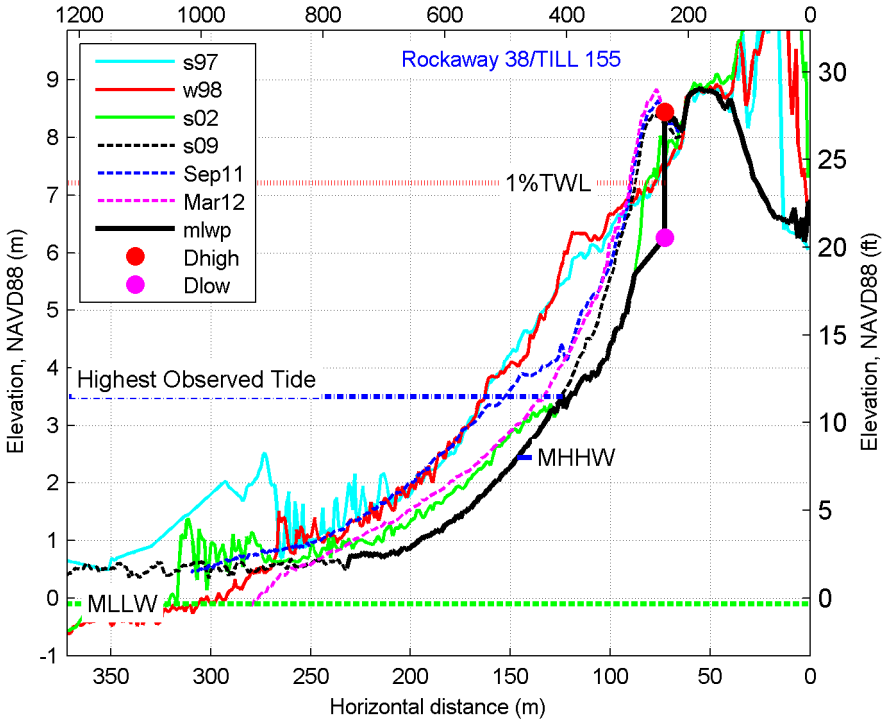

fm_rck 39

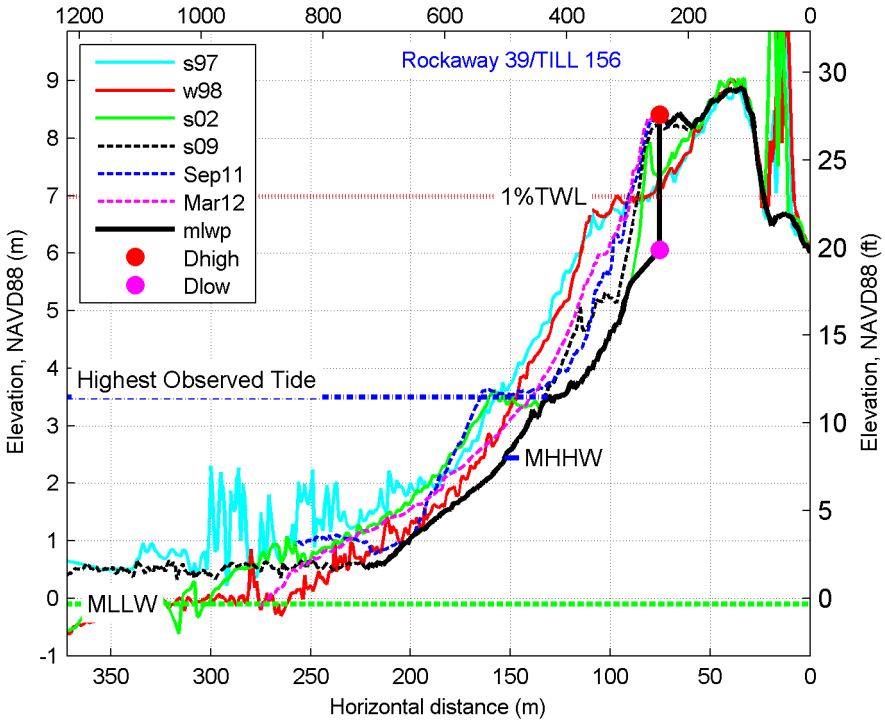

fm_rck 40

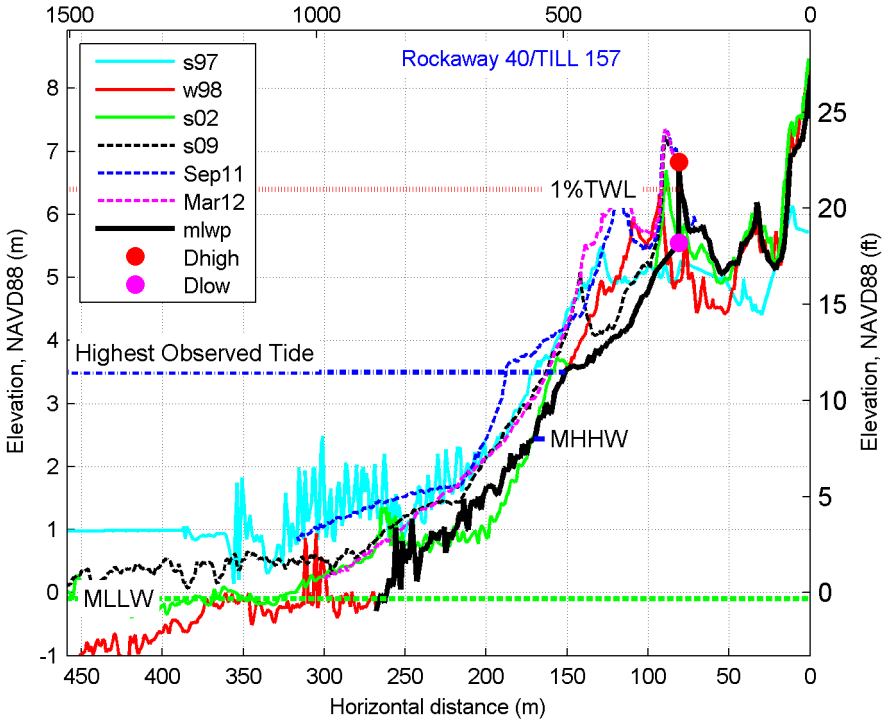

11.4.8 Nehalem Spit

fm_neh 1

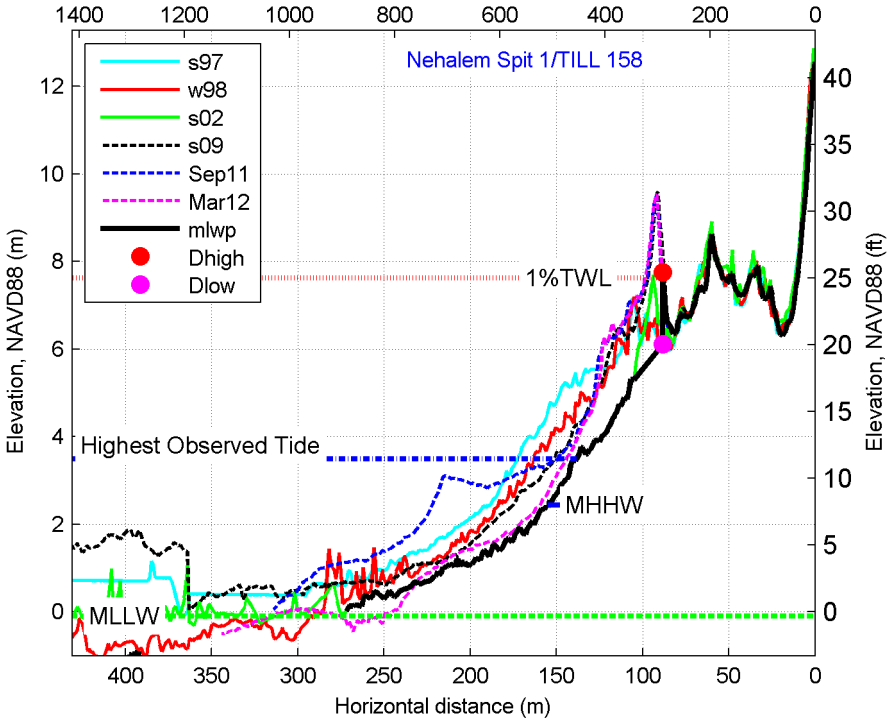

fm_neh 2

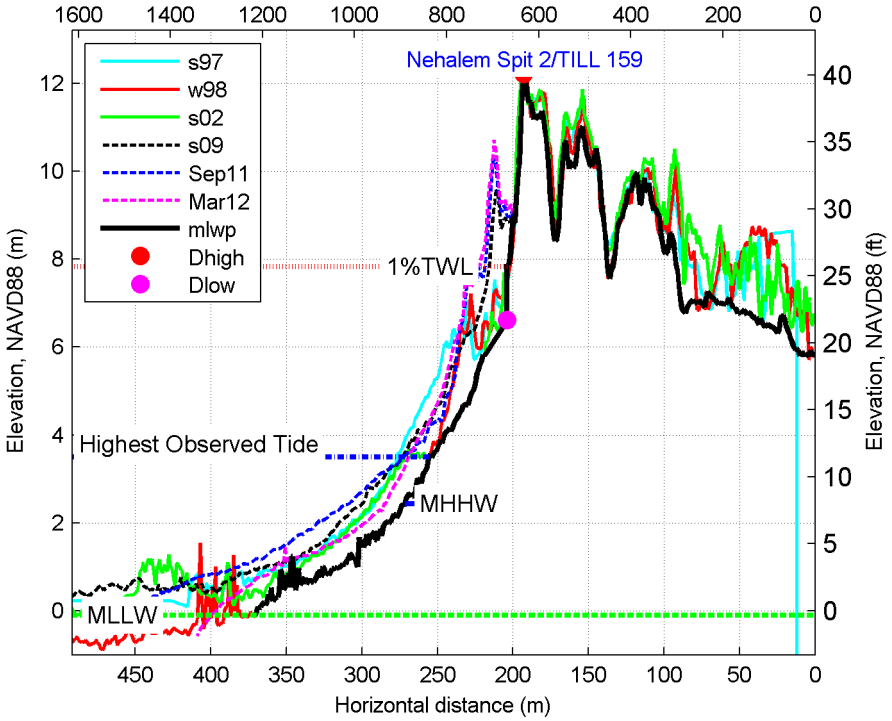

fm_neh 3

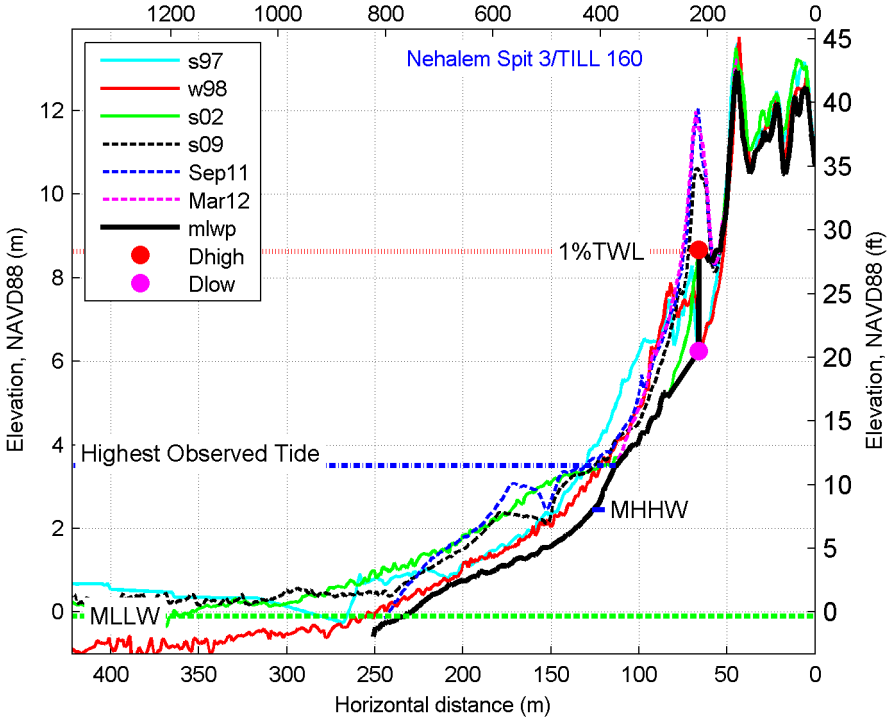

fm_neh 4

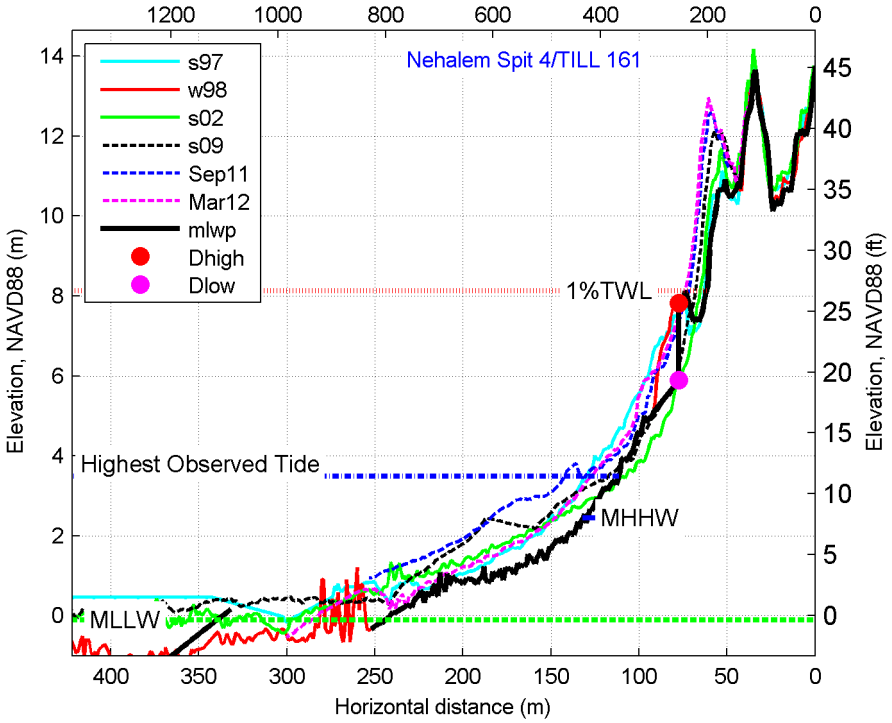

fm_neh 5

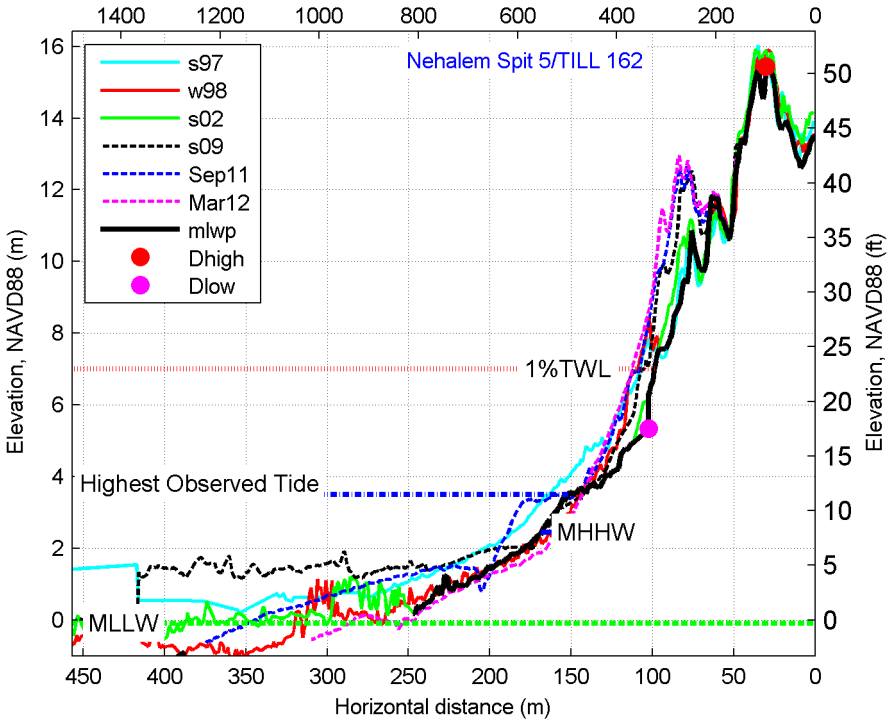

fm_neh 6

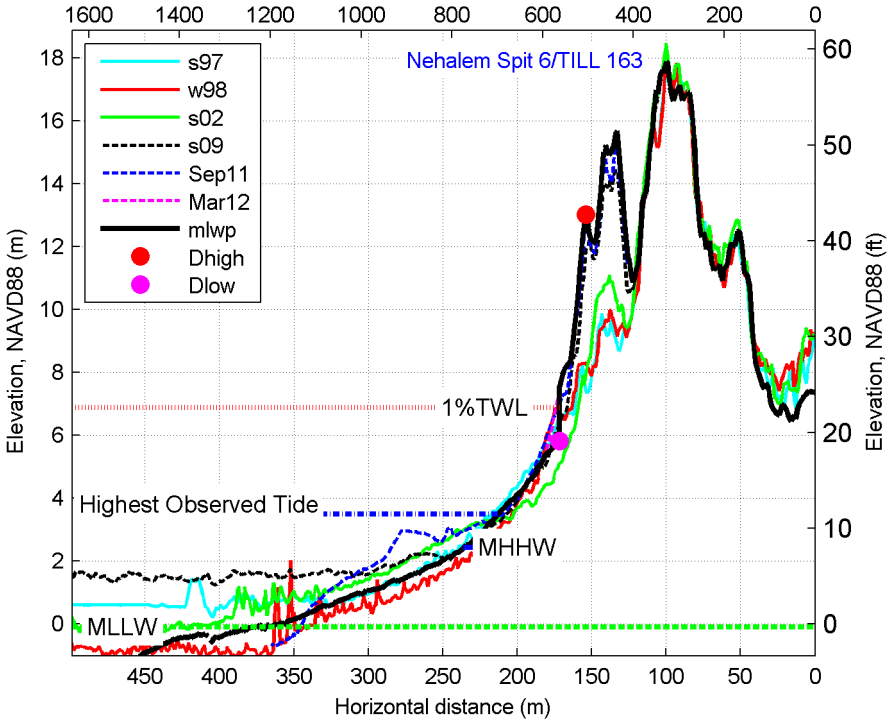

fm_neh 7

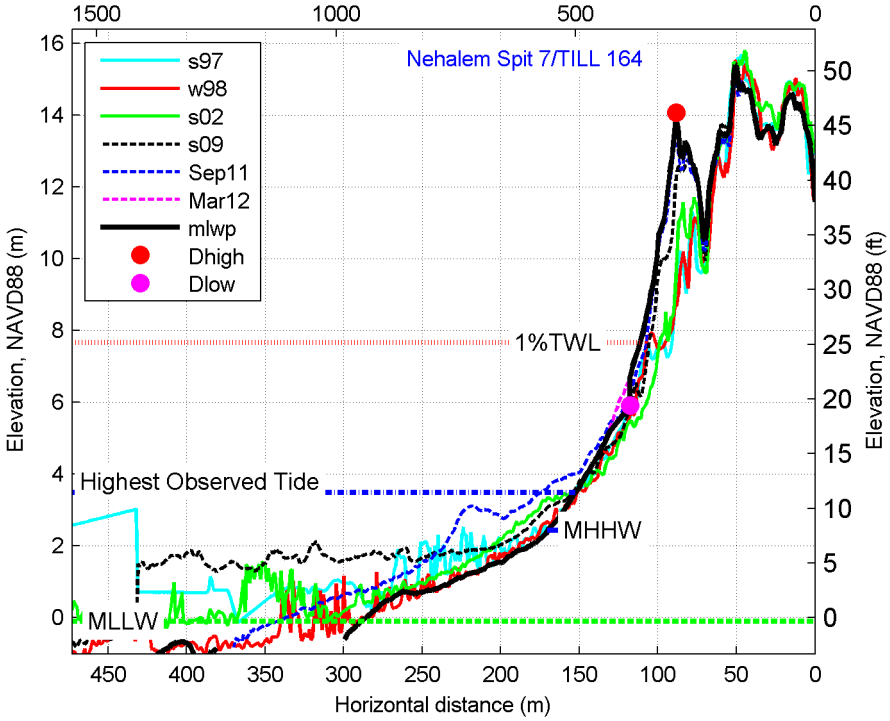

fm_neh 8

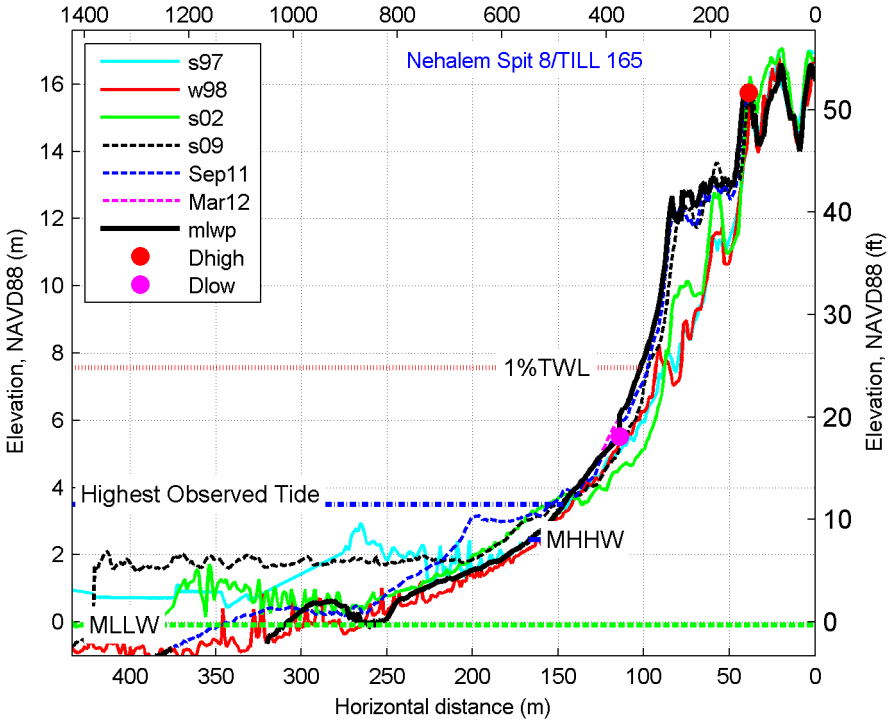

fm_neh 9

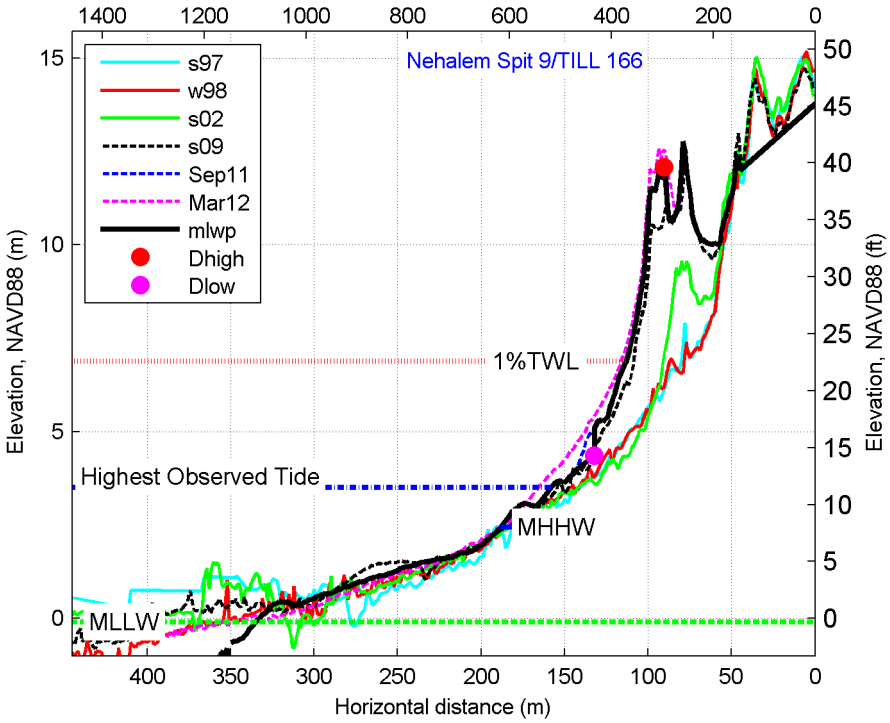

fm_neh 10

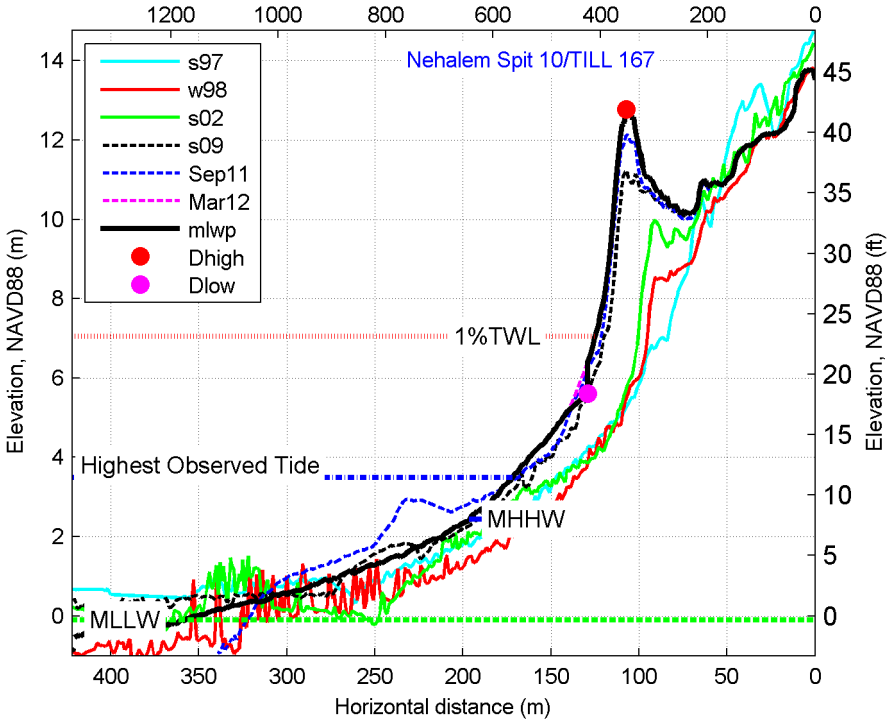

fm_neh 11

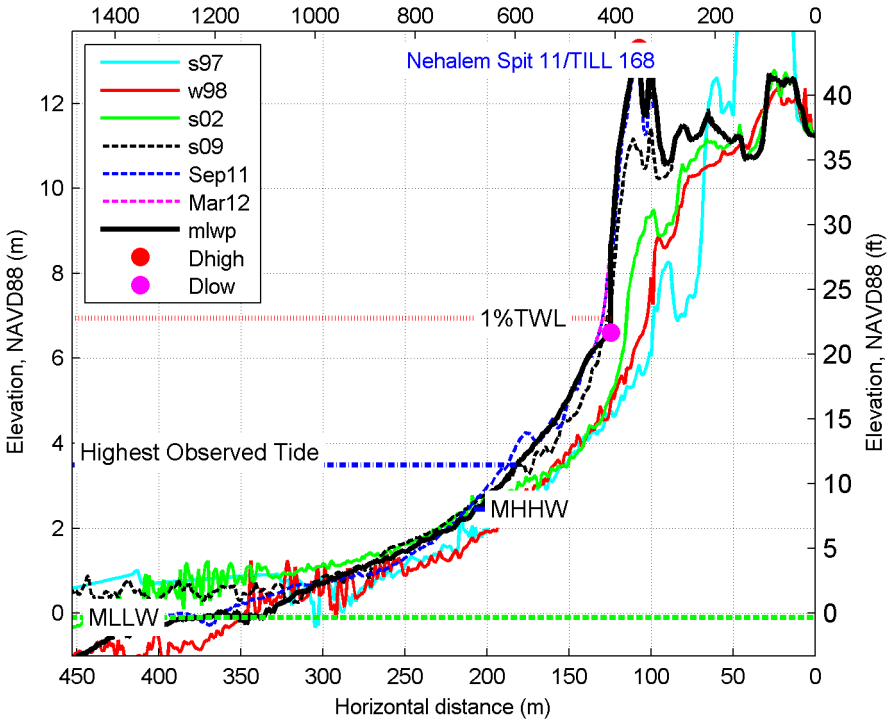

fm_neh 12

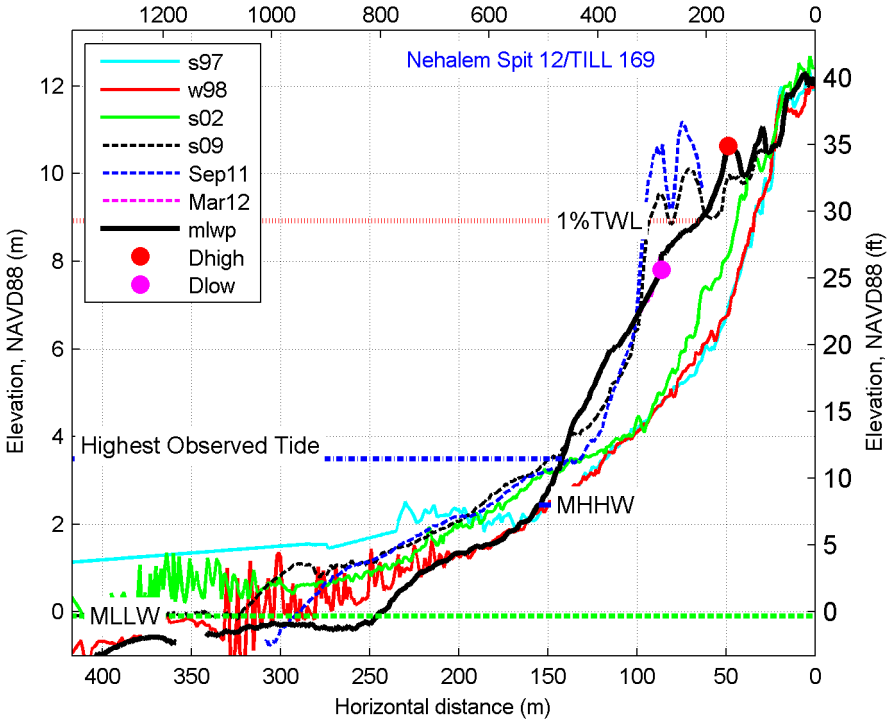

fm_neh 13

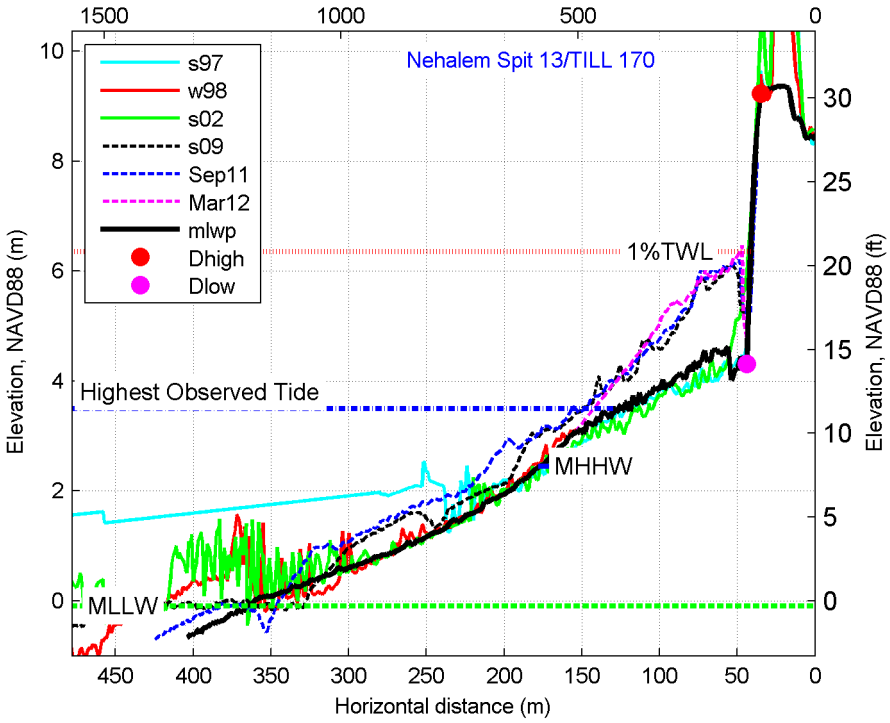

fm_neh 14

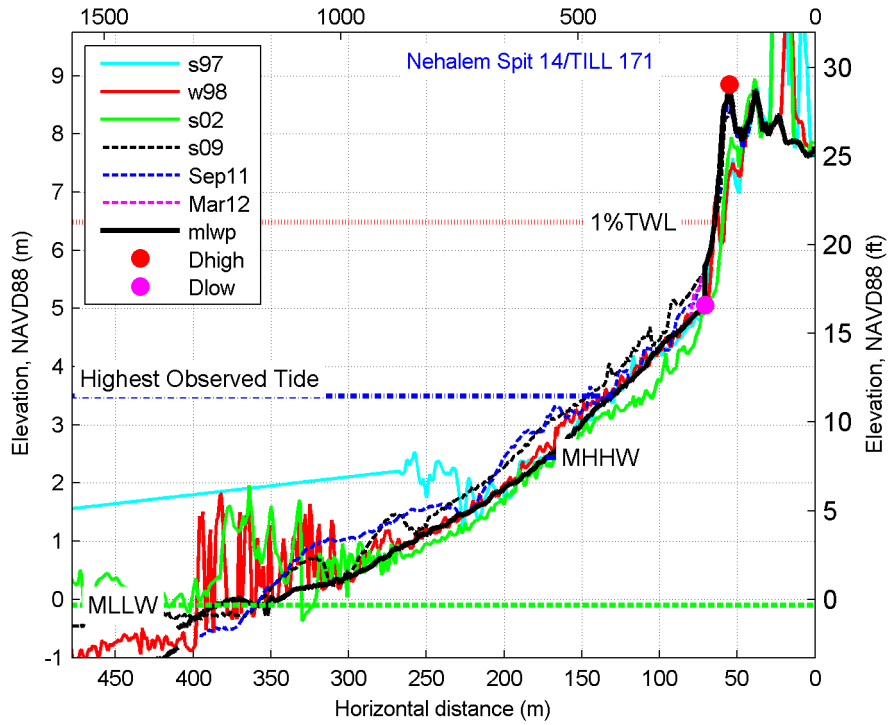

fm_neh 15

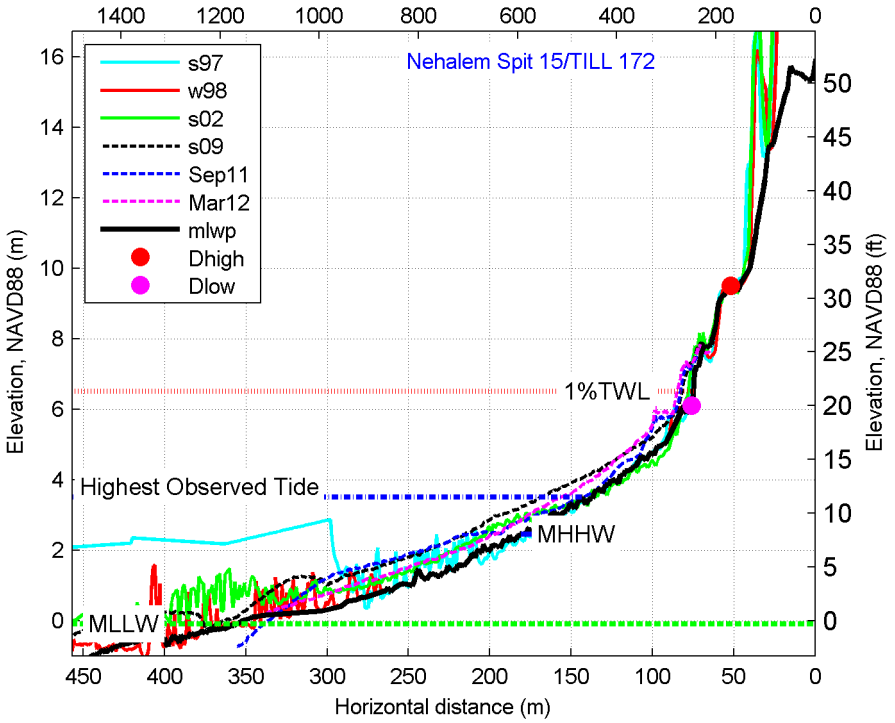

fm_neh 16

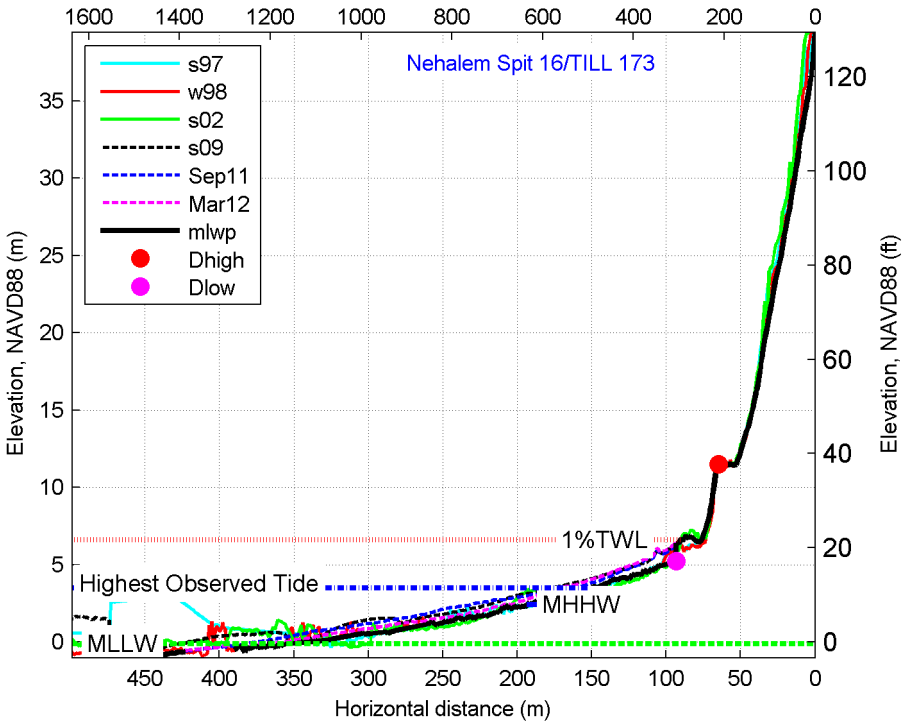

fm_neh 17

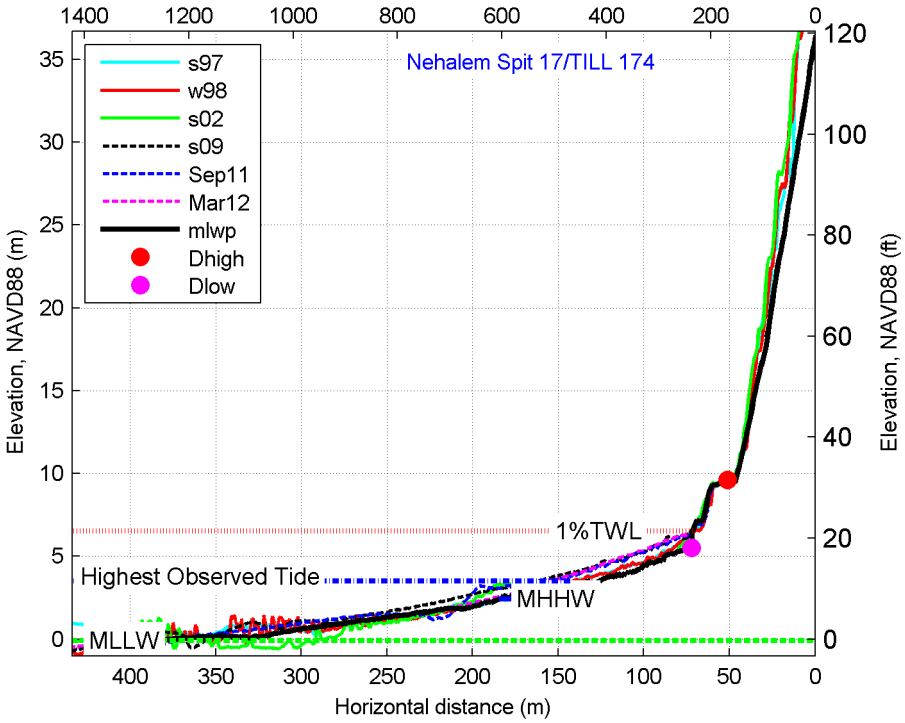

fm_neh 18

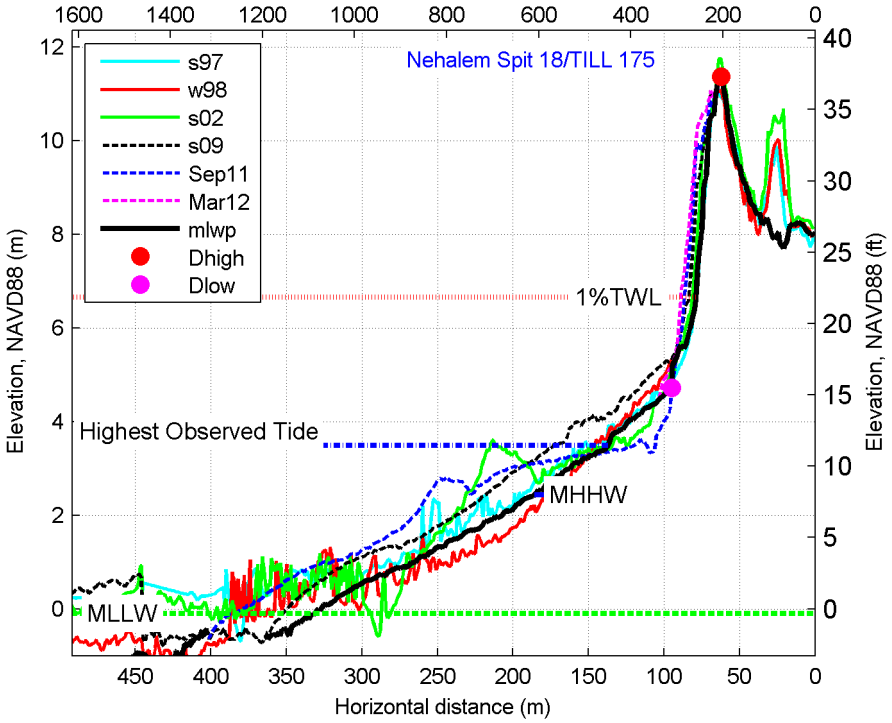

fm_neh 19

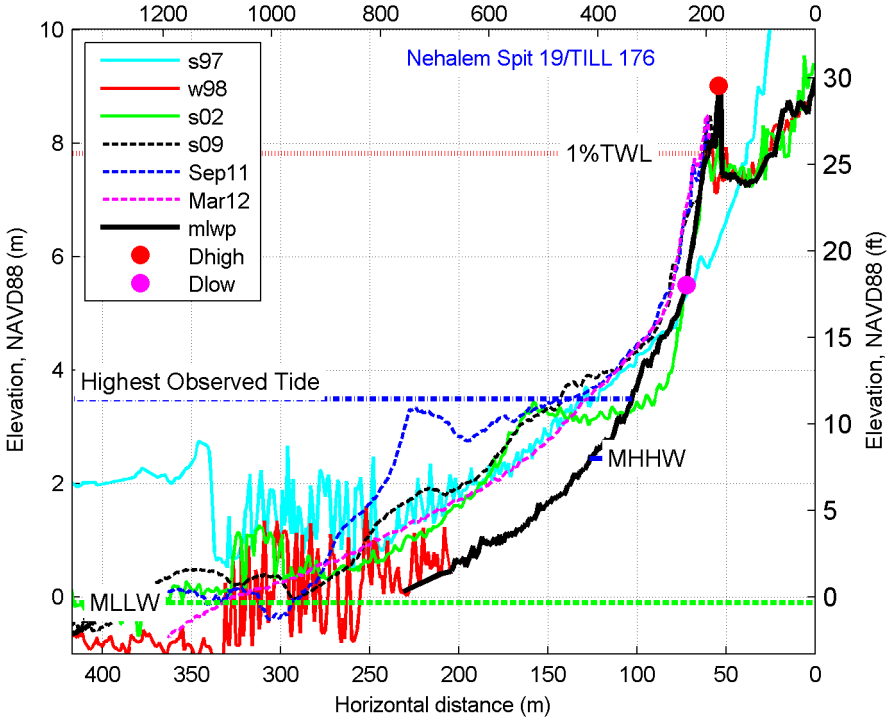

fm_neh 20

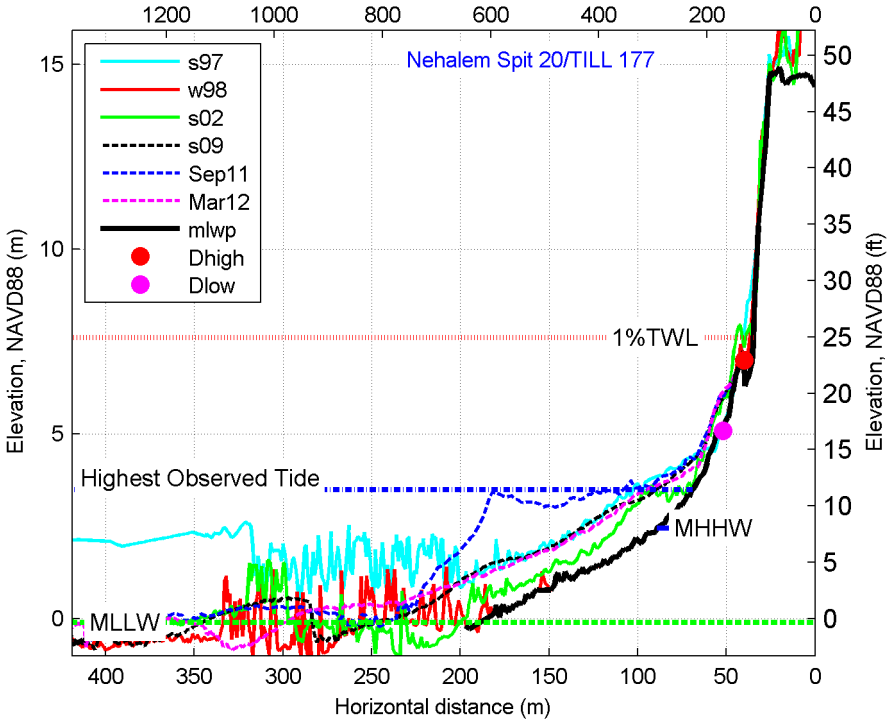

fm_neh 21

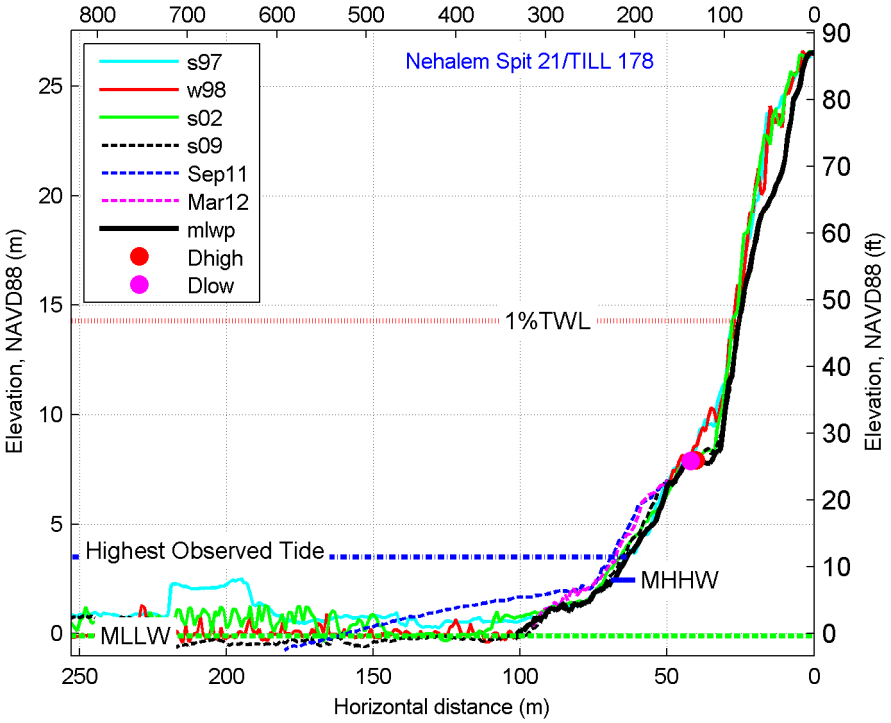
Nehalem Spit 21/TILL 178
s97
w98
s02
s09
Sep11
Mar12
mlwp
Dhigh
Dlow
1%TWL
Highest Observed Tide
MHHW
MLLW
Elevation, NAVD88 (m)
Elevation, NAVD88 (ft)
Horizontal distance (m)
800
700
600
500
400
300
200
100
0
250
200
150
100
50
0
25
20
15
10
5
0
90
80
70
60
50
40
30
20
10
0

11.5 Appendix D: Supplemental Transect Overtopping Table

Profiles	Transect	Dist_3 (≥0.91 m)	Dist_2 (>0.61 <0.91 m)	Dist_1 (≤0.31 m)	*hV*2 > 5.7 m3/s2 (m)	Comment
Neskowin	TILL 2_3524					Mapped to D_{high}
	TILL 2_3521					Mapped to splashdown distance
	TILL 2_3517					Mapped to splashdown distance
	TILL 3_3514					Mapped to D_{high}
	TILL 3_3508					Mapped to D_{high}
	TILL 3_3506					Mapped to D_{high}
	TILL 3_3504					Mapped to D_{high}
	TILL 3_3502			24.98	47.03	Mapped overtopping
Netarts	TILL 79_2035	6.08	45.44	96.74	151.89	Mapped overtopping
	TILL 79_2033					Forced transition from overtopping at TILL 79_2035 to meet the PFD
	TILL 135_857					Mapped to D_{high}
	TILL 135_856					Mapped to D_{high}
	TILL 147_783					Mapped to D_{high}
	TILL 147_778					Mapped to D_{high}